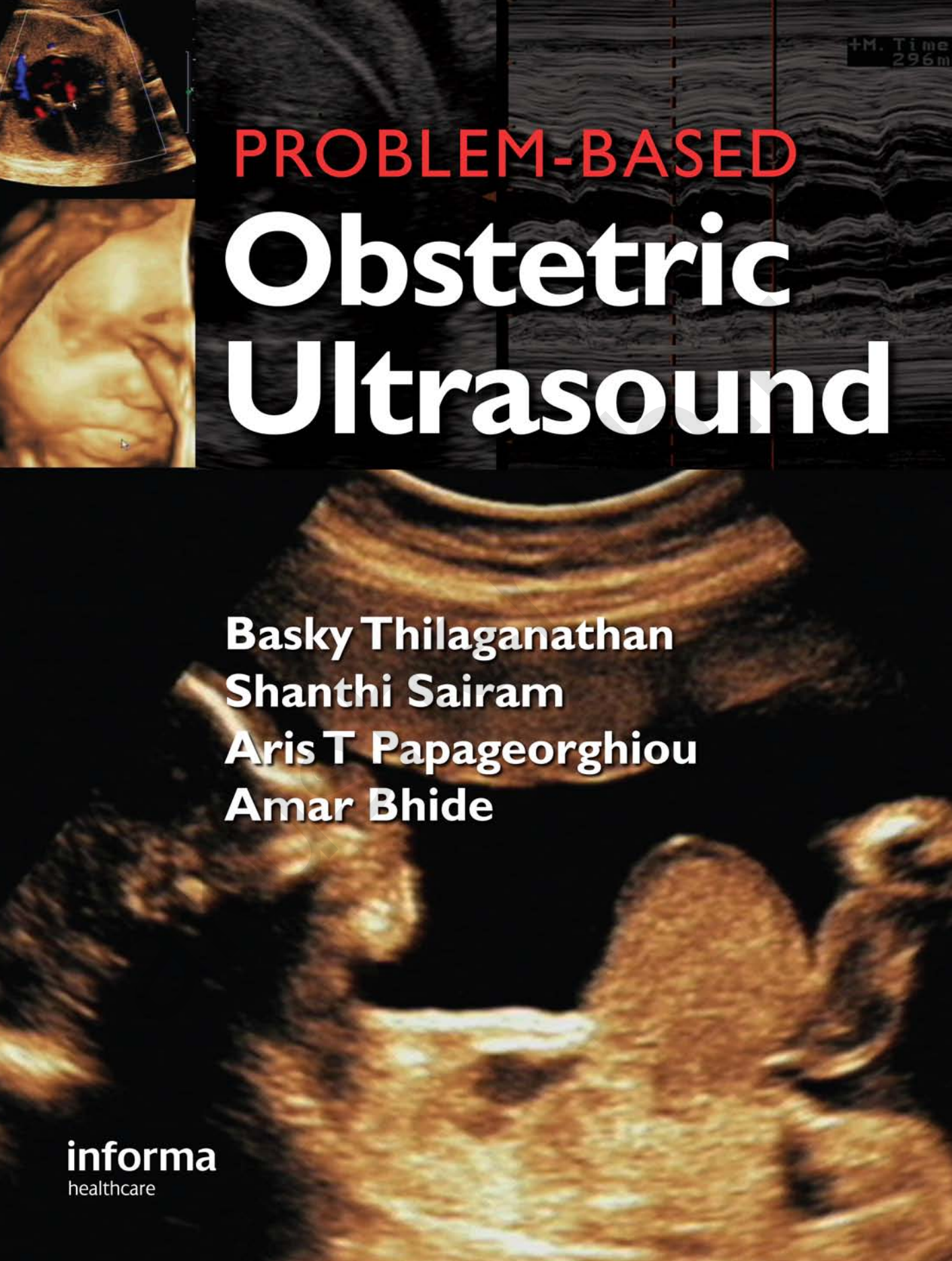


+M. Time
296m



PROBLEM-BASED
Obstetric
Ultrasound

Basky Thilaganathan
Shanthi Sairam
Aris T Papageorghiou
Amar Bhide

informa
healthcare

PROBLEM-BASED OBSTETRIC ULTRASOUND

akusher-lib.ru

akusher-lib.ru

PROBLEM-BASED OBSTETRIC ULTRASOUND

Basky Thilaganathan MD MRCOG

Consultant and Director

Fetal Medicine Unit

St George's Hospital Medical School

London

UK

Shanthi Sairam MD MRCOG

Senior Clinical Fellow

Fetal Medicine Unit

St George's Hospital Medical School

London

UK

Aris T Papageorghiou MRCOG

Consultant Maternal-Fetal Medicine

Fetal Medicine Unit

St George's Hospital Medical School

London

UK

Amar Bhide MD MRCOG

Consultant Maternal-Fetal Medicine

Fetal Medicine Unit

St George's Hospital Medical School

London

UK

informa

healthcare

© 2007 Informa UK Ltd

First published in the United Kingdom in 2007 by Informa Healthcare, 4 Park Square, Milton Park, Abingdon, Oxon OX14 4RN. Informa Healthcare is a trading division of Informa UK Ltd. Registered Office: 37/41 Mortimer Street, London W1T 3JH. Registered in England and Wales number 1072954.

Tel: +44 (0)20 7017 6000

Fax: +44 (0)20 7017 6699

Email: info.medicine@tandf.co.uk

Website: www.informahealthcare.com

All rights reserved. No part of this publication may be reproduced, stored in a retrieval system, or transmitted, in any form or by any means, electronic, mechanical, photocopying, recording, or otherwise, without the prior permission of the publisher or in accordance with the provisions of the Copyright, Designs and Patents Act 1988 or under the terms of any licence permitting limited copying issued by the Copyright Licensing Agency, 90 Tottenham Court Road, London W1P 0LP.

Although every effort has been made to ensure that all owners of copyright material have been acknowledged in this publication, we would be glad to acknowledge in subsequent reprints or editions any omissions brought to our attention.

A CIP record for this book is available from the British Library.
Library of Congress Cataloging-in-Publication Data

Data available on application

ISBN-10: 0 415 40728 1

ISBN-13: 978 0 415 40728 1

Distributed in North and South America by
Taylor & Francis
6000 Broken Sound Parkway, NW, (Suite 300)
Boca Raton, FL 33487, USA

Within Continental USA

Tel: 1 (800) 272 7737; Fax: 1 (800) 374 3401

Outside Continental USA

Tel: (561) 994 0555; Fax: (561) 361 6018

Email: orders@crcpress.com

Distributed in the rest of the world by
Thomson Publishing Services
Cheriton House
North Way

Andover, Hampshire SP10 5BE, UK

Tel: +44 (0)1264 332424

Email: tps.tandfsalesorder@thomson.com

Composition by Exeter Premedia Services Private Ltd., Chennai, India
Printed and bound in India by Replika Press Pvt Ltd

CONTENTS

Foreword	vii
<i>Sabaratnam Arulkumaran</i>	
1. Ventriculomegaly	1
2. Intracranial cysts	5
3. Abnormal skull shape	9
4. Facial clefts	13
5. Absent nasal bones	17
6. Micrognathia	19
7. Chest tumours	23
8. Chest fluid	27
9. Dextrocardia	31
10. Abnormal four-chamber view	35
11. Anterior abdominal wall defect	39
12. Abdominal cysts	43
13. Abdominal echogenicity	47
14. Empty renal fossa	51
15. Cystic kidney	55
16. Fluid filled kidney	59
17. Abnormal bladder	63
18. Short femur length	67
19. Joint abnormalities	71
20. Hand abnormalities	75
21. Spinal abnormalities	79
22. Head and neck masses	83
23. Increased nuchal translucency	87
24. Placental abnormalities	91
25. Single umbilical artery	93
26. Oligohydramnios	95
27. Polyhydramnios	99
28. Amniotic shelf/band	103
29. Hydrops	105
30. Small fetus	109
31. Twin-twin transfusion syndrome	113
Index	117

akusher-lib.ru

FOREWORD

This short textbook on problem-based obstetric ultrasound is an important and needed text for those who scan for fetal anomalies. The book takes a pragmatic approach by first defining an anomaly followed by a decision tree that indicates what other features need to be investigated to reach the definitive diagnosis. In a short text it is difficult to cover the entire pathology seen on scanning, but it covers more than adequately most of the common problems.

In addition to the decision algorithms, the text is well illustrated by the appropriate scan pictures which would be of immense value.

I am delighted that such a book is produced at last by a team of four experts in the field of fetal medicine.

Sabaratnam Arulkumaran

Professor and Head, Obstetrics and Gynaecology

St George's University of London

London

akusher-lib.ru

VENTRICULOMEGALY

The lateral cerebral ventricles are best measured in that part of the posterior horn at the level of the choroids plexus (atrium). The following terminology is followed most often:

- normal: measurement < 10 mm
- mild/borderline ventriculomegaly: 10–12 mm
- moderate ventriculomegaly: 12–15 mm
- severe ventriculomegaly: > 15 mm.

In the majority of cases, the outcome is good for isolated mild/borderline or unilateral ventriculomegaly, suggesting that it is a normal variant. When the ventriculomegaly is bilateral or the measurement is above the 97.5th centile (> 12 mm), the neonatal outcome is associated with the cause of the ventriculomegaly rather than the amount of fluid in the ventricle.

Aneuploidy

Advanced maternal age, high risk screen test results, or the presence of other ultrasound markers of chromosomal abnormality should raise the possibility of fetal aneuploidy. Typically, aneuploidy, if present, is associated with mild rather than moderate or severe ventriculomegaly.

Congenital viral infection

Although rare, the presence of ultrasound features confers a terrible prognosis for congenital fetal viral infection. Typical ultrasound features include severe fetal growth restriction, microcephaly, focal brain hyperechogenicities, and cardiac abnormalities.

Brain haemorrhage

Clots are rarely seen on fetal brain ultrasound, but if seen are characteristic of intracerebral bleed as a cause. In the absence of such a finding, parental blood should be taken to exclude the possibility of fetal alloimmune thrombocytopenia.

Structural brain abnormality

The finding of other structural brain abnormality generally confers a poor neonatal prognosis. The exceptions to this rule are arachnoid cyst (see 'Intracranial cysts') and isolated agenesis of the corpus callosum with normal gyral development.

Bibliography

1. Gaglioti P, Danelon D, Bontempo S et al. Fetal cerebral ventriculomegaly: outcome in 176 cases. *Ultrasound Obstet Gynecol* 2005; 25(4): 372–7.
2. Laskin MD, Kingdom J, Toi A, Chitayat D, Ohlsson A. Perinatal and neurodevelopmental outcome with isolated fetal ventriculomegaly: a systematic review. *J Matern Fetal Neonatal Med* 2005; 18(5): 289–98.

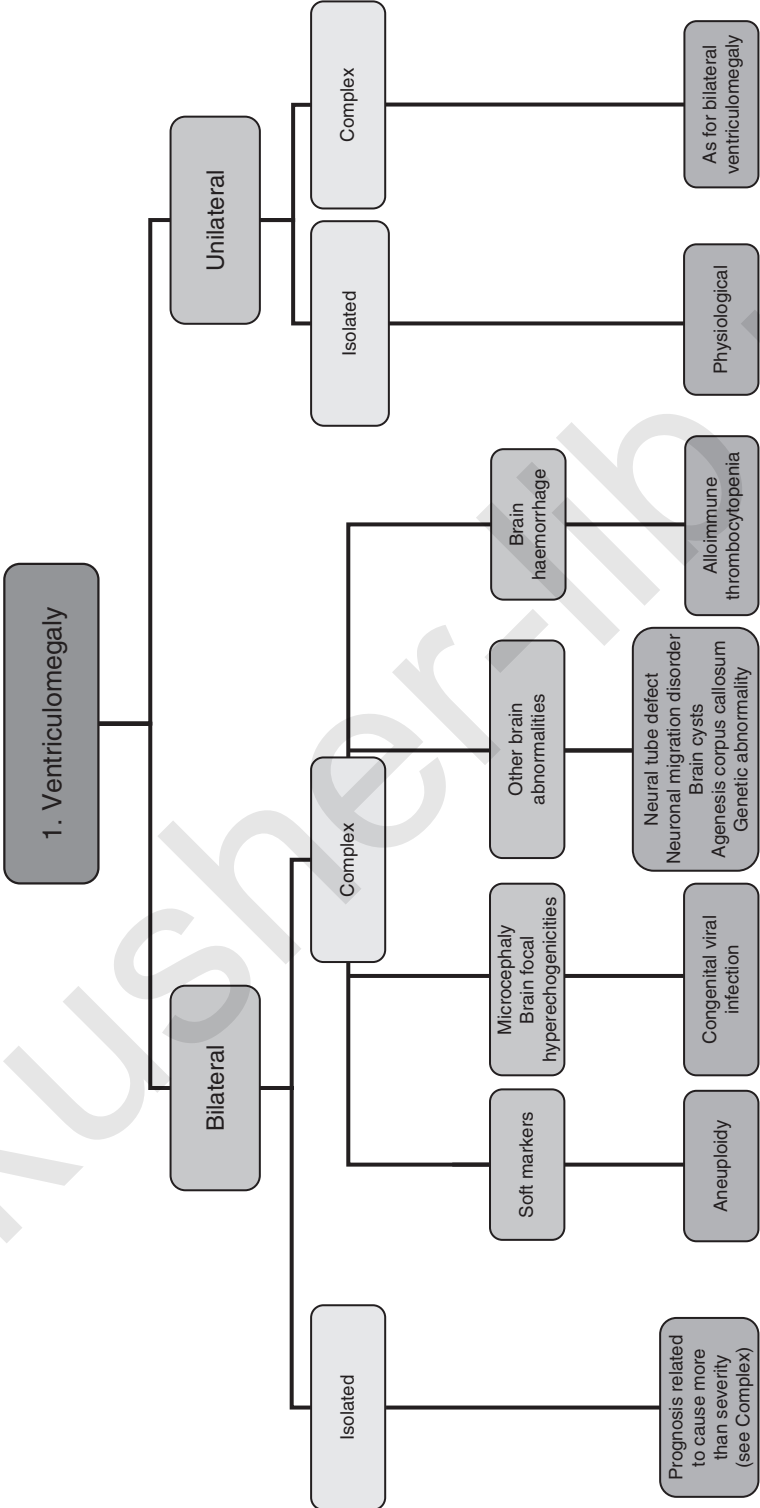




Fig. 1.1 Moderate ventriculomegaly

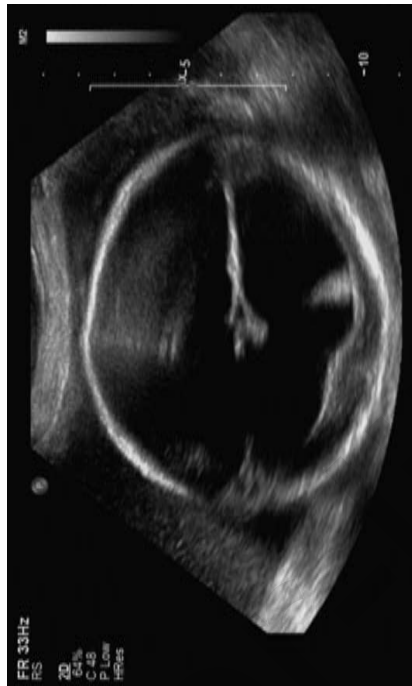


Fig. 1.2 Severe ventriculomegaly

akusher-lib.ru

INTRACRANIAL CYSTS

The origins of intracranial cysts are best identified by their position and associations within the brain as outlined in the diagnostic algorithm.

Choroid plexus cysts

These are collections of the cerebrospinal fluid (CSF) due to blockage of the glands in the choroids plexus. They are seen in 1–3% at the time of the anomaly scan, and occur most commonly in the lateral ventricles. In the absence of associated ultrasound features of fetal aneuploidy, the outlook for the pregnancy is good, with natural resolution in pregnancy being the inevitable outcome.

Arachnoid cysts

These are rare cysts arising from the arachnoid membrane. They are most often isolated, regular, and non-midline, and the size can be very variable. Midline shift of the brain may be seen due to the pressure effect. The outlook is usually good, unless the size is extraordinarily large.

Inter-hemispheric cysts (pseudocysts)

The ultrasound appearance is of a cystic structure in the midline, and they are often mistaken for arachnoid cysts. These pseudocysts result as a consequence of a deficiency in the roof of the third ventricle and agenesis of the corpus callosum. The outlook is guarded because of the structural brain abnormalities associated with this finding.

Posterior fossa cysts

These are variably (and confusingly) termed Dandy–Walker cysts, variant, or malformation. In practical terms it is better to describe the ultrasonographic findings, i.e. posterior fossa cyst with/without agenesis of the cerebellar vermis. The outlook is generally guarded if there is total agenesis of the vermis or the cerebellum is hypoplastic. The prognosis may be good in some cases of apparent partial agenesis of the vermis, due to rotation rather than agenesis of the vermis.

Vascular malformations

Aneurysm of the vein of Galen and dural sinus malformations are rare diagnoses easily made by the use of colour Doppler interrogation of apparent cystic masses in the brain. The prognosis for a vein of Galen malformation is good in the absence of fetal hydrops. In contrast, poor neurodevelopmental outcomes have been reported for dural sinus malformations.

Bibliography

1. Blaicher W, Prayer D, Bernaschek G. Magnetic resonance imaging and ultrasound in the assessment of the fetal central nervous system. *J Perinat Med* 2003; 31(6): 459–68.
2. Pilu G, Visentin A, Valeri B. The Dandy-Walker complex and fetal sonography. *Ultrasound Obstet Gynecol* 2000; 16(2): 115–17.

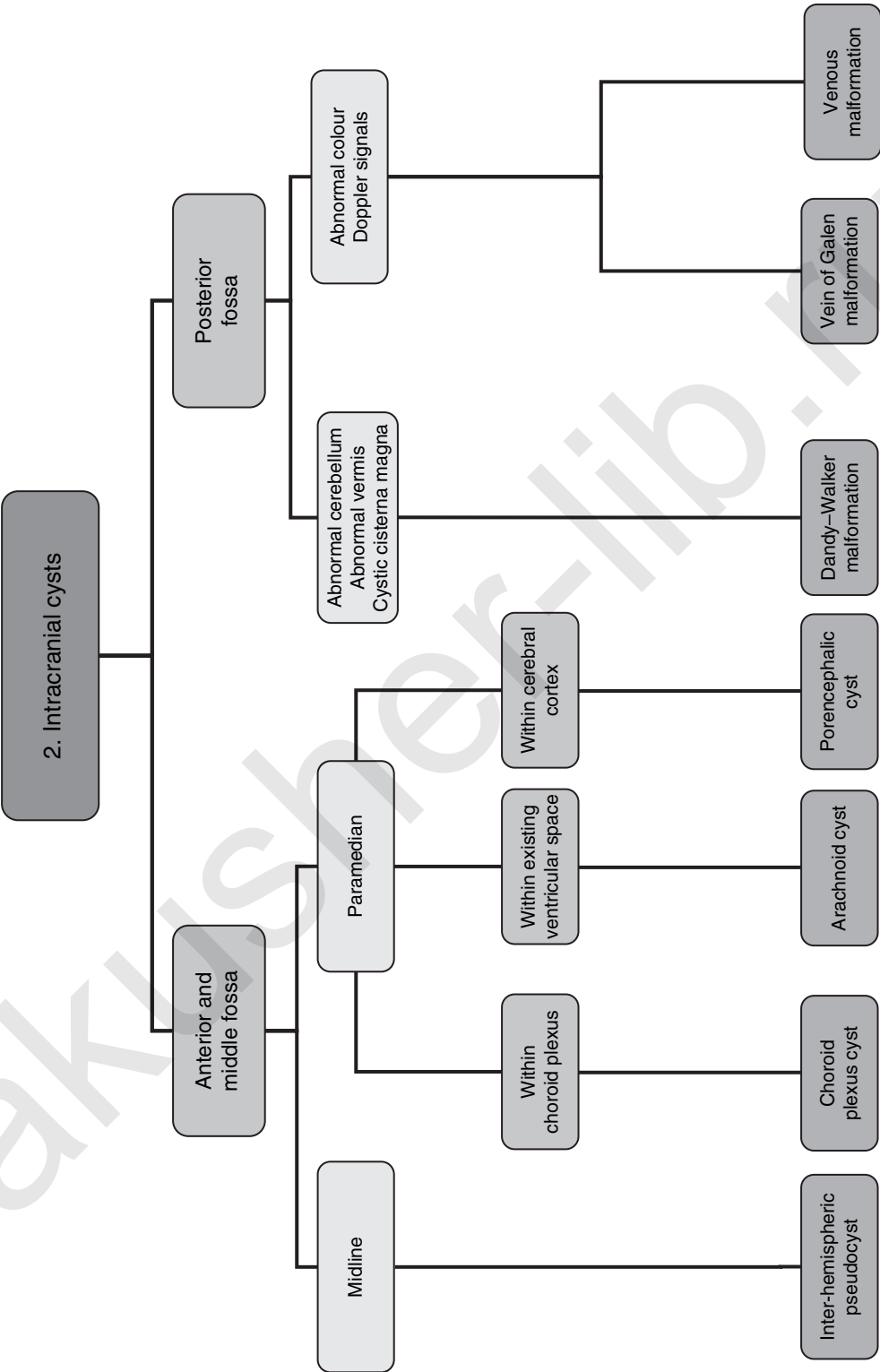




Fig. 2.1 Choroid plexus cyst



Fig. 2.2 Posterior fossa cyst

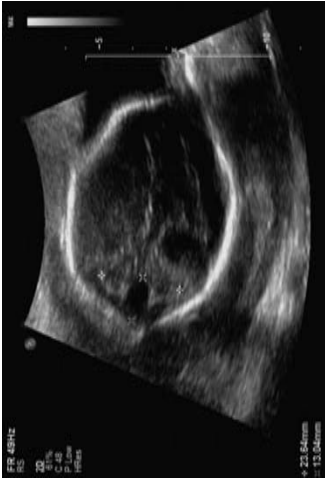


Fig. 2.3 Absent cerebellar vermis



Fig. 2.4 Arachnoid cyst



Fig. 2.5 Midline third ventricular pseudocyst

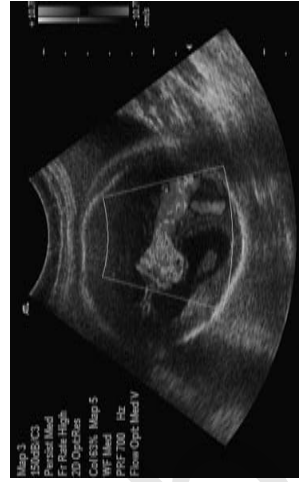


Fig. 2.6 Vein of Galen malformation (see also colour plate)

akusher-lib.ru

ABNORMAL SKULL SHAPE

Abnormalities in skull shape are relatively rare, but quite striking when seen. An ability to recognize the described shapes is invaluable in the diagnosis of the aetiology and associated abnormalities.

Lemon shaped skull

This is a characteristic feature of spina bifida, often associated with a 'banana' shaped cerebellum due to herniation of the cerebellar vermis through the foramen magnum. The lemon shape is most often seen in the middle third of pregnancy, and often resolves in the third trimester. 'Lemon-like' skull without spina bifida has no clinical significance, and therefore a careful search of the spine is indicated before disregarding this finding.

Strawberry shaped skull

This finding should raise the suspicion of trisomy 18 (Edward syndrome). A careful examination should be conducted to exclude other markers of chromosomal abnormality (choroid plexus cysts, ventriculomegaly, clenched fists, congenital heart disease, congenital diaphragmatic hernia, exomphalos, single umbilical artery, and talipes).

Clover-leaf shaped skull

This is typically associated with skeletal dysplasias. Hence, associated findings are shortening of the long bones and narrowing of the chest (thoracic dysplasia) such that the heart appears to fill more of the chest (apparent cardiomegaly).

Encephalocele

The prognosis is generally poor unless the defect contains only meninges without brain matter. When an occipital encephalocele is diagnosed, an effort should be made to exclude Meckel-Gruber syndrome (occipital encephalocele, polycystic kidneys, polydactyly), which has an autosomal recessive pattern of inheritance.

Achondrogenesis

This is a skeletal dysplasia where the skull is very poorly mineralized, and easily deformed by the pressure of the ultrasound probe.

Bibliography

1. Glass RB, Fernbach SK, Norton KI, Choi PS, Naidich TP. The infant skull: a vault of information. *Radiographics* 2004; 24(2): 507–22.
2. Lachman RS, Rappaport V. Fetal imaging in the skeletal dysplasias. *Clin Perinatol* 1990; 17(3): 703–22.

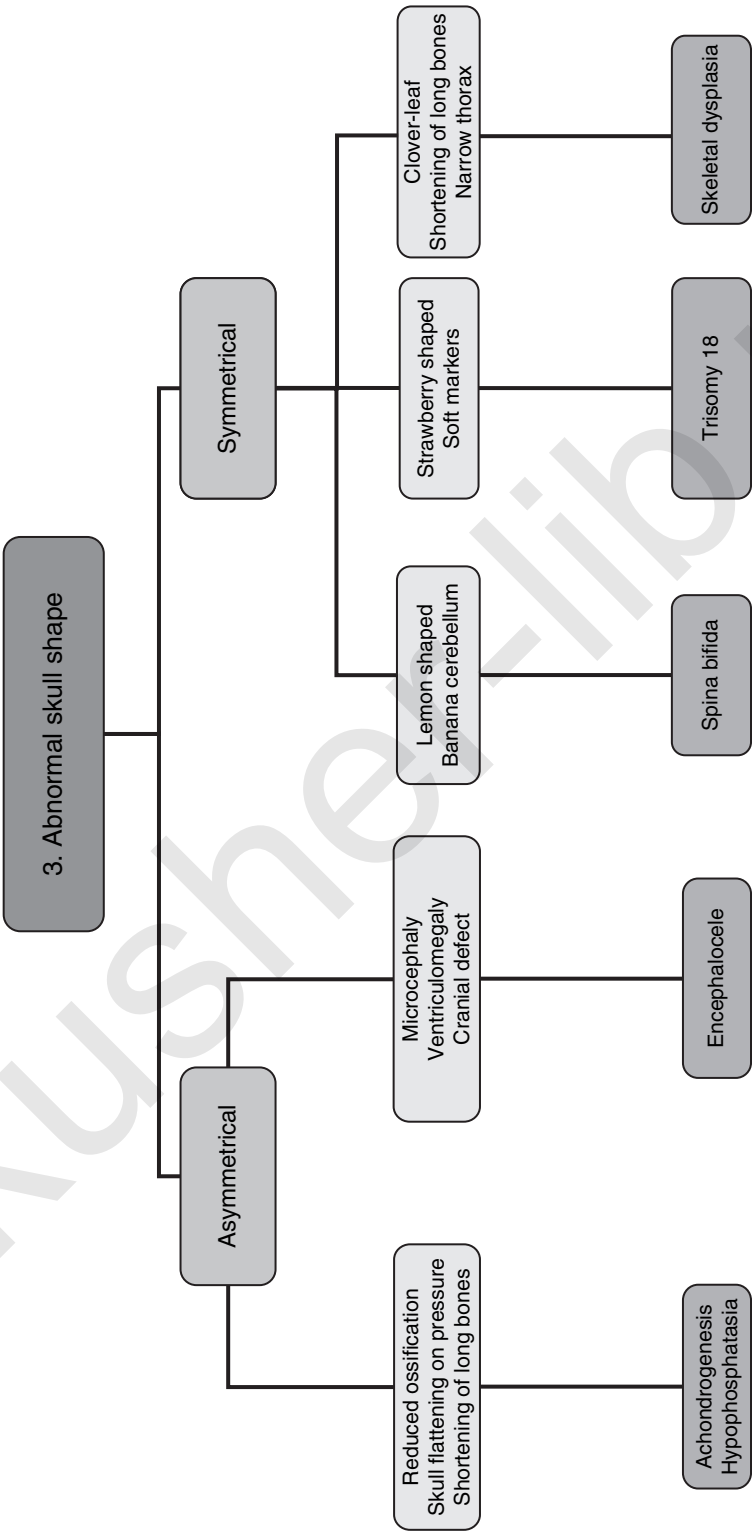




Fig. 3.1 Lemon shaped head

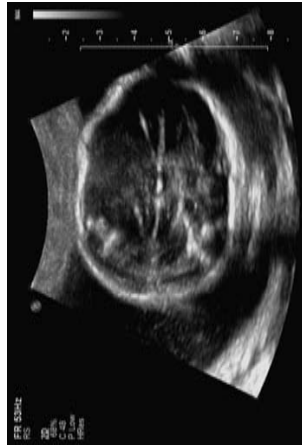


Fig. 3.2 Banana cerebellum

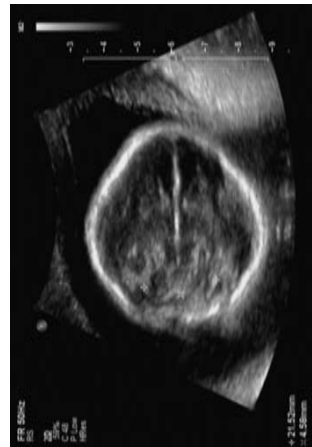


Fig. 3.3 Strawberry shaped head

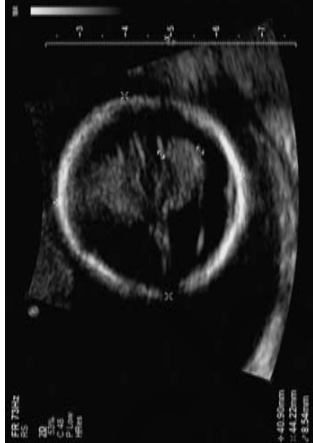


Fig. 3.4 Brachycephaly

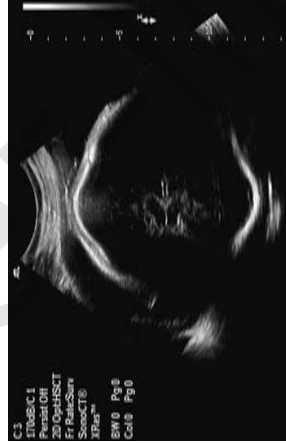
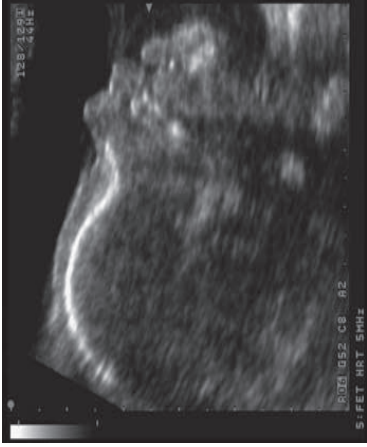


Fig. 3.5 Clover-leaf shaped head



(a)



(b)

Fig. 3.6 (a) Normal mid-sagittal section of face (b) Frontal bossing

akusher-lib.ru

FACIAL CLEFTS

Ultrasound recognition of facial clefts involves obtaining a coronal surface view of the face showing the lips and nostrils. The defect in the alveolar ridge is demonstrable on a transverse view (often mistaken for the primary/hard palate). A profile view may demonstrate a pre-maxillary protrusion in cases of bilateral cleft lip/alveolus. The primary palate is not normally visualized on ultrasound. The defect of the alveolar ridge can be demonstrated by, and in most cases is associated with, a defect of the primary palate. Prenatal diagnosis of cleft palate in the absence of a cleft lip/alveolus is extremely difficult. Recently, the use of 'reverse face view' on three-dimensional ultrasound has been described to improve prenatal identification of defects of the palate.

Facial clefts are typically an isolated finding, but may have a group of conditions associated with them. Median and bilateral facial clefts are associated with a higher risk of underlying chromosomal (trisomy 13) or genetic abnormality. The commonest genetic syndromes typically involve either midline defects of the brain (holoprosencephaly) or defects of the somatic structures. Clefts (usually of the palate) are commonly associated with some craniosynostoses.

Bibliography

1. Campbell S, Lees C, Moscoso G, Hall P. Ultrasound antenatal diagnosis of cleft palate by a new technique: the 3D 'reverse face' view. *Ultrasound Obstet Gynecol* 2005; 25(1): 12–18.
2. Wayne C, Cook K, Sairam S, Hollis B, Thilaganathan B. Sensitivity and accuracy of routine antenatal ultrasound screening for isolated facial clefts. *Br J Radiol* 2002; 75(895): 584–9.

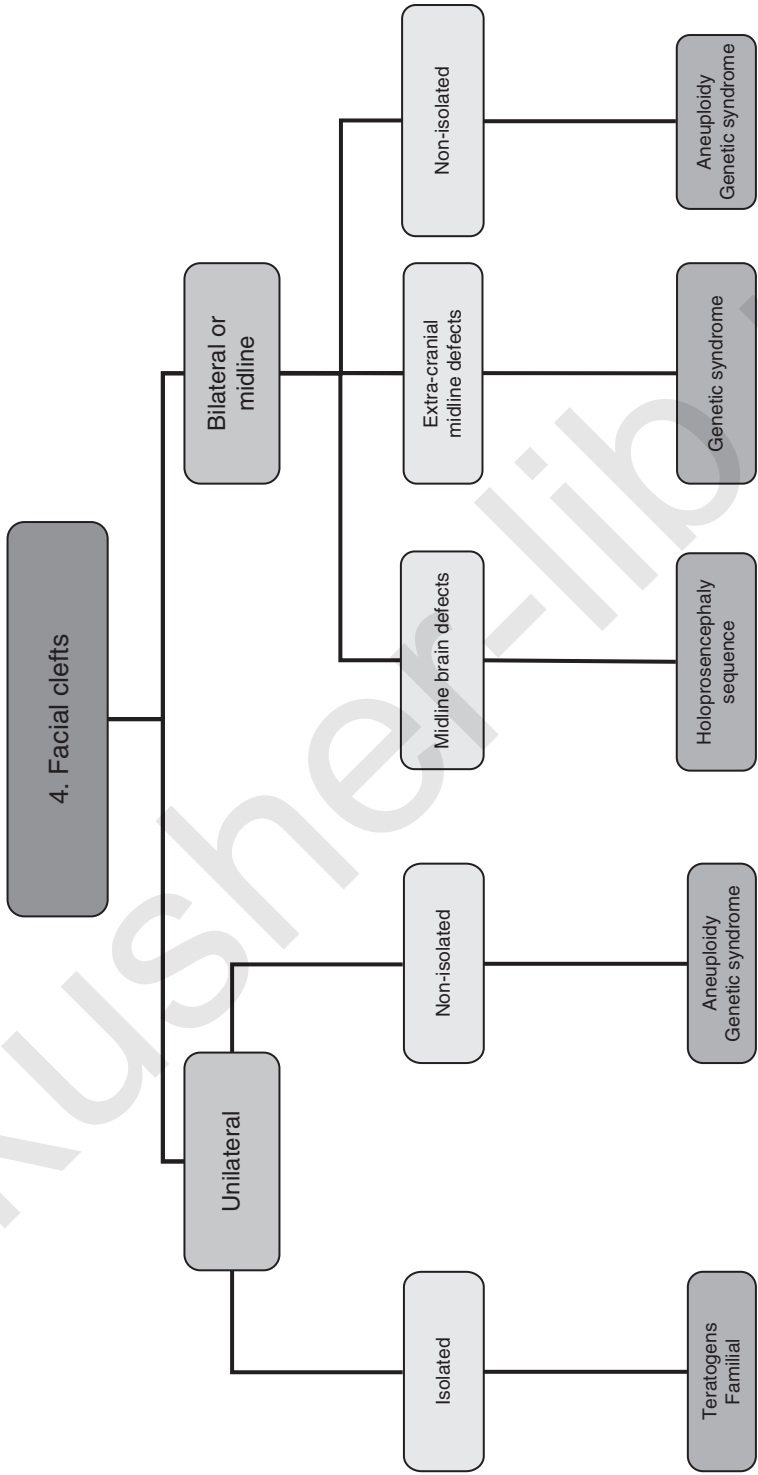




Fig. 4.1 Unilateral cleft lip



Fig. 4.3 Pre-maxillary protrusion



(a)



(b)

Fig. 4.2 (a) Normal alveolar ridge (b) Bilateral cleft alveolus and primary palate

akusher-lib.ru

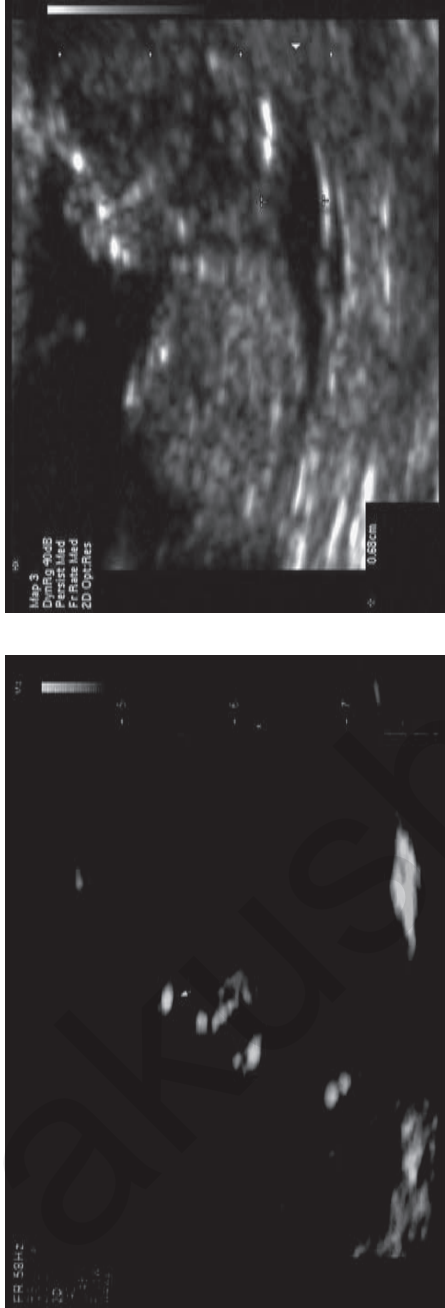
ABSENT NASAL BONES

The association of nasal bone hypoplasia and trisomy 21 is now well established. There are ultrasound studies in low-risk and high-risk populations, and also histopathological studies in fetuses with Down syndrome, which have consistently confirmed this association. Some 50–60% of fetuses with Down syndrome will have absent nasal bones at 11–14 weeks on ultrasound scanning. However, nasal bones may be absent in a small proportion of chromosomally normal fetuses as well. The background prevalence of absent nasal bones in normal fetuses is dependent on the parent's ethnicity and facial structure.

Advanced maternal age, increased nuchal translucency, abnormal serum biochemistry, and abnormalities or soft markers seen on ultrasound are the factors to be considered in determining the a-priori risk for trisomy 21. Absence of the nasal bones would significantly increase the chance of underlying trisomy 21, and an invasive test should be considered. On the other hand, in a population at low risk of trisomy 21, failure to visualize the fetal nasal bone could easily be a variation of normal.

Bibliography

1. Cicero S, Curcio P, Papageorghiou A, Sonek J, Nicolaides K. Absence of nasal bone in fetuses with trisomy 21 at 11–14 weeks of gestation: an observational study. *Lancet* 2001; 358(9294): 1665–7.
2. Prefumo F, Sairam S, Bhide A, Thilaganathan B. First-trimester nuchal translucency, nasal bones, and trisomy 21 in selected and unselected populations. *Am J Obstet Gynecol* 2006; 194(3): 828–33.



(a) (b) **Fig. 5.1** (a) First trimester nasal bones (b) First trimester absent nasal bones



Fig. 5.2 Second trimester hypoplastic nasal bone

MICROGNATHIA

The chin is best visualized on a mid-sagittal profile view of the face. There is no definition for micrognathia, and the diagnosis is subjective. Unless micrognathia is severe, ultrasound diagnosis is extremely difficult. Even when a diagnosis of micrognathia is made, it may be an isolated finding which resolves with advancing pregnancy or with conservative management in the infant period.

Trisomies 13 and 18

A careful examination should be conducted to exclude other markers of trisomy 18 (choroid plexus cysts, ventriculomegaly, clenched fists, congenital heart disease, congenital diaphragmatic hernia, exomphalos, single umbilical artery, and talipes) or trisomy 13 (holoprosencephaly, congenital heart disease, and polydactyly).

Goldenhar syndrome

This is also known as 'hemifacial microsomia'. There is asymmetry between structures on the left/right sides of the face. In addition to craniofacial anomalies, there may be cardiac, vertebral, and central nervous system defects. Most cases are sporadic, but some show autosomal dominant inheritance.

Other genetic syndromes

Many genetic syndromes can be associated with the finding of micrognathia. They include DiGeorge, Treacher Collins, Pierre Robin, and Smith–Lemli–Opitz syndromes. Typically, ultrasound prenatal diagnosis is difficult in these syndromes, as the majority of associated features are not seen on ultrasound or are diagnosed late in pregnancy.

Bibliography

1. Bromley B, Benacerraf BR. Fetal micrognathia: associated anomalies and outcome. *J Ultrasound Med* 1994; 13(7): 529–33.
2. Rotten D, Levailant JM, Martinez H, Ducou le Pointe H, Vicaut E. The fetal mandible: a 2D and 3D sonographic approach to the diagnosis of retrognathia and micrognathia. *Ultrasound Obstet Gynecol* 2002; 19(2): 122–30.

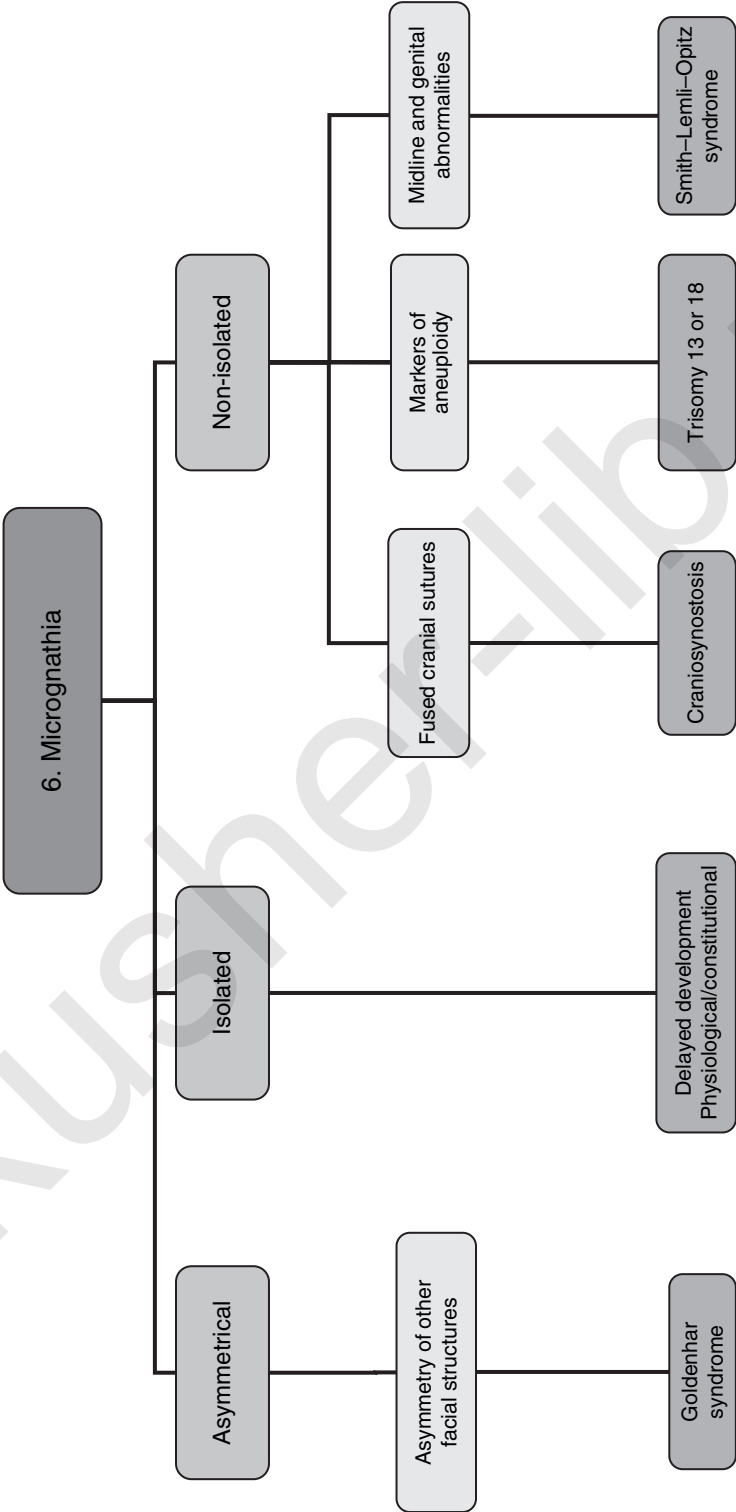




Fig. 6.1 Micrognathia

akusher-lib.ru

CHEST TUMOURS

The majority of fetal chest tumours are benign and tend to be identified in the second trimester. In the absence of fetal hydrops, they usually have a favourable prognosis. The vast majority of chest lesions tend to be unilateral, possibly because bilateral lesions are self-limiting. In many cases they present with mediastinal shift, easily spotted, with the heart axis being deviated to one side (see 'Dextrocardia').

Congenital cystic adenomatoid malformation

These lesions may be unilateral/bilateral and microcystic/macrocystic. Bilateral lesions may cause hydrops and fetal demise as a consequence of cardiac compression.

Pulmonary sequestration

The presence of systemic arterial supply from the thoracic or abdominal dorsal aorta would be characteristic of pulmonary sequestration. These benign tumours may cause hyperdynamic heart failure and hydrops as a consequence of an arterio-venous bypass effect.

Bronchial obstruction

The appearance is similar to a microcystic congenital cystic adenomatoid malformation (CCAM), but typically the diaphragmatic domes are not flattened. Resolution usually occurs in a matter of a few weeks, as opposed to months in the case of CCAM.

Congenital diaphragmatic hernia

The presence of a unilateral lesion with mixed echoes should raise the suspicion of a congenital diaphragmatic hernia (CDH), especially with mediastinal deviation and the lack of a stomach bubble in the normal position.

Congenital high airway obstruction syndrome

The presence of bilateral chest lesions suggests either bilateral CCAM or congenital high airway obstruction syndrome (CHAOS). The latter usually has the additional feature of dilated airways. A significant proportion also present with ascites owing to obstruction to the venous return to the heart.

Midline chest lesions

Midline chest lesions are very rare and may be of enteric, thymic, or pericardial origin. Enteric or bronchogenic midline tumours are usually cystic and tend to be benign. Pericardial tumours are usually teratomas and may present initially as pericardial effusions. Depending on their exact site on the pericardial surface, they may cause rhythm disturbances.

Bibliography

1. Geary MP, Chitty LS, Morrison JJ et al. Perinatal outcome and prognostic factors in prenatally diagnosed congenital diaphragmatic hernia. *Ultrasound Obstet Gynecol* 1998; 12(2): 107–11.
2. Ierullo AM, Ganapathy R, Crowley S et al. Neonatal outcome of antenatally diagnosed congenital cystic adenomatoid malformations. *Ultrasound Obstet Gynecol* 2005; 26(2): 150–3.

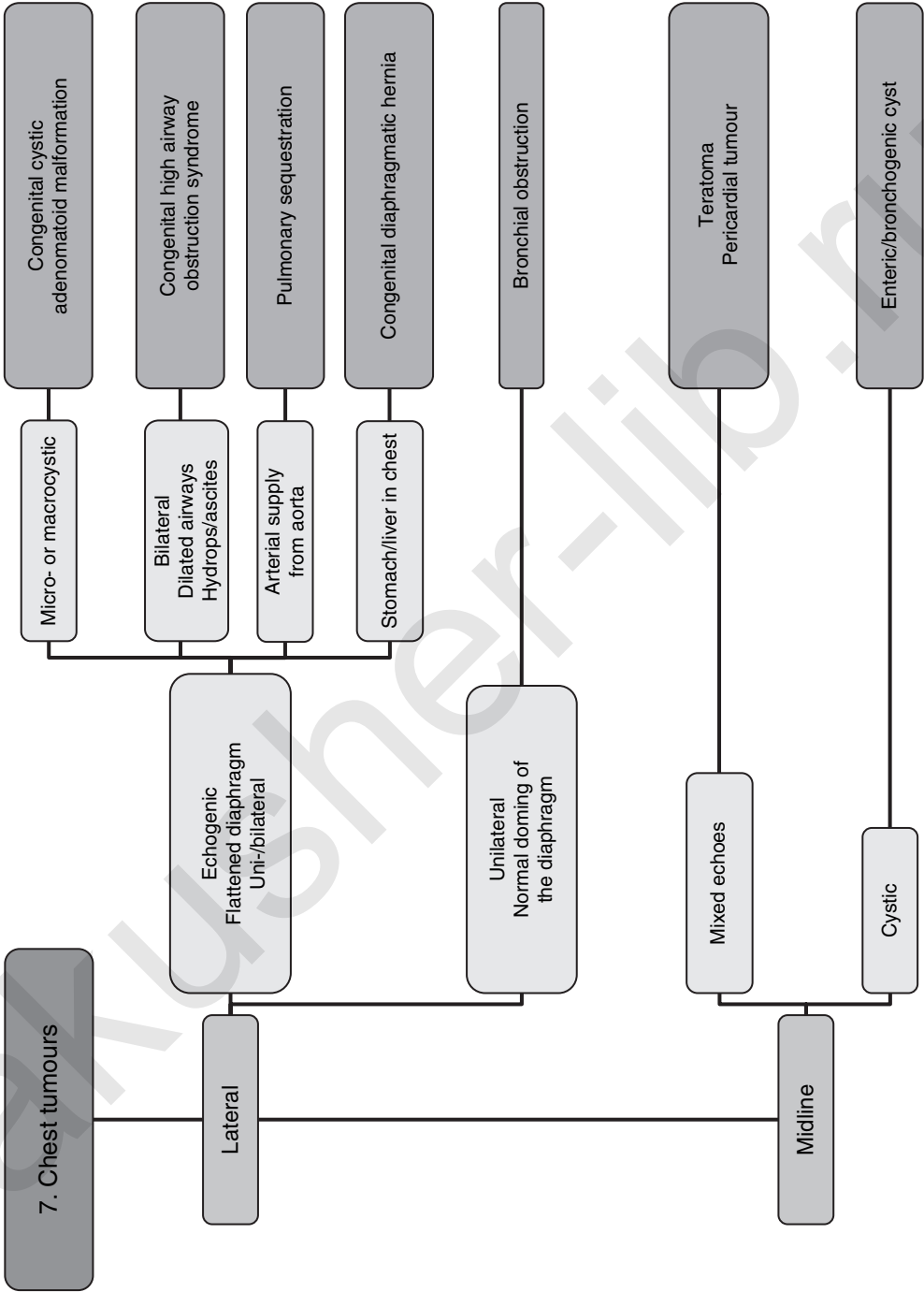




Fig. 7.1 Macrocystic lung lesion



Fig. 7.2 Microcystic lung lesion



Fig. 7.3 Pulmonary sequestration (see also colour plate)

akusher-lib.ru

CHEST FLUID

Fluid in the fetal chest is seen relatively commonly either as a cystic collection or as pleural or pericardial effusion. Cystic collections in the lungs or mediastinum need to be dealt with as chest tumours. Pleural effusion is seen as fluid collection around the compressed lung. Pleural or pericardial effusions may occur simultaneously in some conditions, but usually tend to be independent of each other.

Pleural effusion

This is usually present as part of a fetal hydrops, accompanying a structural anomaly, or, more rarely, an isolated finding. Most primary pleural effusions occur due to either excessive production or reduced reabsorption of lymphatic fluid. Complex or secondary pleural effusions may result from aneuploidy, congenital viral infection, fetal anaemia (usually with skin oedema), and hyperdynamic cardiac failure from arterio-venous shunting (with vascular tumours such as placental chorioangioma). Even in the absence of any other chromosomal marker, pleural effusion carries a 10% risk for chromosomal abnormalities.

Pericardial effusion

Prenatal sonographic identification of a small rim of pericardial fluid is a normal finding. Pericardial effusion is a subjective diagnosis, unless the fluid collection is obviously large. It may be an isolated finding or result from an underlying pericardial tumour or fetal arrhythmia/cardiac structural abnormality, or rarely it may be found with a cardiac aneurysm/diverticulum.

Bibliography

1. Santolaya-Forgas J. How do we counsel patients carrying a fetus with pleural effusions? *Ultrasound Obstet Gynecol* 2001; 18(4): 305–8.
2. Slesnick TC, Ayres NA, Altman CA et al. Characteristics and outcomes of fetuses with pericardial effusions. *Am J Cardiol* 2005; 96(4): 599–601.

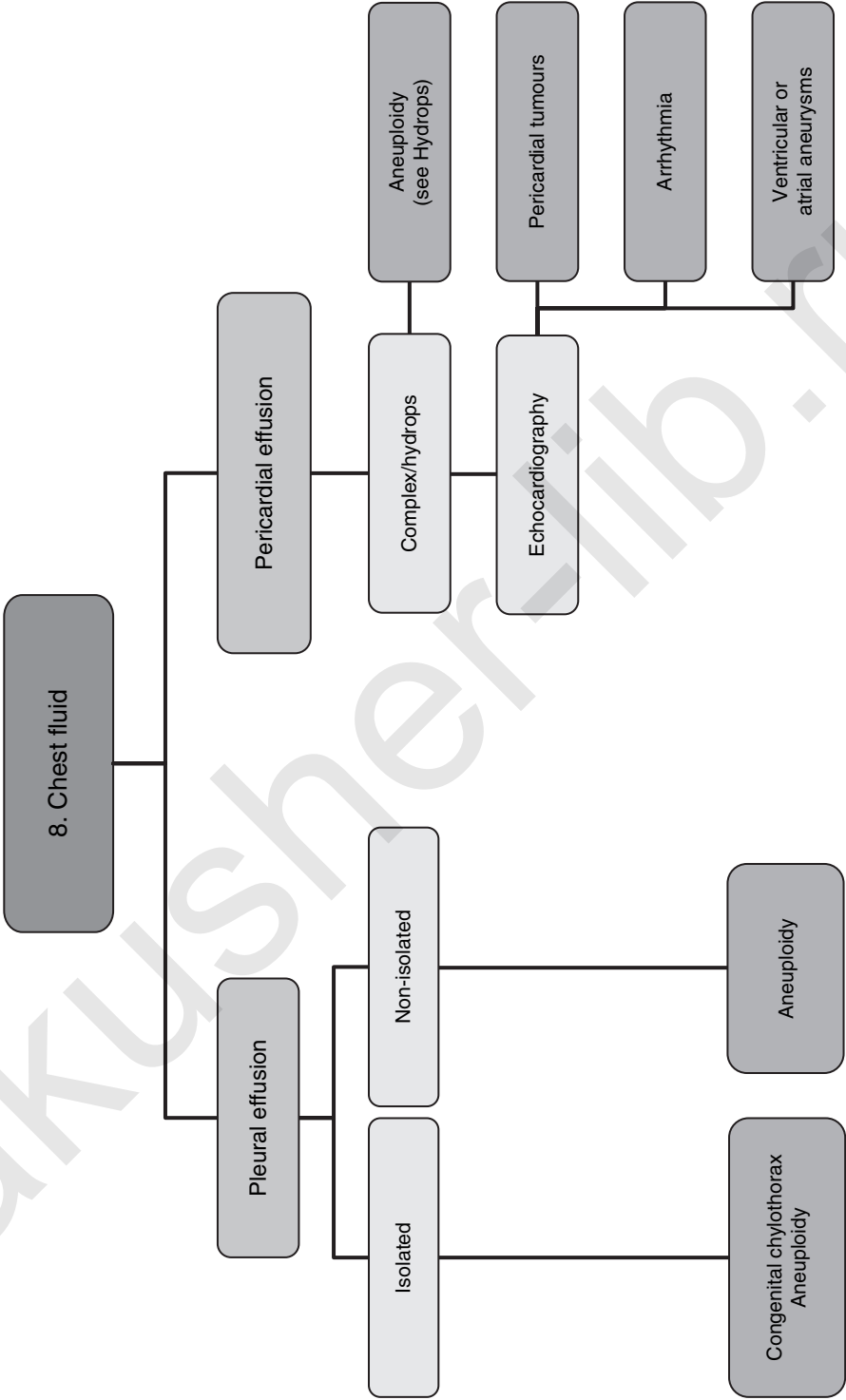




Fig. 8.1 Mild pleural effusion

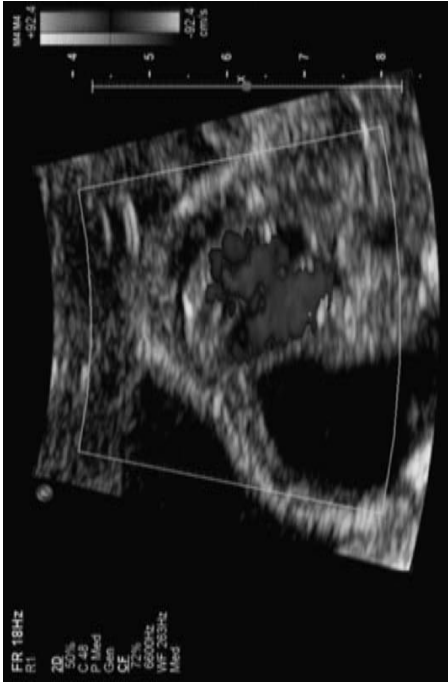


Fig. 8.2 Moderate pleural effusion & mediastinal shift (see also colour plate)



Fig. 8.3 Severe pleural effusion & fetal hydrops



Fig. 8.4 Pericardial effusion

akusher-lib.ru

DEXTROCARDIA

Fetal dextrocardia is a condition in which the major axis of the heart (from the base to the apex along the interventricular septum) points to the right. The term dextrocardia describes only the position of the cardiac axis and conveys no information regarding chamber organization and structural anatomy of the heart. Dextrocardia should be distinguished from dextroposition, in which the heart is shifted into the right chest as a consequence of pathological states involving the diaphragm, lung, pleura, or other adjoining tissues.

Dextroposition

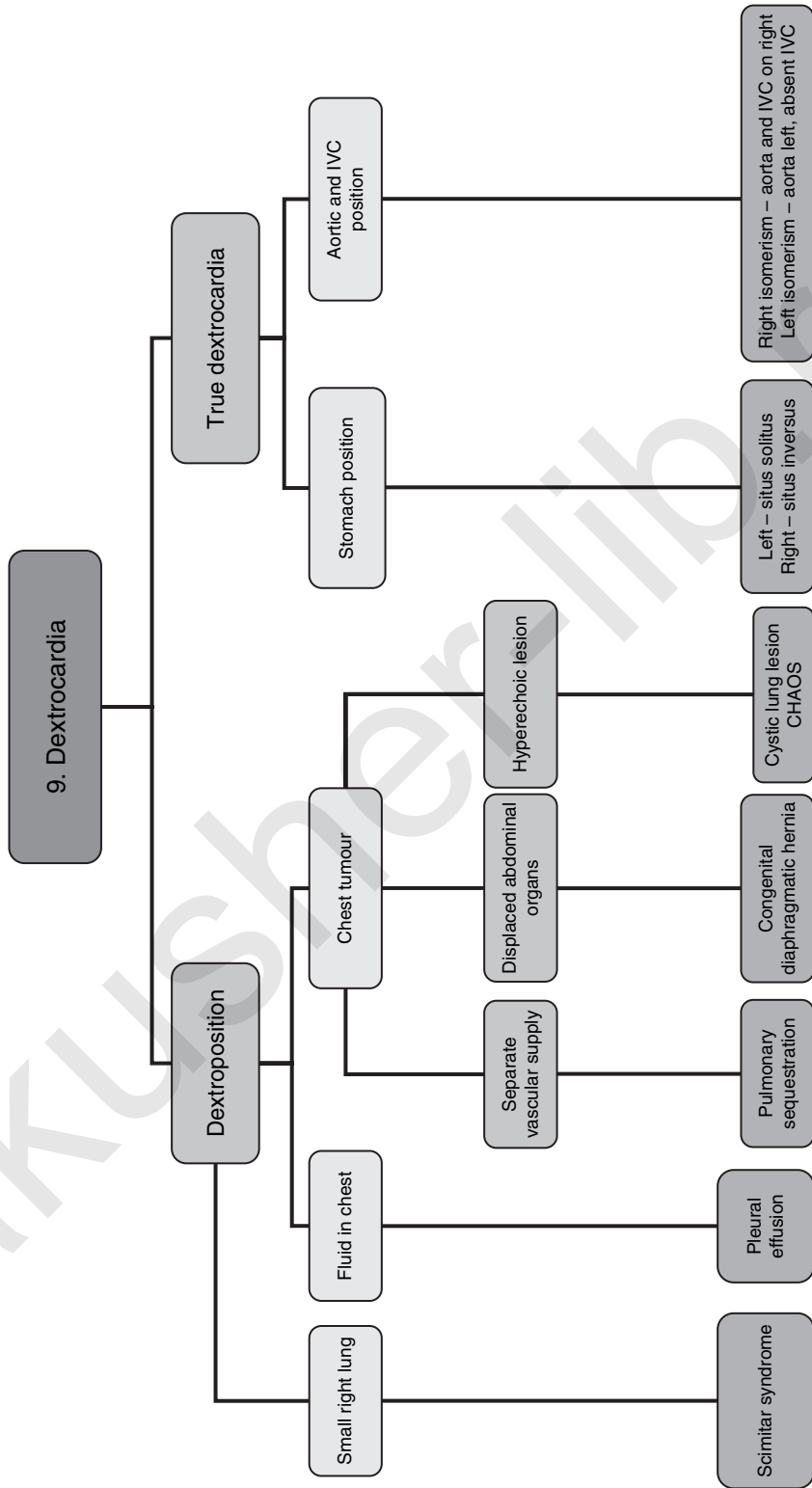
The commonest cause of dextroposition is the presence of chest fluid or a tumour (see previous chapters). In the absence of such space occupying lesions, consideration should be given to the diagnosis of scimitar syndrome: a smaller right side in the fetal chest with hypoplasia of the right lung and anomalous pulmonary venous drainage.

Dextrocardia

True dextrocardia tends to be associated with situs abnormalities. Situs by definition relates to the fetal left–right orientation of chest and abdominal organs. Situs can be assessed at various levels, namely abdominal, atrial, and pulmonary levels, and is usually similar at all levels. Situs solitus refers to the usual (normal) arrangement of left and right sided structures with the dorsal aorta in the left side of the fetal abdomen and the inferior vena cava (IVC) on the right. With true dextrocardia, the likelihood of structural cardiac abnormalities increases, especially of cardiac isomerisms. In the presence of situs inversus and dextrocardia with a structurally normal heart, the child will still need postnatal follow-up for other associated conditions such as Kartagener syndrome (ciliary dyskinesia).

Bibliography

1. Bernasconi A, Azancot A, Simpson JM, Jones A, Sharland GK. Fetal dextrocardia: diagnosis and outcome in two tertiary centres. *Heart* 2005; 91(12): 1590–4.
2. Holzmann D, Ott PM, Felix H. Diagnostic approach to primary ciliary dyskinesia: a review. *Eur J Pediatr* 2000; 159(1–2): 95–8.



CHAOS, congenital high airway obstruction syndrome; IVC, inferior vena cava.

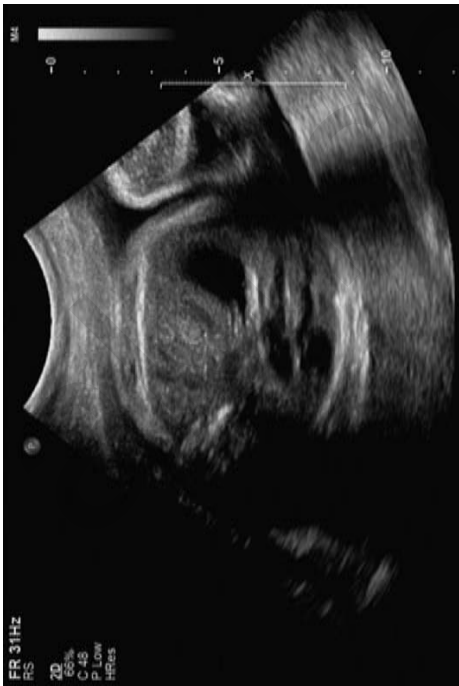


Fig. 9.1 Congenital diaphragmatic hernia

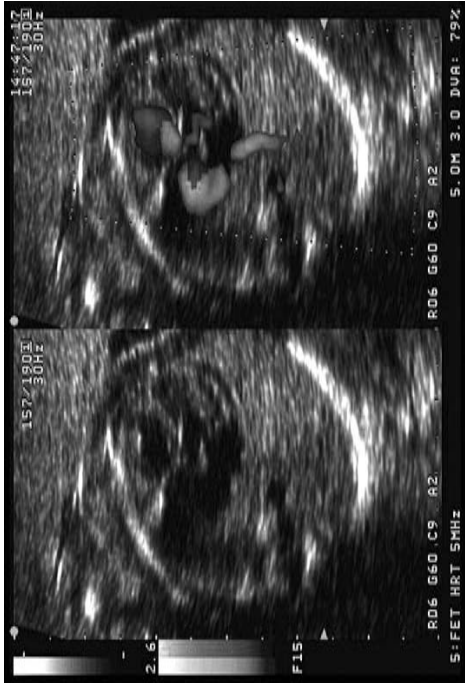


Fig. 9.2 Dextrocardia (see also colour plate)



Fig. 9.3 Axis deviation

akusher-lib.ru

ABNORMAL FOUR-CHAMBER VIEW

It is important to consider what should be routinely examined while checking a fetal heart:

1. Check abdominal situs. First confirm the left and right of the fetus and ensure that the fetal heart and stomach are on the fetal left side.
2. Check that the fetal heart points to the left with the majority of the heart in the left chest.
3. Check that the heart occupies a third of the chest area.
4. Check that there are four chambers with symmetrical ventricles and atria.
5. Ensure that the moderator band is identified and indicates the right ventricle.
6. Check that there are two atrio-ventricular valves opening and closing (cineloop helps) and that their point of attachment to the interventricular septum shows an offset, with the tricuspid valve being closer to the apex when compared to the mitral valve.
7. Check that the septum is intact (preferably examined with the septum horizontally oriented).
8. Further examinations should check the outflow tracts and ensure crossover. Much of this can be assessed using the three-vessel view.

Cardiomegaly

This finding should prompt assessment of the haemodynamic state in the fetus. It is usually secondary to some other fetal pathology including growth restriction, hyperdynamic circulatory states such as anaemia, arterio-venous malformations in the fetus, placental chorioangioma, and occasionally fetal brady- or tachyarrhythmias. Primary causes include major cardiac structural abnormalities, and will need detailed assessment that is beyond the scope of this chapter.

Asymmetry of the cardiac chambers

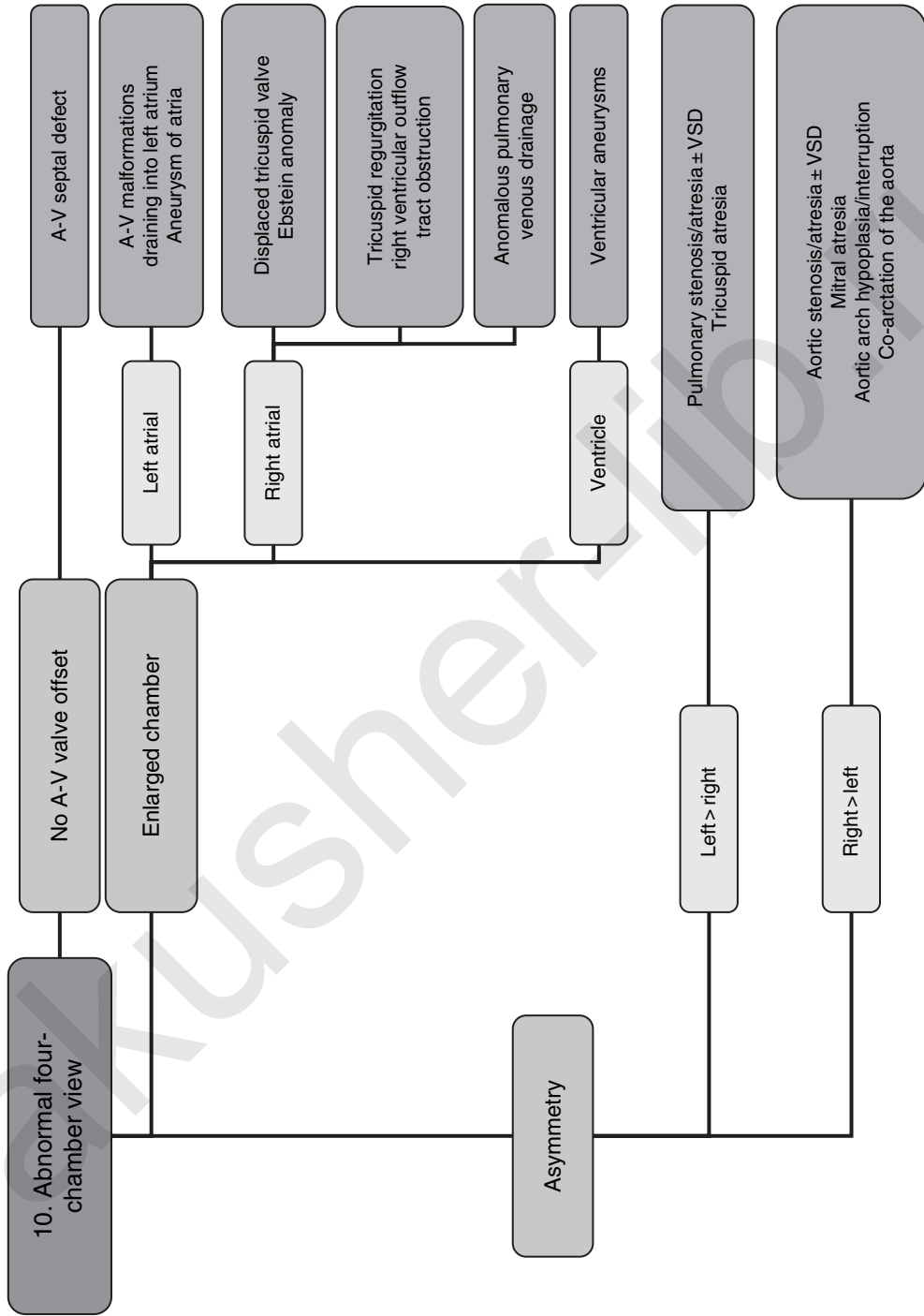
This usually reflects a structural problem in the atrio-ventricular or outflow tract valves. Rare causes include anomalous venous drainage of the pulmonary veins, where the drainage is into the right side of the heart rather than the left side of the heart in one or more veins.

Loss of the atrio-ventricular valve offset

The loss of a normal offset between the atrio-ventricular valves suggests the presence of an atrio-ventricular canal defect called the atrio-ventricular septal defect. This is associated with a 50–60% risk of chromosomal abnormality. A significant proportion of these cases will also have situs abnormalities (see chapter on 'Dextrocardia').

Bibliography

1. Bolnick AD, Zelop CM, Milewski B et al. Use of the mitral valve-tricuspid valve distance as a marker of fetal endocardial cushion defects. *Am J Obstet Gynecol* 2004; 191(4): 1483–5.
2. Del Bianco A, Russo S, Lacerenza N et al. Four chamber view plus three-vessel and trachea view for a complete evaluation of the fetal heart during the second trimester. *J Perinat Med* 2006; 34(4): 309–12.
3. Vergani P, Mariani S, Ghidini A et al. Screening for congenital heart disease with the four-chamber view of the fetal heart. *Am J Obstet Gynecol* 1992; 167(4 Pt 1): 1000–3.



A-V, atrio-ventricular; VSD, ventricular septal defect.

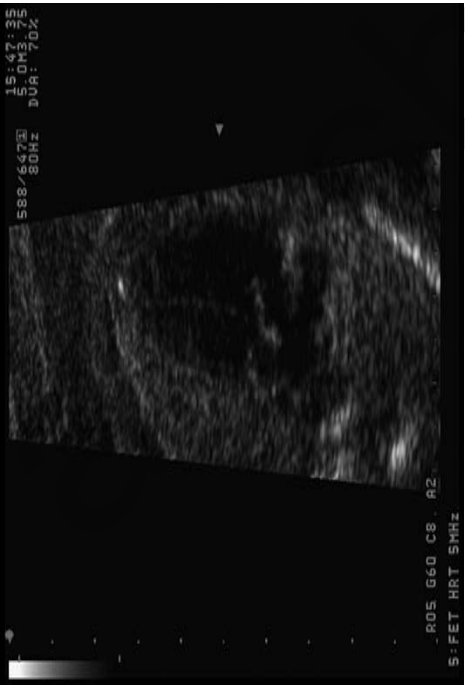


Fig. 10.1 Ventricular asymmetry



Fig. 10.2 Ventricular septal defect



Fig. 10.3 Colour Doppler demonstration of ventriculoseptal defect

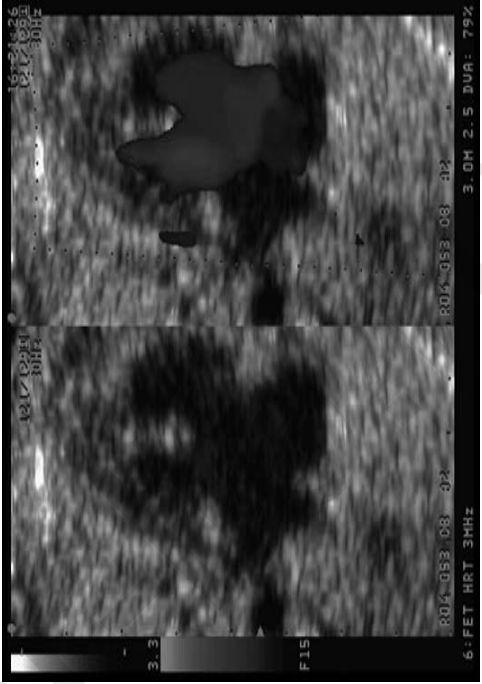


Fig. 10.4 Atrio-ventriculoseptal defect (see also colour plate)

akusher-lib.ru

ANTERIOR ABDOMINAL WALL DEFECT

The physiological gut herniation into the umbilical sac is restored to the normal position by approximately 10–11 weeks. Any abnormality after 11 weeks needs to be assessed carefully.

Exomphalos

The presence of a sac at the umbilicus with gut or liver contained in it is likely to be an exomphalos. The umbilical cord vessels can be seen traversing through this sac, which can vary in size. There is a strong association with chromosomal abnormality.

Bladder and cloacal extrophy

If the defect extends infra-umbilically, it is likely to involve the fetal bladder (non-visualized bladder) and possibly the genitalia (ambiguous genitalia). Under these circumstances, postnatal surgery is likely to involve reconstruction of the external genitalia and possibly gender re-assignment in some fetuses.

Beckwith–Wiedemann syndrome

If the exomphalos is small with features of macrosomia and organomegaly in the fetus, a diagnosis of Beckwith–Wiedemann syndrome can be made, and has implications for follow-up apart from surgery.

Pentalogy of Cantrell

If the anterior wall defect is more extensive superior to the umbilicus, it might involve parts of the diaphragm, pericardium, and the fetal heart as part of the pentalogy of Cantrell.

Body stalk anomaly

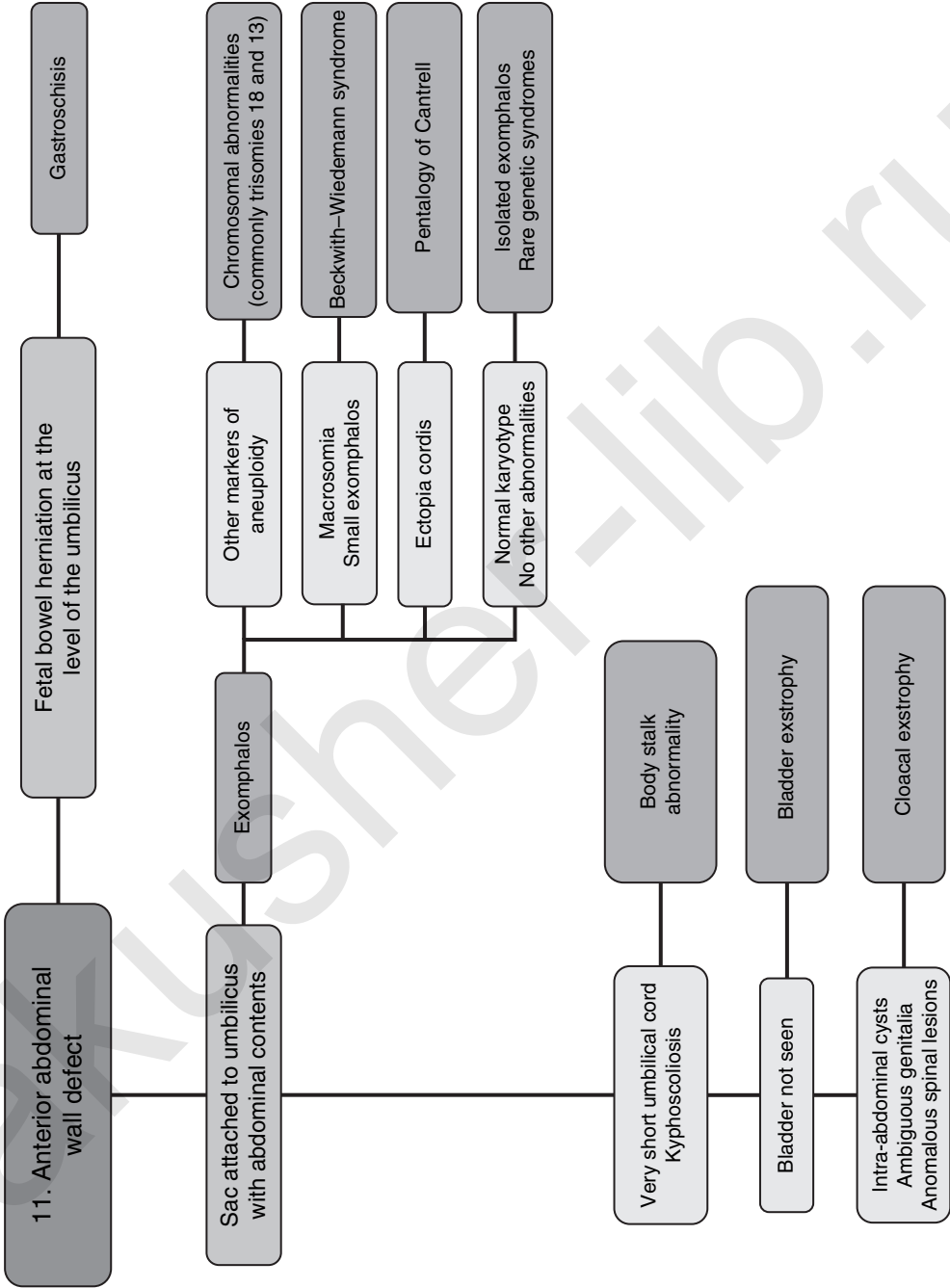
In some cases, a sac with the intra-abdominal contents is seen along with distortion of the spinal cord, poorly developed lower limbs, and a very short umbilical cord. These features form part of the body stalk anomaly or amniotic rupture sequence, and are uniformly associated with very poor prognosis.

Gastroschisis

The bowel is seen herniated without a sac (cauliflower-like appearance), just lateral to the cord insertion. Gastroschisis is usually located to the right of the umbilical cord, which has a normal insertion. The herniated organs usually only include loops of bowel, and there is no association with chromosomal abnormality.

Bibliography

1. Barisic I, Clementi M, Hausler M et al. Euroscan Study Group. Evaluation of prenatal ultrasound diagnosis of fetal abdominal wall defects by 19 European registries. *Ultrasound Obstet Gynecol* 2001; 18(4): 309–16.
2. Smrcek JM, Germer U, Krokowski M et al. Prenatal ultrasound diagnosis and management of body stalk anomaly: analysis of nine singleton and two multiple pregnancies. *Ultrasound Obstet Gynecol* 2003; 21(4): 322–8.
3. Williams DH, Gauthier DW, Maizels M. Prenatal diagnosis of Beckwith-Wiedemann syndrome. *Prenat Diagn* 2005; 25(10): 879–84.



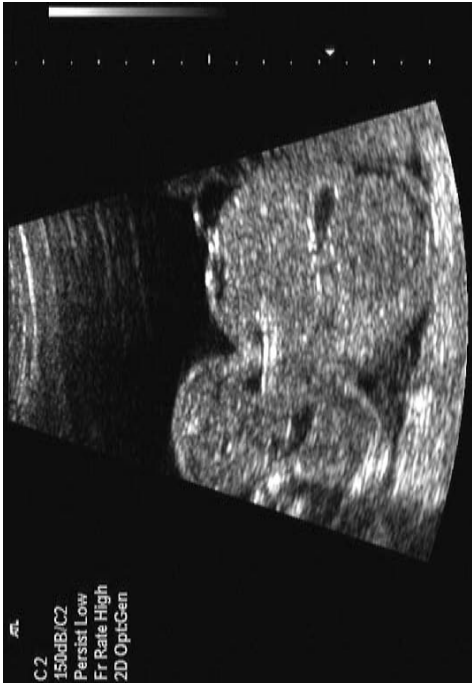


Fig. 11.2 Large exomphalos

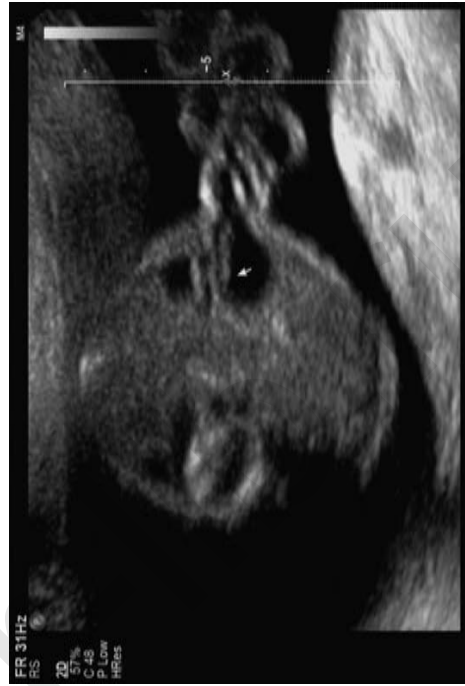


Fig. 11.4 Umbilical cord cyst



Fig. 11.1 First trimester exomphalos

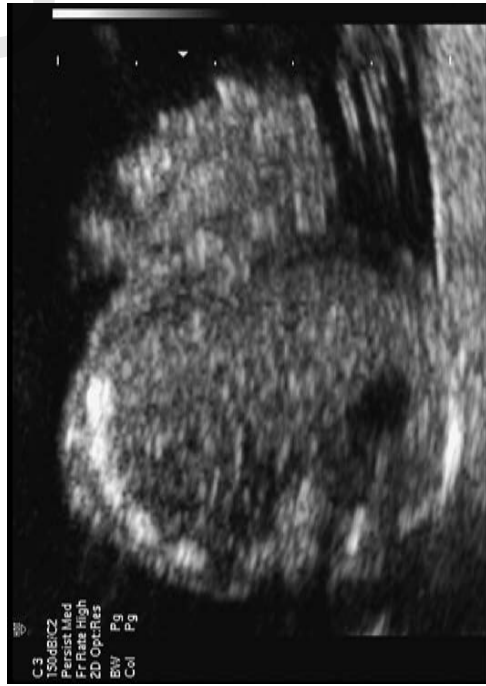


Fig. 11.3 Gastroschisis

akusher-lib.ru

ABDOMINAL CYSTS

Cystic lesions in the fetal abdomen present as either isolated or multiple anechoic areas. The correct diagnosis of these is difficult antenatally and most cysts remain indeterminate in origin. The outcome is usually dependent on the site and origin of these cysts and the presence of any associated abnormalities.

Isolated cystic lesions

Isolated cystic lesions are quite common and are usually considered benign. Their relationship to the fetal bladder is important in determining their origin. A cystic lesion supero-lateral to the fetal bladder (frequently bilateral with septations) is suggestive of an ovarian cyst in a female fetus. In fetuses of either sex, the differential diagnosis would include mesenteric and intestinal duplication cysts. Anterior meningoceles and hydrometrocolpos (female fetus) are seen as cysts posterior to the fetal bladder. Rarely, the cyst may be seen totally unrelated to the bladder and in the upper abdomen. If this is on the right, one should consider a benign liver cyst if the gall bladder is visualized and appears normal. The non-visualization of the gall bladder suggests a choledochal cyst.

Multiple cystic urogenital lesions

Multiple lesions are usually related to either the fetal bowel or fetal kidneys. The presence of hydronephrosis with a dilated, convoluted fluid-filled (echo-free) structure connecting the kidney to the bladder is diagnostic of mega-ureter. The latter usually results from either vesico-ureteric reflux or vesico-ureteric junction obstruction. The presence of a dilated bladder with bilateral mega-ureters is diagnostic of bladder outlet obstruction.

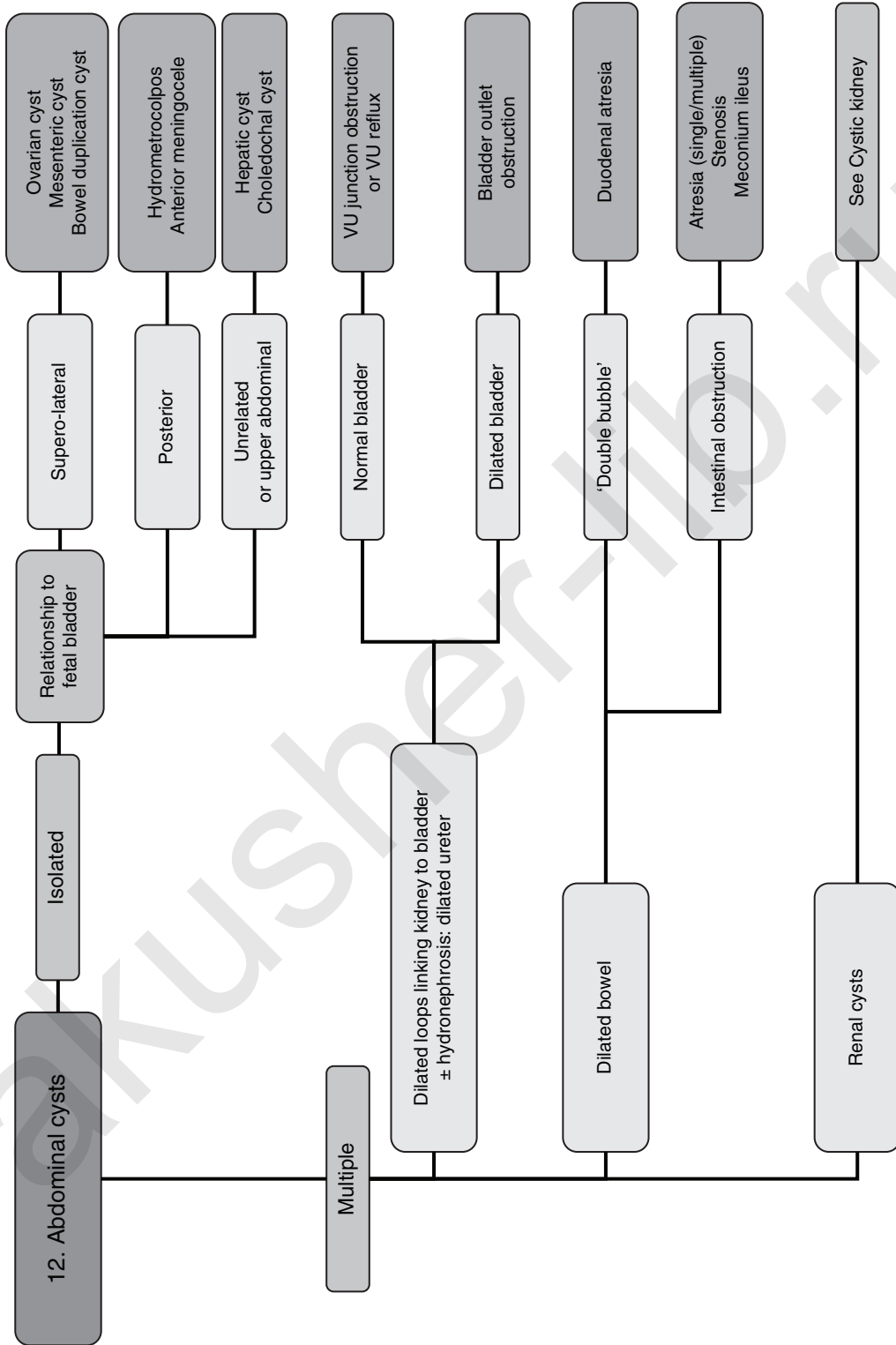
Multiple cystic bowel lesions

Typically, bowel obstruction manifests in the third trimester with multiple linear or discrete cystic spaces that connect with one another. Additionally they have internal echoes that give a speckled appearance. A double bubble appearance in the fetal upper abdomen is suggestive of a high small intestinal obstruction with a high risk for chromosomal abnormality. The exact site(s) or cause (intrinsic: atresia, web; extrinsic: volvulus, peritoneal bands) of the obstruction(s) is not detectable antenatally. Additional features such as echogenic bowel or ascitic fluid collection indicate the possibility of meconium peritonitis which is more common in cystic fibrosis.

Dilatation of the large bowel also manifests in the third trimester, but is usually not detectable on ultrasound.

Bibliography

1. Casaccia G, Bilancioni E, Nahom A et al. Cystic anomalies of biliary tree in the fetus: is it possible to make a more specific prenatal diagnosis? *J Pediatr Surg* 2002; 37(8): 1191–4.
2. Heling KS, Chaoui R, Kirchmair F, Stadie S, Bollmann R. Fetal ovarian cysts: prenatal diagnosis, management and postnatal outcome. *Ultrasound Obstet Gynecol* 2002; 20(1): 47–50.
3. McEwing R, Hayward C, Furness M. Foetal cystic abdominal masses. *Australas Radiol* 2003; 47(2): 101–10.



VU, vesico-ureteric.

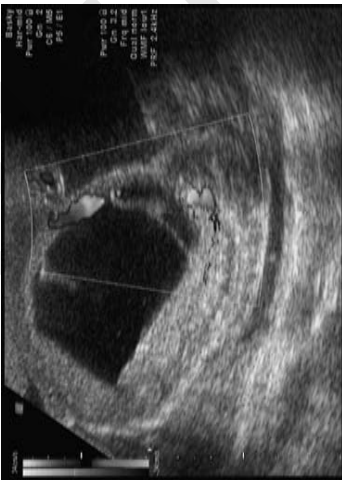


Fig. 12.1 Fetal ovarian cyst (see also colour plate)



Fig. 12.2 Gall bladder



Fig. 12.3 Double bubble

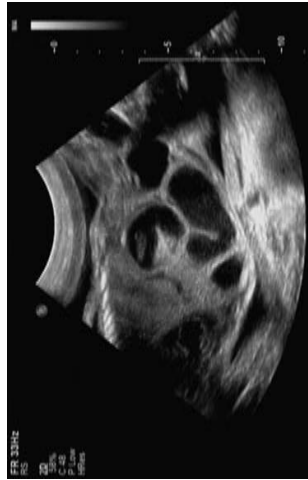


Fig. 12.4 Small bowel obstruction

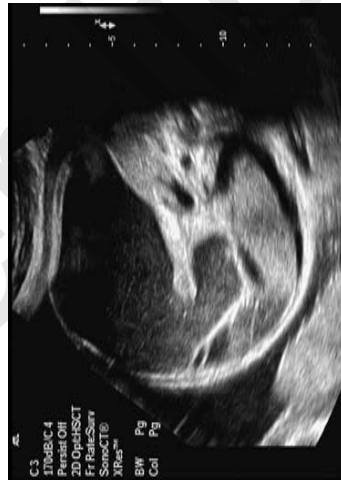


Fig. 12.5 Large bowel dilatation



Fig. 12.6 Volvulus

akusher-lib.ru

ABDOMINAL ECHOGENICITY

The finding of increased echogenicity in the fetal abdomen is common. These hyperechoic areas may be in the fetal bowel, kidneys, or the liver.

Hyperechoic kidneys

Echogenic kidneys in the presence of dilated renal outflow tracts are suggestive of poor function in the kidneys. If the liquor volume is normal, then this is likely to be a normal variant with a normal neonatal outcome. The presence of reduced liquor volume with bright kidneys suggests renal failure, and is likely to be associated with a poor outcome. Infantile polycystic kidneys usually manifest as large bright kidneys without any cortico-medullary differentiation. This invariably presents with anhydramnios and is a lethal malformation.

Hyperechoic bowel

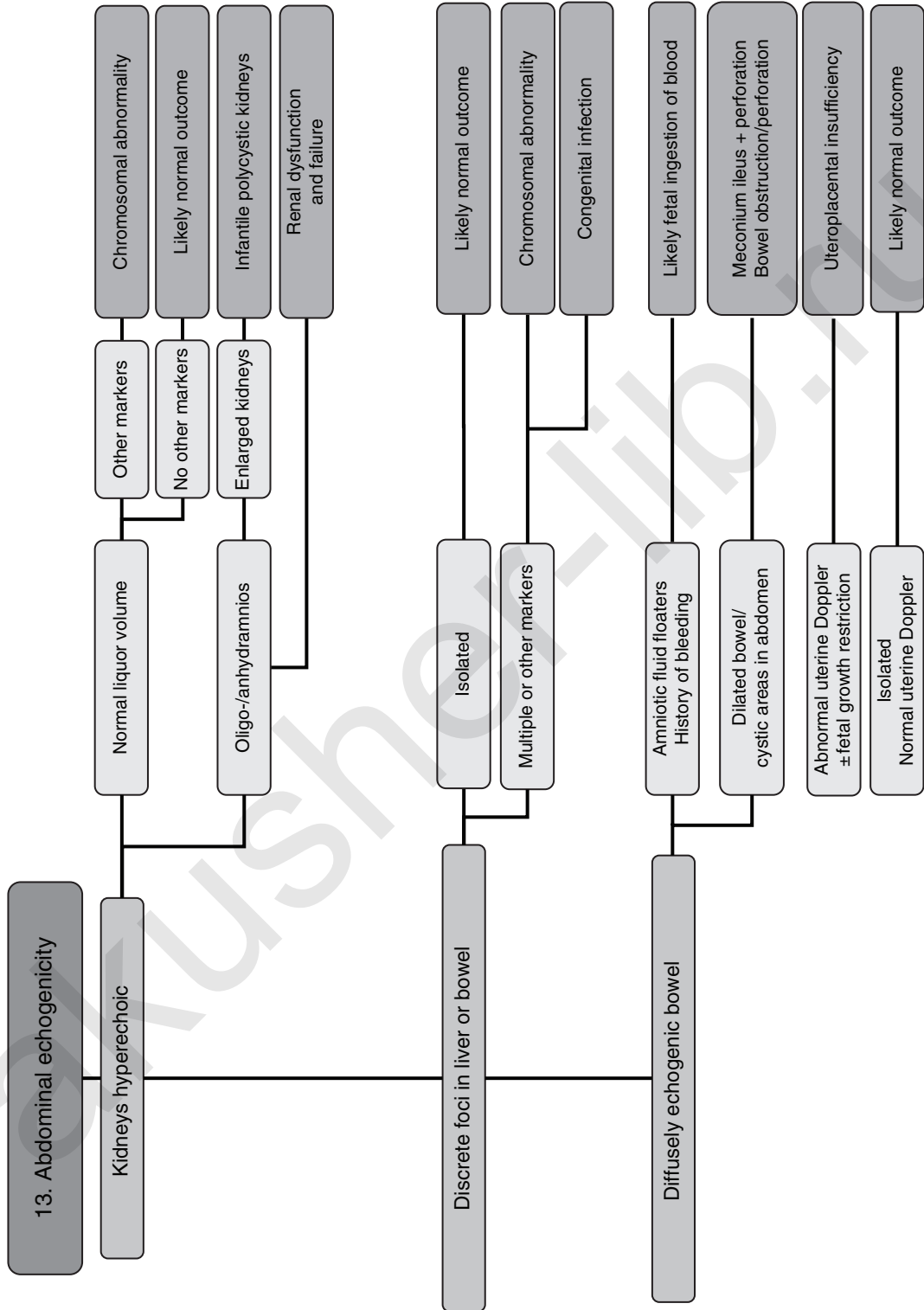
This is the most common echogenic mass in the fetal abdomen. By definition the bowel is considered echogenic only if it is as bright as or brighter than the adjacent bone, namely, the iliac crest. The commonest cause for echogenic bowel is fetal ingestion of blood. This is usually identified as 'floating flakes' in the amniotic fluid and is invariably associated with a history of vaginal bleeding. As an isolated finding, it would not increase the risk for chromosomal abnormalities. The presence of associated bowel dilatation with or without ascitic fluid should raise the possibility of meconium ileus, which is more common with cystic fibrosis.

Discrete hyperechoic foci

Discrete echogenic foci in the fetal abdomen are a common finding at the routine anomaly scan, and are generally associated with a good outcome. The presence of other foci seen in other organs (brain, chest, etc.) is suggestive of congenital viral infection.

Bibliography

1. McNamara A, Levine D. Intra-abdominal fetal echogenic masses: a practical guide to diagnosis and management. *Radiographics* 2005; 25(3): 633–45.
2. Sepulveda W, Leung KY, Robertson ME et al. Prevalence of cystic fibrosis mutations in pregnancies with fetal echogenic bowel. *Obstet Gynecol* 1996; 87(1): 103–6.
3. Simchen MJ, Toi A, Bona M et al. Fetal hepatic calcifications: prenatal diagnosis and outcome. *Am J Obstet Gynecol* 2002; 187(6): 1617–22.



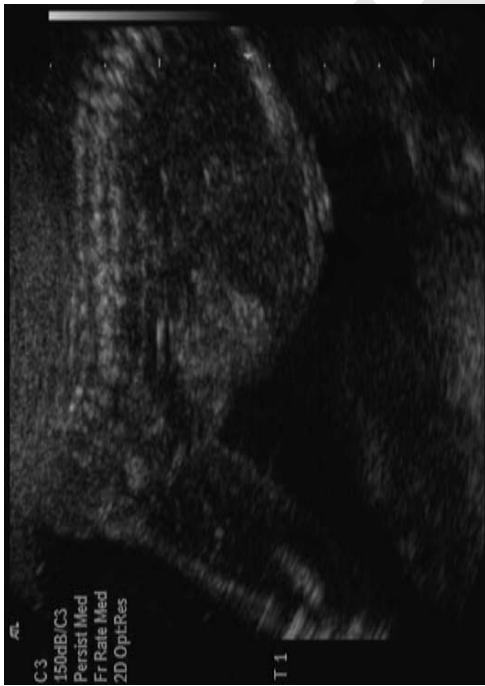


Fig. 13.1 Hyperchogenic bowel



Fig. 13.2 Echogenic focus in liver



Fig. 13.3 Hyperchogenic kidneys

akusher-lib.ru

EMPTY RENAL FOSSA

In fetal life the normal kidneys are imaged with ease in the renal fossae from about 16 weeks of gestation.

Agenesis or ectopic kidney?

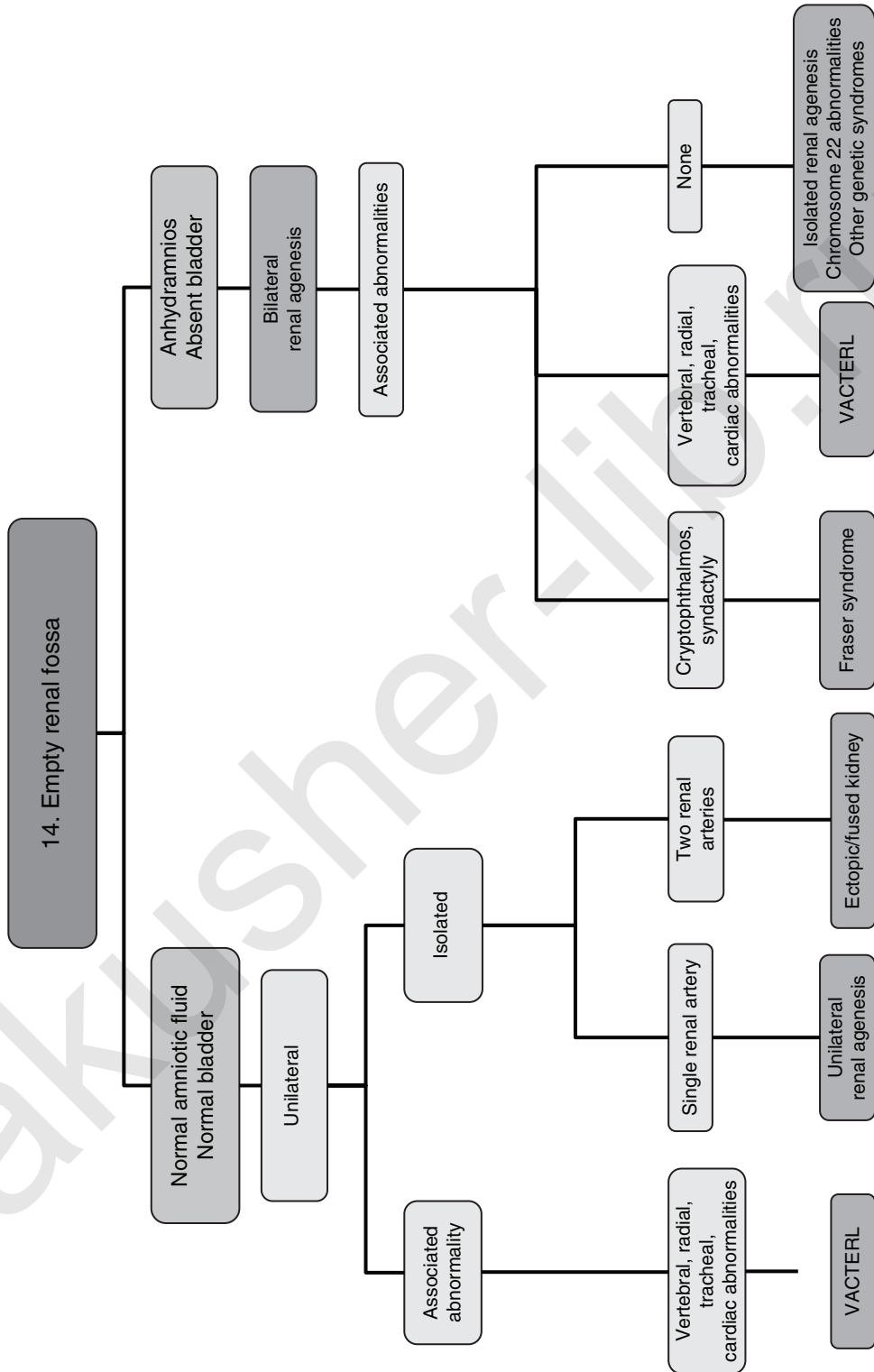
Absence of renal tissue in the normal site, namely the renal fossa, may be due to true agenesis or to ectopic presentation of the kidney. The latter could be either in the fetal pelvis or due to a fusion with the contralateral kidney. In either case, the kidney could show signs of pelvicalyceal dilatation due to the abnormal position and contour of the drainage system. In true agenesis, the renal artery is absent on the ipsilateral side. Ectopic kidneys derive their blood supply from the aorta or the iliac arteries. Unilateral agenesis is usually an isolated finding, but may be part of the VACTERL association (vertebral, anal, cardiac, tracheo-(o)esophageal, (o)esophageal, renal, or limb abnormalities).

Bilateral renal agenesis

Bilateral renal agenesis is usually a diagnosis of exclusion, with the presentation being that of anhydramnios in the second trimester. The renal fossae are hard to image due to the lack of liquor. Additionally, the suprarenal glands occupy the renal fossae, mimicking normal renal tissue on scan. The lack of a normally filled bladder and renal arteries in the setting of anhydramnios would be features in favour of bilateral renal agenesis.

Bibliography

1. Bhide A, Sairam S, Farrugia MK, Boddy SA, Thilaganathan B. The sensitivity of antenatal ultrasound for predicting renal tract surgery in early childhood. *Ultrasound Obstet Gynecol* 2005; 25(5): 489–92.
2. Sepulveda W, Stagiannis KD, Flack NJ, Fisk NM. Accuracy of prenatal diagnosis of renal agenesis with color flow imaging in severe second-trimester oligohydramnios. *Am J Obstet Gynecol* 1995; 173(6): 1788–92.



VACTERL, vertebral, anal, cardiac, tracheo-(o)esophageal, (o)esophageal, renal, limb.

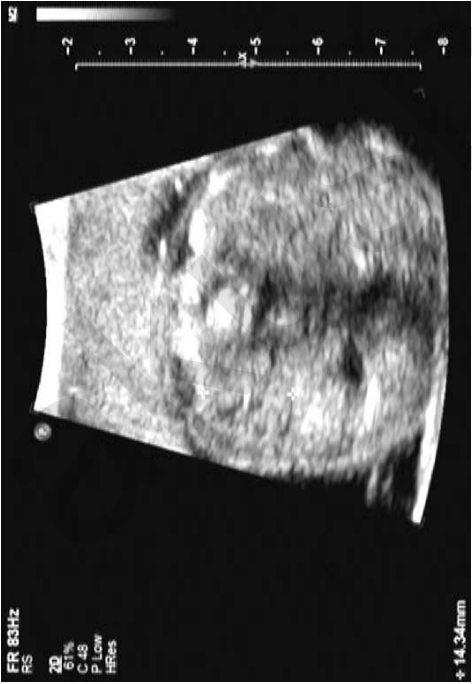


Fig. 14.1 Unilateral renal agenesis

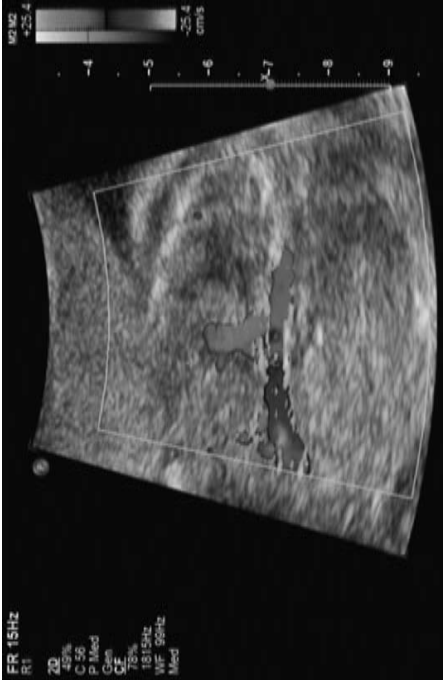


Fig. 14.2 Single renal artery in unilateral renal agenesis (see also colour plate)



Fig. 14.4 Pelvico kidney

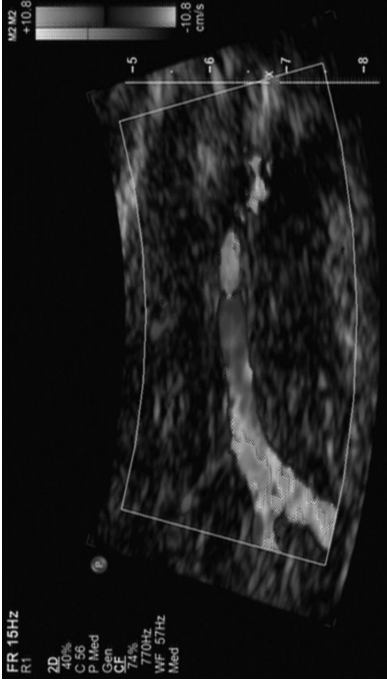


Fig. 14.3 Absent renal arteries in bilateral renal agenesis (see also colour plate)

akusher-lib.ru

CYSTIC KIDNEY

Cystic kidney is a common finding in routine antenatal screening. As a general rule, regardless of the diagnosis, the presence of a normal amniotic fluid volume is indicative of a good prognosis. The finding of anhydramnios in the presence of renal abnormalities would confer a poor prognosis from either pulmonary hypoplasia or renal failure.

Solitary cyst

Solitary cysts in the renal cortex in one or both kidneys may be an isolated finding, but should raise the possibility of adult polycystic disease. In some, there might be demonstrable cysts in the fetal liver and spleen. The bladder and liquor volume are usually normal in this situation. As this is a dominant disorder, the parents should have renal scans.

Isolated multiple cysts

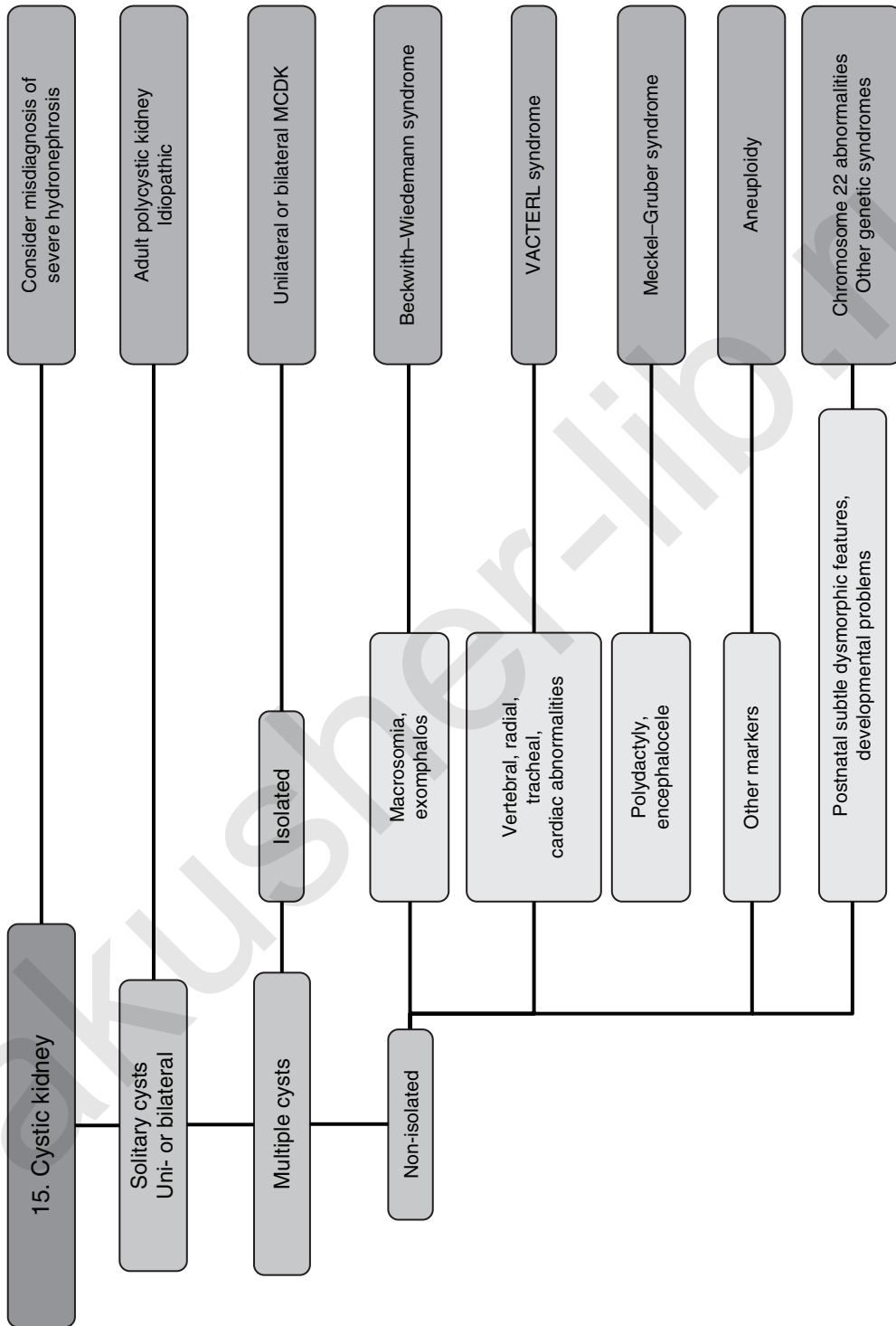
Multiple cysts with a dysplastic kidney can be unilateral (usually normal amniotic fluid volume) or bilateral (usually anhydramnios). There is no clear differentiation between cortex and medulla, with the cysts being randomly distributed, distorting the renal outline. Unilateral multicystic dysplastic kidney has a very good prognosis, provided that the contralateral kidney and amniotic fluid volume are normal.

Multiple cysts with associated findings

Bilateral multicystic kidneys are usually associated with anhydramnios or severe oligohydramnios, and this interferes with the assessment of the rest of the fetal anatomy. However, the identification of macrosomia with a small exomphalos would suggest Beckwith–Wiedemann syndrome. Multisystem abnormalities such as vertebral and cardiac anomalies would favour a diagnosis of VATER (vertebral, anal, tracheo-(o)esophageal, (o)esophageal, renal) or VACTERL (as above, plus cardiac, limb) associations or chromosomal abnormalities such as trisomy 13 or 18. The presence of polydactyly along with an encephalocele would strongly suggest the possibility of the autosomal recessive Meckel–Gruber syndrome. A number of genetic syndromes are diagnosed after a postnatal assessment of the baby or after a post-mortem examination.

Bibliography

1. Lazebnik N, Bellinger MF, Ferguson JE 2nd, Hogge JS, Hogge WA. Insights into the pathogenesis and natural history of fetuses with multicystic dysplastic kidney disease. *Prenat Diagn* 1999; 19(5): 418–23.
2. van Eijk L, Cohen-Overbeek TE, den Hollander NS, Nijman JM, Wladimiroff JW. Unilateral multicystic dysplastic kidney: a combined pre- and postnatal assessment. *Ultrasound Obstet Gynecol* 2002; 19(2): 180–3.



MCDK, multicystic dysplastic kidney; VACTERL, vertebral, anal, cardiac, tracheo-(o)esophageal, (o)esophageal, renal, limb.



Fig. 15.1 Multicystic kidney



Fig. 15.2 Infantile polycystic kidney



Fig. 15.3 Duplex kidney

akusher-lib.ru

FLUID FILLED KIDNEY

Renal pelvis dilatation (hydronephrosis or pyelectasia) is present in approximately 2–3% of all fetuses in mid-gestation. Hydronephrosis is considered to be mild if the antero-posterior dimension of the renal pelvis is 4–7 mm in the absence of calyceal dilatation. Hydronephrosis is classified as moderate/severe if the renal pelvis antero-posterior measurement is over 7 mm or if there is calyceal dilatation.

Risk of chromosomal abnormality

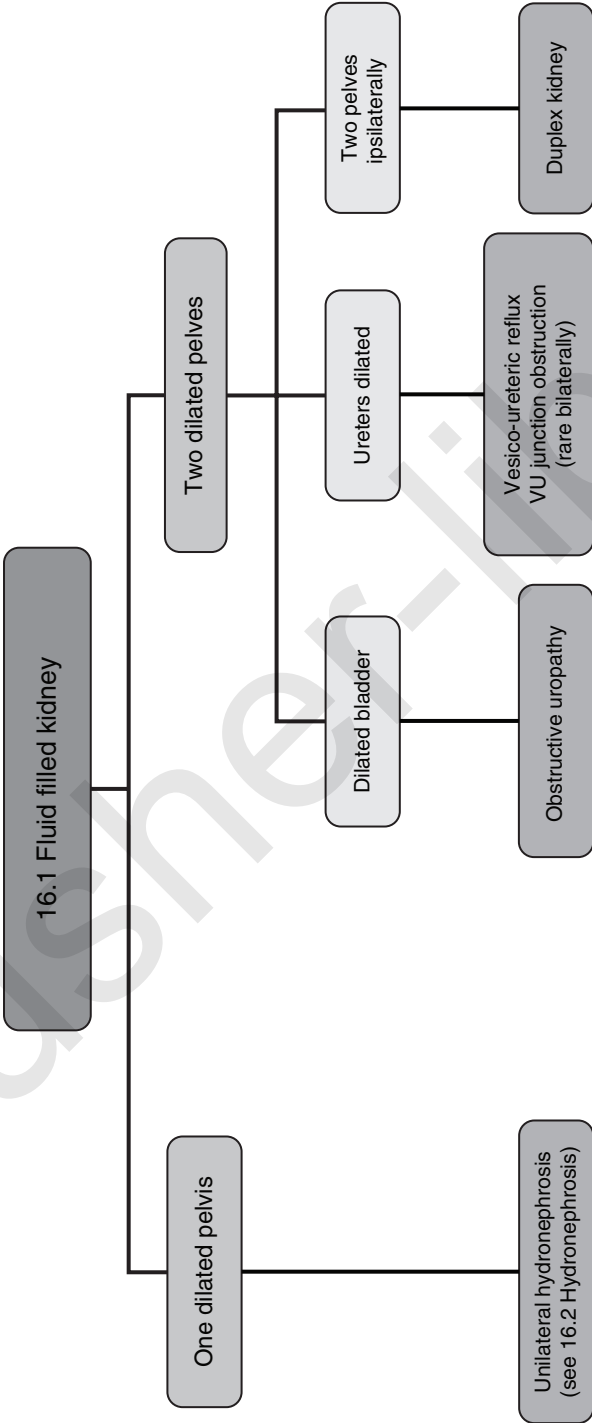
The presence of hydronephrosis should prompt a thorough search for other soft markers for chromosomal abnormalities. In isolation, hydronephrosis does not increase the risk for chromosomal anomalies. The presence of any additional anomalies would significantly increase the background risk of a chromosomal abnormality.

Natural history

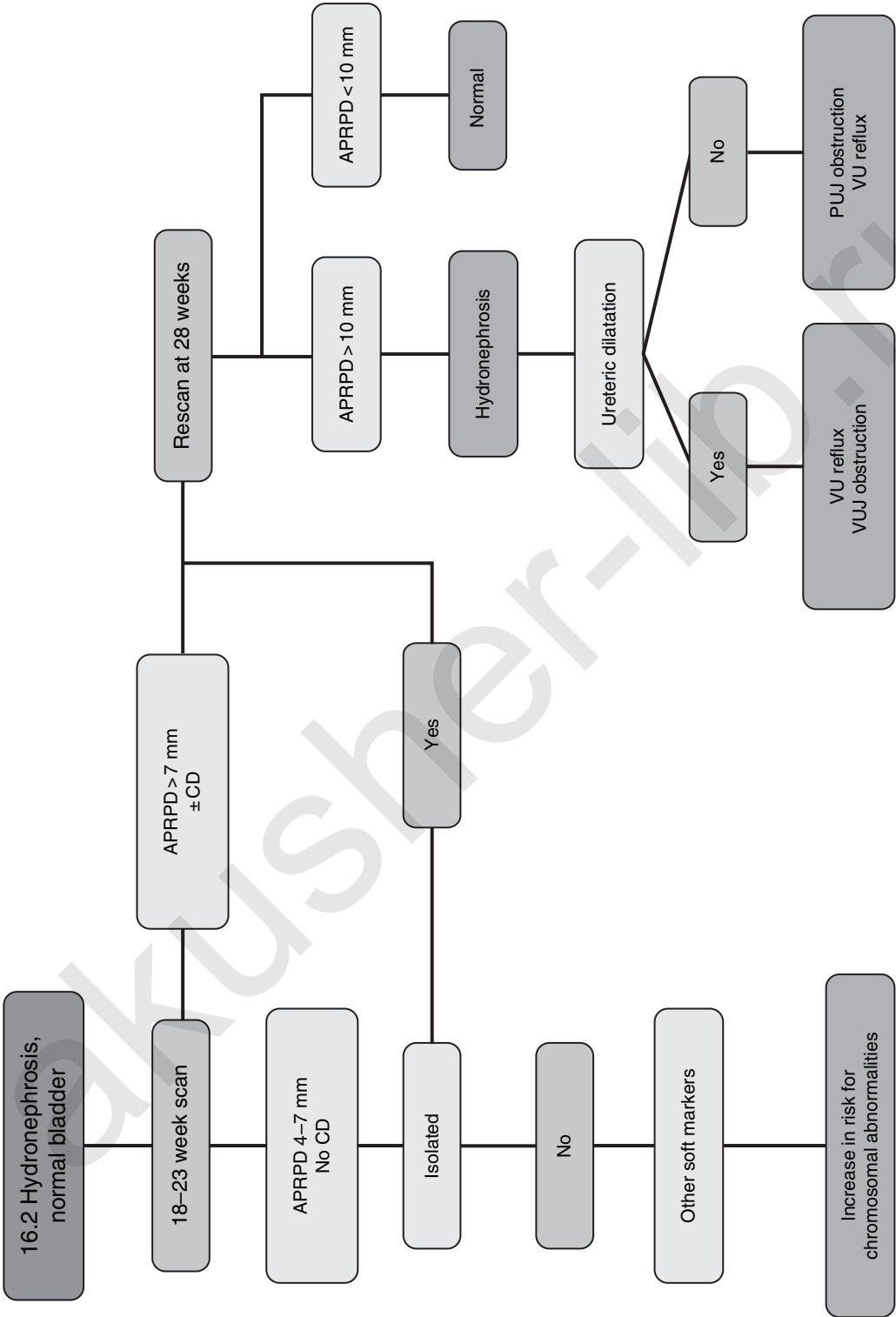
The majority of mild hydronephrosis cases (> 85%) tend to resolve spontaneously, with the remainder only requiring postnatal investigations. Persistent hydronephrosis is defined as a renal pelvis antero-posterior diameter of > 10 mm at > 28 weeks, and suggests the possibility of pelvi-ureteric junction obstruction, or vesico-ureteric junction obstruction or reflux (typically bilateral). With persistent third trimester hydronephrosis, approximately 1 in 3 babies will need postnatal corrective surgery. The presence of ureteric dilatation (vesico-ureteric obstruction or vesico-ureteric reflux) should be noted, as the neonate will need prophylactic antibiotics.

Bibliography

1. Livera LN, Brookfield DSK, Egginton JA, Hawnaur JM. Antenatal ultrasonography to detect fetal abnormalities: a prospective screening programme. *BMJ* 1989; 298(6685): 1421–3.
2. Sairam S, Al-Habib A, Sasson S, Thilaganathan B. Natural history of fetal hydronephrosis diagnosed on mid-trimester ultrasound. *Ultrasound Obstet Gynecol* 2001; 17(3): 191–6.
3. Thompson MO, Thilaganathan B. Effect of routine screening for Down's syndrome on the significance of isolated fetal hydronephrosis. *Br J Obstet Gynaecol* 1998; 105(8): 860–4.



VU, vesico-ureteric.



APRPD, antero-posterior renal pelvis diameter; CD, calyceal dilatation; VU, vesico-ureteric; VUJ, vesico-ureteric junction; PUJ, pelvi-ureteric junction.

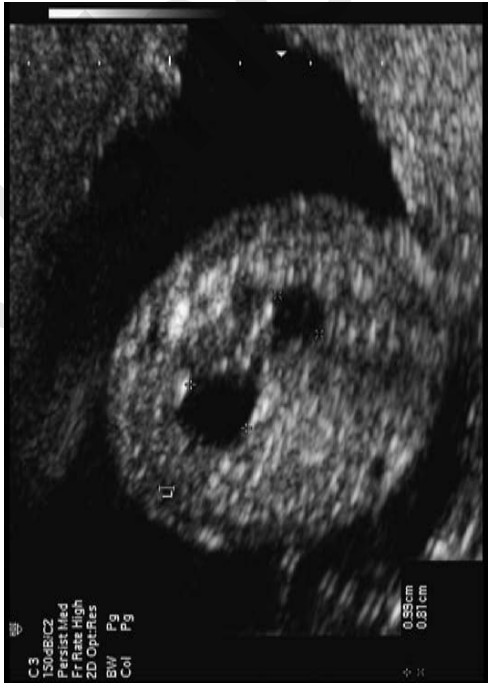


Fig. 16.1 Moderate hydronephrosis



Fig. 16.2 Severe hydronephrosis

ABNORMAL BLADDER

The fetal bladder can be easily visualized in all stages of pregnancy. The bladder should always be assessed in combination with the liquor volume and the kidneys.

Megacystis

In the first trimester, an enlarged bladder > 7 mm (megacystis) should raise the suspicion of either chromosomal abnormalities or obstructive uropathy. Approximately 20% of fetuses with megacystis measuring 7–15 mm have an underlying chromosomal abnormality such as trisomy 13 or 18. If the bladder measures > 15 mm, the risk of an underlying bladder outlet obstruction (urethral atresia, posterior urethral valves, or cloacal abnormalities) is very high and is associated with a very poor prognosis. With megacystis > 15 mm, it is sometimes possible to find echogenic or dysplastic kidneys and reduced liquor volume in the first trimester.

Intermittent/partial urethral obstruction

The finding of an enlarged bladder in the second trimester is usually due to bladder outlet (urethral) obstruction. The presence of normal kidneys suggests that the renal function is likely to be preserved, and is usually confirmed with the additional finding of normal liquor volume. The latter is likely to be due to intermittent/partial outlet obstruction and tends to do well postnatally.

Obstructive uropathy

With posterior urethral valves, there is usually a more severe obstruction of the urethra, resulting in an enlarged and hypertrophied bladder with varying degrees of hydronephrosis and hydroureter, and a spectrum of renal hypoplasia/dysplasia, oligohydramnios, and pulmonary hypoplasia. In some cases, there is associated urinary ascites from rupture of the bladder or transudation of urine into the peritoneal cavity. The combination of an enlarged bladder with abnormal kidneys and reduced or absent liquor volume is indicative of poor renal function, and is generally indicative of poor prognosis.

Bibliography

1. Johnson MP, Freedman AL. Fetal uropathy. *Curr Opin Obstet Gynecol* 1999; 11(2): 185–94.
2. Liao AW, Sebire NJ, Geerts L, Cicero S, Nicolaidis KH. Megacystis at 10–14 weeks of gestation: chromosomal defects and outcome according to bladder length. *Ultrasound Obstet Gynecol* 2003; 21(4): 338–41.
3. Robyr R, Benachi A, Daikha-Dahmane F et al. Correlation between ultrasound and anatomical findings in fetuses with lower urinary tract obstruction in the first half of pregnancy. *Ultrasound Obstet Gynecol* 2005; 25(5): 478–82.

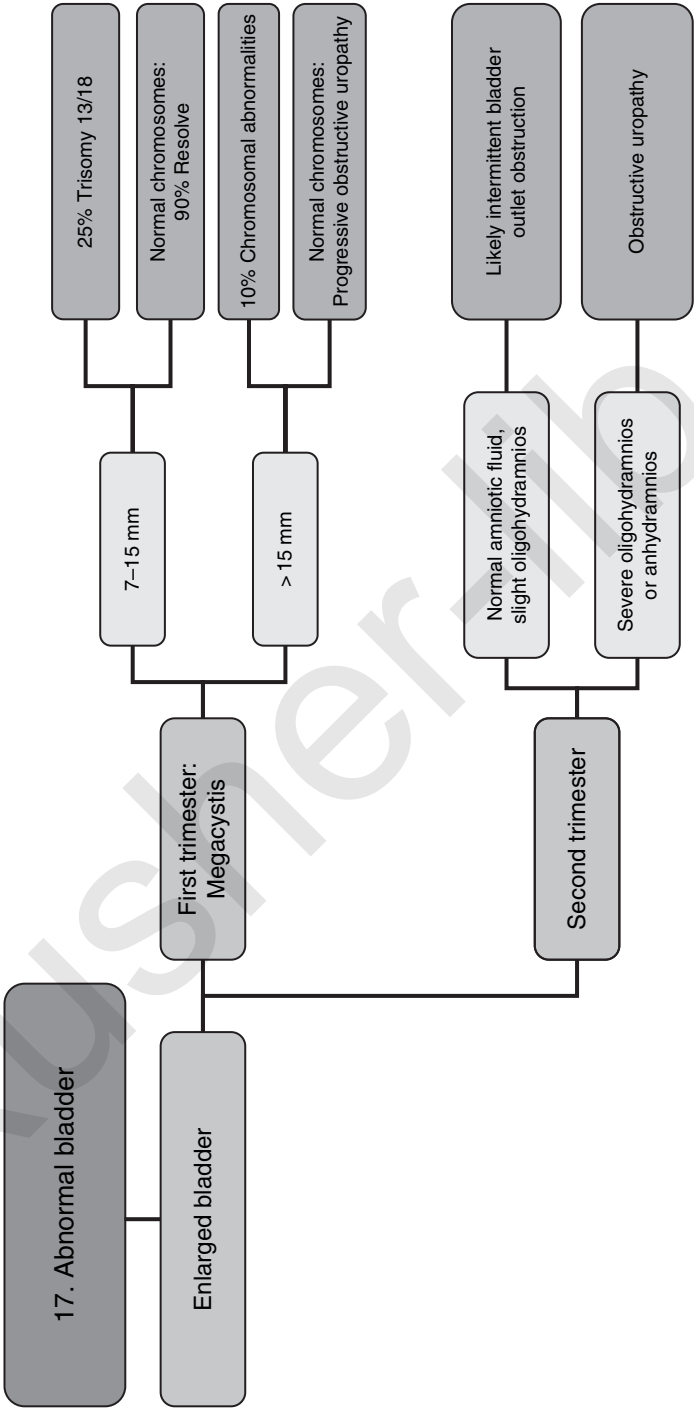




Fig. 17.1 Megacystis

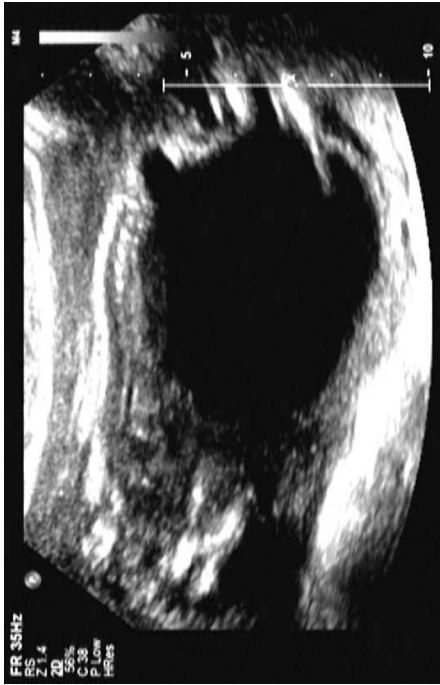


Fig. 17.2 Severe obstructive uropathy



Fig. 17.3 Cystocele

akusher-lib.ru

SHORT FEMUR LENGTH

Shortened femur length is the commonest presentation for suspected skeletal problems, as this is the only bone that is routinely measured in obstetric ultrasound. In the majority of cases, shortening of the long bones is likely to represent inaccurate dating, constitutional smallness, or an early feature of fetal growth restriction. The latter must be excluded before contemplating a diagnosis of a fetal skeletal dysplasia, a heterogeneous group of disorders characterized by abnormalities of cartilage and bone growth. Typically, a diagnosis of a fetal skeletal dysplasia before 24 weeks results in a poor outcome due to thoracic dysplasia.

Fetal growth restriction

Approximately 10–15% of short femur lengths noted at the 20–22 week anomaly scan will subsequently turn out to be due to severe early onset fetal growth restriction secondary to placental insufficiency. The finding of notched, high-resistance uterine artery Doppler indices is characteristic of this diagnosis.

Fetal aneuploidy

Short femur length is a marker for chromosomal abnormality. A thorough search for associated markers of aneuploidy should be undertaken.

Normal bone modelling (< 24 weeks)

Unilateral femoral shortening is suggestive of focal femoral hypoplasia syndromes. Typically the prognosis is good in most of these syndromes. The finding of bilateral shortening is suggestive of achondrogenesis. The latter is a uniformly lethal condition associated with micromelia (extreme shortening of the entire limb) and thoracic dystrophy.

Abnormal bone modelling (< 24 weeks)

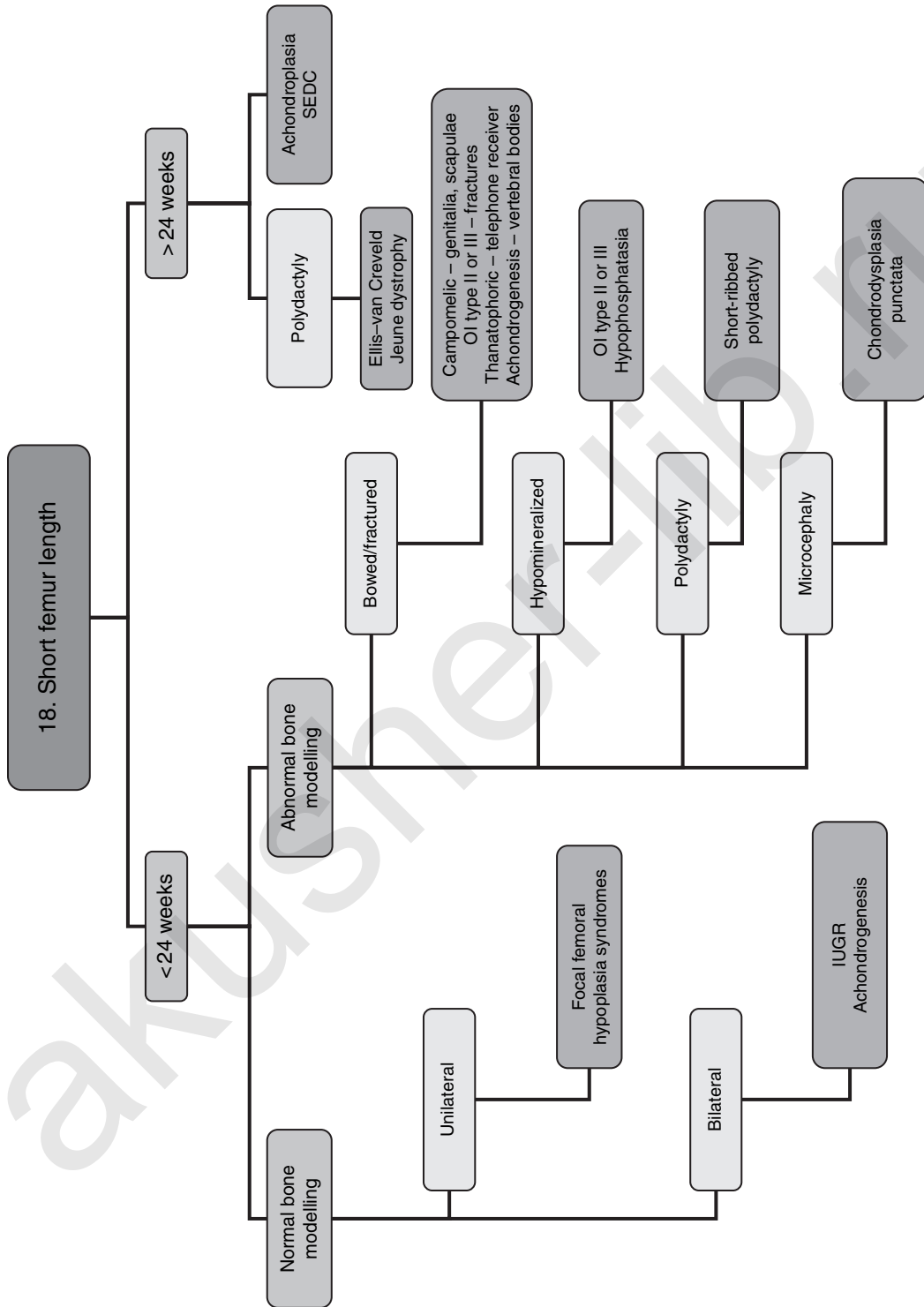
Bowing may be difficult to differentiate from fractures of the long bones, but both suggest the diagnoses of achondrogenesis, thanatophoric dysplasia, campomelic dysplasia, or osteogenesis imperfecta. Definitive hypomineralization is indicative of either hypophosphatasia or osteogenesis imperfecta. Polydactyly is characteristic of short-ribbed polydactyly at this gestation, and microcephaly occurs in chondrodysplasia punctata.

Third trimester diagnosis

The commonest diagnosis in the third trimester is achondroplasia (classical dwarfism). Spondyloepiphyseal dysplasia congenita (SEDC) is an alternative diagnosis, but this is rarely made prenatally as the ultrasound features are subtle. The presence of polydactyly is suggestive of Jeune dystrophy or Ellis–van Creveld syndrome.

Bibliography

1. Krakow D, Williams J 3rd, Poehl M, Rimoin DL, Platt LD. Use of three-dimensional ultrasound imaging in the diagnosis of prenatal-onset skeletal dysplasias. *Ultrasound Obstet Gynecol* 2003; 21(5): 467–72.
2. Lachman RS, Rappaport V. Fetal imaging in the skeletal dysplasias. *Clin Perinatol* 1990; 17(3): 703–22.



IUGR, intrauterine growth restriction; SEDC, spondyloepiphyseal dysplasia congenita; OI, osteogenesis imperfecta.



Fig. 18.1 Short bowed femur



Fig. 18.2 Short bowed forearm



Fig. 18.3 Short fractured femur



Fig. 18.4 Thoracic dystrophy

akusher-lib.ru

JOINT ABNORMALITIES

Typically, joint abnormalities are only diagnosed prenatally when they are severe. However, false positive diagnosis may be made due to the natural joint mobility of fetuses, and the effect of uterine crowding due to advanced pregnancy, oligohydramnios, or multiple pregnancy.

Talipes

This is a varus deformity of the foot, which when diagnosed antenatally is due to abnormal innervation of the muscles of the ankle joint. When unilateral and isolated, the prognosis is very good. A significant proportion of complex/bilateral cases are associated with chromosomal abnormality, genetic syndromes, or neurodevelopmental disorders.

Fixed flexion of multiple joints

These findings fall under the umbrella term arthrogryposis multiplex congenita, which covers many different neuromuscular disorders with guarded postnatal prognoses. The finding of cutaneous webs at the joints is typical of multiple pterygium syndrome. The confinement of abnormalities to the lower limb with an abrupt spinal termination is characteristic of caudal regression syndrome, often associated with diabetic pregnancy. If abnormalities in long bone length, mineralization, or fractures are seen, a skeletal dysplasia should be suspected.

Abnormal tone/posture

Rarely, abnormal posture or tone may be noted in the fetal joints, suggesting a neuromuscular disorder, such as Pena–Shokeir sequence. The latter should only be suspected if the posture is persistently abnormal on several scans on different occasions.

Bibliography

1. Bakalis S, Sairam S, Homfray T et al. Outcome of antenatally diagnosed talipes equinovarus in an unselected obstetric population. *Ultrasound Obstet Gynecol* 2002; 20(3): 226–9.
2. Bonilla-Musoles F, Machado LE, Osborne NG. Multiple congenital contractures (congenital multiple arthrogryposis). *J Perinat Med* 2002; 30(1): 99–104.

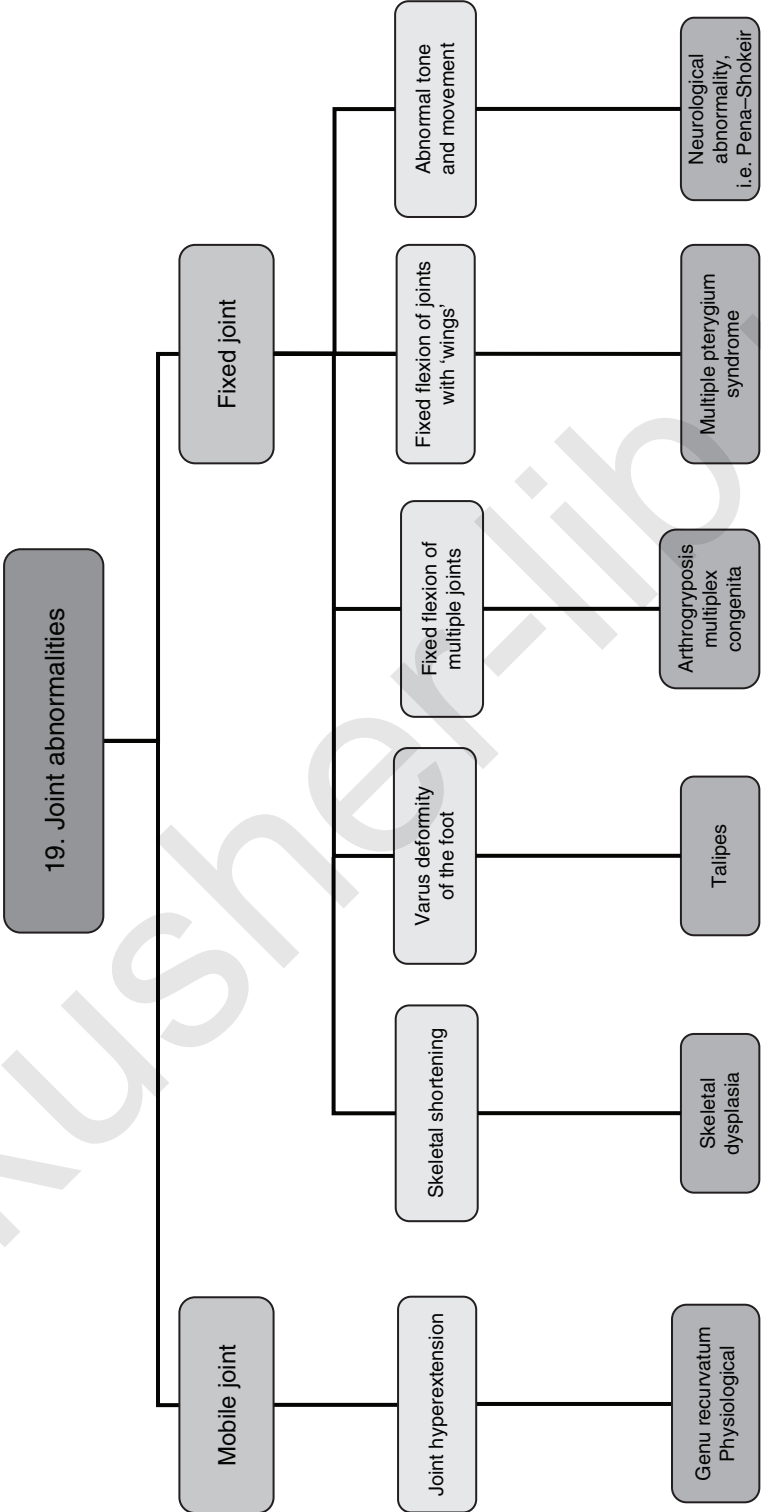




Fig. 19.1 Talipes

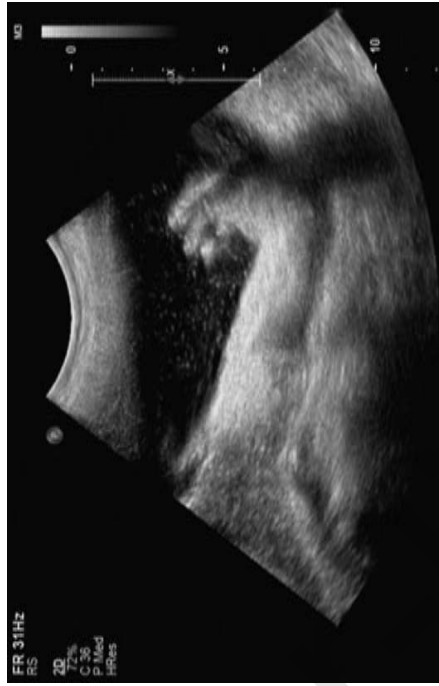


Fig. 19.2 Wrist contracture

akusher-lib.ru

HAND ABNORMALITIES

Typically, abnormalities of the hand are only noted as part of a careful fetal survey after the diagnosis of another abnormality. Under these circumstances, the hand abnormalities are likely to be related to the chromosomal or genetic abnormality diagnosed.

Abnormal hand movement/posture

The presence of overlapping fingers or a clenched hand is suggestive of a chromosomal disorder such as trisomy 18 or a neuromuscular disorder such as Pena–Shokeir syndrome. If the hand is held in a decerebrate, inwardly turned posture, a radial array defect or neurodevelopmental problem should be suspected.

Abnormal hand structure

Polydactyly is a common isolated finding with an excellent prognosis. Associated features suggest a diagnosis such as a trisomy, skeletal dysplasia, Meckel–Gruber, and Smith–Lemli–Opitz syndrome. Missing or prematurely foreshortened digits are characteristic of amniotic band syndrome and terminal transverse limb defects. A split-hand or ‘lobster-claw’ deformity is suggestive of ectrodactyly.

Bibliography

1. Bromley B, Shipp TD, Benacerraf B. Isolated polydactyly: prenatal diagnosis and perinatal outcome. *Prenat Diagn* 2000; 20(11): 905–8.
2. Watson S. The principles of management of congenital anomalies of the upper limb. *Arch Dis Child* 2000; 83(1): 10–17.

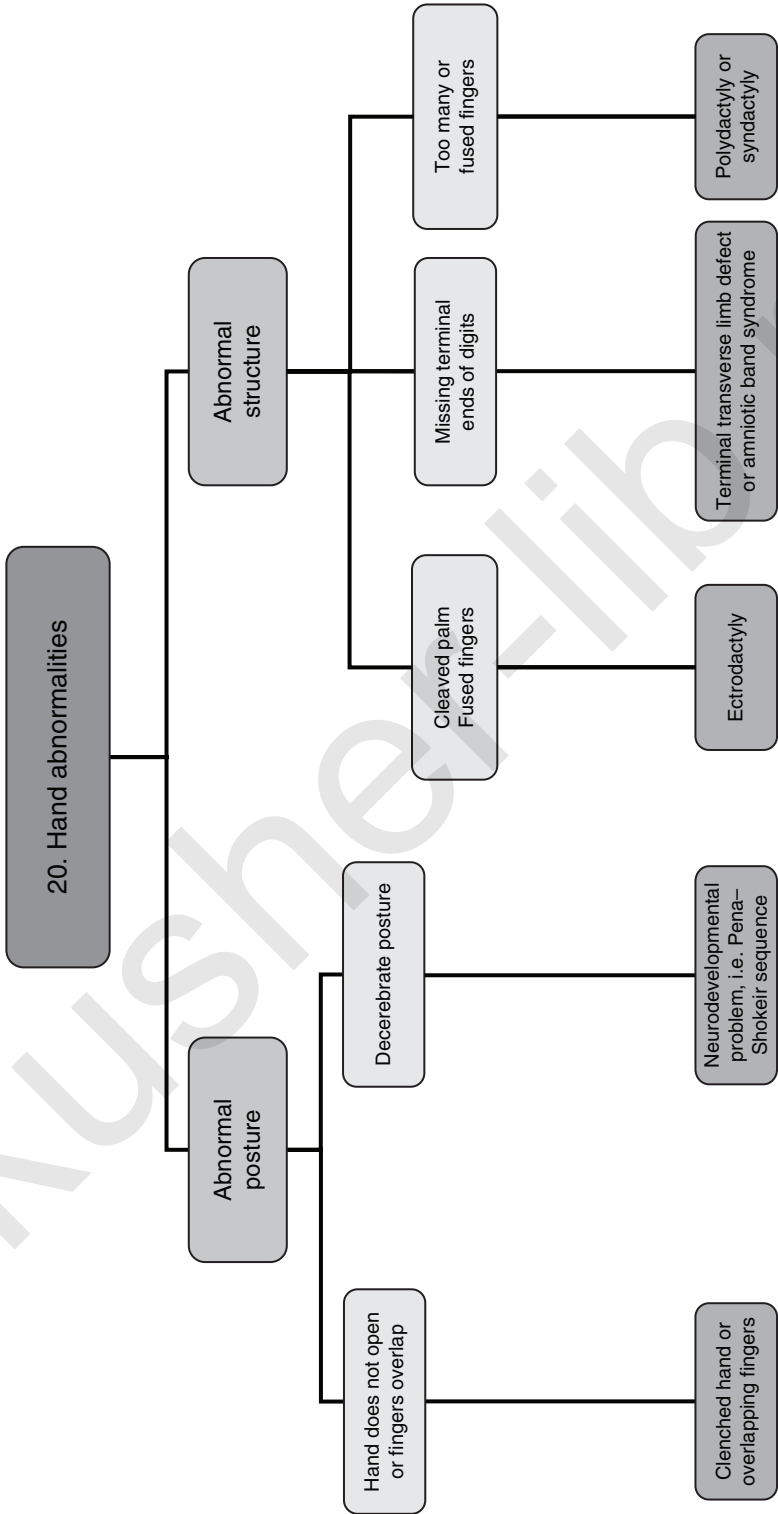




Fig. 20.1 Overlapping fingers



Fig. 20.2 Ectrodactyly of the foot

akusher-lib.ru

SPINAL ABNORMALITIES

The commonest spinal abnormality encountered prenatally is spina bifida. Although other spinal lesions are possible, they are relatively infrequent.

Spina bifida

Typically this is diagnosed on detection of the characteristic 'lemon-shaped' head and 'banana' cerebellum. The level of the lesion, the number of segments involved, and severity of the kyphoscoliosis, ventriculomegaly, and microcephaly determine the prognosis for the neonate.

Sacroccygeal teratoma

This usually presents as a vascular, semi-solid/semi-cystic tumour at the terminal end of the spine. Sacroccygeal teratomas are associated with fetal hydrops and polyhydramnios from high-output cardiac failure related to the arterio-venous shunting within the tumour. These tumours are only rarely malignant, and the prognosis tends to be good after resection.

Spinal angulation

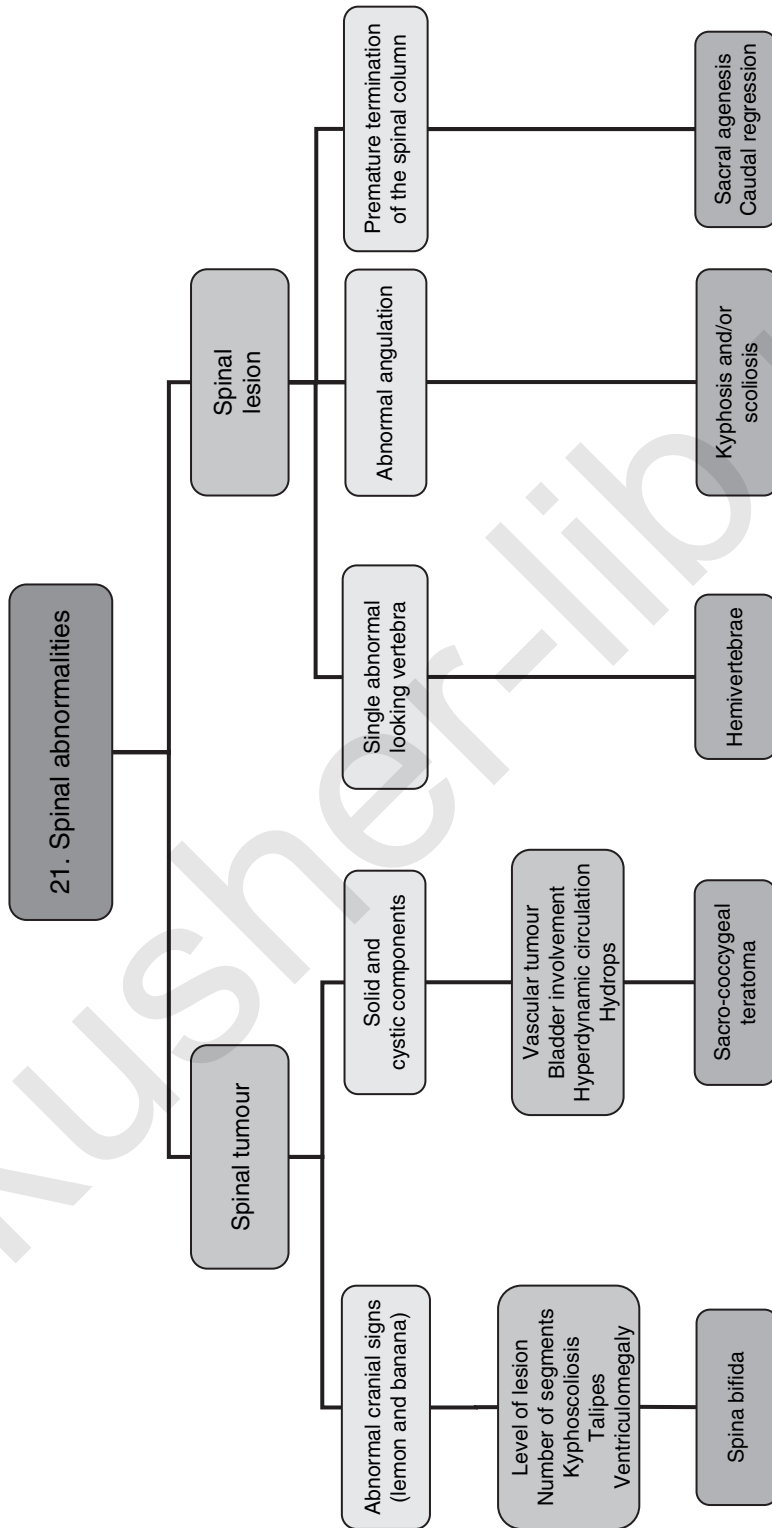
Hemivertebrae are rarely diagnosed prenatally, probably because of the low prevalence and the relatively difficult ultrasound diagnosis. Most cases have a good prognosis, but consideration should be given to the diagnosis of VATER (vertebral, anal, tracheo-(o)esophageal, (o)esophageal, renal) or VACTERL (as above, plus cardiac, limb) associations. Kyphosis (exaggerated hump) and scoliosis (lateral deformity) may be diagnosed prenatally as isolated abnormalities. Occasionally they may be associated with spina bifida, body stalk abnormality, and skeletal dysplasias.

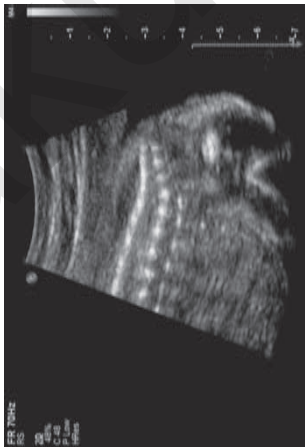
Caudal regression

This can vary in severity from partial sacral agenesis to complete absence of the lumbosacral spine. In an extreme form (sirenomelia), it presents with fusion and hypoplasia of the lower extremities and pelvic structures. Caudal regression occurs more commonly in diabetic pregnancy.

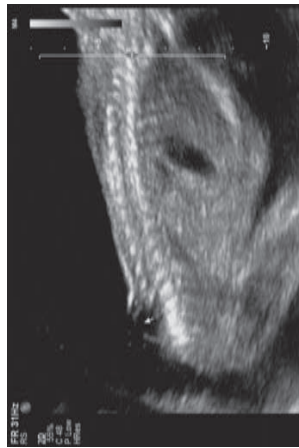
Bibliography

1. Mitchell LE, Adzick NS, Melchionne J et al. Spina bifida. *Lancet* 2004; 364(9448): 1885–95.
2. Nyberg DA. The fetal central nervous system. *Semin Roentgenol* 1990; 25(4): 317–33.





(a)



(b)

Fig. 21.1 (a) Normal spine (b) Sacral meningocele



Fig. 21.2 Lemon shaped head

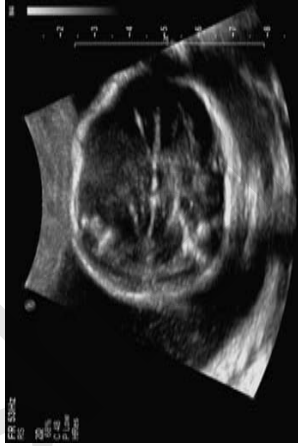


Fig. 21.3 Banana cerebellum



Fig. 21.5 Kyphoscoliosis

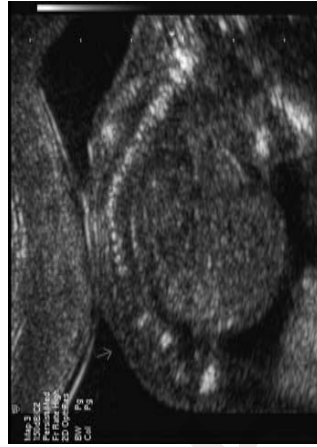


Fig. 21.6 Caudal regression

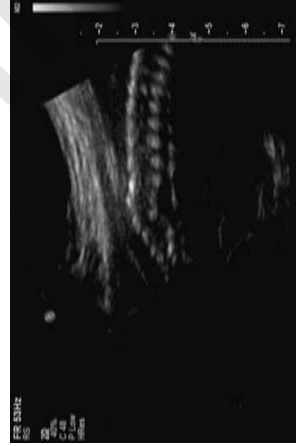


Fig. 21.4 Hemivertebrae

akusher-lib.ru

HEAD AND NECK MASSES

Fetal head and neck tumours are rare. The prognosis of these tumours largely depends on their size. If they are large they can cause compression of the trachea and neonatal airway, requiring ex-utero intrapartum treatment (EXIT) delivery. Fetal hydrops in highly vascular tumours and polyhydramnios due to poor swallowing are both associated with poorer outcomes.

Cervical teratoma

This is a very rare embryonic tumour of the neck with a heterogeneous appearance on ultrasound. They are usually unilateral, solid/cystic, multiloculated masses measuring 5–12 cm, commonly seen with calcifications.

Epignathus

This is a very rare mature teratoma of the oro-pharyngeal region, which presents as a solid tumour of the oral and/or nasal cavities usually associated with polyhydramnios. The tumour is often very vascular, and this can lead to fetal cardiac decompensation and hydrops. The anatomy of the brain must be carefully examined as intracranial extension can occur.

Fetal goitre

This is enlargement of the fetal thyroid gland. It can be due to maternal thyroid disease, but has also been reported in euthyroid women. Ultrasound features are of a symmetrical anterior solid mass which can result in hyperextension of the fetal head.

Cystic hygroma

This is the commonest cause for a fetal neck mass, and is thought to be due to lymphatic malformation. In the first trimester, cystic hygromas can be identified as increased nuchal translucency at the 11–13 + 6 week scan. Second trimester diagnosis is by an ultrasound finding of a thin-walled cystic swelling at the back of the neck with a characteristic midline septum (the nuchal ligament), often with multiple septa. Fetal cystic hygromas are strongly associated with underlying chromosomal abnormalities and genetic syndromes.

Fetal haemangioma

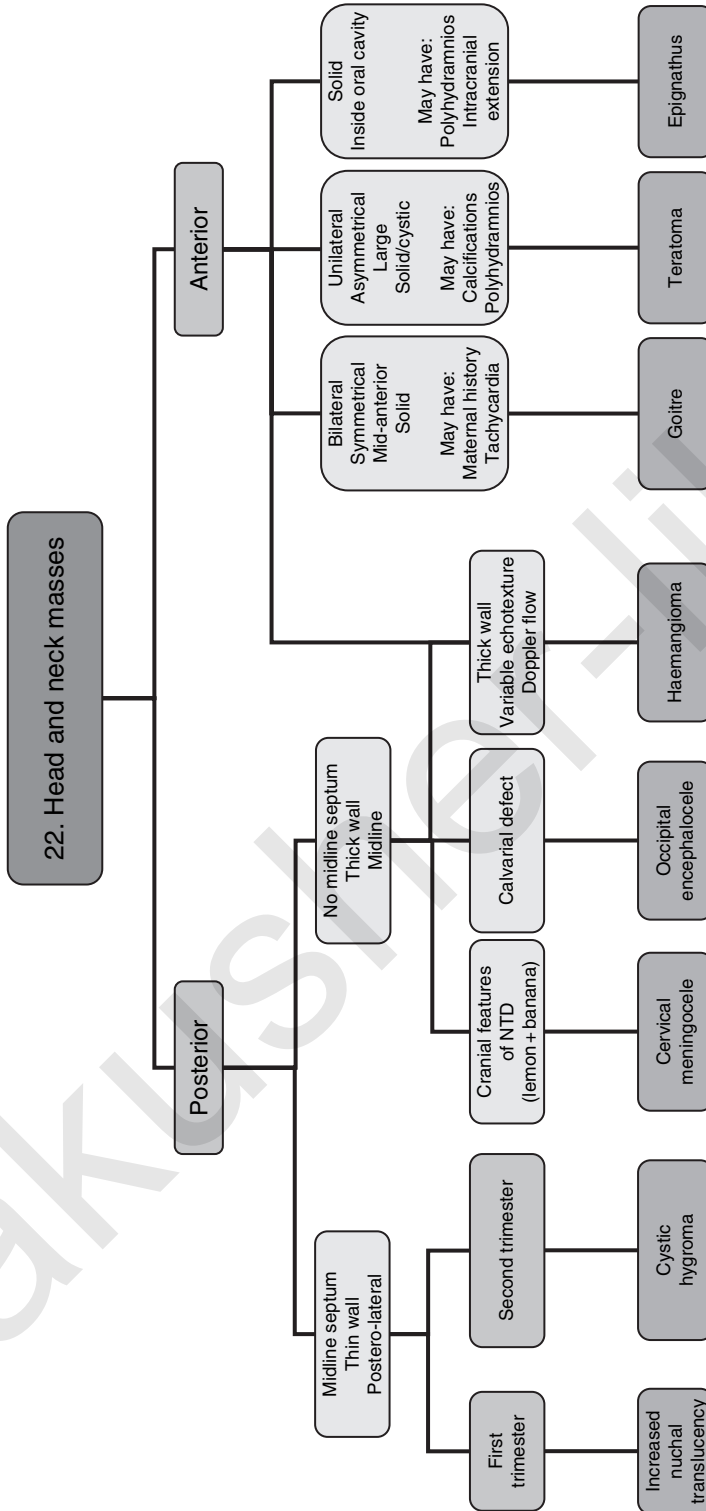
Fetal haemangioma affecting the neck or face is a rare condition, and appears as a thick-walled sonolucent mass with characteristic pulsating Doppler flow signals.

Ex-utero intrapartum treatment (EXIT)

The aim of the procedure is to allow time to secure the airway in the newborn while maintaining uteroplacental gas exchange at Caesarean section. This is achieved by endotracheal intubation or tracheostomy while still connected to the placenta.

Bibliography

1. Chervenak FA, Isaacson G, Touloukian R et al. Diagnosis and management of fetal teratomas. *Obstet Gynecol* 1985; 66: 666–71.
2. Gallagher PG, Mahoney MJ, Gosche JR. Cystic hygroma in the fetus and newborn. *Semin Perinatol* 1999; 23(4): 341–56.
3. Nicolaidis KH. Nuchal translucency and other first-trimester sonographic markers of aneuploidy. *Am J Obstet Gynecol* 2004; 191: 45–67.



In all cases remember to examine for:
 Amniotic fluid
 Other fetal abnormalities
 Hydrops
 Neck position



Fig. 22.1 Encephalocele



Fig. 22.2 Cystic hygroma



Fig. 22.3 Facial cyst

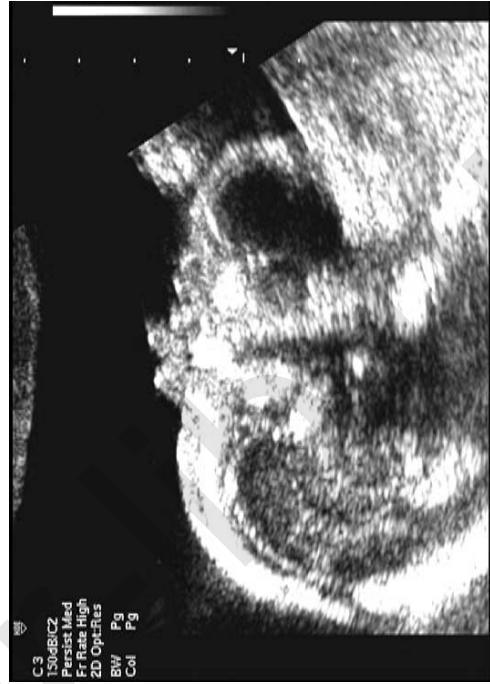


Fig. 22.4 Neck tumour

akusher-lib.ru

INCREASED NUCHAL TRANSLUCENCY

All fetuses have a collection of fluid under the skin behind the neck at 11–13 + 6 weeks of gestation. This nuchal translucency (NT) is visible and measurable on ultrasound. There are many causes of increased NT, and there may not be a single underlying mechanism for its presence.

Chromosomal abnormalities

Nuchal translucency (NT) is the single most important marker for chromosomal abnormalities in the first trimester, and by far the most widely researched. Screening for trisomy 21 by combining NT with maternal age results in a detection rate of about 80% for a 5% invasive testing rate. The NT is increased in other chromosomal abnormalities, and a screening programme for trisomy 21 will also detect the majority of fetuses with other trisomies. Combining NT screening with other first-trimester ultrasound markers (nasal bone, ductus venosus, tricuspid regurgitation) as well as first- and second-trimester maternal serum markers increases the detection rate of chromosomal defects further.

Cardiac defects

Heart abnormalities are associated with increased NT thickness in chromosomally normal fetuses. The prevalence of heart abnormalities is about 7% if the NT is 4.5–5.4 mm, 20% for NT of 5.5–6.4 mm, and 30% for NT of 6.5 mm or more. Using NT as a screening test for major heart defects will significantly improve detection rates for cardiac abnormalities. In pregnancies with increased NT, specialist fetal echocardiography should be considered for fetuses with an NT above the 95th centile.

Fetal abnormalities and movement disorders

Increased fetal NT is associated with a high prevalence of major fetal abnormalities. There is a long and growing list of abnormalities associated with increased NT, and common defects include hydrops, congenital diaphragmatic hernia, exomphalos, body stalk anomaly, skeletal abnormalities, and fetal movement disorders such as fetal akinesia deformation sequence. A careful anatomical survey should therefore be performed in chromosomally normal fetuses with increased NT, and this should include looking for normal fetal movements.

Genetic syndromes

Increased NT has been associated with a large number of genetic syndromes. The rarity of these means that it can be difficult to establish whether the observed prevalence is higher than in the general population, but it appears that congenital adrenal hyperplasia, fetal akinesia deformation sequence, Noonan syndrome, Smith–Lemli–Opitz syndrome, and spinal muscular atrophy are more prevalent than expected in the general population.

Bibliography

1. Makrydimas G, Sotiriadis A, Huggon IC et al. Nuchal translucency and fetal cardiac defects: a pooled analysis of major fetal echocardiography centers. *Am J Obstet Gynecol* 2005; 192(1): 89–95.
2. Snijders RJ, Noble P, Sebire N, Souka A, Nicolaidis KH. UK multicentre project on assessment of risk of trisomy 21 by maternal age and fetal nuchal-translucency thickness at 10–14 weeks of gestation. Fetal Medicine Foundation First Trimester Screening Group. *Lancet* 1998; 352(9125): 343–6.
3. www.fetalmedicine.com.

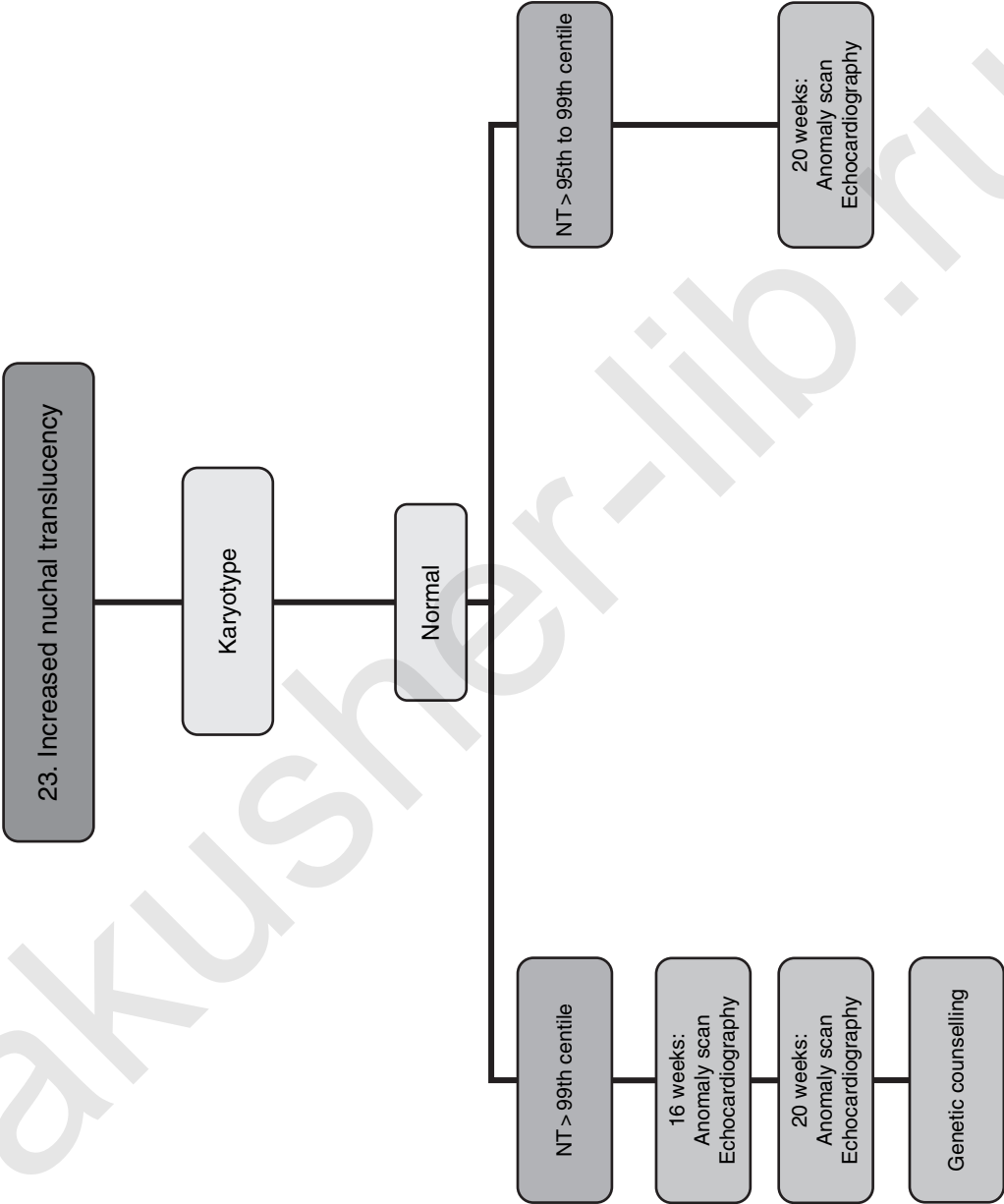




Fig. 23.2 Increased nuchal measurement



Fig. 23.1 Normal nuchal measurement

akusher-lib.ru

PLACENTAL ABNORMALITIES

Molar pregnancy

Hydatidiform mole can be divided into complete (where there is no fetus) and partial/incomplete (where a fetus is present). Ultrasound shows the placenta to be an enlarged complex intrauterine mass containing many small cysts which can be described as grape-like (hydatidiform). The classic image of a snowstorm pattern can sometimes be seen, but the description is based on older ultrasound technology.

Chorioangiomas

These are benign vascular tumours which rarely can result in fetal complications such as cardiomegaly, polyhydramnios, anaemia, hydrops, and occasionally fetal growth restriction. Targeted ultrasound using colour Doppler can help in identifying chorioangiomas in cases with the latter complications.

Placental cysts

These are seen just beneath the chorionic plate and are of no apparent clinical significance. They are thought to be caused by the deposition of fibrin in the intervillous space.

Placental lakes

Placental lakes appear as sonolucent areas in the placenta. They are often seen in cases of fetal growth restriction due to placental insufficiency. However, they are poor in the prediction of uteroplacental insufficiency as they are commonly seen in normal pregnancy, especially with advancing gestation.

Jelly-like placenta

Rarely the placenta can appear thick, with patches of decreased echogenicity. Jelly-like refers to the placenta quivering like jelly in response to sharp abdominal pressure. The finding has been reported as being strongly associated with an adverse pregnancy outcome. In such cases it may therefore be advisable to perform serial growth scans.

Placental grading

Placental grading was used in order to identify pregnancies at risk of fetal growth restriction before the wide availability of Doppler equipment. In addition, the poor correlation of placental grade to neonatal outcome has meant that the effectiveness of reporting Grannum grades in clinical practice is limited and largely historical.

Placenta accreta

In this condition the placenta is adherent to the uterus, and should be suspected in cases of placenta praevia or previous Caesarean section. Ultrasound features include a loss of the hypoechoic area between placenta and myometrium, large intraplacental lakes, or irregular vascular sinuses with turbulent flow within the placenta.

Bibliography

1. Harris RD, Cho C, Wells WA. Sonography of the placenta with emphasis on pathological correlation. *Semin Ultrasound CT MR* 1996; 17(1): 66–89.
2. Thompson MO, Vines SK, Aquilina J, Wathen NC, Harrington K. Are placental lakes of any clinical significance? *Placenta* 2002; 23(8–9): 685–90.

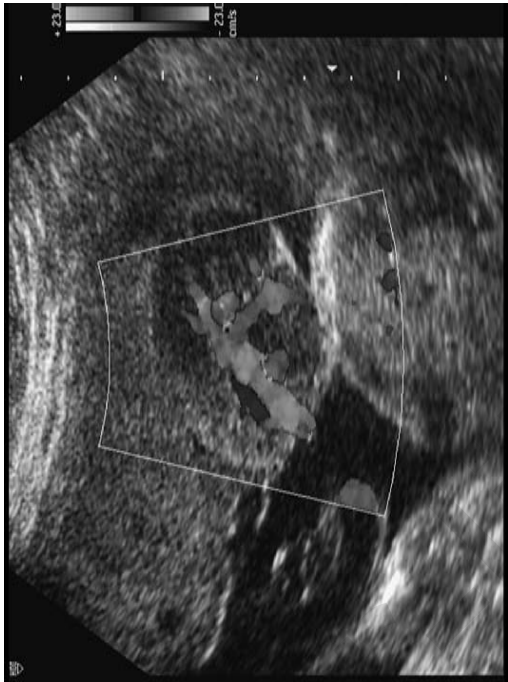


Fig. 24.2 Placental chorioangioma (see also colour plate)



Fig. 24.1 Placenta lakes

SINGLE UMBILICAL ARTERY

The normal umbilical cord contains two arteries and one vein. A single umbilical artery occurs in around 1% of cords in singletons, but the incidence may be higher in women with diabetes, and lower in those of African and Japanese ethnic origin. The antenatal diagnosis can be by examination of a transverse section of the cord using B mode, or by using colour Doppler to image the origin of the umbilical arteries on each side of the fetal bladder.

Chromosomal abnormalities

About 20–30% of fetuses with a single umbilical artery have associated abnormalities, usually chromosomal (trisomy and triploidy). The commonly reported defects are cardiac, abdominal wall, and urinary tract abnormalities.

Isolated two-vessel cord

In a low-risk patient, the finding of an isolated single umbilical artery does not significantly increase the risk for a chromosomal defect. In isolated cases, the perinatal morbidity may be increased due to the association of fetal growth restriction in 10–15% of cases.

Management

Prenatal diagnosis of a single umbilical artery should prompt careful examination for other abnormalities, and fetal karyotyping should be considered if these are found. In ongoing cases serial ultrasound examination to ensure linear fetal growth should be performed.

Bibliography

1. Cristina MP, Ana G, Ines T, Manuel GE, Enrique IG. Perinatal results following the prenatal ultrasound diagnosis of single umbilical artery. *Acta Obstet Gynecol Scand* 2005; 84(11): 1068–74.
2. Predanic M, Perni SC, Friedman A, Chervenak FA, Chasen ST. Fetal growth assessment and neonatal birth weight in fetuses with an isolated single umbilical artery. *Obstet Gynecol* 2005; 105(5 Pt 1): 1093–7.

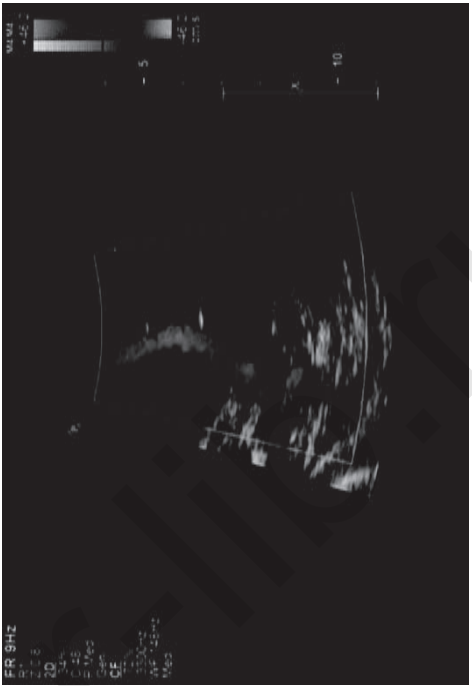
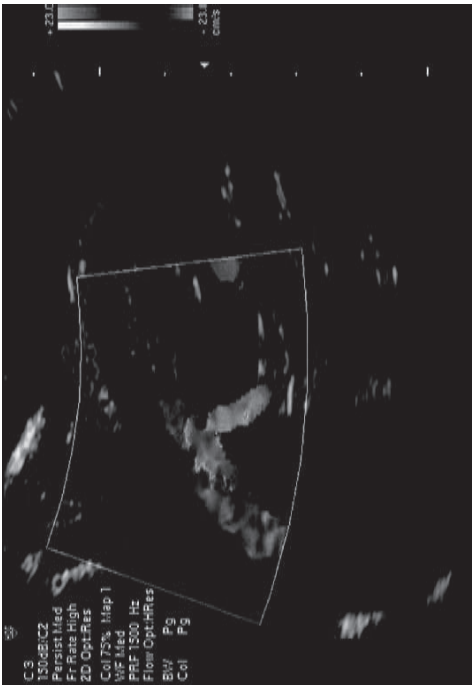


Fig. 25.2 (a) Two umbilical arteries on colour Doppler (b) Single umbilical artery on colour Doppler (see also colour plate)

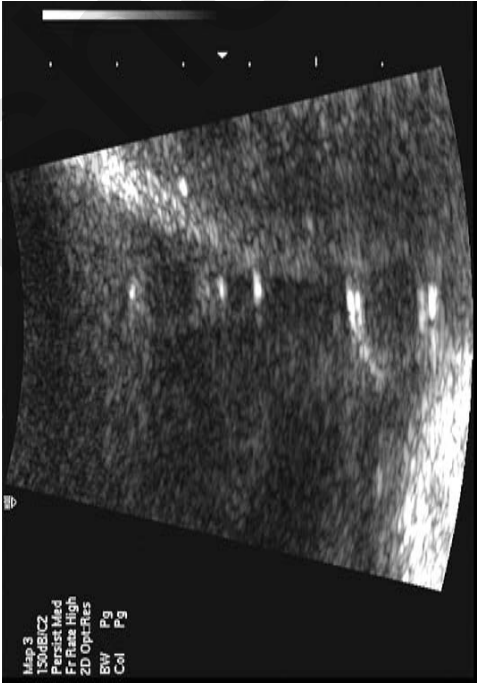


Fig. 25.1 Two-vessel cord in cross section

OLIGOHYDRAMNIOS

Oligohydramnios occurs in 0.5–1% of pregnancies. The diagnosis is usually made subjectively. It is defined as an amniotic fluid index (AFI) of less than 5 cm or a deepest single pocket measurement of 1 cm or less. Oligo-anhydramnios is caused because there is reduced production of fetal urine (e.g. placental insufficiency, renal agenesis), or because the fetus cannot urinate due to an obstruction (e.g. posterior urethral valves), or because the fluid that is produced drains away due to rupture of the membranes (ROM). Anhydramnios means that no amniotic fluid is seen. With anhydramnios there is marked fetal deformation due to fetal compression, including a flattened face, hypertelorism, low-set ears, and micrognathia (Potter syndrome).

Preterm prelabour rupture of membranes

Amniotic fluid is mainly produced by fetal urine, but before 16 weeks the placenta contributes significantly. Therefore oligohydramnios is unusual before 16 weeks, with the exception of preterm prelabour rupture of the membranes (PPROM). Typically, however, this is a diagnosis of exclusion after all other causes have been deemed unlikely.

Renal tract abnormality

The absence of fluid and the associated abnormal posturing of the fetus can make examination for fetal abnormalities difficult. However, a dilated bladder in urethral obstruction and bilateral cystic kidneys are easily seen on ultrasound.

Fetal growth restriction

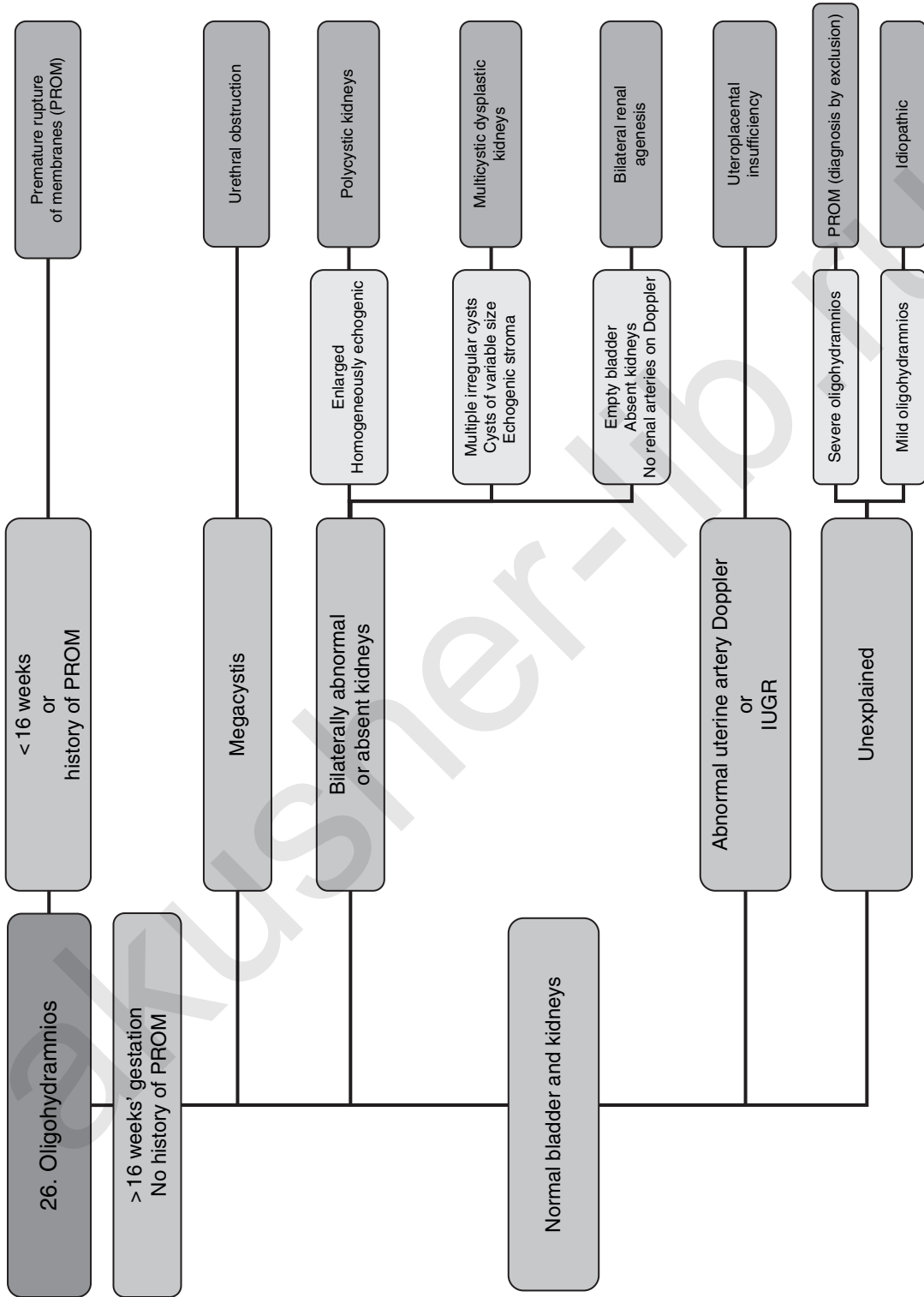
Fetal growth restriction can present with oligohydramnios. This should typically have the characteristic fetal and uterine Doppler profiles indicative of uteroplacental insufficiency.

Prognosis

The prognosis is usually poor with presentations before 24 weeks, mainly because a lack of amniotic fluid causes pulmonary hypoplasia due to compression of the chest and abdomen and limitation of movement of the diaphragm. Fetal compromise may also occur because of severe renal disease or severe fetal growth restriction. When thought to be idiopathic, the prognosis is generally good, with only a moderate increase in fetal and neonatal morbidity.

Bibliography

1. Newbould MJ, Lendon M, Barson AJ. Oligohydramnios sequence: the spectrum of renal malformations. *Br J Obstet Gynaecol* 1994; 101(7): 598–604.
2. Shipp TD, Bromley B, Pauker S, Frigoletto FD Jr, Benacerraf BR. Outcome of singleton pregnancies with severe oligohydramnios in the second and third trimesters. *Ultrasound Obstet Gynecol* 1996; 7(2): 108–13.



IUGR, intrauterine growth restriction.



Fig. 26.1 Anhydramnios

akusher-lib.ru

POLYHYDRAMNIOS

Polyhydramnios is caused by reduced fetal swallowing, or increased fetal urine production. This occurs in 0.5–1% of pregnancies. The diagnosis is usually made subjectively, but it is defined as an amniotic fluid index (AFI) of more than 24 cm or a deepest single pocket measurement of fluid of at least 8 cm. If the deepest pool is greater than 11 cm it is termed moderate, and if more than 15 cm, severe polyhydramnios.

Prognosis

Even in the absence of fetal defects the perinatal mortality rate is about two to three times that of pregnancies with normal amniotic fluid volume. With a fetal or placental malformation the perinatal mortality is as high as 60%.

Twin–twin transfusion syndrome

By far the commonest cause of polyhydramnios in monochorionic twin pregnancy is twin–twin transfusion syndrome (TTTS). This is also one of the very few causes of polyhydramnios at less than 20 weeks of gestation.

Fetal structural abnormalities

Most defects are usually gastrointestinal or in the central nervous system. The presence of multiple abnormalities, or abnormalities that do not explain the polyhydramnios, should raise the suspicion of an underlying chromosomal or genetic syndrome.

Fetal movement disorders

Absent or greatly reduced fetal movement can be suggestive of neuromuscular disease, usually with a guarded postnatal prognosis.

Placental tumours

The presence of a placental tumour, such as a chorioangioma, may cause a hyperdynamic circulation, and subsequent hydrops.

Fetal anaemia

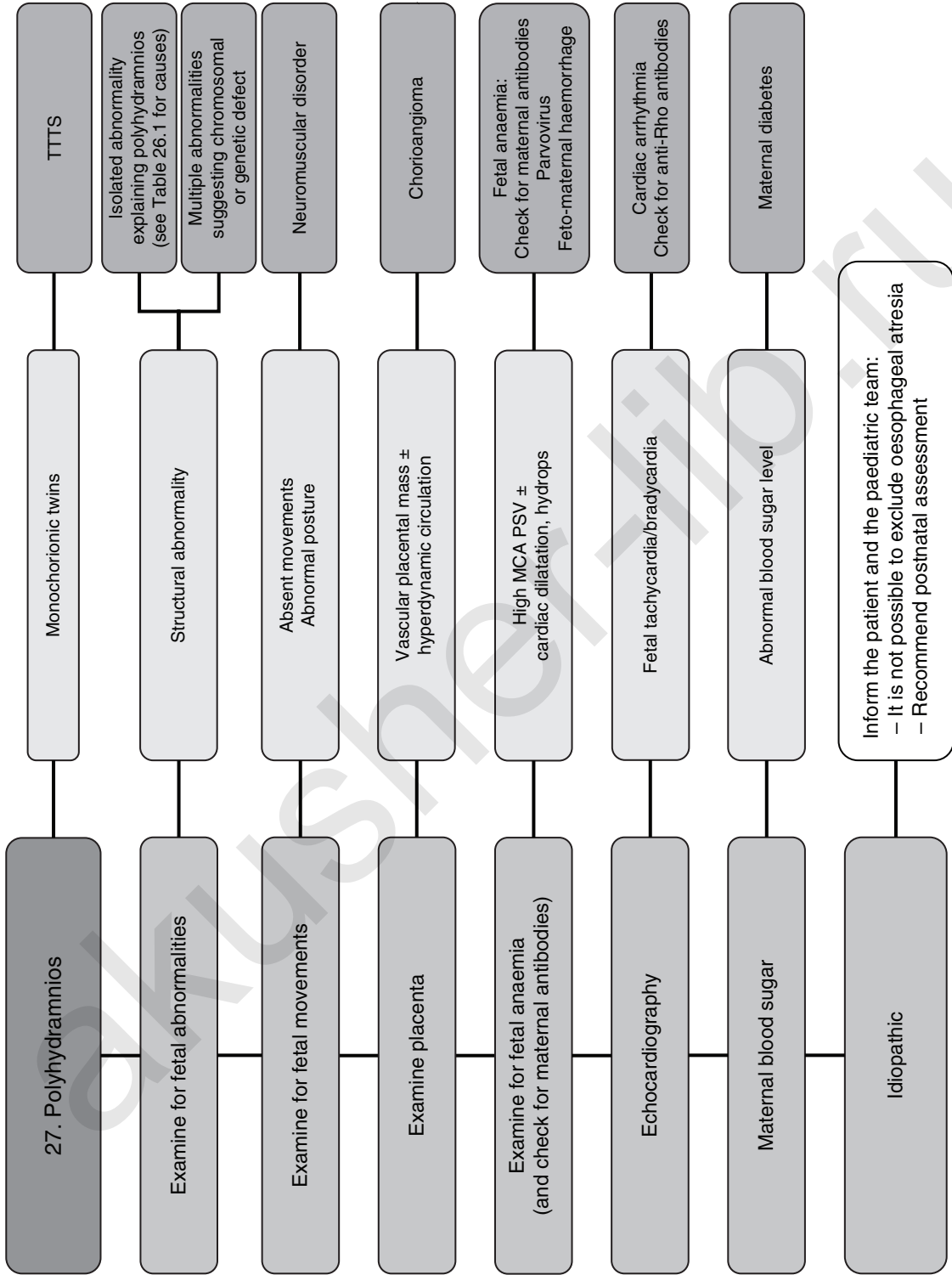
Typically, Doppler examination of the middle cerebral artery should reveal a high peak systolic velocity. Fetal oedema, ascites, or hydrops may be present if the anaemia is severe.

Arrhythmias

Fetal supraventricular tachycardia or heart block can cause polyhydramnios and, subsequently, hydrops.

Bibliography

1. Biggio JR Jr, Wenstrom KD, Dubard MB, Cliver SP. Hydramnios prediction of adverse perinatal outcome. *Obstet Gynecol* 1999; 94(5 Pt 1): 773–7.
2. Desmedt EJ, Henry OA, Beischer NA. Polyhydramnios and associated maternal and fetal complications in singleton pregnancies. *Br J Obstet Gynaecol* 1990; 97(12): 1115–22.



MCA PSV, middle cerebral artery peak systolic velocity; TTTS, twin-twin transfusion syndrome.



Fig. 27.1 Polyhydramnios

akusher-lib.ru

AMNIOTIC SHELF/BAND

Amniotic bands occur as a consequence of a disruption to the amnion, with an intact chorion. In most cases, amniotic bands occur without any associated fetal effects, although occasionally a diagnosis of amniotic band syndrome may be made. Amniotic band syndrome is believed to be caused by the entrapment of fetal parts (usually a limb or digits) in fibrous amniotic bands while in utero. When the amnion ruptures without injury to the chorion, the fetus comes in contact with free-floating sticky amniotic 'bands'. The amniotic bands can entangle various fetal parts, thereby reducing the blood supply and causing congenital abnormalities, typically amputations. Although no two cases are exactly alike, there are several features that are relatively common: syndactyly, distal ring constrictions, shortened bone growth, limb length discrepancy, distal lymphoedema, and congenital bands. Very confusingly, by the time amniotic band syndrome is suspected, the amniotic bands are no longer visible, as the fetal insult probably occurred early in the first trimester.

Bibliography

1. Lockwood C, Ghidini A, Romero R, Hobbins JC. Amniotic band syndrome: reevaluation of its pathogenesis. *Am J Obstet Gynecol* 1989; 160(5 Pt 1): 1030-3.
2. Seeds JW, Cefalo RC, Herbert WNP. Amniotic band syndrome. *Am J Obstet Gynecol* 1982; 144(3): 243-8.

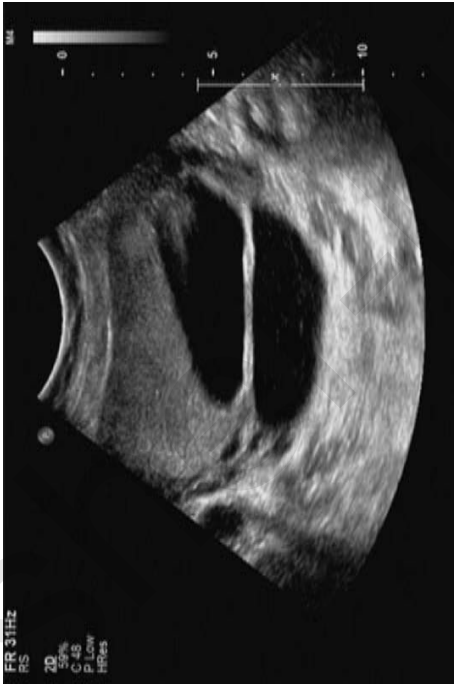


Fig. 28.1 Amniotic band

HYDROPS

Hydrops is defined as an abnormal accumulation of serous fluid in at least two fetal compartments, including ascites, pleural or pericardial effusions, and skin oedema. It is a rare finding and can be the result of cardiac failure, obstructed lymphatic flow, or decreased plasma osmotic pressure.

Monochorionic twin pregnancy

The finding of hydrops in one monochorionic twin is typical of either twin–twin transfusion or twin reversed arterial perfusion syndrome.

Hyperdynamic circulation

The finding of a high peak systolic velocity on middle cerebral artery Doppler is suggestive of hyperdynamic heart failure as the cause of hydrops. The presence of a fetal or placental tumour can cause this by creating an arterio-venous shunt within the fetal circulation. In the absence of a tumour, fetal anaemia is the most likely cause secondary to red blood cell allo-immunization, parvovirus infection, or feto-maternal haemorrhage, or due to inherited fetal anaemias.

Fetal structural abnormality

Cardiac failure as a consequence of congenital heart defects and arrhythmias is the commonest cause of hydrops in this group. The other reason for hydrops is thoracic compression leading to cardiac failure. Typically, the fetal abnormalities associated with this are cystic adenomatoid malformation and diaphragmatic hernia.

Fetal syndromes

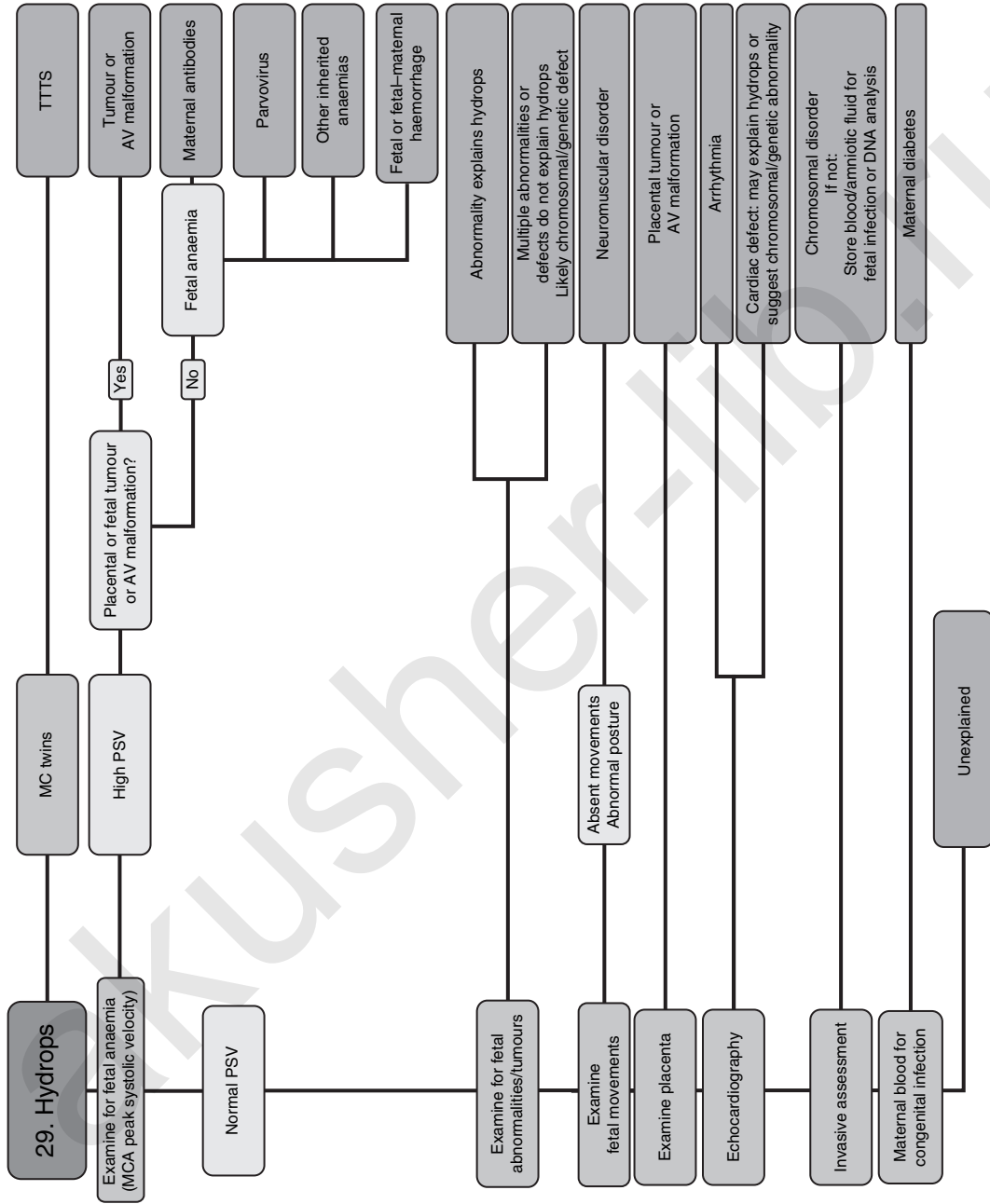
These include chromosomal (trisomy and Turner syndrome), genetic (Noonan syndrome), and metabolic disorders (glycogen storage diseases, lysosome storage diseases).

Fetal congenital infections

These are most commonly due to early pregnancy congenital infection with cytomegalovirus, toxoplasmosis, coxsackievirus, or *Listeria*.

Bibliography

1. Bukowski R, Saade GR. Hydrops fetalis. Clin Perinatol 2000; 27(4): 1007–31.
2. Sohan K, Carroll SG, De La Fuente S, Soothill P, Kyle P. Analysis of outcome in hydrops fetalis in relation to gestational age at diagnosis, cause and treatment. Acta Obstet Gynecol Scand 2001; 80(8): 726–30.



MCA, middle cerebral artery; PSV, peak systolic velocity; MC, monochorionic; AV, arterio-venous; TTTS, twin-twin transfusion syndrome.



Fig. 29.1 Severe fetal hydrops

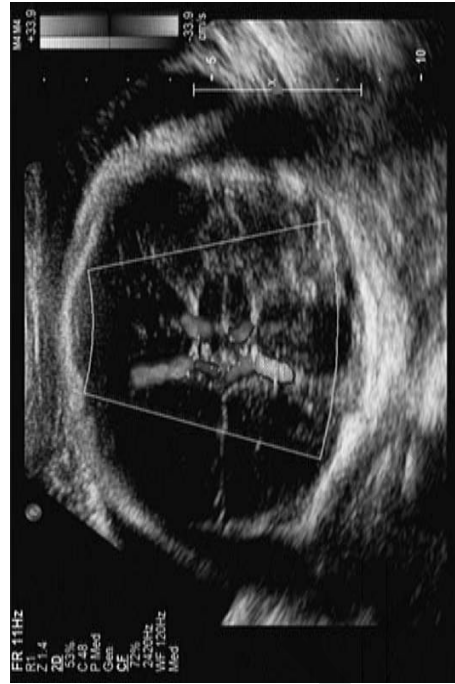


Fig. 29.2 Middle cerebral artery colour Doppler (see also colour plate)

akusher-lib.ru

SMALL FETUS

Fetal growth restriction (FGR) is defined as growth below the 5th centile for gestational age. Broadly speaking, there are four causes for this finding: incorrect dating, constitutionally small fetus, placental insufficiency, or fetal abnormality.

Incorrect dating

1. Check the pregnancy history for a previous dating scan. Earlier scans will be more reliable, particularly if done between 10 and 14 weeks. **Once the pregnancy has been dated in this way, do not change the gestational age again.**
2. If no previous scans are available, date by the last menstrual period (LMP).
3. In cases where pregnancies are dated late or there is a question regarding the gestation, a scan in 3–4 weeks should be performed to ensure that fetal growth continues on the same centile. If there is a further fall in growth, consider an alternative diagnosis.

Constitutionally small baby

1. The mother and/or father may be of small stature.
2. Previous babies have been small for gestational age.
3. Be aware of ethnic differences in birth weight.
4. A follow-up growth scan will often show a slight fall from the centile line.
5. The uterine and fetal Doppler studies are entirely normal.

Placental insufficiency

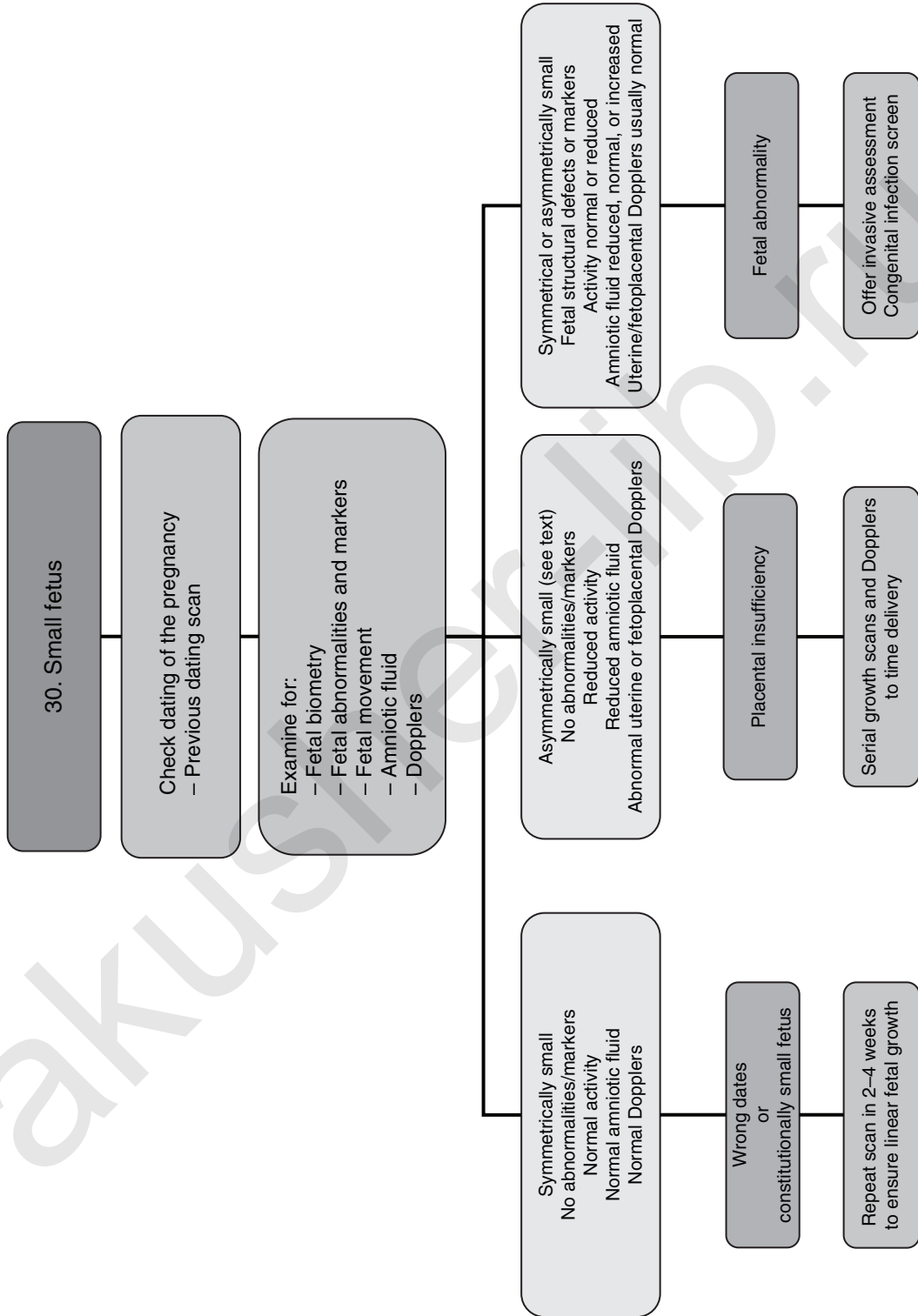
1. Previous pregnancies may have been affected by placental insufficiency, pre-eclampsia, or placental abruption.
2. FGR is asymmetrical. In general, the abdominal circumference is smaller than the head circumference. In some cases of severe early onset growth restriction, femur length may be the first index to be affected. Doppler studies are abnormal, with the usual sequence of abnormal Doppler waveforms present first in the uterine, then the umbilical, and then the middle cerebral arteries.

Fetal abnormality

1. The presence of FGR in the presence of fetal structural abnormalities, markers for chromosomal defects, or polyhydramnios makes the presence of congenital or acquired fetal abnormality likely.
2. Causes include: chromosomal abnormality, congenital fetal infection, fetal alcohol syndrome, and genetic abnormality (e.g. uniparental disomy, Silver–Russell syndrome).

Bibliography

1. Baschat AA. Pathophysiology of fetal growth restriction: implications for diagnosis and surveillance. *Obstet Gynecol Surv* 2004; 59(8): 617–27.
2. Baschat AA, Galan HL, Bhide A et al. Doppler and biophysical assessment in growth restricted fetuses: distribution of test results. *Ultrasound Obstet Gynecol* 2006; 27(1): 41–7.



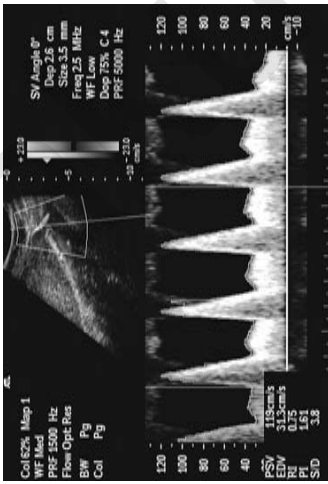


Fig. 30.1 High resistance uterine artery Doppler (see also colour plate)

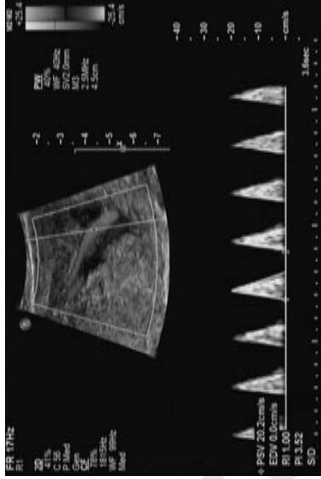


Fig. 30.2 Absent end-diastolic flow in the umbilical artery (see also colour plate)

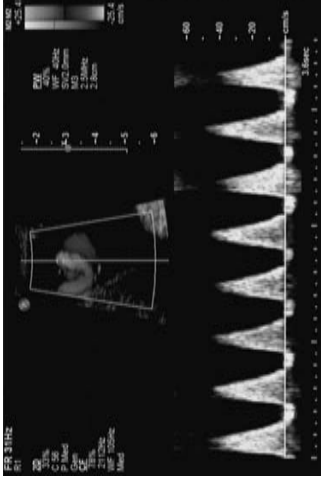


Fig. 30.3 Reversed end-diastolic flow in the umbilical artery (see also colour plate)

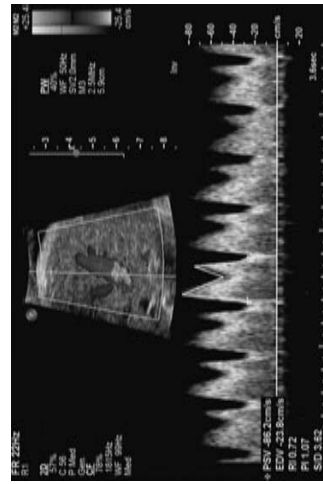


Fig. 30.4 High resistance ductus venosus Doppler (see also colour plate)

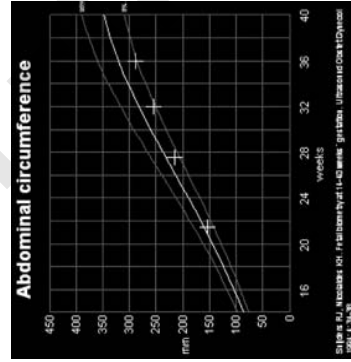


Fig. 30.5 Normally small growth velocity

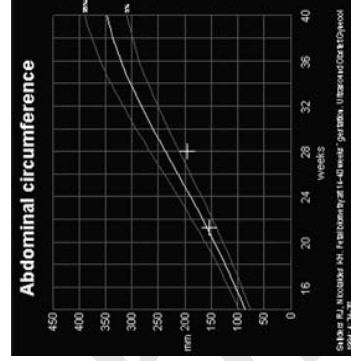


Fig. 30.6 Growth velocity in placental insufficiency

akusher-lib.ru

TWIN–TWIN TRANSFUSION SYNDROME

About 10–15% of monochorionic (MC) twin pregnancies are complicated by severe twin–twin transfusion syndrome (TTTS) as a consequence of a chronic circulatory imbalance in the vascular anastomoses that occur in virtually all MC placentae. TTTS typically presents in the mid-second trimester. The diagnosis is based on the donor presenting with oligo-anhydramnios and the recipient having polyhydramnios. The donor appears to be stuck, with restricted growth and an absent/small bladder. The recipient appears to be of average/increased weight with a big bladder. Doppler changes may accompany these findings and usually signify worsening TTTS. The donor twin may have absent/reversed end-diastolic flow in the umbilical artery. The recipient and, less commonly, the donor may show absent or reversed flow during atrial contraction in the ductus venosus.

Staging of twin–twin transfusion syndrome

The natural history of TTTS has been classified into five stages (Table 31.1). The differential diagnoses from TTTS are much rarer, and include acute inter-twin transfusion and selective fetal growth restriction.

Acute inter-twin transfusion

Acute inter-twin transfusion usually occurs as a consequence of an acute vascular imbalance in previously healthy MC twins. It presents in the late second or third trimester with acute polyhydramnios in normally grown MC twins. Amniodrainage may be required to reduce the risk of preterm labour from the polyhydramnios, and in the majority of cases the symptoms do not recur.

Selective fetal growth restriction

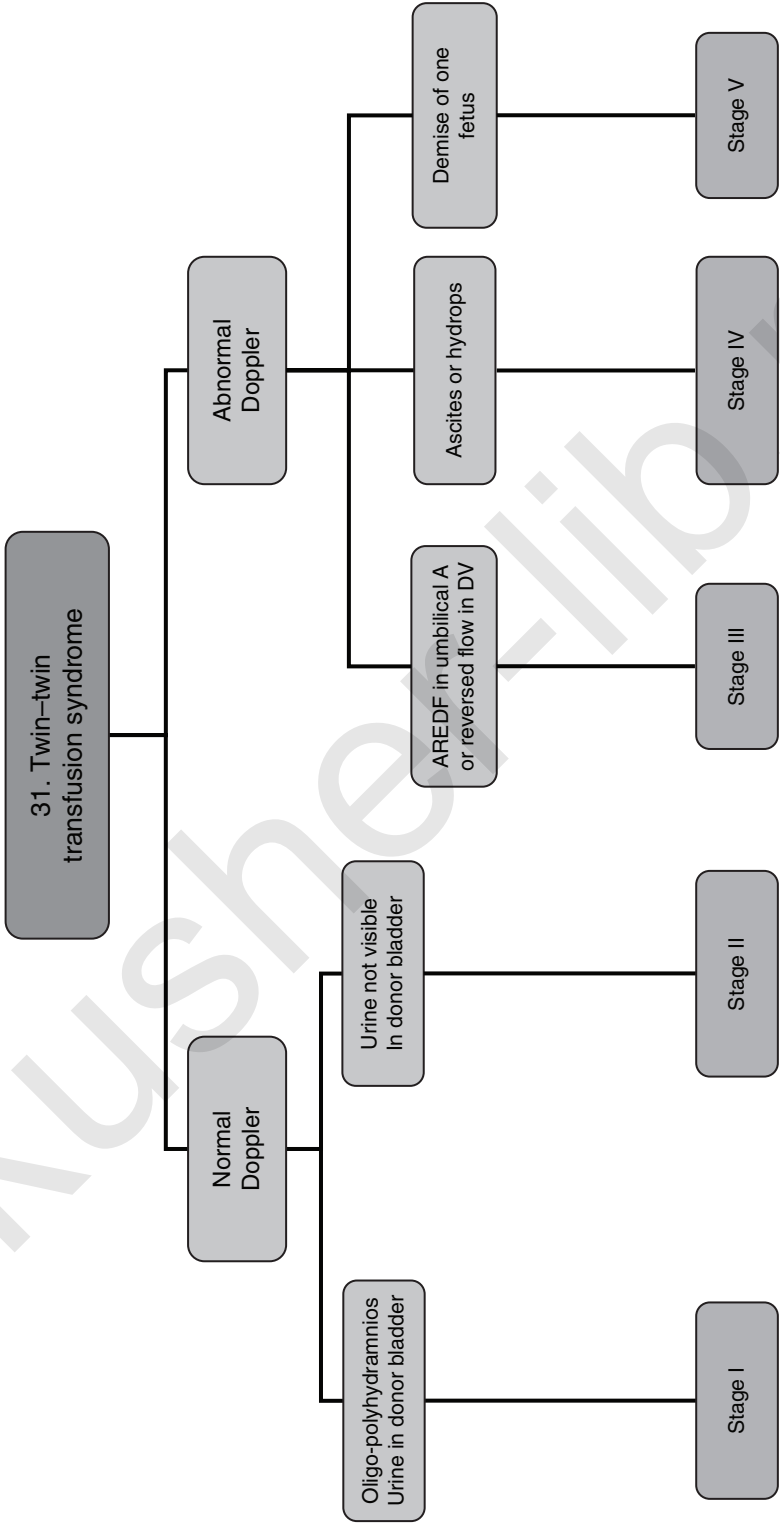
This presents in the second trimester with one growth restricted twin (as in TTTS) and one apparently healthy, normally grown twin. The majority of cases can be managed conservatively, but fetoscopic laser may sometimes be required if preterm death of the growth restricted twin seems likely.

Table 31.1 *Natural history of twin–twin transfusion syndrome*

Stage	Poly-oligo hydramnios	Bladder in donor	Abnormal Dopplers	Hydrops	Demise
I	Yes	Yes	No	No	No
II	Yes	No	No	No	No
III	Yes	No	Yes	No	No
IV	Yes	No	Yes	Yes	No
V	Yes	No	Yes	Yes	Yes

Bibliography

1. Robyr R, Quarello E, Ville Y. Management of fetofetal transfusion syndrome. *Prenat Diagn* 2005; 25(9): 786–95.
2. Senat MV, Deprest J, Boulvain M et al. Endoscopic laser surgery versus serial amnioreduction for severe twin-to-twin transfusion syndrome. *N Engl J Med* 2004; 351: 136–44.



AREDF, absent/reversed end-diastolic flow; A, artery; DV, ductus venosus.

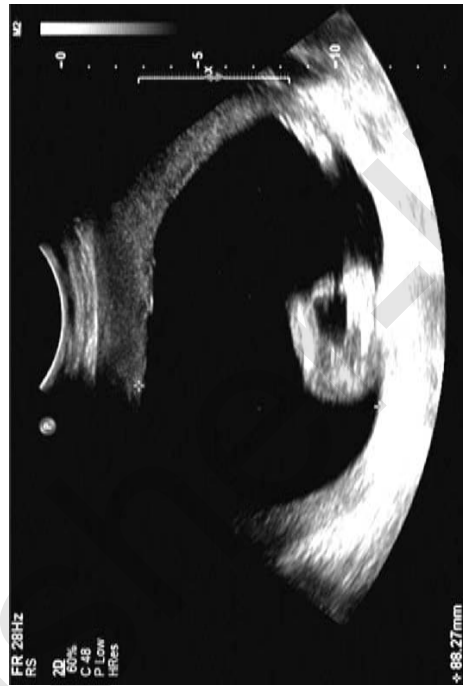


Fig. 31.1 TTTs recipient with enlarged bladder

akusher-lib.ru

INDEX

- abdominal cysts 40, 43, 44, 45
achondrogenesis 9, 10, 67, 68
achondroplasia 67, 68
agenesis
 of cerebellar vermis 5, 7
 of kidney 51, 52, 53
 bilateral 51, 52, 53, 96
 sacral 79, 80
ambiguous genitalia 39, 40
amniotic band syndrome 75, 76, 103
amniotic bands 103, 104
anaemia 27, 99, 100, 105, 106
aneuploidy
 chest fluid and 27, 28
 facial clefts and 14
 polycystic kidney and 56
 short femur length and 67
 ventriculomegaly and 1
aneurysm
 cardiac 27, 28, 36
 vein of Galen 5, 6, 7
anhydramnios 47, 48, 51, 52, 55, 64, 95, 97
anterior abdominal wall defects 39, 40, 41
aortic arch hypoplasia/interruption 36
aortic stenosis/atresia 36
arachnoid cysts 5, 6, 7
arrhythmias 99, 100, 106
arterio-venous shunting 27
arthrogryposis multiplex congenita 71, 72
atrio-ventricular malformations 35, 36
atrio-ventricular septal defect 35, 36, 37
atrio-ventricular valve offset, loss of 35, 36
banana shaped cerebellum 9, 10, 11, 79, 80, 81
Beckwith-Wiedemann syndrome 39, 40, 55, 56
bilateral renal agenesis 51, 52, 53, 96
bladder 63, 64, 65
 absent 51, 52
 exstrophy 39, 40
 megacystis 63, 64, 65
 outlet obstruction 43, 44, 63, 64, 65
blood ingestion 47, 48
body stalk anomaly 39, 40, 79
bone modelling 67, 68
bowel
 duplication cysts 43, 44
 hyperechoic 47, 48, 49
 obstruction 43, 44, 45, 48
brachycephaly 11
brain hemorrhage, ventriculomegaly and 1
bronchial obstruction 23, 24
bronchogenic cysts 24
campomelic dysplasia 67, 68
cardiac chamber asymmetry 35
cardiac defects 87, 106
cardiomegaly 35
caudal regression 71, 79, 80, 81
cervical teratoma 83
chest fluid 27, 28, 29, 32
chest tumours 23, 24, 25, 32
choledochal cyst 43, 44
chondrodysplasia punctata 67, 68
chorioangioma 27, 91, 92, 99, 100
choroid plexus cysts 5, 6, 7

- chromosomal abnormalities 87
see also aneuploidy; *specific trisomies and conditions*
- ciliary dyskinesia (Kartagener syndrome) 31
- cleft alveolus 13, 15
- cleft lip 13, 15
- cleft palate 13, 15
- cloacal exstrophy 39, 40
- clover-leaf shaped skull 9, 10, 11
- co-arcuation of the aorta 36
- congenital chylothorax 28
- congenital cystic adenomatoid malformation 23, 24
- congenital diaphragmatic hernia 23, 24, 32, 33
- congenital high airway obstruction syndrome (CHAOS) 23, 24, 32
- congenital infections 105
 viral 1, 27, 47
- craniosynostoses 13, 20
- cryptophthalmos 52
- cystic fibrosis 43, 47
- cystic hygroma 83, 84, 85
- cystocele 65
- cysts
 abdominal 40, 43, 44, 45
 bronchogenic 24
 facial 85
 intracranial 5, 6, 7
 placental 91
 umbilical cord 41
see also kidney
- Dandy–Walker cysts 5, 6
- dextrocardia 31, 32, 33
- dextroposition 31, 32, 33
- diaphragmatic hernia 23, 24, 32, 33
- DiGeorge syndrome 19
- double bubble appearance 43, 44, 45
- Down syndrome, nasal bone absence 17
- duodenal atresia 44
- dural sinus malformations 5
- dwarfism 67
- Ebstein anomaly 36
- ectopia cordis 40
- ectopic kidney 51, 52, 53
- ectrodactyly 75, 76, 77
- Edward syndrome 18
- Edward syndrome *see* trisomy
- Ellis–van Creveld syndrome 67, 68
- encephalocele 9, 10, 55, 56, 84, 85
- epignathus 83, 84
- ex-utero intrapartum treatment (EXIT) 83
- exomphalos 39, 40, 41, 55, 56
- facial clefts 13, 14, 15
- facial cyst 85
- femur, short length 67, 68, 69
- fetal abnormalities 87, 99, 105
- fetal growth restriction 67, 68, 91, 95, 96, 109, 110, 111
 constitutionally small baby 109, 110
 fetal abnormality 109, 110
 incorrect dating 109, 110
 placental insufficiency 109, 110, 111
 selective 113
- fetal movement disorders 87, 99
- floating flakes 47, 48
- four-chamber view abnormalities 35, 36, 37
- Fraser syndrome 52
- gall bladder 45
- gastroschisis 39, 40, 41
- genetic syndromes 87
see also specific syndromes
- glycogen storage diseases 105
- goitre 83, 84
- Goldenhar syndrome 19, 20
- haemangioma 83, 84
- hand abnormalities 75, 76, 77
- head masses 83, 84, 85
- heart block 99
- hemifacial microsomia 19
- hemivertebrae 79, 80, 81
- hepatic cyst 43, 44
- holoprosencephaly 13, 14
- hydatidiform mole 91
- hydrometrocolpos 43, 44
- hydronephrosis 43, 44, 56, 59, 60–1, 62
- hydrops 27, 28, 29, 105, 106, 107
- hyperdynamic circulation 105
- hyperechoic foci 47, 48
- hypophosphatasia 10, 67, 68
- inter-hemispheric cysts (pseudocysts) 5, 6, 7
- intestinal duplication cysts 43, 44
- intestinal obstruction 43, 44, 45, 48
see also bowel
- intracranial cysts 5, 6, 7
- intrauterine growth restriction (IUGR) *see* fetal growth restriction
- jelly-like placenta 91
- Jeune dystrophy 67, 68
- joint abnormalities 71, 72, 73

- Kartagener syndrome (ciliary dyskinesia) 31
- kidney
 agenesis 51, 52, 53
 bilateral 51, 52, 53, 96
 cystic 55, 56, 57
 multicystic dysplastic 55, 56, 96
 polycystic 47, 48, 55, 56, 57, 96
 solitary cyst 55, 56, 57
 duplex 57, 60
 ectopic 51, 52, 53
 fluid filled 59, 60–1, 62
 hyperechoic 47, 48, 49
- kyphoscoliosis 40, 79, 80, 81
- kyphosis 79, 80
- left isomerism 32
- lemon shaped skull 9, 10, 11, 79, 80, 81
- liver
 cyst 43, 44
 hyperechoic 48, 49
- lobster-claw deformity 75
- lysosome storage diseases 105
- macrosomia 40, 55, 56
- Meckel–Gruber syndrome 9, 55, 56, 75
- meconium ileus 43, 44, 47, 48
- mega-ureter 43
- megacystis 63, 64, 65, 96
- meningocele 43, 44
 cervical 84
- meningomyelocele 81
- mesenteric cysts 43, 44
- microcephaly 10, 67, 68, 79
- micrognathia 19, 20, 21
- mitral atresia 36
- molar pregnancy 91
- multicystic kidney *see* kidney
- multiple pterygium syndrome 71, 72
- nasal bone hypoplasia 17, 18
- neck masses 83, 84, 85
- Noonan syndrome 105
- nuchal translucency (NT) 87, 88, 89
- obstructive uropathy 43, 44, 63, 64, 65, 96
- oligohydramnios 55, 64, 95, 96
 prognosis 95
- osteogenesis imperfecta (OI) 67, 68
- ovarian cyst 43, 44, 45
- overlapping fingers 75, 76, 77
- pelvi-ureteric obstruction 61
- Pena–Shokeir syndrome 71, 72, 75, 76
- pentalogy of Cantrell 39, 40
- pericardial effusion 27, 28, 29
- Pierre Robin syndrome 19
- placenta accreta 91
- placental abnormalities 91, 92, 99
- placental grading 91
- placental insufficiency 109, 110, 111
- placental lakes 91, 92
- pleural effusion 27, 28, 29, 32
- polycystic kidney *see* kidney
- polydactyly 55, 56, 67, 68, 75, 76
 short-ribbed 67, 68
- polyhydramnios 83, 84, 99, 100, 101
 prognosis 99
- porencephalic cyst 6
- posterior fossa cysts 5, 6, 7
- pre-maxillary protrusion 13, 15
- preterm prelabour rupture of membranes (PPROM) 95, 96
- pseudocysts 5, 6, 7
- pulmonary sequestration 23, 24, 25, 32
- pulmonary stenosis/atresia 36
- pulmonary venous drainage anomalies 35, 36
- pyelectasia 59
- renal agenesis 51, 52, 53
 bilateral 51, 52, 53, 96
- renal artery absence 51, 52, 53
- renal fossa, empty 51, 52, 53
- renal tract abnormality 95
- right isomerism 32
- right ventricular outflow tract obstruction 36
- sacral agenesis 79, 80
- sacrococcygeal teratoma 79, 80
- scimitar syndrome 31, 32
- scoliosis 79, 80
- sirenomelia 79
- situs abnormalities 31, 32
 situs inversus 31, 32
- skeletal dysplasia 9, 10, 67, 71, 72, 75, 79
- skull shape abnormalities 9, 10, 11
- Smith–Lemli–Opitz syndrome 19, 20, 75
- spina bifida 9, 10, 79, 80
- spinal abnormalities 79, 80, 81
 angulation 79, 80
- split hand deformity 75
- spondyloepiphyseal dysplasia congenita (SEDC) 67, 68
- strawberry shaped skull 9, 10, 11
- supraventricular tachycardia 99
- syndactyly 76

- talipes 71, 72, 73, 80
teratoma 23, 24, 84
 cervical 83
 epignathus 83, 84
 sacrocoxygeal 79, 80
terminal transverse limb defect 75, 76
thanatophoric dysplasia 67, 68
thoracic dysplasia 67, 69
Treacher Collins syndrome 19
tricuspid atresia 36
tricuspid regurgitation 36
tricuspid valve displacement 36
trisomy 13 13, 19, 20, 40, 55, 63, 64
trisomy 18 9, 10, 19, 20, 40, 55, 63, 64, 75
trisomy 21 17, 87
Turner syndrome 105
twin reversed arterial perfusion syndrome 105
twin-twin transfusion syndrome (TTTS) 99, 100,
 105, 106, 113, 114, 115
 natural history 113
 selective fetal growth restriction 113
 staging 113, 114
umbilical artery, single 93, 94
 management 93
umbilical cord cyst 41
urethral obstruction 63, 96
 see also obstructive uropathy
uteroplacental insufficiency 48, 96
VACTERL 51, 52, 55, 56, 79
vascular malformations 5, 6
VATER 55, 79
vein of Galen malformation 5, 6, 7
ventricular septal defect (VSD) 36, 37
ventriculomegaly 1, 2, 3, 10, 79, 80
vesico-ureteric obstruction 43, 44, 59, 60, 61
vesico-ureteric reflux 43, 44, 59, 60, 61
viral infections, congenital 1, 27, 47
volvulus 45
wrist contracture 73

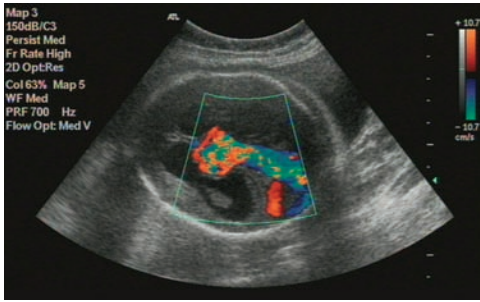


Fig. 2.6 Vein of Galen malformation

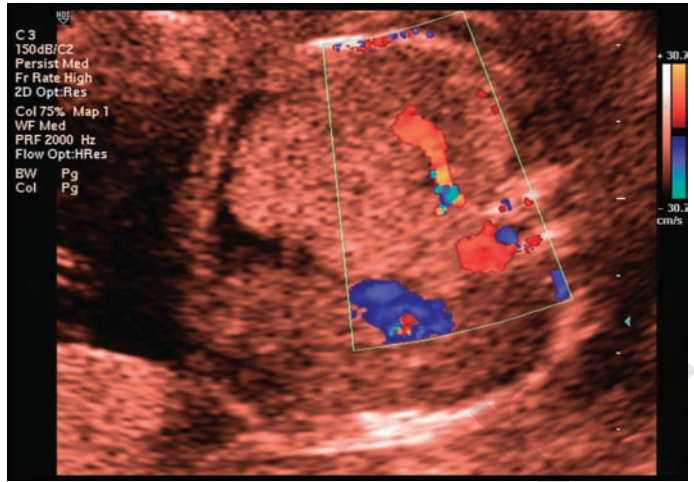


Fig. 7.3 Pulmonary sequestration

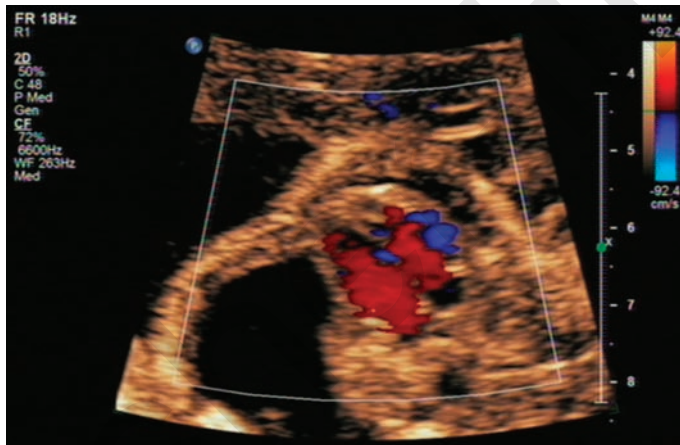


Fig. 8.2 Moderate pleural effusion & mediastinal shift

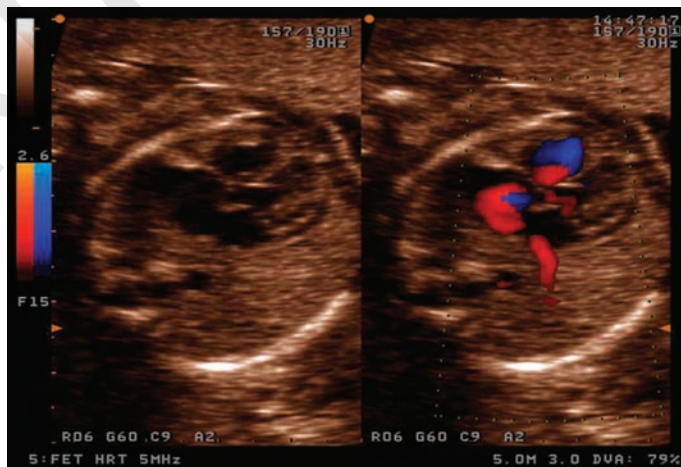


Fig. 9.2 Dextrocardia

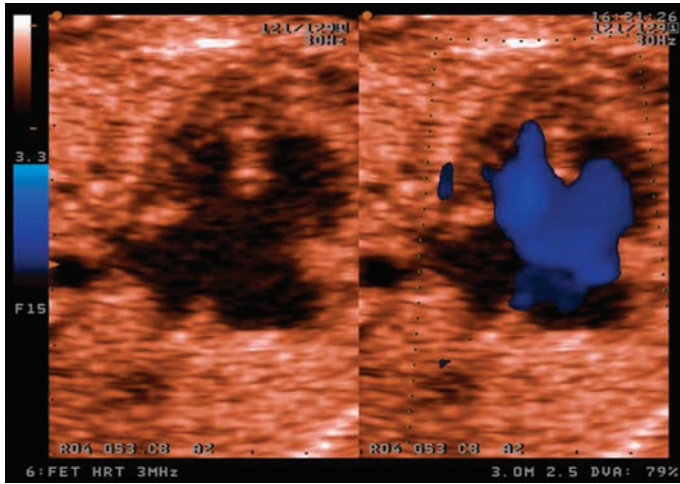


Fig. 10.4 Atrio-ventriculoseptal defect

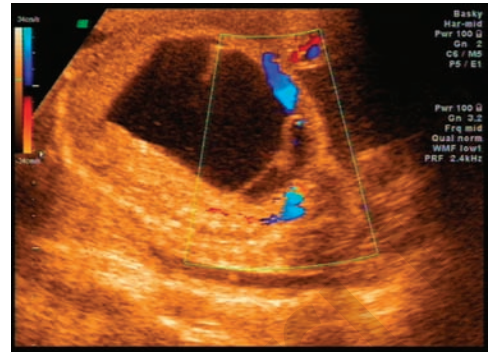


Fig. 12.1 Fetal ovarian cyst

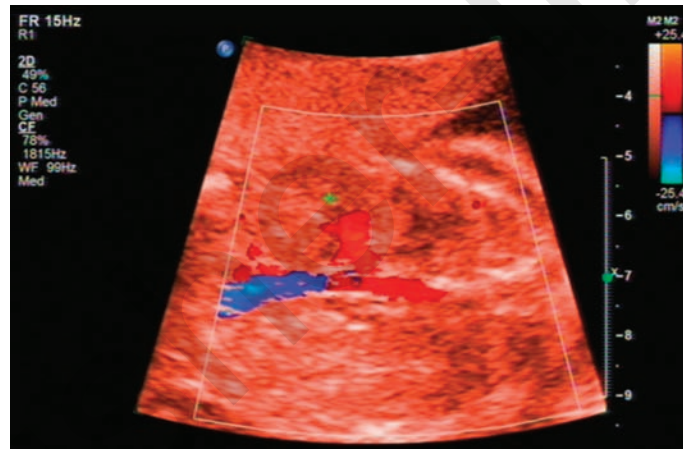


Fig. 14.2 Single renal artery in unilateral renal agenesis

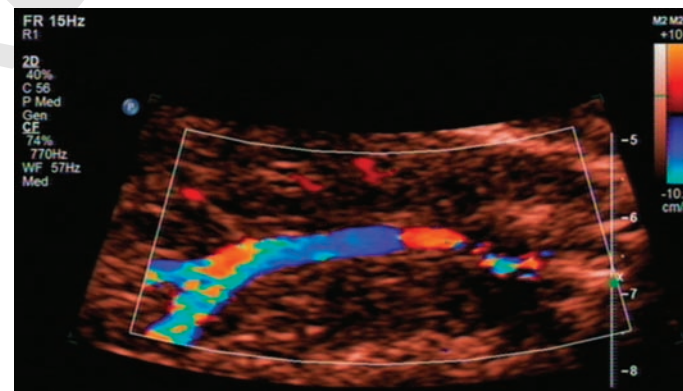


Fig. 14.3 Absent renal arteries in bilateral renal agenesis

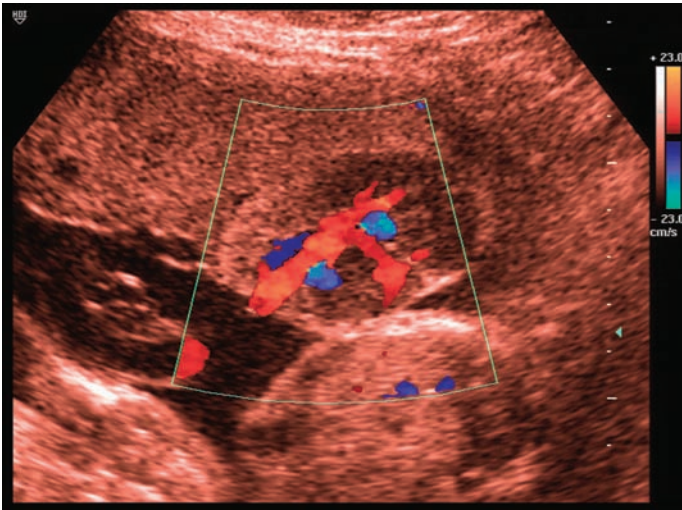
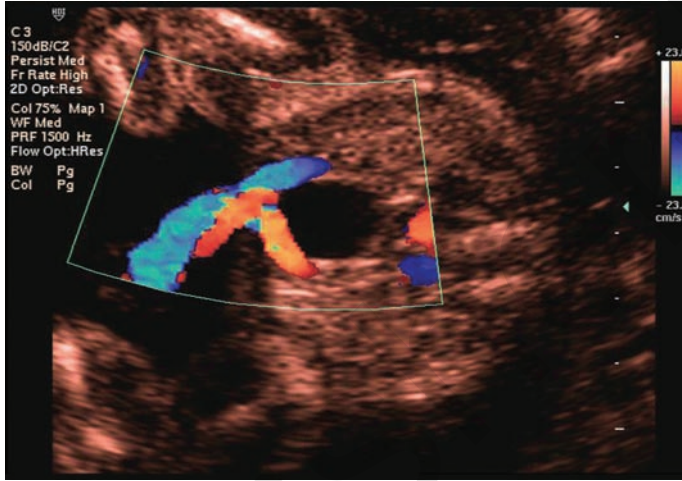
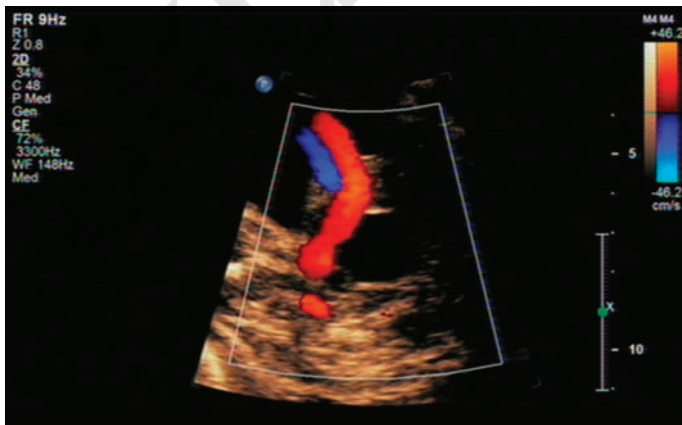


Fig. 24.2 Placental chorioangioma



(a)



(b)

Fig. 25.2 (a) Two umbilical arteries on colour Doppler (b) Single umbilical artery on colour Doppler

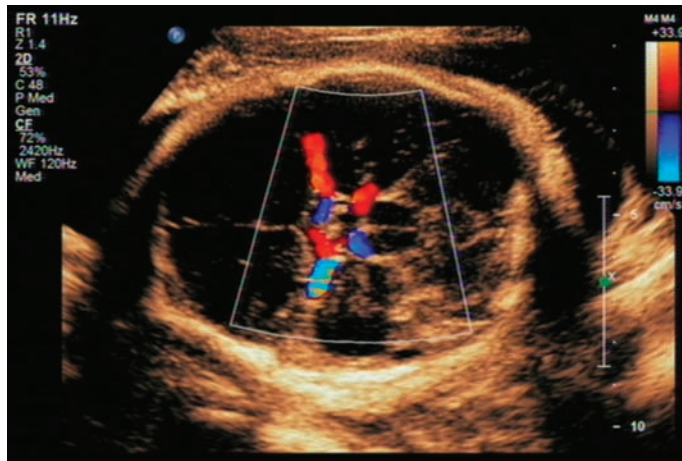


Fig. 29.2 Middle cerebral artery colour Doppler

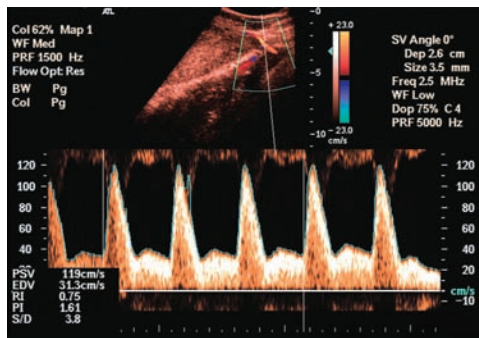


Fig. 30.1 High resistance uterine artery Doppler

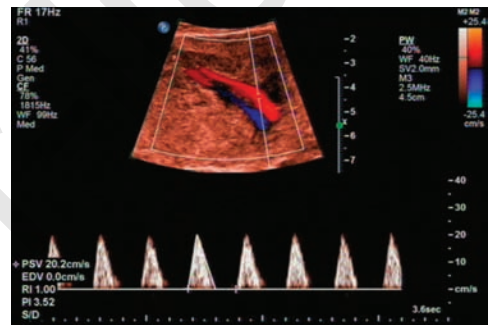


Fig. 30.2 Absent end-diastolic flow in the umbilical artery

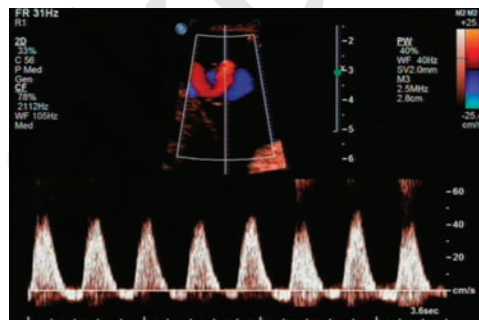


Fig. 30.3 Reversed end-diastolic flow in the umbilical artery

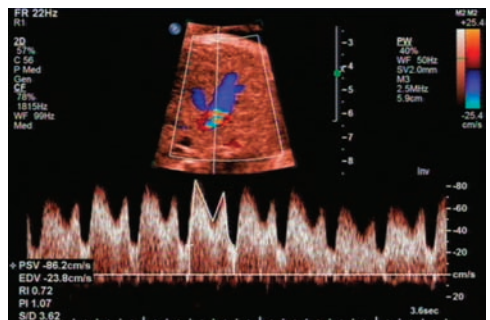
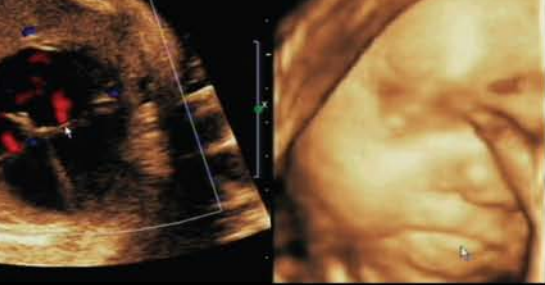


Fig. 30.4 High resistance ductus venosus Doppler



PROBLEM-BASED Obstetric Ultrasound

This handbook on problem-based obstetric ultrasound is an important and invaluable text for those who scan for fetal anomalies: it takes a pragmatic approach by first defining an anomaly, then giving an algorithm indicating other investigations and illustrating diagnoses. The most likely and the most significant abnormalities have been covered, making this text a very useful adjunct and reference for the busy clinician.

With over 100 illustrations, including 16 in colour.

Basky Thilaganathan MD MRCOG is Consultant and Director, Fetal Medicine Unit, St George's Hospital Medical School, London, UK

Shanthi Sairam MD MRCOG is Senior Clinical Fellow, Fetal Medicine Unit, St George's Hospital Medical School, London, UK

Aris T Papageorghiou MRCOG is Consultant in Maternal-Fetal Medicine, Fetal Medicine Unit, St George's Hospital Medical School, London, UK

Amar Bhide MD MRCOG is Consultant in Maternal-Fetal Medicine, Fetal Medicine Unit, St George's Hospital Medical School, London, UK

With a Foreword from Professor Sabaratnam Arulkumaran

informa
healthcare
www.informahealthcare.com



**EXPOSURE CRITERIA FOR
MEDICAL DIAGNOSTIC
ULTRASOUND: II. CRITERIA
BASED ON ALL KNOWN
MECHANISMS**



Exposure Criteria for Medical Diagnostic Ultrasound: II. Criteria Based on all Known Mechanisms

**Recommendations of the
NATIONAL COUNCIL ON RADIATION
PROTECTION AND MEASUREMENTS**

Issued December 31, 2002

**National Council on Radiation Protection and Measurements
7910 Woodmont Avenue, Suite 400 / Bethesda, Maryland 20814**

LEGAL NOTICE

This Report was prepared by the National Council on Radiation Protection and Measurements (NCRP). The Council strives to provide accurate, complete and useful information in its documents. However, neither the NCRP, the members of NCRP, other persons contributing to or assisting in the preparation of this Report, nor any person acting on the behalf of any of these parties: (a) makes any warranty or representation, express or implied, with respect to the accuracy, completeness or usefulness of the information contained in this Report, or that the use of any information, method or process disclosed in this Report may not infringe on privately owned rights; or (b) assumes any liability with respect to the use of, or for damages resulting from the use of any information, method or process disclosed in this Report, *under the Civil Rights Act of 1964, Section 701 et seq. as amended 42 U.S.C. Section 2000e et seq. (Title VII) or any other statutory or common law theory governing liability.*

Library of Congress Cataloging-in-Publication Data

National Council on Radiation Protection and Measurements. Scientific Committee 66 on Biological Effects of Ultrasound.

Exposure criteria for medical diagnostic ultrasound II, Criteria based on all known mechanisms / National Council on Radiation Protection and Measurements.

p. ; cm. — (NCRP report ; no. 140)

“Prepared by Scientific Committee 66”—Pref.

“December 2002.”

Includes bibliographical references and index.

ISBN 0-929600-73-8

1. Diagnosis, Ultrasonic—Safety measures. 2. Ultrasonics in medicine—Toxicology. I. Title. II. Series

[DNLM: 1. Ultrasonography—adverse effects. 2. Equipment Safety—standards. 3. Hyperthermia, Induced. 4. Ultrasonic Therapy—adverse effects. 5. Ultrasonics. 6. Ultrasonography—instrumentation.

WB 208 N277e 2002]

RC78.7.U4 N374 2002

616.07'543'0289—dc21

2002071873

Copyright © National Council on Radiation
Protection and Measurements 2002

All rights reserved. This publication is protected by copyright. No part of this publication may be reproduced in any form or by any means, including photocopying, or utilized by any information storage and retrieval system without written permission from the copyright owner, except for brief quotation in critical articles or reviews.

[For detailed information on the availability of NCRP publications see page 556.]

Preface

This Report is the third in a series that includes NCRP Report No. 74, *Biological Effects of Ultrasound: Mechanisms and Clinical Implications* and NCRP Report No. 113, *Exposure Criteria for Medical Diagnostic Ultrasound: I. Criteria Based on Thermal Mechanisms*. These three reports were prepared by Scientific Committee 66 under the chairmanship of Wesley L. Nyborg. Dr. Nyborg and the Committee responded admirably to its mandate to address the topic “Biological Effects of Ultrasound and Exposure Criteria.”

As has been pointed out in the earlier reports, the use of diagnostic ultrasound in medicine has an enviable record for safety. However, new applications, new procedures, and new kinds of equipment are continually being introduced, higher output levels have become available for some applications, and the extent of usage continues to increase. Hence, it is important that users be informed as well as possible for judging conditions under which the benefit/risk ratio is or is not favorable.

It is the purpose of this Report, and its two predecessors, to present background for a scientifically based approach to safety assessment for diagnostic ultrasound. These three reports are intended to help the medical community take advantage of new developments in clinical practice, while maintaining its safety record.

In preparing the present Report, Scientific Committee 66 benefitted greatly from comments received through the NCRP processes of critical and Council review. In addition, many helpful suggestions were received from J.S. Abramowicz, G.R. Harris, T.A. Siddiqi, and M.E. Stratmeyer, all of whom are members of the American Institute of Ultrasound in Medicine, a Collaborating Organization of the NCRP. The NCRP is also grateful for the assistance given to Scientific Committee 66 by S.H.P. Bly, National Research Council of Canada, and the detailed and cogent comments received from F. Duck, Chairman of the European Committee for Medical Ultrasound Safety.

This publication was made possible, in part, by Grant Number R24 CA74296-05 from the National Cancer Institute (NCI) and its contents are the sole responsibility of the NCRP and do not necessarily represent the official views of the NCI, National Institutes of Health.

Serving on Scientific Committee 66 during the preparation of this Report were:

Wesley L. Nyborg, *Chairman*
University of Vermont
Burlington, Vermont

Members

Paul L. Carson
University of Michigan Medical
Center
Ann Arbor, Michigan

Edwin L. Carstensen
University of Rochester
Rochester, New York

Floyd Dunn
University of Illinois
Urbana, Illinois

Douglas L. Miller
University of Michigan Medical
Center
Ann Arbor, Michigan

Morton W. Miller
University of Rochester
Medical Center
Rochester, New York

Horace E. Thompson
University of Colorado
Denver, Colorado

Marvin C. Ziskin
Temple University School of
Medicine
Philadelphia, Pennsylvania

Consultants

Robert E. Apfel*
Yale University
New Haven, Connecticut

Charles C. Church
University of Mississippi
Oxford, Mississippi

Lawrence A. Crum
University of Washington
Seattle, Washington

NCRP Secretariat

Constantine J. Maletskos, *Consultant* (1999–2002)

Eric E. Kearsley, *Staff Scientist* (1998–1999)

James A. Spahn, Jr., *Senior Staff Scientist* (1993–1998)

Cindy L. O'Brien, *Managing Editor*

The Council wishes to express its appreciation to the Committee members for the time and effort devoted to the preparation of this Report.

Thomas S. Tenforde
President

*deceased

Contents

Preface	iii
1. Executive Summary	1
2. Introduction	5
3. Nonthermal Mechanisms for Bioeffects in the Absence of Cavitation	16
3.1 Introduction	16
3.2 Acoustic Radiation Force and Radiation Pressure	16
3.2.1 Application to Measurements of Acoustic Power	16
3.2.2 Auditory Response to Pulsed Ultrasound	17
3.2.2.1 Electrical Response in the Cat Auditory System	17
3.2.2.2 Human Sensing of Modulated Ultrasound Applied to the Middle Ear	18
3.2.2.3 Possibility of Hearing Pulsed Ultrasound by Bone Conduction	20
3.2.2.4 Audible Sound Produced <i>In Utero</i> by Ultrasound Scanning	21
3.2.2.5 Auditory Phenomena During Insonation of the Basilar Artery	21
3.2.3 Reversible Modification of Membrane Potential by Ultrasound Bursts	22
3.2.4 Tactile Perception of Pulsed Ultrasound	23
3.2.5 Acoustic Radiation Force Applied to the Eye	24
3.2.6 Effects of Acoustic Radiation Forces on the Heart	26
3.2.7 Acoustic Radiation Forces and Torques on Small Particles	26
3.3 Acoustic Streaming and Microstreaming	31
3.3.1 Theory	31
3.3.2 Acoustic Streaming Produced by Diagnostic Ultrasound	33
3.3.3 Heat Transport by Acoustic Streaming	34
3.3.4 Cellular Inactivation by Heat and Shear	34

3.3.5	Enhanced Agglutination and Aggregation by Acoustic Streaming	36
3.3.6	Contraction of Myocardial Cells	37
3.3.7	Theory: Small-Scale Acoustic Streaming (Microstreaming)	37
3.3.8	Experiments with Acoustic Microstreaming in Cells and in Cell Suspensions	38
3.3.9	<i>In Vivo</i> Experiments with Acoustic Microstreaming	40
3.4	Unidentified Nonthermal Mechanisms	42
3.4.1	Introduction	42
3.4.2	Modification of Electrical Potentials and Currents	42
3.4.3	Effects on Cardiac Performance	44
3.4.4	Stimulation of Bone Repair	44
3.4.5	Fetal Hemorrhage Caused by Lithotripsy	47
3.4.6	Effects of Lithotripsy Under Noncavitating Conditions	48
3.5	Summary	48
4.	Noninertial Cavitation; Gas-Body Activation	50
4.1	Noninertial Cavitation Involving Free Bodies	50
4.1.1	Introduction	50
4.1.2	Radial Pulsation of a Spherical Gas Bubble	52
4.1.3	The Damping Constant for a Spherical Bubble	56
4.1.4	Bubble Stability, Diffusion and Rectified Diffusion	60
4.1.5	Scattering, Harmonics and Bubble Detection	62
4.1.6	Surface Waves	64
4.2	Activation of Stabilized Gas Bodies	65
4.2.1	Gas-Body Structures and Stability	66
4.2.2	Bubbles Stabilized in Viscoelastic Media	68
4.2.3	Gas Trapped in Pits or Pores	71
4.2.4	Gas-Filled Channels	76
4.2.5	Gas Bodies in Mammals	77
4.3	Contrast Agents for Diagnostic Ultrasound	78
4.3.1	Engineering of Stabilized Gas Bodies	78
4.3.2	Physics of Contrast-Agent Excitation	81
4.3.3	Stability and Nucleation of Inertial Cavitation	84
4.3.4	Exploitation for Medical Purposes	88
4.4	Physical Consequences of the Vibration of Bubbles or of Stabilized Gas Bodies	92

4.4.1	Acoustic Power Radiated and Heat Generated by a Vibrating Bubble	93
4.4.2	Acoustic Radiation Force on a Gas Bubble, Bubble Motion, and Associated Hydrodynamic Shear	95
4.4.3	Acoustic Radiation Force on a Particle Near a Free Bubble or Stabilized Gas Body	99
4.4.4	Acoustic Microstreaming Near a Vibrating Free Bubble	100
4.4.5	Acoustic Microstreaming Near a Stabilized Gas Body	104
4.5	Summary	105
5.	Nonlinear Bubble Response; Inertial Cavitation	107
5.1	Introduction	107
5.2	Cavitation Theory; General	109
5.3	Theory: Stable Noninertial Cavitation with Spherical Symmetry	113
5.4	Theory: Inertial Cavitation with Spherical Symmetry	116
5.5	Theory: Cavitation Produced by Very Short Pulses of Ultrasound	120
5.6	Indeterminate Motion and Chaos	125
5.7	Surface Disturbances and Jet Formation	127
5.8	Experimental Studies of Repetitive Inertial Cavitation	129
5.9	Sonoluminescence	131
5.10	Sonochemistry	135
5.11	Acoustical Parameters as Predictors of Inertial Cavitation	138
5.12	Summary	142
6.	Bioeffects of Noninertial Cavitation Involving Free and Stabilized Gas Bodies in Non-Mammalian Systems	146
6.1	Introduction	146
6.2	Studies with Cell Suspensions	147
6.2.1	Gas-Filled Micropores	147
6.2.2	Ultrasound Contrast Agents	150
6.3	Tissues with Internal Gas Bodies	159
6.3.1	Plants	159
6.3.2	Insects	161
6.4	Biophysical Analysis of Effects	165
6.4.1	Shear-Stress Hypothesis	165
6.4.2	Applications of the Shear-Stress Hypothesis	167
6.4.3	Other Mechanisms	169
6.5	Summary	169

7. Bioeffects of Inertial Cavitation <i>In Vitro</i>	171
7.1 Introduction	171
7.1.1 Advantages and Disadvantages of Studies Using Cells <i>In Vitro</i>	171
7.1.2 Exposure Systems	173
7.1.3 Biological Effects	176
7.1.4 Mechanisms of Action of Ultrasound <i>In Vitro</i>	177
7.2 Cell Lysis	179
7.2.1 Influence of Various Aspects of Exposure Conditions	179
7.2.1.1 Exposure Parameters	179
7.2.1.2 Rotation of Exposure Tube and Attenuation of Ultrasound by Bubbles ..	180
7.2.1.3 Mechanical Stirring	183
7.2.1.4 Standing Waves	183
7.2.1.5 Bubble Recycling	184
7.2.1.6 Alternating the Ultrasound Propagation Direction	186
7.2.2 Mechanisms of Lysis	187
7.2.2.1 Near-Boundary Streaming	187
7.2.2.2 Shear Near Moving Bubbles and Cell- Bubble Collisions	188
7.2.2.3 Bubble Implosion and Jets	189
7.2.2.4 Free Radicals and Other Sonochemicals	190
7.2.3 Influence of Various Aspects of Cells and Media	192
7.2.3.1 Nucleation	192
7.2.3.2 Cell Concentration	196
7.2.3.3 Ultrasound Contrast Agents	198
7.2.3.4 Viscosity of the Medium	199
7.2.3.5 Multicellularity	200
7.2.3.6 Gas Content of the Medium	200
7.2.3.7 Temperature	200
7.2.3.8 Superposed Ionizing Radiation or Chemotherapeutic Agents	201
7.3 Effects on Viable Cells	202
7.3.1 Structure and Function	202
7.3.1.1 Cell Morphology	202
7.3.1.2 Electrical Excitability and Phagocytic Activity	202
7.3.1.3 Growth	204
7.3.2 Effects on Deoxyribonucleic Acid	204
7.3.3 Membrane Permeabilization	206
7.4 Bioeffects and Lithotriptors	208
7.5 Summary	211

8. Bioeffects of Acoustic Cavitation in Mammalian	
Tissues	213
8.1 General Evidence for the Occurrence of Cavitation in	
Tissues	213
8.1.1 Studies of Brain and Liver	213
8.1.2 Muscle	215
8.1.3 Paraplegia	217
8.1.4 Intestine	218
8.1.5 Blood	219
8.1.6 Urine	220
8.1.7 Summary	220
8.2 Evidence of Cavitation <i>In Vivo</i> from Lithotripsy	220
8.2.1 Kidney and Liver	221
8.2.2 Embryos	222
8.2.3 Lung	222
8.2.4 Intestine	223
8.2.5 Heart	223
8.2.6 Blood	224
8.2.7 Negative Lithotripter Fields	224
8.2.8 Hemorrhage Near Fetal Bone	225
8.3 Cavitation Effects with Diagnostically Relevant	
Acoustic Fields	226
8.3.1 Lung	226
8.3.2 Intestine	230
8.3.3 Heart	231
8.3.4 Blood	231
8.3.5 Hemorrhage Near Fetal Bone	232
8.3.6 Synergism	232
8.3.7 Summary	232
8.4 Related Reports of Biological Effects	233
8.4.1 Endothelial Damage to Blood Vessels	233
8.4.2 Ultrasonic Enhancement of Thrombolysis and	
Perfusion	234
8.4.3 Contrast Agents	235
8.4.4 Sonochemical Tumor Treatment	237
8.5 Summary	238
9. Models for Exposure Estimation in Human Beings ...	240
9.1 Introduction	240
9.2 General Diagnostic Considerations	247
9.2.1 Patient-Specific Adjustment of the	
Homogeneous Attenuation Model	247
9.2.2 Nonlinear Propagation and Other Effects	
Limiting the Accuracy of Tissue Models for	
Exposure Estimates	252

9.2.3	Considerations with Use of Microbubble Contrast Agents	254
9.3	Obstetrics	254
9.3.1	Introduction	254
9.3.2	Measurements of Path Lengths in Individual Tissues Overlying the Fetus	256
9.3.3	Insertion-Loss Measurement <i>In Vivo</i>	257
9.3.4	Obstetrical Attenuation Models	262
9.3.5	Patient-Specific Models	270
9.4	Scanning Sensitive Tissues Through Saline During Surgery and Other Cases of Minimally Attenuating Fluid Paths	272
9.5	Lung and Other Respiratory Tract	272
9.5.1	Indirect Lung Exposure During Echocardiography	272
9.5.2	Other Indirect Lung Exposures and Direct Lung Studies	273
9.5.3	Thyroid and Other Organs Near the Respiratory Tract	274
9.6	Digestive Tract	274
9.6.1	Air Cavities	274
9.6.2	Esophageal and Other Intracavitary and Intraoperative Probes (with Bubbles Possibly Trapped in the Coupling Fluid)	275
9.7	The Neonatal Head	276
9.8	Transcranial Doppler	276
9.9	Ophthalmic Ultrasound	277
9.10	Summary	277
10.	Employed and Needed Sound Pressure Waveforms	280
10.1	Introduction	280
10.2	Outputs from Existing Diagnostic Systems and Historical Trends	282
10.2.1	General Comments	282
10.2.2	Output-Labeling Guidance and Requirements	282
10.2.2.1	FDA 510(k) Guidance	282
10.2.2.2	AIUM Output Measurement and Labeling Standard and Corresponding NEMA Standard	284
10.2.2.3	Thermal- and Mechanical-Index Data	288
10.2.2.4	Acoustic Data Provided in Compliance with the Output Display Standard	289
10.2.2.5	IEC 61157 Data and Requirements ..	292

10.2.2.6	Other Current Sources of Output Data Provided in Operators' Manuals and Reference Manuals	294
10.2.3	Recent Independently-Measured Output Data and Comparisons with Manufacturer-Reported Data	298
10.2.3.1	Recent Independently-Measured Output Data and Historical Trends in System Output	298
10.2.3.2	Comparison of Manufacturer-Supplied and Independently-Measured Output Data	298
10.2.4	Other Exposure Quantities	299
10.2.4.1	Frequencies	299
10.2.4.2	Pulse Durations and Repetition Rates	300
10.2.4.3	Beam Dimensions and Focal Gain ..	301
10.2.4.4	Nonlinear Propagation	302
10.3	Bioeffects Particularly Relevant to Possible Changes in Diagnostic Equipment Design	303
10.3.1	General Wave Shape and Polarity Observations	303
10.3.2	General Observations Related to Pulse Duration	303
10.3.3	Effects of Repetition Rate, Duty Factor, and Dwell Time	304
10.3.4	Summary of Effects of Pulse Duration, Repetition Rate, and Dwell Time	305
10.4	Dependence of Information Content on Acoustic Pressure	305
10.4.1	General Factors Relating Pressure and Diagnostic Information	305
10.4.2	Effects of Increased Output on Effective Penetration	307
10.4.3	Effects of Increased Output on Other Image and Signal Quality Measures	310
10.4.4	Experimental Studies: Dependence of Image Quality on Output	313
10.5	Pulse Compression as a Possible Tool for Reduction of Peak Pressure	314
10.6	Equipment Features for Reducing Acoustic Pressures	316
10.6.1	General	316
10.6.2	Single-Knob Output Control	316

10.6.3	Multiple-Receive Lines on a Single-Transmit Pulse (Explososcan Techniques)	317
10.7	Summary and Conclusions	318
11.	Temperature Elevation and Its Biological Effects ...	319
11.1	Introduction	319
11.2	Biological Responses to Temperature Change	320
11.2.1	General Conclusions	320
11.2.2	Maternal and Fetal Core-Temperature Relations	321
11.2.3	Thermally Induced Teratogenesis	324
11.2.4	Heat-Shock Proteins	332
11.2.5	Investigations Involving Ultrasound Exposures of Mammalian Embryos or Fetuses <i>In Vivo</i> and <i>In Vitro</i>	334
11.3	Re-evaluation of Data on Thermally Induced Teratogenicity	337
11.4	Role of Temperature in Biological Effects of Ultrasound	349
11.5	Computations of Temperature Rise	351
11.6	Measurements of Temperature Rise in Models	357
11.7	Measurements of Temperature Rise in Mammalian Tissues	362
11.8	Ultrasonic Hyperthermia and Temperature-Related Surgery	369
11.9	Summary	376
12.	Epidemiology of Ultrasound Exposure	379
12.1	Introduction	379
12.2	Epidemiologic Methodology	380
12.3	Causality	382
12.4	Clinical Surveys	382
12.4.1	Studies of Fetal Exposure	383
12.4.2	Effect on Fetal Activity	388
12.4.3	The RADIUS Study	389
12.4.4	The Newnham Study	392
12.4.5	The Campbell Study	395
12.4.6	Statistical Considerations	397
12.4.7	Commentary on Results from Human Epidemiology	402
13.	Summary and Conclusions	404
13.1	Introduction	404

13.3	Nonthermal Mechanisms for Bioeffects in the Absence of Cavitation	404
	13.3.1 Summary	404
	13.3.2 Conclusions	405
13.4	Noninertial Cavitation; Gas-Body Activation	406
	13.4.1 Summary	406
	13.4.2 Conclusions	407
13.5	Nonlinear Bubble Response; Inertial Cavitation	408
	13.5.1 Summary	408
	13.5.2 Conclusions	410
13.6	Bioeffects of Noninertial Cavitation Involving Free and Stabilized Gas Bodies in Non-Mammalian Systems	410
	13.6.1 Summary	410
	13.6.2 Conclusions	411
13.7	Bioeffects of Inertial Cavitation <i>In Vitro</i>	412
	13.7.1 Summary	412
	13.7.2 Conclusions	413
13.8	Bioeffects of Acoustic Cavitation in Mammalian Tissues	414
	13.8.1 Summary	414
	13.8.2 Conclusions	416
13.9	Models for Exposure Estimation in Human Beings	417
	13.9.1 Summary	417
	13.9.2 Conclusions	419
13.10	Employed and Needed Sound Pressure Waveforms	420
	13.10.1 Summary	420
	13.10.2 Conclusions	421
13.11	Temperature Elevation and Its Biological Effects ..	422
	13.11.1 Summary	422
	13.11.2 Conclusions	424
13.12	Epidemiology of Ultrasound Exposure	425
	13.12.1 Summary	425
	13.12.2 Conclusion	426
13.13	The Thermal and Mechanical Indices	427
	13.13.1 Introduction	427
	13.13.2 Conclusions	429
14.	Recommendations	430
	14.1 Introduction	430
	14.2 Exposure Quantities	431
	14.3 Safety Criteria	432

14.4 Equipment Features; Output and Product Information	433
14.5 Responsibilities of Users	434
Appendix A. Mechanical Equilibrium of Free Bubbles .	435
Appendix B. Output Display Standard	439
B.1 Introduction	439
B.2 Equations for the Indices	440
B.3 Maximal Values of the Thermal Indices	444
B.4 Accuracy of the Output Display Standard Indices	445
B.4.1 Nonlinear Propagation	445
B.4.2 Estimation of Attenuation	446
B.4.3 The Cranial Thermal Index and the Bone Thermal Index	447
B.4.4 The Soft Tissue Thermal Index	448
B.4.5 Frequency Dependence of the Threshold for Nonthermal Damage	449
B.4.6 Spatial Distribution of Acoustic Pressure	449
B.4.7 Recent Tests of the Accuracy of the Output Display Standard Thermal Indices	450
Appendix C. Nepers and Decibels	452
Appendix D. Nonlinear Propagation: An Update	454
D.1 Introduction: Conclusions of NCRP Report No. 113 on Nonlinear Propagation	454
D.2 Nonlinear Propagation in Tissue	456
D.2.1 Intensity	456
D.2.2 Derating Intensities	458
D.2.3 Heating Rates	459
D.2.4 Temperature Increments	462
D.2.5 Acoustic Pressures	464
D.2.6 Derating Pressures	466
D.2.7 Nonlinear Propagation and the Mechanical Index	468
D.3 Summary	471
Glossary	473
Symbols	475
References	479
The NCRP	547
NCRP Publications	556
Index	566

1. Executive Summary

In developing background for scientifically based exposure criteria, this Report gives much emphasis to the means by which ultrasound can bring about changes in biological structures or processes. The intent is to consider all known mechanisms, thermal and nonthermal. Nonthermal mechanisms are taken up in Sections 3 through 8 and are divided, for convenience, into two classes: those that involve acoustic cavitation, *i.e.*, the many-faceted activities of gas-filled cavities, and those that do not. It is the former on which there is, by far, the most information, and to which the greater part of this Report is devoted; however, the latter is of much interest, and is discussed in Section 3.

Effects of nonthermal mechanisms that do not involve cavitation include: tactile response to, and hearing of, pulsed ultrasound; aggregation of cells in blood vessels; reversible alteration of electrical and other properties of cell membranes; and irreversible cell damage. These depend on acoustic radiation pressure, radiation force, radiation torque, or acoustic streaming, all of which are time-averaged quantities that are consequences of acoustic nonlinearity.

Acoustic cavitation phenomena include a wide variety of possibilities. The kind of activity that occurs depends on the size of the cavity as well as on the nature of its immediate surroundings; it is also dependent on the characteristics of the ultrasound field, the pressure amplitude being especially important. The response to an ultrasound field of low or moderate pressure amplitude may be a periodic volume pulsation, so that the cavity becomes a secondary source of sound; this response underlies the effectiveness of the gas-based contrast agents that are now widely used to enhance ultrasound imaging. Other phenomena that occur at moderate amplitudes are best seen in modeling experiments with plants, insects and *in vitro* cell suspensions, but have their counterparts in mammalian tissues when contrast agents, bubbles or other gas bodies are present. These phenomena include fluid movements, bubble-particle interactions, and shearing action in the neighborhood of gas bodies with consequent effects on properties of cell membranes. The movements and actions can be partially accounted for as special forms of acoustic radiation force and small-scale acoustic streaming.

If a beam of pulsed ultrasound from commercial diagnostic ultrasound equipment is projected into water or another aqueous medium and if contrast agents or other suitable small gas bodies are present, the pressure amplitude during the pulse is often sufficient to produce inertial cavitation. This is a violent activity in which a cavity expands during part of a sonic cycle, then collapses suddenly to a very small volume which persists for a few nanoseconds, during which time the pressure and temperature of the contents are very high. If the collapse occurs near a solid boundary, a liquid jet may be formed that impinges on the boundary at high speed. Inertial cavitation is usually involved during *in vitro* investigations of effects of ultrasound on cell suspensions or cellular monolayers; the cell killing, which is commonly observed, appears to be mostly from the associated mechanical forces. Biochemical damage may result from the highly reactive chemicals, including free radicals, that are often produced during the moments of high pressure and temperature that follow collapse events. *In vitro* experiments have led to much information on the possible biological consequences of inertial cavitation.

While experiments with model systems, together with relevant theory, have led to valuable insights on basic mechanisms, the results cannot usually be applied with confidence to clinical situations, unless they have been tested by experiments with living animals. This is especially true when considering possibilities for nonthermal biological effects caused by various aspects of acoustic cavitation. In mice, rats, swine and other laboratory animals, diagnostic ultrasound has been shown capable of rupturing small blood vessels, with consequent leakage of red cells into extravascular space, but only under special conditions. The conditions are that the vessel walls must be near gas bodies that either (1) are present normally, as in adult lung and intestine or (2) have been injected into the blood stream, as when gaseous contrast agents are used. The use of contrast agents can significantly increase the potential for ultrasound to affect processes in organs or tissues that do not normally contain obvious gas bodies, as is shown by the recent findings of increased incidence of premature ventricular contractions when the heart is examined with ultrasound. In general, gas bodies are found to play a critical role, serving as sites where diagnostic ultrasound can alter biological structures and processes *via* nonthermal mechanisms.

Biological effects produced by thermal mechanisms are taken up in Section 11, as an extension of the detailed treatment of this subject in NCRP Report No. 113. In that earlier Report, attention was given to teratological effects of heat, on which topic the information comes mostly from “whole-body” exposures in which small pregnant

laboratory mammals are subjected to elevated temperatures in heated air chambers or water baths. In the present Report, the analysis of results from such exposures is extended, in order to obtain information on situations where heat is applied more directly to the fetus, as it is when focused ultrasound is used clinically to examine the human fetus. Also included here is a review of recent advances in experimental and theoretical methods for measuring or estimating temperature fields produced by ultrasound in model systems and in mammals.

A review of existing human epidemiological studies (Section 12) of patients examined with ultrasound leads to the encouraging conclusion that these studies do not provide sufficient justification for finding ultrasound to be the cause of any of the adverse effects investigated. It is pointed out, though, that these studies would not have detected a small percentage increase in a common event. Also, it is noted that the studies are based on procedures using ultrasound equipment manufactured before 1991, and that important changes in equipment and procedures have occurred since then.

In the course of discussions in this Report on the status of knowledge about biological effects of ultrasound, specific values are given for physical parameters that define conditions of relative safety or concern; these are the "criteria" to which the title of this Report refers. For example, approximate values are given of the lowest pressure amplitudes for which lung damage has been observed in laboratory animals. These are *in situ* values of the pressure amplitude, *i.e.*, they apply at the surface of the animal lung. In using these criteria for human exposures, it is necessary to estimate the pressure-amplitude values existing at the surface of the human lung. In order to do this, knowledge is required of the acoustic pressure amplitudes produced by the diagnostic equipment at various parts of the human body. These quantities cannot be measured directly but, in the United States, are estimated by manufacturers from measurements made in water, together with assumptions about ultrasound propagation characteristics in tissues. Section 9 includes a discussion of present knowledge on attenuation of ultrasound in the human body, with special consideration of obstetrical applications. Present standards adopted by the Food and Drug Administration (FDA) for estimating the attenuation appear to be sufficiently accurate for several large classes of obstetrical examinations. However, they can seriously overestimate the attenuation (and thus underestimate the exposure) in situations where there is a large fluid component in the path to the target tissue. Proposals are offered for improving the estimates.

Section 13 contains conclusions reached by weighing the information presented in the preceding sections of this Report, and Section 14 contains recommendations. The latter recognize the responsibilities users have in making decisions about procedures to be followed and control settings to be used. It is necessary to be knowledgeable about ultrasonic dosimetry and effects, and about acoustical characteristics of the equipment used, in addition to the particular characteristics of the patient being examined. Modern equipment for diagnostic ultrasound is complex, and users need considerable assistance in making decisions. The on-screen display of thermal indices (TI) and a mechanical index (MI), now provided by many manufacturers in response to requirements of the FDA, mark a significant step forward in making safety information available to users. It is recommended that there be continuous efforts to make this information more accurate and complete. In Section 14, criteria are expressed both in terms of these displayed indices, and in terms of the basic physical quantities involved.

It is noted that an appropriate benefit/risk decision does not always call for a choice of pressure amplitude, or other acoustic output parameter, low enough to assure that there is no risk. For some situations, it may be determined that the improved imaging capabilities that can come from increased output level, as discussed in Section 10, or from use of contrast agents, may offer enough benefit to make increased risk acceptable.

It is the purpose of this Report to present background for a scientifically based approach to safety assessment for diagnostic ultrasound, so that users can make informed decisions, while taking advantage of new developments in equipment and procedures.

2. Introduction

Pulsed ultrasound as an imaging tool in medicine has been used for nearly half a century. Its use for this purpose was first described by Howry and Bliss (1952) at the University of Colorado, by Wild (1950) at the University of Minnesota, and by a group working with Kikuchi (Tanaka *et al.*, 1952) in Japan. Since that time it has rapidly been established as an extremely useful diagnostic tool in many areas of medicine, especially in radiology, obstetrics, cardiology and ophthalmology. At the present time it is one of the most widely used diagnostic techniques in the physician's armamentarium. Probably more than 75 percent of all infants born in the United States (Moore *et al.*, 1990) and likely a similar or larger number in some other developed countries of the world, has been examined with ultrasound *in utero*. The corresponding number in underdeveloped countries of the world is not known, but the use of diagnostic ultrasound there is considerable and growing.

The widespread and rapidly increasing use of ultrasound in diagnosis is, in part at least, attributed to a number of factors: (1) the relatively low cost of acquiring and operating the equipment; (2) ease of interpretation, both by the physician and the patient; (3) availability for office use; (4) superiority as an imaging modality that allows the visualization and differentiation of soft tissues, as well as detection and measurement of blood flow and structural size; and (5) its familiarity to both physicians and patients as a modality, unrelated to ionizing radiation and magnetic energy, from whose use there has been little fear of adverse effects.

The diagnostic information gleaned from the use of ultrasound simplifies and enhances the understanding of so many abnormalities and disease processes in the patient that the physician and the patient have readily become dependent on its use. The public has been quick to accept this new technology and although there has been some concern about its safety, it has been minimal in comparison with concerns about other imaging modalities, especially those that depend on ionizing radiation. Few energy sources to which the human body is exposed have been more exhaustively studied for adverse effects. Its safety record is unsurpassed by any other human tissue imaging modality to date.

However, even a procedure whose risk has appeared to be small must be continually examined for safety when it is used as widely as diagnostic ultrasound. In employing any medication or power source for the purpose of therapy or diagnosis, the provider (manufacturer or supplier) and user must be aware of the appropriate dosage to safely accomplish the desired goal. The provider must supply information about the product which will adequately inform the user. In turn, the user must be adequately educated about the product in order to be able to inform and protect the patient. This is especially true with ultrasound since here the dosage may be adjusted to meet the needs for a particular patient and procedure. The need for information and education has become of special concern since October 1991, when FDA relaxed its guidelines (FDA, 1991) to allow the manufacturer to market equipment with an estimated *in situ* spatial-peak temporal-average (SPTA) intensity of 720 mW cm^{-2} for all applications (except ophthalmology). For fetal scanning, this was almost an eight-fold increase in the SPTA intensity (compared to the earlier upper limit of 94 mW cm^{-2}) and carries the possibility of harm. This change was made by the FDA in anticipation of a standard, commonly called the Output Display Standard, with an acronym "ODS" (AIUM/NEMA, 1992). The latter was based on a measurement standard which had been developed jointly by the American Institute of Ultrasound in Medicine (AIUM), the National Electrical Manufacturers Association (NEMA), and other organizations (AIUM/NEMA, 1992; 1998).¹ The higher intensities allowed by the above-mentioned change in guidelines makes increased diagnostic power available to users. At the same time, the possibilities for excessive heating are increased. This increased intensity is available only on equipment that is provided with features for display of prescribed safety information.

Other recent advances in the practice of diagnostic ultrasound include the introduction of gaseous contrast agents, and techniques involving harmonic imaging. Both significantly improve the quality of ultrasound images and, also, add elements of risk which must be considered. This increased potential for both benefit and harm in present practice presents opportunities and responsibilities to manufacturers, users, educators and others to see that the new capabilities are used wisely.

In this Report, the status of knowledge on biological effects of ultrasound is reviewed, and conclusions are drawn about its

¹Some aspects of ODS were adapted from criteria and algorithms developed by NCRP (1992), though there are important differences discussed in the body of this Report.

implications for the practice of diagnostic ultrasound, particularly in respect to exposure criteria. Thermal mechanisms were discussed in detail in NCRP Report No. 113 (NCRP, 1992) while this Report deals with all known mechanisms.

In 1980, the National Council on Radiation Protection and Measurements (NCRP) created Scientific Committee No. 66 with the assigned topic, "Biological Effects of Ultrasound and Exposure Criteria." In preparing its first report (NCRP, 1983), the Committee reviewed existing scientific information on biological effects of ultrasound and mechanisms, especially material considered relevant to safety of medical diagnostic ultrasound. Also, recommendations were made for future research, instrument characterization, and safety-related aspects of clinical practice. Following that report, the Committee accepted a bold challenge: To make safety recommendations more specific by formulating *quantitative* exposure criteria. In doing this, it was decided to proceed by utilizing physical mechanisms, both thermal and nonthermal, as the basis for making quantitative recommendations. The known mechanisms and their relationships to each other are shown in Figure 2.1. Thermal mechanisms were addressed first, and the results were summarized in NCRP Report No. 113 (NCRP, 1992). Besides reviews of required background information, the latter contains tables, graphs, mathematical formulas, and decision schemes which are recommended for determining and choosing conditions under which biological damage from heating can be avoided.

This Report complements Report No. 113 (NCRP, 1992) by providing (1) an update on thermal considerations and (2) analogous

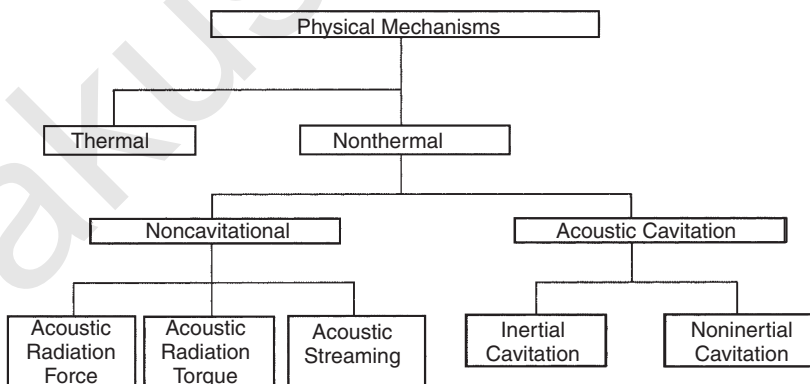


Fig. 2.1. Classification of physical mechanisms by which ultrasound can produce changes in biological systems.

material on biological effects of ultrasound for which the physical mechanisms are nonthermal. The nonthermal mechanisms include acoustic radiation forces and torques, acoustic streaming, and a variety of phenomena associated with acoustic cavitation (see Glossary and Figure 2.1). While results are included for a wide range of conditions, the emphasis is on the frequency range (2 to 10 MHz) and other conditions representative of much of the commercial equipment presently used in clinical diagnostic practice.

Information on conditions under which biological effects of ultrasound occur, or might be expected, are obtained partly from experiments and partly from computations. In experimental studies, biological systems of interest are exposed to ultrasound under specified conditions and selected endpoints are investigated. *In vitro* studies involve exposure of cells or spheroids suspended in aqueous media, while *in vivo* mammalian studies involve exposure of laboratory animals ranging from mice to monkeys. In still other experiments, the test objects are plant tissues or insect larvae. The ultrasound is delivered in a continuous-wave (CW) mode, or in a pulsed mode. Results obtained often depend on the extent to which gas-filled cavities are present in the exposed system.

Computations based on known principles have proved valuable for interpreting experimental findings and for quantifying the limiting conditions under which ultrasound will produce biological effects. However, because the basic equations of acoustics are nonlinear, computations relating to nonthermal mechanisms pose special mathematical difficulties. There are both similarities and differences between ultrasound and other forms of radiation. While acoustic radiation forces and torques, and acoustic streaming, have their parallels in electromagnetic fields and in ionizing radiation, the varied phenomena of cavitation are unique to acoustics and hydrodynamics.

The material presented in Sections 3 through 8 of this Report relates to biological effects of ultrasound for which the mechanism is, or appears to be, nonthermal. In many experiments, the evidence that observed effects are not a result of temperature elevation comes directly from thermometry. In others, the evidence is more indirect and may be based mostly on calculations of the kind discussed in NCRP Report No. 113 (NCRP, 1992). Sections 9 through 12 deal with: ultrasound attenuation in the human body, the extent to which high acoustic outputs are needed for some diagnostic applications, updated information on thermal considerations, and findings from human epidemiology. Finally, in Sections 13 and 14, conclusions are drawn on the clinical implications of the material presented. These conclusions include recommendations on limiting conditions for prudent use of diagnostic ultrasound.

Section 3 deals specifically with biological effects of ultrasound for which neither heat nor cavitation appears to be responsible. Acoustic radiation force, the time-averaged force exerted on an object by a sound field, is sometimes found to be the cause. This mechanism is involved in applications and effects as diverse as (1) techniques for measuring total power, or local intensity, in an ultrasound beam; (2) production of auditory responses when pulsed ultrasound is focused on the brain of a living animal; and (3) separation of cells into a series of bands when blood vessels are exposed to standing waves *in vivo*. A special kind of acoustic radiation force exists between neighboring particles in a sound field, causing them to attract or repel each other. Sound also can act on an object *via acoustic radiation torque* (see Glossary) to produce rotation or, at least, a tendency to rotate. If the object possesses symmetry about its axis of rotation, and is free of elastic constraints, steady spinning occurs. If the object is not spherically symmetric (*e.g.*, if it is discoid), or if there are elastic constraints to the motion, it may rotate to an equilibrium orientation and remain there as long as the sound field is maintained. In a liquid-filled space, ultrasound produces acoustic streaming, *i.e.*, steady circulatory flow. When the flow is of small geometric scale, called “microstreaming,” and it occurs in a fluid containing biological cells, the associated viscous stress exerted on the cells may cause them either to lyse, or to be otherwise affected.

Sections 4 through 8 address biological effects of ultrasound in which the mechanism is acoustic cavitation. This is an activity associated with gas-filled cavities or bubbles in a liquid, quasi-liquid or soft tissue, and is designated as being either *inertial* or *noninertial* (Figure 2.1). Inertial cavitation involves implosions of bubbles; it may be accompanied by the production of shock waves, by the emission of visible and ultraviolet light (*sonoluminescence*), and by the generation of highly reactive chemical species. Noninertial cavitation occurs at lower levels of the acoustic pressure and does not lead to the production of light or of new chemical species; in liquids, it is associated with vigorous motions within bubbles and in the surrounding fluid, and with attendant heat generation. Noninertial cavitation can also occur in selected tissues of plants, insects and mammals which contain stable gas bodies; here, the detailed mechanisms are only partially understood.

Sections 4 and 5 address, respectively, the physics of noninertial and inertial cavitation. Much of the theory in Section 4 is based on linear approximations, which are valid when the acoustic pressure is relatively low. Under these conditions a sound field causes volume oscillations of any small gaseous inclusion, analogous to those of the forced harmonic oscillator of classical physics. The gas body then

becomes a secondary source of sound and radiates (scatters) energy in the form of an outward-going ultrasound wave. Small gas-containing particles are exceptionally effective as scatterers of ultrasound, especially if they are of near-resonance size; such particles, stabilized by thin viscoelastic shells (now commercially available) are employed widely as contrast agents for diagnostic ultrasound.

At moderate levels of the acoustic pressure, but still within the conditions of noninertial cavitation, heat production by gas bodies can become significant. Other significant factors may include acoustic radiation forces which can cause individual bubbles to travel at high speed through a liquid, forces between bubbles which may cause them to coalesce, and forces of attraction between bubbles and neighboring particles. Bubble growth occurs, partly through the above-mentioned coalescence and partly through *rectified diffusion*; the latter occurs when the amount of gas diffusing from the bathing liquid into the bubble during part of a cycle exceeds that diffusing outward during the rest of the cycle. Vigorous microstreaming occurs within oscillating gas bodies, and in the immediately surrounding medium if it is fluid; this stirring action can enhance reaction rates at surfaces, and can also exert shearing stresses on neighboring structures.

In Section 5, other aspects of cavitation are treated which manifest themselves at pressure amplitudes high enough to produce significant nonlinearity in the bubble response. Nonlinear differential equations are presented and discussed in Section 5. They have been solved numerically to determine the radius (R) as a function of time (t) for a spherical bubble of a given size in a specified acoustic driving field. Under conditions of nonlinearity, features appear in the function $R(t)$ which are absent under linear conditions. For example, if the driving acoustic field is a CW in which the acoustic pressure varies sinusoidally with time, the function $R(t)$ can, under nonlinear conditions, contain spectral components of *harmonic*, *subharmonic* and *ultraharmonic* frequencies. This complexity is reflected in the spectra of the acoustic pressure [$p(t)$] in the acoustic field scattered by the bubble. While “resonance” retains significance, it takes on new features under nonlinear conditions. Still another consequence of nonlinearity is the occurrence of *deterministic chaos*, a condition under which the function $R(t)$ is multiply valued, and is predictable only in a statistical sense.

As the pressure amplitude increases further, the contraction phase of the bubble motion approaches a condition often referred to as “collapse.” When a critical amplitude is reached, dramatic changes occur in the predicted rate of collapse, as well as in the predicted pressure and temperature reached in the bubble during a brief

interval when its volume is near its minimal value. It is the bubble activity and associated processes which accompany violent collapse that are referred to in this Report as *inertial cavitation* (see Glossary and Figure 2.1). Although the heated sphere which exists momentarily following a collapse may be less than a hundred nanometers in diameter, and the high temperature state may persist only a few tens of nanoseconds, the mechanical and chemical damage done to a biological system can be severe when inertial cavitation occurs.

When the oscillations are not spherically symmetric, other phenomena appear. In a sound field at low amplitudes, waves like those on a vibrating drumhead may be set up at the gas-liquid interface which bounds a bubble. At higher amplitudes, the waves become distorted and chaotic; microbubbles may be formed on the liquid side of the interface, while jets of liquid are formed on the gaseous side. A special kind of inertial cavitation occurs when a bubble rests above a solid boundary and undergoes collapse in an asymmetric manner, such that liquid above the bubble plunges downward through it and impinges on the boundary as a high-speed jet.

Physical theory has been used to define limiting acoustical conditions for the occurrence of cavitation, and has provided helpful guidance to the medical community. Sections 6 through 8 deal with experimental studies of biological effects that are produced by ultrasound through the action of gas bodies or bubbles, and hence are results of acoustic cavitation, either inertial or noninertial (see Figure 2.1). In water and other liquids used for experiments with biological systems *in vitro*, small gas bodies may always be present, to some extent, and provide sites for cavitation activity; they are commonly called *cavitation nuclei* (see Glossary). Such nuclei are present only because means are available for stabilizing them; without stabilization, the gas bodies would dissolve or float out of the region of interest. In commonly performed experiments, the nuclei occur randomly in association with small particles which may exist in the liquid or with pits, cracks, etc. at the container walls. In Section 6, it is shown how stabilized gas bodies can be made available in a more controlled manner by using hydrophobic membranes with uniform gas-containing pores. Vigorous acoustic microstreaming occurs near these pores during exposure to ultrasound at relatively low amplitudes.

In special biological structures, such as those of plants and insects, gas-filled spaces occur as part of the natural anatomy. When these tissues are exposed to ultrasound, the gas bodies in these spaces become active in various ways, through gas-body activation (GBA), a special form of noninertial cavitation. In leaves, roots and other plant tissues, many of the cells are surrounded by gas-filled channels, and most of the cell interior is occupied by a large vacuole containing

fluid with water-like viscosity. In an ultrasound field, the gas bodies undergo volume oscillations which produce vibrations in the cell walls; the latter, in turn, cause acoustic microstreaming to occur within the cell vacuoles.

In an insect, gas bodies are present throughout the interior in the form of channels which constitute the respiratory system. Experiments have shown that the development of insect larvae can be arrested by exposure to pulsed ultrasound, even at low values of the time-averaged intensity, after the respiratory system has filled with air. Observations during ultrasonic exposure showed no evidence of microstreaming in the tissue outside the respiratory channels; details of the mechanisms for the ultrasonic action remain incomplete.

Section 7 deals with findings of investigations in which cell suspensions were exposed to ultrasound in any of a wide variety of arrangements and observations were made of resulting changes in cellular structure and/or function. In most studies, acoustic cavitation was apparently involved in bringing about the changes observed. In a common experimental arrangement, a cell suspension of interest is contained in a test tube which is positioned in a temperature-controlled water bath and exposed to a beam of ultrasound. A surprising finding for this arrangement is that while a cellular effect, such as lysis, may be minimal when the tube is stationary, it can be greatly enhanced when the tube is slowly rotated about its axis, the latter being perpendicular to the direction of propagation of the ultrasound. It appears that the biological changes are mainly a result of mechanical stresses acting on cells during close interactions with bubbles and that the tube rotation recycles bubbles through the suspensions, thereby increasing the probability of cell-bubble interaction. This explanation is supported by findings that enhancement of the cellular effect can also be achieved by alternating the direction of ultrasound propagation with the exposure vessel fixed.

An important finding from experiments with suspensions of red cells is that the fraction of cells damaged is less, while the absolute number is greater, when the concentration of cells is increased. Experiments done to test suggested explanations for this concentration effect are described in Section 7, along with the findings that the amount of ultrasound-induced hemolysis is increased in the presence of a pulse-echo contrast agent comprised of tiny bubbles. Also discussed is the critical question of whether hereditary effects can occur; possibilities are suggested by the finding that hydrogen peroxide produced outside the cells (by inertial cavitation) can produce single-strand deoxyribonucleic acid (DNA) breaks within viable cells. Still other results show that ultrasound exposure can cause cells in suspension to become temporarily permeable to large molecules.

The investigations discussed in Section 8 concern effects produced by ultrasound on cats, rats, mice and other laboratory animals, in which the mechanism appears to be acoustic cavitation. These studies are particularly relevant to the safety of medical ultrasound because the ultrasonic properties of tissues and the characteristics on which acoustic cavitation depends are generally similar for all mammalian species. For example, in a mammal, an obvious location of naturally occurring gas-filled spaces, and hence a likely site for GBA, is the lung. In fact, the aerated lung has proved to be unusual among mammalian organs in its susceptibility to nonthermal damage from ultrasound. Hemorrhage occurs in the lung of the living mouse and other mammals when exposed to pulses of ultrasound with center frequency 0.5 to 5 MHz for which the maximum acoustic pressure is of the order of 1 MPa. (These conditions sometimes prevail at the focus of an ultrasound beam used in diagnostic medicine, and the focus may occasionally fall on the surface of the lung.) The detailed mechanism for the hemorrhaging is not known, but the high air content of postnatal lung is evidently an important factor. Similar experiments have implicated air bubbles in intestinal hemorrhage. It has been established that the fetal lung, which is not aerated, does not show this enhanced susceptibility to ultrasound.

In mammalian organs which do not contain known gas bodies, the threshold for damage from short pulses of ultrasound is higher. For example, lesions which appeared to arise from some form of cavitation were observed in exposures of cat brain *in vivo* to a single focused ultrasound pulse of 1 MHz frequency and a duration of less than 40 ms, but not unless the pressure amplitude was 8 MPa or greater. In contrast to lesions produced by longer exposures at lower amplitudes, where the mechanism is believed to be thermal, the lesions produced at the higher pressure amplitudes were irregularly shaped (showing gross tissue disruption), occurred preferentially at boundaries of fluid-filled spaces such as ventricles and blood vessels, and appeared immediately after sound exposure when examined with light microscopy.

Section 9 takes up the difficult problem of determining exposure quantities (usually the acoustic power, pressure and intensity, or quantities expressed in terms of them) in patients during applications of diagnostic ultrasound. Errors arise in expressing safety criteria in terms of these exposure quantities, because the latter are not measured *in situ*, but, instead, are estimated; the actual measurements are made in water or other standard media. The estimates depend on assumptions, expressed in terms of simplified models, about the attenuation of ultrasound as it propagates in the body. In Section 9, various models are discussed and compared with available

data on attenuation. The concepts of *typical* estimates and *reasonable-worst-case* estimates are introduced, the latter being appropriate when it is especially important that the relevant exposure quantities not exceed critical values. Attention is given to the propagation paths involved in examinations of the fetus, and to other special situations.

It is widely agreed that the values of exposure quantities employed in the practice of diagnostic ultrasound should be no greater than what is needed to obtain required medical information. In Section 10, data are presented on maximum values which manufacturers have made available in widely used commercial instruments. The data show that the values have increased during the last two decades. Since these values sometimes approach or exceed levels at which biological effects can occur, it is evidently believed by the manufacturer that users sometimes need the highest values which safety considerations allow. For use in critical situations, instruments should be designed and constructed so that maximum diagnostic information can be obtained while the probability of biological effects is minimized. Considerations involved in optimum design (and prudent use) of diagnostic equipment are discussed in Section 10.

Since NCRP Report No. 113 was published (NCRP, 1992), there has been continued progress in understanding the response of biological systems to temperature change, and in knowledge of temperature increases which occur when biological systems, or models of them, are exposed to ultrasound. Recent findings are reviewed in Section 11. Additional evidence has been found for hyperthermia as a teratogen in laboratory animals. Investigations have been made into the increase of temperature produced by ultrasound in fetal brain, fetal soft tissue, and neonatal brain. In studies involving brain within the skull, it was found, as expected, that the temperature was greatest near the skull. There has been further development of theory and its application to medical ultrasound. Also, numerous investigations have been done involving measurements of temperature rise produced by ultrasound in tissue-mimicking materials (TMM), *i.e.*, in gels designed to have acoustical and thermal characteristics similar to those of mammalian tissues (except that perfusion is usually absent). It appears from this work that the temperature field produced by a well-defined ultrasound beam in a homogeneous medium of known characteristics can be predicted well by available theory. However, in other situations, the temperature rise can be affected significantly by (1) extra heating arising from the transducer itself, (2) cooling produced by acoustic streaming, or (3) extra absorption when an accumulation of small gas-filled cavities is in the field.

In this Report, as in NCRP Report No. 113 (NCRP, 1992), exposure criteria were arrived at primarily by using information from

laboratory studies of biological effects in animals or other biological systems, under conditions where the mechanisms for the effects were reasonably well understood. From such information, it is possible to extrapolate to human beings; that is, it is possible to draw conclusions about the conditions under which the effects will occur in human patients. In addition, some information about effects on human patients can be learned from epidemiology, although the use of human subjects in studies of biological effects is very limited for ethical reasons. The results of epidemiological studies of patients who had been medically examined with diagnostic ultrasound are reviewed in Section 12, with emphasis on several studies that have been done since an earlier review of the subject in NCRP Report No. 74 (NCRP, 1983).

In Section 13, the findings of this Report are summarized and conclusions are drawn. Recommendations are presented in Section 14.

3. Nonthermal Mechanisms for Bioeffects in the Absence of Cavitation

3.1 Introduction

There have been numerous investigations of changes produced by ultrasound in biological systems under conditions where, apparently, neither temperature elevation nor cavitation was significantly involved. Instead, when the causes were identified, they included such mechanisms as acoustic radiation force or torque, or acoustic streaming. These topics are examined briefly and the reader is referred to more extended discussions in the cited literature.

3.2 Acoustic Radiation Force and Radiation Pressure

Relevant aspects of the general subject have been reviewed by Nyborg (1978; 1991), Rooney (1981), and ter Haar (1986). When sound interacts with an object, the temporal average of the force exerted on it (usually not zero) is called the *acoustic radiation force*. Theoretical expressions have been developed for the acoustic radiation force in various applications and are the basis for acoustic measurements, as well as the basis for analysis of biological effects of sound.

3.2.1 Application to Measurements of Acoustic Power

When a beam of ultrasound travels through a liquid, such as water, and impinges on an immersed object (the target) which absorbs all of the incident energy, the magnitude of the radiation force (F_{rad}) on the target is given by the simple expression:

$$F_{\text{rad}} = \frac{W}{c}, \quad (3.1)$$

where W is the total acoustic power incident on the target and c is the speed of sound in the liquid. Taking c to be $1,500 \text{ m s}^{-1}$ (the

speed of sound in water) and the power to be 1 W, one obtains 6.67×10^{-4} N or 667 μ N for F_{rad} , approximately equal to the weight of a 68 mg mass at Earth's surface. Equation 3.1 is a working equation for radiation balances used to measure the total power in a beam (Carson *et al.*, 1978). If the intensity (I) at the target is uniform over the cross-sectional area (S), the power (W), is the product IS . If the *acoustic radiation pressure* (p_{rad}) at the target is defined as the ratio F_{rad}/S , one obtains from Equation 3.1:

$$p_{\text{rad}} = \frac{I}{c}. \quad (3.2)$$

If S is 10^{-4} m² (1 cm²) and if, as before, the acoustic power is 1 W, one obtains 10^4 W m⁻² (1 W cm⁻²) for I and 6.67 Pa for p_{rad} .

3.2.2 Auditory Response to Pulsed Ultrasound

3.2.2.1 Electrical Response in the Cat Auditory System. Foster and Wiederhold (1978) found that electrical responses were elicited in the cat auditory system when the brain was exposed to pulsed ultrasound, and explained them in terms of acoustic radiation pressure. In their experiment, ultrasound was produced in the cat brain by means of a piezoelectric ceramic transducer (6 mm diameter) placed in intimate contact with the dura mater through a hole (10 mm diameter) in the skull. The ultrasound was transmitted in pulses of about 10 to 70 μ s duration, 5 MHz center frequency, and 10 Hz repetition frequency; the spatial-average temporal-average (SATA) intensity during a pulse at the transducer position was 3×10^5 W m⁻² (30 W cm⁻²).

The same investigators made recordings of cochlear microphonics and neural responses to the ultrasound pulses, as well as to audible tone pips, the latter being produced in air and presented to the eardrum. While the signal amplitudes generated in the cochlea by the ultrasound pulses were comparable to the background noise, reproducible patterns were obtained by averaging recorded data from many cycles. Features of the responses were very dependent on the pulse duration. Recordings produced with ultrasound pulses of given duration were similar to those produced by tone pips of the same duration, the pressure amplitude for the latter being about 2 mPa and the frequency between 5 and 10 kHz.

To explain these findings, the authors made the reasonable assumption that the repeated ultrasound pulses produced a second-order sound field in the brain with a broad spectrum whose

fundamental frequency was 10 Hz and which was superposed on the ultrasound field. This was expected, because the brain, a medium in which the 5 MHz ultrasound was rapidly attenuated (analogous to the absorbing target discussed in Section 3.2.1), was subjected to a steady force during each pulse. This force was distributed throughout the volume of tissue traversed by the ultrasound beam, its total value being given by F_{rad} in Equation 3.1. To maintain equilibrium during each pulse, this force was balanced by steady second-order stresses established in the tissue. These consisted partly of an increase of time-averaged pressure during the pulse, *i.e.*, the postulated radiation pressure, and partly of shearing stresses. During passage of the repeated pulses, the radiation pressure at any point varies with time, and the spatial distribution of this time-varying pressure constitutes an audio-frequency sound field superimposed on the ultrasound field. In this field, the radiation pressure at any point can be represented by a Fourier series with its fundamental at 10 Hz and a very large number of harmonics. For a series of rectangular pulses of height p_{rado} (the radiation pressure during the pulse at a given point in the medium), duration (τ) and repetition period (T), the amplitude (p_n) of the n th harmonic is:

$$p_n = \frac{2(-1)^n}{n\pi} \sin(n\pi\phi) p_{\text{rado}}, \quad (3.3)$$

where ϕ is the duty factor τ/T . The energy associated with each harmonic is proportional to p_n^2 and the authors found reasonable agreement with experimental findings by assuming the stimulus proportional to Σp_n^2 , where the lower limit of n is 1,000, corresponding to a frequency of 10 kHz; this corresponds to an assumption that the hearing system acts as a high-pass filter, passing frequencies above 10 kHz. Drawing inferences from experiments of von Bekeky (1960), the authors suggest that this behavior may result from skull resonances, the lowest of which is in the range of 10 kHz for the cat. According to this suggestion, the cochlear microphonics and neural responses caused by pulsed ultrasound are not produced directly by the audio-frequency, radiation-pressure sound field, but more indirectly through the influence of this field in exciting skull vibrations. The mechanisms are thus similar to those for hearing by bone conduction. This idea gains some support from other experiments in which Foster and Wiederhold (1978) found that the response to pulsed ultrasound was about the same, whether the transducer was applied to the skull or directly to the dura mater.

3.2.2.2 Human Sensing of Modulated Ultrasound Applied to the Middle Ear. Gavrilov and co-workers have conducted many studies

of the sensory response of animals, including human beings, to pulsed or modulated ultrasound (Gavrilov, 1984a; 1984b). These include studies in which modulated ultrasound was used to produce a sense of hearing in human subjects; typical results are shown in Figure 3.1 (Tsirulnikov *et al.*, 1988). In obtaining data of the kind seen in Figure 3.1, focused ultrasound of frequency in the range 0.4 to 4 MHz, sinusoidally modulated at frequencies in the audible range, was passed along a water path into the subject's head, with the beam directed at the middle ear. The plotted points show the lowest focal intensity (averaged over the focal area, measured in water) at which the subject senses the ultrasound, at various frequencies. In this set of data, the minimum value of this intensity, 1 W cm^{-2} , occurs at 500 Hz. The primary mechanism responsible for the sensation is believed to be time-varying radiation pressure acting on the middle ear.

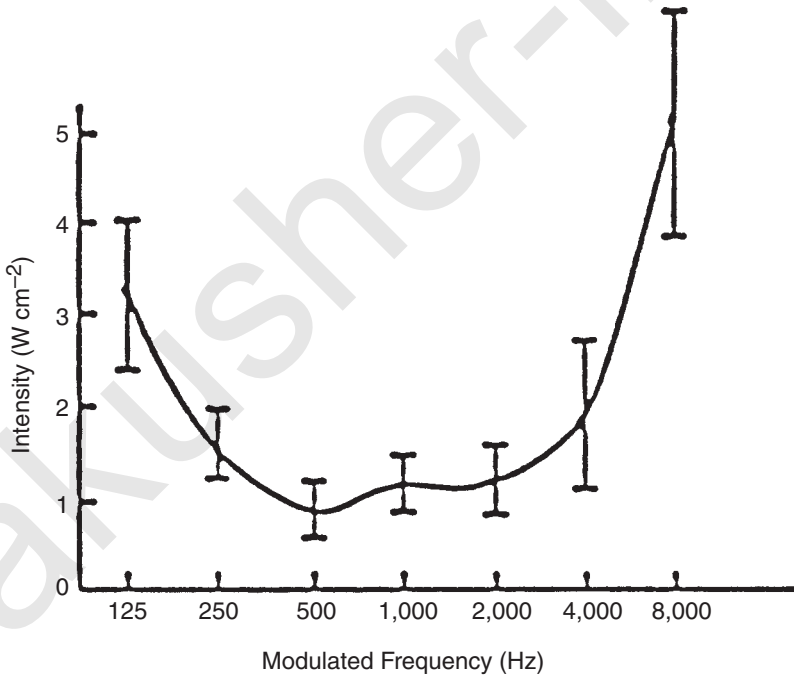


Fig. 3.1. Threshold of sensation for sinusoidally modulated ultrasound applied to the middle ear of persons with normal hearing. The intensity plotted is as measured in water; actual intensities at the middle ear are less because of attenuation (Tsirulnikov *et al.*, 1988).

3.2.2.3 Possibility of Hearing Pulsed Ultrasound by Bone Conduction. Data on thresholds for hearing by bone conduction, taken together with theory for acoustic radiation force, suggest that human beings would be able to sense repeated pulses of ultrasound from existing diagnostic equipment if these were focused on a sensitive area of the skull. Experiments have shown (ANSI, 1992) that when a vibrator is placed in contact with the mastoid, thus exerting localized force which varies sinusoidally with time, the force amplitude required for hearing is minimum at a frequency in the range of 2 to 3 kHz (Table 3.1). In this frequency range, the threshold force amplitude is about 31 dB (decibel) referred to 1 μN , *i.e.*, $10^{(31/20)}$ μN or 35 μN (see Table 3.1 footnote). If the vibrator were replaced by repeated pulses of diagnostic ultrasound focused on the mastoid, the radiation force would typically be applied in short pulses separated by large intervals in comparison with the pulse duration. Representing the force-versus-time relationship as a Fourier spectrum, the frequency (f_1) of the fundamental component would be the pulse repetition frequency (*PRF*). If the latter is in the vicinity of 3 kHz, one would expect the hearing system to respond primarily to this frequency, and very little to harmonics with frequencies of 6 kHz and higher (von Bekesy, 1960).

From Fourier analysis for repeated rectangular pulses, the amplitude of the fundamental (F_1) is equal to $2\phi F_p$, where F_p is the force applied during each pulse and ϕ the duty factor. If the repetition

TABLE 3.1—Selected thresholds of the force amplitude (in decibels)^a referred to 1 μN , for hearing a sinusoidally varying force applied to the mastoid bone.^b

Frequency (Hz)	Threshold (dB)
250	67.0
400	61.0
630	52.5
800	47.0
1,000	42.5
1,500	36.5
2,000	31.0
3,000	30.0
4,000	35.5

^aThe force amplitude (F) in decibels referred to 1 μN is defined as $20 \log_{10} F$ when F is expressed in micronewtons. A decibel ratio of X corresponds to $F = 10^{X/20}$.

^bANSI (1992).

frequency is 3 kHz, results (ANSI, 1992) show that an auditory sensation would be produced when F_1 is as small as $32 \mu\text{N}$, the corresponding force (F_p) (in micronewtons) being $16/\phi$. Bone is highly absorbent (NCRP, 1992) so, for purposes of a rough estimate, the bone may be considered to be a perfect absorber and use made of Equation 3.1. Taking c to be $1,500 \text{ m s}^{-1}$ and setting F_{rad} equal to $16/\phi \mu\text{N}$, one obtains $0.024/\phi$ for the power in watts needed during each pulse to cause an auditory sensation. Multiplying by ϕ to obtain the corresponding time-averaged power, one finds the latter to be 24 mW , well within the range of existing Doppler equipment. This reasoning suggests that ultrasound from existing diagnostic equipment might, when focused on a sensitive part of the human skull (such as the mastoid bone), produce a sensation of hearing. However, this possibility has not been confirmed experimentally.

3.2.2.4 Audible Sound Produced In Utero by Ultrasound Scanning. Arulkumaran *et al.* (1991) reported studies involving patients scheduled for induction of labor. In one such patient, a hydrophone (apparently uncalibrated) was introduced into the uterine cavity after rupture of membranes, and placed near the fetal ear. When the beam of a commercial ultrasound scanner imaged the hydrophone, a clicking noise was heard from a receiver connected to the hydrophone. An oscillographic display of the electrical signal showed a 10 Hz repetition frequency, equal to the framing rate of the scanner. The authors suggest that the sound resulted from modulated acoustic radiation pressure generated by passage of the ultrasound beam through absorbing maternal tissue. They further suggest that ultrasound scanning of the fetal head might generate sound within the head which would be audible to the fetus.

Suggestions that ultrasonic scanning can be sensed by the human fetus [which had been tested in earlier studies briefly reviewed in Section 5.6.4 of NCRP (1983)] appear to be supported in results reported recently by Fatemi *et al.* (2001). The authors investigated a group of nine normal pregnancies and healthy fetuses at gestational ages 25 to 40 weeks. In each experiment the fetus was exposed to ultrasound at the focus of a 2 MHz commercial ultrasound scanner, either pulsed or CW, SPTA intensity being about 280 mW cm^{-2} . During each exposure, a fetal monitor recorded whether movement occurred or not. Results showed that the fetuses moved more often when exposed to pulsed ultrasound than when exposed to CW ultrasound of the same intensity, or when no ultrasound was applied. The results were attributed to fetal sensing of the audio-frequency sound field associated with modulated acoustic radiation pressure produced by incidence of pulsed ultrasound on bones of the fetal head.

3.2.2.5 Auditory Phenomena During Insonation of the Basilar Artery. Magee and Davies (1993) made observations on 15

volunteers, in which the basilar artery was examined with 2 MHz Doppler ultrasound. The acoustic path was through the *foramen magnum* and thus did not include transmission through bone. For 10 of the volunteers a commercial device was used, for which the SPTA intensity (measured in water) was varied from 50 to 435 mW cm⁻², *PRF* being automatically varied simultaneously. Each of these 10 subjects experienced high-pitched tones during the examination; the tones being described as noises similar to loud, marked tinnitus. The effect was highly directional and varied from subject to subject. The noise was not affected by directing the beam at the cochlea. The other five subjects were examined with equipment which allowed the relevant parameters to be varied independently. It was found that increasing SPTA intensity (from 0 to 500 mW cm⁻²) caused the perceived loudness to increase, increasing *PRF* (from 500 Hz to 10 kHz) increased the pitch, and changing the pulse duration (from 2 to 10 μs) had no effect. The authors did not identify a specific mechanism, but considered acoustic radiation pressure as one of several possibilities.

3.2.3 *Reversible Modification of Membrane Potential by Ultrasound Bursts*

Mihran *et al.* (1990) applied focused ultrasound *in vitro* to whole sciatic nerves from frogs of the species *Rana pipiens*, and observed changes which they attributed to localized radiation force. Frequencies of 2 to 7 MHz, a burst duration of 0.5 ms, and focal diameters (half-power widths) from 1 to 3 mm were used. The intensity during the burst varied from 100 to 800 W cm⁻². Each nerve was excited electrically at various times after a single burst of ultrasound had been applied to the nerve, and compound action potentials (CAPs) were observed. It was found that the ultrasound usually produced either of two types of response from a given nerve: an early-suppression type in which CAP was suppressed or an early-enhancement type in which it was enhanced. For either type the lifetime of the modification was short, less than 50 ms.

The temperature rise produced during the short ultrasound pulse was estimated to be of the order of 0.1 °C or less. While the rate of temperature rise was rather high, and some cavitation may have occurred, a test done using direct mechanical stimulation provides good evidence that the mechanism was neither thermal nor cavitational. In this test, effects on CAPs similar to those produced by an ultrasound burst were obtained by applying a mechanical impulse to the nerve with a transducer-driven glass stylus 3 mm in diameter.

Further evidence against thermal and cavitation mechanisms came from the finding that, using ultrasound bursts of a given intensity, the effect on CAPs was increased by decreasing the focal diameter. The authors conclude (1) that the changes in CAPs are produced by bursts of localized acoustic radiation force exerted on the nerve by the focused ultrasound and (2) that the force causes local stretching of the membrane, thus producing changes *via* stretch-activated channels of the kind investigated by Guharay and Sachs (1984) and others. Additional examples of brief and reversible modification of cellular excitability by short bursts of ultrasound are described by Mihran *et al.* (1996). Again, the action is apparently not a result of temperature elevation or cavitation; instead, it is attributed to membrane stretching produced by radiation force.

Other findings of reversible effects produced on nervous tissue by ultrasound were reported much earlier by Wulff *et al.* (1951). These investigators exposed ganglia excised from the crayfish ventral abdominal nerve cord to ultrasound of frequency 1 MHz and intensity 35 W cm^{-2} during time intervals up to about 40 s. They observed changes from the normal spike potentials which differed from changes that would have been expected from an increase in temperature. These changes recovered in a few seconds after the exposure and could be repeated. Measurements of the temperature rise under the conditions of the experiments indicated a maximal temperature rise of 1°C . The acoustical conditions differed considerably from those used by Mihran *et al.* (1990) and it is not known whether the same mechanisms were operative in the two situations. There was no evidence of cavitation, but its existence was not excluded.

3.2.4 *Tactile Perception of Pulsed Ultrasound*

Gavrilov *et al.* (1977a; 1977b) and Gavrilov (1984a; 1984b) reported that ultrasound focused on the skin produced sensations of touch, temperature and pain. In these studies the frequency range varied from 0.5 to 3 MHz and the temporally averaged intensity (spatially averaged over the focal area) from 400 to $7,500 \text{ W cm}^{-2}$. The ultrasound was delivered continuously or in pulses, singly or repetitively, with pulse durations from 0.01 to 5,000 ms. The temporal characteristics of tactile perception in the pulse-repetition-frequency range of 20 to 1,000 Hz have been studied by Sato (1961) and Verrillo (1962; 1963; 1965) using mechanical sources of vibration, while Moore (1968) employed electric fields to generate audio-frequency (3 Hz to 20 kHz) stresses on the skin. Dalecki *et al.* (1995a) exploited the properties of acoustic radiation force to study tactile response of the

human finger and upper forearm as functions of pulse-repetition-frequency (50 to 1,000 Hz) and pulse length (0.1 to 100 ms). The latter authors provide evidence that direct tactile perception of ultrasound by the skin is actually the response of its sensors to the radiation force exerted on the tissue by absorption of acoustic energy.

All approaches to the subject agree that maximum tactile sensitivity to force varying sinusoidally with time occurs at frequencies in the range of 100 to 200 Hz. For the finger, the 50 percent response levels for the amplitude are of the order of 0.5 mN. For single rectangular pulses of force, 1 to 100 ms in duration, the threshold forces are greater by an order of magnitude. Comparison of perception thresholds with and without a reflecting material over the tissue are consistent with the hypothesis that the tactile sensation experienced when tissue is exposed to ultrasound results primarily from its response to the radiation force associated with transfer of momentum from the sound field to the tissue medium (Dalecki *et al.*, 1995a). A similar conclusion was reached by Gavrillov *et al.* (1996) from studies of the tactile response to focused ultrasound applied to the human hand.

3.2.5 Acoustic Radiation Force Applied to the Eye

Equation 3.1 applies when a beam impinges on a totally absorbent object. The radiation force on an object with a perfectly reflecting plane surface on which the ultrasound is incident perpendicularly is given by $2Wc^{-1}$, twice the value in Equation 3.1. When ultrasound is focused on the surface of adult bone or lung, most of the energy is absorbed or diffusely scattered, and the radiation force on the surface of incidence is of the order of Wc^{-1} . However, the radiation force on an individual soft-tissue layer is much less, since only a relatively small fraction of the acoustic energy is reflected or absorbed by the layer. Nevertheless, it can sometimes be biologically significant, if the beam is focused and its acoustic power concentrated in a small area. For example, Purnell *et al.* (1964a; 1964b) applied radiation force to the retinas of rabbit eyes by means of focused 7 MHz ultrasound, and found that detached retinas could be retrodisplaced by this means. They also found that the initial application of focused ultrasound to a retina caused reversible blanching in a small area. Lizzi *et al.* (1978) extended this work, using a beam of 9 MHz ultrasound, focused to an area 0.4 mm in diameter in the chorioretinal region. The energy was delivered CW or in bursts (pulses of long duration) 0.1 s in duration at different values of *PRF* from 1 to

8 Hz. The lesions were considered to be of thermal origin. Figure 3.2 shows the SATA intensity (temporal-average, averaged over the cross-sectional area) threshold for lesion production with 50 percent probability as a function of total exposure duration (including both “on” and “off” time) for CW and pulsed conditions.

Assuming the lesions are solely a result of temperature elevation, and that the time-averaged rate of heat generation is proportional to the time-averaged intensity, one might expect the SATA intensity threshold to be about the same for CW and all the pulsed modes. Instead, for the longer exposure durations, *e.g.*, 10 s, the threshold is greatly reduced when *PRF* is decreased from 8 to 1 Hz. The authors attribute this *PRF* effect to blood flow interruptions produced by each burst at the lower values of *PRF*. These interruptions reduce the perfusion and produce a higher rise in temperature. One reason the interruptions are more effective, for a given SATA intensity, when *PRF* is 1 Hz is that the intensity during the 0.1 s burst is eight times greater than when *PRF* is 8 Hz. According to Equation 3.2, the radiation force applied during each burst is then eight times greater for the 1 Hz than for the 8 Hz *PRF*. Another possible contribution to *PRF* effects seen in Figure 3.2 is increased nonlinear heating

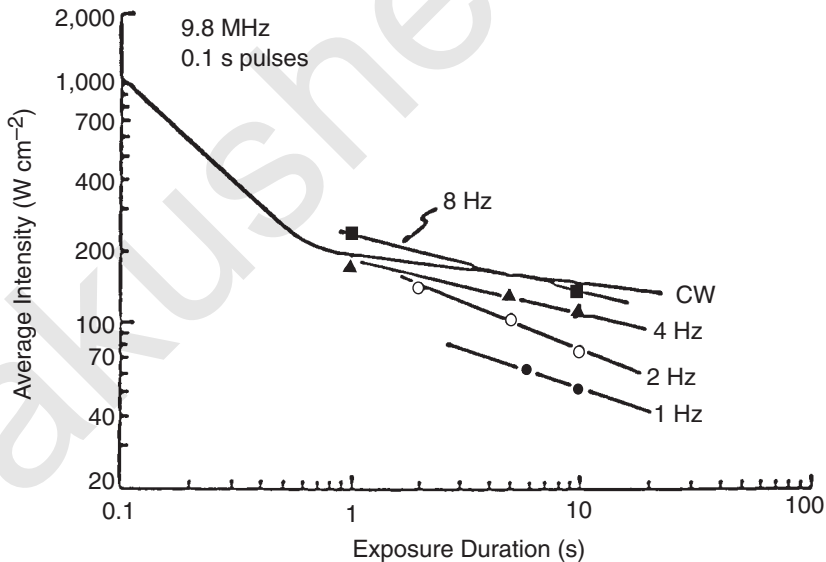


Fig. 3.2. Threshold values of the SATA intensity for production of chorioretinal lesions versus total exposure time for CW ultrasound and for pulsed ultrasound with indicated values of *PRF* (Lizzi *et al.*, 1981).

associated with the high intensities that exist during the bursts at the lower values of *PRF* (NCRP, 1992).

3.2.6 *Effects of Acoustic Radiation Forces on the Heart*

High intensity pulsed ultrasound in the frequency range of 1 to 4 MHz has been shown to change the performance of the frog heart *in vivo* (Dalecki *et al.*, 1993a). Threshold levels for these effects occurred at acoustic pressure amplitudes of the order of 10 MPa. Two qualitatively different effects were observed. Their occurrence depended upon the phase of the heart cycle when the pulse arrived. It appeared that the physical mechanisms responsible for the two effects were different and neither could be explained by the ultrasonic heating of the heart muscle (Dalecki *et al.*, 1993b). If the pulse of ultrasound arrives when the heart is relaxed (late diastole), it may cause premature ventricular contraction. This phenomenon does not appear to be driven by radiation forces and is discussed in greater detail in Section 8.

If the acoustic pulse coincides with maximum activity of the heart muscle (systole), the pulse causes either a reduction in the strength of contraction, as measured by the aortic pressure, or an increase in the rate of relaxation of the heart muscle. This phenomenon can be demonstrated either by direct exposure of the heart muscle to the ultrasound field, or by covering the heart with acoustically reflecting material prior to ultrasound exposure (Dalecki *et al.*, 1997a). The reflector transmits radiation force to the heart tissue, but eliminates any direct interaction of the sound with the heart and therefore excludes heating or cavitation as contributing mechanisms. The reflector technique was like that used in studies of the response of nerves to radiation forces (Sections 3.2.3 and 3.2.4). There are marked similarities in the response of neural and cardiac tissues. Threshold levels are comparable; relatively long pulses, compared to those used in diagnostic ultrasound, are required to produce these responses. With cardiac tissues, there is rapid increase in the effectiveness of the ultrasound with an increase in pulse length in the range from 1 to 10 ms. The effect was not observed in the frog heart under the most extreme exposure conditions used in modern Doppler ultrasound devices (Dalecki *et al.*, 1997a). Other studies of cardiac performance as affected by ultrasound are discussed in Section 3.4.3.

3.2.7 *Acoustic Radiation Forces and Torques on Small Particles*

Sections 3.2.2 through 3.2.6 address situations in which acoustic radiation force is produced by a beam of ultrasound traversing a

tissue volume whose dimensions lateral to the beam direction are larger than the acoustic wavelength (λ). For these situations, the relationships in Equations 3.1 and 3.2 are found to be useful. For the situations in this Section, the objects with which the ultrasound interacts are biological cells or other particles surrounded by fluid where the particle dimensions are much less than λ . Here, the applicable relationships are very different from those in Equations 3.1 and 3.2. The acoustic force exerted by an ultrasound field on a small particle surrounded by liquid depends on the properties of the particle, the liquid and the local ultrasound field. Because of these forces, exposure of a cell suspension to ultrasound may cause redistribution of the cells, including aggregation. Acoustic radiation torque may cause re-orientation or spinning of the particles. Examples of these phenomena have been observed in blood vessels *in vivo*, and have been employed in the automated processing of cells.

According to an equation (Gorkov, 1962; Nyborg, 1978; 1991) which applies rather generally to small particles (*i.e.*, those with dimensions small compared to the acoustic wavelength), the acoustic radiation force on a sphere of volume (v) and density (ρ_s) in a liquid of density (ρ_0) is:

$$F_{\text{rad}} = vD_p \nabla \langle E_k \rangle - v(1 - \beta_r) \nabla \langle E_p \rangle, \quad (3.4)$$

where ∇ is the gradient operator; β_r is the ratio of the compressibility of the particle to that of the surrounding medium; $\langle E_k \rangle$ and $\langle E_p \rangle$ are the time-averaged densities of the kinetic energy and potential energy, respectively; and D_p is defined by:

$$D_p = \frac{3(\rho_s - \rho_0)}{2\rho_s + \rho_0}. \quad (3.5)$$

More general expressions, which take viscosity and thermal conductivity into account, have been published by Doinikov (1996; 1997a; 1997b; 1997c).

An important application of equations such as Equation 3.4 is the determination of the force on biological cells in a stationary wave. There, $\nabla \langle E_p \rangle$ is equal and opposite to $\nabla \langle E_k \rangle$ so that F_{rad} can be written as $C\nabla \langle E_k \rangle$, where C is a constant equal to $v(D_p + 1 - \beta_r)$. If the cells are more dense and less compressible than the surrounding fluid, as is usually true for cells in saline solutions or in body fluids, then C is positive and the radiation force is in the direction of $\nabla \langle E_k \rangle$. Because the kinetic energy density (E_k) and the potential energy density (E_p) are proportional to the squares of the velocity amplitude and pressure amplitude, respectively, it follows that cells in saline solutions will usually move toward velocity-amplitude maxima and away from pressure-amplitude maxima. Experiments with cell

suspensions exposed to standing waves support the conclusion that in uniform planar fields, cells collect in bands one-half wavelength apart. However, in nonplanar waves the distribution is more complex (Weiser *et al.*, 1984; Whitworth and Coakley, 1992).

Techniques employing acoustic radiation forces on small objects are finding applications in biotechnology. Ultrasonic fields are used to separate, concentrate and/or transport cells and other biological particles (Allman and Coakley, 1994; Bardsley *et al.*, 1989; Benes *et al.*, 1993; Grundy *et al.*, 1995; Hawkes and Coakley, 1996; Thomas and Coakley, 1996; Trampler *et al.*, 1993; Weiser and Apfel, 1982; Whitworth *et al.*, 1991).

Separation of cells into bands has also been observed *in vivo*. Observations of small blood vessels during the application of ultrasound, under special conditions where stationary waves were established, have shown that a series of evenly spaced clear regions may appear in an otherwise opaque interior of the vessel (see Figure 3.3).

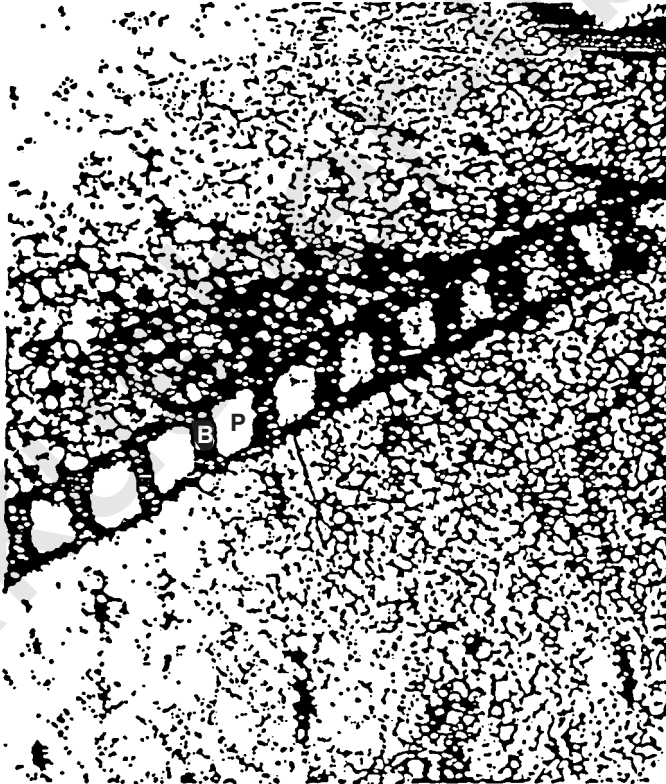


Fig. 3.3. Banding of red cells in a blood vessel of chick embryo during exposure to ultrasound (Dyson *et al.*, 1971).

Between the clear spaces are bands of packed red cells, the distance between band centers being about a half wavelength. When the ultrasound is turned off, the cells typically disperse and blood flow continues normally. A pressure amplitude of about 0.2 MPa, corresponding to a traveling-plane-wave intensity of 1 W cm^{-2} , was found sufficient to produce the banding in vessels where the blood is moving slowly (Dyson *et al.*, 1971; 1974). Such intensities are commonly produced in therapy devices, and are sometimes encountered in the focal regions of beams used in Doppler techniques; however, in pulsed Doppler, standing waves exist only in very small regions (several wavelengths in extent along the propagation path) when oppositely directed pulses are superposed. Reflections leading to standing waves can occur at interfaces with bone or with gas-filled spaces. The possibility of adverse effects from the banding can be avoided or reduced by minimizing the time during which the beam is maintained in a single location.

Equation 3.4 provides an explanation for the attraction of particles to a vibrating bubble, a phenomenon discussed in Section 4.3.3. The scattered field from a small spherically vibrating bubble is essentially that from a monopole; near the bubble, E_k dominates over E_p . Since $\nabla\langle E_k \rangle$ is directed toward the bubble, so is F_{rad} , when D_p is positive.

A related application of Equation 3.4 is the determination of the force between two particles in a sound field. This situation is somewhat more complex than the bubble-particle interaction since the scattered field of a particle such as a biological cell (whose compressibility is much less than that of a bubble) is a combination of monopole and dipole fields. The force of attraction between the particles is given by the equation:

$$F = F_0 (1 - 3 \cos^2 \theta). \quad (3.6)$$

Here, θ is the angle between the direction of the particle-particle axis and the direction of oscillatory motion in the surrounding fluid, while the factor (F_0) is given by:

$$F_0 = \frac{2 \pi (\rho - \rho_0)^2 u_0^2 a_1^3 a_2^3}{3 \rho_0 r^4}, \quad (3.7)$$

where ρ and ρ_0 are the densities of the particle material and the fluid, respectively; a_1 and a_2 are the radii of the two particles; r is the distance between centers of the spherical particles; and u_0 is the velocity amplitude of the oscillatory fluid motion (Nyborg, 1989).

It is seen from Equation 3.6 that the force F is repulsive when θ is zero (the direction of the particle-particle axis being then the same as that of the oscillatory fluid motion) and attractive when θ is $\pi/2$

(the two directions being at right angles). Therefore, particle doublets tend to form whose axes are perpendicular to the local acoustic particle velocity. Furthermore, these doublets may combine with other doublets or singlets to form chains, all with the same alignment. An example is seen in Figure 3.4, where particles in suspension form roughly parallel lines in response to an ultrasound field. The lines of particles seen here are analogous to the “pearl chains” observed in microwave fields (Herrick, 1958).

Another application of Equation 3.4 is to the “acoustic tweezers” developed by Wu (1991). Here, two opposing focused beams create an acoustic force field in which a small biological object, such as a frog egg, can be trapped in a small region where the two foci are superposed. The object can then be manipulated by using mechanical or electronic methods to translate the combined ultrasound field.

In general, a body suspended in a sonicated liquid will be subject, not only to acoustic radiation force, but also to an allied phenomenon, *acoustic radiation torque*. If the body is free to rotate, this torque may set it into steady spinning, or may cause it to seek a preferred orientation, depending on the degree of asymmetry possessed by the body. In a review of the subject, Nyborg (1978) discussed acoustical theory for different situations. For example, the acoustic radiation torque on a disc causes it to seek an orientation where its axis is

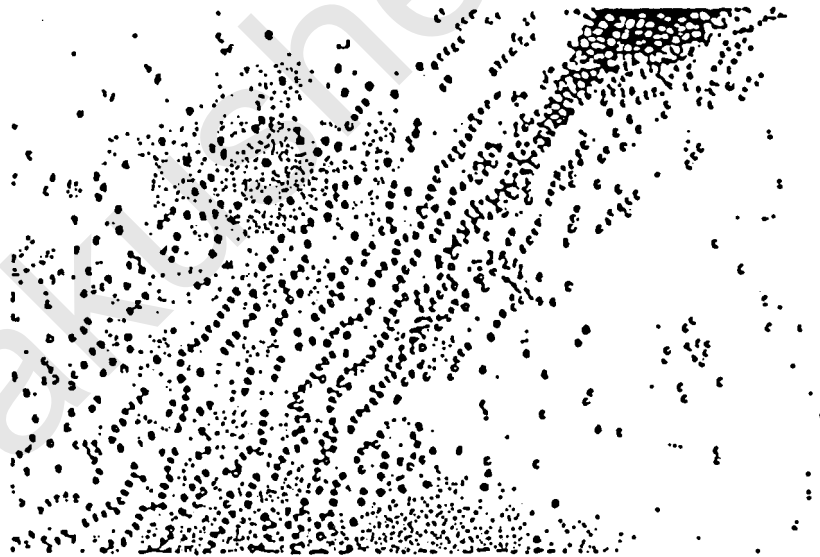


Fig. 3.4. Pearl chains formed from osmotically sphered erythrocytes in a 1 MHz ultrasound field (Nyborg *et al.*, 1975).

parallel to the oscillatory velocity in the local sound field. Trenchard (1987) showed that an optical method for assessing the alignment of platelets in an ultrasound field can be utilized in assessing platelet morphology. When a spherical particle, such as a nucleolus in a marine egg or a chloroplast in a plant cell, is exposed to a nonuniform ultrasound field, it may be set into a continuous spinning motion.

3.3 Acoustic Streaming and Microstreaming

3.3.1 Theory

An ultrasound field in a fluid usually gives rise to *acoustic streaming*, i.e., to a pattern of steady circulatory flow, which may be too slow to be observed at low values of the acoustic pressure, but becomes increasingly obvious as the pressure increases. As illustrated in Figure 3.5, a beam of ultrasound passing through the interior of a fluid-filled, cylindrically-symmetric vessel produces a flow along the axis of the beam with a return flow along the outer part of the vessel. This kind of motion is sometimes called “quartz wind.” The speed of the flow depends on the ratio of lateral dimensions for the beam and vessel, and is proportional to the total power in the beam, assuming linear propagation (Eckart, 1948). The flow results from the

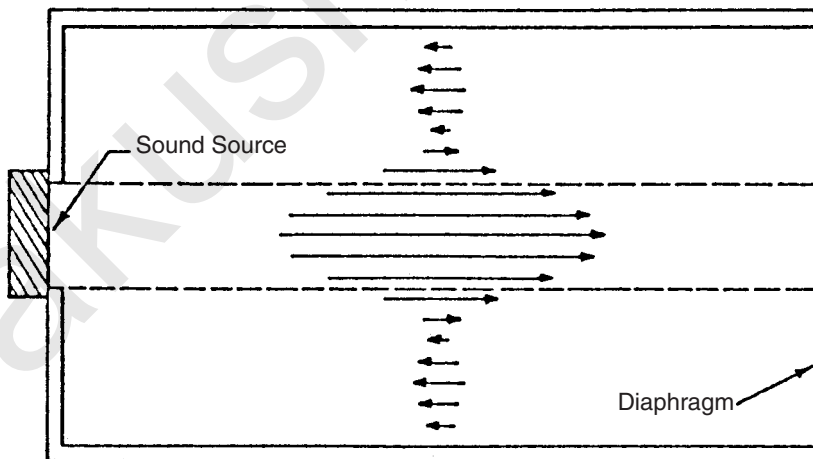


Fig. 3.5. Acoustic streaming in a fluid-filled space produced by a beam of ultrasound passing through a nonreflecting boundary (Liebermann, 1949).

radiation force per unit volume (F_v) exerted on the fluid traversed by the beam. In a homogeneous fluid, F_v is proportional to the local values of the absorption coefficient (α) and the intensity. For given values of other parameters, the streaming speed at a given point is proportional to the ratio α/η , where η is the coefficient of shear viscosity for the fluid (Nyborg, 1953; Piercy and Lamb, 1954). Under conditions of nonlinear propagation (NLP), as in the experiments described in Section 3.3.2, the theory must be modified; promising methods which have been developed for this purpose are described by Rudenko *et al.* (1996).

Eckart (1948) considered the simplified situation of an ultrasound beam of uniform radius (r_1) and intensity (I) propagating coaxially in a liquid-filled cylindrical tube of inner radius (r_0). His expression for the streaming velocity (U_0) along the axis can be written:

$$U_0 = \frac{\alpha W \phi(\beta)}{\pi \eta c}, \quad \phi(\beta) = \frac{\beta^2}{2} - \frac{1}{2} - \ln \beta, \quad (3.8)$$

where W is the total acoustic power ($\pi r_1^2 I$) in the beam, c is the speed of sound in the liquid, and β is the ratio r_1/r_0 . In water at 20 °C and under conditions of linear propagation, *i.e.*, at low amplitudes, the combination $\alpha/\pi \eta c$ has the value $4.7 \times 10^{-15} f^2$ in SI units, f being the frequency. For example, if f is 10^6 Hz, the power W is 1 W and β is 0.5, one obtains 0.0015 m s^{-1} for U_0 . The velocity (U) at different distances from the axis is considered to be always parallel to the axis, as indicated in Figure 3.5, though it reverses direction at a distance (r) which depends on the ratio (β). The maximal gradient $\partial U/\partial r$ occurs at the edge of the beam $r = r_1$ and has the value U_0/r_1 . If α is proportional to η , as is approximately true for some fluids, the speed is independent of α and η . However, α/η is increased, and the speed is enhanced if the absorption is primarily from causes other than shear viscosity, *e.g.*, molecular relaxation.

In some biological fluids, the ratio α/η is much greater than for water. For example, using data on attenuation in blood (NCRP, 1983) and in water (Herzfeld and Litovitz, 1959) as well as data on the viscosity of blood in the normal human body (Burton, 1965), one finds that α/η for blood is about 30 times that for water at 37 °C. In other fluids, such as urine or amniotic fluid, the value of α/η is comparable to that for water under linear conditions and, as for water, can become much larger under conditions of NLP (Carstensen *et al.*, 1980; Dalecki *et al.*, 1991a; NCRP, 1992). This can lead to correspondingly large increases in streaming velocity (Starritt *et al.*, 1989; 1991).

3.3.2 Acoustic Streaming Produced by Diagnostic Ultrasound

Acoustic streaming of the “quartz wind” type (Section 3.3.1) is likely to occur in any fluid-filled space through which an ultrasound beam passes, if the dimensions of the space are not too small. This means that a “stirring” action would be expected in some regions of a patient’s body (*e.g.*, the bladder) which are in the interrogation path during an ultrasound examination. Starritt *et al.* (1989) investigated the streaming produced in a water tank by ultrasound beams, including those from commercial diagnostic ultrasound equipment. The highest speeds occurred on the axis in the focal region and beyond, and were greatly enhanced under conditions of NLP. Commercial equipment produced the highest speeds (up to 14 cm s^{-1}) when operated in pulsed-Doppler modes, and the lowest (up to about 1 cm s^{-1}) in imaging modes. Hartley (1997) made studies of acoustic streaming in fluids at higher frequencies, using a pulsed-Doppler system, both to generate the flow in an open container and to measure its speed. With the use of 1 mm diameter disc transducers to produce ultrasound beams, each with an acoustic power of $\sim 4 \text{ mW}$, the maximal streaming speed produced in canine blood was 0.6 mm s^{-1} at a frequency of 10 MHz and 3 mm s^{-1} at 20 MHz.

Medical applications of acoustic streaming are under development. Stavros and Dennis (1993) have reported that simple (benign) breast cysts can be distinguished from complex ones by observations of ultrasound-produced flow. These authors explain that floating cholesterol crystals, visible in an ultrasound image, may develop in the internal fluid of some cysts; if these can be set into streaming motion by an ultrasound beam, the cyst will have been shown to be a simple one. Nightingale *et al.* (1995) describe a pilot study in which commercial color-Doppler equipment (Siemens SI 1200 Phased Array Ultrasound Scanner, modified to allow control of the pulse length) was used to obtain detailed information on streaming motions in cysts of volunteer patients. The center frequency and *PRF* were 6.75 MHz and 3.5 kHz, respectively; the pulse duration varied from 0.44 to 3.1 μs . Motion was observed in six out of seven of the cysts examined. Measured streaming speeds varied from 1 to 4 cm s^{-1} . Temporal average intensities at the focus, as measured in water, varied from 1.4 W cm^{-2} (the minimum for producing observable flow) to 4.4 W cm^{-2} ; the spatial-peak pulse-average (SPPA) intensity and peak rarefactional pressure were held constant at 470 W cm^{-2} and 3.3 MPa, respectively. The authors suggest that improved techniques for observing slower flow will allow use of lower intensities.

3.3.3 *Heat Transport by Acoustic Streaming*

It would be expected that when flow speeds of the magnitude discussed above (1 to 4 cm s^{-1}) occur in a body region, any existing gradients of temperature or of solute concentration would be altered. The possibilities here are seen in the findings of Wu *et al.* (1994) who measured the temperature rise produced by ultrasound under various conditions (see Section 12). In these studies a beam of ultrasound was transmitted into each of several phantoms designed to provide simplified models of clinical situations. CW 3.5 MHz ultrasound was generated by a concave focusing transducer for which the acoustic power output was 180 mW, the focal length was 5.1 cm, and the 6 dB beamwidth (in the focal plane) was 2 mm. The beam was transmitted through layers of water and/or TMM, and focused on a specimen of bone (human post-mortem femur). Measurements of the temperature rise at the bone surface were made with a small imbedded thermocouple after ultrasound exposures of 600 s. Of the various findings, those of special interest here are the differences observed when the transmission path from transducer to bone was either (1) entirely through water or (2) entirely through TMM. It was found that for a given acoustic power incident on the bone, the temperature rise under Condition 1 was less, by nearly a factor of 15, than under Condition 2. The cooling effect was attributed largely to convection of heat away from its source (the bone) by acoustic streaming; the latter was observed to occur in the water under Condition 1. The cooling effect was greatly reduced when the bone was covered by a TMM layer of 1 mm thickness.

3.3.4 *Cellular Inactivation by Heat and Shear*

Studies in which cell suspensions are irradiated with ultrasound at elevated temperatures (motivated by the possibility of therapeutic applications of ultrasonically produced hyperthermia) have shown that when the temperatures are in the hyperthermia range, *viz* 42 to 45 °C, the amount of cell killing that results from ultrasound exposure is greater than that which would be accredited to temperature rise alone (Li *et al.*, 1977; ter Haar *et al.*, 1980). In one investigation, heating to 43 °C reduced the surviving fraction to 10^{-1} in approximately 70 min, while simultaneously maintaining the same temperature and exposing the suspension to 3 MHz continuous unfocused ultrasound at a spatial-average intensity of 3 W cm^{-2} produced the same reduction in surviving fraction in approximately 30 min (ter Haar *et al.*, 1980).

An observed feature of these experiments with ultrasound is that the fluid medium is kept in motion by induced acoustic streaming, insuring that cells do not settle out of suspension (ter Haar *et al.*, 1980). The possibility was considered that the ultrasonically induced streaming might have a significant influence on the results. To test this hypothesis, the flow pattern produced by the sound in a typical ultrasound irradiation chamber was examined and the attending shear stresses estimated. Cell suspensions were then exposed to shear stresses produced by a nonacoustic method, while heated simultaneously in a water bath (Dunn, 1985). In estimating the stress produced by the streaming, use was made of the theory for “quartz-wind” streaming which is discussed briefly in Section 3.3.1. In applying Equation 3.8, the absorption coefficient (α) for the cell suspension was estimated to be $\sim 0.2 \text{ Np (nepers) cm}^{-1}$ by considering energy losses to arise primarily from finite amplitude absorption [see NCRP (1992); the conditions for Figure A.3 in Appendix A were comparable to those applicable to these experiments]. Also, the radii r_1 and r_0 were estimated to be 0.35 and 1.25 cm, respectively, and the average intensity over the beam area (πr_1^2) to be 3 W cm^{-2} (the total power W then being 1.15 W). Taking η to be $1.5 \times 10^{-3} \text{ Pa s}$ (1.5 cP) and c to be as for water, yields 2.77 m s^{-1} for U_0 and 1.2 Pa (12 dyn cm^{-2}) for the maximal stress.

This shear stress was simulated by experiments in which velocity gradients were established in Couette flow between two concentric cylinders, of which the outer cylinder was held fixed and the inner one rotated. Chinese hamster lung fibroblast V-79-379A cells, grown in suspension (Stratford and Adams, 1977), were employed. After treatment by heat and shear, the cells were resuspended, counted, serially diluted, plated in MEM (minimal essential medium) plus 15 percent fetal calf serum and incubated at 37°C in an atmosphere of 95 percent air plus five percent CO_2 for 7 d and the colonies stained with methylene blue. Colonies so identified were scored as survivors and the surviving fraction was calculated as the number of colonies counted divided by the initial number of cells plated. It was found that the “heat-and-shear” surviving-fraction curves appeared much the same as those for “heat-and-ultrasound.” For the indicated temperature and shear stress, the treatment time required for reducing the surviving fraction to 10^{-1} was about 50 min, compared to 100 min for the heat alone (Dunn, 1985). For the same temperature and the indicated ultrasound conditions the corresponding values were 30 and 70 min, respectively (ter Haar *et al.*, 1980). These findings suggest that a significant mechanism for ultrasonic interactions with biological cells in suspension at elevated temperatures is that of shear stress resulting from acoustic streaming.

It is unclear whether events similar to those just described will occur *in vivo* following exposure to ultrasound or to ultrasound and heat. Cellular structures *in vivo* are generally well anchored in fixed anatomical positions, with little opportunity to be displaced in response to mechanical forces, though fluid-like media may be forced to move past anchored structures, possibly producing shear stresses of significant magnitude. Also not revealed in these studies is the nature of the heat-and-ultrasound and heat-and-shear interactions with cell suspensions. It is not presently possible to determine whether simple additivity of these agents is involved or whether the interactions are more complicated, involving, for example, phase transitions in cellular membranes as considered by Krizan and Williams (1973; 1977).

It should be recognized that the shear stresses applicable to this study, and the associated treatment times, are orders of magnitude different than those involved in the acoustic-microstreaming situations discussed in Sections 3.3.7 through 3.3.9.

3.3.5 *Enhanced Agglutination and Aggregation by Acoustic Streaming*

Pohl *et al.* (1995) studied the rate of aggregation of human erythrocytes produced by exposure to CW ultrasound beams, focused at frequencies of 2 and 10 MHz, and unfocused at a frequency of 1.55 MHz. In preparing the test specimens, erythrocytes were removed from plasma by centrifugation, washed and resuspended in buffered saline at a predetermined hematocrit, usually three percent. Agglutination was induced by adding antisera to the cell suspension for specific cell groups, and aggregation by adding dextran, blood plasma, or alcian blue. The degree of aggregation/agglutination was determined with a Doppler device during the exposure and after the exposure (of fixed cells) with a Coulter counter. It was found, for example, that 10 min of exposure to unfocused ultrasound of frequency 1.55 MHz and pressure amplitude 106 kPa caused an increase of about 50 percent in the agglutination volume. The effect was reversible; the cells returned to normal in a few minutes after the exposure ceased.

The authors provided evidence that neither temperature rise nor cavitation was responsible for the observed enhancement and that, instead, the mechanism was acoustic streaming of the kind discussed in Section 3.3.1. For example, increase of pressure amplitude (p_0) caused the enhancement to increase with the square of p_0 in the range from about 100 to 200 kPa, as might be expected from theory

for the acoustic streaming. When p_0 is increased further, the enhancement peaks, then decreases. It was found that similar enhancement was obtained by introducing flow by nonacoustic means (using mechanical pumps) and that here, too, the enhancement was maximum for an optimal choice of flow speed. It was also found that increasing the ultrasound frequency (from 2 to 10 MHz) caused an increase in enhancement, as might be expected from theory for acoustic streaming. The authors proposed that flow increases the rate of agglutination by either or both of two means: (1) by altering ionic distributions external to the cells and (2) by increasing the collision rate between cells.

3.3.6 *Contraction of Myocardial Cells*

Salz *et al.* (1997) describe experiments in which isolated myocardial cells of Wistar rats were stimulated electrically while being exposed to CW ultrasound. When the frequency of the applied ultrasound was 10 MHz and the pressure amplitude 0.25 MPa, the ultrasound caused a significant (10 percent) decrease in the voltage threshold for producing sarcomere contractions but no significant change in their magnitude. When the frequency was 2.25 MHz and the pressure amplitude 0.45 MPa, there was no significant change in either the threshold or the magnitude. Evidence was given for ruling out cavitation or temperature rise as the cause of the threshold lowering produced by the 10 MHz ultrasound, and the effect was attributed to acoustic streaming of the suspending fluid.

3.3.7 *Theory: Small-Scale Acoustic Streaming (Microstreaming)*

Small-scale acoustic streaming associated with vibrating gas bubbles and gas bodies is discussed in Section 4.3. Here the subject is treated more generally, although only briefly. Relevant aspects of the topic have been reviewed by Nyborg (1965; 1978; 1991), Rooney (1981), and Miller (1987).

When a sound field exists in a fluid, acoustic boundary layers are set up near surfaces of walls or immersed objects. Near these surfaces the tangential component (u_{tan}) of the acoustic particle velocity is highly nonuniform. At a solid wall, where a nonslip condition applies, u_{tan} drops abruptly to zero in a short distance (Δ) called the “acoustic boundary thickness.” At the surface of a semi-solid object, such as a biological cell, u_{tan} is not zero, but differs from its value in the fluid. As before, an acoustic boundary layer of thickness Δ exists near the

surface in which there is a relatively high gradient of u_{\tan} . The quantity Δ depends on the viscosity coefficient (η) and density (ρ_0) of the fluid, as well as the frequency (f), as follows:

$$\Delta = \left(\frac{\eta}{\pi \rho_0 f} \right)^{1/2}. \quad (3.9)$$

For water at room temperature and at a frequency of 1 MHz, the boundary layer thickness is 0.56 μm and is thus comparable to a wavelength of visible light. It is the existence of boundary layers that is responsible for the generation of acoustic streaming near surfaces of objects when there is relative motion between the fluid and the object.

Theory for acoustic streaming has been developed for a number of basic situations. For summaries of the theoretical findings on this topic, the reader is referred to the reviews cited above. In the much-investigated topic of streaming near a fixed cylinder in an oscillating fluid (which presents essentially the same streaming situation as an oscillating cylinder in a quiescent fluid) it is found that the streaming flow is characterized by high velocity gradients in a thin boundary layer near the cylinder surface. If the cylinder diameter is not too small, and the oscillatory amplitude not too great, the acoustic-streaming boundary layer thickness is approximately equal to Δ , the boundary layer thickness for the oscillatory field, given in Equation 3.6. An approximate expression for the viscous stress (S) at the cylinder surface, associated with the acoustic streaming, is:

$$S = \frac{2 \pi \eta f \xi_0^2}{R_0 \Delta}, \quad (3.10)$$

here ξ_0 is the amplitude of the fluid oscillation relative to the cylinder and R_0 is the cylinder radius (Rooney, 1972).

3.3.8 *Experiments with Acoustic Microstreaming in Cells and in Cell Suspensions*

Experiments have been done using vibrating tungsten wires with which stresses of the order of 100 Pa are easily achieved. Exposing cells and large biomolecules to the action of a vibrating wire has elicited a variety of effects, including erythrocyte lysis, altered phagocytic index for leucocytes, clumping of platelets, and deactivation

of enzymes (Rooney, 1981; Williams, 1983). Figure 3.6 shows the streaming, sometimes called *microstreaming* because of its small scale, near the rounded tip of a 250 μm diameter wire, oscillating transversely at a frequency of 20 kHz. Small polystyrene spheres in the surrounding liquid followed flow lines similar to those which would be expected if the spheres were replaced by biological cells. The eddying brings suspended cells or molecules very near the vibrating tip for a brief exposure to the high viscous stress which exists in the boundary layer (Kashkooli, 1977; Rooney, 1981).

Similar motions can be produced in the interior of cells if the contents are sufficiently fluid. This comes about because microstreaming is generated in fluids adjacent to vibrating surfaces if the vibration pattern is sufficiently nonuniform. In their reviews, Williams (1983) and Miller (1987) describe experiments involving acoustic microstreaming produced in marine eggs, muscle fibers, and plant cells, leading to disturbances of various kinds.

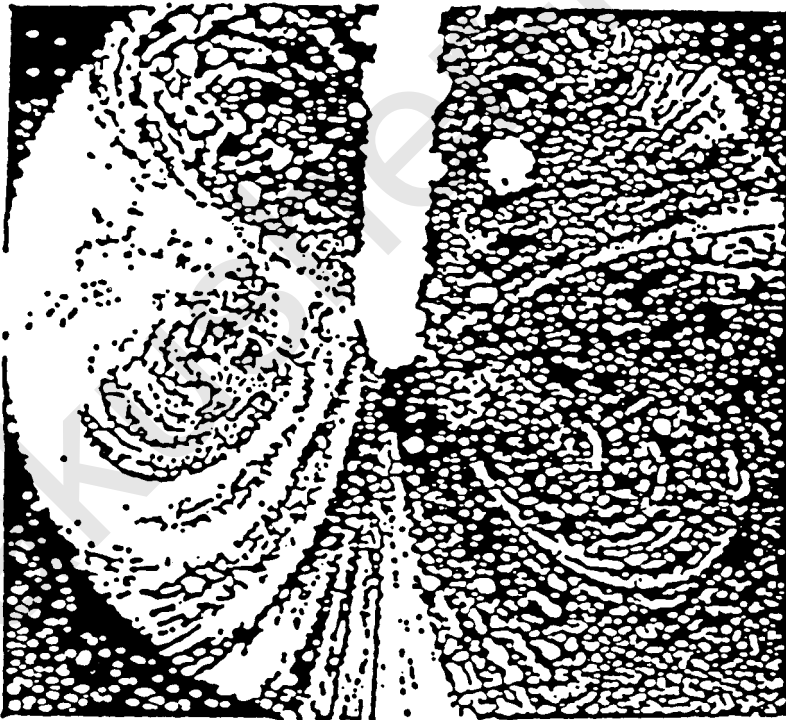


Fig. 3.6. Acoustic microstreaming near the tip of an oscillating wire (Rooney, 1981).

Figure 3.7 shows evenly spaced dark regions, representing accumulations of cytoplasm, within and near the surface of a large plant cell (*Hydrodictyon reticulatum*). These resulted when the plant specimen, immersed in water, was exposed to CW ultrasound at pressure amplitudes between 1 and 2 MPa in the absence of any obvious cavitation (Miller, 1986). It is believed that the ultrasound produced standing transverse waves in the cell wall and that these, in turn, generated microstreaming eddies, which shifted the cytoplasm into the observed pattern. The spacing between accumulations was found to be approximately equal to the calculated half-wavelength for transverse waves on a membrane under tension because of turgor pressure in the cell.

3.3.9 *In Vivo Experiments with Acoustic Microstreaming*

Motions similar to those produced in Figure 3.6 have also been observed within blood vessels of living animals. Figure 3.8 shows results of bringing the tip (about 25 μm in diameter) of a metal probe against the wall of a 200 μm diameter mouse mesenteric blood vessel

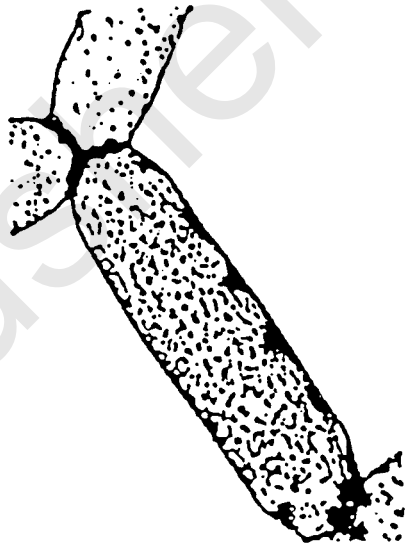


Fig. 3.7. Low magnification photomicrograph of a cell in a colony of *Hydrodictyon reticulatum*, showing evenly spaced striations corresponding to accumulations of cytoplasm produced by ultrasound. It is believed that the accumulations are produced by acoustic microstreaming associated with standing transverse waves in the cell wall (Miller, 1986).

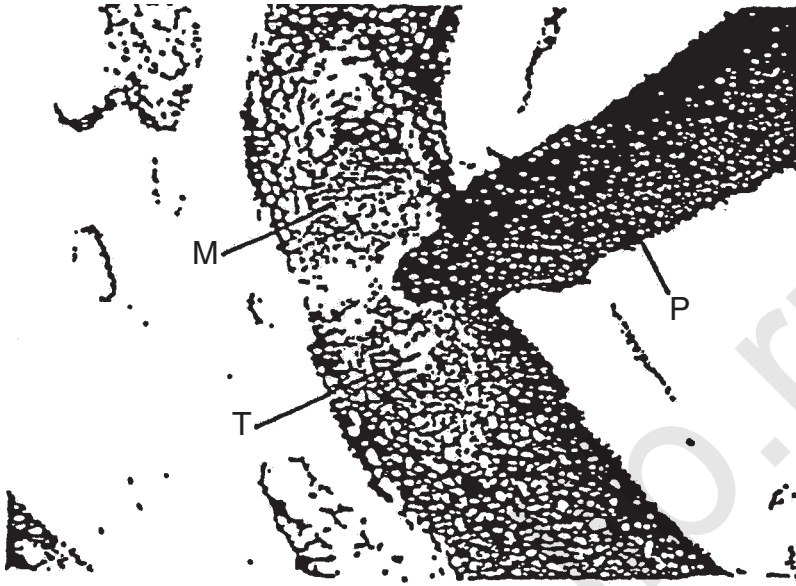


Fig. 3.8. Photomicrograph of the microstreaming vortices (M) produced within a mouse mesenteric blood vessel *in vivo* by the external application of a metal probe (P) oscillating at 85 kHz. A platelet thrombus (T) can be seen within one of the microstreaming vortices (Williams, 1985).

in vivo, and setting the probe into 85 kHz vibration with a displacement amplitude of about 5 μm . Vortices can be seen within the vessel, as well as a thrombus which evidently resulted from the shearing stresses (Williams, 1985).

Results of the kind shown in Figure 3.8 have also been obtained at frequencies in the megahertz range. For example, microstreaming flow has been seen in the semi-transparent fish *Xiphophorus maculatus* (Martin *et al.*, 1983). Microstreaming eddies were generated in blood vessels near cartilaginous rods in fish exposed at 0.78, 1.5 and 3 MHz. These eddies presumably arose from boundary layers at the surfaces of the rods resulting from oscillatory motion relative to the rods in the local ultrasound field.

In an analogous experiment, Frizzell *et al.* (1986) insonated blood vessels in surgically exposed mesentery of a living mouse at a frequency of 1 MHz, while observing the vessels by microscopy. Vigorous microstreaming was observed when a small external object (part of a micropipette) was pressed against the vessel wall during the exposure. The flow was similar to the acoustic streaming known to be established when oscillatory flow occurs relative to a fixed cylinder (the pipette, in this case) (see, *e.g.*, Nyborg, 1965). Thrombogenesis

resulted, apparently from platelet damage caused by viscous stresses associated with the microstreaming. The velocity amplitude in the ultrasound field was estimated to be comparable to that of a plane traveling wave with an intensity of a few watts per square centimeter; the viscous stress was estimated to be in the range 4 to 40 Pa.

3.4 Unidentified Nonthermal Mechanisms

3.4.1 Introduction

In numerous investigations, it has been reported that exposure of a biological system to ultrasound causes changes under conditions where nonthermal mechanisms are indicated, but where the actual mechanisms have not been identified specifically. There is little or no evidence of cavitation in any of these, but it usually is not possible to rule out the possibility of some form of cavitation activity.

3.4.2 Modification of Electrical Potentials and Currents

Wulff *et al.* (1951) exposed spinal cords of intact frogs to CW ultrasound of 1 MHz frequency and intensity 35 W cm^{-2} , and found that exposures of 7.3 s produced permanent paralysis of the hind legs. Additional studies of this phenomenon were done by Wall *et al.* (1951). Fry (1953) reviewed these and other findings, and presented detailed arguments for concluding that the ultrasonically induced changes were a result of neither temperature rise nor cavitation.

In a study involving isolated frog skin, Coble and Dunn (1976) observed a nonthermal ultrasound-induced effect under conditions where there was no evidence of cavitation activity. Here the specimen was supported in an adaptation of the Ussing chamber (Ussing and Zehran, 1951) which provided continuous perfusion of the specimen, and was exposed to 1 MHz ultrasound in the intensity range 1 to 100 W cm^{-2} . This study provided quantitative information about short-term reversible changes elicited from a biological specimen exhibiting membrane-like properties; the transmembrane potential of the abdominal skin of the frog *Rana pipiens* is determined by the sodium concentration outside and the potassium concentration inside (Ussing and Zehran, 1951). With standard Ringer's solution bathing both sides of the membrane, the membrane potential (MP) is sensitive to solution pH, temperature, and membrane metabolic state. The magnitude of the sodium-linked short-circuit current

(SCC) flowing when the MP is driven to zero is known, under a variety of conditions, to be equal to the sodium flux. MP and SCC were monitored continuously before, during and after the ultrasound exposure. An example of the findings is shown in Figure 3.9. The magnitudes of the ultrasonically induced changes in both parameters were found to be proportional to the acoustic intensity, though the MP decreased while the SCC increased. In addition to MP decrease and SCC increase during each pulse, the time courses of these two parameters were also substantially different in that MP reached its plateau quickly, within less than 0.5 s, and maintained that level during the exposure period, whereas SCC increased nearly linearly with time during the duration of the pulse. The authors explain that these findings eliminate thermal processes as the principal mechanism for the observed effects, since increasing the temperature (in the absence of ultrasound) causes both MP and SCC to increase at the rate of 6.9 percent per degree Celsius. Instead, they suggest that mass transport *via* microstreaming and radiation force altered the ion concentration gradients at the two skin surfaces. These results differ from those of an earlier study with frog skin (Lehmann and Biegler, 1954) in which MP changes produced by ultrasound, using longer exposure times and lower intensities, were readily duplicated by heating.

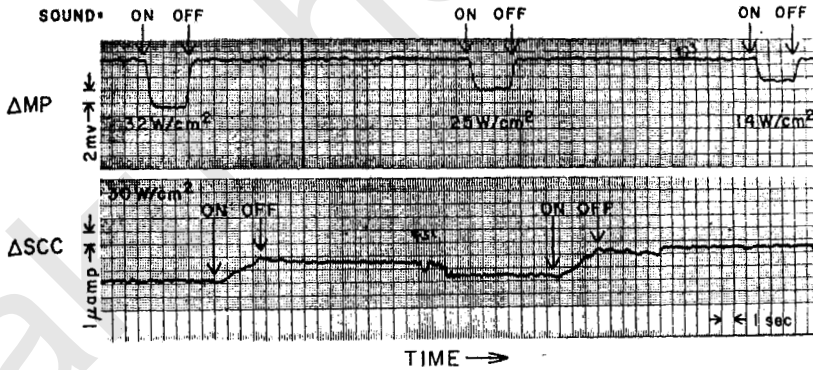


Fig. 3.9. Change of transmembrane potential (ΔMP) and short-circuit current (ΔSCC) for frog skin exposed to CW 1 MHz ultrasound. The figure shows a segment of a strip-chart recorder tape with biological responses superposed over the tape gridlines. The upper half shows the membrane-potential responses for three different intensities of 32, 25 and 14 W cm⁻², while the lower half shows two SCC responses for the same intensity of 30 W cm⁻² (see text for discussion) (Coble and Dunn, 1976).

In later studies, also with frog skin exposed to ultrasound, Dinno *et al.* (1989a) and Al-Karmi *et al.* (1994) observed effects which they attributed to microstreaming and other phenomena associated with cavitation.

3.4.3 *Effects on Cardiac Performance*

Several investigations have shown that ultrasound can affect the contractile characteristics of rat papillary muscle *in vitro*. Mortimer *et al.* (1978) showed that exposure of isolated papillary muscle to 1 MHz CW ultrasound at a spatially-averaged intensity of 2.4 W cm^{-2} , caused the resting tension of the muscle to decrease when the muscle had been stimulated to make three contractions per minute. In later studies of cat heart exposed *in vivo* (Mortimer *et al.*, 1986), it was found that application of 1 MHz CW ultrasound (with a spatially-averaged intensity of 2 W cm^{-2}) improved performance of the cat heart, by increasing the systemic and left ventricular blood pressure, when electrical stimulation was used to pace the heart at a faster rate than normal, but not otherwise. The changes were opposite to those observed with temperature increase alone. The specific mechanism is unknown.

In a study with isolated rat papillary muscle, Mortimer and Trollope (1987) found that 1 MHz pulsed ultrasound (pulse duration $10 \mu\text{s}$, repetition rate 1 kHz, SATA intensity 0.5 W cm^{-2}) caused a significant increase in the developed force during the period of exposure.

3.4.4 *Stimulation of Bone Repair*

Dyson and Brookes (1983) found that the repair of fibular fractures in adult female Wistar rats was accelerated and modified by treatment with ultrasound. Bilateral complete transverse fractures were made in fibulae of 70 rats; in each of these, one fracture was treated with ultrasound and the contralateral was sham-irradiated. The ultrasound was transmitted through degassed water in pulses of 2 ms duration repeated every 10 ms for 5 min. The SATA intensity was 100 mW cm^{-2} and the spatial-average pulse-average intensity was 500 mW cm^{-2} . Different groups of rats were treated at various times after injury and at a frequency of either 1.5 or 3 MHz.

The progress of repair was assessed by histology and microradiography of the fracture site at two, four and six weeks after injury. Under the best conditions, ultrasound produced improved repair in

over 75 percent of the animals. The treatment was most effective if given during the first two weeks after injury, rather than at later times, and 1.5 MHz was superior to 3 MHz in the results produced. The latter finding indicates, as suggested by the authors, that a nonthermal mechanism was involved in accelerating the repair, since the absorption coefficient in the tissue increases with frequency (NCRP, 1992). However, it is possible that the ultrasound caused a small temperature increase in the fracture region and that this, also, may have contributed to the improved repair.

In other studies of bone repair, the influence of temperature elevation seems to have been reduced further, if not eliminated. In one of a series of papers reporting accelerated healing of bone resulting from application of ultrasound, Pilla *et al.* (1990) describe experiments with New Zealand rabbits. In test animals, a cut was made in the tibular shaft of each hind limb. Transducers (about 4 cm² in area) capable of generating ultrasound at a frequency of 1.5 MHz were coupled to each limb. During experiments, one of the transducers was activated while the other was not, the latter serving as a contralateral sham control. A series of 200 μ s pulses of ultrasound at 1,000 μ s intervals was applied, the duty factor thus being 0.2. The intensity, averaged over the cross section of the beam and over the entire pulsing cycle, was reported as 30 mW cm⁻²; the corresponding spatially-averaged intensity, averaged over a pulse, would then be 150 mW cm⁻². Treatments of 20 min duration were administered daily for as many as 28 d.

Tests made on fibulae excised from animals sacrificed after 14 d of treatment showed that the torsional stiffness and breaking torque for treated fibulae were 1.7 times greater than for the sham-treated fibulae. The improvement factor decreased with time such that after 28 d the difference in mechanical strength between ultrasound- and sham-treated fibulae was not significant. Therefore the treatment apparently accelerates the healing process, but not the final strength of the repair.

Calculated estimates of the temperature rise in the experiments described above indicate that this was probably in the vicinity of 1 °C or less. At the low intensities used, inertial cavitation is not expected. The mechanisms responsible for the observed effects remain unknown.

Wang *et al.* (1994) obtained additional evidence that low-intensity pulsed ultrasound can accelerate fracture repair. In their investigations, bilateral closed femoral shaft fractures were made in 22 male Long-Evans rats. In 16 animals, ultrasound was applied to one limb for 15 min daily 10 times within the first 14 postoperative days. The treated limbs received a 200 μ s burst of 1.5 or 0.5 MHz sine waves

repeated at 1 kHz at a temporal average spatial-average intensity of 30 mW cm^{-2} ; all exposures were made in the near field. Contralateral limbs served as nontreated controls. Six remaining animals with fractures and six additional animals without fractures received sham ultrasound treatment to control for the effects of anaesthesia and handling. Fracture repair was evaluated by radiography, mechanical testing in torsion, and histology on postoperative day 21. Five of the 16 ultrasound-treated fractures showed obliteration of the fracture gap on radiographs, while none of the 28 controls did. The average maximum torque withstood by fractures treated with either frequency was 22 percent greater than that of contralateral controls ($p < 0.05$). The stiffness of treated fractures was greater than that of control fractures, but the difference was significant only in animals treated at a frequency of 1.5 MHz ($p < 0.02$). Sham treatment did not affect repair in the control group.

Several clinical trials report results which are consistent with those from the animal experiments discussed above. Heckman *et al.* (1994) examined 67 closed or Grade-1 open fractures of the tibial shaft in a prospective, randomized, double-blind evaluation of use of an ultrasound stimulating device as an adjunct to conventional treatment with a cast. Thirty-three fractures were treated with the active device and 34 with a placebo control device. At the end of the treatment, there was a statistically significant decrease in the time to clinical healing ($86 \pm 5.8 \text{ d}$ in the active-treatment group compared with $114 \pm 10.4 \text{ d}$ in the control group; $p = 0.01$) and also a significant decrease in the time to overall (clinical and radiographic) healing ($96 \pm 4.9 \text{ d}$ in the active-treatment group compared with $154 \pm 13.7 \text{ d}$ in the control group; $p = 0.0001$). The frequency of the ultrasound was 1.5 MHz delivered in bursts of duration $200 \mu\text{s}$ at a repetition frequency of 1 kHz. The SATA intensity was 30 mW cm^{-2} and the spatial-average intensity during each burst was 150 mW cm^{-2} .

In another clinical trial (Kristiansen *et al.*, 1997), ultrasound was applied in a similar way to healing of dorsally angulated fractures (negative volar angulation) of the distal aspect of the radius that had been treated with manipulation and a cast. Sixty patients (61 fractures) were enrolled in the study within 7 d after the fracture. The patients used either an active ultrasound device (30 fractures) or a placebo device (31 fractures) daily for 20 min at home for 10 weeks. The two types of devices were identical except that the placebo devices emitted no ultrasound energy. Clinical examination was performed and radiographs were made at 1, 2, 3, 4, 5, 6, 8, 10, 12 and 16 weeks after the fracture by each site investigator. The time to union was significantly shorter for the fractures that were treated with ultrasound than it was for those that were treated with the

placebo (mean and standard error, 61 ± 3 d compared with 98 ± 5 d; $p < 0.0001$). Each radiographic stage of healing also was significantly accelerated in the group that was treated with ultrasound as compared with that treated with the placebo. Compared with treatment with the placebo, treatment with ultrasound was associated with a significantly smaller loss of reduction (20 ± 6 percent compared with 43 ± 8 percent; $p < 0.01$), as determined by the degree of volar angulation, as well as with a significant decrease in the mean time until the loss of reduction ceased (12 ± 4 d compared with 25 ± 4 d; $p < 0.04$).

In a third similar clinical trial (Cook *et al.*, 1997), a similar low-intensity ultrasound device was investigated as an accelerator of cortical and cancellous bone fracture healing in smokers and nonsmokers. Statistically significant reductions in healing time for smokers and nonsmokers were observed for tibial and distal radius fractures treated with an active ultrasound device compared with a placebo control device. The healing time for a tibial fracture was reduced 41 percent in smokers and 26 percent in nonsmokers with the active ultrasound device. Similarly, distal radius fracture healing time was reduced by 51 percent in smokers and 34 percent in nonsmokers with the active device. Treatment with the active ultrasound device also substantially reduced the incidence of tibial delayed unions in smokers and nonsmokers.

3.4.5 Fetal Hemorrhage Caused by Lithotripsy

Considerable evidence has accumulated that ultrasound with acoustic pressures of the order of 1 MPa can produce rupture of blood vessels, leading to hemorrhage, in the vicinity of gas bodies, such as exist normally in adult mammalian lung or intestines (Section 8). A recent finding, for which an explanation has not yet been established, is that lithotripter pulses, with acoustic pressures less than 1 MPa, can rupture capillaries in late-term fetuses, where there are no obvious gas bodies (Dalecki *et al.*, 1997b). Hemorrhage occurred most often in tissues near developing bone, including the head, limbs and ribs. Temperature elevations were determined to be negligible. No hemorrhage was observed in other experiments, in which murine fetuses were exposed earlier in pregnancy, prior to development of skeletal modeling, even though much higher acoustic pressures were used. It was not determined in this work whether diagnostic levels of pulsed ultrasound can produce similar effects on the late-term murine fetus (see Section 8.2.8).

3.4.6 *Effects of Lithotripsy Under Noncavitating Conditions*

Recent publications describe *in vitro* experiments in which lithotripter shock waves produce damage under conditions where cavitation is believed to be absent, and temperature elevation is negligible. Howard and Sturtevant (1997) investigated damage to nitrocellulose membranes and demonstrated the importance of heterogeneity in the medium through which the shock waves are transmitted. Membranes suffered no damage when exposed while immersed in a homogeneous medium such as castor oil in the absence of cavitation, but showed tears and holes after exposure when small glass spheres, or muscle tissue, were dispersed in the medium through which the shock waves passed. The authors explained this by pointing out that the heterogeneities introduced into the path of the shock waves made the latter nonuniform so that they produce nonuniform displacement of the membrane and consequent shearing strain.

Williams *et al.* (1999) found that red cells were lysed after exposure to shock waves even when the cells were under very high hydrostatic pressure (more than 12 MPa) during exposure to prevent cavitation. They offer several possible mechanisms for their findings, including the shear mechanism proposed by Howard and Sturtevant (1997) and acoustic streaming.

3.5 Summary

There are important examples of biological changes produced by ultrasound in which it appears that neither cavitation nor thermal enhancement is involved, and in which the operative mechanism is acoustic radiation force, acoustic radiation torque, or acoustic streaming. Radiation force can be localized, as in applications where focused ultrasound is used to exert a force on part of the retina. By modulating the acoustic power, the radiation force can be made to vary with time. Localized pulsed radiation force applied to nerve can alter its response to electric excitation. When applied to the middle ear, time-varying radiation force can give rise to an auditory response; when applied to the skin it can elicit a tactile response; when applied to the heart it can affect cardiac function. Ultrasound fields can be designed to redistribute cells in suspension, or to manipulate small biological objects, by the action of radiation force.

Large-scale acoustic streaming can occur in any fluid-filled region through which a beam of ultrasound passes; it can affect transport of heat or matter, or affect cells. Microstreaming, of small scale, occurs near small obstacles to the sound field; in a blood vessel

exposed to ultrasound, the shearing stresses can lead to thrombogenesis if a small obstacle is present.

Ultrasound alters MPs and currents, and accelerates healing of bone fractures, under conditions where the intensities are much lower than those typical of ultrasound therapy as generally applied. The specific mechanism has not been identified.

akusher-lib.ru

4. Noninertial Cavitation; Gas-Body Activation

As pointed out in Section 2, a volume of free gas (or vapor) in a liquid medium, *i.e.*, a *bubble*, interacts strongly with an ultrasonic wave due to its high compressibility and low density. In this interaction, the bubble engages in acoustic cavitation, an activity with many aspects. Inertial cavitation, treated in Section 5, can occur if the bubble is of appropriate size and the pressure amplitude is sufficiently high.

This Section deals with various forms of noninertial cavitation; these can occur at lower amplitudes. Here the sites of activity are bodies of gas, which may be free or constrained. A free gas body (bubble) is mostly surrounded by liquid, while a constrained body may be partially contained in a pore or crevice in a solid or may be entirely surrounded by structures, as in biological tissues. As explained in Section 4.1.4, a small free gas bubble will dissolve quickly (unless the surrounding liquid is highly supersaturated with the gas), while constrained gas bodies may be stabilized against diffusion by surrounding structures. When gas bodies are activated by ultrasound, biological effects can be produced at relatively low pressure amplitudes through a variety of physical mechanisms. Basic equations governing noninertial cavitation are included in this Section for reference. These equations apply to the activation of either free or constrained gas bubbles.

4.1 Noninertial Cavitation Involving Free Bodies

4.1.1 Introduction

In its simplest form, noninertial cavitation can be treated theoretically by an approximation in which (free or constrained) gas bodies are considered to be simple harmonic oscillators. In much of Section 4, this approximation is made; it is assumed that the acoustic perturbations are relatively small. For a sound field generated by a source which vibrates sinusoidally in time with frequency (f), let A be

proportional to the source amplitude and consider some acoustic quantity, such as the acoustic pressure (p), at a point in the field. The quantity p is a function of space and time, as well as of the amplitude (A). It can be expressed in the form of a series as follows:

$$p = p_0 + p_1 + p_2 + \dots \quad (4.1)$$

Then the contributions p_0, p_1 and p_2 are called, respectively, the *zero-, first-, and second-order* contributions to p . The zero-order contribution is the static pressure which exists in the absence of sound, while the first-order contribution varies sinusoidally in time with frequency (f) and amplitude proportional to A . The second-order contribution consists of two parts: a time-independent part whose magnitude is proportional to A^2 and a second-harmonic part whose amplitude is also proportional to A^2 . (It will be recognized that the expressions given in Section 3 for radiation force, acoustic streaming, etc. are second-order approximations.) Higher-order terms contain contributions to the pressure whose typical magnitudes are proportional to A^3, A^4 , etc.

One can similarly define the contributions of various orders to the density, the particle velocity, and other field quantities. Equations which are valid to first order involve acoustic quantities of order "one" or "zero." To simplify notation in subsequent text, quantities of first order will be written without subscripts, as p, u , etc. For example, the first-order equation of motion with spherical symmetry for a nonviscous fluid is:

$$\partial p / \partial r = -\rho_0 \partial u / \partial t, \quad (4.2)$$

where ρ_0 is the zero-order approximation to the density and r is the distance from the center of symmetry, while p and u are first-order approximations to the pressure and the (radially directed) particle velocity, respectively. Thus, ρ_0 is the constant undisturbed density (independent of A) while p and u are each proportional to A .

As exemplified by Equation 4.2, an equation of first order is linear. The corresponding first-order (*i.e.*, linear) wave equation, for spherical symmetry, is:

$$\partial^2 p / \partial r^2 + (2/r)(\partial p / \partial r) = (\partial^2 p / \partial t^2) / c^2, \quad (4.3)$$

where c is the (zero-order approximation to the) speed of sound. A solution of Equation 4.3, representing an outgoing spherical wave, is (the real part of):

$$p = (B/r)^{j(\omega t - kr)}, \quad (4.4)$$

where ω is the angular frequency, equal to $2\pi f$, and f is the frequency; k is the propagation constant, given by ω/c or $2\pi/\lambda$, where λ is the

wavelength. By using Equations 4.2 and 4.4 the velocity (u) can be expressed in terms of the pressure (p):

$$\begin{aligned} u &= p(1 + jkr)/j\omega\rho_0r \\ u &= -jp/\omega\rho_0r \text{ for } kr < 1 \\ u &= p/\rho_0c \text{ for } kr > 1 \end{aligned} \quad (4.5)$$

It is seen from Equations 4.4 and 4.5 that when kr is small (*i.e.*, at points near the origin, such that $r \ll \lambda$) the velocity (u) and pressure (p) differ in phase by $\pi/2$; also, u is inversely proportional to r^2 . When this condition applies, the volume rate of fluid flow outward through any spherical surface of radius (r), centered at the origin, at any given time, is a constant equal to $4\pi r^2u$. Thus, in a region of small kr , the flow is as if the fluid were incompressible. For large kr (*i.e.*, at distances from the origin large compared to the wavelength) we see from the third of Equations 4.5 that p and u are in phase, and are related as in a plane traveling wave.

4.1.2 Radial Pulsation of a Spherical Gas Bubble

The bubble considered in Figure 4.1 is a body of gas surrounded by liquid. In the absence of sound the bubble is spherical with radius (R_0); it responds to a sound field by pulsating as a sphere whose radius (R) varies with time. Its equation of motion can be derived by considering the energy possessed by a "bubble system" consisting of the bubble itself plus that part of the surrounding medium which lies under its influence. The potential energy of the system comes

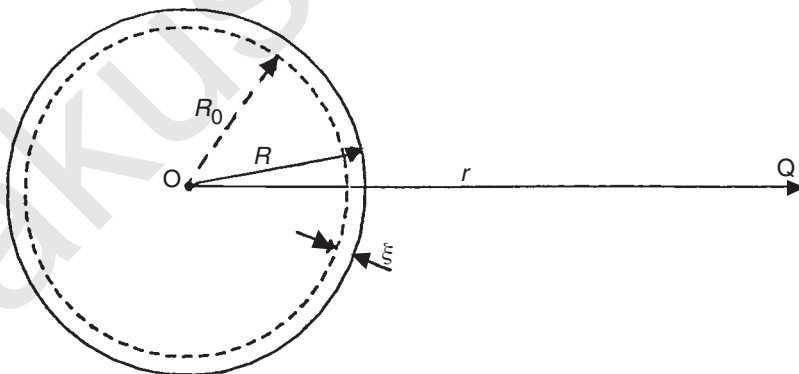


Fig. 4.1. A spherical gas bubble centered at O, with equilibrium radius (R_0) and instantaneous radius (R). The observer point Q is at a distance r from the center.

almost entirely from the compression or expansion of the gas in the bubble, and the change in curvature of the gas-liquid interface. An expression for the instantaneous potential energy E_p of the system can be obtained by considering the work done in a change of radius from R_0 to R , corresponding to a change of volume from V_0 to V , in somewhat the same way as the potential energy of a stretched spring is calculated. Here the “spring” comes partly from the gas and partly from the gas-liquid surface tension. A “restoring force” exists since an increase in R leads to a decrease of the pressure (p_i) inside the bubble. Let Γ be the polytropic index for the gas and let σ be the gas-liquid surface tension. Also let ξ be the increase in radius considered, *i.e.*:

$$\xi = R - R_0. \quad (4.6)$$

In a small increase of the radius (R) from R_0 to $R_0 + \xi$, the fractional increase in radius is ξ/R_0 and the fractional increase in volume is approximately $3 \xi/R_0$. At the new value of R the pressure is given for an ideal gas approximately by:

$$p_i = p_{i0} - 3 \Gamma p_{i0} \xi/R_0, \quad (4.7)$$

where p_{i0} , the initial value of the pressure in the gas, is given by:

$$p_{i0} = P_0 + 2 \sigma/R_0, \quad (4.8)$$

with P_0 the hydrostatic pressure. As R changes, the potential energy (E_p) of the bubble system changes, partly because of work done on the gas and partly because of work done through an increase of surface area. The change dE_p is equal to:

$$dE_p = (P_0 - p_i)dV + \sigma dA; \quad (4.9)$$

here, dV is the increase in volume and dA is the increase in area. Further, dV is equal to $4 \pi R^2 dR$ and dA is equal to $d(4 \pi R^2)$, *i.e.*, to $8 \pi R dR$. Noting that R is $R_0 + \xi$, and making use of Equations 4.7 and 4.8, one finds, approximately, that:

$$dE_p = k_s \xi dR, \quad (4.10)$$

where:

$$k_s = 12 \pi \Gamma P_0 R_0 + 8 \pi \sigma (3 \Gamma - 1). \quad (4.11)$$

In Equation 4.10 the coefficient of dR is valid to first order in ξ . Replacing ξ by $R - R_0$ and integrating from R_0 to R yields:

$$E_p = (1/2)k_s \xi^2, \quad (4.12)$$

an expression valid to second order. The constant k_s is an effective “spring constant” for the bubble system.

Since the density of the liquid outside the bubble is usually much greater than that of the gas inside it, the kinetic energy of the system lies primarily in the liquid. In a spherical shell of infinitesimal thickness (dr) and radius (r), the kinetic energy is equal to one-half the product of the mass $4 \pi \rho_0 r^2 dr$ and the square of the velocity. As is seen later, the most active bubbles are small, with radii much less than the wavelength (λ). In the region of interest outside the bubble, the velocity (u) is given approximately by the second of Equations 4.5 and thus, with p given by Equation 4.4, varies inversely with r^2 . Because $d\xi/dt$ is the velocity at the bubble surface, approximately at $r = R_0$, the velocity (u) can be written:

$$u = \frac{d\xi}{dt} \frac{R_0^2}{r^2}. \quad (4.13)$$

To obtain the kinetic energy in the liquid associated with the bubble motion, an integration of the kinetic energy for each differential volume element outside the bubble is taken from $r = R$ to infinite r . Since the integrand is significant only at small values of r , little error is incurred by considering u to be given by Equation 4.13 (even though this is incorrect at large r). The result for the total kinetic energy (E_k), valid to second order in $d\xi/dt$, can be written:

$$E_k = 1/2 m \left(\frac{d\xi}{dt} \right)^2, \quad (4.14)$$

where the *effective mass* (m) is given by:

$$m = 4 \pi \rho_0 R_0^3. \quad (4.15)$$

The quantity m is just three times the mass of liquid which would fill the bubble volume.

One can now proceed to write a governing equation for the bubble system based on energy principles. At any instant the total energy of the system is the sum of E_p and E_k . This sum changes with time, partly because energy is lost from the system through several mechanisms, and partly because energy is being added to the system by sound sources. It is assumed here that the energy lost can be represented (in a second-order approximation) by the term $b(d\xi/dt)^2$, where b is constant with respect to time; processes contributing to this term are discussed in Section 4.1.3.

Energy is added to the system at a rate equal to the product of $-dV/dt$, the rate of volume decrease, and the acoustic pressure $p_0 e^{j\omega t}$ applied to the bubble. The energy-based governing equation now becomes:

$$\frac{d(E_p + E_k)}{dt} + b \left(\frac{d\xi}{dt} \right)^2 = - \frac{dV}{dt} p_0 e^{j\omega t}. \quad (4.16)$$

Using expressions for E_p and E_k from Equations 4.12 and 4.14, and setting dV/dt equal (as a first approximation) to $4 \pi R_0^2 d\xi/dt$, one obtains:

$$m \frac{d^2 \xi}{dt^2} + b \frac{d\xi}{dt} + k_s \xi = -4 \pi R_0^2 p_0 e^{j\omega t}. \quad (4.17)$$

This linear differential equation is of a familiar type in physics and engineering. A solution is:

$$\xi = \xi_0 e^{j(\omega t + \beta)}, \quad (4.18)$$

where ξ_0 is the displacement amplitude of the bubble surface and β is the phase angle between the displacement and the acoustic pressure. In the following expressions, ξ_0 and β are related to other quantities:

$$\xi_0 = (4 \pi R_0^2 p_0 / k_s) \chi(\Omega, \delta), \quad (4.19)$$

where:

$$\chi(\Omega, \delta) = [(1 - \Omega^2)^2 + \Omega^2 \delta^2]^{-1/2}, \quad (4.20)$$

$$\beta = \arctan[\Omega \delta / (\Omega^2 - 1)], \quad (4.21)$$

$$\Omega = \omega / \omega_0, \quad (4.22)$$

$$\omega_0 = (k_s / m)^{1/2} = 2 \pi f_0, \quad (4.23)$$

$$\delta = b / m \omega_0 = \omega_0 b / k_s, \quad (4.24)$$

$$m = 4 \pi \rho_0 R_0^3, \quad (4.25)^2$$

$$k_s = 12 \pi \Gamma P_0 R_0 + 8 \pi \sigma (3 \Gamma - 1) \quad (4.26)^2$$

and in these expressions, f_0 is the resonance frequency of the bubble system and ω_0 the corresponding angular frequency; δ is the damping constant (see below). The branch of the arctangent is chosen for which β decreases from π to zero as Ω increases from zero to infinity; the displacement ξ is opposite in phase to the acoustic pressure at low frequencies (as would be expected) and is in phase at high frequencies. Some values of the bubble radius at the linear resonance

²These two equations, which are identical to Equations 4.15 and 4.11, respectively, are repeated here for clarity and convenience.

frequency are given in Table 4.1; in calculating these, the surface tension was assigned the value of 0.072 N m^{-1} and the polytropic index the value of 1.044. Features of the bubble resonance are seen in Figure 4.2.

4.1.3 The Damping Constant for a Spherical Bubble

If a small air bubble in liquid is set into oscillation by a sound field, and the sound is shut off, the bubble may continue to oscillate. However, its frequency of oscillation will be somewhat less than the resonance frequency, and the amplitude will quickly decrease. Specifically, the amplitude will drop by a factor of e , the base of the natural logarithms ($e \approx 2.718$) in a characteristic time (τ) given by:

$$\tau = 2 m/b = 2/\omega_0 \delta \quad (4.27)$$

provided that $\omega_0 \tau < 1$.

TABLE 4.1—*Ultrasonic characteristics of free bubbles and gas bodies from 1 to 10 MHz.*

Characteristics	Frequency (MHz)			
	1	3	5	10
Free spherical bubbles:				
Resonance diameter (μm)	6.4	2.4	1.6	0.96
Damping coefficient	0.13	0.19	0.23	0.31
Rectified diffusion threshold (kPa) ^a	10	40	80	220
Shell-encapsulated bubbles^b (12 nm shell):				
Resonance diameter (μm)	13	6	4.2	2.6
Damping coefficient	0.25	0.85	1.5	3
Gas-filled cylindrical micropores^c ($a = h$):				
Resonance diameter (μm)	5.8	2.7	1.9	1.2
Damping coefficient	0.08	0.12	0.14	0.17
Gas-filled channels with four walls^d:				
Resonance diameter (μm)	11.5	6	4.7	3.4
Damping coefficient	0.43	0.50	0.54	0.62

^a See Section 4.1.4.

^b Church (1988a).

^c See Section 4.2.3.

^d See Section 4.2.4.

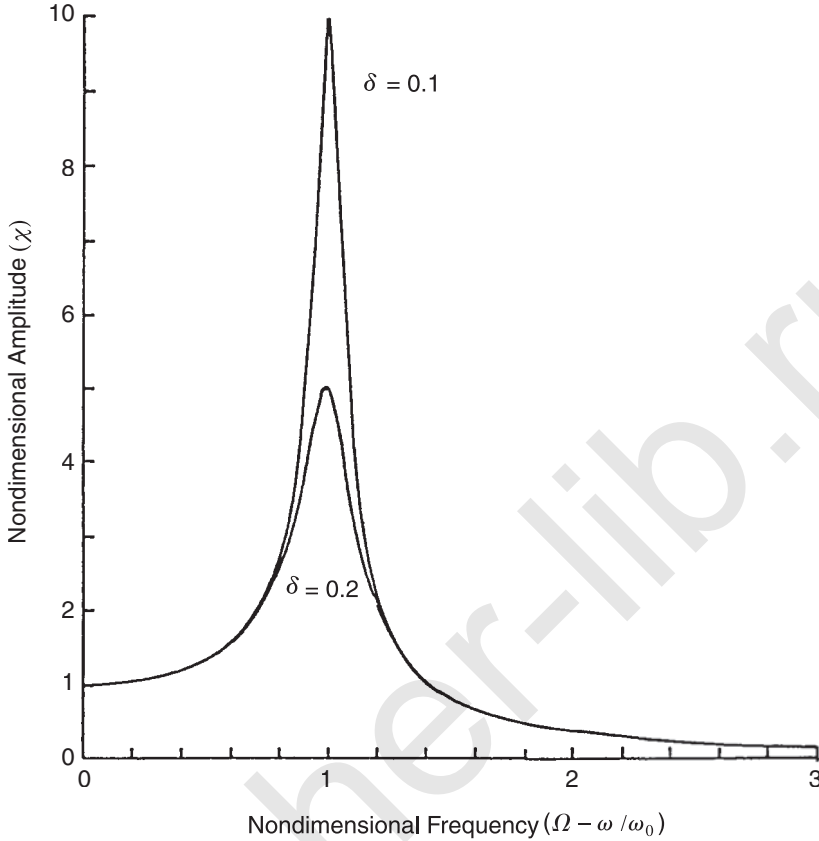


Fig. 4.2. Plots of the nondimensional amplitude (χ) versus the nondimensional frequency ($\Omega - \omega / \omega_0$) for two values of the damping constant (δ) (based on Equation 4.20).

Mechanisms for damping of the oscillations are fairly well known for spherical air bubbles in water, and for comparable situations. Most of the energy loss appears to be accounted for by considering the damping to be made up from three contributions indicated as follows:

$$\delta = \delta_{\text{rad}} + \delta_{\text{vis}} + \delta_{\text{th}}. \quad (4.28)$$

Here, δ_{rad} accounts for losses which occur because of sound radiation from the bubble, δ_{vis} for losses through viscous dissipation and δ_{th} for losses of thermodynamic origin.

In obtaining expressions for the contributions to δ , one calculates second-order quantities such as $\langle pu \rangle$, where p and u are quantities varying sinusoidally in time with angular frequency ω and $\langle \rangle$

indicates the time average over one or more complete cycles. It is convenient to use complex expressions for p and u , although the physical quantities represented are the real parts, which we designate as $\text{Re}(p)$ and $\text{Re}(u)$, respectively. In evaluating $\langle pu \rangle$, one can, of course, literally use real parts in carrying out the averaging. However, it is often expedient to use the following identity, which is easily verified. If p and u are complex quantities, each proportional to $e^{i\omega t}$, the following holds:

$$\langle \text{Re}(p) \times \text{Re}(u) \rangle = 1/2 \text{Re}(pu^*), \quad (4.29)$$

where u^* denotes the complex conjugate of u .

One of the contributions to δ is the radiation term δ_{rad} . As the bubble oscillates, it acts as the source of an outgoing spherical wave. The energy required to do this is lost from the bubble system and it is this loss which is accounted for by δ_{rad} . If $p(R)$ is the acoustic pressure in the liquid at the surface of the bubble, the time-averaged rate at which work is done by the bubble in generating the spherical wave is given by:

$$\langle \text{Work/time} \rangle = \langle 4 \pi R^2 \frac{d\xi}{dt} p(R) \rangle, \quad (4.30)$$

where $d\xi/dt$, as before, is the velocity of the bubble surface. The right hand side of Equation 4.30 is a nonlinear quantity, the product of three time-dependent variables: R , $d\xi/dt$, and p . Each of the latter variables can be represented as a sum of contributions of different order in the amplitude-parameter (A), as illustrated in Equation 4.1. It is sufficient to evaluate the right hand side of Equation 4.30 to second order, yielding a result in which R is replaced by R_0 while $d\xi/dt$ and $p(R)$ are first-order contributions.

In evaluating δ_{rad} , use can be made of the expression for an outgoing spherical wave in a nonviscous fluid, valid to first order, which was discussed in Section 4.1. At the bubble surface the first of Equations 4.5 is used, with $u = d\xi/dt$, $r = R$, and $p = p(R_0)$. The right hand side of Equation 4.30 can then be evaluated to second order and the result can be equated to $\langle b(d\xi/dt)^2 \rangle$ since, by Equation 4.16, $b(d\xi/dt)^2$ represents the rate of energy loss for the bubble system. An expression for b results. If δ_{rad} is then set equal to $b/m\omega_0$, as in Equation 4.24, one obtains:

$$\delta_{\text{rad}} = \omega^2 R_0 / \omega_0 c, \quad (4.31)$$

assuming $k^2 R_0^2 \ll 1$, since $R_0 \ll \lambda$ for conditions of interest.

Viscous dissipation contributes to the damping through the term δ_{vis} . When spherically symmetrical, radially directed flow $u(r)$ occurs in a Newtonian fluid, a field of stress is set up. Normal to any spherical surface of radius (r), centered at the origin, a tensile stress

exists, given by $2 \eta \partial u / \partial r$, where η is the coefficient of shear viscosity (Lamb, 1945). In the liquid near a small bubble vibrating as a pulsating sphere, the velocity is given by Equation 4.13. The rate at which the bubble does work against the stress is, in the time average, given by:

$$\langle \text{Work/time} \rangle = - \left\langle \left(4 \pi R^2 \frac{d\xi}{dt} \right) \left(2 \eta \frac{\partial u}{\partial R} \right) \right\rangle \quad (4.32)$$

Again, as in connection with Equation 4.30, a second-order approximation will suffice, in which R becomes R_0 while $d\xi/dt$ and u are first-order quantities. Setting the right hand side of Equation 4.32 equal to $\langle b(d\xi/dt)^2 \rangle$ yields an expression for b ; dividing this by $m \xi_0$ yields:

$$\delta_{\text{vis}} = 4 \eta / \rho_0 \omega_0 R_0^2. \quad (4.33)$$

The thermal contribution to the damping arises because of temperature changes which occur in the gas during the volume changes. Heat flows out of the bubble when the gas temperature is relatively high, and inward when the temperature is low. This “vibratory heat flow” would, by itself, produce a net flow of entropy into the bubble. It follows that a mean temperature elevation occurs inside the bubble, which produces a steady outward flow of heat and entropy, so that the net entropy flow is zero, as required by thermodynamics. The existence of steady heat flow from the bubble means, of course, that the vibration is continually generating heat in the gas, at the expense of vibrational energy.

Detailed theory for the thermal contribution (δ_{th}) to the damping coefficient is too lengthy to treat here. Instead, the reader is referred to analysis and results given by Devin (1959). In Figure 4.3 the thermal damping coefficient (δ_{th}) for a resonant bubble is plotted against a nondimensional parameter $2 \phi R_0$. The quantity ϕ is defined as the reciprocal of the thermal diffusion layer thickness in the gas, and is given by:

$$\phi = (\omega/2 \kappa)^{1/2}; \quad \kappa = K/\rho_0 s_p. \quad (4.34)$$

Here, κ is the thermal diffusivity, K the thermal conductivity coefficient, ρ_0 the density, and s_p the specific heat at constant pressure, all for the gas phase. For air at room temperature, κ is approximately equal to $0.18 \text{ cm}^2 \text{ s}^{-1}$. At large values of $2 \phi R_0$, the thermal diffusion layer is small compared to the bubble radius; thermal gradients then are confined mainly to a thin layer next to the bubble surface, and most of the gas in the bubble responds nearly adiabatically during a vibrational cycle. At small values of $2 \phi R_0$ the diffusion layer is

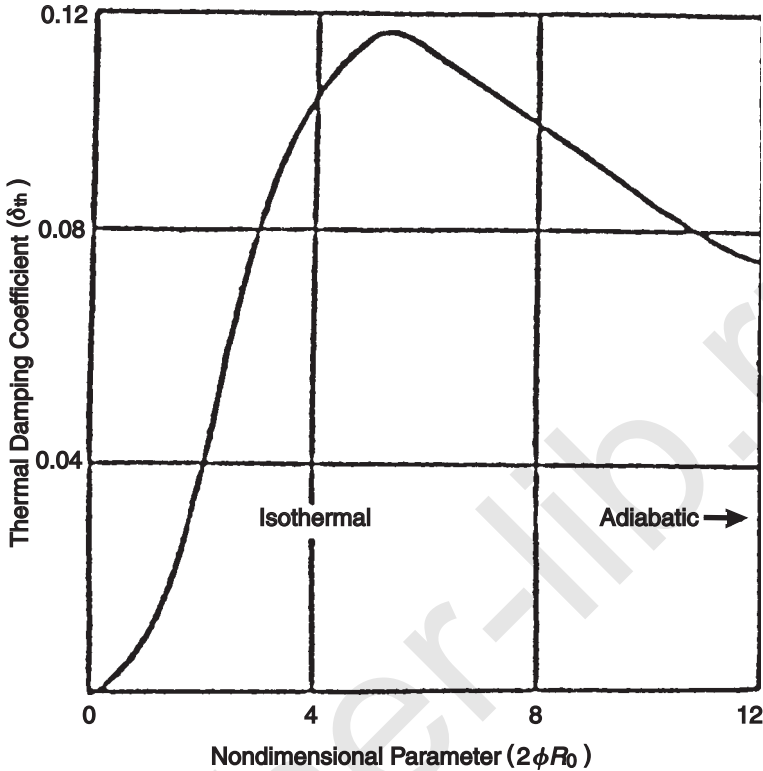


Fig. 4.3. Plot of thermal damping coefficient (δ_{th}) for a resonant gas bubble in water versus a nondimensional parameter ($2\phi R_0$) (ϕ defined in Equation 4.34) (Devin, 1959).

large, so that the temperature is nearly uniform throughout the bubble; the temperature in the gas then hardly varies during a cycle. In Table 4.1 some values are shown of the total damping constant (Equation 4.28) at resonance for free bubbles and stabilized gas bodies.

4.1.4 Bubble Stability, Diffusion and Rectified Diffusion

A volume of gas in a liquid will form a spherical bubble under the interfacial surface tension (σ). If the liquid is under constant hydrostatic pressure (P_0), the total pressure (p_i) internal to the bubble is given by:

$$p_i = p_v + p_g = P_0 + 2 \sigma/R \quad (4.35)$$

in which p_v is the vapor pressure and p_g the gas pressure in the bubble, while R is the radius of the bubble. For an air bubble in water, air may diffuse into or out of the bubble to achieve equilibrium with the air dissolved in the water. If the water is in contact with air at atmospheric pressure and is saturated with air at this pressure, it will be undersaturated relative to the air in the bubble since, according to Equation 4.35, the internal pressure (p_i) is greater than the atmospheric pressure (P_0). Hence, air will flow outward from the bubble and dissolve into the surrounding water. The decrease in bubble radius, which results from the air loss, further increases the excess internal pressure. Thus, a bubble shrinks at an accelerating rate, and small bubbles quickly dissolve. For example, a 1 μm radius bubble will have an excess internal pressure of 1.4 times atmospheric pressure (*i.e.*, a total internal pressure of 2.4 atmospheres, or 0.24 MPa), and will dissolve in a few milliseconds even in air-saturated water (Epstein and Plesset, 1950). This is a significant finding since (as shown in this Section and in Section 5), at frequencies relevant to diagnostic ultrasound, bubbles of micron size are of special importance as sites of either inertial or noninertial cavitation. In the absence of ultrasound, free gas bubbles of this size are quite ephemeral, and must be continuously replenished, if the bubble-related activity is to continue.

However, in the presence of ultrasound, the tendency of free bubbles to shrink is countered and, in fact, they are caused to grow, under some conditions. The process involved is called “rectified diffusion.” Theory for the movement of gas into the bubble was developed by Hsieh and Plesset (1961). Strasberg (1961) compared this theory for bubble growth to theory for shrinkage and pointed out that the combination yields a threshold for bubble stability. The rectified diffusion threshold depends strongly on the bubble and exposure parameters, and is lowest for a bubble of resonance size. This concept is important because it defines a threshold for stable cavitation involving free spherical bubbles. Subsequently, the subject was theoretically treated by Crum and Hansen (1982a), Church (1988a; 1988b), Eller and Flynn (1965), Safar (1968), and Skinner (1970). Experimental studies have been conducted at low frequencies (Crum and Hansen, 1982b; Eller, 1969; 1972). A complicating factor is acoustic microstreaming near pulsating bubbles which can greatly enhance bubble growth (Gould, 1974), apparently by refreshing the liquid in the vicinity of the bubble (Church, 1988b). Church (1988a) made a computational study of rectified diffusion over the frequency range 1 to 10 MHz and found the threshold for bubble growth by this

process to be little different from the threshold for inertial cavitation, except for narrow ranges of bubble size.

Rectified diffusion has been invoked in explaining results of cavitation, both inertial and noninertial at megahertz frequencies. Alternating growth and shrinkage periods occur during burst mode exposure, resulting in optimum bubble size distributions under some conditions (Ciaravino *et al.*, 1981a; Flynn and Church, 1984) and loss of cavitation activity for long off-periods (Miller and Williams, 1992). Also, growth-shrinkage cycles were observed by Miller (1977a) during experiments with CW ultrasound; in these experiments, bubbles of near-resonance size became trapped in rapid translational oscillation in a standing wave field. Radiation forces (discussed in Section 4.3.2) were apparently involved. The bubbles were seen to shrink at the pressure minima until smaller than resonance size, then to move toward increasing pressure amplitude until they grew above resonance size and were forced back toward the minima. Rectified diffusion has been proposed by Crum and Hansen (1982a; 1982b) as an explanation of the bubble growth observed by ter Haar and Daniels (1981) and ter Haar *et al.* (1982) in gels and animal tissue (see Section 4.2.2).

4.1.5 Scattering, Harmonics and Bubble Detection

Any oscillating bubble is a source of sound; if the vibration is symmetrical about the bubble center, the sound field generated is a spherical wave, whose characteristics are seen in Equations 4.4 and 4.5. The bubble motions are themselves brought about by a sound field (Section 4.1.2). This sound field may be called the *ambient* field (or *primary* field, or *driving* field) and the wave generated by the bubble is called the *scattered* field. Letting p_s be the sound pressure amplitude in a spherical wave scattered by a bubble of small radius (R_0), we obtain from Equations 4.4 and 4.5 that:

$$p_s = \frac{j\omega\rho_0 R_0^2}{r} \frac{d\xi}{dt} \quad (4.36)$$

where $d\xi/dt$ is the velocity amplitude at the bubble surface. Using Equations 4.18 through 4.26 for $d\xi/dt$ (given by $j\omega\xi$) the result can be written:

$$|p_s| = (\Omega^2 p_0 R_0 / r) \chi(\Omega, \delta). \quad (4.37)$$

It is interesting to compare this expression with that for scattering from a solid or liquid sphere of similar size. According to Rschevkin (1963) the analogous expression for scattering from a small liquid

sphere of radius (R_0), density (ρ) and compressibility (β), in a medium of density (ρ_0) and compressibility (β_0) is:

$$p_s = \frac{p_0 k^2 R_0^3}{3 r} \Phi, \quad (4.38)$$

where:

$$\Phi = 1 - (\beta/\beta_0) + 3(\rho - \rho_0) \cos \theta / (2\rho + \rho_0); \quad (4.39)$$

here θ is the angle between the direction of particle velocity in the sound field and the direction to the observation point from the scattering object. Calculations for typical situations of interest show that the scattered pressure from a small gas bubble is larger by several orders of magnitude than that from a liquid or solid sphere, or biological cell, of comparable size. Advantage is taken of this fact when "contrast media," containing gas bubbles, are introduced into the blood to improve ultrasonic imaging of the circulation (Section 4.2.5). In addition, the strong scattering provides a convenient means to detect the presence of bubbles even *in vivo*, either by pulse-echo imaging (Daniels *et al.*, 1979; Watmough *et al.*, 1991) or in moving blood with Doppler instruments (Evans and Walder, 1970; Nishi, 1972).

When a gas bubble exists in a liquid where the ambient field is of frequency (f), the bubble vibrates with a displacement (ξ) which can be represented as a series of contributions of differing order, in the sense defined in Section 4.1.1. The first-order contribution has already been discussed in Section 4.1.2; for this the frequency is the same as that of the ambient field. As explained in Section 4.1.1, the pressure in the wave radiated (scattered) by the bubble can be represented as the sum of a first-order contribution, a second-order contribution, and contributions of higher order. The second-order contribution has two parts, one of which varies sinusoidally in time with frequency ($2f$), *i.e.*, with frequency equal to the second harmonic of the ambient frequency.

Theory for the second harmonic generated by vibrating bubbles has been treated by Miller (1981), and used to develop a method for detecting bubbles, and determining their size, based on measurements of second harmonic fields radiated by the bubbles. It is shown that techniques based on measurements of radiated second harmonic are superior to techniques based on detection of first harmonic, in that the former have a much greater ability to distinguish resonant bubbles from larger ones. The method can be used for detecting decompression bubbles (Christman *et al.*, 1986) or stable cavitation bubbles *in vitro* (Miller *et al.*, 1984) or *in vivo* (Gross *et al.*, 1985).

A related technique for detecting and sizing bubbles has been reported by Newhouse and Shankar (1984). In this method, however, the bubbles are exposed to two superimposed sound fields, one of frequency f_1 and the other of frequency f_2 . As the bubble vibrates it radiates a field which contains, not only the original two frequencies, but also the sum and difference frequencies. This method is reported to have advantages similar to those of methods involving second-harmonic detection and, in addition, offers the possibility of determining the bubble location (Cathignol *et al.*, 1990). Other cavitation detection techniques depend on the manifestations of inertial cavitation and are discussed in Section 5. Techniques for ultrasonic imaging based on detection of the second-harmonic component in the waves scattered by gas-containing contrast agents are discussed in Section 4.3.

4.1.6 Surface Waves

While much can be learned about bubble dynamics by using a model with spherical symmetry, the actual situation is usually more complex. Waves are often set up on the bubble surface; these can be simple or complex, coherent or chaotic. If θ and ϕ are polar and azimuthal angles, respectively, the radial displacement amplitude at the bubble surface for a particular mode is given as a function of angle by :

$$\xi(\theta, \phi) = a_{mn} P_n^m(\cos\theta) \cos m\phi, \quad (4.40)$$

where $P_n^m(\cos\theta)$ is a Legendre function and a_{mn} is a constant dependent on the function $\xi(\theta, \phi)$. For $m = 0$, the mode has axial symmetry; a few examples of the Legendre functions which then apply are (omitting the “m” superscript):

$$P_0 = 1; P_1 = z; P_2 = 1/2 (3 z^2 - 1). \quad (4.41)$$

Of these, the P_0 mode (a “breathing” mode) has spherical symmetry, the P_1 mode is a rigid translation and the P_2 mode is the lowest mode involving a change in shape of the surface. In this last mode, the surface contracts along its equator while it expands along the axis of symmetry, and *vice versa*. The characteristic angular frequencies for axisymmetric modes are given (Lamb, 1945) by:

$$\omega_n^2 = (n - 1)(n + 1)(n + 2)\sigma/\rho_0 R_0^3. \quad (4.42)$$

When surface waves occur they can have considerable influence on cavitation activity by affecting heat transport and mass transport (Gould, 1966; 1974). At amplitudes (commonly achieved) such that

the waves are distorted and unstable, jets of liquid are formed which lead to erosion of solid surfaces to which the bubbles are adjacent (Coleman *et al.*, 1987); see Section 5.8. Also, the unstable surface waves lead to fragmentation of the primary bubble into much smaller bubbles, sometimes in great numbers (Nyborg and Hughes, 1967; Storm, 1974); these smaller bubbles may then act as sites for further cavitation (Neppiras and Fill, 1969).

The surface waves may be excited *linearly*, in such a way that the frequency is the same as that of the ambient field, and the wave amplitude is proportional to the pressure amplitude of the ambient field. Alternatively, and perhaps usually, they are excited *parametrically*; the wave amplitude then varies nonlinearly with p_0 and the frequency is typically a subharmonic of the ambient-field frequency (Benjamin and Ursell, 1954; Coakley and Nyborg, 1978).

4.2 Activation of Stabilized Gas Bodies

The term *gas-body activation* (GBA) applies to a body of gas stabilized by a structure which partially or completely surrounds it. The body is activated when it is set into oscillation by ultrasound. While GBA is a sub-category of cavitation, it has special manifestations and is conveniently discussed as a separate subject. For commonly observed cavitation in water or other fluids, many cavities suddenly appear when the pressure amplitude exceeds an ultrasonic cavitation threshold. The violent implosions associated with inertial cavitation generate characteristic noise, shockwaves, light, free radicals, and other chemical species (Section 5). The cavities appear to vanish or to evolve into large inactive bubbles that rise at the cessation of ultrasonic exposure. For GBA, a pre-existing gas body is often readily observable in the medium (acoustically or optically) and is set into oscillation at any non-zero level of ultrasound. There is no threshold for GBA. The oscillation often involves a membrane-like motion of an interface or structure (gas volume changes being less dramatic than for inertial cavitation) and may test “negative” for many tests applicable to inertial cavitation. At the cessation of ultrasonic exposure, even when biological effects are produced, the gas body and its stabilizing structure may be completely unchanged. The importance of GBA for risk assessment in medical ultrasound lies in its subtle nature (since GBA can fail tests for other kinds of cavitation), its occurrence below the threshold for cavitation involving free bubbles in liquids, and its potential for occurrence in any medium with gas bodies.

GBA was first observed in leaves of the aquatic plant *Elodea* by Harvey and Loomis (1928). The gas bodies in *Elodea* are gas-filled

channels which run between the cells and serve in respiratory functions. Pfirsch (1958) first demonstrated the critical role of the gas-filled channels in generating biological effects of ultrasound in *Elodea*. Gershoy *et al.* (1976) found this same phenomenon in other plant tissues, such as pea roots. Miller (1977b) introduced the term “gas-body activation” to distinguish this phenomenon from “free-bubble cavitation.” GBA has also been identified in experiments with insect eggs and larvae (Carstensen *et al.*, 1983a), with mammalian lung (Section 8) and with small gas-containing bodies employed clinically as contrast media (Section 4.3). In addition, “artificial” gas bodies which promote GBA can be created by trapping air in pores in hydrophobic sheets of plastic (Nyborg *et al.*, 1977). GBA is a developing subject with many aspects under study at this time. This Section draws upon and updates a previous review of the topic (Miller, 1984) and Section 4.3 takes up the topic of gas-body-based ultrasound contrast agents.

4.2.1 Gas-Body Structures and Stability

Bodies of gas may be stabilized by containment in a solid or within a walled structure or shell. Gas in a pore or pit in a solid can be stable even with a free air-water interface provided that the curvature $1/r$ results in a value of internal pressure equal to the external pressure. For example, a flat interface ($1/r = 0$) eliminates the excess pressure due to surface tension. Structures of this type (*i.e.*, pits or crevices in solids) are thought to provide sites for cavitation nuclei, *i.e.*, small, gas bodies from which free bubbles can grow and become active in a sound field. The existence of such nuclei links GBA with other forms of cavitation, and indicates some potential for GBA at levels below the threshold for inertial cavitation in virtually any medium with cavitation nuclei. Gas bodies can also be stabilized within pores in hydrophobic membranes, such as are used in Nuclepore® filters (Nuclepore Corporation, Pleasanton, California), and studied at megahertz frequencies (Miller, 1982). An example of a gas-filled micropore is shown in Figure 4.4. For this type of gas body, the need for a nearly flat interface places requirements on the shape of the pore or pit and on the contact angle of the three-phase line (where gas, liquid and solid meet). For the micropore with straight sides, a hydrophobic surface is needed in order to have the requisite 90 degree contact angle fall within the advancing and receding contact angles of the surface (Miller, 1982).

The difference in the advancing and receding angles is known as contact-angle hysteresis (Johnson and Dettre, 1969). If the material

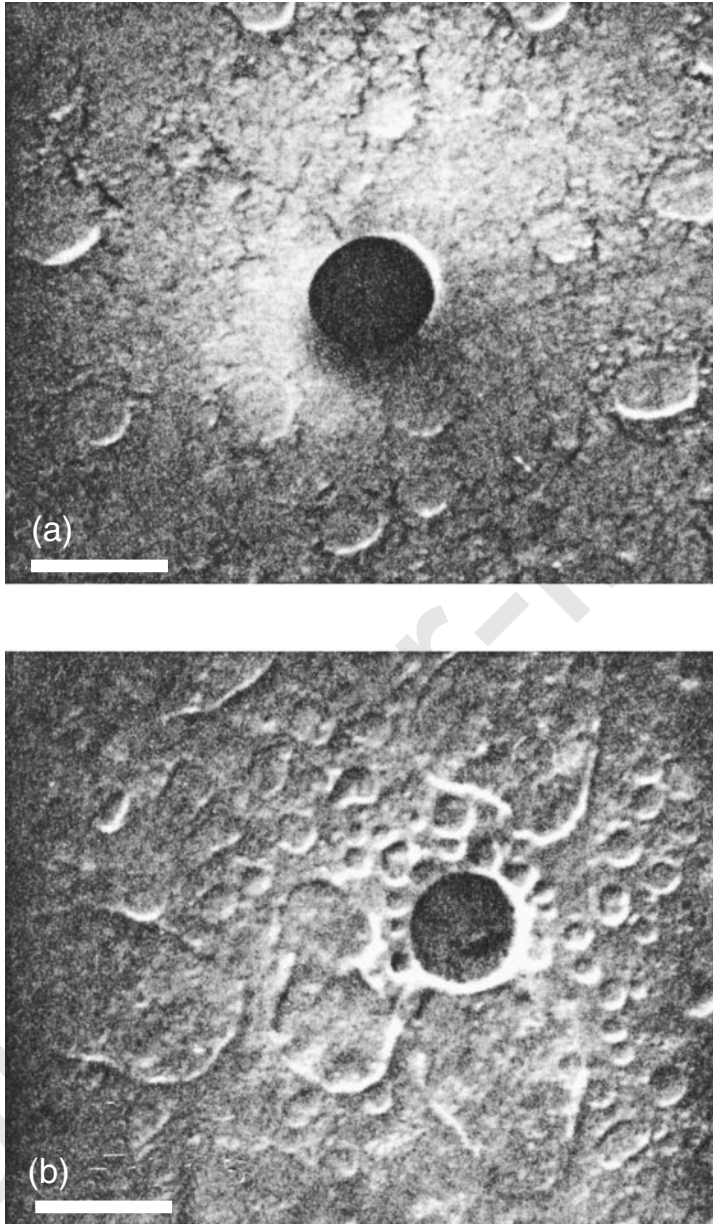


Fig. 4.4. Scanning electron photomicrographs of micropores in hydrophobic sheets: (a) an open micropore and (b) a micropore in a sheet covered with hydrophobic coating material. Nonuniformity in the hydrophobic coating leads to some variability in results with these micropore sheets. The scale bar indicates $5\ \mu\text{m}$ (Miller, 1982).

is hydrophilic, then the advancing angle is less than 90 degrees, the three phase line advances, a positive radius of curvature results in excess internal pressure, and the gas body dissolves. Therefore, gas stabilization in a pore or pit may not be readily achieved for systems, including some biological subjects, which primarily have hydrophilic materials and surfaces.

Gas may also be stabilized by walls or shells. This type of stabilization is relatively common in biological subjects, particularly in association with respiratory functions. The gas-filled channels in many plant tissues are examples of this type of gas body, which has been employed for bioeffects studies at megahertz frequencies (Miller, 1983a). A gas-filled channel in an *Eloдея* leaf is shown in Figure 4.5a (Miller, 1984). Gas-filled channels also occur in insect larvae, as shown in Figure 4.5b (Carstensen *et al.*, 1983b), and form the respiratory network of the animal.

Gas bodies may become unstable under some conditions, particularly for ultrasonic activation at high amplitudes. On the one hand, certain gas bodies serving as cavitation nuclei can become unstable as they grow explosively into inertial cavities (Atchley and Prosperetti, 1989). On the other hand, gas-filled micropores become unstable and lose gas at incident ultrasound levels capable of nonlinear excitation, even for short-duration pulses (Neppiras *et al.*, 1983). Gas-filled channels in *Eloдея* leaves tend to fill with liquid when the ultrasonic exposure results in the death of the adjacent cells (Miller, 1985a). Even the gas in the respiratory channels of fruit-fly larvae retreats under some conditions (Carstensen *et al.*, 1983a). Recent evidence suggests that pulsed-mode exposure can excite the channel gas bodies into nonlinear oscillation which may correspond in some respects to the inception of inertial cavitation (Carstensen *et al.*, 1990a).

4.2.2 *Bubbles Stabilized in Viscoelastic Media*

While ultrasonic cavitation has been studied primarily as it occurs in aqueous solutions, a substantial amount of theoretical research has been conducted on the dynamics of cavities in viscoelastic media. These include not only non-Newtonian liquid media, such as polymer solutions, but also soft solids, such as gels and rubber compounds. This body of work may be important here, since biological media include a variety of viscoelastic materials; these range from liquids (urine, synovial fluid, extracellular fluid, blood, vitreous humor) to solids (soft tissue, cartilage and bone).

Theory for cavities in viscoelastic fluids indicates that the collapse behavior may, under some conditions, be less violent in such fluids

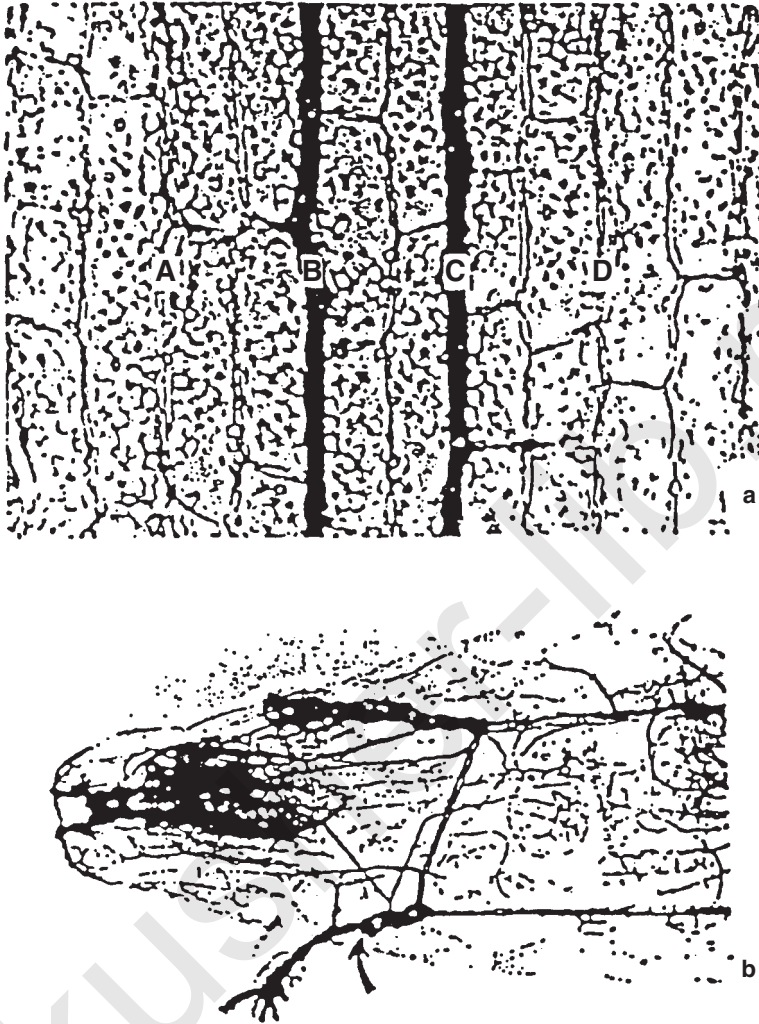


Fig. 4.5. Examples of *in vivo* gas bodies: (a) a transmitted-light photomicrograph of a partially degassed *Elodea* leaf. Intercellular channels (vertical in the figure), spaced about 50 μm apart, occur at A, B, C and D. The channels at B and C are filled with gas and appear black, while those at A and D are water-filled and transparent (Miller, 1979a). (b) *Drosophila* larva. The main gas channels (the tracheae) are indicated by an arrow (Carstensen *et al.*, 1983a) (composite figure from Miller, 1987).

than in water. Fogler and Goddard (1970) concluded that in media with long-range memory in the stress-strain relations, relaxation effects will have a considerable influence on the collapse of a cavity if the relaxation time is long compared to the time for collapse in water. The influence of combined viscosity and elasticity (Oldroyd model) were considered further by Tanasawa and Yang (1970), who calculated the radius (R) versus time (t) for a gas-filled bubble subjected to a sudden increase in the external pressure. Yang and Lawson (1974) similarly calculated R versus t curves for a gas-filled bubble in a sound field, finding that both the transient and the steady-state response (including the resonance frequency) are affected by the combined viscosity and elasticity (Oldroyd model).

Blood may be approximated by theoretical models of liquid suspensions (Shima and Tsujino, 1978). The oscillation amplitude of a gas-filled bubble in blood, produced by changes in the external pressure, is reduced from that in water (as expected for higher viscosity, see Section 4.1.3), but nonlinear oscillation appears for higher pressure amplitudes. Analysis of bubble response to oscillating pressure fields at frequencies up to 300 kHz indicates that collapse behavior may also occur in blood when the pressure amplitude is 0.1 MPa or more (Tsujino and Shima, 1980).

The influence of the addition of polymers on cavitation behavior in water has been studied with regard to cavitation suppression and reduction of cavitation damage. The addition of polymers theoretically adds to the non-Newtonian viscosity affecting the motion (Shima *et al.*, 1985). The resonance frequency of a bubble at small amplitudes is unchanged from that in water, except for small bubbles (high frequencies) for which a critical radius exists. Below the critical radius, which depends on the concentration of the additive, the bubble is overdamped, and no resonance frequency is obtained. For bubble excitation at relatively high amplitudes, the bubble response is reduced from that in water, but nonlinear behavior is still possible.

In experimental studies, damage to solid surfaces caused by acoustic cavitation (at a frequency of 19.5 kHz) was found to be reduced by polymer additives; however, the sound pressure level of harmonics and subharmonics produced were actually higher than in water (Tsujino, 1987).

Daniels and ter Haar (1986) observed the growth of gas bubbles in agar gel as well as in animal tissue at a frequency of 0.75 MHz and at spatial-average intensities up to 1 W cm^{-2} . When the gel was supersaturated with gas, thresholds for the bubble growth could be determined from the visual appearance of bubbles in the gel during exposure. In subsequent work, the threshold was found to increase for higher frequencies, shorter pulse durations and longer duty cycles

(Daniels *et al.*, 1987). It was found that the observed behavior of growing bubbles could be modeled by rectified-diffusion theory for bubbles in water (Crum *et al.*, 1987).

The oscillation of a spherical hole in a solid, which poses a relatively difficult theoretical problem, has been treated by a few investigators. The rigidity of a solid provides an elastic restoring force which is lacking in a liquid, and which can predominate over the inertial forces (Blake, 1952). Meyer *et al.* (1958) and Gaunard and Uberall (1978) theoretically considered the behavior of cavities in rubber at low frequencies and found that pulsation could occur, but with complex dependence on parameters such as the Poisson's ratio of the solid. Application of these theories to cavitation at high frequencies in biological material would require extensive development.

4.2.3 Gas Trapped in Pits or Pores

Theory has been developed for the low amplitude activation of gas-filled micropores (Miller and Neppiras, 1985; Miller and Nyborg, 1983) and cylindrical bubbles and gas-filled channels in plants (Miller, 1979b). These theories are based on linear approximations, as for the theory discussed in Section 4.1. In this Report, this linear modeling method is extended to include the possibility of stabilizing shells on the spherical and cylindrical bubbles. Linear approximations allow the relatively simple theoretical framework for harmonic oscillators to be applied to models of the gas bodies. The linear theories will be briefly presented in this Section as applied to gas trapped in a pore or pit with a circular air-water interface, for cylindrical bubbles with a thin shell (again for stability) and for the gas-filled channels bounded by three or four cell walls in plant tissues. These gas bodies and their presumed modes of oscillation are illustrated in Figures 4.6, 4.7 and 4.8.

In all cases, the oscillation is assumed to be a sinusoidal function of time at the frequency (f) of the incident sound wave. The displacement amplitude (ξ_0) of the response of a vibrating gas body may be written in the form of Equation 4.19 as:

$$\xi_0 = \frac{F_p}{k_s} \chi(\Omega, \delta) \quad (4.43)$$

in which F_p is the driving force, k_s is the stiffness, and $\chi(\Omega, \delta)$ is given in Equation 4.20. With this standard solution, the problem of modeling the behavior of a gas body is reduced to specifying appropriate expressions for the oscillation constants F , k_s , δ and the resonance frequency (Equation 4.23).

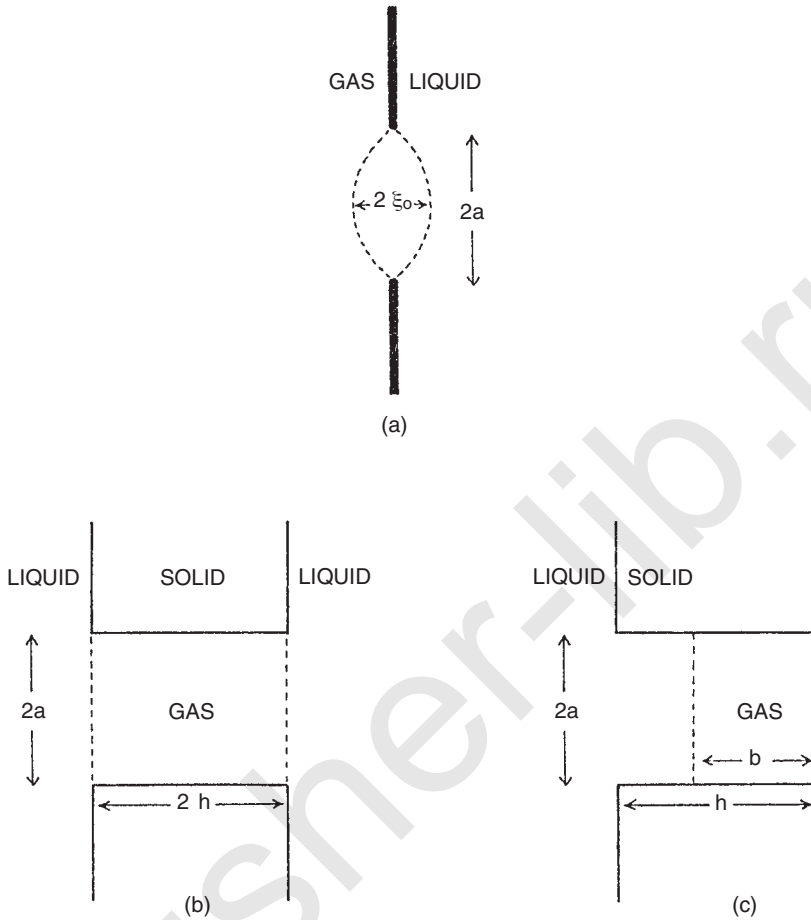


Fig. 4.6. Three configurations of a stable gas-liquid interface. (a) At a hole in a membrane which is bounded on one side by gas, and on the other by liquid, (b) at the ends of a gas-filled channel in a solid sheet enclosed by liquid on both sides, and (c) at the end of a gas pocket in a pit (Miller and Nyborg, 1983).

For both the gas-filled pit, which is a model for cavitation nuclei, and the gas-filled micropore, which passes through a membrane, the gas-liquid interfaces execute transverse oscillations in which the three-phase line (the line at which gas, liquid and solid meet) apparently remains fixed for low-amplitude oscillations (Miller and Neppiras, 1985; Miller and Nyborg, 1983). The mathematical formalism is the same for the pit and the through-membrane pore; the latter is equivalent to two identical opposing pits (see Figure 4.6).

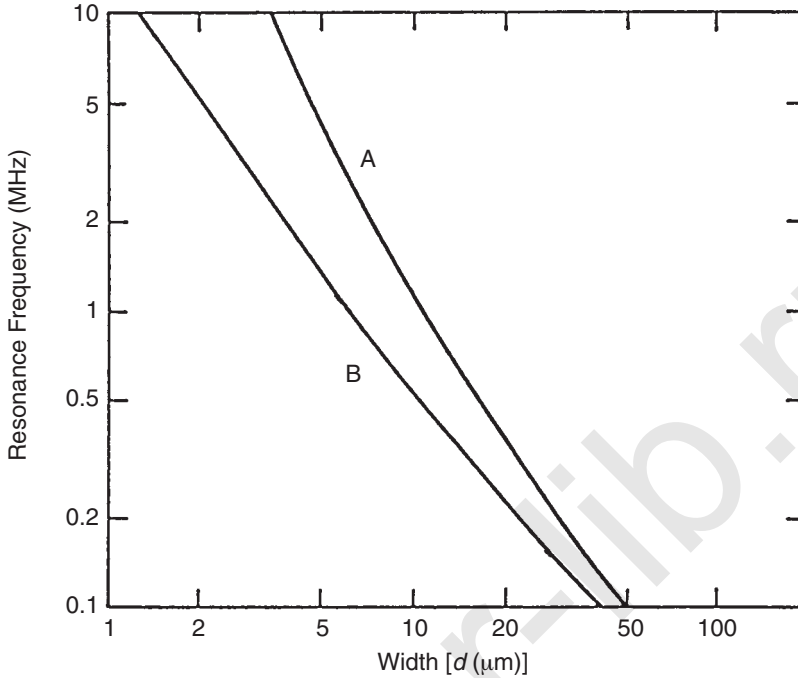


Fig. 4.7. Theoretical resonance frequencies for gas bodies. (A) Gas-filled channels formed by a ring of four cells with walls of $0.5 \mu\text{m}$ thickness and width (d) (see Figure 4.8) in *Elodea* leaves. (B) Gas-filled micropores (see Figure 4.6b) with equal diameter ($d = 2a$) and length ($2h$) (Miller, 1984).

Assuming a circular interface in a gas-filled pit of depth (h) [or pore of length ($2h$)], and radius (a) and for an incident pressure amplitude (p_0), the oscillation constants are (Miller and Nyborg, 1983):

$$F_p = \pi a^2 p_0, \quad (4.44)$$

$$k_p = 8 \pi \sigma_s + \pi \Gamma P_0 a^2 h^{-1}, \quad (4.45)$$

$$m_p = \frac{32}{15} \rho a^3, \quad (4.46)$$

and

$$f_p = \frac{1}{2\pi} \left[\frac{120 \pi \sigma h + 15 \pi \Gamma P_0 a^2}{32 \rho a^3 h} \right]^{1/2}, \quad (4.47)$$

in which the surface tension (σ) is 0.070 N m^{-1} (70 dyn cm^{-1}), mass density (ρ) is $1,000 \text{ kg m}^{-3}$ (1 g cm^{-3}), polytropic exponent (Γ) is one and ambient pressure (P_0) is 0.1 MPa (10^6 dyn cm^{-2}). The damping

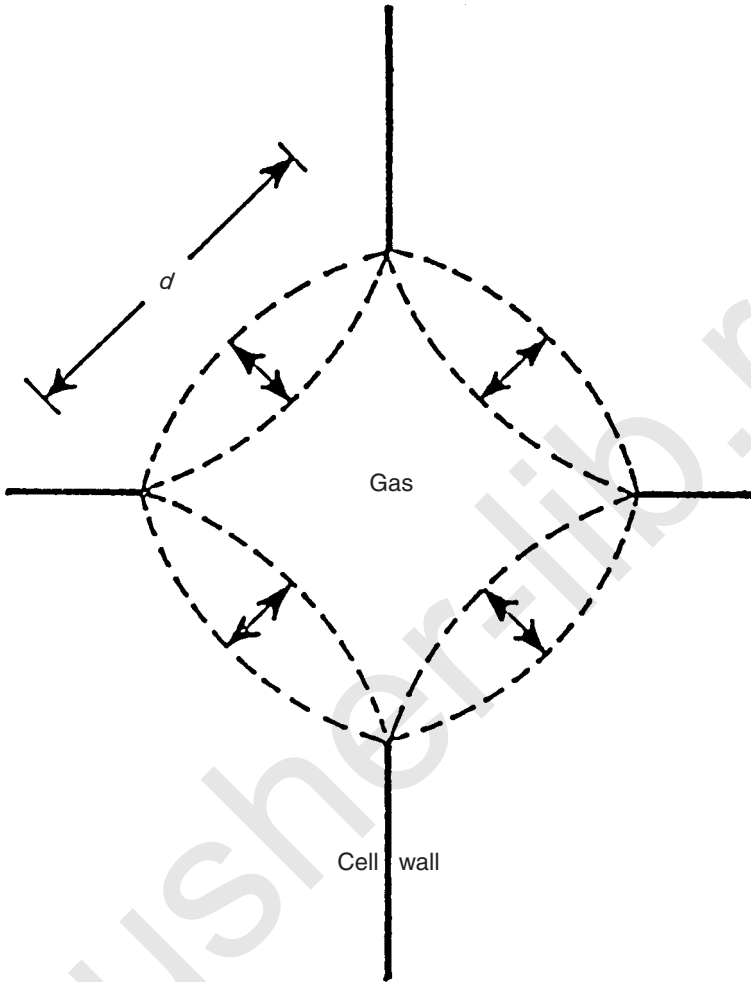


Fig. 4.8. Diagram of the oscillation mode expected for a four-walled gas-filled channel in an *Elodea* leaf (Miller, 1984).

of the oscillation results from the sum of viscous, boundary layer, and radiation losses of energy, given by:

$$\delta_p = \frac{1}{2 \pi f_0 m_p} \left[2 \pi \eta a + \frac{\pi^2 \rho f \ell a^2}{8} + \frac{4 \pi^3 f_0^2 a^4}{3 c} \right] \quad (4.48)$$

in which $c = 1.5 \times 10^3 \text{ m s}^{-1}$ is the speed of sound and the viscosity (η) is typically about 1 MPa s (1 cP). The thickness (ℓ) of the viscous boundary layer at the solid surface around the micropore is $(\eta/\pi \rho f^c)^{1/2}$.

For example, a 2 μm radius micropore would be resonant at 1.7 MHz, with a damping constant of 0.09 giving a fairly sharp resonance (Miller and Nyborg, 1983). These expressions change if the pore or pit is not completely full of gas (Miller and Nyborg, 1983). The resonance frequency for different sizes of micropores with $a = h$ is shown in Figure 4.7.

Gas-filled micropores in hydrophobic membranes have been investigated for use in bioeffects studies at medically relevant frequencies. Micropores of 1 to 5 μm radius in hydrophobic polycarbonate membranes about 12 μm thick have been used with pore number densities of 100 mm^{-2} to more than 1,000 mm^{-2} (Miller, 1982). These are available in sheets amenable to simple transmission and reflection measurements for the purpose of determining the physical behavior of the gas-filled micropores. These gas bodies are strongly activated over a broad frequency range from about 0.3 MHz to more than 3 MHz, which deviates from the sharp resonance behavior expected on the basis of the theory for a single gas-filled micropore (Miller, 1982). More recent observations of micropore behavior using different methods have also shown relatively broad frequency spectra (Quain *et al.*, 1991; Wu and Nyborg, 1989).

The broadening of the response appears to be due to two complicating factors: (1) many micropores only partly retain air upon immersion and (2) acoustically activated gas bodies interact. If the micropores only partly retain air when immersed in aqueous media, the behavior changes (Miller and Nyborg, 1983). In particular, the resonance frequency can shift to lower values due to increased mass of the system. For example, a 2 μm radius micropore can have a resonance frequency ranging from about 0.85 MHz (when about half-filled with air) to 1.7 MHz (when filled with air). Partial filling in an asymmetrical fashion can lead to even greater broadening, which appears to be sufficient to explain the observed response range (Miller and Neppiras, 1985). The acoustical interaction arises from the fact that the pressure driving the gas body is the sum of the incident ultrasonic wave and the waves radiated by all the other gas bodies on the sheet. This phenomenon has been analyzed by Miller (1980) using a theoretical model developed by Weston (1966). Essentially, the incident wave is reduced to p_1 , given by:

$$p_1 = p_0 \left(1 + \frac{15 \pi \lambda a N}{64 f_0 \delta} \right)^{-1} \quad (4.49)$$

in which N is the number density of micropores and λ the ultrasonic wavelength (c/f). This interaction behaves much like an increased damping and tends to reduce the resonance peak, thus broadening

the response. When the effects of partial gas filling and acoustical interaction are taken into account, the theory and experiment appear to be in approximate agreement (Miller, 1984; Miller and Neppiras, 1985).

4.2.4 Gas-Filled Channels

Plant tissue gas bodies have a variety of forms, each of which might require a specific theoretical model. A model has been developed for long narrow channels bounded by three or four thin plant cells walls, which is of interest for *Elodea* leaves and plant roots. The model is depicted in Figure 4.8 and presumes that the oscillation consists of transverse motion of the channel walls (rather than a pulsation, as in the cylindrical bubble). The oscillation constants for a channel with n walls of width d are (Miller, 1979b):

$$F_c = ndp_0 \quad (4.50)$$

$$k_c = \frac{n\pi^4 T_w}{8d} + \frac{n\pi^6 h_w^3 Y}{12d^3(1-\sigma^2)} + 4\pi\Gamma P_0 \quad (4.51)$$

$$m_c = -\frac{n^2 d^2 \rho}{2\pi} \left[\ln\left(\frac{ndf}{c}\right) + 0.577 \right] \quad (4.52)$$

and the resonance frequency is f_c :

$$f_c = \frac{1}{2\pi} \left(\frac{k_c}{m_c} \right)^{1/2} \quad (4.53)$$

in which the wall properties are thickness $2h_w$, tension $T_w = 10 \text{ N m}^{-1}$ (10^4 dyn cm^{-1}) (estimate based on turgor of 6.5 times atmospheric pressure in *Elodea* leaves), Young's modulus $Y = 10^3 \text{ MPa}$ ($10^{10} \text{ dyn cm}^{-2}$) (estimate based on values for algae), Poisson's ratio $\sigma = 0.3$ and the polytropic index $\Gamma = 1$. The damping is primarily due to radiation loss, and is given by:

$$\delta_c = -\frac{\pi}{2} \left[\ln\left(\frac{ndf}{c}\right) + 0.577 \right]^{-1}. \quad (4.54)$$

The resonance frequency of $n = 4$ walled gas channels with $2h_w = 0.5 \mu\text{m}$ thick walls is shown in Figure 4.7. For calculating the response of gas-filled channels, Ω should be modified to account for the weak dependance of the effective mass on frequency (Miller, 1979b).

Experimental study of cylindrical bubbles and gas-filled channels at megahertz frequencies has not been extensive due to the lack of suitable subjects. These types of gas bodies are also expected to be

resonant, although the damping is much higher than for micropores. For example, a four-walled channel with $d = 6 \mu\text{m}$, resonance occurs at about 3 MHz (Figure 4.7) and the damping constant is about 0.5. Gas-filled channels are also subject to acoustical interaction, which can be considered theoretically for a leaf in the same way as for sheets of micropores (Miller, 1984). For more complicated situations, such as the three dimensional arrays of gas-filled channels found in plant roots (Gershoy *et al.*, 1976), the outer channels may tend to shield the inner channels (but this has apparently not been quantified). As noted above, there is little direct experimental data available on the behavior of these gas bodies. However, the resonance response of the gas-filled channels in *Elodea* is evident in the occurrence of biological effects in the leaf cells examined as a function of frequency (Carstensen *et al.*, 1990b; Miller, 1979a).

The gas bodies in fruit-fly larvae are long thin channels. Child *et al.* (1992) noted that these gas bodies appear to behave like cylindrical bubbles. The intensity threshold for death of the larvae displayed a minimum at about 0.26 to 0.54 MHz (see Section 6). This range of frequencies for strong activation was predictable from theory for the oscillation of a cylindrical bubble from Miller (1979b). Assuming negligible tension and Young's modulus in Equations 4.51 through 4.53, the resonance frequency for a free cylindrical bubble of $4 \mu\text{m}$ radius (for which d in Equations 4.51 and 4.52 equals $\pi/2$ times the radius, assuming $n = 4$) is 0.3 MHz, in good agreement with the minimum in the threshold data.

4.2.5 Gas Bodies in Mammals

Stable bodies of gas also exist naturally in the body. The lung is a prominent gas-containing tissue. Its interior cannot be imaged, and intervening lung tissue must be avoided in order to visualize cardiac structures. If the alveoli are considered to be gas bodies, then the resonance frequencies are relatively low [*i.e.*, in the sonar range around 25 kHz (Smith and Hunter, 1980)]. The lung does appear to be susceptible to damage, presumably related to its pre-existing gas content, from lithotripter shockwaves (Delius *et al.*, 1987) and even from short bursts or pulses of ultrasound (Child *et al.*, 1990). Prudent use of ultrasound includes consideration of potential effects on lung tissue, as discussed in Section 8.

Small gas bodies apparently also exist in the body, and these serve as cavitation nuclei (*e.g.*, in lithotripter shockwave exposure) and sites for formation of bubbles in decompression (*e.g.*, the bends). Presently, the nature and distribution of these gas bodies are not

well known, so that potential risks from exposing them to medical ultrasound is problematical.

4.3 Contrast Agents for Diagnostic Ultrasound

4.3.1 *Engineering of Stabilized Gas Bodies*

The success of diagnostic ultrasound depends on differences in the acoustic signal reflected or scattered back to the receiving transducer from different sites in the tissue on which the ultrasound is incident (see, *e.g.*, Dickinson, 1986). Diagnostic ultrasound images often fail to show a contrast between features of interest due to the homogeneous nature of many tissues and fluids. Blood, for example, often appears as vacant space even in the heart. Doppler imaging methods can partly rectify this situation under some conditions, but can be too insensitive for imaging slow venous flow or tissue perfusion unless image contrast is enhanced by injecting material with superior echogenicity. Another application for ultrasound contrast agents derives from the lack of contrast when tissue structural differences are small, as in many liver metastasises, or when the object of interest composes a small fraction of the ultrasound sample volume. For example, liver tumors as large as 4 cm in diameter may go undetected using present ultrasound techniques (Masatoshi and Hasegawa, 1988). For these reasons, various compounds and preparations have been considered for use as possible ultrasound contrast agents throughout the development of diagnostic ultrasound. Contrast agents are also used for medical imaging with x rays or magnetic resonance imaging (MRI), but each modality requires specially designed materials. Ultrasound contrast agents are unique in their acoustic properties as active agents; that is, they are activated by the incident wave to become secondary point sources. The topic has been the subject of detailed reviews describing the uses of these agents (de Jong, 1996; Goldberg *et al.*, 1994; Ophir and Parker, 1989; Roelandt, 1982; Schlieff, 1991; Wight, 1995; Ziskin *et al.*, 1972). Contrast agents have found the greatest acceptance and use in echocardiology (Kaul, 1997; Paelinck and Kasprzak, 1999), but techniques utilizing the agents are also finding applications in radiology (Burns, 1998) and in obstetrics and gynecology (Abramowicz, 1997). In this Report, the present status of contrast agents developed for diagnostic ultrasound will be reviewed and discussed with emphasis on their ultrasonic behavior and the potential for nonthermal bioeffects.

Early contrast-enhancement effects were noted with free gas bubbles in suspension (Gramiak *et al.*, 1969; Kremkau *et al.*, 1970). Clinical researchers utilized existing radiographic contrast agents (Corday *et al.*, 1984), which were found to act through the stabilization of bubbles (Meltzer *et al.*, 1980). An early specific ultrasound agent utilized gel-encapsulated microbubbles (Carroll *et al.*, 1980). These agents are based on the pronounced ability of gas bodies to scatter ultrasound (see discussion in Section 4.1.5), producing a bright echo on an image. In a recent study, even a bolus of microbubbles generated directly in the aorta during cavitation by high power focused ultrasound has been proposed as a novel contrast agent (Ivey *et al.*, 1995). Compounds not based on gas bodies can also provide contrast under some conditions, including liquid impedance and speed of sound agents (Mattrey and Pelura, 1997; Mattrey *et al.*, 1983; Tyler *et al.*, 1981), and particulate agents (Parker *et al.*, 1987).

The 100 to 1,000 times greater scattering by gas compared to a particle like a red blood cell of the same size gives added contrast which is difficult to match with a gasless particle. For this reason, the first generation of successful commercially developed ultrasound contrast agents (Table 4.2) were simply stabilized bodies of air (see Table 4.1). The two agents SH U-454 (Echovist®) and SH U-508 (Levovist®), gas bodies developed by Schering AG (Berlin, Germany), consist of dry galactose particles which are manually reconstituted from a dry powder for use (Smith *et al.*, 1984). These agents can be difficult to characterize acoustically due to the brief lifetime of the gas bodies and the range of particle-gas configurations created. The ultrasonic attenuation produced by Levovist® gas bodies, which are stabilized by palmitic acid, peaks at about 2 to 3 MHz, indicating a typical bubble size of 2.7 μm (Schlief *et al.*, 1993). The shell-stabilized agent Albunex® (Molecular Biosystems, Inc., San Diego) has been available clinically for several years, and has been the subject of several characterization studies (Bleeker *et al.*, 1990; Christiansen *et al.*, 1994). This suspension is created by sonication of a five percent solution of human serum albumin, which creates numerous small gas bodies. These have stable shells of heat-denatured albumin about 15 nm in thickness (Hellebust *et al.*, 1993). The product contains about $2 \times 10^8 \text{ mL}^{-1}$ gas bodies between 4 and 10 μm in diameter which are stable under refrigeration for several years (Christiansen *et al.*, 1994).

A number of “second-generation” commercial agents are presently under development and clinical testing, see Table 4.2. In general, these new agents are intended to improve the persistence of the gas bodies in the circulation, and especially to improve the transpulmonary contrast level obtained in studies of the left side of the heart

TABLE 4.2—*Examples of some commercially-developed ultrasound contrast agents.*

Agent Designation	Stabilization	Gas	Associated Company	Exemplary Citation
Echovist ^a	Galactose particle	Air	Schering AG	Schlief (1991)
Albumex ^a	Denatured albumin shell	Air	Mallinckrodt Medical, Inc.	Bleeker <i>et al.</i> (1990)
Levovist ^a	Palmitic acid	Air	Schering AG	Schlief (1991)
Optison (FS069) ^a	Denatured albumin shell	Perfluoropropane	Mallinckrodt Medical, Inc.	Killam and Dittrich (1997)
Definity (MRX)	Phospholipid coating	Perfluoropropane	Dupont Pharmaceuticals Co.	Unger <i>et al.</i> (1997)
Sonovue (BR1)	Phospholipid coating	Sulfur hexafluoride	Bracco Diagnostics	Schneider <i>et al.</i> (1995)
EchoGen (QW3600)	Liquid droplet	Dodecafluoropentane	Abbott Laboratories	Correas <i>et al.</i> (1997)
Sonogen (QW7437)	Droplet/surfactant	Dodecafluoropentane	Sonus Pharmaceutical	Yasu <i>et al.</i> (1999)
Imagent US (AFO150)	Surfactants	Perfluorohexane	Alliance Pharmaceutical	Mattrey and Pelura (1997)
Sonovist (SH U-563A)	Polymer shell	Air	Schering AG	Fritsch <i>et al.</i> (1997)
Sonozoid (NC100100)	Polymer shell	N/A ^b	Nycomed Imaging AS	Sontum <i>et al.</i> (1999)
Quantison	Thick albumin shell	Air	Andaris Ltd.	Frinking and de Jong (1998)
Myomap	Thick albumin shell	Air	Andaris Ltd.	Frinking and de Jong (1998)
AI-700	Polymer shell	Perfluorocarbon	Acusphere, Inc.	

^aAgents which are presently in clinical use.^bN/A = not available from the literature.

or of perfusion of other organs. Optison® (Mallinckrodt Medical, St. Louis, Missouri) is related to the earlier product Alunex®, but contains perfluoropropane, a gas which is much less soluble in aqueous media than is air. Other agents employ phospholipids or other surfactants to form a skin on bubbles of low-solubility gases. Recent developments include the manufacture of polymeric microballoons with biodegradable polymer shells (Fritzsche *et al.*, 1997; Schneider *et al.*, 1992). Perfluoropentane has been used to form liquid droplets at room temperature (Echogen and Sonogen) which form gaseous microbubbles at body temperature (Correas *et al.*, 1997), although vaporization of the droplets appears to be required prior to injection (Forsberg *et al.*, 1998a; 1998b). These agents all are undergoing clinical trials for safety and efficacy. The specific consideration of potential bioeffects resulting from the interaction of gas bodies with ultrasound has not been extensively evaluated (see Section 6.2.2).

Research reports of new agents continue to appear in the literature for this rapidly developing field. PESDA, which has been developed for echocardiology applications, is produced by sonicating a solution of dextrose and albumin with perfluorobutane gas (Porter *et al.*, 1996). Contrast agents BY963 with a phospholipid coating (Seidel *et al.*, 1998) and ST44 and ST68 with surfactant coatings (Forsberg *et al.*, 1999a) have been used to show superior behavior of low solubility gases (perfluoropentane or sulphur hexafluoride) on stability and scattering. Several agents have been developed specifically for therapeutic applications including chemotherapeutic drug delivery (Unger *et al.*, 1998), targeting of gas bodies to cell receptors (Klibanov *et al.*, 1998) and binding to thrombi for enhancement of thrombolysis (Wu *et al.*, 1998). The rapid growth of this area of medical ultrasound is expected to continue. Each new gas-body-based contrast agent may be expected to have different acoustical characteristics, and possibly different potential for biological effects.

Bubbles for contrast enhancement in ultrasound images do not necessarily need to be injected. Microbubbles generated *in vivo* by cavitation in blood could serve as contrast agents downstream. Microbubble boluses have been generated by 1.8 MHz focused ultrasound in the canine abdominal aorta and detected by diagnostic ultrasound B-mode imaging and spectral Doppler (Ivey *et al.*, 1995). Intensities of 19,000 W cm⁻² in 12 ms bursts or 4,300 W cm⁻² in 25 ms bursts were needed for robust cavitation in the aorta. This concept has also been applied to a urinary bladder model, for the purpose of developing a method to aid detection of urinary reflux (Hwang *et al.*, 1998).

4.3.2 *Physics of Contrast-Agent Excitation*

Most contrast agents currently under commercial development for clinical use consist of some form of stabilized microbubble in

suspension. It had been argued from early work that microbubbles show no resonant behavior in whole blood, but Schrope *et al.* (1990) have shown that to be a misconception. Bleeker *et al.* (1990) investigated the commercial product Alunex[®], which consists of albumin-encapsulated microspheres of air averaging a few micrometers in diameter. By measuring the attenuation of ultrasound as it passed through suspensions of these microspheres, they demonstrated distinct resonances in the range 3 to 4.5 MHz. Measurements of scattering showed that these air bodies are more effective, by orders of magnitude, as scatterers of ultrasound than are cells of the blood; this is consistent with considerations in Section 4.1.5. Recent measurements of signal loss through Alunex[®] suspensions indicate maximal loss at about 2 MHz (see Figure 4.9). The modification of the theory for pulsation of free bubbles needed to account for a stabilizing film or shell has been considered by several investigators including Church (1995), de Jong *et al.* (1994a), Fox and Herzfeld (1954), Glazman (1983; 1984), Roy *et al.* (1990), and Ye (1996). These theories are particularly applicable to contrast agents with shells, like Alunex[®], and measurements have demonstrated reasonable agreement with theory for this agent (de Jong and Hoff, 1993; de Jong *et al.*, 1994b). The theory for small amplitudes is based on

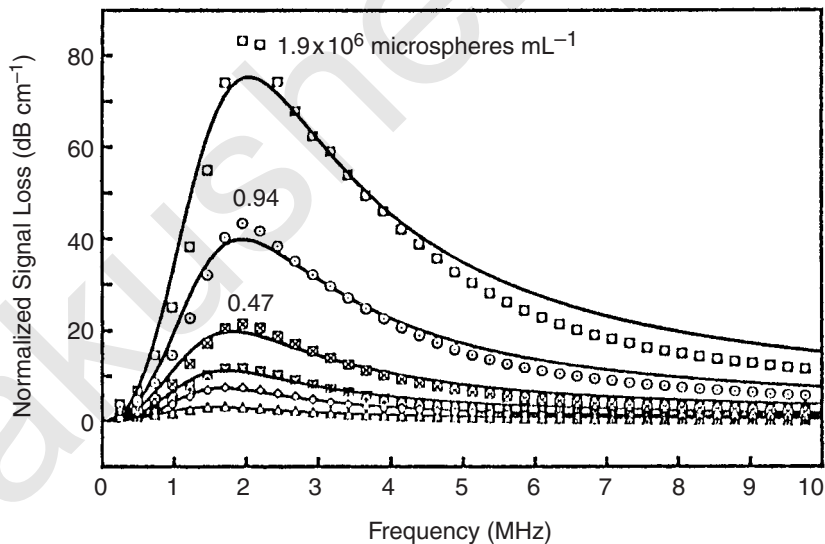


Fig. 4.9. Data on the signal loss through Alunex[®] suspensions at the indicated concentrations ($1.9, 0.94, 0.47, 0.23, 0.12$ and 0.05×10^6 microspheres per milliliter) as a function of frequency compared to theoretical calculations (lines) (Marsh *et al.*, 1997).

the linear models discussed in Section 4.1. Essentially, the shell adds a component k_{sh} to the stiffness of the oscillating bubble (in addition to the gas stiffness), given by:

$$k_{\text{sh}} = 8 \pi S_s. \quad (4.55)$$

Here, the shell parameter (S_s) has been determined to be about 8 N m^{-1} for Alburnex[®], corresponding to a Young's modulus of 466 MPa for a 12 nm thick shell and Poisson's ratio of 0.3 (de Jong *et al.*, 1994a). This added stiffness increases the resonance frequency of a given size gas-body, relative to a free bubble. In addition, the shell contributes to the damping of the oscillations, with an additional damping coefficient given by:

$$\delta_{\text{sh}} = \frac{S_f}{m \omega} \quad (4.56)$$

in which m is the effective mass (Equation 4.25) and the shell viscosity parameter (S_f) has been determined to be about $4 \times 10^{-6} \text{ N s m}^{-1}$ for Alburnex[®] (de Jong *et al.*, 1994a). The additional damping reduces the response of the gas body relative to a free bubble. This model has also been applied to relatively thick-shelled ($\sim 200 \text{ nm}$) gas bodies in Quantison[®] (Andaris Ltd., Nottingham, United Kingdom), which have higher elasticity and friction parameters than Alburnex[®] gas bodies (Frinking and de Jong, 1998). Church (1995) presents several detailed calculations of the response of shelled gas bodies. The resonance frequency as a function of gas-body size is shown in Figure 4.10 for several values of shell rigidity. The value of shell rigidity corresponding to the shell parameter of de Jong *et al.* (1994a) is 88.8 MPa (Church, 1995). In general, the response of the encapsulated gas bodies is reduced from that of free bubbles, particularly for harmonics such as the second harmonic. This restricted behavior also reduces the effect of gas body suspensions on speed of sound, attenuation and scattering cross section relative to free bubbles. Nevertheless, Alburnex[®] can produce large scattering effects at moderate concentrations due to the great number of gas bodies present. Marsh *et al.* (1997) found through transmission losses up to 80 dB at about 2 MHz for a concentration of $1.9 \times 10^6 \text{ mL}^{-1}$. Theoretical consideration of these results indicated a shell elasticity of 4.2 N m^{-1} , and a shell viscosity parameter of $5.4 \times 10^{-6} \text{ N s m}^{-1}$. Calculations of the resonance size and damping coefficient based on these parameter values are listed in Table 4.1. Clearly, the engineering of ultrasound contrast agents involves trade-offs in terms of stability (enhanced with thick shells), as opposed to contrast effectiveness relative to free bubbles.

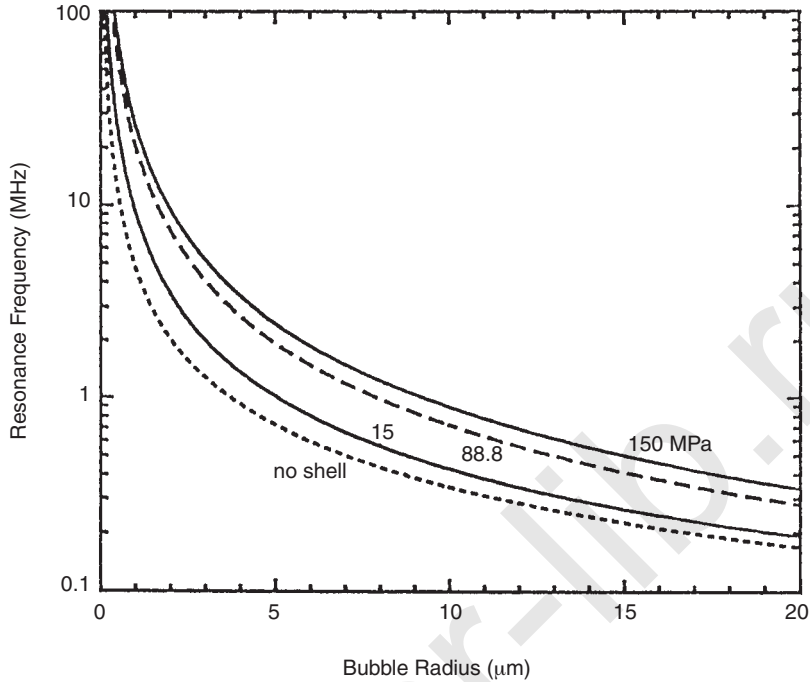


Fig. 4.10. Resonance frequencies of encapsulated bubbles as a function of radius and the shell elastic parameter in megapascal (Church, 1995).

4.3.3 Stability and Nucleation of Inertial Cavitation

Although gas body contrast agents are stable in storage for extended periods, they can become unstable during handling and use. The stability of Albunex[®] has been extensively studied. The contrast effect can be modified by modest pressures such as are found in the circulation (Vuille *et al.*, 1994), and the gas bodies can even be destroyed at physiologic pressures (Brayman *et al.*, 1996c; Gottlieb *et al.*, 1995). The gas bodies are also susceptible to destruction by ultrasound. At 2.5 MHz, backscatter decreased *in vitro* for pulse-pressure amplitudes greater than 0.15 MPa and decreased readily for pulse pressures greater than 0.33 MPa (Vandenberg and Melton, 1994).

The interaction of ultrasound with a gas body contrast agent is, by definition, a form of cavitation. Determination of how this “engineered” cavitation compares and relates to “natural” GBA, noninertial cavitation, and inertial cavitation represents a key problem for assessing the potential for nonthermal bioeffects as contrast agents

become widely used in the clinic. As noted in Section 4.3.2 in regard to GBA, Albunex® behaves as expected from theory for shell-encapsulated gas bodies for low-amplitude measurements of ultrasonic scattering. Comparison to cavitation phenomena occurring at higher amplitudes is more difficult. Using active cavitation detection methods *in vitro*, Albunex® has been shown to produce emissions indicative of cavitation (Holland and Apfel, 1990; Roy *et al.*, 1990). In contrast, this response could not be demonstrated with Albunex® using a diagnostic ultrasound system at 2.5 MHz nor at 5 MHz for peak negative pressures up to 1.2 MPa (even though hydrophobic polystyrene microspheres did initiate cavitation) (Holland *et al.*, 1992).

The presence of stabilizing shells inhibits the pulsation of contrast-agent gas bodies. However, the shells are readily broken and other agents merely have surfactant coatings which are expected to inhibit oscillation less than elastic shells do. Albunex® is particularly subject to ultrasonic destruction (Vandenberg and Melton, 1994), but most agents appear to be susceptible to destabilization (Walker *et al.*, 1997). After destabilization the resulting entity may behave like a free bubble, before dissolving away, which helps to explain “stimulated-emission,” “flash,” or “transient-response” effects (Section 4.3.4). Therefore, much of the interaction of diagnostic ultrasound with contrast agents appears to involve essentially free bubbles, which exhibit cavitation-like behavior. The breakage of encapsulated gas bodies such as Quantison® has been noted to provide a robust vehicle for localized delivery of free-gas bubbles, which were considered to be the ultimate contrast agent (Frinking *et al.*, 1999).

In addition to the expected second-harmonic response, the agent Albunex® returns subharmonic signals, an established cavitation indicator, at modest exposure amplitudes (Lotsberg *et al.*, 1996; Miller and Bao, 1998). One factor in this strong subharmonic response appears to be the larger size of resonant shelled gas bodies relative to free bubbles. A resonant Albunex® gas body might liberate a free bubble about twice the linear resonance diameter for the frequency employed, which is the size most likely to exhibit subharmonic oscillation (Miller, 1998). This signal was returned from Optison® at a pressure amplitude of about 10 kPa, which was lower than expected from theory for the pulsation of the gas bodies (Shankar *et al.*, 1999). This rather low threshold may indicate unexpected behavior, different from simple linear pulsation, which may be related to the destabilization of the gas bodies.

The destabilization can lead to a full spectrum of acoustic emission. This phenomenon has been observed with SH U-563A (Sonovist®, Shering AG, Berlin, Germany), which has a polymer shell, and the

resulting nonlinear response has been termed “acoustically stimulated acoustic emission” (Uhlendorf and Hoffman, 1994). Frequency spectra of the emissions for 5 MHz pulses of 35 cycles and 1 MPa amplitude include sub- and ultra-harmonics at odd multiples of 2.5 MHz. The full range of harmonics, as well as the half-harmonic and its multiples, have been detected in signals from Optison® exposed to 4 MHz pulses *in vitro* (Shi and Forsberg, 2000). The spectrum changes with exposure pressure amplitude, as shown in Figure 4.11. Some of the characteristic nonlinear behavior appears to have application to diagnostic imaging procedures as discussed in Section 4.3.4.

These emissions received when the shell-encapsulated gas bodies break are essentially as expected of freely occurring ultrasonic cavitation. In work with the rotating tube system for *in vitro* cavitation studies, both Alunex® and Levovist® have been shown to be able to nucleate inertial cavitation when “natural” cavitation nuclei have been depleted (Miller and Thomas, 1995a). After nucleation, free cavitation bubbles contain air in which the temperature may rise dramatically upon collapse, generating free radicals and sonochemicals, such as hydrogen peroxide, with potential biological consequences (see Section 5.10). For continuous exposure at 2.95 MHz, both agents initiated significant hydrogen peroxide production at 0.58 MPa or higher, but not for 3.8 MHz up to 1.16 MPa.

The coatings on many contrast agents may inhibit the collapse behavior. In addition, newer contrast agents typically use perfluorocarbon gases, which have a high heat capacity. Theoretical modeling of the high-amplitude collapse response of perfluorocarbon bubbles indicate that the high temperature free radicals are greatly diminished (Church and Brayman, 1998).

Alunex® was found to nucleate vigorous cavitation activity for 1.28 MHz focused ultrasound even in canine whole blood, for 20 μ s duration pulses and 2 ms pulse repetition period, but with a threshold of 7.6 MPa temporal peak pressure amplitude (Miller and Thomas, 1996a). In this experiment, the biological effect of hemolysis was used as the cavitation indicator (see Section 6.2.2).

A similar result was found with high-intensity focused ultrasound at 1.1 MHz (Poliachik *et al.*, 1999). Alunex® concentrations as low as 0.28 μ L mL⁻¹ in whole blood exposed for 1 s to 2,360 W cm⁻² (approximately 8.4 MPa) lead to significant hemolysis relative to sham exposure or exposure without added contrast agent. The hemolysis was correlated with both the number of cavitation events and with the integrated cavitation emission signal detected with a passive ultrasound receiver.

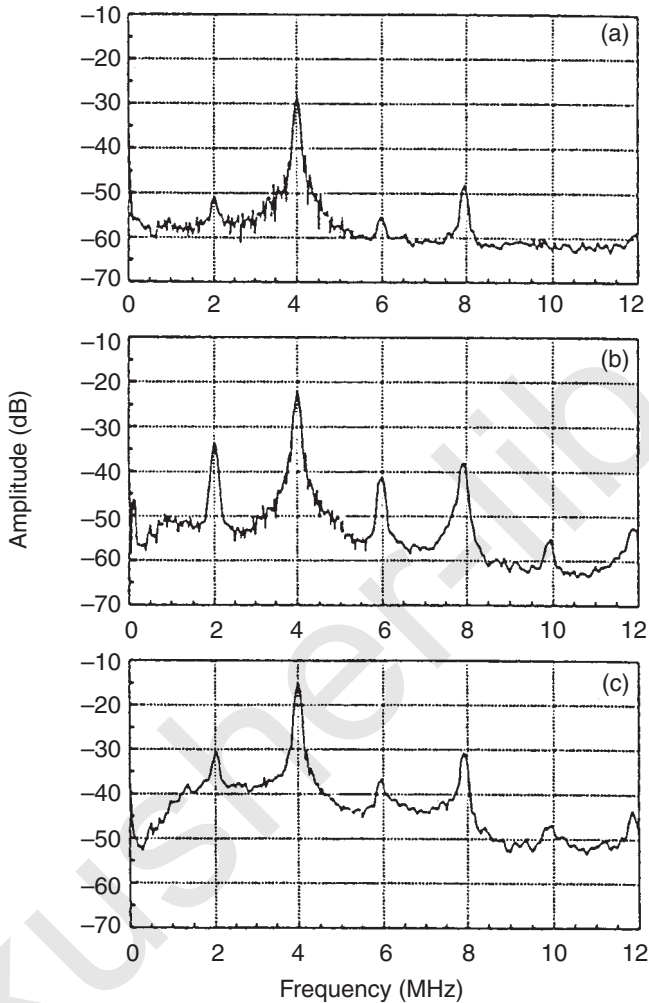


Fig. 4.11. Spectra of the scattered signals from Optison® microbubbles insonified at pressure amplitudes of: (a) 0.8 MPa, (b) 1.6 MPa, and (c) 2.4 MPa. These spectra were not corrected for the frequency response of the receiving transducer. The experiment for each spectrum was carried out at around 1 min post injection using an Optison® microbubble suspension with a concentration of $0.10 \mu\text{L mL}^{-1}$. Acoustic pulses with a center frequency of 4 MHz and a length of 32 cycles were transmitted at a *PRF* of 10 Hz (Shi and Forsberg, 2000).

In an experiment using the rotating tube exposure system, some cavitation nuclei of some form were found to survive the apparent destruction of Alburnex[®] gas bodies (Brayman and Miller, 1997). When a normally cloudy solution of five percent human serum albumin with 3.6 percent Alburnex[®] was treated with 1 MHz ultrasound with 0.8 MPa rarefactional amplitude pulses 10 μ s in duration (0.5 duty cycle), the suspension cleared due to gas-body destruction. When an equal volume of whole blood was added, and the mixture re-exposed, significant hemolysis relative to shams of 0.4 percent was produced, indicating that some form of nucleating entity survived. This persistence of nuclei appears likely to be related to the ability of albumin to stabilize gas bodies; for example, Alburnex[®] itself is produced by sonicating human serum albumin solution.

4.3.4 *Exploitation for Medical Purposes*

The medical utilization of contrast agents for diagnostic purposes has developed along with the agents and the literature on this area of diagnostic ultrasound continues to grow rapidly. A complete review of all medical uses and procedures of ultrasound contrast agents lies outside the scope of this Report; however, some developments that might have a bearing on the safety question are briefly noted in this Section.

One difficulty with early agents is that often not enough of the available small (2 to 7 μ m) gas bodies get through the lung to be detected well in the distal human circulatory system although they are visualized in the human heart and distal systems of small animals (Goldberg *et al.*, 1994). This problem is being reduced with the advent of better agents as reported by Simon *et al.* (1992) and Unger *et al.* (1992) where lipid structures have been used to stabilize the bubble. The detection of any of these small bubbles in low densities may require relatively high amplitude ultrasound.

After intravenous injection, most agents are depleted from the circulation by the lungs, which acts as an effective filter for microbubbles (Butler and Hills, 1979). Even good transpulmonary agents are rapidly removed from the blood by the reticuloendothelial system. Nearly 80 percent of Alburnex[®] injected into rats is cleared from the blood within 2 min and ends up inside the Kupffer cells of the liver (Walday *et al.*, 1994a). In pigs, most of the agent was retained by the lungs (Walday *et al.*, 1994a). The injected agent gradually disappears from the body as it is degraded, and only trace amounts of radio-labeled Alburnex[®] material could be found in internal organs after 24 h (Walday *et al.*, 1994b). Some lipid coated microbubbles may

persist longer in the circulation and appear to be taken up by tumor cells, which may enhance tumor visualization by ultrasound (Barbarese *et al.*, 1995).

Improvements in contrast agents should eventually lead to the advent of an agent with considerable longevity and stability. At the present time, such attributes are still somewhat elusive. For both general contrast generation and bolus transit measurements (Segil *et al.*, 1988), a contrast enhancement system has been investigated experimentally and theoretically (Fowlkes *et al.*, 1992a; 1992b) to create bubbles and/or regrow bubbles from injected agents, at a subcapillary size, to a larger size for visualization of a small number of bubbles. This bubble stabilization outside the lungs may be similar to that found in sea water in which bubbles persist for hours longer than expected. The resonance properties of bubbles can also be exploited for diagnostic measurements of blood pressure (Fairbank and Scully, 1977).

The most straightforward use of gas-body contrast agents is to enhance the display of blood flow on diagnostic imaging systems. In B-mode imaging, scattering from the gas bodies simply increases the brightness of regions containing blood, although this can be at the expense of shadowing of tissue image behind the enhanced region (Uhlendorf, 1994). Using theory for scattering, the brightness and shadowing effects can be described by taking into account the shell parameters (Soetanto and Chan, 2000). The kinetics of the Doppler enhancement consist of a rapid increase in brightness, followed by a slow decline and can be modeled by simple indicator-dilution theory (Schwarz *et al.*, 1996). Using measurements of scattering and transmission loss, a scattering-to-attenuation ratio can be determined to characterize the effectiveness of different contrast agents (Bouakaz *et al.*, 1998), but this single quantity may not be sufficient for a complete comparison of different agents (Marsh *et al.*, 1999).

Mainframe ultrasound machines can display images in real time, with pulsed-Doppler information coded in color (as directional flow or "power Doppler") and contrast agents are used to increase sensitivity and accurately depict pulsatile flow velocities. Several artifacts can hinder the use of contrast agents for this purpose (Forsberg *et al.*, 1994). For example, color blooming (*i.e.*, display of color-Doppler information indicated in areas without flow) occurs immediately after injection of an agent, obscuring tissue information. The agents can also cause the indication of higher Doppler shifts (high blood speed) than was present before injection. In addition, it is possible for the gas bodies to create "bubble noise," which apparently is a result of cavitation activity induced by the imaging ultrasound and appears as large excursions on Doppler M-mode recordings.

Contrast agents rapidly disappear from the circulation, which tends to produce time varying enhancement and to limit the examination time. Such problems can be reduced by using a continuous infusion of contrast agent, rather than a simple bolus injection (Weissman *et al.*, 2000). Another scheme takes advantage of the retention of larger gas bodies in the tissue capillaries (Kasprzak *et al.*, 1998). The agent Myopmap[®] (also called Quantison Depot[®]), which has relatively large gas bodies averaging about 10 μm in diameter (Frinking and de Jong, 1998), is deposited in the myocardium and remains after the bulk of the agent injected through an atrial catheter washes out of the chambers. The myocardial mass is then enhanced and readily delineated in the ultrasound images.

Contrast agents can sometimes disappear into an image, so that the regions with agent blend-in with the other tissue. One method which is under development for enhancing the contrast produced by gas-body contrast agents takes advantage of the nonlinear response of the gas bodies. The second harmonic is particularly useful for this purpose (Schrope *et al.*, 1992). Using a sending beam centered at 3 MHz for example, the image would be formed from the 6 MHz component of the returning echoes. Because pulsating gas bodies are especially effective in converting some of the incident ultrasound to the second harmonic, the method can, in principle, result in a display that emphasizes the configuration of contrast agent in the tissue. Laboratory research on this method has shown promise (Chang *et al.*, 1996; Schrope and Newhouse, 1993). Second-generation agents such as FS069 may be better suited to this purpose than first-generation agents like Albunex[®] (Krishna and Newhouse, 1997). With newer transpulmonary contrast agents, for example, blood flow in the coronary arteries might be visualized by this method (Mulvagh *et al.*, 1996) and tumor vasculature may be more readily recognized (Forsberg *et al.*, 1998a; 1998b). Further, for a method commonly called "harmonic imaging," clinical instruments have been developed to form images from other returned frequencies (in addition to the second harmonic) above the transmitted central frequency. This imaging method also finds particularly advantageous application to contrast agents (Burns, 1998). Still another method that takes advantage of the nonlinear behavior of the contrast-agent gas bodies is known as "pulse inversion imaging" (Burns *et al.*, 2000; Harvey *et al.*, 2000). In this method, pulses of alternating sign (*i.e.*, 180 degrees out of phase) are transmitted into tissue, and the resulting echos are summed. Because gas bodies respond differently to pulses with initially negative or positive half-cycle, while tissues do not, the tissue signal tends to cancel, leaving the gas-body signal to be displayed in the resulting image. This method may allow use of sufficiently low amplitudes to

avoid breakage of the gas bodies (Burns *et al.*, 2000). Undoubtedly, other novel imaging methods will be devised for taking advantage of the unique properties of contrast agents.

As noted in Section 4.3.3, contrast agents can generate nonlinear emissions, which may be useful for medical imaging. The subharmonic signal may be especially suitable for this purpose because it is not normally returned from tissues of the body (Shankar *et al.*, 1998). This strategy appears to be useful for pulse echo imaging (Shi *et al.*, 1999a). In addition, the subharmonic may be useful for assessment of hydrostatic pressure (*e.g.*, in the heart), owing to the variation in the signal strength with hydrostatic pressure (Shi *et al.*, 1999b).

Another imaging method utilizes the nonlinear behavior of stimulated acoustic emission from the gas bodies to form a color- or power-Doppler image (Uhlendorf and Scholle, 1996). The phenomenon is short-lived, and seems to depend on breakage of the gas bodies rather than their movement (*i.e.*, the Doppler detection appears to be falsely generated by the gas-body behavior), because it can be produced with Sonovist® gas bodies fixed in a gel phantom (Forsberg *et al.*, 1999a; 1999b). The phenomenon can be produced with other agents, for example, Levovist® (Blomley *et al.*, 1998). The contrast effect appears as a random mosaic pattern of color in color-Doppler mode and can be detected after the vascular contrast effect has diminished. The method has diagnostic value particularly in the liver. The retention of the gas bodies in the liver may result from the action of the reticuloendothelial system, which localizes the effect to normal regions of tissue and accentuates the presence of tumors by its absence (Blomley *et al.*, 1999a; Hauff *et al.*, 1997). Although the effect can be seen in the other tissues such as kidney soon after injection, the late phase of imaging method appears to be confined to the liver and spleen (Blomley *et al.*, 1999b). The imaging of the mosaic pattern seems to require relatively high pressures, as it depends on focal zone placement and on penetration depth at different frequencies.

The transient nature of the intense contrast reaction has been noted in gray-scale images and imaging methods have been developed to accommodate this behavior. Flash echo imaging utilizes the first frame in a real-time B-mode image sequence to accentuate the contrast agent (Kamiyama *et al.*, 1999). In order to take full advantage of this method, special imaging software may be needed to intermittently collect frames while avoiding contrast destruction. A similar procedure, transient-response imaging, has been used with harmonic imaging of the heart (Porter *et al.*, 1996). This method requires the triggering of the ultrasound at slow frame rates, such as once per cardiac cycle, which allows the tissue to refill with contrast agent from the circulation. In an application to imaging the perfusion of the brain, this method has

been performed with triggering every four cardiac cycles (Postert *et al.*, 1998). The exact nature of the transient phenomenon in these methods is not completely clear, but appears to stem from the destabilization of the contrast-agent gas bodies which results in their dissolution.

The contrast-agent destruction caused by ultrasound can also be exploited in a different way. If a relatively high power ultrasound beam is aimed at the artery feeding an organ, then the contrast agent can be completely destroyed for a desired period. This action produces a negative bolus with sharp rise time in the tissue, which allows simple wash-in, wash-out measures of blood flow (Fowlkes *et al.*, 1998). A 1.8 MHz beam was used to generate 0.25 to 1 s tone bursts for contrast interruption in the femoral artery, which was observed by diagnostic ultrasound imaging in a rabbit tumor model. In the method, imaging fields can be relatively low amplitude in the tissue of interest because the contrast-agent destruction occurs elsewhere.

4.4 Physical Consequences of the Vibration of Bubbles or of Stabilized Gas Bodies

As explained in Section 4.1, the nonlinear equations which govern acoustics can be used to evaluate physical quantities to various orders of approximation. In a CW sound field, the first-order quantities vary sinusoidally with time so that, by the first-order approximation, all particles of the medium return to their original positions every cycle. To account for net changes in the medium (such as biological effects) one must use an approximation of higher order. It is found for the phenomena taken up in this Section, as for the applications treated in Section 3, that the second-order approximation (see Section 4.1.1) leads to a great deal of useful information and is adequate for many purposes. In a sound field where the sources vibrate sinusoidally in time, with frequency (f) and typical amplitude (A), a second-order quantity has these characteristics, at any point in space: (1) it consists of two parts, one of which varies sinusoidally in time with (second-harmonic) frequency ($2f$), while the other is time-independent; and (2) the magnitude of each part is proportional to A^2 . The time-independent part of a second-order quantity (q) is the same as the time average of q over one or more (complete) cycles.

Examples of second-order quantities, applicable to vibrating bubbles, are the time-averaged energy densities, $\langle E_p \rangle$ and $\langle E_k \rangle$, for which expressions are given in Equations 4.12 and 4.14. Other examples of time-independent phenomena, treated in subsequent sections, include acoustic power, the rate of heat generation, radiation forces, and acoustic streaming.

4.4.1 Acoustic Power Radiated and Heat Generated by a Vibrating Bubble

We let $\langle W \rangle$ represent the total rate of energy lost from a vibrating bubble. In Equation 4.16 the term $b(d\xi/dt)^2$ gives W ; making use of Equation 4.24 we obtain:

$$\langle W \rangle = m \omega_0 \delta \left(\frac{d\xi}{dt} \right)^2 = 1/2 m \omega_0 \omega^2 \delta \xi_0^2 \quad (4.57)$$

because $d\xi/dt$ is equal to $\omega\xi$ and $\langle \xi^2 \rangle$ is equal to $1/2 \xi_0^2$. At resonance for a spherical bubble, we obtain from Equations 4.19 through 4.26 that the power lost by the bubble in an ambient sound field of pressure amplitude (p_0) is:

$$\langle W \rangle = \frac{2 \pi R_0 p_0^2}{\rho_0 \omega_0 \delta}. \quad (4.58)$$

If the ambient field is a traveling plane wave, the above equation can be expressed in terms of the intensity (I), because the latter is equal to $1/2 p_0^2/\rho_0 c$. The result can be written:

$$\langle W \rangle = sI, \quad (4.59)$$

where s has units of area and can be interpreted as a cross section. The quantity $\langle W \rangle$ in Equation 4.57 represents loss from radiation as well as from heat production; the radiation is referred to as *scattering* and the heat production as *absorption*. Then s is the absorption-scattering cross section for the bubble; comparing Equations 4.58 and 4.59 yields a result for s at resonance which can be written:

$$s = \left(\frac{2 \lambda_0}{\pi R_0 \delta} \right) \times \pi R_0^2. \quad (4.60)$$

Here, λ_0 is the acoustic wavelength ($2 \pi c/\omega_0$) in water at the resonance frequency. The parenthetical expression by which πR_0^2 is multiplied in Equation 4.60 gives the ratio of s to the geometric cross section for the spherical bubble. This ratio is typically very large for a resonant air bubble in water. For example, at a frequency of 2 MHz [where the resonance radius (R_0) is 1.7 μm , λ_0 is 0.75 mm, and δ is 0.16] the cross section is 1,700 times as large as the geometric cross section and is $1.6 \times 10^{-8} \text{ m}^2$. That part of the energy loss which is due to scattering can be obtained as the product of $\langle W \rangle$, given by Equation 4.57, and the ratio ($\delta_{\text{rad}}/\delta$); the remainder of $\langle W \rangle$ is due to absorption. The scattering cross section (s_{sc}) is, similarly, the product

of s , given by Equation 4.60 and the ratio $(\delta_{\text{rad}}/\delta)$; the absorption cross section (s_{abs}) is just $(s - s_{\text{sc}})$.

A plane wave traveling through a medium in which there are bubbles will be attenuated because of energy loss to them. Suppose there are N identical bubbles per unit volume, and that N is small, so that the bubbles respond independently to the sound field. Then, for a wave traveling along x , the intensity will be given as:

$$I = I_0 e^{-2ax}, \quad (4.61)$$

where I_0 is constant and the attenuation coefficient (a) is:

$$a = Ns/2. \quad (4.62)$$

For example, if the frequency is 2 MHz and $N = 1 \text{ mm}^{-3}$, one obtains 0.08 Np cm^{-1} for a ; this may be compared with a typical value of 0.1 Np cm^{-1} for the attenuation coefficient of liver at 2 MHz. Equations 4.59 through 4.62 give us a ready means of calculating the heat production by a traveling sound wave in a bubble medium. Letting $\langle Q \rangle$ be the time-averaged rate at which heat is produced per unit volume one obtains, simply:

$$\langle Q \rangle = 2 \alpha I = N s_{\text{abs}} I, \quad (4.63)$$

where s_{abs} is the absorption cross section and α is equal to $1/2 N s_{\text{abs}}$. Letting $\langle q \rangle$ be the time-averaged rate of heat production by a single bubble, we see from Equation 4.63 that this is given by $s_{\text{abs}} I$. Alternatively, an expression for $\langle q \rangle$ is obtained (for a resonant bubble) by proceeding from Equation 4.58:

$$\langle q \rangle = (2 \pi R_0 p_0^2 / \rho_0 \omega_0) \times (\delta_{\text{vis}} + \delta_{\text{th}}) / \delta^2. \quad (4.64)$$

Solving the steady-state heat conduction problem for a spherical heat source of radius (R_0) yields for the temperature rise at the bubble surface:

$$\Delta T = \langle q \rangle / 4 \pi K R_0, \quad (4.65)$$

where K is the coefficient of thermal conductivity for the liquid. Combining Equations 4.64 and 4.65, one can calculate ΔT ; however, the results will be accurate only when the governing equation, Equation 4.17, is valid, *i.e.*, only under conditions of linearity. This requirement puts a limit on the pressure amplitude. In water at 1 MHz, the damping constants δ_{rad} , δ_{vis} and δ_{th} have the values 0.014, 0.06 and 0.07, respectively (Coakley and Nyborg, 1978). Using values of ρ_0 and K for water and choosing the modest value 10^4 Pa for p_0 , one obtains $0.08 \text{ }^\circ\text{C}$ as the temperature rise ΔT at the surface of a resonant bubble in water at a frequency of 1 MHz. According to this linear model, the predicted temperature rise is proportional to p_0^2 .

Wu (1998) has estimated that a 2 MHz ultrasound beam of intensity 110 mW cm^{-2} can produce a temperature rise of about 2°C in 10 s if contrast agents are present. Calculations of the temperature rise expected for the much higher values of p_0 often used in medical applications require use of nonlinear theory for the bubble dynamics; recent findings on this have been published by Hilgenfeldt *et al.* (2000).

4.4.2 Acoustic Radiation Force on a Gas Bubble, Bubble Motion, and Associated Hydrodynamic Shear

In a sound field, a bubble (or any other object) is acted on by stresses at its surface. As a result, a net force may exist on the object. Like other acoustic quantities, as discussed in Section 4.1.1, the force can be expressed as the sum of contributions of varying order. In an acoustic field of frequency (f), the first-order contribution to the force varies sinusoidally in time with frequency (f) and causes the object to oscillate with the same frequency. There are two parts to the second-order contribution; one varies sinusoidally in time with the second-harmonic frequency ($2f$), while the other is time-independent. It is the latter contribution which is called the *acoustic radiation force*, and is under discussion here.

Consider a sound field in which the acoustic pressure is an arbitrary function of space and a sinusoidal function of time with frequency (f). Suppose a gas bubble of momentary volume (V) exists at a location where the momentary acoustic pressure is p and its gradient is ∇p . Then (when effects of viscous stresses are neglected) the radiation force (F) is given by the time-averaged second-order approximation to $-V\nabla p$. For this purpose it suffices to use first-order approximations to V and ∇p . For V , this leads to:

$$V = V_0(1 + 3 \xi/R_0), \quad (4.66)$$

where V_0 is the undisturbed bubble volume ($4 \pi R_0^3/3$) and the vibrational displacement (ξ) is as obtained in Section 4.1.2 and given in Equations 4.18 through 4.26. As in Section 1.2, we take p to be given by $p_0 e^{j\omega t}$ but now consider p_0 to be, in general, a function of space expressed as a complex quantity; thus:

$$p_0 = p_{0m} e^{j\psi}, \quad (4.67)$$

where the amplitude (p_{0m}) and phase (ψ) are both real, and may both be the functions of space. Using the identity in Equation 4.29 and letting (p^* , p_0^*) be the complex conjugates of (p , p_0) respectively, we obtain:

$$F = -(3 V_0/2 R_0) \operatorname{Re}(\xi \nabla p^*), \quad (4.68)$$

recognizing that the time-average of $V_0 \nabla p^*$ is zero because p^* is approximated as a first-order quantity. Referring to Equations 4.18 through 4.26 we find that one can write:

$$\xi \nabla p^* = \xi_0 \nabla p_0^* e^{j\beta}. \quad (4.69)$$

Using Equation 4.19 for ξ_0 and $2 \pi R_0^2$ for $3 V_0/2 R_0$ we obtain a result that can be written as:

$$F = -(8 \pi^2 R_0^4 / k_s) X, \quad (4.70)$$

where:

$$X = \chi \operatorname{Re}(p_0 \nabla p_0^* e^{j\beta}). \quad (4.71)$$

Using Equation 4.67 one obtains:

$$\nabla p_0^* = [\nabla p_{\text{om}} - j p_{\text{om}} \nabla \psi] e^{-j\psi}. \quad (4.72)$$

Making use of Equations 4.20, 4.21, 4.71 and 4.72 one can write:

$$X = \chi^2 [1/2(\Omega^2 - 1) \nabla p_{\text{om}}^2 + \Omega \delta p_{\text{om}}^2 \nabla \psi]. \quad (4.73)$$

Examining Equation 4.73 we see that the radiation force (F) on a bubble depends on the nature of the ultrasound field and on the radius of the bubble relative to the resonance value. By considering different situations one arrives at the following rules:

1. In a plane traveling wave (constant amplitude) the radiation force on a bubble is in the direction of sound propagation, regardless of the bubble size.
2. In a plane standing wave (where the phase is essentially constant between the minima of the pressure amplitude) the radiation force on a bubble is toward (away from) a pressure maximum if it is smaller (larger) than resonance size.
3. In the region very near a small sound source, at distances from it small compared to the wavelength, the phase is essentially constant and the radiation force on a bubble is toward (away from) the source if it is smaller (larger) than resonance size.

The above qualitative rules are very useful in understanding the motion of bubbles in a sound field. For example, under suitable viewing conditions it is common to see bubbles traveling along the axis of an ultrasound beam in water, the speed being especially great for bubbles of resonance size. During *in vitro* bioeffects studies the speeds of resonance size bubbles in a traveling wave field can become biologically significant in terms of hydrodynamic stress (Miller *et al.*,

1991a). In a rotating exposure system, the translational motion of bubbles seems to be particularly important, as bubbles shuttle across the chamber. The radiation force (F_r) on a resonant bubble is given, if surface tension $\sigma = 0$, from Equations 4.70 and 4.73 (Coakley and Nyborg, 1978) as:

$$F_r = V_0 k p_0^2 / 2 \Gamma \delta P_0, \quad (4.74)$$

in which V_0 is the bubble volume, k the wave number, P_0 the ambient static pressure, and p_0 the acoustic pressure amplitude. The polytropic exponent (Γ) may be approximated by unity when R_0 is small. Because the force depends on p_0^2 , it is proportional to the incident intensity. For slow motion, the viscous drag (F_v) on the bubble is given as $6 \pi \eta a U$ by the Stokes formula (Coakley and Nyborg, 1978), in which η is the shear viscosity coefficient (1 MPa s = 1 cP in water), and U is the translational velocity. The bubble will rapidly attain a terminal velocity, which is found by equating F_r and F_v , then solving for U . The velocity is sufficient, however, that the use of the simple Stoke's formula is questionable. This drag formula is only accurate for slow motion, for which the Reynold's number (N_r) is:

$$N_r = \rho_0 a U / \eta < 1, \quad (4.75)$$

in which $\rho_0 = 1 \text{ g cm}^{-3}$ is the density of the medium. For higher Reynold's numbers, the drag is increased above the amount expected from the simple formula. A correction equal to $1 + 3 N_r / 8$ can be used to multiply the simple value, but this is still only valid for $N_r < 1$ (Happel and Brenner, 1983). Neppiras and Coakley (1976) use the approximate correction $(1 + 0.2 N_r)$ for high Reynolds numbers [Neppiras and Coakley (1976) specifically use $(1 + 0.1 R_e)$, in which $R_e = 2 N_r$]. Using this approximation yields:

$$U = k a^2 p_0^2 / [9 \eta \Gamma \delta P_0 (1 + 0.2 N_r)]. \quad (4.76)$$

Interactive calculation with the values given above, and p_0 , P_0 both equal to 100 kPa, yields $U = 1.35 \text{ m s}^{-1}$, with $N_r = 2.8$. This is a relatively high speed for a pressure-amplitude level equivalent to an intensity of only 0.33 W cm^{-2} in a traveling plane wave. The dependence of drag on N_r means that increasing the force on a bubble, which is already moving fast, produces less than the expected increase in bubble speed (*i.e.*, less than proportional to the intensity). For very high Reynolds numbers in this approximation, the velocity is expected to be roughly proportional to the pressure amplitude (*i.e.*, the square root of the intensity). At such speeds, the extra energy taken up by the extra drag raises the level of perturbation of the medium, with the possible generation of a turbulent wake behind

the bubble. The calculation using Equation 4.76 is only a rough approximation; however, improved theory, which takes into account the nonlinear behavior of bubbles, also indicates that speeds of the order of 10 m s^{-1} can be expected for typical experimental conditions (Carstensen *et al.*, 1993).

The hydrodynamic flow around the bubble can be estimated from simple theory. For a small sphere, with a nonslip boundary condition as expected for a small bubble (Happel and Brenner, 1983), fluid velocity components in the radial and angular directions are:

$$v_r = -1/2 U \cos\theta[(a/r)^3 - 3(a/r) + 2] \quad (4.77)$$

and

$$v_\theta = -1/4 U \sin\theta[(a/r)^3 + 3(a/r) - 4]. \quad (4.78)$$

The shear stress is given by the product of the viscosity and the gradient of the fluid velocity, and can arise in several different ways in the flow field of Equations 4.77 and 4.78. For example, a large radial stress (S_r) exists for v_θ at the sides of the bubble ($\theta = 90$ degrees), which is maximal at the bubble surface $r = a$ and given by:

$$S_r = 3 \mu U/2 a \quad (4.79)$$

For $a = 2.05 \mu\text{m}$ and $U = 10 \text{ m s}^{-1}$, the shear stress is $S_r = 7.3 \text{ kPa}$.

In a standing wave field, small bubbles tend to move to pressure maxima, remain there until they grow above resonance size, then move to pressure minima. Large bubbles are commonly seen to become locked into the planes defined by a standing wave field when stable cavitation occurs in a tank of water. As noted in Section 4.1.4, bubbles tend to shrink when not pulsating, and grow when the pulsation amplitude exceeds a threshold. The combination of radiation forces, which reverse at resonance size, and the threshold for growth near a pressure minimum in a standing wave field causes large bubbles to shrink at a pressure minimum, then move toward pressure maxima only to grow again and move back to the minima. This leads to an experimentally observed translational oscillation of bubbles (Miller, 1979b), which provides experimental confirmation of the theory.

In regard to biological effects, as pointed out by Church *et al.* (1982), biological cells in suspension tend to migrate *via* radiation force to pressure minima in a standing wave field. Thus, in an undisturbed medium, the radiation forces on cells tend to move them to regions where there is little cavitation action (due to the low pressure amplitude). Thus, *in vitro* biological effects are minimal in a standing wave field. Rotating or stirring the suspension so that the cells and

active bubbles will be brought together before the bubbles over-grow may encourage bioeffects.

Rule 3 (following Equation 4.73) is very much involved in the dynamics of bubbles in a sound field. A bubble is itself a small sound source and the rule explains much of the behavior of other bubbles in its vicinity. Thus, two bubbles smaller than resonance size attract each other and (if surface films do not prevent it) coalesce to form a single bubble. This process is a principal one in causing bubble growth, being complementary to the process of “rectified diffusion” discussed in Section 4.1.4. In applying the theory to bubble-bubble interactions, however, it must be realized that the total field consists of the ambient field plus that scattered by the bubble. For a bubble much smaller than resonance size, the scattered acoustic pressure at the bubble surface is in phase with the local acoustic pressure in the ambient field, as can be verified by examining Equations 4.21 and 4.22 together with Equation 4.36; hence, the resultant pressure amplitude decreases with radial distance and a second small bubble would be attracted to the first. For a bubble much larger than resonance size, the scattered pressure at the bubble surface is opposite in phase to the ambient pressure, so that the two tend to cancel; hence, the resultant pressure amplitude first increases with radial distance, then decreases after passing through a maximum, and small bubbles would tend to move to the position of this maximum.

4.4.3 *Acoustic Radiation Force on a Particle Near a Free Bubble or Stabilized Gas Body*

Cells and other suspended particles tend to collect at vibrating bubbles because of time-averaged forces, *i.e.*, radiation forces, exerted on them by the scattered field. In the immediate vicinity of a spherical bubble the force on a small solid or liquid particle is proportional to the gradient of the time-averaged acoustic kinetic energy density in the liquid (Section 3.2.7). This force gives rise to migration of the particle toward the bubble, with a speed equal to the magnitude of the radiation force divided by the frictional constant for the particle. For a small spherical particle of radius (a_s), its migration speed (v) toward the bubble is:

$$v = v_0 \left(\frac{R_0}{r} \right)^5, \quad (4.80)$$

where:

$$v_0 = \left[\frac{3 \rho_0}{\rho + 2 \rho_0} \right] \frac{s_c \omega^2 \xi_0^2}{R_0}. \quad (4.81)$$

Here, r is the distance between centers of the bubble and particle, ρ is the density of the particle, ξ_0 (as before) is the vibrational amplitude of the spherical bubble, R_0 is the undisturbed bubble radius, and s_c is the sedimentation constant for the particle. For a spherical particle of radius (a_s) in a liquid whose shear viscosity coefficient is η , one obtains:

$$s_c = \frac{2 a_s^2 (\rho - \rho_0)}{9 \eta} \quad (4.82)$$

The sedimentation coefficient (s_c) is employed in biophysics for characterizing biological particles by their migration under gravity or in a centrifuge; it is defined, for a particle falling under gravity in a viscous fluid, as the ratio of its terminal speed to the gravitational constant. By calculations it has been shown that a vibrating bubble can cause migration of nearby particles (including large molecules) at speeds comparable to those in a high-speed centrifuge.

Collection of particles or biological cells to ultrasonically activated gas-filled micropores is experimentally observable at megahertz frequencies (Miller, 1988b). Red blood cells are drawn to each active micropore (for example, 3.4 μm diameter micropores) at 2.1 MHz, and form patterns as shown in Figure 4.12. Presumably, similar phenomena occur near free bubbles in suspensions, but are not readily observable. In dilute biological suspensions, this process of particle collection at bubbles probably enhances the action of ultrasound, since it causes cells to move toward regions where shearing action occurs. When the cell concentration is high, the collection of cells at the boundary may inhibit the bubble vibration (see Section 7.2.3.2).

4.4.4 Acoustic Microstreaming Near a Vibrating Free Bubble

Experiments are described in Section 6, in which biological cells are perturbed or destroyed by ultrasound at low amplitudes in the presence of small stabilized gas bubbles. The action is probably chiefly a result of acoustic streaming, or of closely related phenomena. Acoustic streaming is a stable pattern of flow set up by a sound field; it is treated mathematically by theory based on a second-order approximation (Nyborg, 1965). The flow occurs in a fixed quantity of fluid and thus is circulatory in nature. Near a vibrating gas bubble

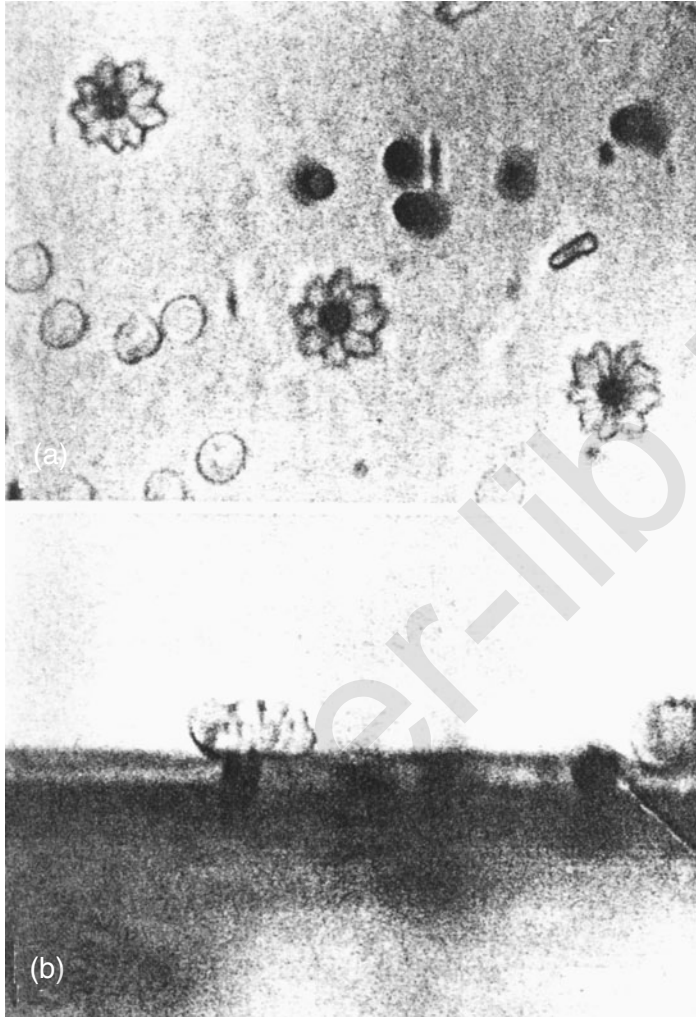


Fig. 4.12. Red blood cells attracted to ultrasonically activated gas-filled micropores (which appear black). (a) Viewed from above and (b) viewed from the side (Miller, 1988a).

located on a solid surface, or contained in a cavity at the surface, vigorous flow occurs in the form of circulations or vortices whose typical dimensions are comparable to those of the bubble or cavity. Because bubble-associated flow is of very small (“microscopic”) scale, it is appropriately called microstreaming.

In general the theory is complex, and only a few problems have been solved with high accuracy. For present purposes an approximate

solution will suffice. An expression has been obtained, which is applicable to the microstreaming produced by a body of gas contained in a small cavity and set into oscillation by a sound field (Nyborg, 1965). The flow under consideration occurs near the solid surface immediately surrounding the cavity. Let U be the streaming velocity parallel to the surface and directed radially outward from the cavity. From theory, the velocity (U) at a distance (r) from the center of the cavity, and at a distance (z) above the solid boundary, is given by:

$$U = U_L(1 - e^{-2Z} - 3e^{-Z}\sin Z), \quad (4.83)$$

$$U_L = Q_f^2/4 \pi^2 \omega r^5, \quad (4.84)$$

$$Z = z/\Delta, \quad (4.85)$$

$$\Delta = (2 \eta/\rho\omega)^{0.5}. \quad (4.86)$$

Here Q_f is the maximum during a cycle of the volume flow at the opening of the cavity; it is equal to $\omega \xi_{av} A$, where ω is the angular frequency, A the area of the opening, and ξ_{av} the average displacement amplitude of the gas-liquid interface over this area. The length (Δ) is called the acoustic boundary layer thickness; it refers to a (typically thin) layer of fluid near a solid boundary in which the tangential component of first-order velocity changes rapidly with distance from the boundary.

Figure 4.13 is based on Equations 4.83 through 4.86 and shows, using nondimensional quantities, how the streaming velocity (U) varies with distance from the boundary. At the boundary, U is zero, as required by a nonslip condition. At values of Z (*i.e.*, z/Δ) less than 1.1 the streaming velocity (U) is negative, that is, it is directed toward the cavity. The velocity is zero when Z is equal to about 1.1, and is positive for larger values of Z . As Z increases, U/U_L approaches unity, having the value 0.81 when Z is 2.4. Thus, according to Equations 4.83 through 4.86 the streaming velocity (U) approaches a limiting value U_L when z is large compared to the boundary layer thickness (Δ). Also, the velocity gradient at the boundary is given, in magnitude, by the simple expression:

$$|dU/dz|_{z=0} = U_L/\Delta. \quad (4.87)$$

The associated viscous stress (S_{rz}) is the product of the shear viscosity coefficient and velocity gradient; hence, at the boundary:

$$|S_{rz}|_{z=0} = \frac{\eta U_L}{\Delta}. \quad (4.88)$$

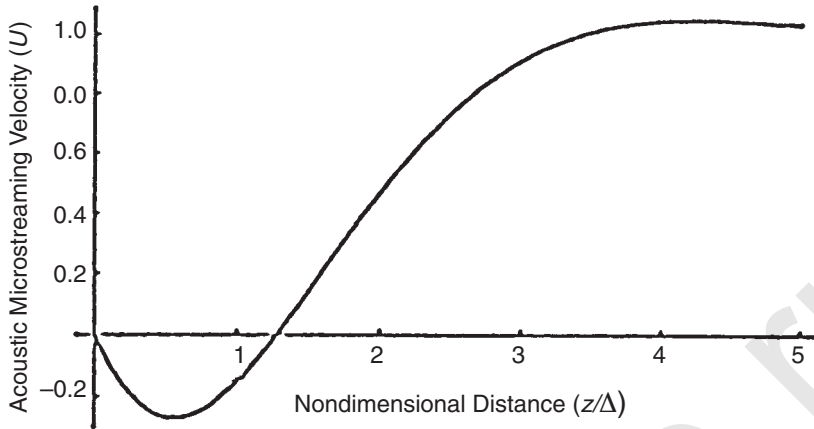


Fig. 4.13. Acoustic microstreaming velocity (U) (arbitrary units) parallel to a boundary near a small vibrating gas body versus distance (z/Δ) from the boundary, according to theory in which the vibrating gas body is modeled as a small sound source (Equations 4.83 to 4.86). In the boundary layer region, in which z is comparable to the boundary layer thickness (Δ), the velocity (U) varies rapidly with z ; here velocity gradients are relatively high and, hence, viscous stresses exerted on cells or other particles caught up in the flow are correspondingly high.

Equation 4.88 gives the largest value of the stress. The actual value varies with z , as is clear from examining the plot in Figure 4.13. The average magnitude of S_{rz} over the Z range from zero to two is about 0.6 times the boundary value given in Equation 4.88.

A biological particle passing along a solid boundary near a vibrating bubble, or gas-filled cavity, is subjected to viscous stresses associated with a nonuniform flow field. The shear stress can cause membrane damage in biological cells (Section 6). There is some evidence that the damage done to a cell in the microstreaming field near a vibrating bubble, or gas-filled cavity, occurs in a single pass, or in just a few passes, through the small critical region in which the velocity gradients are high. The time required for a single cell to be affected is thus very short, say, of the order of milliseconds. However, a much longer time is typically required for a suspension of cells to be affected, since this requires that all, or most, of the cells pass through a critical near-bubble region one or more times.

It should be realized that the theory given in Equations 4.83 through 4.86 is based on a series of assumptions, whose validity varies with the circumstances. While this simplified theory has been proven useful for predicting conditions under which cells will be affected by bubble vibration, it is not highly accurate. Lewin and

Bjorno (1982), while discussing applications of the microstreaming theory, have also pointed out some of its limitations.

4.4.5 Acoustic Microstreaming Near a Stabilized Gas Body

The acoustic microstreaming near an ultrasonically activated gas-filled micropore is closely related to that discussed above for the gas-filled bubble on a boundary. The flow can be observed by adding indicator particles to the liquid, which are taken up in the highly localized flow (Miller, 1988b). The flow is in the form of a toroidal eddy, which decreases in size as the ultrasonic frequency is increased. For example, the flow extends about $3 \mu\text{m}$ outward from $3.4 \mu\text{m}$ diameter micropores activated at 2.1 MHz. Red blood cells attracted to the micropores were caught up in larger flow patterns, but tended simply to rotate at the edge of a micropore for flow patterns smaller than the cell.

A qualitatively different phenomenon occurs for ultrasonically activated gas-filled channels in plant tissue. The acoustic microstreaming occurs entirely within a cell adjacent to the channel, and may be restricted to only a part of the cell's interior (Gershoy *et al.*, 1976). The microstreaming at the oscillating wall of the gas-channel can be theoretically considered using near-boundary streaming theory (Miller, 1985a) and the theory for resonance oscillation (see Section 4.2.4). The limiting streaming velocity (U_c) is given by:

$$U_c = - \left(\frac{3 u_0^2}{16fd} \right) \sin\left(\frac{2 \pi x}{d}\right). \quad (4.89)$$

in which x is the tangential distance from the center of a vibrating segment (see Figure 4.8), u_0 is the (transverse) velocity amplitude at the center of the segment, d is the width of the segment, and f is the ultrasound frequency. The maximal shear stress (S_c) expected inside the cell is then obtained by dividing the maximum value of U_c by the boundary layer thickness (Δ) (see Equation 3.9) and multiplying by η the coefficient of shear viscosity of the cytoplasm:

$$S_c = 3 \frac{\eta u_0^2}{16 fd \Delta}. \quad (4.90)$$

If sufficient shear stress is applied to a biological membrane it will yield, and this membrane disruption can lead to the death of a cell. Thus, the utility of Equation 4.90 can be tested experimentally by observing the cell death threshold in *Elodea* leaves, as discussed in Section 6.

Because the shear stress generated in the microstreaming is a static quantity (*i.e.*, not oscillating at the ultrasonic frequency), the threshold shear stress should be independent of frequency. Under this assumption, the frequency dependence of the lowest expected cell death threshold (*i.e.*, for resonance conditions) can be derived from the theory above (Miller and Thomas, 1993a). At resonance frequency (f_0), the transverse velocity amplitude at the center of the wall is given by:

$$u_0 = \frac{2 \pi d p_e}{b} = \frac{p_e}{4 \rho f_0 d}, \quad (4.91)$$

where p_e is the pressure amplitude at the leaf and b is a damping constant (compare Sections 4.1.2 and 4.1.3), given for this situation by $8 \pi \rho d^2 f_0$. The shear stress (Equation 4.90) at resonance is then:

$$S = \frac{3 \eta p_e^2}{256 \rho^2 f_0^3 d^3 \Delta} = \frac{3 \pi^{0.5} \eta^{0.5} p_e^2}{256 \rho^{1.5} f_0^{2.5} d^3}. \quad (4.92)$$

Proceeding from Equation 4.92, the dependence on frequency is simplified by recognizing that viscosity and density are constants with respect to frequency, and assuming that the intensity (I) is proportional to p_e^2 . In addition, for the range of frequencies considered, $d^2 f_0$ is roughly constant; specifically, between 0.5 and 20 MHz, $d^2 f_0$ is approximately 1.2 for d in centimeters and f_0 in megahertz. Therefore, the shear stress at resonance may be written:

$$S_t = C \frac{I}{f_0^{2.5} d^3} \propto \frac{I}{f_0} \quad (4.93)$$

in which C is a constant with respect to frequency. Because the critical shear stress is expected to be approximately constant at the cell-death threshold, regardless of resonance frequency in this range, I/f_0 is approximately constant. Thus, the intensity threshold for cell death is expected to be approximately proportional to frequency, other factors being equal. This approximate relationship has been observed for *Elodea* leaves (Section 6).

4.5 Summary

Low pressure amplitude ultrasound can interact with a bubble or gas body to produce a nearly sinusoidal oscillation of small amplitude. In this context, small amplitude refers to a balance in the equations of motion, giving a mass and spring type oscillation, in contrast to the dominance of the inertial terms at higher amplitudes,

giving inertial cavitation. The small amplitudes of oscillation can take on many forms, including the radial pulsation of spherical gas bodies in ultrasound contrast agents, the drumhead-like motion of the air-water interface of gas trapped in a pore, or transverse oscillation of plant cell walls around a gas-filled intercellular channel. In each case, the oscillation concentrates acoustic energy and enhances the operation of physical mechanisms in the vicinity of the oscillation, potentially by orders-of-magnitude above that expected in the absence of the localized oscillation. An ultrasonically activated gas body can act to attract small particles by the radiation force mechanism and to stir the liquid in its vicinity by the acoustic microstreaming mechanism.

The importance of these phenomena to the consideration of biomedical ultrasound arises from the initiation of the activity at any non-zero level of exposure, provided that bubbles or gas bodies are present in the ultrasonic field. The thresholds for adverse biological effects in this case are related to the biological thresholds for mechanical damage. For example, cells can be attracted to an oscillating gas body and may tend to gather near the body at very low levels; when caught up in the local microstreaming flow, the cells can be lysed if the time-averaged shear stress exceeds the threshold for membrane rupture. Other perturbations relate directly to the instantaneous pulsation of the gas bodies, as has been noted in the fruit-fly larvae. These physical mechanisms can operate during diagnostic ultrasound examinations when suitable gas bodies are present. This may occur for gas-bearing tissues of lung and intestine, although these tissues are not common subjects of diagnostic ultrasound. The situation most pertinent to clinical medicine occurs with the use of gas-body-based contrast agents, which are specifically designed to be suitable for strong activation or cavitation. The gas-body or bubble activity creates secondary point sources, which gives strong echos used to enhance diagnostic images in various ways, and generates mechanical perturbation in their local vicinity. That is, the enhancement of the image contrast and of nonthermal bioeffects mechanisms originate from the same phenomena. Because the contrast effect and the bioeffects mechanisms are linked, improvements in delivery, persistence and response not only improve the diagnostic effectiveness of gas-body-based contrast agents but also tend to increase the potential for bioeffects.

The effectiveness of gas-body agents for enhancing biological effects has led to their use in therapeutic applications of ultrasound. The present knowledge of bioeffects induced by the interaction of ultrasound with gas bodies and bubbles is presented in Sections 6, 7 and 8.

5. Nonlinear Bubble Response; Inertial Cavitation

5.1 Introduction

In this Section, as in Section 4, the center of attention is a small body of gas surrounded by liquid, *i.e.*, a *bubble*, and its response to an ultrasound field. While in Section 4 the analysis is restricted to conditions in which the ultrasound causes only relatively small changes in bubble volume, in the present section there are no such restrictions. In a CW, monofrequency ultrasound field of frequency (f), the nature and vigor of the bubble response will depend critically on the pressure amplitude. In a pulsed field the bubble response depends on features of a more complex pressure-time relationship. These features appear in the waveform, a display of acoustic pressure (p) versus time during a pulse (“acoustic pressure” being the excess of the instantaneous pressure over its mean value). The waveform exhibits alternating positive and negative intervals of the acoustic pressure. During the positive intervals, the medium is being compressed. The greatest of the maximal values of p is referred to as p_+ (or, alternatively, as p_c). During negative intervals, the medium is being expanded and the greatest value of the magnitude of p is referred to as p_- (or, alternatively, as p_r). Especially when distortion occurs during NLP, p_- and p_+ may not be equal. The “peak positive pressure” (p_+) and the “peak negative pressure” (p_-) have proven useful for characterizing pulsed diagnostic ultrasound (Section 5.11). At low pressure amplitudes, the waveform may be symmetrical, in which case $p_+ = p_-$, and it is possible to define the wave simply by its pressure amplitude (p_0).

In some situations the waveform at the source is essentially sinusoidal with frequency (f_0), and the ultrasound bursts are long enough so that each burst contains several complete periods. As the wave propagates under nonlinear conditions the waveform becomes distorted but remains periodic with period $1/f_0$. It can then be represented approximately as a Fourier series whose fundamental frequency is f_0 . The pressure amplitude (p_f) of the fundamental can be determined

experimentally by suitable filtering of the distorted waveform. It has been found (Ayme and Carstensen, 1989a) that p_f is a useful indicator of biological effects caused by ultrasound under nonlinear conditions.

When a gas bubble in a liquid is exposed to ultrasound, the nature of its response changes as the pressure amplitude in its vicinity increases. From the theory discussed in Section 4.1, it is seen that when a spherical bubble is exposed to a CW field of frequency (f) at a relatively low pressure amplitude (p_0), its radial displacement ($R - R_0$) varies sinusoidally with time (after a brief transient) at the same frequency, according to a first-order, linear, approximation. As p_0 increases, the displacement-versus-time function acquires a second-harmonic component of frequency ($2f$), for which the displacement amplitude is proportional to p_0^2 , according to a second-order approximation (Section 4.1.5). With further increase of the driving pressure amplitude (p_0), the latter approximation is no longer valid, the predicted R versus t plot becomes increasingly distorted, and the associated frequency spectrum of the acoustic pressure becomes increasingly rich in components above and below the fundamental frequency. Under some conditions, the theoretical R versus t plot becomes highly dependent on initial conditions, a characteristic which implies deterministic chaos.

Under a very important class of conditions, the predicted R versus t plot follows a course whose primary features are (1) an expansion interval during which the bubble is larger than at the beginning of the ultrasound exposure and, following this, (2) a “collapse” interval during which the bubble rapidly contracts to a much smaller size. During the latter interval, the R versus t curve resembles one (sometimes called the *Rayleigh collapse curve*) derived by Rayleigh (1917) for the contraction of a spherical cavity (Section 5.2). The predicted collapse can be violent, leading momentarily to a pressure of hundreds of megapascals within the gas, orders of magnitude greater than the acoustic pressures that stimulated the bubble, and internal temperatures in thousands of kelvins. The violence of the collapse results from the rush of water toward the bubble center; this inward rush is maintained by the inertia of the surrounding liquid, in spite of increasing gas pressure. In this Report, bubble collapse of the kind just described is referred to as *inertial cavitation*.³

³In earlier publications violent bubble collapse was referred to as *transient cavitation* (Flynn, 1964). This term was chosen initially with the recognition that, in practice, violent collapse of a bubble is often associated with its disappearance through fragmentation (the latter occurring because of surface instabilities). However, in most existing theory for dynamics of a gas bubble in a monofrequency sound field, it is assumed that the bubble remains spherical and intact as its volume changes. According to such theory, a bubble can collapse and rebound repeatedly for an indefinite period of time; recent experiments show that this does indeed occur under suitable conditions. Choice of the term *inertial* emphasizes the role of fluid inertia without implication as to the continued existence of the bubble.

There is considerable experimental evidence confirming predicted features of inertial cavitation (Section 5.8). Also, its significance for effects of ultrasound on chemical reactions has been demonstrated, although mainly for unspecified bubble populations, rather than for single bubbles (Section 5.9).

While most of existing theory for cavitation assumes a single spherical bubble in a homogeneous medium away from boundaries, this situation is seldom realized. Instead, bubbles of interest are often on or near solid boundaries, and their motion is therefore not spherically symmetric. Even the motion of bubbles distant from the boundary is often not symmetric, because of surface waves generated at the air-water interface. Because of the asymmetry, phenomena occur which would otherwise be absent. Particularly significant for bubbles near a solid boundary are the microscopic liquid jets that form at the perturbed air-water interfaces, and are projected toward the solid boundary. The erosion of solid surfaces which is sometimes produced by cavitation has been attributed to these jets.

The remainder of Section 5 deals with the topics of nonlinear bubble response, indeterminate motion and inertial cavitation, both symmetrical and asymmetrical.

5.2 Cavitation Theory; General

When bubbles are exposed to pressure amplitudes of the order of 0.1 MPa near their resonance frequency, their response becomes highly nonlinear. Analytical models of the associated physical processes date back to the work of Rayleigh (1917) and Lamb (1879; 1945). As shown by Young (1989) and Leighton (1996), many investigators have taken part in the development of theory for hydrodynamically and acoustically generated cavitation. Each theoretical model is based on laws of conservation of mass, momentum and energy, and also on assumptions for the equations of state for liquid and gaseous media, and for the transfer of heat between gas and liquid. The models differ in their assumptions regarding the velocity of sound in the liquid. Rayleigh's model assumes the liquid to be incompressible, which corresponds to an infinite velocity of sound in the liquid. Herring's model (Herring, 1941; Knapp *et al.*, 1970) is based on the so-called acoustical approximation, namely that the compressibility of the liquid is a constant and corresponds to the small amplitude speed of sound in the liquid. Gilmore's (1952) model assumes that the compressibility of the liquid and its speed of sound is a function of the pressure. A comparison of these models by Lastman

and Wentzell (1981) showed that, for small amplitudes of motion, all models predict similar results. For moderate amplitudes, all models that recognize the compressibility of the liquid are in good agreement. But, at large amplitudes, the results of the predictions of the three classes of models depart significantly and the most complex assumptions regarding the properties of the fluid are needed to deal with the violent motion of the bubble (Vokurka, 1986).

With the assumptions that the liquid is incompressible and inviscid, conservation of momentum gives Raleigh's equation which can be written in the form:

$$\frac{dU}{dt} = \frac{1}{\rho_0 R} [P(R) - P_\infty(t)] - \frac{3}{2} \frac{U^2}{R}. \quad (5.1)$$

where R is the radius of the bubble, $U = dR/dt$, ρ_0 is the equilibrium density of the liquid, $P(R)$ and $P_\infty(t)$ are the total pressure at the surface of the bubble and at infinity, respectively. In this form, Equation 5.1 shows that two quantities, of different natures, drive the bubble, *i.e.*, contribute to the acceleration dU/dt . Flynn (1964) referred to these as the pressure acceleration function (PF) and the inertial acceleration function (IF); they are given by:

$$PF = \frac{1}{\rho_0 R} [P(R) - P_\infty(t)] \quad (5.2)$$

Except when $U = 0$, as at the time of maximum expansion, the inertial acceleration function (IF) is an inward acceleration. The pressure acceleration function (PF) is an inward acceleration at maximumal:

$$IF = -\frac{3}{2} \frac{U^2}{R}. \quad (5.3)$$

expansion, but as the bubble collapses PF becomes a very large outward acceleration that eventually arrests the collapse. When the right hand side of Equation 5.1 is dominated by PF , the oscillation of the bubble is relatively small. Most of the phenomena discussed in Section 4 occur in this regime.

If the function IF dominates, inertial cavitation occurs.⁴ It has been shown (Flynn, 1975b) for a range of conditions that this occurs if the largest value (R_{\max}) of the bubble radius during its oscillation is comparable to or greater than twice its equilibrium value (R_0). As an approximate predictor of the threshold for inertial cavitation, the

⁴Following Flynn (1964), the primary definition of the threshold for inertial cavitation is the condition that $PF = IF$ at the minimal value for PF .

criterion $R_{\max}/R_0 > 2$ has proven to be useful for a wide range of conditions.

When inertial cavitation occurs, the bubble collapse is violent, leading to extremely large temperatures and pressures in the compressed gas. In addition, spherically diverging shock waves are generated in which the instantaneous pressures are very high.

Although developed primarily for hydrodynamical applications, the Rayleigh model gives a good semiquantitative description of the behavior of bubbles during collapse in acoustic fields. As noted above, more realistic assumptions about the properties of the media lead to improved descriptions of cavitation phenomena.

The Flynn equation for the motion of a bubble in an acoustic field (Flynn, 1975a; 1975b) can be written as:

$$R \left(1 - \frac{U}{c_0} \right) \frac{dU}{dt} + \frac{3}{2} \left(1 - \frac{U}{3c_0} \right) U^2 = \frac{R}{\rho_0 c_0} \left(1 - \frac{U}{c_0} \right) \frac{dP}{dt} + \frac{1}{\rho_0} \left(1 + \frac{U}{c_0} \right) \left[\left(P_0 + \frac{2\sigma}{R_0} \right) \left(\frac{R_0}{R} \right)^{3\gamma} + P_{v_0} - \frac{2\sigma}{R} - \frac{4\eta U}{R} - P_0 + p_0 \sin(\omega t) \right], \quad (5.4)$$

where c_0 is the small-signal speed of sound in the liquid, σ is the surface tension of the liquid, η is the shear viscosity of the liquid, and Γ is a parameter (the polytropic exponent) that varies between unity for the isothermal case to the ratio of the specific heats of the gas for the adiabatic case. (By varying Γ between these limits, it is possible to explore the effects of heat conduction on the cavitation process.) Also, P_0 is the hydrostatic pressure, P_{v_0} is the vapor pressure (usually negligible in comparison with the total gas pressure), p_0 and ω are the pressure amplitude and (angular) frequency, respectively, of the driving field; and R_0 is the equilibrium radius of the bubble. Equation 5.4 corresponds to Equation 5.1 except that the compressibility of the liquid is introduced to a first approximation and the pressure at the bubble $P(R)$ is given more explicitly. Equation 5.4 can be rearranged, for comparison with Equations 5.1 through 5.3, so that dU/dt is alone on the left-hand side and the sum ($PF + IF$) on the right, if the latter functions are written as:

$$PF = \frac{1}{\rho_0 c_0} \frac{dP(R)}{dt} + \frac{\left(1 + \frac{U}{c_0} \right)}{\rho_0 R \left(1 - \frac{U}{c_0} \right)} [P(R) - P_{\infty}(t)] \quad (5.5)$$

and

$$IF = -\frac{3}{2} \frac{\left(1 - \frac{U}{3c_0}\right) U^2}{\left(1 - \frac{U}{c_0}\right) R}. \quad (5.6)$$

In Equation 5.5, the bracket $[P(R) - P_\infty(t)]$ replaces the lengthy bracket “[. . .]” in Equation 5.4, $-P_\infty(t)$ replaces the expression “ $-P_0 + p_0 \sin(\omega t)$,” and $P(R)$ replaces the remaining terms. During the interval when the bubble is larger than its equilibrium size, the interface moves slowly, allowing time for heat exchange (Figure 5.1). Here PF dominates the movement of the bubble and heat exchange is rapid enough so that the process approaches isothermal conditions ($\Gamma \rightarrow 1$). During violent collapse, the process is nearly adiabatic; then Γ approaches the ratio of specific heats for the gas. All of these cavitation models require complex numerical integration methods. Generalizations must be made on the basis of the solutions for numerous specific cases. For a more complete description of this model and techniques for its evaluation, the reader is directed to Flynn (1975a; 1975b).

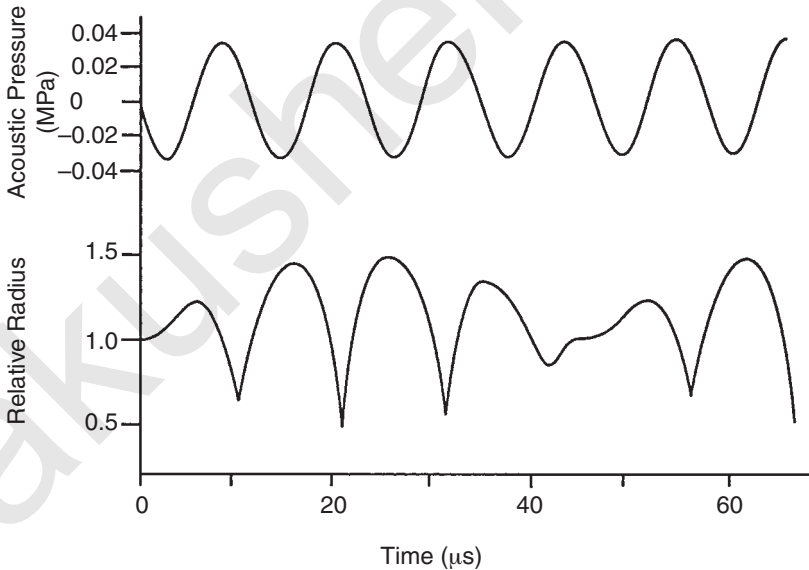


Fig. 5.1. Radius versus time for a bubble driven at a pressure amplitude below the threshold for inertial cavitation. Equilibrium radius, 26 μm ; acoustic frequency, 83 kHz; acoustic pressure amplitude, 0.033 MPa (adapted from Flynn, 1964).

Gilmore's (1952) model differs qualitatively from other classes of models by including the nonlinear properties of the liquid and acknowledging that the speed of sound is a function of the acoustic pressure. Specifically:

$$c = \left(\frac{dp}{d\rho} \right)^{1/2} \Big|_{r=R_0} \quad (5.7)$$

where p is the pressure and ρ is the density at an arbitrary point in the medium. With this, the equation of motion of the bubble becomes:

$$R \left(1 - \frac{U}{c} \right) \frac{dU}{dt} + \frac{3}{2} \left(1 - \frac{U}{3c} \right) U^2 = \left(1 + \frac{U}{c} \right) H + \frac{R}{c} \left(1 - \frac{U}{c} \right) \frac{dH}{dt}. \quad (5.8)$$

where c and H , both functions of time and both evaluated at the bubble surface, are the speed of sound and the enthalpy, respectively. The enthalpy is given by:

$$H = \int_{p_\infty(t)}^{p(R)} \frac{dp}{\rho}, \quad (5.9)$$

and includes the pressure in the driving field. For more details on the model and techniques for numerical evaluation (Ayme and Carstensen, 1989b).

5.3 Theory: Stable Noninertial Cavitation with Spherical Symmetry

Under some conditions, cavitation occurs in events of short duration, as when a bubble disintegrates through fragmentation in the course of a single expansion-contraction cycle, or in only a few such cycles. Under other conditions the cavitation is stable, in that the bubbles involved maintain their identities while continuing to oscillate over a relatively long period of time. Stable cavitation can be linear or nonlinear, inertial or noninertial, spherically symmetric or asymmetric. In this Section, the discussion is limited to noninertial cavitation involving radial oscillations of a spherical bubble in which the motion possesses spherical symmetry.

Any of the cavitation models discussed in Section 5.2 can be linearized for small amplitudes of motion by assuming $R = R_0 + \xi$, where $\xi \ll R_0$. In that case, the equation of motion for a bubble becomes that of a simple harmonic oscillator with a resonance frequency (f_0) inversely related to the equilibrium radius of the bubble (Section 4.1.2).

For example, according to Table 4.1, f_0 is about 1 MHz for a spherical air bubble in water with radius 3.2 μm and is about 3 MHz if the radius is 1.2 μm . Also, under linear conditions, when the acoustic pressure in the driving field varies sinusoidally in time with frequency (f), the radial displacement (ξ) of the bubble likewise varies sinusoidally in time with the same frequency. Furthermore, if the bubble is driven in a fluid of low viscosity, such as water, at a series of different frequencies [at constant driving pressure amplitude (p_0)] the peak value of R , which occurs each cycle, will have its maximum value (R_{max}) when f is approximately equal to f_0 , independent of p_0 .

Complications occur when a bubble is driven at pressure amplitudes high enough to produce a nonlinear response. Under nonlinear conditions, even though the driving pressure varies sinusoidally with time, the radial displacement (ξ) no longer does so. Also, in a plot of bubble radius (R) against time, an “ R versus t ” curve, deviations of R from its mean value in the positive direction are no longer symmetric with those in the negative direction. An example of an R versus t curve exhibiting these features of nonlinearity is seen in Figure 5.1. This figure is for a bubble being driven below its linear resonance frequency at a driving pressure amplitude of 0.033 MPa (one-third atmosphere). Only in a rough sense do the maxima in the radius occur at the minima in acoustic pressure. Even at this modest pressure amplitude, the bubble response is beginning to show the sharp minima that result from the inertial forces associated with the rushing water. At the minimum value for the radius of the bubble in this figure, the gas pressure is calculated to be 0.8 MPa, *i.e.*, more than 24 times the driving pressure amplitude. A close inspection of the bubble response (over a time scale extending well beyond that shown in Figure 5.1) shows that it is periodic but with a global period four times the acoustic period. Thus, the bubble response includes, among other frequencies, a subharmonic at one-fourth the driving frequency.

Lauterborn (1976) showed that the concept of “resonance” for a bubble must be modified when it is driven under nonlinear conditions. In examining R versus t curves for different frequencies (f) and pressure amplitudes (p_0) [all for the same initial bubble radius (R_0)] he observed for each frequency and pressure amplitude the largest value (R_{max}) of the radius and calculated the nonlinear relative amplitude, defined as $(R_{\text{max}} - R_0)/R_0$. The plots in Figure 5.2 show this nonlinear amplitude as a function of normalized driving frequency (f/f_0) for an initial bubble radius (R_0) of 1 μm and for different values of the driving pressure amplitude (p_0), the latter varying from 0.01 to 0.16 MPa. Plot a, for the lowest value of p_0 (0.01 MPa), resembles the corresponding plot of amplitude versus frequency for linear

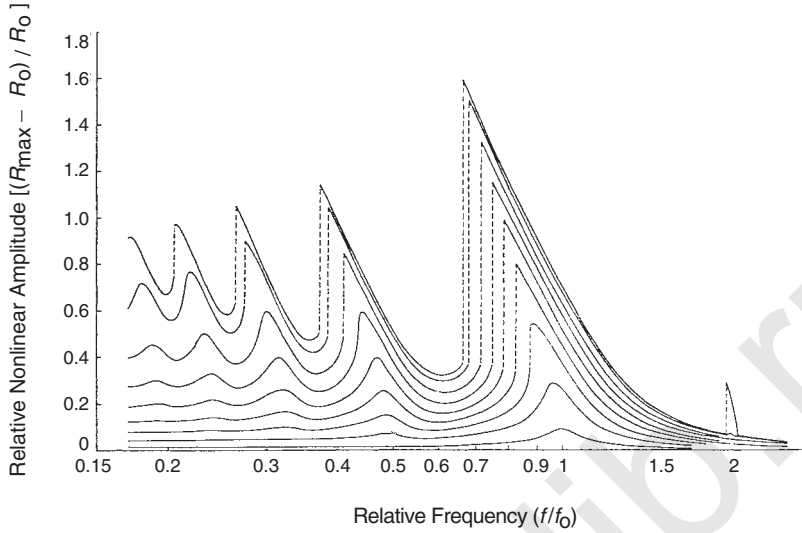


Fig. 5.2. Computed plots of relative nonlinear amplitude $(R_{\max} - R_0)/R_0$ versus f/f_0 ; f is the frequency of the driving field and f_0 the linear resonance frequency for the bubble. The pressure amplitudes (p_0) for the different plots are: (a) 0.01, (b) 0.03, (c) 0.05, (d) 0.07, (e) 0.09, (f) 0.11, (g) 0.13, (h) 0.15, and (i) 0.16 MPa. In the far right ($f/f_0 \sim 2$), the plot represents bubble oscillation with repetition frequency equal to its resonance frequency and also equal to half the frequency (f) of the driving field. For all other plots the bubble repetition frequency is equal to f ; nonlinear resonances are seen when f is in the vicinity of submultiples of the resonance frequency (adapted from Lauterborn, 1976).

conditions in Figure 4.2; a maximum occurs at the frequency for linear resonance (for which $f/f_0 = 1$) and the amplitude decreases monotonically as the frequency increases above, or decreases below, that frequency. In Plot b, for a driving pressure amplitude p_0 of 0.03 MPa, the major peak, defining the major nonlinear resonance frequency, is greatly increased in relative amplitude and occurs when f/f_0 is about equal to 0.95; furthermore, a smaller peak occurs when f/f_0 is a little less than 0.5. In Plot c, for $p_0 = 0.05$ MPa, the major resonance peak has increased further in amplitude and occurs when f/f_0 is somewhat less than 0.9; the nonlinear relative amplitude changes precipitously on the low-frequency side of this peak, and two minor resonances appear, occurring when f/f_0 is 0.48 and 0.33.

The other R versus t curves in Figure 5.2 show that the main nonlinear resonance peak, as well as other peaks occurring at higher as well as lower frequencies, all shift continuously to lower frequencies as p_0 increases, and become very asymmetric. On the

low-frequency sides of the peaks, the vertical dotted lines indicate instability. At frequencies near one of these lines, a small change in frequency or other condition (in a computation) or a small disturbance in a laboratory situation can cause the bubble motion to jump suddenly from one mode to another. The jumps are characterized by hysteresis: for example, suppose that slowly increasing the frequency to f_a causes a jump from a low-amplitude mode to one with higher amplitude; then, if the frequency is slowly decreased the reverse jump does not occur until the frequency is less than f_a . (The hysteresis is not shown in Figure 5.2 because the plots are all made with frequency increasing.)

Another consequence of nonlinearity is that the repetition period (T_R) of the function $R(t)$ is not, in general, equal to the period ($T = 1/f$) of the driving pressure field. Lauterborn (1976) found that if the pressure amplitude (p_0) is not too high, the function $R(t)$ will approach a steady-state in which T_R is an integral multiple of T ; thus $T_R = m T$, in which $m = 1, 2$, leading to the generation of subharmonic modes. The motion may also contain harmonic components whose frequencies are integral multiples of f . In computations for bubbles with different initial radii (R_0), he found a multiplicity of nonlinear resonances.

Under these nonlinear conditions, the R versus t curve deforms so that maxima and minima are no longer symmetrical, and the increase in gas pressure during compression is greater than its decrease during rarefaction. Also, at the higher values of p_0 , the nonlinear resonance frequency decreases from its linear resonance value with increasing p_0 . In addition, when the driving pressure is sinusoidal with frequency (f), the Fourier spectrum of the R versus t curve includes harmonics and subharmonics of f .

5.4 Theory: Inertial Cavitation with Spherical Symmetry

As the driving pressure amplitude (p_0) increases toward the threshold for inertial cavitation, the violence of collapse increases precipitously. In Figure 5.3, two R versus t curves are shown for a bubble with equilibrium radius $26 \mu\text{m}$ and linear resonance frequency 125 kHz (the same as for Figure 5.1), driven at a frequency of 25 kHz . When the pressure amplitude (p_0) is 0.07 MPa (Curve A), the bubble radius (R) increases slowly to a broad maximum of about 1.5 times the equilibrium value (R_0), then decreases rapidly. During collapse, the inward velocity of the bubble surface ($-dR/dt$) reaches the magnitude $0.02 c_0$, where c_0 is the speed of sound in water.

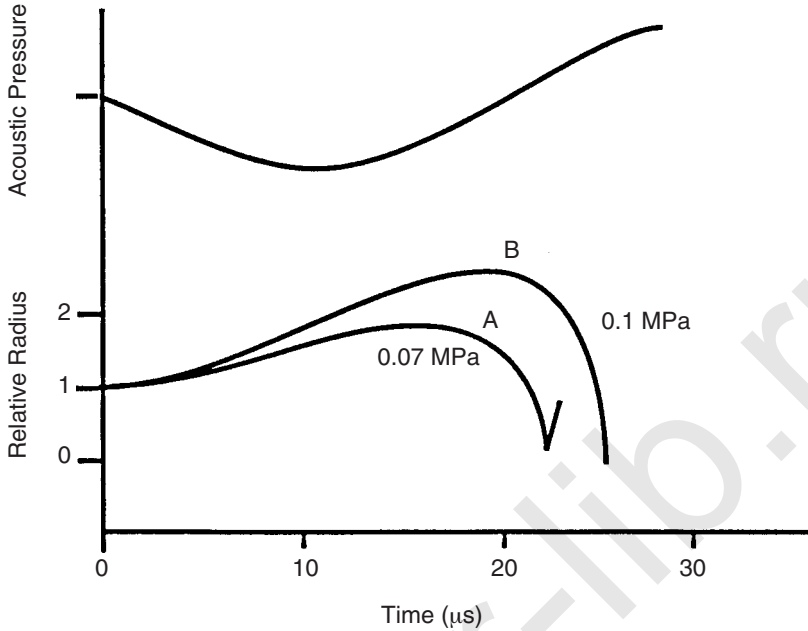


Fig. 5.3. Radius versus time for a bubble driven near the threshold for inertial cavitation. Equilibrium radius, $26 \mu\text{m}$; acoustic frequency, 25 kHz ; acoustic pressure amplitude, 0.07 and 0.10 MPa (adapted from Flynn, 1964).

For Curve B, the driving pressure amplitude (p_0) is increased to 0.1 MPa (about 1 atm); although this increase (from 0.07 to 0.1 MPa) is modest, it greatly affects the collapse. After an expansion phase in which R increases to about twice R_0 , contraction occurs in which the inward speed of the bubble surface becomes very large; in fact, it exceeds c_0 , according to the theory used in generating the curve. This result is invalid, since it is inconsistent with an assumption in the theory (that $|dR/dt|$ is small compared to c_0), but nevertheless it is clear that the collapse in Curve B is markedly different from that in Curve A. It is found that the conditions of Curve B lead to inertial cavitation.

When R versus t curves are calculated for different conditions, it is found that these vary greatly with driving frequency, equilibrium bubble size and driving pressure amplitude and depend upon properties of the media, such as liquid viscosity and surface tension at the bubble surface. It often occurs that R versus t curves for different values of p_0 , with other parameters held constant, reveal a threshold, as in Figure 5.3. That is, curves for which p_0 exceeds the threshold value p_{0c} by a small amount exhibit inertial cavitation while those for

which $p_0 < p_{0c}$ do not. When inertial cavitation occurs (as in Curve B of Figure 5.3) the bubble radius increases appreciably during the expansion phase, the inward velocity of the bubble surface reaches high values during the collapse phase, and high temperatures exist in the gas when the radius has its minimal value.

In Section 5.2 it has been shown for a range of conditions that inertial cavitation will occur if R_{\max} , the largest value the bubble radius (R) reaches during an expansion, exceeds the equilibrium bubble radius (R_0) by about a factor of two. Apfel (1986) pointed out that when the bubble contains a perfect gas whose pressure during changes of bubble radius (R) is proportional to $R^{-3\Gamma}$ (where Γ is the polytropic index; see Equation 5.4), the temperature reached at the time of minimum radius is equal to $T_0(\Gamma - 1)(R_{\max}/R_0)^3$, where T_0 is the ambient temperature in kelvins. Hence, under the stated assumptions, choosing the ratio R_{\max}/R_0 as the criterion for inertial cavitation is equivalent to choosing the maximum temperature reached during collapse as the criterion. For air and other diatomic gases, the ratio of specific heats is 1.4; choosing this value for Γ , choosing 300 K for T_0 , and setting R_{\max}/R_0 equal to two yields 960 K for the maximum temperature.

An accurate theoretical determination of whether or not inertial cavitation will occur for a given set of conditions requires computation of a numerical solution to the governing differential equations. Flynn and Church (1988) computed a large number of R versus t curves for a spherical air bubble in water using a modification of the Gilmore equation (Equation 5.8) suggested by Akulichev (1971). This equation takes into account compressibility and viscosity of the liquid, as well as surface tension at the bubble surface. For each computed curve, the driving field consisted of exactly five cycles in which the acoustic pressure varied sinusoidally in time, with f and p_0 equal to 3 MHz and 0.5 MPa, respectively. One objective of the work was to determine ranges of the equilibrium bubble radius (R_0) for which inertial cavitation was produced for given values of p_0 and f , using the criterion $R_{\max}/R_0 \geq 2$.

It was found in these computations that under some conditions inertial cavitation occurs during the first cycle of the driving field. A summary of conditions is presented in Figure 5.4 for a spherical air bubble in water with equilibrium radius (R_0) in a driving field of frequency (f) and pressure amplitude (p_0) equal to 0.5 MPa. For f in the range 0.1 to 10 MHz, ranges of R_0 are shown for which the maximal radius (R_{\max}) exceeds $2R_0$ (indicating that inertial cavitation occurs) in the first cycle. For example, when f is 3 MHz the predicted range of R_0 is 0.18 to 1.8 μm and, when f is 7 MHz, the range is 0.22 to 0.62 μm . The upper limit of R_0 is roughly comparable to the

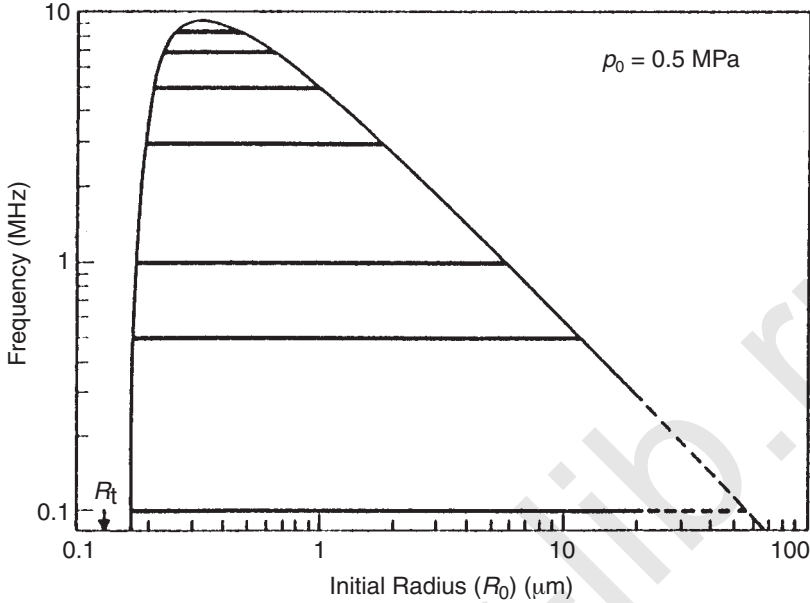


Fig. 5.4. Ranges of radius (R_0) at different frequencies for bubbles from which inertial cavitation is elicited in one cycle when p_0 is 0.5 MPa (adapted from Flynn and Church, 1988). R_t is the Blake threshold radius, discussed in Appendix A.

computed radius for linear resonance, which (assuming $\Gamma = 1.4$) is 1.4 μm at 3 MHz and 0.7 μm at 7 MHz, while the lower limit is comparable to, but greater than a limit for mechanical stability discussed by Blake (see Appendix A). At frequencies above 9 MHz, inertial cavitation is not produced during the first cycle regardless of bubble size when p_0 is 0.5 MPa.

It was also found by Flynn and Church (1988) that under some conditions inertial cavitation does not occur in the first cycle, but does so in the second, third or later cycle. For example, when f is 1 MHz, the maximum radius (R_{max}) exceeds $2 R_0$ in the third cycle, but not earlier, for R_0 in the range 2.8 to 3.8 μm and for p_0 equal to only 0.1 MPa. (When f is 1 MHz, the computed radius for linear resonance is 3.7 μm when $\Gamma = 1.4$.)

To obtain further information on the significance of the equilibrium bubble radius (R_0), Flynn and Church (1988) determined R_{max} from each of a family of R versus t curves, all for the same value of f and p_0 , but for a range of R_0 values, and generated plots of R_{max}/R_0 versus R_0 . In so doing, they found that for a family of curves in which inertial cavitation occurs during the first cycle, the plot of R_{max}/R_0 versus R_0

has a rather simple shape (Figure 5.5, Curve a); the ratio R_{\max}/R_0 is maximal at a small value of R_0 , just a little greater than the lower limit of the R_0 range, then decreases monotonically as R_0 increases. However, plots of R_{\max}/R_0 versus R_0 for the second or later cycles are much more complex and contain peaks associated with resonances to harmonics and subharmonics (see Figure 5.5, Curves b through e).

5.5 Theory: Cavitation Produced by Very Short Pulses of Ultrasound

Many pulse-echo imaging devices utilize ultrasound pulses that are only one or two cycles in duration; they must be short to yield the required resolution. (Doppler pulses are somewhat longer to allow velocity determinations.) Flynn (1982) investigated theoretically the behavior of spherical argon bubbles 0.1 to 5 μm in diameter exposed in water to such short pulses with carrier frequencies between 1 and 10 MHz and relatively modest driving pressure amplitudes from 0.1 to 1 MPa. He obtained numerical solutions to equations which take into account the compressibility, heat conductivity, and viscosity of the water as well as the water-air surface tension. Figure 5.6 shows a typical pulse as well as the R versus t curve for a bubble exposed to it for a particular set of conditions. This pulse consists of a sine wave of frequency 2.25 MHz modulated with a Gaussian envelope whose maximum is 0.48 MPa and whose duration (the time interval between instants at which the envelope height is e^{-1} times its maximal value) is 1 μs . Figures 5.7 to 5.10, based on that work, show the strikingly nonlinear relationship between the "collapse pressure" (the gas pressure when R is minimal) and the driving pressure amplitude (p_0) when the latter exceeds a threshold value.

For Figure 5.7, the bubble radius is 1 μm and for Figure 5.8 it is 0.1 μm . For center frequencies of 1 and 2 MHz, the 1 μm bubble shows an order-of-magnitude increase in collapse pressure for an increase in driving pressure amplitude (p_0) from 0.12 to 0.14 MPa (Figure 5.7), giving a dramatic meaning to the concept of a threshold for this aspect of cavitation. For the same (1 μm) bubble, there is no comparable abrupt increase in collapse pressure when the carrier frequency is greater than 5 MHz so the threshold concept loses meaning for this bubble at these high frequencies. For a 0.1 μm bubble (Figure 5.8), the threshold shifts to somewhat higher acoustic pressure levels, and sharply defined thresholds occur up to higher frequencies. A summary of the thresholds for inertial cavitation

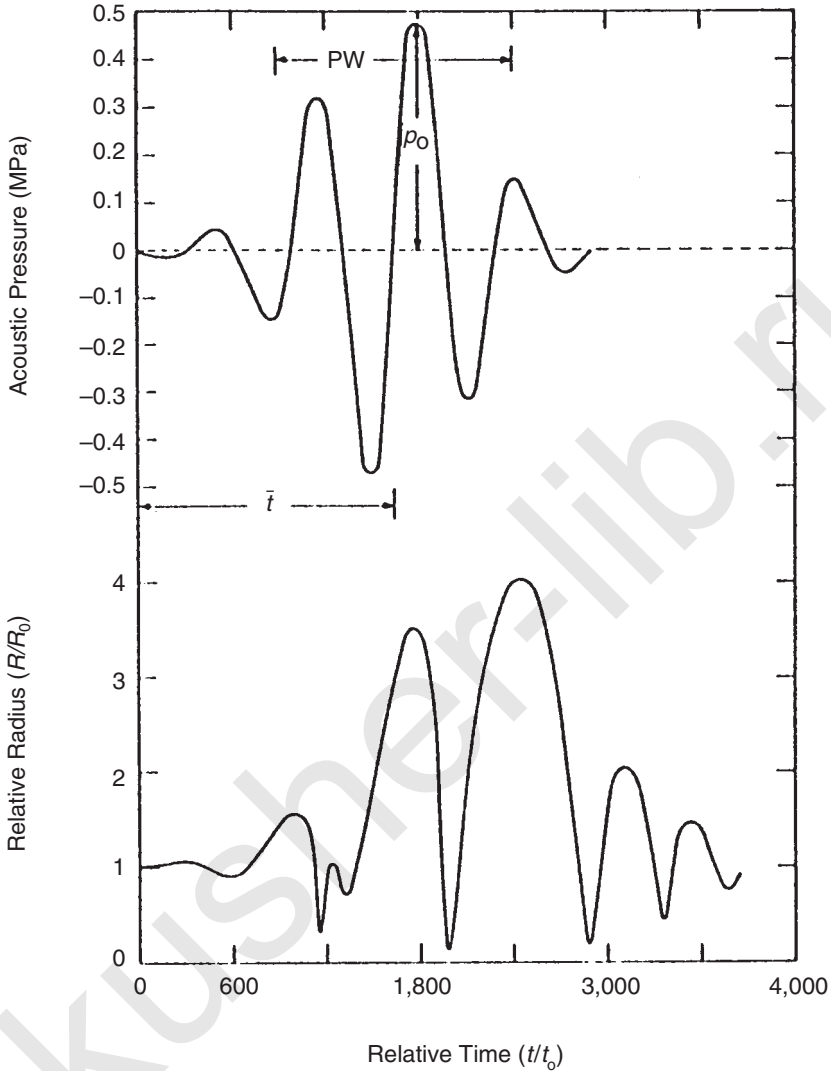


Fig. 5.6. Gaussian pressure pulse and resulting cavity motion. In the acoustic driving field, the frequency (f) is 2.25 MHz and the peak acoustic pressure (p_0) is 0.48 MPa and the initial radius (R_0) 1 μm ; the pulse width (PW) 1 μs ; and the time from $t = 0$ to the center of the pulse $\bar{t} = 2.5/f$; and t_0 is the ratio of R_0 to the speed of sound in the liquid (adapted from Flynn, 1982).

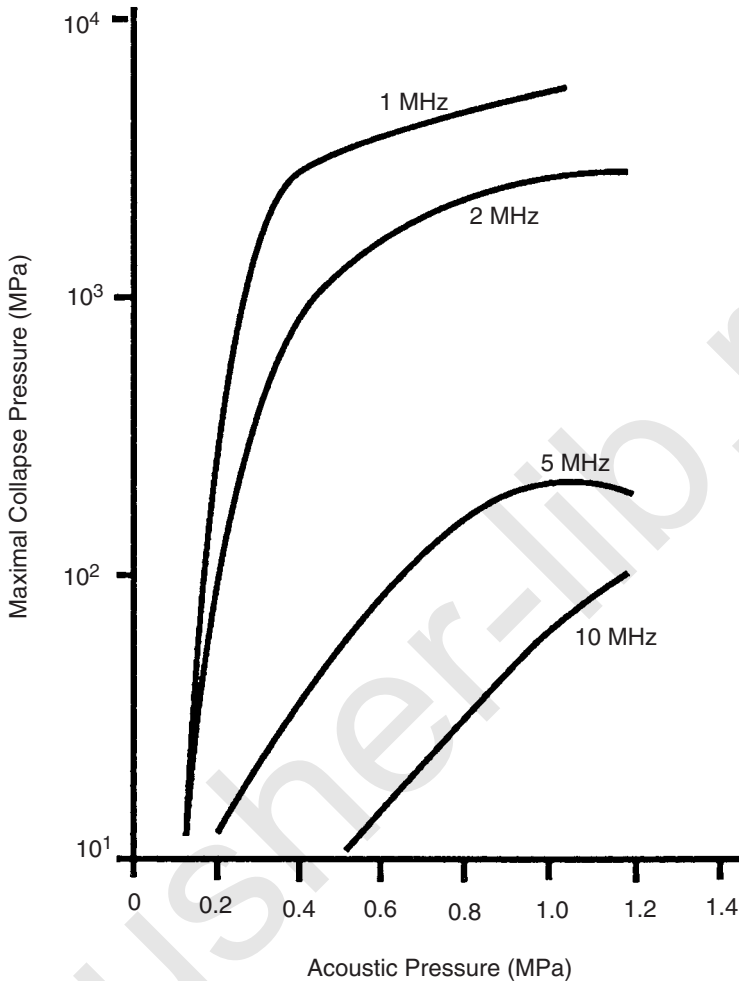


Fig. 5.7. Maximal collapse pressure for a bubble of $1 \mu\text{m}$ radius driven by a $1 \mu\text{s}$ pulse with carrier frequencies from 1 to 10 MHz (adapted from Flynn, 1982).

for bubbles exposed to pulsed ultrasound is given in Figure 5.9 (Flynn, 1982).

To complement the above results, which are based on numerical solutions of an applicable differential equation, Apfel and Holland (Apfel, 1986; Holland and Apfel, 1989) developed an approximate analytical expression for the threshold. While results obtained from its use are less accurate than those obtained from numerical

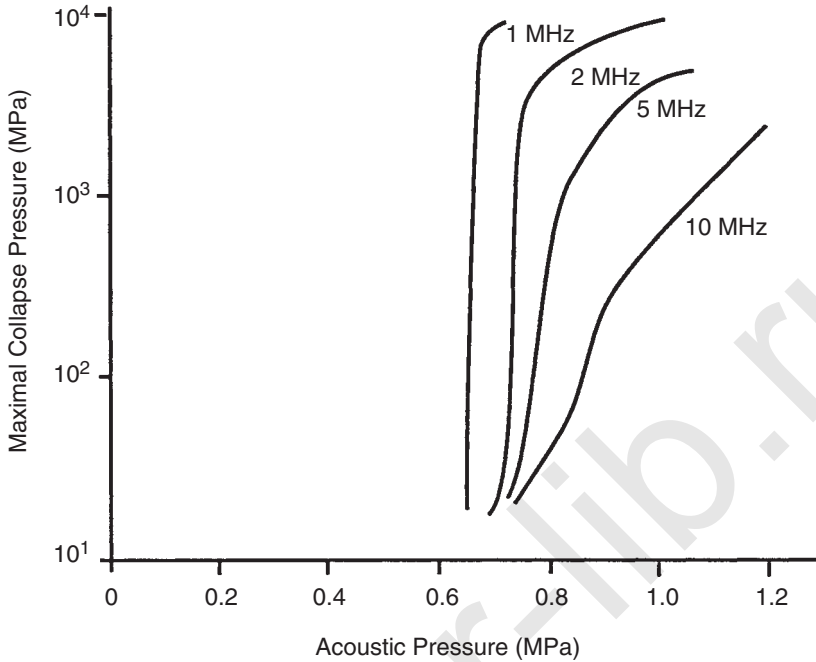


Fig. 5.8. Maximal collapse pressure for a bubble of $0.1 \mu\text{m}$ radius driven by a $1 \mu\text{s}$ pulse with carrier frequencies from 1 to 10 MHz (Flynn, 1982).

solutions, they have proven useful because of the relative ease with which the influence of variables can be studied. This expression was used (Apfel and Holland, 1991) to calculate the pressure amplitude required to produce inertial cavitation during a single cycle of the driving acoustic field, for a range of values of the equilibrium bubble radius and the driving frequency. The criterion used was that the temperature reached at the time of minimal radius should be 5,000 K, corresponding roughly to a value of 3.5 for R_{max}/R_0 , assuming adiabatic conditions. Results are shown in Figure 5.10; here the pressure amplitude threshold is plotted against R_0 for several frequencies. For each frequency, the plot shows a minimum (p_{min}) of the threshold for an optimum value of R_0 ; for example, at 5 MHz the optimum value of R_0 is about $0.3 \mu\text{m}$ and p_{min} is 0.6 MPa. From results of this kind for many values of the frequency, the series of points in Figure 5.11 was obtained, showing p_{min} for an air bubble in water as a function of frequency. The solid curve fitted to the points would apply if $p_{\text{min}}^{2.1}/f$ were constant; it follows that p_{min} is approximately proportional to $f^{0.5}$. From Figure 5.11, this threshold

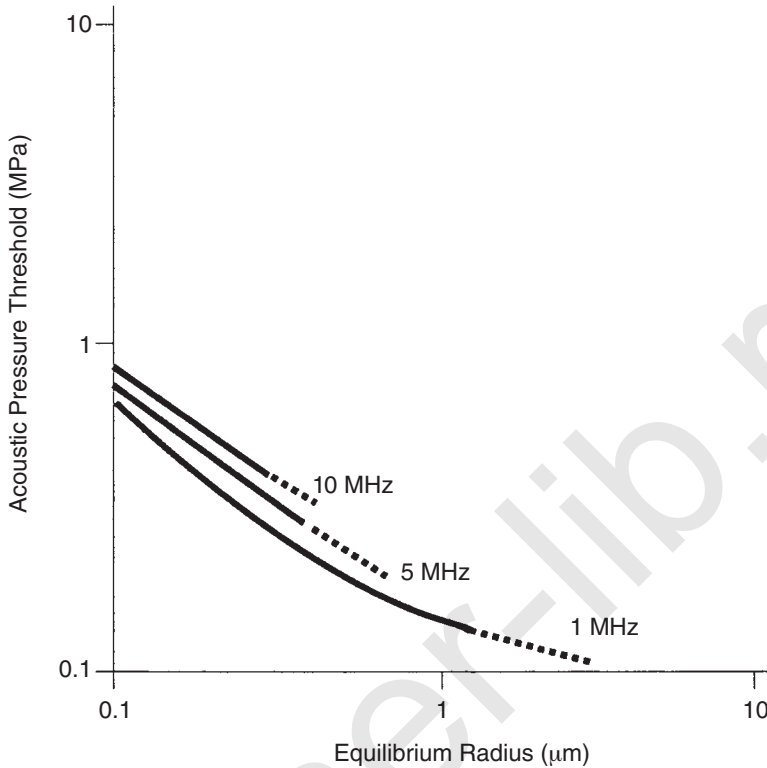


Fig. 5.9. The acoustic pressure threshold for inertial cavitation for bubbles driven by $1 \mu\text{s}$ pulses with carrier frequencies between 1 and 10 MHz (adapted from Flynn, 1982).

is about 0.45 MPa at 3 MHz and in the frequency range 1 to 10 MHz is given (in megapascal) approximately by $0.26 f^{0.5}$, where f is in megahertz.

The thresholds calculated by Apfel and Holland (1991) are somewhat higher than those given by Flynn and Church (1988), as is reasonable since achieving a maximal temperature of 5,000 K, as required by the former authors, evidently requires R_{max} to be greater than the value ($2 R_0$) required by the latter. It is stated by Apfel and Holland (1991) that when the same criterion for inertial cavitation is used in both methods they give results which are in reasonable agreement.

5.6 Indeterminate Motion and Chaos

It is shown in Section 5.3 that, because of nonlinearity in the governing equation for cavitation (*e.g.*, Equation 5.4), several features

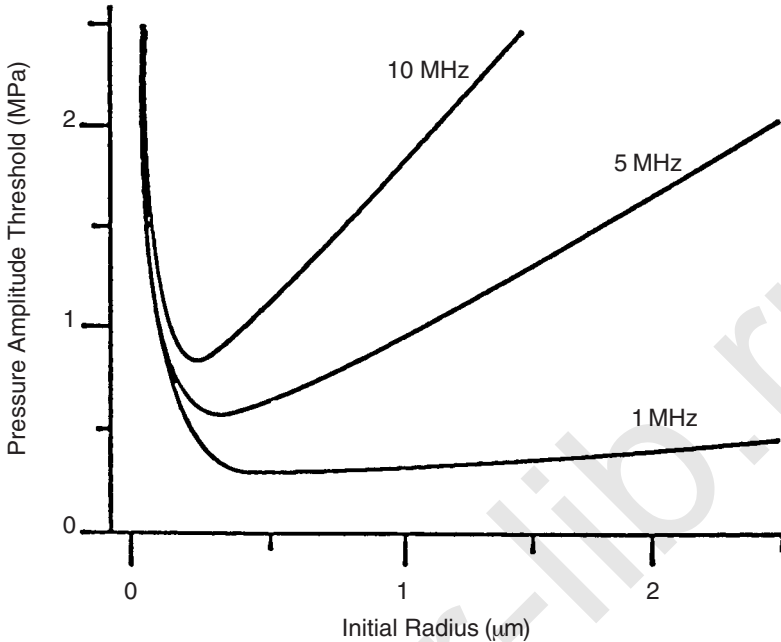


Fig. 5.10. Plot of pressure-amplitude threshold for inertial cavitation versus equilibrium bubble radius (R_0). The minimum of each curve gives the threshold (p_{\min}) for the applicable frequency when a bubble (cavitation nucleus) of optimum size is present (adapted from Holland and Apfel, 1989).

of the solutions appear (nonlinear resonances, harmonics, etc.) which would not be present if the equations were linear. Another such feature is the instability which occurs when the pressure amplitude is sufficiently high. Suppose, for example, that R versus t curves are plotted for a given bubble in a driving field of frequency (f) at a series of p_0 values, starting from low values where linear conditions apply, and gradually increasing. As this is done, changes occur in the R versus t curves, but these take place gradually until a critical value of p_0 is reached, at which a *bifurcation* occurs. At this and higher values of p_0 (up to another critical value) computations yield R versus t curves leading to either of two steady-states, depending on the initial conditions: either a steady-state in which $R(t)$ is periodic with frequency (f), or one in which it is periodic with the subharmonic frequency ($f/2$). If p_0 is increased further until the next critical value is reached, a second bifurcation occurs, and another R versus t curve becomes possible in which the steady-state $R(t)$ is periodic with frequency ($f/4$). It is also likely that bifurcations leading to other

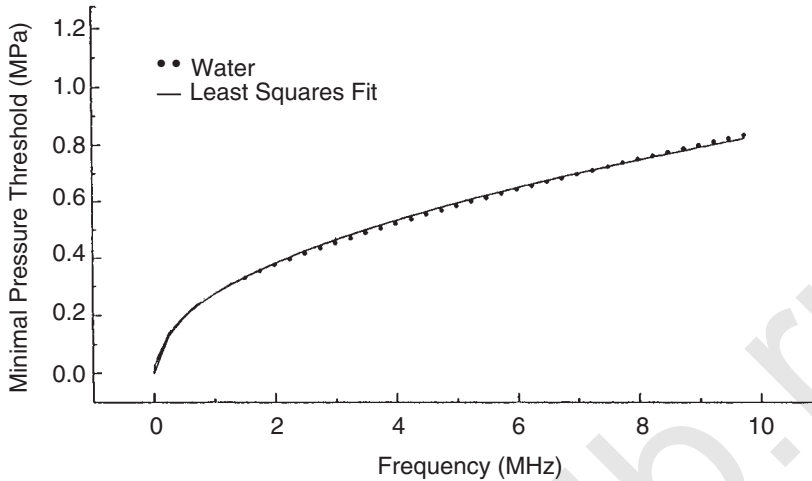


Fig. 5.11. Minimal pressure threshold versus frequency for inertial cavitation in water. Dots show values of p_{\min} from calculated curves such as those in Figure 5.10. Solid curve is a least-squares fit to the relationship $p_0/f^{0.5} = \text{constant}$ (Apfel and Holland, 1991).

frequencies will appear at closer and closer intervals as p_0 is increased still further, until a value is reached at which the motion is completely indeterminate and *chaos* ensues. The spectrum of sound emanating from the bubbles then includes a continuous band of noise.

The topic of *deterministic chaos* as applied to nonlinear systems generally has many aspects, and has developed rapidly in the last decade. Primary concepts of the subject, especially as they apply to cavitation, are defined and explained in reviews by Lauterborn and Parlitz (1988) and by Lauterborn (1991).

5.7 Surface Disturbances and Jet Formation

In Sections 5.2 through 5.6, the gas bubble is assumed to vibrate with spherical symmetry. Actually, however, complete symmetry probably exists only under restricted conditions, especially, for a vigorously vibrating bubble. Surface waves are frequently set up on the gas-liquid interface, as discussed in Section 4.1.6. Also bubbles are often situated on or near solid boundaries; liquid jets may then form at the bubble surfaces and impinge on the solid surface with high speed. Insight on the problem comes from studies by Plesset

and Chapman (1971). These investigators used numerical methods to obtain an approximate description of the collapse of a bubble near a solid wall. (Except for presence of the wall, which introduced asymmetry, the situation is similar to that considered earlier by Rayleigh (1917); see Section 5.1.) Plesset and Chapman (1971) assumed that, initially, the bubble is spherical and is nearly empty, containing only a small amount of vapor. It shrinks in response to ambient pressure in the liquid. Figure 5.12 shows computed surface profiles of a bubble just above a wall at various times given in the figure caption. Liquid flows toward the wall from the region above the bubble, the speed being greatest on the axis of symmetry. A jet forms, which impinges on the wall.

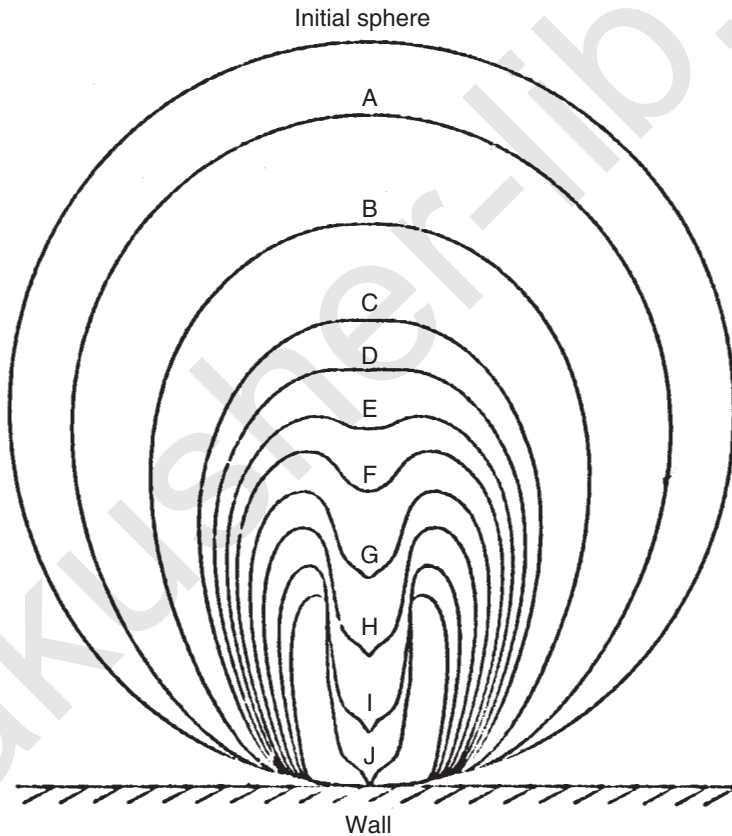


Fig. 5.12. Computed bubble surfaces at various times (in microseconds) after the beginning of collapse, as follows (see text). (A) 0.63, (B) 0.885, (C) 0.986, (D) 1.013, (E) 1.033 (F) 1.048, (G) 1.066, (H) 1.082, (I) 1.098, (J) 1.119 (Plesset and Chapman, 1971).

The phenomenon of jet formation has also been studied experimentally. Vogel *et al.* (1989) have used high-speed photography, up to 10^6 frames per second, to study the dynamics of laser-produced bubbles (radii ≈ 2 mm) collapsing near or on a solid boundary. Jet formation is seen clearly in their published photographs, as are other features. Coleman *et al.* (1987) investigated cavitation produced by an extracorporeal shockwave lithotripter (ESWL). Figure 5.13, from their publication, shows depressions in aluminum foil produced by exposing it to ESWL waves in a water bath. The depressions are believed caused by jets associated with collapsing bubbles.

5.8 Experimental Studies of Repetitive Inertial Cavitation

Although an extensive literature exists on theory for inertial cavitation involving a single spherical bubble oscillating continuously in a purely radial mode, it is only recently that this situation was realized experimentally. Gaitan and Crum (1990) and Gaitan *et al.* (1992) succeeded in finding conditions under which a single gas

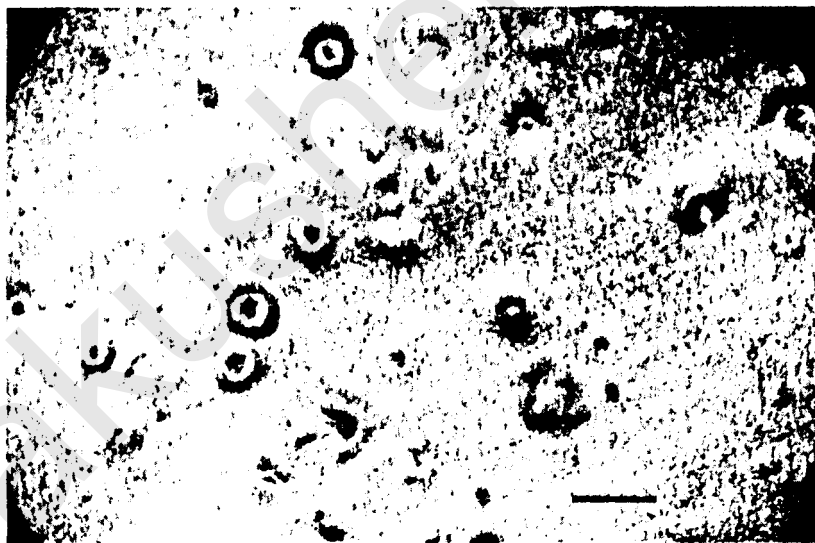


Fig. 5.13. General view of 0.02 mm thick section of aluminum foil exposed to shock waves from an ESWL. The deep depressions in the foil are probably caused by the impact of high-speed liquid jets developed in collapsing bubbles. The photo obtained by light microscopy. The length of the bar is 1 mm (Coleman *et al.*, 1987).

bubble executes large radial pulsations continuously for thousands of acoustic cycles; under these conditions flashes of light are emitted by the bubble, synchronously with the pulsations, giving evidence that high temperatures are produced. Records of the bubble radius (R) as a function of time were obtained experimentally with optical methods developed and used previously by Hansen (1984), Holt (1988), and Horsburgh (1990). It was found, with high temporal precision, that the light flashes coincided with minima in the R versus t curves (Section 5.9).

Techniques for measuring the bubble radius during its rapid changes were developed further by Barber and Putterman (1992). In Figure 5.14, the dotted curve shows the experimental R versus t data obtained by them for an air bubble in water; the driving frequency and pressure amplitude were 26.5 kHz and 0.108 MPa, respectively. The solid curve is based on theory similar to Equation 5.4. The evident agreement between theory and experiment gives strong support to current theory as a means of obtaining important information on inertial cavitation.

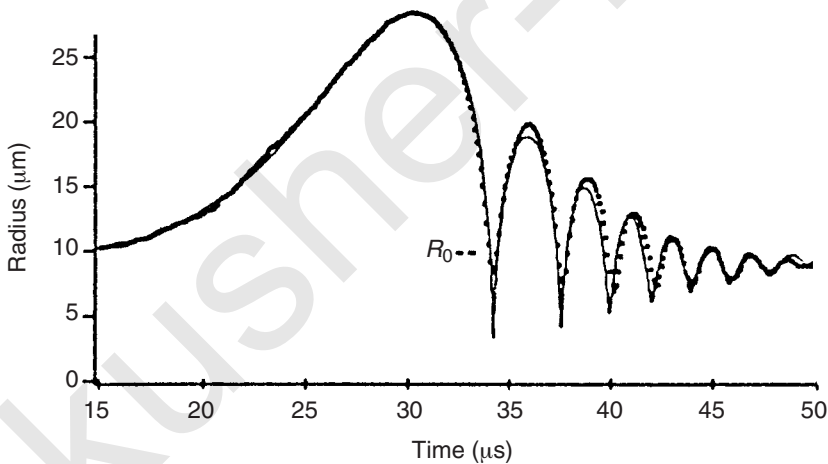


Fig. 5.14. One cycle of the radius versus time curve for an air bubble (initial radius $10.5 \mu\text{m}$) in water. The points are experimental data and the curve is from theory similar to that in Equation 5.4 but simplified by neglecting compressibility of the liquid, as in the “Rayleigh” models (Section 5.2). The pressure amplitude in the driving field is 0.108 MPa and the frequency is 26.5 kHz. Under these conditions, no observable light is emitted from the bubble (Barber and Putterman, 1992).

5.9 Sonoluminescence

Two qualitatively different physical phenomena occur during inertial cavitation that may be important from a biological point of view. The first is thermochemical. Such high temperatures and pressures are developed in the gas that the chemistry within the bubble may be qualitatively different than that which would occur at room or body temperatures. Both short-lived (free radicals) and relatively long-lived, potentially toxic products may be generated (Section 5.10). The second is mechanical. Upon rebound, the bubble sends forth very large, extremely short (subnanosecond) pressure spikes. As an example, calculations based on Gilmore's model indicate that, for an acoustic pressure of 2 MPa, the pressure spike at the surface of a 0.5 μm bubble as it begins to expand is of the order of 10^6 MPa and even at 50 μm from the bubble center is of the order of 100 MPa (Ayme-Bellegarda, 1990). For perspective, the shock waves generated by lithotriptors that are used to break kidney stones have focal pressures between 20 and 100 MPa.

During the brief interval when the gas is maximally compressed, its temperature briefly reaches thousands of kelvins. As an example, Figure 5.15 gives the maximum predicted collapse temperature of a 0.5 μm bubble exposed to a 1 μs pulse with a center frequency of 1 MHz (Flynn, 1982). Temperatures of this magnitude are great enough to generate free radical species that on recombination emit light (Sehgal *et al.*, 1980a; 1980b). This light emission may have biological significance in itself, since it extends into the ultraviolet end of the spectrum (see Section 7.4). Also, the light emission is an indicator of the occurrences of high temperatures associated with inertial cavitation and of the associated potentially adverse chemical reactions. If this sonoluminescence is observed experimentally, there can be little doubt that inertial cavitation is taking place.

Crum and Fowlkes (1986) have used sonoluminescence to investigate the conditions that are required to produce cavitation with short pulses of ultrasound. They report a threshold for sonoluminescence in an aqueous liquid at approximately 2 MPa for a 1 μs pulse with a carrier frequency of 1 MHz. The threshold falls gradually with increasing pulse length to about 1 MPa with 1 ms pulses. Duty cycle also influences the threshold. For 1 μs on-times and very long off-times, the threshold is roughly 2 MPa, but the threshold approaches 1 MPa at an on/off ratio of one in three.

In these studies, light emission was enhanced by addition of luminol to water. Thus, the light came primarily from reaction of the free radicals with molecules in the liquid surrounding the gas space. The light occurred in streaks suggesting that bubbles moved

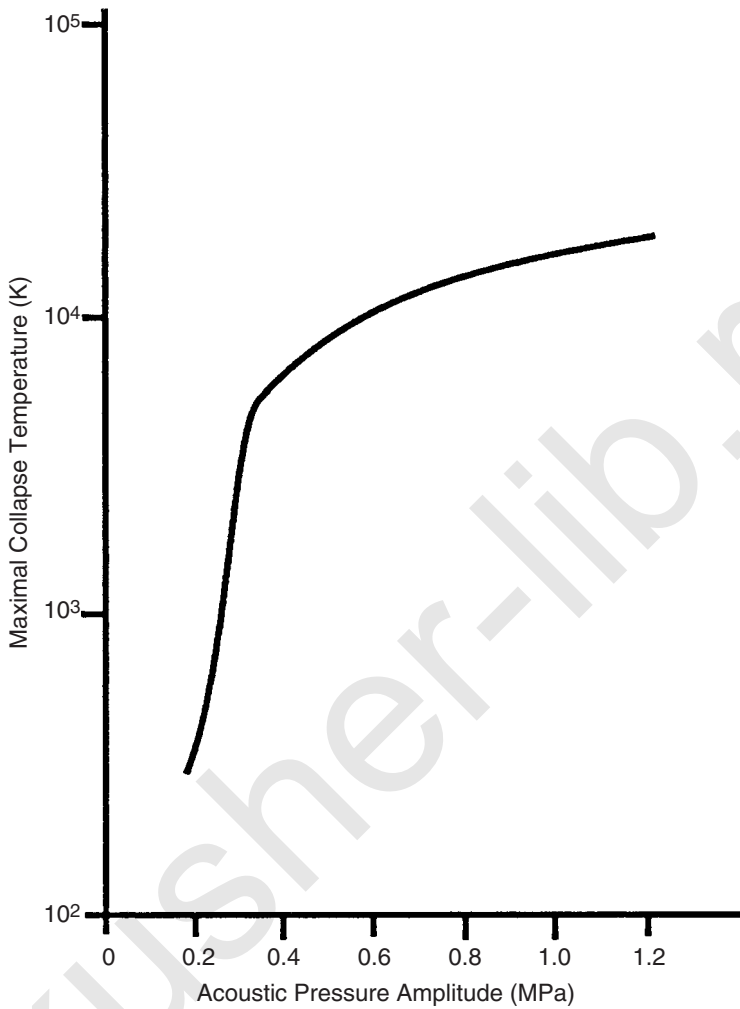


Fig. 5.15. Maximal collapse temperature for a bubble of $0.5 \mu\text{m}$ radius exposed to a $1 \mu\text{s}$ pulse with a carrier frequency of 1 MHz (adapted from Flynn, 1982).

rapidly through the medium under the influence of radiation forces (Section 4.4.2), while collapsing repetitively and generating light as they moved.

In their experiments with a single bubble, Gaitan *et al.* (1992) were able to record the intensity of light emitted from it and relate the temporal variation of light intensity with that of the bubble

radius (R). In Figure 5.16, the three curves give the driving pressure, the bubble radius and the light intensity, all as periodic functions of the time. The light is emitted in a single pulse each cycle; its duration is so short that it appears on the plot as a vertical line. It is seen that the light appears when the radius has its first minimum following the major collapse; this is as expected from theory, assuming the light intensity is greatest when the temperature in the bubble is highest.

Kamath *et al.* (1993) performed a detailed analysis of the chemistry underlying sonoluminescence, combining theory for bubble dynamics with theory for chemical kinetics. Their chemical model (for an argon bubble in water) includes 19 simultaneous reactions between radical species. They consider, as did previous workers, that the observed peak at 310 nm in the sonoluminescence spectrum results from radiative transitions of excited hydroxyl radicals.

The finding that inertial cavitation, involving a repetitive collapse cycle, can be maintained continuously with a single bubble has attracted considerable interest. The production of light from a repetitively collapsing bubble has been termed *single-bubble sonoluminescence* (SBSL). Some of the general features of the phenomenon have been discussed by Crum (1994) and by Putterman (1995). The

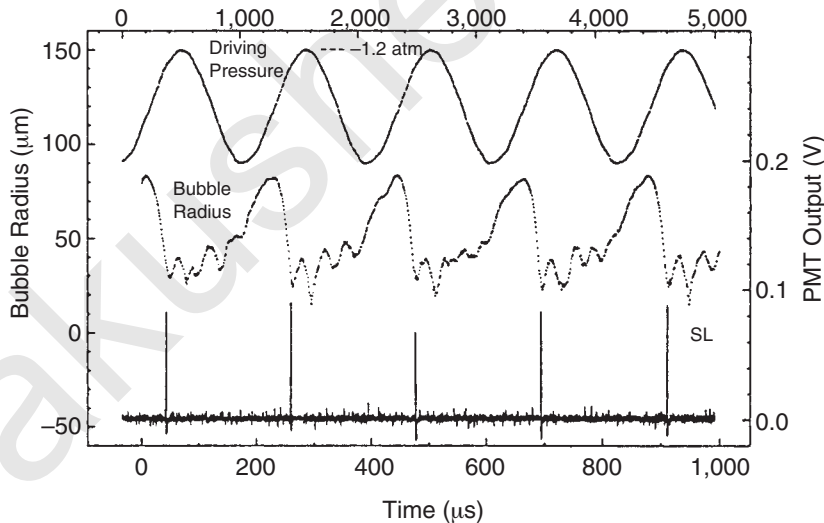


Fig. 5.16. Simultaneous plots of the driving acoustic pressure (top), bubble radius (middle), and intensity of sonoluminescence (SL) emitted by a single bubble (bottom). Pressure amplitude, 0.12 MPa; frequency, 22.3 kHz (Gaitan *et al.*, 1992).

spectral density of the light emitted by a single air bubble in water, shown in Figure 5.17 (Hiller *et al.*, 1992), extends well into the ultraviolet and agrees over much of the range with expectations for radiation from a 25,000 K blackbody. It is found that the light intensity is increased by a factor of more than a hundred when the water temperature is lowered from 35 to 1 °C. The spectrum is very sensitive to gas content in the bubble; for example, the emission of light from a bubble containing nitrogen is increased by about a factor of 30 when the argon content is increased from zero to one percent (Hiller *et al.*, 1994).

Crum (1994) points out that characteristics of SBSL are very different from those of the *multibubble sonoluminescence* (MBSL), produced in typical experiments with liquids. Whereas the spectrum of MBSL in water contains discrete lines characteristic of free radicals, such lines are not seen in the SBSL spectrum (*e.g.*, Figure 5.17). It

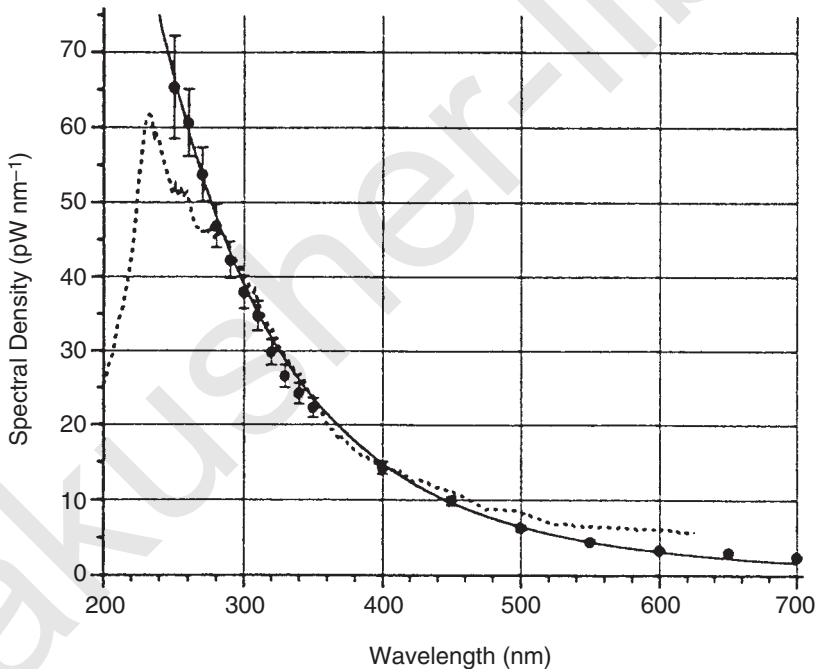


Fig. 5.17. Spectral density of the sonoluminescence from an air bubble in water at 22 °C, driven at a frequency of 27 kHz. The two sets of data (1) large dots and (2) dotted curve, are based on two methods of calibrating the light detector, and are in good agreement, except for wavelengths less than 300 nm. The solid curve is from theory for radiation from a blackbody at a temperature of 25,000 K (Hiller *et al.*, 1992).

is probable that the conditions of single-bubble inertial cavitation (involving symmetry in the driving pressure field) can lead to production of much higher temperatures in the gas than are produced in the more typical experimental conditions where many bubbles are active. Investigations of mechanisms continue. At present, it is not known to what extent results of SBSL experiments, done with special arrangements at relatively low frequencies (in the range of about 10 to 30 kHz), are relevant to conditions typical of medical diagnostic ultrasound.

5.10 Sonochemistry

As noted in previous sections, temperatures in a collapsing bubble can reach thousands of kelvins, even for modest excitation amplitudes (as noted in Section 5.9), and can thus create a favorable environment for unusual chemical reactions. A primary event for sonochemistry in aqueous media is the decomposition of water into the radical species of hydrogen and hydroxyl (Henglein, 1987). Hence, acoustical cavitation resembles some aspects of ionizing radiation, in that both are capable of generating free-radicals and biologically active sonochemicals. This aspect of cavitation is potentially critical for considerations of bioeffects and risks of biomedical ultrasound, because it introduces free radical damage, chemical toxicology, and genetic damage into the deliberations.

Richards and Loomis (1927) were among the first to investigate the chemical activity of ultrasound. Many studies followed and, at the present time, sonochemistry is an active field which has led to useful industrial processes, especially in the low ultrasonic frequency range 20 to 50 kHz (see, for example, Mason and Lorimer, 1988). The broad topic can be divided into two areas: (1) homogeneous sonochemistry, which deals with reactions in water and many other liquids (Suslick, 1988) and (2) heterogeneous sonochemistry, which involves reactions at interfaces between liquids and solids (Boudjouk, 1988). The many aspects of sonochemistry will be only briefly reviewed here, with emphasis on phenomena occurring in the megahertz frequency range relevant to biomedical applications.

The highly reactive hydrogen and hydroxyl radicals rapidly recombine or combine with nearby chemicals in other ways to yield a variety of species, especially molecular hydrogen, molecular oxygen, and hydrogen peroxide. Many other unstable and stable chemicals can be generated, depending on what chemical species are available in the medium. For example, with dissolved nitrogen present in

water, nitrous (HNO_2) and nitric (HNO_3) acids, ammonia (NH_3) and nitrous oxide (N_2O) are formed (Mead *et al.*, 1975). A wide variety of reactions can be initiated or enhanced: in biological media, a vast array of reactions and biochemical products is possible (Riesz and Kondo, 1992).

Sonochemicals are readily measured by chemical tests, which also provide a means of detecting cavitation as well as of quantifying its activity. Since sonoluminescence, discussed in Section 5.9, arises from chemical reactions, techniques based on observation of this phenomenon have potential for detection of cavitation and sonochemical activity.

Many chemical dosimeters have been developed for the detection of free radicals produced by ionizing radiation (Draganic and Draganic, 1971) and these can be adapted for ultrasonic cavitation. For example, terephthalic acid is converted to a fluorescent product by ultrasound which is readily measured (McLean and Mortimer, 1988). Such chemical dosimeters for cavitation are conveniently calibrated in terms of the equivalent gamma-ray dose. However, this nomenclature does not imply that an equivalent level of biological damage is produced, since the physical or chemical damage mechanisms may be different for ultrasound and ionizing radiation. A widely used cavitation assay is the liberation of free iodine from sodium iodide in the presence of carbon tetrachloride (Ciaravino and Miller, 1983; Coakley and Sanders, 1973; Weissler *et al.*, 1950). Alternatively, some experimental situations allow the convenient and sensitive detection of hydrogen peroxide (Miller and Thomas, 1993b; Weissler, 1958). A particularly powerful technique for detecting free radical production involves use of spin trapping chemicals and the electron spin resonance technique (Edmonds and Sancier, 1983; Makino *et al.*, 1983; Riesz and Kondo, 1992).

The production of sonochemicals is dependent on cavitation physics. In the absence of inertial cavitation, ultrasound does not form any sonochemicals. Techniques which initiate or enhance inertial cavitation also enhance sonochemical production. For example, freshly made phosphate buffered saline contained in a rotating tube exposure system is particularly efficacious for sonochemical production at megahertz frequencies (Clarke and Hill, 1970; Miller and Thomas, 1993b). Other factors influencing cavitation activity also influence sonochemical activity, such as temperature, viscosity, vapor pressure, etc. Pulsed ultrasound can lead to enhanced effect for relatively long pulses around 10 ms duration (Ciaravino *et al.*, 1981a), but generally gives decreasing sonochemical yield for decreasing pulse duration and decreasing repetition frequency (Clarke and Hill, 1970; Fowlkes and Crum, 1988) (see Section 7.2.1.2

including Figure 7.2). However, it should be noted that cavitation and free radical production are possible even for short pulses (Christman *et al.*, 1987; Crum and Fowlkes, 1986). The yield of H_2O_2 is strongly dependent on ultrasonic frequency, and the apparent threshold for production is proportional to frequency in the rotating tube system (Hill and Joshi, 1970; Miller and Thomas, 1993a), as shown in Figure 5.18. Sonochemical production by inertial cavitation has been reported to be difficult to detect above about 4 or 5 MHz; for example, no effect could be detected in the rotating tube system for 4.9 MHz focused exposures up to 2.8 MPa (Miller and Thomas, 1993a).

Chemical yields are also altered in several different ways by the chemical composition of the medium. As noted above, the presence

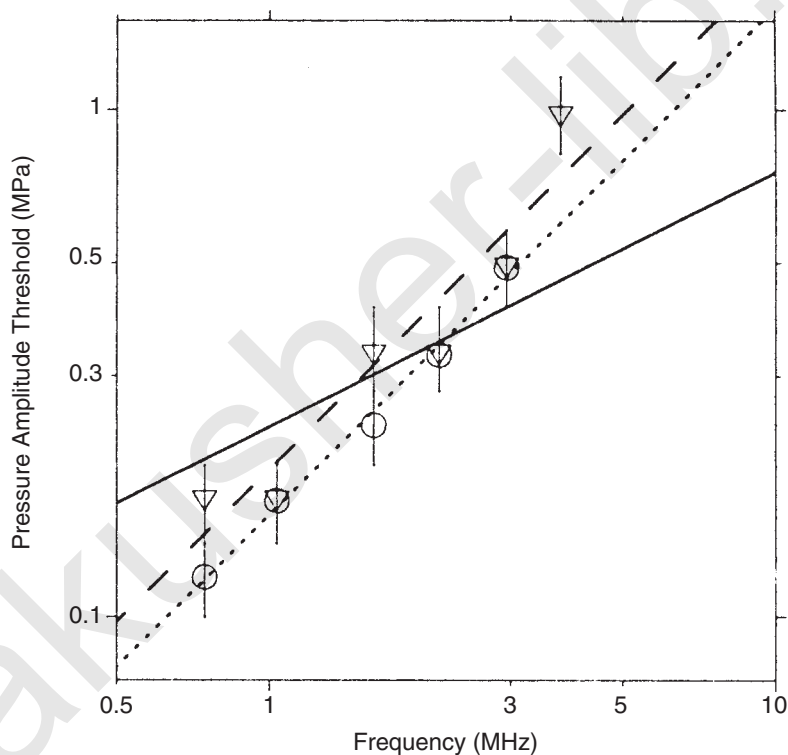


Fig. 5.18. Frequency dependence of cavitation thresholds in the rotating tube system for hemolysis (circles with fitted dotted line) and H_2O_2 production (triangles with fitted dashed line) with a 3 dB range of uncertainty. Exposure duration was 15 s for the hemolysis results but 15 min was needed to accumulate readily measurable hydrogen peroxide. The solid line represents the relationship $p_0 = c f^{1/2}$, where c is a constant (Miller and Thomas, 1993a).

of different chemical species such as nitrogen result in their participation in free-radical reactions. Dissolved noble and other gases present in the collapsing cavity alter the thermodynamics of the collapse, and the resulting sonochemistry (Suslick, 1988). For example, relative to yields with dissolved air, dissolved argon enhances but dissolved nitrous oxide eliminates the sonochemical reaction of uracil in the medium (McKee *et al.*, 1977). Various solutes have an effect on hydrogen peroxide yields, and some are efficient scavengers of the hydroxyl radical (Henglein and Kormann, 1985). Addition of a scavenger, such as cysteamine, can be used as a test for free-radical effects (Armour and Corry, 1982; Dooley *et al.*, 1984; Fu *et al.*, 1980).

5.11 Acoustical Parameters as Predictors of Inertial Cavitation

Formulation of quantitative safety guidelines to assist users of diagnostic ultrasound presents challenges because of the complex spatial and temporal configurations of the ultrasound fields made available by modern equipment. In the interests of simplicity and convenience, efforts have been made to characterize the fields in terms of a few selected acoustical quantities (AIUM/NEMA, 1992; IEC, 1992; NCRP, 1983; Nyborg and Wu, 1993; Preston, 1991). In particular, suitable quantities have been sought in terms of which guidelines can be stated for avoiding the occurrence of cavitation, especially inertial cavitation, which might cause biological damage.

For CW fields, in which the pressure varies sinusoidally with time, the local acoustic pressure amplitude is the quantity usually chosen to indicate whether inertial cavitation can occur at a given site. For beams in which the wave form has become distorted by NLP, the pressure does not vary symmetrically about its mean value; instead, the positive peaks of the acoustic pressure tend to become larger than the negative peaks, while the latter become broader and the former narrower. When the waveform becomes distorted by NLP, the concept of pressure amplitude loses meaning. Therefore, the term acoustic pressure amplitude is reserved in this Report for linear conditions and sinusoidal waveforms. For acoustic fields that have been affected by NLP, the peak negative pressure is often taken to be the critical quantity in defining threshold conditions for inertial cavitation.

For pulsed ultrasound fields in which the waveform for each pulse is essentially a sinusoidal function of time with frequency (f) (the “carrier” frequency), the acoustic pressure amplitude (p_0) is the

critical predictor of inertial cavitation if the pulse duration (t) is sufficiently long compared to the ultrasound period ($1/f$). This condition is usually satisfied in Doppler ultrasound studies, where the product tf is typically three or more. The peak negative pressure is often used as the critical parameter in these circumstances.

The ultrasound pulses used in imaging are very short, such that the product tf is of the order of unity. For such a pulse the ultrasound spectrum is not characterized by a single frequency, but by a frequency band. These pulses can be viewed to a first approximation as a carrier modulated by a Gaussian envelope. When $tf \sim 1$, the modulation itself can make the pulse asymmetric even under linear conditions. In that case, the acoustic pressure amplitude is arbitrarily defined as the mean of the absolute values of the maximum positive and maximum negative pressures in the pulse.

If distortion is produced by NLP, the ultrasound field becomes very complex and it is difficult to determine general criteria for the production of inertial cavitation. However, insight on the problem has come from theoretical studies. Ayme and Carstensen (1989b) made computations in which the waveform was represented under linear conditions as a sinusoidal function with "carrier" frequency (f) and pressure amplitude (p_0) multiplied by a Gaussian function whose width determined the pulse duration (t). After distortion had occurred as a result of NLP, the waveform was represented by the same Gaussian function multiplied by a Fourier series in which the first term, *i.e.*, the fundamental, was the original sinusoidal function with altered amplitude. Using theory for inertial cavitation they found that either the pressure amplitude of the fundamental or the peak negative pressure of the pulse could serve satisfactorily in defining the threshold for inertial cavitation, when the pulse becomes distorted as a result of NLP. In an experimental situation, it may not be feasible to make an accurate measurement of the fundamental pressure amplitude as defined above; however, it may be possible to measure an approximation to it by appropriate filtering of the waveform.

It has been shown that some kind of temporal peak as opposed to a temporal average property of the sound field will correlate with the occurrence of cavitation (Apfel, 1982; Carstensen and Flynn, 1982; Carstensen *et al.*, 1983b; Flynn, 1982). Several quantities have been used to describe the temporal-peak field values for diagnostic ultrasound devices. These include the peak positive pressure, the peak negative pressure, the pulse-average intensity, and the maximum intensity. In principle, the pulse-average intensity is the energy per unit area per pulse divided by the pulse length or, in effect, the intensity averaged for the time that the sound is on. It is feasible

to measure this quantity with modern technology but it is still an average and not precisely a peak indication of the sound field. It is possible to devise two different pulse envelopes with the same pulse average intensity but which have qualitatively different biological effects (Carstensen *et al.*, 1983c). In fact, it is probable that there is no single peak measurement quantity which completely predicts the onset of inertial cavitation for all conditions and waveforms.

To be useful as a predictor of cavitation, any descriptive parameter must be able to work with the asymmetrically distorted waveforms that result from diffraction in the presence of NLP at high output intensities particularly, when the ultrasound has passed a significant distance through water or other weakly attenuating liquid. As illustrated in Figure 5.19, the waveform (in water) at the focus of a typical large amplitude diagnostic device has a nearly discontinuous rise to its peak positive pressure, and a rapid fall to a comparatively slowly varying negative phase. Frequently, under conditions where the waveform is highly distorted the peak positive pressure is more than twice the amplitude of the peak negative pressure (Section 10). A sharp spike in pressure, be it positive or negative, is a poor predictor of inertial cavitation because the spike comes from high frequency components in the wave, which are much less effective in driving bubble motion than lower frequencies. Therefore, the peak positive pressure is not a good candidate as a primary predictor of inertial cavitation.

The maximal intensity (I_m) (NCRP, 1983) was defined as the intensity averaged over the largest half cycle of the pulse. Since the "largest" half cycle in a diagnostic pulse is ordinarily the positive half, I_m suffers from the same problems in a nonlinearly distorted wave as the peak positive pressure (although to a lesser degree).

In general, bubbles in water expand during the negative phase of the acoustic pressure cycle. The violence of the collapse is linked to the degree of expansion. It is reasonable, therefore, to conclude that the amplitude of the negative phase of the acoustic pressure may have a causal relationship to the violence of the collapse. Of course, the positive pressure plays a role in the behavior of the bubble as well. One can incorporate both negative and positive pressures into the descriptive parameter of the field without emphasizing the high frequency components of the positive pressure spike by using the fundamental frequency component of the pulse (Ayme and Carstensen, 1989a; 1989b).

For a typical diagnostic pulse (*e.g.*, Figure 5.19), the negative pressure amplitude, the amplitude of the fundamental frequency component of the wave or pulse average intensity are probably equally good as predictors of inertial cavitation in water given the present

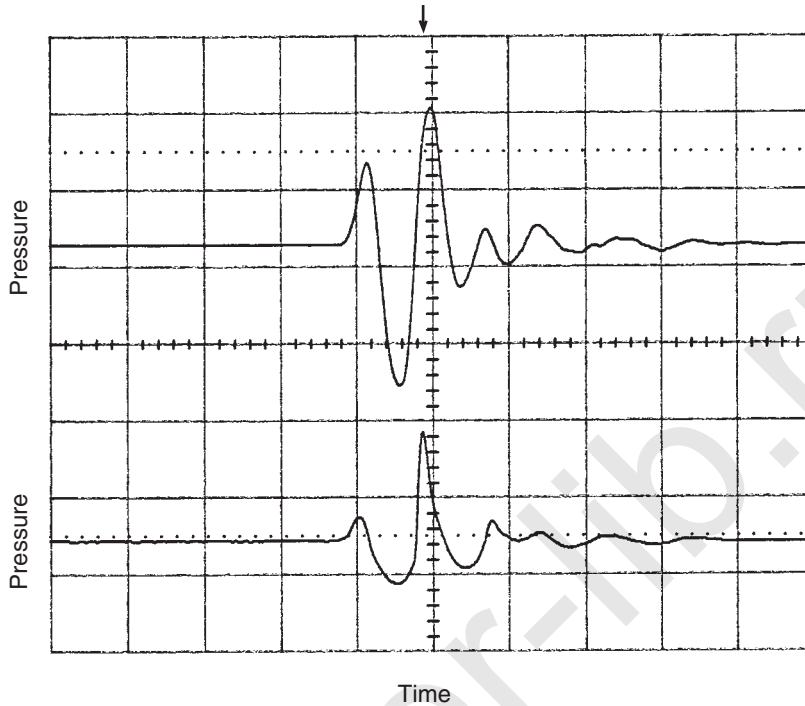


Fig. 5.19. Typical waveforms for commercial diagnostic ultrasound equipment, operating in M-mode at nominal frequency 2.5 MHz; the time scale is $0.5 \mu\text{s}$ per division. The upper plot was sampled near the transducer and the lower waveform was recorded after propagation to the far field through water. Near the source the waveform within the pulse is nearly sinusoidal. After propagation at high amplitude to the far field the waveform is characterized by a much shorter rise time to the peak amplitude and by asymmetry. In this example, the peak positive pressure (indicated by the arrow) is nearly twice the maximal negative pressure.

state of knowledge. Other parameters that influence the threshold and intensity of cavitation include pulse duration and pulse repetition rate (Ciaravino *et al.*, 1981a; Fowlkes and Crum, 1988).

In summary, the occurrence and intensity of acoustic cavitation depend strongly on the local pressure amplitude of the sound field and, of course, the existence and character of gaseous nuclei and their local environment; they also depend, though to a lesser extent, on the pulse length and center frequency. A step in the development of a specific predictor for inertial cavitation called the *mechanical index* (MI) has been proposed by consensus groups in the United States (AIUM/NEMA, 1992) (see Appendix B).

Almost all of the discussion of cavitation up to this point has assumed that the environment of the bubble is water. Within the body, the physical properties of the media may differ significantly from those of water. Two approaches to more realistic models of cavitation *in vivo* suggest that the violence of cavitation in the body may be less than it is in water for similar local acoustic fields.

One approach to this problem is simply to assume that tissues have a higher viscosity than water when modeling bubble behavior through the Gilmore equation. It is not clear what value of viscosity is appropriate to use in such a model. However, in a specific example, calculations based on an assumed five-fold increase in viscosity over that of water resulted in more than a 100-fold reduction in the computed local body forces near the most active collapsing bubbles in a 1 MHz, 8 W cm⁻² field (Carstensen *et al.*, 1993). In experiments done under these exposure conditions, approximately 80 percent of erythrocytes were lysed when suspended in a medium with a viscosity of 1×10^{-3} Pa s (1 cP), whereas less than 20 percent were lysed when the suspending medium had a viscosity of 5×10^{-3} Pa s (5 cP). It is difficult to interpret experiments whose results depend on the action of bubbles when the size, number, location and surface condition of the bubbles is unknown. In the example cited, the added agent not only changed the viscosity measurably but it also may have changed the processes of bubble generation, fragmentation and recombination because of the tendency of polymers to form skins on the bubble surfaces.

An analytically more complicated approach is to limit bubble expansion in the negative phase of the acoustic cycle. It is quite possible that bubbles in tissues are contained within structures that dominate their radial motion. Because inertial cavitation depends on a significant expansion of the bubble during the negative phase of the acoustic wave, it is reasonable to expect a significant reduction in collapse pressure if the containing structures inhibit the expansion of the bubble. Ding and Gracewski (1994) modeled this situation by giving the bubble a shell which had no effect on the bubble for radii less than equilibrium values but had a large stiffness that opposed expansion. These bubbles were subjected to positive and negative pressure pulses. The effects of constraint are most pronounced with small bubbles. In the example of Figure 5.20, bubbles that were constrained in their expansion had collapse pressures several orders of magnitude smaller than free bubbles.

5.12 Summary

When free bubbles of gas are exposed to ultrasound at the acoustic pressure levels used in most applications of diagnostic ultrasound,

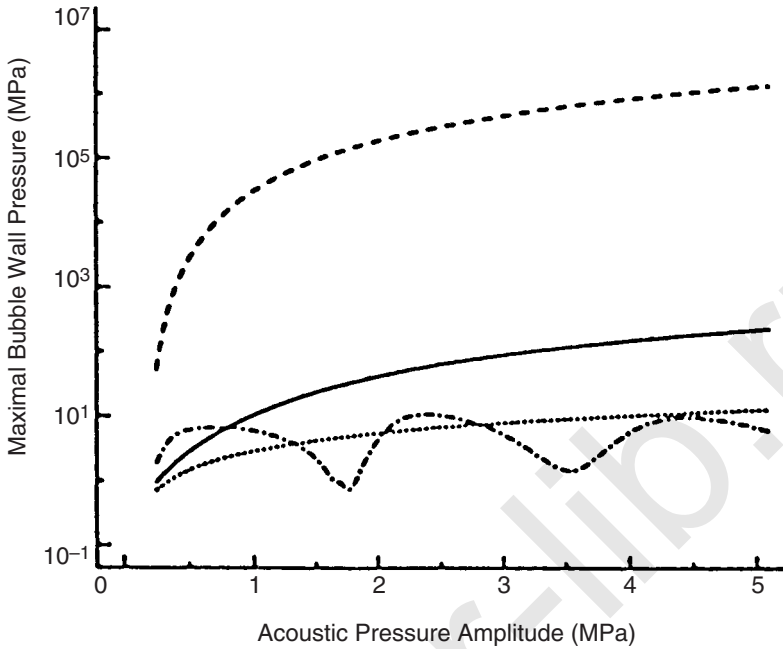


Fig. 5.20. Maximal bubble wall pressure $[P(R)]$ of a $2\ \mu\text{m}$ bubble. The upper (dashed) curve gives the response of an unconstrained bubble to a purely negative pressure pulse while the solid curve is the response of the same bubble to a purely positive pulse. When the bubble is constrained by a stiff shell, the bubble wall pressure is reduced: dashed-dotted curve is for a negative and the dotted curve is for a positive pulse (Ding and Gracewski, 1994).

the bubble response is nonlinear. Resonance characteristics are modified or absent. The spectrum of ultrasound scattered from the bubbles contains components which are integral and nonintegral multiples and submultiples of the incident frequency. Often the motion is chaotic and the spectrum contains noise. Under specialized conditions a free bubble maintains a spherical shape during nonlinear oscillations, but more often the surface becomes severely contorted. Under the latter conditions small microbubbles of gas are created at the interface; also, jets of liquid are formed which project inward.

When the pressure amplitude of the field driving the bubble exceeds a critical value, inertial cavitation occurs; then the phase of motion during which the radius is decreasing is dominated by an implosion or collapse, as the surrounding liquid rushes inward. The bubble decreases to a minimum volume which is a small fraction of

its original value. This highly compressed state persists for a very short time, after which the fate of the bubble varies; it may rebound or it may disintegrate into very small fragments, some of which dissolve and some of which may become active bubbles. During the state of greatest compression the pressure and temperature of the gas are very high. If the bubble is near a boundary when it collapses, a liquid jet may form which impinges on the boundary at high speed. The term inertial cavitation is given to the activity described above, since the vigor of the collapse comes from inertia (or momentum) of the inward rushing liquid.

All of the above characteristics of inertial cavitation are expected from physical theory in the form of nonlinear differential equations; these are solved numerically for conditions of interest by using special computational programs. The model chosen for most computations is a single spherical bubble which contains a gas of known properties; it exists in a Newtonian fluid well away from boundaries and maintains a spherical shape as it oscillates. Such theory has been shown to agree well with important features of the observed oscillatory motion of single bubbles in special arrangements. However, in a typical experiment where ultrasound is applied to a liquid in a test tube or other container, it is difficult to compare results with predictions from theory. This is primarily because cavitation activity is strongly dependent on the number, size and location of cavitation nuclei, and information on these is not known unless special steps are taken. The use of contrast agents consisting of small stabilized gas bodies of controlled size as cavitation nuclei has made it possible to make more specific predictions of cavitation activity in liquids.

When ultrasound is applied to a liquid which has not been "prepared" by adding cavitation nuclei, the onset of cavitation requires the occurrence of such nuclei accidentally on vessel walls or on small impurity particles, the latter being ubiquitous unless the liquid has been very thoroughly filtered. These accidental nuclei are typically small, and the acoustic pressure levels required to activate them are also high enough to produce inertial cavitation. Hence, when cavitation activity is produced in an unprepared liquid, inertial cavitation is likely to dominate, although noninertial cavitation may be present also. If stabilized gas bodies of suitable size are added to a liquid, cavitation activity of a noninertial type can occur at levels of the acoustic pressure too low for the production of inertial cavitation (Section 4).

It is known from many experiments that chemical reactions of widely varying nature are accelerated by exposure of liquids to ultrasound. These chemical effects can often be attributed to free radicals

produced during the short pulses of high temperature expected when inertial cavitation occurs. Some of these reactions are accompanied by sonoluminescence, *i.e.*, by the production of light. Techniques for detecting and measuring chemical reaction products, or the light output when sonoluminescence occurs, have proven useful for assessing the extent to which inertial cavitation occurs in a liquid. Sonoluminescence, and hence inertial cavitation, was found to occur in water exposed to short pulses of ultrasound.

An approximate theoretical result has proven convenient for predicting the lowest acoustic pressure level at which inertial cavitation can be produced in a liquid by a single cycle of ultrasound when cavitation nuclei of optimum size are present (see Figure 5.11). According to this result, for frequencies in the range 1 to 10 MHz, the threshold value of the peak negative pressure (p_-) is proportional to the square root of the frequency (f), *i.e.*, proportional to f^n , where $n = 0.5$. Although this relationship has undergone little testing under conditions assumed in the theory, it was found to agree with experiments done in which water, containing contrast agents or other cavitation nuclei, was exposed to pulsed ultrasound; an ultrasonic method was used to detect cavitation events. In other experiments, the frequency dependence has varied, the exponent n usually ranging from 0.5 to 1 or more. Under most conditions n is equal to, or greater than, 0.5.

6. Bioeffects of Noninertial Cavitation Involving Free and Stabilized Gas Bodies in Non-Mammalian Systems

6.1 Introduction

The physical interaction of ultrasound with stable bodies of gas is reviewed and discussed in Section 4. When gas bodies are set into oscillation by ultrasound, they may affect biological cells or tissues in their vicinity. The bioeffects of noninertial cavitation and GBA can be conveniently divided into two types: (1) effects of stabilized gas bodies *in vitro*, including gas-filled micropores and gas-body-based contrast agents for diagnostic ultrasound, reviewed in Section 6.2, and (2) effects of gas bodies stabilized in biological tissue *in vivo*, including plant and insect tissues, reviewed in Section 6.3. The physical phenomenon of GBA may occur at any level of exposure. Thus, bioeffects of GBA may potentially occur at relatively low amplitude levels, well below the threshold for inertial cavitation. This feature has allowed the analysis of some bioeffects using relatively simple linear-oscillation theory, which is applicable at low amplitudes. Furthermore, certain effects (*e.g.*, the membrane damage arising from shear stress in acoustic microstreaming flow) appear to be amenable to description in terms of the action of single mechanisms in contrast to the more complex analysis required for the higher level exposures associated with inertial cavitation, when many mechanisms operate simultaneously. Although the physical phenomenon of GBA has no threshold, thresholds can typically be defined for its biological effects, which are, for example, related to the shear-stress threshold for membrane breakage. Applications of shear stress and other physical mechanisms to the description of ultrasonic bioeffects is reviewed in Section 6.4

6.2 Studies with Cell Suspensions

In vitro bioeffects of ultrasound on cell suspensions result primarily from cavitation. Noninertial cavitation involving free bubbles, as described in Section 4.1, should theoretically be a part of the phenomena occurring during cavitation bioeffects studies. However, specific examples of *in vitro* bioeffects of this type of cavitation are not available as a separate subject in the literature, except for studies with added ultrasound contrast agents discussed in Section 6.2.2. Without stabilized gas bodies pre-existing in the suspension, ultrasound fields must be high enough to generate suitable bubbles from available cavitation nuclei, and these levels are typically also high enough to generate inertial cavitation. Thus, in general, bioeffects on suspensions of cells occur above the inertial cavitation threshold in the megahertz frequency range, and it is impossible to observe separately the effects of noninertial bubbles. In order to study possible bioeffects of noninertial cavitation, it is necessary to work with media containing stabilized gas bodies. This Section is devoted to research with stabilized gas bodies, while Section 7 deals with bioeffects of ultrasound on cell suspensions where inertial cavitation is the dominant mechanism.

6.2.1 Gas-Filled Micropores

As detailed in Section 4, one means of stabilizing small bodies of gas for use in ultrasonics research is to trap gas in microscopic pores (*i.e.*, micropores) in hydrophobic membranes immersed in an aqueous medium. When the air-water interfaces in the micropores are driven to oscillation by ultrasonic exposure, acoustic microstreaming flow develops in the liquid near the micropore. In addition, small particles, including biological cells, are attracted to the activated micropores by radiation force. In a cell suspension, these phenomena result in a gathering of cells to active micropores and damage to the cells taken up in vigorous microstreaming flow.

This process was first observed for ultrasound in the medically relevant frequency range by Nyborg *et al.* (1977). Human blood platelets formed semi-solid clumps at 3 to 5 μm diameter micropores exposed for 15 min of 1 MHz ultrasound at 125 mW cm^{-2} . The clumping of platelets, which is a physiological response related to blood clotting, could be observed at intensities as low as 32 mW cm^{-2} (about 31 kPa pressure amplitude) and increased with increasing intensity (Miller *et al.*, 1978). The effect was also obtained using a 2.1 MHz CW Doppler ultrasound instrument (Miller *et al.*, 1979).

Barnett and Kossoff (1984) observed clumping of platelets at 4 μm diameter micropores after 4 MHz exposures at 30 mW cm^{-2} with 30 μs pulses repeated at a frequency of only 30 Hz.

The effects of ultrasonically activated gas-filled micropores include membrane damage. Williams and Miller (1980) developed a test for release of ATP from erythrocytes, using the sensitive firefly luminescence method, which could be conducted simultaneously with ultrasonic exposure. For 2 MHz ultrasound with 3.4 μm diameter micropores, ATP release was approximately proportional to the square of SPTA intensity in the range 5 to 100 mW cm^{-2} for both continuous and pulsed (1 μs pulses, one in nine duty cycle) 100 s exposures (Miller and Williams, 1983); this response is shown in Figure 6.1. The response was roughly proportional to exposure duration but independent of pulse duration for 1 to 100 μs pulses (one in nine duty cycle). The lack of a clearly defined threshold for the ATP release was an important feature of the results (Miller and Williams, 1983), and illustrates a difference between inertial cavitation bioeffects, which only occur above the inertial cavitation threshold, and GBA effects, which potentially can occur at much lower levels.

The micropore exposure system also induced cell lysis in murine spleen cell suspensions observed after 1.6 MHz ultrasound exposure above 75 mW cm^{-2} SPTA intensity (Vivino *et al.*, 1985). The cells were stimulated to divide with the mitogen Concanavalin A so that effects on DNA synthesis could be followed. Incorporation of DNA label was reduced by exposure for cells exposed and labeled 24 and 48 h after stimulation, but not 7 or 13 h after stimulation, indicating that the cells were more sensitive in the later stages of stimulation. In this study, the direct effect of lysis also appeared to cause an indirect effect by the action of the cell lysate on surviving cells.

Release of type-B red-cell antigens into the medium was observed after 1.7 MHz exposure of three percent hematocrit suspensions with 4 μm diameter gas-filled micropores (Miller and Lamore, 1987), following a report of reversible removal of cell surface antigens by ultrasound (Pinamonti *et al.*, 1982). However, this effect appeared to be a byproduct of hemolysis induced by GBA, rather than a sublethal effect on the cell surface (Miller and Lamore, 1987).

Various biophysical factors influence hemolysis by ultrasonically activated gas-filled micropores. Suspensions of erythrocytes from 0.1 to 30 percent hematocrit and whole blood (hematocrit = 47 percent) were exposed at 37 $^{\circ}\text{C}$ to 1.7 MHz ultrasound with 4 μm diameter micropores in an exposure chamber which was continuously moved in an orbital motion to maintain the suspensions (Miller, 1988a). Significant hemolysis was observed after 16 min exposures at

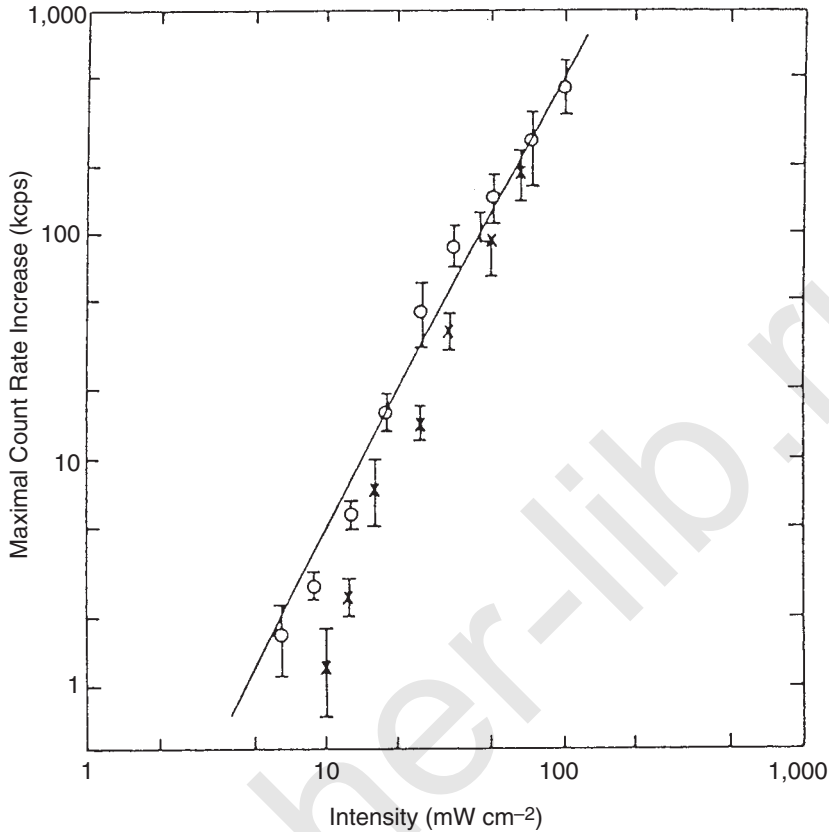


Fig. 6.1. ATP release, indicated by the maximal count rate increase (MCRI) of luminescence, from erythrocytes during 2 MHz exposures with 3.4 μm diameter gas-filled micropores. The 100 s exposures used 1 μs pulses with 0.1 duty cycle and variable pulse-maximal intensity (open circles) or variable duty cycle with 1 W cm^{-2} pulse-maximal intensity (crosses). The quantity plotted along the horizontal axis is the SPTA intensity. The straight line indicates proportionality of MCRI to the square of the SPTA intensity (Miller and Williams, 1983).

90 mW cm^{-2} (approximately 50 kPa) or above. The number of cells lysed remained roughly constant for hematocrit above one percent, but this constant number represented a decreasing percentage of hemolysis for increasing hematocrit (Miller, 1988a). This suggests that a fixed number of bubbles is limited in its ability to lyse cells. Thus, at high cell number densities, effects from a few bubbles might easily be lost in the background. This phenomenon helps to explain the cell-density effect observed by several investigators (Section 7),

in which effects seen in sparse cell suspensions become increasingly difficult to detect at higher cell number densities.

Hemolysis induced in five percent hematocrit suspensions by 1.9 MHz activation of 3.4 μm micropores at pressure amplitudes up to 0.1 MPa was not strongly influenced by exposure temperature (15, 25, 37 and 48 °C) or pre-treatment with heat (48 or 50 °C) or variations in osmolarity (180, 290 or 580 mOsm) (Miller and Thomas, 1990). Since elevated temperatures tend to make red cells more sensitive to shear stress (Krizan and Williams, 1973), the results for various temperatures were interpreted to mean that the sensitivity to shear is not critical in the results. Apparently, the shear stress is well above the lysis threshold, and the amount of lysis is determined by the number of cells which encounter the active micropores. Increasing viscosity of the liquid (0.7 to 4.2 cP) reduced the effect, and increased mass density (1.12 g cm⁻³) increased the effectiveness of the exposures. The latter finding is interesting because the increased mass density eliminated the density difference between the cells and the medium, which might have been expected to reduce the radiation force on the cells and to reduce the effectiveness of the exposures (Miller and Thomas, 1990). Katz (1992) suggested that surface forces on small particles explain part of this unexpected phenomenon, in which surface forces cause particles to accumulate on the surface of the micropore sheet. Another possible explanation arises from detailed theoretical consideration of the radiation forces on small particles (Doinikov, 1997a; 1997b; 1997c). Due to viscous and thermal boundary-layer effects, a droplet in the vicinity of a spherical-wave source would be expected to undergo an attractive force regardless of its specific properties.

6.2.2 *Ultrasound Contrast Agents*

Small bodies of gas can strongly scatter incident ultrasound, making stabilized gas bodies excellent candidates for the formulation of contrast agents for diagnostic ultrasound (Section 4.3). Clinical testing of ultrasound contrast agents has found them to be generally “safe and efficacious” as defined by the drug-approval process; however, the potential for effects to result from interaction of diagnostic sound with gas bodies would not be examined specifically during this process. Results of bioeffects research, such as from gas-filled micropores (Section 6.2.1), show a potential for significant bioeffects to occur from GBA at low continuous or pulsed ultrasonic intensities, and stimulate interest in the potential for bioeffects (either harmful or therapeutically beneficial) from gas-body-based contrast agents.

Presently, few data are available on this topic due in part to the lack of standardized and readily available commercial products. Several recent reviews have noted a growing collection of studies that indicate a potential for cell-membrane damage and perturbation of the microvasculature (AIUM, 2000; ECMUS, 1999; Fowlkes and Hwang, 1998; Miller, 2000; Mornstein, 1997). Most studies have been conducted with Levovist[®], Echovist[®] or Alburnex[®], which are commercially available. In several studies, the contrast agents have been added to blood cell suspensions and exposed to ultrasound with hemolysis as the bioeffects endpoint, under the assumption that blood would be the primary tissue affected by injection of contrast agents during diagnostic ultrasound examinations. Some recent studies have begun to examine effects other than hemolysis and to utilize different systems, such as cells in monolayer culture.

Normally, cavitation is difficult to produce in clean or sterile biological media, because of the relative lack of cavitation nuclei. Addition of gas bodies in sterile contrast agents alters this picture and allows a measure of control over the cavitation phenomena. However, it is not yet completely clear how the interaction of ultrasound with contrast agents should be classified relative to the other forms of cavitation. At high exposure amplitudes the agents can serve as nuclei for inertial cavitation (Miller and Thomas, 1995a) and can dramatically reduce the cavitation threshold in whole blood (Miller and Thomas, 1996a). Bioeffects of inertial cavitation are discussed in Section 7, with or without added contrast agents (although, given the vague distinction in many reports between noninertial and inertial cavitation, some overlap occurs in Sections 6 and 7). Of particular interest in Section 6 is the potential for induction of bioeffects at relatively low amplitudes either by GBA, when the contrast agent remains stable during exposure, or by oscillation of free bubbles, when the contrast agent is modified. In the latter case, effects would result from the initiation of free-bubble cavitation, rather than by direct action of the stable gas bodies. For example, Alburnex[®] gas bodies are acoustically labile and begin to disappear at 0.15 to 0.33 MPa during exposure to 2.5 MHz pulsed ultrasound (Vandenberg and Melton, 1994). The destruction of gas bodies in contrast agents during exposure at higher pressure amplitudes may involve liberation of free bubbles (*i.e.*, noninertial cavitation bubbles), which quickly dissolve when the ultrasound ceases.

Williams *et al.* (1991) examined the effects of an experimental contrast agent SH U-454 (Echovist[®]) on cell lysis in the rotating tube exposure system at 0.75 MHz. For hematocrits below two percent, the addition of the agent enhanced the observed lysis, especially at the lowest SATA intensity of 0.5 W cm^{-2} . The enhancement was most

evident in a stationary tube, for which the lysis is normally minimal. At higher intensities, lysis sometimes decreased with added contrast agent. At hematocrits greater than 5.5 percent, lysis was not observable, and addition of the contrast agent did not produce detectable lysis. Given the small effects, even in the sensitive rotating-tube exposure system, it seems unlikely that use of Echovist® clinically would result in appreciable amounts of cell lysis (Williams *et al.*, 1993). In similar experiments at 1 MHz using Albunex® at $33 \mu\text{L mL}^{-1}$, Miller *et al.* (1995a) found that hemolysis essentially did not occur in the rotating-tube system for hematocrits above 10 percent with exposures up to 5 W cm^{-2} spatial peak. These results with added contrast agents are similar to other results for the rotating tube system without added gas bodies, and thus may represent augmented nucleation of the normal cavitation phenomena in a rotating tube exposure system. In some cases, ultrasonically induced hemolysis at higher hematocrits may simply be undetectable in the background hemolysis, and may become observable for low background, depending on the frequency, intensity and other factors. For example, Daniels *et al.* (1995) noted that a small amount of hemolysis was produced in 21 percent hematocrit suspensions of blood cells in saline by exposures at 0.75 MHz for several minutes duration at intensities as low as 9.4 W cm^{-2} (about 0.53 MPa pressure amplitude) without tube rotation or added contrast agent, and associated this effect with acoustic emissions indicative of cavitation.

Brayman *et al.* (1995) observed hemolysis with $35 \mu\text{L mL}^{-1}$ added Albunex® for burst-mode 1.1 MHz exposures [1 ms burst at 20 Hz PRF at 420 W cm^{-2} (4.5 MPa peak positive and -2.7 MPa peak negative pressure amplitudes)] in a 200 rpm rotating tube for relatively high cell concentrations, including even whole blood. The fraction of cells lysed decreased for increasing hematocrits in the range 5 to 40 percent, but the number of cells lysed was approximately constant, which is similar to the observation noted above for micro-pore-stabilized gas bodies (Miller, 1988a) except at much higher amplitudes. Brayman *et al.* (1996a) have found that hemolysis could be induced by 1 MHz pulsed ultrasound for pulses of $5 \mu\text{s}$ to 1 ms duration. Hemolysis increased for increasing pulse duration at constant intensity, or for increasing pressure amplitude at a constant pulse duration. For $5 \mu\text{s}$ pulses, the hemolysis increased dramatically above about 3 MPa peak negative pressure amplitude, but some hemolysis was observed even at amplitudes less than 1 MPa. Brayman *et al.* (1996b) analyzed the hemolysis effect by considering theoretically the process of cell-bubble encounters. The results for predicted cell lysis could be fitted to experimental data and indicated that increasing hematocrits should not limit cell lysis, which may

actually increase with increasing cell numbers, given sufficient available gas bodies.

The frequency dependence of effects related to gas-body-based contrast agents has been examined in several studies, with particular interest in comparing findings with the relationship adopted by AIUM/NEMA (1992) (see Appendix B). Such comparisons are of particular interest in judging the utility of MI for estimating thresholds for bioeffects. Brayman *et al.* (1997) examined hemolysis with $36 \mu\text{L mL}^{-1}$ Alunex[®] added to 40 percent hematocrit suspensions in the 1 to 3.4 MHz frequency range. Focused ultrasound was used in the rotating tube system with 20 and 200 μs pulses and 0.01 or 0.001 duty factors in 60 s exposures. Hemolysis was observed with or without rotation. For a given exposure amplitude above the cavitation threshold, hemolytic yield declined dramatically with increasing frequency, being proportional to the inverse third or fourth power of frequency.

For example, the ultrasonically induced hemolysis for 3 MPa decreased from about 60 percent at 1 MHz to about 0.5 percent at 3.4 MHz. In a related study, the dependence of hemolysis on pulse number and duration was examined (Brayman and Miller, 1999). Pulses of 3.6 MPa peak negative pressure at 1 MHz were delivered at 1 Hz *PRF*. Hemolysis was statistically significant for 50 or more 20 μs pulses, or one or more 200 μs , or longer, pulses. Approximately constant hemolysis was produced by exposure with different pulse numbers and durations when the total on-time was the same.

Miller *et al.* (1997) examined the hemolysis due to ultrasonic activation of Alunex[®] for relatively high cell and gas-body concentrations. The near-field ultrasound exposures were conducted with 1 mm thick disc-shaped exposure chambers which were not rotated. For 2.25 MHz exposures, the apparent threshold for the pressure amplitude (p_0) in 50 percent hematocrit, 50 percent Alunex[®] suspensions was 0.28 MPa for 1 s continuous exposure and 0.58 MPa for 100 s pulsed exposures (10 μs pulses repeated at 1 ms intervals). In these near-field exposures, p_+ and p_- are nearly equal, and are equated to p_0 . Continuous exposure durations as short as 10 ms produced about 4.5 percent hemolysis, which only increased slightly to about 5.5 percent after 100 s. At a constant 1.6 MPa, hemolysis increased with increasing gas body concentration and with decreasing cell concentration; a high ratio of gas-bodies to cells was needed for observable effects at moderate exposure amplitudes. This observation confirms and extends the results of Miller (1988a) and Brayman *et al.* (1995) in regard to the cell-density effect. Hemolysis thresholds decreased with increasing frequency in a 50/50 mixture of whole blood and Alunex[®] (about 25 percent hematocrit) with

pressure-amplitude thresholds rising from 0.12 MPa continuous (1 s) and 0.47 MPa pulsed (10 μ s on, 1 ms off for 100 s) at 1.06 MHz to 0.47 MPa continuous and 1.9 MPa pulsed at 5.3 MHz, respectively. This represents a roughly linear dependence on frequency for the apparent threshold, as shown in Figure 6.2. This may be compared to the threshold relationship adopted in ODS (AIUM/NEMA, 1992), which is based on the assumption that the threshold value of the

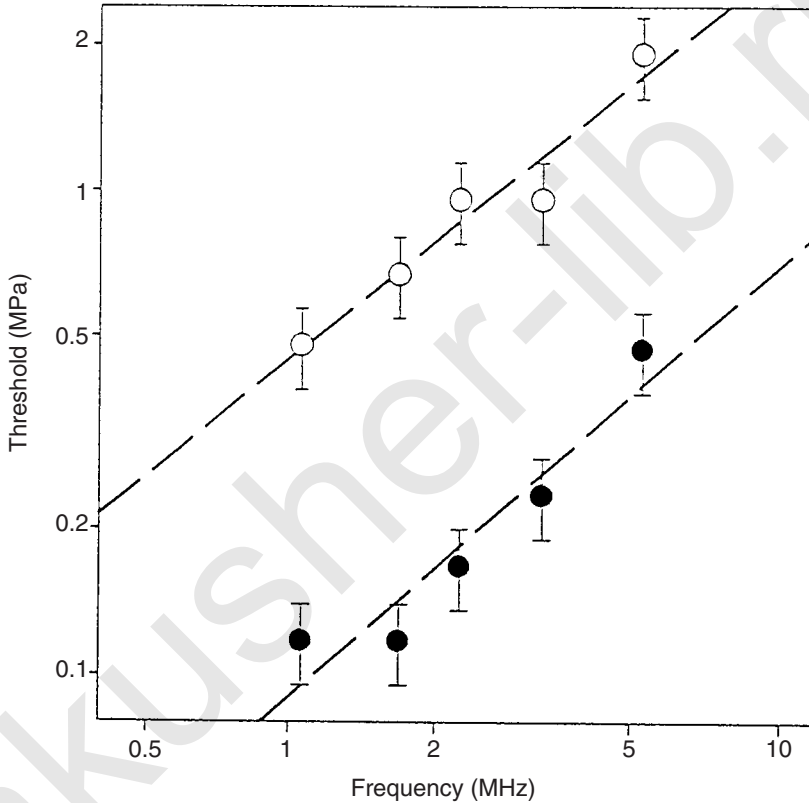


Fig. 6.2. Pressure-amplitude thresholds for hemolysis in 25 percent hematocrit suspensions with 50 percent Alunex[®] contrast agent for 1 s continuous exposure (filled circles) and for 100 s pulsed exposure with 10 μ s pulses and 1 ms pulse repetition period (open circles). The error bars extend between the lowest pressure amplitude which produced significant hemolysis and the highest pressure amplitude which did not, with the threshold plotted at the midpoint. The dashed lines were fitted by linear regression to the logarithmic data, and have slopes (frequency exponents) of 0.89 and 0.94 for the continuous and pulsed data, respectively (Miller *et al.*, 1997).

peak negative pressure is proportional to the square root of the frequency.

As described in Section 4, contrast agents for diagnostic ultrasound have been modified from simple bubbles in order to achieve greater persistence in the circulation. Miller and Gies (1998a) investigated the induction of hemolysis by four different contrast agents. Canine whole blood mixed with 50 percent concentrations of the agents was exposed in 1 mm thick chambers in the nearfield of a 2.4 MHz ultrasound beam in a 37 °C water bath. The contrast agents included Albunex® and Levovist® which are “first generation” air-based agents and the experimental agents FS069 (Optison®) and modified MRX-130 (ImaRx Pharmaceutical Corporation, Tucson, Arizona), which are “second generation” perfluorocarbon-based contrast agents. No significant ultrasonically-induced hemolysis was detected for the phosphate-buffered saline or Levovist® suspensions under the conditions tested. For 1 s continuous exposure, ultrasonically induced hemolysis was significant for Albunex® at 0.4 MPa or higher pressure amplitudes, for FS069 at 0.2 MPa and for modified MRX-130 at 0.4 MPa. Again, in these near-field exposures, $p_+ > p_-$, being nearly equal, are equated to p_0 . Hemolysis found after pulsed exposure with 10 μ s pulses and 1 ms pulse repetition period was significant for Albunex®, FS069 and modified MRX-130 above thresholds of 1.1, 0.57 and 1.6 MPa, respectively, for the pressure amplitude. Reduced concentrations of gas-bodies gave increased thresholds and reduced hemolysis. The perfluorocarbon agent FS069 led to more hemolysis after pulsed mode exposures of 1 s or longer duration than did Albunex®. This result indicates that improvements in persistence of contrast agents, which increase their clinical utility, can increase their potential for inducing cavitation bioeffects.

Bioeffects of ultrasound with contrast agents have also been investigated for cultured cells (Bao *et al.*, 1997). Cultured Chinese hamster ovary (CHO) cells in suspension with 10 percent Albunex® were exposed to 2.25 MHz ultrasound in sterile 4.5 mL rotating tubes at 37 °C. After exposure, cells were tested for lysis, sonoporation, which involves the sublethal permeabilization and resealing of cell membranes, and DNA transfer, which occurred when DNA in the suspending medium was trapped inside permeabilized cells. Sonoporation, indicated by uptake of large fluorescent dextran molecules by some cells, was observed for spatial-peak pressure amplitudes as low as 0.1 MPa. The “mean pressure amplitudes” (obtained by averaging p_+ and p_-) were specified, but the p_- were also provided (given here in parentheses where different). Significant lysis occurred for 0.2 MPa (0.18 MPa, p_-), and increased rapidly for exposures above the inertial cavitation threshold (using the H₂O₂ production test) of

about 0.4 MPa (0.18 MPa, p_-). In the DNA transfection tests, 20 $\mu\text{g mL}^{-1}$ luciferase reporter plasmid was added to the suspension during exposure, and cells were assayed for proliferation ability and for luciferase gene expression 2 d after exposure. Cell proliferation was greatly reduced above the cavitation threshold. Luciferase production was significant for 0.2 MPa (0.18 MPa, p_-) and higher exposure. The luciferase production was greater for cells exposed in medium supplemented with serum than for cells exposed in serum-free medium. Cells harvested for exposure either in the log-phase or in the stationary phase of culture gave similar proliferation and transfection results. The effects essentially disappeared when the Alunex[®] was omitted from the suspension and the tube was not rotated. The addition of stabilized gas bodies to suspensions can therefore lead to biological effects at ultrasound exposures below the threshold for inertial cavitation. Lysis and sonoporation have also been demonstrated in cervical cancer cells with 2 MHz ultrasound at 0.2 MPa in a rotating tube system (Ward *et al.*, 1999). The effect occurred either with added Alunex[®] (12 percent) or Optison[®] (6.5 percent) and the presence of a contrast agent was required for producing the effect with burst-mode ultrasound.

The work noted above on CHO cells was expanded to a range of frequencies from 1 to 7.15 MHz (Miller *et al.*, 1999). For 10 percent Alunex[®], rarefactional amplitude thresholds for sonoporation were 0.084 MPa for 1 to 3.3 MHz, and 0.27 MPa at 5.3 and 7.15 MHz. These levels were about the same as the levels needed to destabilize the gas bodies. The sonoporation effect represents membrane damage which adversely impacts the cells. Plating efficiency after sorting a flow cytometer was 19 percent for sonoporated (fluorescent) cells (0.2 MPa at 2.25 MHz), compared to 67 percent for exposed but nonsonoporated cells.

Many cells are normally grown as monolayers in culture, and this represents a quite different situation for ultrasound exposure than cells in suspension. Lysis of cultured CHO cells attached to thin mylar sheets was investigated by Miller and Bao (1998) for 3.3 MHz ultrasound exposure in the presence of five percent Alunex[®]. The ultrasound beam was directed upward at a thin exposure chamber with the monolayer on the inside of the upper acoustic window. The near-field position of the chamber minimized finite amplitude distortion of the ultrasound, so p_+ and p_- were nearly equal. Cell membrane damage was detected by measuring ATP release with the firefly enzyme assay. A receiving transducer was used to detect the subharmonic, fundamental and second-harmonic scattered signals, which were recorded on a spectrum analyzer. ATP release increased monotonically with increasing pressure amplitude above apparent

thresholds of 0.28 MPa for 1 s continuous and 0.56 MPa for 100 s pulsed (10 μ s pulses, 1 ms pulse repetition period) exposures with five percent Alburnex[®]. The subharmonic signal and, to a lesser extent, the second-harmonic signal both increased with the cell membrane damage. If the monolayer was positioned on front window of the exposure chamber, cell membrane damage was greatly reduced, which confirmed the protective influence of this configuration of monolayers previously reported in the literature (Section 7). The effect decreased both at high (50 percent) or low (0.5 percent) concentrations of Alburnex[®]. The utility of contrast agents resides in their strong nonlinear scattering of ultrasound. In addition, the scattered signals appear to indicate the level of cavitation activity and to correlate with the cellular membrane damage, at least in this *in vitro* model system.

Pulsed ultrasound interaction with Alburnex[®] can also cause erosion of cells from a monolayer (Brayman *et al.*, 1999). Fibroblast monolayers grown on a window of a stationary chamber were exposed to 20 μ s pulses at 500 Hz *PRF* in the presence of three percent Alburnex[®]. The removal of cells increased with increasing peak negative pressure, with some of the removed cells remaining viable. Thresholds were increased from 0.5 MPa at 1.02 MHz, to 1 MPa at 3.52 MHz. The effect was not strongly dependent on the position of the monolayer on the proximal or distal side of the chamber for the horizontally-oriented exposures. This *in vitro* system may simulate to some extent the potential for erosion of endothelial cells (Brayman *et al.*, 1999).

Many of the studies reviewed above have noted the induction of biological effects for research exposure systems with parameters, such as peak negative pressure amplitude, frequency, pulse duration and *PRF*, falling within the range of diagnostic ultrasound conditions. A recent study employed an actual diagnostic ultrasound machine *in vitro*, which mitigates possible uncertainty as to whether the research systems truly duplicate diagnostic parameters (Miller and Quddus, 2000a). Human (A431 epidermoid carcinoma) cells were grown as monolayers on 5 μ m thick mylar sheets, that formed one window for a 1 mm thick, 23 mm diameter disc-shaped exposure chamber. A 3.5 MHz curved linear array transducer (Acoustic Imaging model 5200B) was aimed upward at the chamber so that the beam passed vertically through the chamber. Optison[®] was present in the medium and the gas bodies were allowed to rise and rest against the cell monolayer on the inside of the upper window before exposure. Sonoporated cells (up to about 10 percent of cells in the beam) were noted for both spectral Doppler with 5 μ s pulses and 4.4 kHz *PRF* and for two-dimensional (2D) scan mode with 0.46 μ s

pulses and 27 Hz frame rate, as shown in Figure 6.3. Effects were significant relative to controls exposed without contrast agent for all the available power levels with or without a tissue-mimicking phantom. The effect was only weakly dependent on pulse duration, *PRF* or exposure duration, but was strongly dependent on contrast agent concentration below two percent. This result demonstrates that diagnostic ultrasound activation of contrast agent gas bodies using actual diagnostic ultrasound exposure parameters can produce cell membrane damage. The lowest value of the pressure amplitude for which significant sonoporation was produced was 0.23 MPa. At the frequency of 4 MHz, this is about 15 times smaller than the maximum allowed in the United States [by $MI = 1.9$ limit in ODS

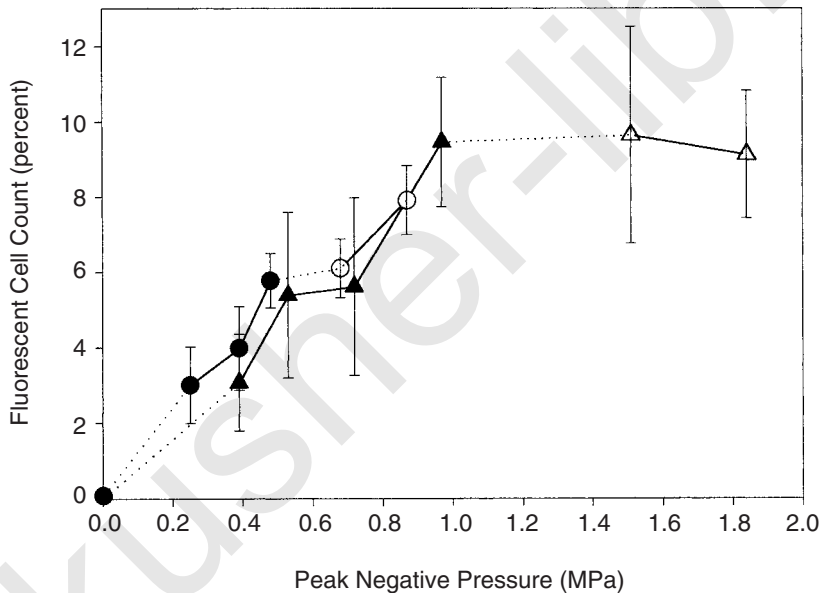


Fig. 6.3. The percentage of monolayer cells within a microscopic field of view that exhibited fluorescence due to sonoporation. Exposure was from a 3.5 MHz diagnostic ultrasound scanner in Doppler (circles) or 2D scan (triangles) modes, in the presence of one percent Optison® ultrasound contrast agent. Exposures were 1 min duration with a water path (open symbols) or with a tissue mimicking phantom (filled symbols) in the beam path having an attenuation of about $0.3 \text{ dB cm}^{-1} \text{ MHz}^{-1}$. The data under the different conditions are joined by dotted lines to indicate extrapolation of complete curves. All exposures produced a statistically significant effect relative to sham exposure or to exposure without added gas bodies (Miller and Qudus, 2000a).

(AIUM/NEMA, 1992); see Appendix B] for the estimated *in situ* value of the peak negative pressure.

6.3 Tissues with Internal Gas Bodies

6.3.1 Plants

Research on plant tissues has yielded an important fraction of our knowledge of the bioeffects of GBA for megahertz frequency ultrasound. In excess of 100 research reports exist in the literature on botanical effects of ultrasound and include a wide range of observations and potential applications. This topic has been reviewed previously (Miller, 1983a; NCRP, 1983), and will be only briefly reviewed in this Section with emphasis on mechanistic studies and studies reported since 1980.

Microscopical observations of mechanical (*i.e.*, nonthermal) activity in *Elodea* leaves exposed to ultrasound extend back to the earliest studies by Harvey and Loomis (1928). Pfirsch (1958) recognized that the vulnerability of *Elodea* to ultrasound was related to the intercellular gas channels in the leaves. Gershoy *et al.* (1976) also recognized this phenomenon and noted that it appears to pertain to many plant tissues, such as root tips used for studies of the effect of ultrasound on root growth rates. Studies of leaves and roots have been of particular interest due to the exceptional sensitivity of these gas-body-containing tissues to medically-relevant pulsing regimes (Child *et al.*, 1975; Miller, 1977b). As noted in Section 4, the linear resonance frequencies of the gas-filled channels in *Elodea* leaves may be estimated theoretically for the range of sizes of channels in the leaves (Miller, 1979b). This theoretically predicted resonance behavior is evident in the variation of the cell death threshold with frequency in the 0.45 to 10 MHz frequency range for each of several regions of the leaves with different sizes of channels (Miller, 1979a).

Although *Elodea* leaves have been convenient for mechanistic studies, other plant tissues also contain intercellular gas-filled channels and are therefore subject to similar phenomena. Plant roots are a particularly important subject for bioeffects studies related to GBA because the rapidly growing root tips have a rich biology which potentially can be affected in many ways. The nonthermal, cavitation-related nature of effects of ultrasound on plant roots has been noted by Carstensen *et al.* (1979), Gershoy *et al.* (1976), Graham *et al.* (1980), Leeman and Harrison (1982), and Morris and Coakley (1980).

Elodea leaves have regular arrays of cells and gas-filled intracellular channels which allow detailed study of the cell death effect. Focused 5.25 MHz ultrasound aimed at the area between the midrib and edge of leaves produced effects above about 0.35 W cm^{-2} spatial peak intensity (about 0.1 MPa) continuous (Miller, 1983b). The cells near activated channels showed two types of progressive degradation for higher intensities: (1) the breakage of the vacuolar membrane and detachment of organelles (e.g., chloroplasts which could then be centrifuged to the ends of the cells), and (2) the breakage of the plasma membrane (shown by uptake of stain). A photomicrograph of a leaf with damage localized in the focal spot is shown in Figure 6.4. Both types of damage were apparently lethal, since Type 1 damaged cells took up the vital stain within an hour. The membrane damage observed in *Elodea* appears to result from shear stress associated with microstreaming flow near the ultrasonically activated gas-filled intercellular channels (Miller, 1985a), as discussed in Section 6.3.2.

Carstensen *et al.* (1990b) reported observations of effects in *Elodea* leaves, which tend to confirm the gas-channel resonance hypothesis

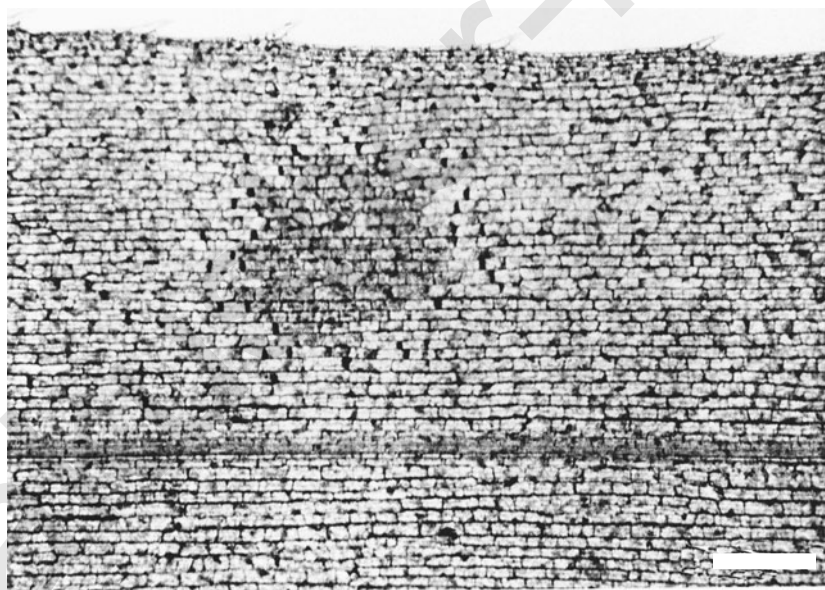


Fig. 6.4. An *Elodea* leaf exposed to 5.25 MHz focused continuous ultrasound for 100 s at a spatial peak intensity of 2 W cm^{-2} ($\sim 0.24 \text{ MPa}$) and then simultaneously stained and centrifuged at 500 g. The dark circular region contains cells stained by a vital stain, while a band of cells around this region have organelles displaced to the centrifugal end of the cells. The bar indicates $500 \mu\text{m}$ (Miller, 1983b).

for continuous exposures. Very short pulses, 3 or 5 μs in duration, seemed to produce a flatter frequency response behavior than CW exposure for 1, 2.5 and 3.8 MHz ultrasound. It was suggested that the short pulses, with high pulse-average intensities relative to the temporal average intensity, might represent a qualitatively different phenomenon (from low-intensity resonance-related effects) (Carstensen *et al.*, 1990b). In particular, the decreasing probability of lysis appeared to level off and to remain approximately constant for progressively lower pulse repetition frequencies (as low as 100 Hz) for 3 μs pulses of 2.5 MHz ultrasound.

Cell death in *Elodea* from pulsed ultrasound in the range 0.745 to 15 MHz followed a frequency dependence roughly similar to that previously observed for continuous exposure (Miller and Thomas, 1993c). However, thresholds were higher for the pulsed modes: for example, the threshold for cell death was 166 W cm^{-2} spatial-peak pulse-average (SPPA) ($\sim 2.2 \text{ MPa}$ pressure amplitude) for 1 μs pulses and 1 kHz *PRF* of 6 MHz ultrasound for 60 s compared to 12 W cm^{-2} ($\sim 0.6 \text{ MPa}$ pressure amplitude) for 60 ms continuous exposure (*i.e.*, the same total on-time). The threshold gradually increased for progressively lower *PRF* down to 10 Hz. The results were compared to linear theoretical analysis, which appeared to be appropriate for use up to about 10 MPa, and to estimates of the shear-stress thresholds for membrane damage (Section 6.4.2). Theory and observation indicated that the minimum cell death threshold intensity (corresponding to the most active channels on a leaf) was proportional to the frequency in the 0.745 to 15 MHz range. This trend is shown in Figure 6.5. Specifically, the cell death thresholds expressed in terms of pressure amplitude had a constant value of the quantity $pf^{-1/2}$ of about $0.95 \text{ MPa MHz}^{-1/2}$ for 3 μs pulses with 0.2 to 2 kHz *PRF* and 60 ms total on-time (Miller and Thomas, 1993c).

6.3.2 *Insects*

In early studies using therapeutic ultrasound exposure of insect tissues, Fritz-Niggli and Boni (1950), Lotmar (1952), and Selman and Counce (1953) reported bioeffects such as the death of eggs and larvae, delayed death and abnormal development. Subsequent investigations demonstrated that the abnormalities were not due to mutations, but confirmed the remarkable sensitivity of insect tissues to ultrasound (NCRP, 1983). This sensitivity has been associated with the presence of gas-filled channels in insect larvae, which conceptually links them to GBA phenomena in plant tissues. This review will concentrate on mechanistic studies and reports appearing after

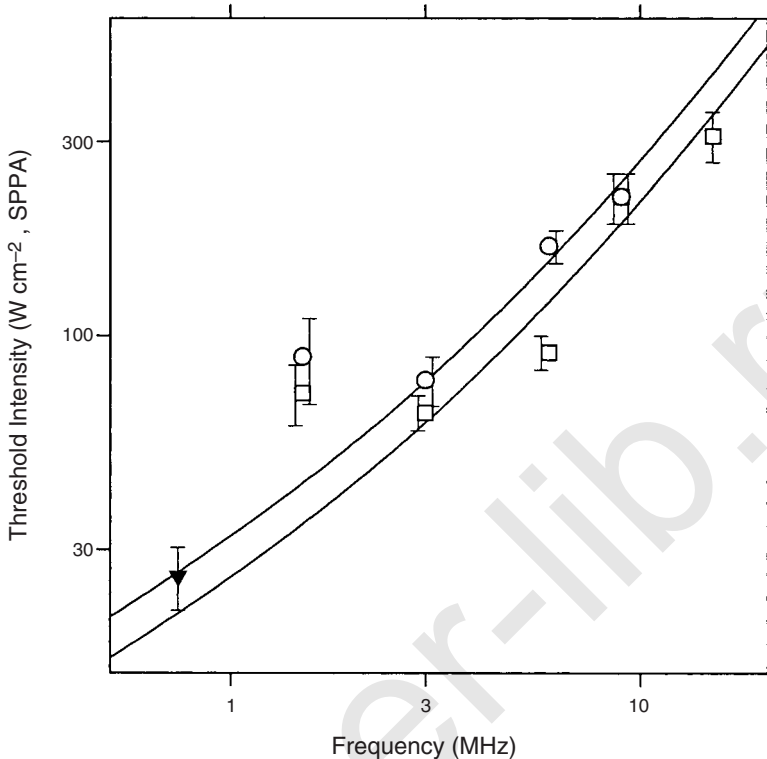


Fig. 6.5. Frequency dependence of the minimal cell death intensity thresholds in *Elodea* leaves for pulsed mode exposures. Data are for 5.9 μ s pulses and 1 kHz *PRF* for 10 s at 0.745 MHz (triangles), and 3 μ s pulses and 2 kHz *PRF* for 10 s (circles), or 200 Hz *PRF* for 100 s (squares) at 1.5, 3, 6, 9, 15 MHz. The lines are theoretical curves of relative intensity calculated for constant shear stress and fitted to the data (upper and lower curves are for circles and squares, respectively) (Miller and Thomas, 1993c).

about 1980, which were not included in NCRP Report No. 74 (NCRP, 1983).

As for plant tissues, insect tissue gas bodies provide a fertile subject for the study of effects of pulsed ultrasound. Pizzarello *et al.* (1978) and Child *et al.* (1981) showed that *Drosophila* larvae are quite sensitive to pulsed ultrasound. For example, larvae were killed by 2.5 min exposure to 2.4 MHz ultrasound with 1 μ s pulses and 50 Hz to 5 kHz *PRF* at SPPA intensities above 10 $W\ cm^{-2}$ (Child *et al.*, 1981). Berg *et al.* (1983) used 1 μ s pulses with 1 kHz *PRF* to explore the sensitivity of larvae to megahertz frequencies (described below). The maximal intensity during a pulse appears to be a better

indicator for judging the effectiveness of pulsed exposure than is pulse-average intensity (Carstensen *et al.*, 1983c). SPPA intensity is a better indicator than temporal average intensity, which has no predictive value for killing of larvae (Child *et al.*, 1981; Pay and Barrick, 1987). Insect tissue is therefore significantly affected by low intensity ultrasound at medically relevant frequencies and pulsing regimes.

Effects on insect tissues have long been thought to be nonthermal in origin. Selman and Counce (1953) microscopically observed vigorous stirring motions in *Drosophila* eggs during exposure to 1 MHz ultrasound. Child *et al.* (1980) conclusively demonstrated the nonthermal nature of effects on eggs. The frequency dependence of effects on eggs observed by Hayes *et al.* (1983) at 43, 123 and 447 kHz supports the nonthermal hypothesis because the eggs were more sensitive to the lower frequencies. Many insect tissues contain specialized gas-filled channels for respiration, and these appear to mediate the nonthermal effects. Child and Carstensen (1982) found that the exceptional sensitivity of *Drosophila* eggs to 2.25 MHz ultrasound with 1 μ s pulses and 500 Hz PRF develops just before hatching when the respiratory system fills with air, as shown in Figure 6.6. The *Drosophila* eggs contain up to four percent of gas by volume, and the microscopically observable streaming motions associated with the gas during exposure are like those seen in *Elodea* (Carstensen *et al.*, 1983a). Therefore, the interaction of ultrasound with insect tissues which leads to observed bioeffects is classified as a form of GBA.

The threshold for killing larvae has a minimum at about 300 kHz, which is the approximate resonance frequency expected of a cylindrical gas channel of 4 μ m radius (Child *et al.*, 1992). This observation indicates that studies using frequencies in the diagnostic range actually expose the channels in *Drosophila* larvae well above their resonance frequencies. Berg *et al.* (1983) examined the frequency dependence of the killing of *Drosophila* larvae by ultrasound in the medically relevant range, specifically, 2.2, 5.6 and 9.6 MHz. The 2.5 min exposures utilized 1 μ s pulses with a 1 kHz repetition frequency. The relative survival of the larvae increased markedly with frequency at a constant intensity; for example, at 40 W cm⁻² spatial-average temporal-peak (SATP) intensity, survival was zero at 2.2 MHz, about 20 percent at 5.6 MHz and nearly 100 percent at 9.6 MHz.

Phenomena related to those in plant and insect tissues appear to occur in lung as a result of pulsed ultrasound or lithotripter shock-wave exposures; this topic is discussed with other mammalian effects in Section 8. Threshold levels similar to those for adult murine lung

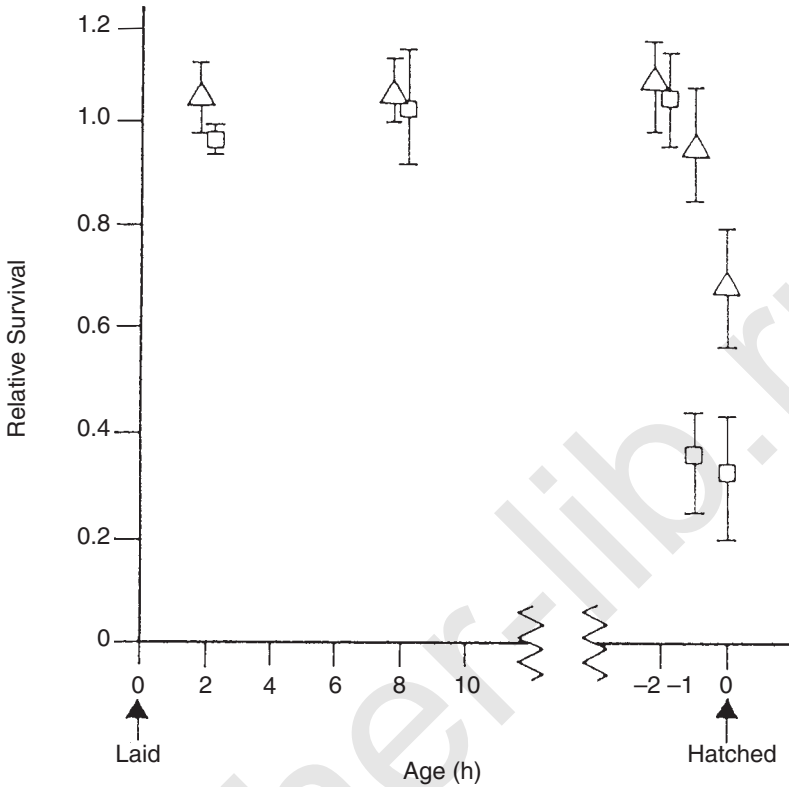


Fig. 6.6. Survival of *Drosophila* eggs after exposure to pulsed ultrasound. The 2.25 MHz ultrasound was delivered as 1 μ s pulses and 500 Hz PRF at 40 W cm⁻² SATP (triangles) or 10 W cm⁻² SATP (squares) (Child and Carstensen, 1982).

have been found for the killing of larvae of the fruit fly, *Drosophila melanogaster* (Carstensen *et al.*, 1990c). It may be accepted that this comparatively simple biological material provides a model with properties that, from the point of view of bubble-ultrasound interaction, are qualitatively similar to those of mammalian lung. Larvae contain small gas bodies stabilized within their respiratory systems (Carstensen *et al.*, 1983a). These bubbles are inhibited in their capacity to expand by the surrounding tissues (Carstensen *et al.*, 1990c). Furthermore, because of metabolic activity, the gas is enriched with CO₂. Approximately one-half of a population of *Drosophila* larvae is killed by exposure to 3 to 10 lithotripter shocks having a compressional pressure of 2 to 3 MPa. In contrast with the predictions of classical theory for inertial cavitation, adding a rarefactional phase

to the exposure has little influence on the killing rate or its threshold pressure (Bailey *et al.*, 1996; Carstensen *et al.*, 1990c).

6.4 Biophysical Analysis of Effects

6.4.1 Shear-Stress Hypothesis

The lethal cellular effect that has been associated with GBA results from membrane damage (rather than, for example, DNA damage). The mechanism responsible for this damage seems to be hydrodynamic shear stress applied to cells caught up in microstreaming flow near vibrating surfaces, as first suggested by Hughes and Nyborg (1962). This idea was developed into a quantitative hypothesis by Rooney (1970; 1972) and by Williams *et al.* (1970) in applications to wires and bubbles vibrating at 20 kHz. This topic has been reviewed by NCRP (1983) and Williams (1983); in the present Section, recent developments pertinent to megahertz-frequency ultrasound are emphasized. Shear stress can produce a variety of damage to mammalian cells, such as induction of stress proteins and platelet aggregation (McIntire and Rajagopalan, 1993), but cell lysis has been emphasized in studies involving ultrasonic cavitation.

Information on the shear stress required for cell lysis comes from a variety of different types of hydrodynamic flow (Miller, 1987; Rooney, 1973). Among other factors, the threshold shear stress for hemolysis depends on the duration of the shear. For steady, uniform shear, the threshold has been measured to be about 42 Pa for 10 min at 20 °C (Williams, 1973a). For shear lasting an estimated 30 μ s in a jet of liquid, the threshold is about 6 kPa (Bernstein *et al.*, 1967). Other thresholds for intermediate times are listed in Table 6.1, and these data are plotted in Figure 6.7 to show the weak dependence of the threshold on duration of shear. In regard to cavitation and GBA, it should be noted that for a cell caught up in microstreaming flow, the duration of high shear is limited to the short time the cell is in the boundary layer; for example, Rooney (1970) calculated a threshold of 450 Pa in 1.3 ms for hemolysis near a bubble oscillating at 20 kHz. The shear-stress threshold is different for different cells; for example, the threshold for 5 min of shear is about 10 Pa for platelets compared to about 60 Pa for red cells (see Table 6.1). Thresholds of mechanical hemolysis, for example in liquid jets, also depend on the size of the red cells, and is higher for the small blood cells of goats and sheep than for the larger blood cells of human beings (Blackshear and Blackshear, 1987). The threshold also varies with

TABLE 6.1—Shear-stress thresholds for lysis of red blood cells.^a

Method ^b	Duration (s)	Threshold (Pa)	Point Number ^c	Source
Viscometer	60, 300, 600	86, 59, 42	1, 2, 3	Williams (1973a)
Viscometer	100	150	4	Leverett <i>et al.</i> (1972)
Viscometer	300	10	5	Brown <i>et al.</i> (1975)
Capillary	0.02	500	6	Bacher and Williams (1970)
Bubble	0.0013	450	7	Rooney (1970)
Wire	0.0005	560	8	Williams <i>et al.</i> (1970)
Capillary	0.00045	3,000	9	Coakley <i>et al.</i> (1977)
Jet flow	0.00005	6,000	10	Bernstein <i>et al.</i> (1967)

^aExcept for Brown *et al.* (1975) who used platelets.

^bDifferent methods used by different authors provide a range of stress-duration values (estimate from data provided in the source).

^cThe data are plotted in Figure 6.7 with each point assigned a number as listed in this column.

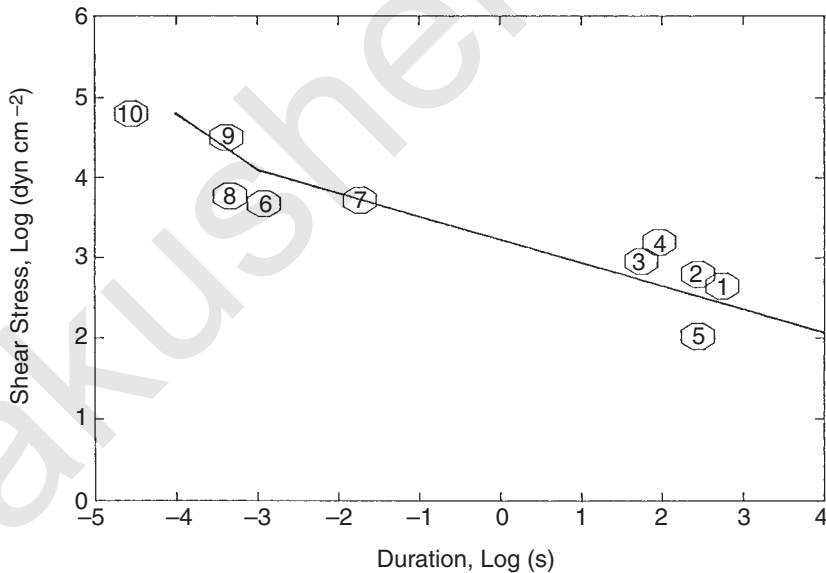


Fig. 6.7. Shear-stress threshold values for cell lysis as a function of the duration of stress. The solid line represents theoretical estimates of shear stress using data from *Elodea* leaves exposed to 1 MHz ultrasound and the numbered points are from the studies listed in Table 6.1 (Miller, 1985a).

temperature; thresholds for 5 min of shear are about 60 Pa at 20 °C and about 30 Pa at 45 °C, above which the threshold rapidly falls to zero at about 49 °C (Krizan and Williams, 1973).

6.4.2 Applications of the Shear-Stress Hypothesis

The hypothesis that membrane damage from noninertial cavitation and GBA results from microstreaming shear stress can be applied to many different experimental situations. In this way, the etiology of the bioeffects can be examined with regard to mechanisms and dosimetry. In practice, this research strategy can be quite difficult to realize, however, and only a few semi-quantitative examples exist.

Theoretically, noninertial cavitation could produce cell damage by microstreaming shear stress at very low levels of exposure. The physics of this phenomenon is presented in Section 4.4.4. By extrapolation from observations at 20 kHz, Nyborg (1977) speculated that a 3 μm bubble resting on a surface and exposed to 1 MHz ultrasound might cause membrane damage at an intensity of only 0.5 mW cm^{-2} (~ 0.004 MPa in a CW field).

For *in vitro* experiments with suspended cells, microstreaming shear is thought to be the cause of cell lysis during GBA. Erythrocytes may be observed to collect at ultrasonically activated gas-filled micropores and participate in the microstreaming flow near the micropores (Nyborg and Miller, 1982a; 1982b). However, the flow patterns near the micropores do not appear to follow the model of the interaction of cells with the microstreaming boundary layer developed for lower frequencies (Miller, 1988b). For 1 μm diameter polystyrene spheres as indicator particles, entire microstreaming eddies were shown to be equal to, or smaller in size than an erythrocyte for frequencies in the range 0.7 to 3.5 MHz and micropores 2.5 to 4 μm in diameter.

A shear-stress model for cell death has been developed for ultrasonic activation of the gas-filled intercellular channels in *Elodea* leaves. The oscillation of the gas-channel walls (presumably including the cellulose wall and plasma membrane) generates acoustic microstreaming within the cells, which is readily seen by microscopical observation during exposure (Gershoy *et al.*, 1976). The thresholds for cell death are related to the hydrodynamic shear stresses generated within the cells. The intracellular flow velocities and the shear stresses can be estimated by theory (outlined in Section 4.4.5) for acoustic microstreaming (Miller, 1985a). Since the flow and stress occur inside the cells (rather than in brief periodic encounters of cells with the boundary layer as in the low-frequency model), the

duration of shear equals the exposure duration. The shear-stress thresholds estimated for *Elodea* are in rough agreement with shear-stress thresholds for cell-membrane breakage found for other ultrasonic and hydrodynamic situations, and are plotted as the straight line in Figure 6.7.

Thresholds for cell death in *Elodea* were measured for frequencies in the range 0.745 to 15 MHz, and theoretical calculations of the shear stress were also made over the range 0.5 to 20 MHz (Miller and Thomas, 1993c). For a model in which acoustical interaction of the channels is ignored, the channels in a typical leaf act independently and have a range of resonance frequencies. The cell death threshold is then associated with the channel which is resonant (or most nearly so) at the specific frequency. The relative intensity required for constant shear stress is plotted as a function of resonance frequency in Figure 6.5 as the two lines, which were fitted to the data points for cell death thresholds at 3, 6 and 9 MHz for a *PRF* of 200 Hz and 2 kHz. The 1.5 MHz data do not fit these lines, and it may be that no channels were resonant at this frequency. The thresholds at 0.745 and 15 MHz, which presumably involve the different populations of cells near the large channel at the midrib (0.745 MHz) and the smaller channels near the edge (15 MHz), do fall near these lines. Therefore, the theory and experimental observation of the cell death thresholds at resonance follow similar trends, which lends support to the shear-stress hypothesis.

These intensity thresholds for cell death increase roughly in proportion to frequency (*i.e.*, If^{-1} is constant), see Figure 6.5, and this roughly linear relation can be calculated from the theory for microstreaming shear stress in the *Elodea* leaf cells (Miller and Thomas, 1993c). This frequency dependence of threshold intensities, if expressed in terms of pressure amplitude, is similar to the frequency dependence of MI (that is, $pf^{-1/2}$ is constant) which has been adopted for display on diagnostic ultrasound instruments for characterizing clinical exposures (AIUM/NEMA, 1992) in the United States. As stated in Section 6.3.1, the pressure relation corresponding to *Elodea* cell death thresholds for 3 μ s pulses, 0.2 to 2 kHz *PRF* and 60 ms total on-time is approximately $pf^{-1/2} = 0.95 \text{ MPa MHz}^{-1/2}$. The pulse duration, *PRF* and exposure duration selections were chosen to be in the medically relevant range. The index value would change depending on the specific choices for all these factors. For example, results for CW exposures (Miller, 1979a) would have a much smaller value for the constant. Specifically, the threshold for 100 s exposures at 5.25 MHz was 0.18 W cm^{-2} , which implies $pf^{-1/2} = 0.03 \text{ MPa MHz}^{-1/2}$. The possibility of using the same frequency dependence for describing the bioeffects potential of widely different exposure

situations would be an important simplification of the overall safety problem, if this were to be established in more medically relevant situations.

6.4.3 Other Mechanisms

Other physical mechanisms of action are undoubtedly operative during GBA. There may be localized heating with elevated temperatures, particularly if many gas bodies are present. Both plant roots (Eames *et al.*, 1975) and fruit-fly eggs (Carstensen *et al.*, 1983a) have larger absorption coefficients than soft mammalian tissues with a corresponding potential for heating. In addition, radiation forces on small particles and radiation torque on cells or small particles near ultrasonically activated gas bodies may also be important in the etiology of some bioeffects (Nyborg, 1978). However, the reported bioeffects appear to be primarily the result of shear stress-induced membrane damage.

6.5 Summary

Research on ultrasonic activation of stable bodies of gas *in vitro* and *in vivo* has generated basic information on potential bioeffects. The primary experimental subjects are gas-filled micropores and contrast agent gas-bodies *in vitro*, and gas-filled channels in plants and insects *in vivo*. In many cases, the physical oscillation of the gas bodies can be described theoretically (Section 4), which is a critical step in generalization beyond the immediate experiment. Biophysical analysis has yielded an understanding of some pertinent mechanisms, including radiation forces and acoustic microstreaming. The predominant effect of cell death appears to result from membrane rupture in regions of high hydrodynamic shear stress. However, other mechanisms may be involved in, for example, insect tissue.

The recent emergence of gas-body based contrast agents for diagnostic ultrasound has been of special interest for nonthermal bioeffects research. These agents can introduce a potential for nonthermal bioeffects of ultrasound into situations, such as sterile culture media or blood samples, for which cavitation phenomena are normally absent, due to the lack of cavitation nuclei. Reports of research concerning the potential of these agents to mediate bioeffects of diagnostic ultrasound are beginning to appear in the literature. Observed effects appear to be related to destabilization of contrast-agent gas bodies and can be enhanced by improvements in the agents

which enhance, for example, persistence between pulses. The effects also appear to be correlated to some extent with acoustic emissions from the gas bodies, such as the second harmonic or subharmonic, which suggests a possible correlation of bioeffects potential with contrast-associated features in images formed from received emissions. The microscale effects would likely be clinically subtle, and their medical significance remains to be determined. As information accumulates, the possibilities for bioeffects, such as hemolysis, sonoporation, lysis and erosion of monolayers, can be related to potential clinical risks and weighed against the clinical benefits contrast agents provide to the diagnostic process.

The knowledge gained from research on GBA in plant and insect tissue, though basic in nature, has a strong relevance to the problem of defining the potential for bioeffects of medical ultrasound. Many effects are readily produced by pulsed ultrasound, even with short pulses and low duty cycles characteristic of diagnostic applications. The frequencies of maximum oscillation for some gas bodies are near or within the range of medically relevant frequencies. The frequency dependence of most observed effects of GBA in tissue are similar, with threshold intensities roughly proportional to frequency (pressure amplitudes roughly proportional to the square root of frequency). This frequency dependence and some selected thresholds are summarized in Figure 8.1. Mammalian lung appears to represent a situation related to the plant and insect subjects discussed in this Section, and thus might be expected to exemplify GBA in human beings. Research on lung has supported the expectation of low amplitudes for effects of pulsed ultrasound (Section 8), and data for lung are also summarized in Figure 8.1.

7. Bioeffects of Inertial Cavitation *In Vitro*

7.1 Introduction

Sections 6 and 7 deal with the action of acoustically activated bubbles on biological systems, with Section 6 also including but not limited to certain bioeffects *in vitro*. In general, the acoustic pressure amplitudes used to study GBA bioeffects (Section 6) are substantially less than those used to study inertial cavitation bioeffects *in vitro* (Section 7). For the former, the stabilized gas body is not destroyed but is subjected to acoustic conditions which cause it to oscillate, sometimes continuously for a substantial number of cycles. The bubble oscillations cause physical processes, *e.g.*, microstreaming currents in the medium surrounding the bubble, which can cause bioeffects. For the latter, bubbles are violently activated, with concomitant generation of potentially biologically effective physical (*e.g.*, shear forces, photonic emissions) and chemical (*e.g.*, sonochemicals) insults. Theory has shown that inertial cavitation is to be expected from pulsed ultrasound (Flynn and Church, 1988) (see Section 5). The literature on the subject of inertial cavitation-induced bioeffects *in vitro* is analyzed in this Section to learn as much as possible about the details of the interaction of these violent cavitation events with cells in suspension. The recent availability of ultrasound contrast agents has provided sources of well characterized bubble populations, stabilized by a variety of proprietary methods, which are useful in the study of inertial cavitation. Bioeffects studies involving the use of contrast agents are analyzed here as well as in Sections 6 and 9.

7.1.1 *Advantages and Disadvantages of Studies Using Cells In Vitro*

Cell suspensions have been used in many studies of the basic mechanisms of action of ultrasound on cells and their components. *In vitro* cell systems offer the investigator many advantages, including considerable control of environmental, biological and exposure

parameters. For instance, an investigator can choose to use cells of known genetic origin and defined cell suspension density, contained in a chosen medium with a specified and readily measured amount of gas in solution. With the development of pulse-echo contrast agents, which presently consist of populations of stabilized microbubbles, it is also possible to have some control over the extent of gas nucleation of the medium, *i.e.*, over the extent to which the medium contains cavitation nuclei (Section 4.2.1). Exposure conditions and experimental logistics are generally much simpler than those for animal studies. Additionally, cells *in vitro* can be exposed to a carefully determined level of ultrasound under conditions which minimize thermal complications and enhance specific nonthermal mechanisms of action of ultrasound. Compared with *in vivo* exposures involving high ultrasound absorption, it is easy to avoid heating of cell suspensions, allowing specific studies of nonthermal mechanisms of action. Finally, the experimental control afforded by *in vitro* systems can provide exceptional levels of sensitivity, essentially down to single cell effects, which may not be achieved *in vivo*.

There are several limitations of the use of cells *in vitro* for dealing with questions that relate to safety of medical ultrasound. Firstly, the nonthermal mechanisms of action may be different in cell suspensions from those which occur in tissues and organs where little fluid generally exists in the spaces between and among cells. For example, in cell suspensions, bubbles may undergo growth to many times their original sizes (Sections 4 and 5), whereas growth of gas-filled cavities (spaces, bodies, etc.) in tissues may be restricted by tissue architectural features. Secondly, the gas content of, and nucleation processes in, cell suspension media may be very different from those occurring in the fluids surrounding cells of tissues and organs *in vivo*. Thirdly, while *in vitro* systems provide possibilities for detailed investigation of bubble-related activities at the cellular level, the results may be tied to specific exposure systems and protocols, with the possibility of reduced relevance to cellular events *in vivo*. Multicellular aggregates of cells *in vitro* (Section 7.2.3.2.4.) may provide results having more direct relevance to questions of health and safety, but spheroids are often more difficult to study than suspensions of single cells and offer less precision for studying events at the cellular level. Most importantly, cavitation is generally more likely to occur *in vitro* than *in vivo*, except in tissues containing gas bodies.

The importance of studies using cells *in vitro* lies in the opportunity to study basic mechanisms of action. Models for describing the cavitation-related, nonthermal impact of ultrasound on cells must be developed to understand the observed bioeffects and to allow application

of insights to the medical safety question. All present models of effects *in vitro* assume that bubbles and cavitation are involved, except for certain systems, wherein steps were taken to avoid cavitation or to rule it out as a significant factor (Section 3). The models need to account for two basic processes. The first process concerns the mechanism by which cells and acoustically activated bubbles are brought close enough together to permit their interaction. The second process concerns the physical action by which the bubbles, in the vicinity of the cells, produce an effect on the cells. Moreover, the models need to take into account the nucleation and growth of bubbles, the production of large bubble populations from a few nuclei, the translation of bubbles through the medium such that they are brought into association with cells, and the mechanism by which the bubble-cell interaction leads to effects. Current models are limited, and it is likely that a combination of features presented in the various current models may be needed to account for the observed effects.

7.1.2 Exposure Systems

A variety of systems for exposing cells *in vitro* to ultrasonic fields has been reported (see Figure 7.1 for graphic illustrations and Table 7.1 for respective references). Generally, the cell suspensions are in closed containers (vessels) of various types (Figure 7.1; No. 2 to 15), but, in one scheme, the rotifers and amoebae were placed directly on the transducer (Figure 7.1; No. 1), and in another the exposure vessel was not mentioned (hence, the question mark for No. 13 in Figure 7.1). Ordinarily, at frequencies in the megahertz range, the sound sources are piezoelectric elements in the shape of discs which generate beams whose lateral dimensions are large compared to the acoustic wavelengths, except in the focal regions of focused beams. At lower ultrasonic frequencies, the studies are sometimes performed with sources in the shape of needles or wires (Figure 7.1; No. 12) whose lateral dimensions are small compared to the wavelength. In general, the exposure of a subject suspension is far from uniform, because the acoustic fields are nonuniform and smaller than the exposure chamber dimensions (to avoid interaction with chamber walls). Thus, it is exceedingly difficult to define a clear response in relation to any single exposure parameter (in contrast to defined dosages in ionizing radiation research).

In experiments with cell systems *in vitro*, the vessel containing the experimental material can have a marked influence on the character of the ultrasound exposure. A plastic test tube, oriented relative

"EXPOSURE" SYSTEMS

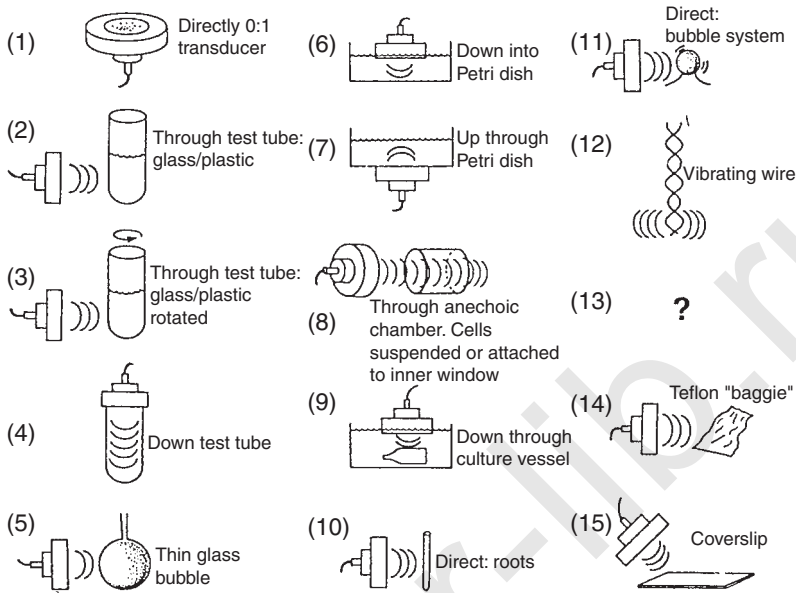


Fig. 7.1. Some systems (No. 1 to 15) used for ultrasound exposure of cells *in vitro* (see Table 7.1 for references to use for each system).

to the sound field as illustrated in Figure 7.1, No. 2, will generally result in a standing wave field within the tube because of the difference in the acoustic impedance of the vessel walls and the vessel contents and exterior medium. Air/water interfaces yield nearly perfect reflection of any incident ultrasound field, such that a Petri dish placed directly on an ultrasound transducer will establish within the fluid contents a nearly perfect standing wave in which the pressure amplitude is nearly zero at its minima. A very thin "flexible" plastic film, such as dialysis tubing, will have a minimal effect on the incident ultrasound field in the low megahertz frequency range. The vessel walls may contain cracks and/or surface irregularities which may also contribute cavitation nuclei (Brayman and Miller, 1993; Carstensen *et al.*, 1993; Williams, 1982; Williams and Miller, 1989) which subsequently affect cells. Tube rotation during insonation may enhance the effect of ultrasound on the cells by preventing cell accumulation at positions where there is little cavitation activity (Church and Miller, 1983; Church *et al.*, 1982), by recycling bubbles into the medium (Williams and Miller, 1989), and by increasing fluid nucleation (Brayman and Miller, 1994; Carstensen *et al.*, 1993;

TABLE 7.1—References to illustrate the use of various exposure systems shown in Figure 7.1.

Exposure System (No.)	Reference
1.	Hawley, S.A. and Dunn, F. (1964). "UHF acoustic interaction with biological media," <i>Naturwissenschaften</i> 51 , 555–556.
2.	Conger, A.D., Ziskin, M.C. and Wittels, H. (1981). "Ultrasonic effects on mammalian multicellular tumor spheroids," <i>J. Clin. Ultrasound</i> 9 , 167–174.
	Clarke, P.R. and Hill, C.R. (1970). "Physical and chemical aspects of ultrasonic disruption of cells," <i>J. Acoust. Soc. Am.</i> 47 , 649–653.
3.	Clarke, P.R. and Hill, C.R. (1970). "Physical and chemical aspects of ultrasonic disruption of cells," <i>J. Acoust. Soc. Am.</i> 47 , 649–653.
	Kaufman, G.E. and Miller, M.W. (1978). "Growth retardation in Chinese hamster V-79 cells exposed to 1 MHz ultrasound," <i>Ultrasound Med. Biol.</i> 4 , 139–144.
4.	Liebeskind, D., Bases, R., Mendez, F., Elequin, F. and Koenigsberg, M. (1979a). "Sister chromatid exchanges in human lymphocytes after exposure to diagnostic ultrasound," <i>Science</i> 205 , 1273–1275.
5.	Harvey, W., Dyson, M., Pond, J.B. and Graham, R. (1975). "The <i>in vitro</i> stimulation of protein synthesis in human fibroblasts by therapeutic levels of ultrasound," pages 10 to 21 in <i>Proceedings of the Second European Congress Ultrasonics in Medicine</i> , Kazner, E., de Vlieger, M., Muller, H.R. and McCready, V.R., Eds., International Congress Series No. 363 (Excerpta Medica, Amsterdam).
6.	Loch, E.G., Fischer, A.B. and Kuwert, E. (1971). "Effect of diagnostic and therapeutic intensities of ultrasonics on normal and malignant human cells <i>in vitro</i> ," <i>Am. J. Obstet. Gynecol.</i> 110 , 457–460.
7.	Martins, B.I., Raju, M.R., Hayes, T.L. and Tobias, C.A. (1977). "Survival of cultured mammalian cells exposed to ultrasound," <i>Radiat. Environ. Biophys.</i> 14 , 243–250.
8.	Armour, E.P. and Corry, P.M. (1982). "Cytotoxic effects of ultrasound <i>in vitro</i> dependence on gas content, frequency, radical scavengers, and attachment," <i>Radiat. Res.</i> 89 , 369–380.

TABLE 7.1—References to illustrate the use of various exposure systems shown in Figure 7.1. (continued)

Exposure System (No.)	Reference
9.	Morton, K.I., ter Haar, G.R., Stratford, I.J. and Hill, C.R. (1982). "The role of cavitation in the interaction of ultrasound with V79 Chinese hamster cells <i>in vitro</i> ," Br. J. Cancer (Suppl.), 45 , 147–150.
10.	Gregory, W.D., Miller, M.W., Carstensen, E.L., Cataldo, F.L. and Reddy, M.M. (1974). "Non-thermal effects of 2 MHz ultrasound on the growth and cytology of <i>Vicia faba</i> roots," Br. J. Radiol. 47 , 122–129.
11.	Miller, D.L., Nyborg, W.L. and Whitcomb, C.C. (1979). "Platelet aggregation induced by ultrasound under specialized conditions <i>in vitro</i> ," Science 205 , 505–507 (discussed in Sections 6.2.1 and 6.3.1).
12.	Williams, A.R. (1973b). "A possible alteration in the permeability of ascites cell membranes after exposure to acoustic microstreaming," J. Cell Sci. 12 , 875–885.
13.	Wagai, T. and Kikuchi, Y. (1965). "Destruction of transplantable ascites tumors by means of intense ultrasound," pages 179 to 189 in <i>Ultrasonic Energy: Biological Investigations and Medical Applications</i> , Kelly, E., Ed. (University of Illinois Press, Urbana).
14.	Kaufman, G.E., Miller, M.W., Griffiths, T.D., Ciaravino, V. and Carstensen, E.L. (1977). "Lysis and viability of cultured mammalian cells exposed to 1 MHz ultrasound," <i>Ultrasound Med. Biol.</i> 3 , 21–25.
15.	Holmer, N.G., Johnsson, A. and Josefsson, J.O. (1975). "Effects of ultrasonic irradiation upon <i>Amoeba proteus</i> ," Z. Naturforsch. 28c , 607–609.

Williams, 1982). Thus, factors which may seem innocuous, such as rotation of the exposure tube to keep cells suspended, can have greater effects on results than many-fold increases in intensity or duration of exposure.

7.1.3 Biological Effects

A very wide spectrum of biological effects has been reported to be induced in cells *in vitro* by ultrasound. For the purposes of this

Report, these effects are conveniently separated into: (1) the cell lysis effect, and (2) effects on cells which survive the ultrasound exposure. Red blood cell lysis (hemolysis) was among the earliest reported effects of ultrasound (Harvey, 1930). Later workers studied lysis of cultured cells as the primary effect of cavitation *in vitro* (e.g., Ciaravino *et al.*, 1981b; 1981c; Clarke and Hill, 1970). Hemolysis in dilute suspensions is useful as a cavitation indicator in studies of nucleation and evolution of cavitation (Miller and Williams, 1989). Since cell lysis occurs in exposures resulting in noninertial cavitation at modest levels of the acoustic pressure, if suitable gas bodies are present (Section 6.2.1), it is reasonable that it should occur even more readily in exposures resulting in inertial cavitation, for which the pressure amplitudes are higher.

Effects on surviving cells may include alterations of structure or function, or they may include genetic effects. For example, cell morphology alterations have been reported (e.g., Liebeskind *et al.*, 1979b). DNA strand breakage (e.g., Miller *et al.*, 1989a; 1991b; 1991c; 1995b), chromosome breakage (Macintosh and Davey, 1970), sister chromatid aberrations (Barnett *et al.*, 1983; Liebeskind *et al.*, 1979a), cell transformation (Liebeskind *et al.*, 1979b), and mutation (e.g., Kaufman, 1985) have been reported to occur as results of ultrasound exposure of cell suspensions, but some of the reports have proven more repeatable than others (see also Section 7.2.3.1).

7.1.4 Mechanisms of Action of Ultrasound In Vitro

For many of the publications reporting on the bioeffects mentioned above, there were no *a priori* hypothesized mechanisms of action, rendering them of limited value for identifying and understanding the basic physical actions responsible for the observed endpoints. For some, scrutiny of the protocols can reveal characteristics and conditions which are suggestive of a mechanism of action where bioeffects are induced. For some others, there have been unsuccessful attempts at independent verification of a reported bioeffect, thus calling into question the accuracy of the reported association of ultrasound exposure with the effect. Additionally, much literature in the bioeffects area is of little use in understanding basic mechanisms of action and thus is briefly summarized only to update NCRP Report No. 74 and No. 113 (NCRP, 1983; 1992).

There are three general mechanisms for bioeffects of cavitation *in vitro*: (1) enhanced heat production, (2) mechanical action, and (3) production of free radicals and/or other sonochemicals. Thermal mechanisms and thermally mediated effects of ultrasound on cell

systems *in vitro* were reviewed in NCRP Report No. 113 (NCRP, 1992) and are updated in Section 11 of this Report. In most experiments of the effects of ultrasound on cell suspensions, the highly localized heat production near bubbles (Section 4.3.1) is rapidly dissipated through convection. In gels, however, the presence of bubbles can contribute significantly to the temperature elevation in the exposed sample. At the moment of violent inertial collapse, temperatures within the bubble may reach several thousands of degrees; this probably is responsible for sonochemical production. Even at relatively low levels of ultrasound, where the oscillation of the bubbles is quasilinear, the presence of bubbles in the sound field can greatly enhance the absorption coefficient of the medium (Section 4). As an example, Watmough *et al.* (1993) investigated the effects of bubbles on ultrasound-induced temperature changes in a gel and its interface. A gel (5.7 percent weight/volume) made from bovine hide was insonated for 1 min (1 W cm^{-2} , 0.75 MHz, CW), and its temperature increased by $2.3 \text{ }^\circ\text{C}$; when gelatin foam was mixed into the gel, and it was subsequently insonated, the temperature increase was about $12 \text{ }^\circ\text{C}$. An Astralux[®] card (200 μm thick and containing irregular holes whose sizes ranged from 2 to 10 μm) (Star Paper Ltd., Feniscowles, Blackburn, Lancashire, United Kingdom) was used as a fixed source of bubbles. The card was sandwiched between two layers of gel, and a 0.125 mm thick copper constantan thermocouple was inserted into the gel with the thermocouple juncture in close proximity to the card target. Ultrasound exposures (1 W cm^{-2} , 0.75 MHz, 60 s duration) were CW. There was a correlation between ultrasound-induced temperature rise and gel "concentration." For instance, the mean ultrasound-induced temperature rises for gels of 11, 8 and 5 percent weight/volume concentration were 41, 24 and $17 \text{ }^\circ\text{C W}^{-1} \text{ cm}^2 \text{ min}$, respectively; for a degassed Astralux[®] card in a five percent gel concentration, the temperature rise was $7 \text{ }^\circ\text{C W}^{-1} \text{ cm}^2 \text{ min}$. This work is discussed further in Section 11.5.

In most studies of the effects of ultrasound on cell suspensions, however, the contribution of bubbles to the bulk heating of the medium is minimal. When biological samples have been shown to be heated during exposure, the usual source of the excess heating has been from absorption of sound by the sample container. Brayman and Miller (1993) noted that for an insonated polystyrene exposure vessel containing physiological saline and set within a large water bath, the tube walls absorbed a small amount of energy which was converted to heat, leading to increased partial degassing of the medium. However, the thermal effect is, even under these conditions, very small and may be totally absent in other containers providing

minimal acoustic absorption. For the latter (*i.e.*, bubble-related acoustic heating), the theory for heat produced by vibrating bubbles is discussed in Section 4.3.1).

Cavitation, discussed in Sections 4 and 5, is a mechanically vigorous phenomenon. It is clear that cavitation, both inertial and noninertial, including activation of stabilized gas bodies (Section 6), can induce cell lysis *in vitro*. As discussed in Section 7.2.2, considerable information is available on how ultrasound may cause this bioeffect. Acoustic streaming, near-boundary microstreaming, hydrodynamic flow around moving bubbles, expansion and collapse (asymmetric or symmetric) of bubbles, and bubble-bubble and bubble-cell “collisions” (also discussed in Sections 4 and 5) are all possibilities for how cavitation might lyse cells in suspension.

Inertial cavitation is a particularly vigorous form of cavitation, and generates temperature elevations during collapse sufficient to produce free radicals and sonochemicals (Suslick *et al.*, 1985; 1986). Suslick and Hammerton (1986) have shown that the imploding bubble is composed of two zones, an inner, central vapor cavity and a thin, surrounding liquid layer. During an inertial event, sonochemical reactions occur in the imploding center cavity due to the very high temperatures (the transient “hot spot”), which causes secondary reactions in the surrounding liquid layer. This mechanism enlarges the study of cavitation-related bioeffects to include not only purely mechanical processes but also secondary, chemically mediated processes arising in consequence of the occurrence of inertial cavitation (Section 7.2.2.4). For example, hydrogen peroxide is readily detectable after modest exposures which produce inertial cavitation (Section 5.11) and can damage DNA in viable cells *in vitro* (Miller *et al.*, 1991c; 1995b).

7.2 Cell Lysis

7.2.1 Influence of Various Aspects of Exposure Conditions

Whether or not a specific ultrasound exposure regimen is biologically effective depends on a large number of physical, chemical and biological factors. The main factors affecting the potential for ultrasound to induce bioeffects *in vitro* are discussed below.

7.2.1.1 Exposure Parameters. The outcome of *in vitro* ultrasound exposures may be influenced by other ultrasound parameters, in addition to the acoustic pressure amplitude.

Pulsing parameters are especially important, since virtually all diagnostic imaging devices employ pulse-echo techniques. Several assessments of the effect of ultrasound pulse durations, including CW, and frequencies higher than about 1 MHz on bioeffects *in vitro* have been made. Clarke and Hill (1970) showed that cavitation and cell lysis decrease markedly for short pulses, or for low pulse repetition frequencies. There are data on pulse lengths which suggest that bursts of about 1 ms or longer are effective, and pulse lengths less than 1 ms are not effective in inducing biological effects in aerated cell culture media (Clarke and Hill, 1970; Dooley *et al.*, 1983; Kober *et al.*, 1989). However, a recent report by Brayman *et al.* (1994) indicates significant ultrasound-induced (1 MHz, 5 W cm⁻² SPPA intensity, 0.4 MPa pressure amplitude) cell lysis at pulse lengths of 50 μs, employing a stationary exposure vessel and acoustically balanced, opposing continuously gated transducers. Kober *et al.* (1989) showed that, for Reh cells *in vitro* insonated with increasing pulse lengths of 0.775 MHz ultrasound at 3.6 or 6.4 W cm⁻² SPPA intensity (0.35 or 0.45 MPa pressure amplitude), cell damage increased with increase in pulse length over the range of 16 to 1,000 μs, with the 3.6 W cm⁻² regimen having a pulse length threshold of about 125 μs, whereas that for the 6.4 W cm⁻² regimen was about 32 μs. These results are in agreement with theoretical assessments of cavitation activity (as discussed in Section 5 in this Report), indicating an expected increase in cavitation activity with increase in ultrasound intensity and pulse length, and a decrease in cavitation activity with increase in hydrostatic pressure or ultrasound frequency.

Ciaravino *et al.* (1981b) showed that for 1 MHz CW exposures of V-79 cells *in vitro*, there was more lysis at 10 than at 5 W cm⁻² and that a higher atmospheric pressure was needed to eliminate lysis for the former relative to the latter exposure.

7.2.1.2 Rotation of Exposure Tube and Attenuation of Ultrasound by Bubbles. For investigations in the megahertz frequency range in which heating of the medium is avoided, the physical mechanism of action for most of the bioeffects on cells *in vitro* involves some action of bubbles on the cells. Often, as the ultrasound exposure intensity is increased, an apparent threshold for a bioeffect coincides approximately with the threshold for inertial cavitation. Above this threshold, cavitation activity occurs as the ultrasound exposure intensity increases, and the resulting biological effect may exhibit a maximum and then decline. Figure 7.2 shows results for 1 MHz exposures in a rotating tube, with reduced cell survival as the observed bioeffect and with cavitation activity indicated by iodine release (Clarke and Hill, 1970). These authors used an experimental

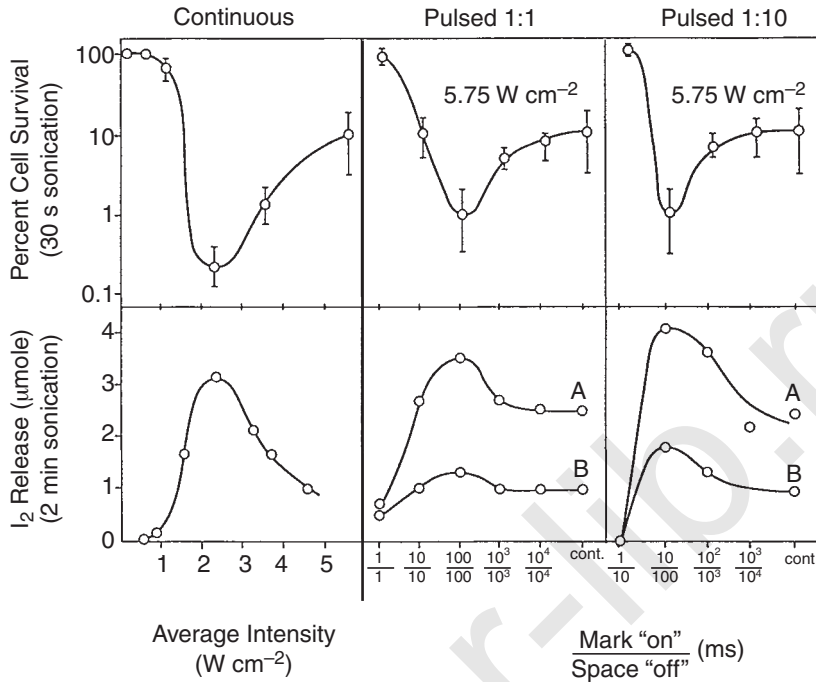


Fig. 7.2. Variation of cell survival and iodine release with ultrasonic intensity and pulsing conditions at 1 MHz [(A) 3.1 W cm^{-2} , (B) 4.6 W cm^{-2}]. For the continuous exposures (cont.), the intensity is spatially averaged, the spatial peak being about three times higher. For the pulsed exposures (on:off), the SPPA intensity is shown (adapted from Clarke and Hill, 1970).

setup similar to that shown in Figure 7.1, No. 3, in which the tube was upright and perpendicular to ultrasound beam direction and was rotating about its long axis.

The occurrence and extent of inertial cavitation is greatly influenced by various aspects of the exposure system. In general, in the arrangement represented schematically by No. 3 in Figure 7.1, rotation of the tube at low speed (*e.g.*, 100 revolutions per minute) enhances ultrasound-induced, nonthermal effects in mammalian cell suspensions, and whether or not an exposure tube is rotated can determine whether or not effects are observed. This phenomenon was initially observed by Clarke and Hill (1970). They explained the effect in terms of centripetal forces and the continually changing direction of the sound field; a detailed analysis of this postulate is given by Carstensen *et al.* (1993). Many subsequent reports have confirmed that tube rotation is generally necessary to observe

extensive cell lysis *in vitro* (Brayman and Miller, 1992; 1994; Carstensen *et al.*, 1993; Conger *et al.*, 1981; Sacks *et al.*, 1982; 1983).

There are two principal aspects of the ultrasound intensity-biological response relationships shown in Figure 7.2. The first deals with the initially increasing severity of the bioeffect with initial increase in ultrasound intensity. The second deals with the subsequent decrease in bioeffect severity as the ultrasound exposure intensity increases above that which caused a maximum effect, a phenomenon which Clarke and Hill referred to as "anomalous." They did speculate on possible reasons for the "falloff" in cell killing and iodine release at the higher ultrasound intensities, hypothesizing, (1) that bubbles may be swept out of the central region by the higher streaming forces associated with the higher ultrasound intensities, (2) the development of surface waves on the bubbles which would disrupt or reduce microstreaming, or (3) a rapid bubble development resulting in a shorter period of resonance vibration. Miller *et al.* (1989b) hypothesized that the reduction in cell lysis with increase in ultrasound intensity is related to the ultrasonically-induced "cloud" of bubbles in the fluid between the transducer and exposure vessel. The bubble "cloud" has the effect of reducing the sound intensity in the vessel, thus reducing cell lysis in the exposure vessel. Support for the hypothesis was obtained by noting a significant increase in bubble numbers in the fluid between transducer and the exposure vessel, and a significant increase in bubble numbers in that fluid with increases in ultrasound intensity above the maximum intensity for cell lysis.

Carstensen *et al.* (1993), however, provided an alternative explanation to the observation that above some ultrasound intensity level the amount of sonolysis *in vitro* diminishes. They observed that the intensity of the sound field at or behind the exposure vessel was linearly related to the source power and proposed instead that at relatively high ultrasonic pressures, the radiation forces act to return the bubbles to the back side of the exposure vessel in increasingly shorter arcs of the revolution, thus foreshortening the path of the bubble. With a reduced path, there is less chance for a bubble to encounter a cell, and lysis declines as the intensity of the ultrasound is increased above that required to produce a maximum lytic effect.

Considerable effort in the study of bioeffects *in vitro* has been directed at understanding the tube rotation effect. This is discussed in some detail because an essential step in modeling the influence of exposure vessel rotation deals with mechanisms for bringing cells and bubbles close enough together so that interaction between the two can occur. There are two detailed, and probably complementary, rotation-effect models which attempt to explain the interaction of

lytically effective bubbles and cells in an exposure vessel: (1) the *standing wave model* involves radiation forces which can lead to segregation of cells and bubbles in an exposure system; and (2) the *bubble recycling model* involves the return of bubbles, which are sent to the rear of a tube by the traveling wave radiation force, to the front of the tube by the rotation where they can renucleate the medium and retransit through the medium. Both models have been developed through the use of relatively dilute cell suspensions, being of the order of about a one percent or less cell volume concentration. The rationale for using relatively dilute cell suspensions is that apparent ultrasound induced lytic yields, expressed in relative terms (e.g., percent cell lysis) generally decrease with only modest increases in cell number density. For example, Williams *et al.* (1991) and Miller *et al.* (1995a) have noted that relative ultrasound-induced cell lysis diminishes rapidly with increase in hematocrit from 1 to ~10 percent (Section 7.2.3.2).

7.2.1.3 Mechanical Stirring. Exposure vessel rotation is, however, not indispensable to observing ultrasound-induced bioeffects in *in vitro* systems. A report by Williams (1982) showed that when the contents of a stationary tube were stirred mechanically during insonation, cell lysis increased with increase in stirring speed up to 30 rpm. The above report can be viewed as providing independent confirmation of the effectiveness of rotating fluid in mediating ultrasound-induced cell lysis. Williams (1982) also showed that percussive impacts on the tube wall or vibration (13 Hz) of the tube increased sonolytic activity and suggested that vibration of the container enhanced gas nucleation processes at the wall-fluid interface. Saad and Williams (1985) suggested that the impacts can arise *via* contact of the magnetic stirrer bar with the vessel. Additionally, Watmough *et al.* (1990) noted that streaming-related internal mixing within a chamber can depend critically on its placement in an ultrasound beam.

7.2.1.4 Standing Waves. As indicated above, the purported necessity for tube rotation to increase ultrasound-induced cell lysis was originally reported by Clarke and Hill (1970) and subsequently confirmed by a number of independent investigators (e.g., Brayman *et al.*, 1992; 1994; Conger *et al.*, 1981; Sacks *et al.*, 1982). A somewhat complicated mechanism involving bubbles trapped by standing waves was subsequently proposed by Church and Miller (1983). A typical experimental setup involved a polystyrene tube placed in a bath of degassed water (e.g., Figure 7.1, No. 2). It had long been recognized that standing waves were produced in a polystyrene tube

during CW insonation. Under these conditions in which the tube is not rotated, cells congregated at the pressure minima of the standing wave, while lytically effective bubbles somewhat smaller than resonance size congregated at the pressure maxima. Thus, bubbles capable of lysing the cells were segregated from the cells, and cell lysis was generally absent or minimal during insonation ("segregation" in this manner is a result of acoustic radiation forces acting on the cells and bubbles, each having different acoustic properties, as discussed in Sections 3.2.7 and 4.4.2). As the cells are held by relatively weak forces, tube rotation during insonation sweeps the cells through the arrays of lytically effective bubbles, and cell lysis results. Studies showed that inertial cavitation, as evidenced by an iodine-release assay, is associated with the occurrence of cell lysis (Ciaravino *et al.*, 1981a; Clarke and Hill, 1970). Thus, tube rotation in the presence of standing waves brings cells into association with bubbles; the violent implosion of the bubble was deemed to produce the shear forces which ruptured the membranes of nearby cells. Support for the hypothesis of Church *et al.* (1982) and Church and Miller (1983) was obtained (1) by the visual demonstration of a standing wave (*i.e.*, a dilute aqueous suspension of activated charcoal showing half-wave length longitudinal bands) within the tube during CW insonation, (2) by an increase in cell lysis with increase in rotation speed, and (3) from the report by Verrall and Sehgal (1988) of sonoluminescence at pressure amplitude maxima in a standing wave. Church and Miller's (1983) model recognized that there were also nontrapped bubbles and that they may be brought into proximity with cells by a different process.

7.2.1.5 Bubble Recycling. A detailed model has been proposed (Miller and Williams, 1989; Miller *et al.*, 1991a) which does not involve the presence of standing waves in the medium. This model proposes that cavitation bubbles of near-resonance size travel to the side of the tube away from the transducer (*i.e.*, in the direction of the traveling wave) under the influence of traveling-wave radiation forces. Tube rotation brings the bubbles around from the distal inner vessel wall (*i.e.*, furthest from the sound source) to the inner proximal tube wall for another radiation force-driven transit through the medium. Without tube rotation, bubbles are postulated to be driven to, and collect at, the far-inside of the tube. Support for the bubble recycling mechanism comes from several observations. Red blood cells insonated in a tube system which greatly reduces the presence of standing waves undergo lysis, so that robust standing waves *per se* are not necessary for sonolytic activity. When focused 1.45 MHz ultrasound was turned on for half a rotation and off for half, which

would not cause bubble recycling, results (*i.e.*, amount of ultrasound-induced cell lysis) were similar to those for a nonrotated tube. When on-off cycles were synchronized to a quarter rotation, which would cause bubble recycling, results were similar to those obtained using a continuously rotating tube. The establishment of a rotation effect could also be obtained with relatively short bursts of ultrasound (Williams and Miller, 1989), using a cylindrical chamber rotated perpendicular to its axis with exposure only while the tube was aligned with the beam each half turn. This system allows the study of various nonacoustic factors in the etiology of *in vitro* effects, such as the distance across the tube and vessel wall materials. The bubbles appear to move through the medium at speeds up to 10 m s^{-1} in recycling across the tube (Miller *et al.*, 1991a). The detailed mechanisms by which the bubbles mechanically tear the cell membranes can range from the nearly inertial-cavitation implosions (Carstensen *et al.*, 1993) to the hydrodynamic shear stresses arising in the hydrodynamic flow around such rapidly moving bubbles (Miller *et al.*, 1991a) (Section 7.2.2).

A series of experiments was undertaken in an effort to explore the standing wave (Church and Miller, 1983) and bubble recycling mechanisms (Williams and Miller, 1989). Brayman and Miller (1992) constructed an exposure tank such that the angle of insonation was approximately 54 degrees upward relative to the axis of the insonated vessel. Under these conditions, and with tube rotation, a bubble (by virtue of its being propelled diagonally upward and across the tube by the radiation force) would make at most about two transits through the medium before being removed from the sound field. A styrofoam reflector could be placed in the tank to induce a strong standing wave field. The amount of ultrasound-induced (1 MHz, 5 W cm^{-2} , 5 min CW exposures) cell lysis was studied. A polystyrene tube which contained the cell suspension, was rotated and was either perpendicular (90 degrees) or angled (54 degrees) to the sound field. When insonations occurred at 90 degrees, a large amount (97 percent) of cell lysis occurred. When insonations were performed at a 54 degree angle, a small amount of lysis (five percent) was observed when an acoustic absorber was present, and a large amount (37 percent) of lysis was observed when an acoustic reflector was used. These results suggest that, under conditions which produce strong standing waves, trapped bubbles may be effective in lysing cells, but that two-thirds of the cells are lysed by some other mechanism. Doida *et al.* (1992a) further tested the importance of standing waves by translating polystyrene tubes back and forth in a standing wave field. Because the tube was not rotated, only bubbles trapped in the standing wave would be expected to interact with

suspended cells. It was postulated that if bubble recycling is needed to induce sonolysis, one would not expect cell lysis to occur with insonation under these conditions. If, however, standing waves retain cells and lytically effective bubbles at different but discrete locations in the medium, then by moving the tube back and forth, one would effectively “mix” cells and lytically effective bubbles, and lysis should occur. When a high amplitude wave was present (through the use of an acoustic reflector), there was a small but significant increase in cell lysis however, it was less than that observed with continuous tube rotation. These results were also suggestive of a small involvement of standing waves in inducing cell lysis but that the dominant mechanism appeared to be associated with recycled translating bubbles.

Carstensen *et al.* (1993) observed that as few as two full turns (in 180 degree steps) spaced over a 5 min period were sufficient to produce a significant increase in hemolysis in comparison with a similar exposure in a stationary vessel. This suggested that locations on the container walls could act as nucleation sites giving off bubbles for many seconds before being depleted of gas. This was confirmed by observations of chemiluminescence under similar exposure conditions. Only rarely could the light be seen in a stationary tube. However, once rotation started the whole tube would light up. Furthermore, luminescence continued for a short time after rotation stopped. When the inner wall of the container was deliberately scratched to provide more sites for stabilization of bubbles, the luminescence was enhanced and the glow continued for longer times after rotation stopped. Brayman *et al.* (1994) independently verified the results of Carstensen *et al.* (1993) using a different cell line that provided a more rigorous control over background levels of lysis. The results exhibited a small but significant amount of cell lysis in nonrotated tubes, but a very substantial increase with only one complete rotation (two 180 degree steps) during a 5 min exposure duration.

7.2.1.6 Alternating the Ultrasound Propagation Direction. The bubble recycling hypothesis for induction of cell lysis *in vitro* suggests that it is the translation of the bubble which facilitates interaction between lytically effective bubbles and cells. A test of this hypothesis was undertaken by Brayman *et al.* (1994) in which a stationary polystyrene tube with a dilute suspension of cells (2×10^5 cells mL⁻¹) was insonated for 15 to 300 s alternatively from opposite directions (1 MHz, 5 W cm⁻²) with various opposing pulsing regimens of the transducers; the exposure arrangement was similar to that shown in Figure 7.1, No. 2 except there was an additional transducer facing

the exposure vessel on the side opposite that shown in the figure. Under these conditions, it was postulated that the lytically effective bubbles would be translated back and forth across the tube without the necessity of tube rotation. The objectives of the study were to attempt confirmation of the bubble recycling hypothesis in the absence of exposure vessel rotation, and to assess indirectly the average translational speed of lytically effective bubbles. As long as each transducer's pulse duration was greater than 0.5 ms, very substantial cell lysis was obtained; the longest pulse length was 5 s. As the pulse length was decreased below 0.5 ms, a progressive decline in cell lysis occurred. No cell lysis was observed at pulse lengths of 5 μ s or at any pulse length if only one transducer was activated.

Presumably, the primary site for nucleation was the wall of the exposure tube. Thus, on the one hand, if the direction of the bubble travel reversed before significant movement relative to tube size (diameter), only a negligible fraction of the cell suspension was exposed to bubbles. On the other hand, if the direction of the sound did not change (*i.e.*, only one transducer was used in CW), bubbles made one pass through the medium, nucleation was restricted, and the total effective time of exposure was negligible. The increase in total lysis as the period increased up to a plateau of about 1 ms pulse duration suggests it took about 1 ms to complete transit across the tube, corresponding to a linear velocity for the bubble of about 10 m s⁻¹, a value consistent with theory and other experimental results (Miller *et al.*, 1991a). The results of this experiment are consistent with the hypothesis that rotation of the exposure vessel in the conventional experiment increases lysis by recirculating bubbles.

If it were assumed that it takes about 1 ms for a bubble to transit the diameter of the tube, it is clear that translation of about 20 percent of the total distance should be sufficient to result in some cell lysis and that at translational distances amounting to only a few cell diameters no effect would be noted. The failure of the 5 μ s pulse regimen to lyse cells may be related to the relatively short translational distance of the bubble (about 25 μ m, or two to three cell diameters) and the large separation distances between cells, or to the possibility that cavitation activity is occurring in very limited areas due to the short translational distance. The data therefore appear to support the hypothesis. Bubble translation thus appears to be important in achieving cell lysis due to the increased possibility of interaction between a cell and an active bubble.

7.2.2 Mechanisms of Lysis

7.2.2.1 Near-Boundary Streaming. Hemolysis observed near ultrasonically activated gas-filled micropores in plastic sheets (Section 6)

is apparently the result of shear stress applied to the cells as they are taken up in the near-boundary fluid flow (*i.e.*, microstreaming) at the surface of the plastic. In studies of cavitation effects, one plausible mechanism of cell lysis is near-boundary microstreaming near bubbles which have been forced against or into the distal wall of the exposure tube or chamber. Williams and Miller (1989) and Miller *et al.* (1991a) found that “soft” walls (*i.e.*, agar or silicone grease) of an exposure vessel, which would prevent near boundary streaming, only slightly reduced the effectiveness of exposure. This implies that near-boundary microstreaming contributes only a small part of the overall sonolytic activity in rotating tubes. Presumably, the majority of lytic events occur in the bulk of the medium through encounters of free cells and bubbles, and not at container boundaries.

7.2.2.2 *Shear Near Moving Bubbles and Cell-Bubble Collisions.*

Because sonolysis in a rotating tube seems to occur predominately in the bulk medium, with rapidly moving bubbles encountering cells, a plausible picture of bullet-like bubbles colliding with cells was hypothesized (Church and Miller, 1983). This is a useful model, although the exact nature of a “collision,” which occurs on microscopic and microsecond scales, is somewhat difficult to establish. A translating bubble might be considered to physically and directly collide with a cell and might not travel in a straight line because of bubble-bubble as well as bubble-cell attractions and repulsions. However, a bubble passing near a cell, but failing to make direct contact with it, might also be considered to have undergone a “collision” with a cell. Miller *et al.* (1991a) suggested that a bubble translating through an aqueous medium might approach speeds of 10 m s^{-1} (as is consistent with the results discussed in Section 7.2.2.1) and that hydrodynamic flow around a bubble moving at such speeds might be sufficient to lyse cells.

The idea of bubbles colliding with cells, as initially proposed by Church and Miller (1983), is useful for estimating the number of bubbles involved in lysis, given a known number of cells (Miller and Williams, 1989). A simple model was developed to describe the lytic process (Miller and Williams, 1992), in which all the cells encountered within a cylindrical volume along the bubble path were lysed. Bursts of 1.61 MHz ultrasound were synchronized with the rotation of a cylindrical exposure chamber. Cavitation induced hemolysis was dependent on nucleation, apparently sometimes by only few nuclei (or even a single nucleus), and proliferation of the nuclei into thousands of active bubbles within a few rotations. For 11 ms bursts, for example, 0.33 percent of the cells were lysed for each burst, which represents, for a $10 \text{ }\mu\text{m}$ diameter lytic cylinder, 3,300 bubbles lysing

315 cells each. In experiments involving a 2.17 MHz ultrasound exposure and an acoustic pressure amplitude at 0.8 MPa, Miller and Thomas (1994a) estimated that approximately 7,100 bubbles were involved in lysis during a 10 ms burst. This estimate was made by dividing the number of cells lysed in a single burst by the number of cells contained within the volume of a “lytic chamber” associated with the transit of a single bubble. The apparently higher sensitivity for sonolysis of 15 μm diameter CHO cells, relative to 5 μm diameter red blood cells is consistent with a collision model of bubble-cell interactions, *i.e.*, big cells are easier targets to hit than are small cells (Brayman *et al.*, 1996b). It is interesting to note that Blackshear and Blackshear (1987), in evaluating mechanical hemolysis of a large range of red blood cell types (from human beings to goats), noted that as cell size decreased there was a corresponding and dramatic increase in critical shear stress needed to rupture the membrane. For example, human red blood cells have a volume of approximately 84 μm^3 and a critical shear stress value of approximately 40,000 dyn cm^{-2} , whereas bovine red blood cells have a volume of approximately 32 μm^3 and a critical shear stress value of approximately 118,600 dyn cm^{-2} . These factors appear likely to play a role in the differing sensitivities of cells to ultrasound (Brayman *et al.*, 1996b) and may be important in understanding the different sensitivities of cells to ultrasound shown in Figure 7.3. Miller and Brayman (1997) tested the hypothesis that lymphocytes would be significantly more sensitive than erythrocytes to a lytically effective ultrasound exposure because of the former’s larger size (1,083 versus 76 μm^3 , respectively). The hypothesis was supported in that the larger cells had greater amounts of relative cell lysis than smaller cells; the mean levels of lysis in insonated lymphocyte and erythrocyte populations were 90 and 79 percent, respectively ($p < 0.005$).

7.2.2.3 Bubble Implosion and Jets. During inertial cavitation events, a bubble undergoes a rapid expansion to more than twice its original radius, then collapses and upon rebound, generates extremely large local stresses (Section 5.8). If a boundary is nearby, an asymmetric collapse can occur with formation of a water jet directed toward the surface. Physical constraints and observations indicate that jet formation, while involving the same general physical requirements for inertial cavitation in general, is more likely to occur when a bubble is near a boundary of the medium or next to another bubble (Apfel, 1986; Coleman *et al.*, 1987; Crum, 1979; 1992; Shima *et al.*, 1983; Tomita and Shima, 1986; Vogel and Lauterborn, 1988). The jets may be sufficiently forceful to erode metals (Coleman *et al.*, 1987), and so it is not surprising that cells encountering such violent

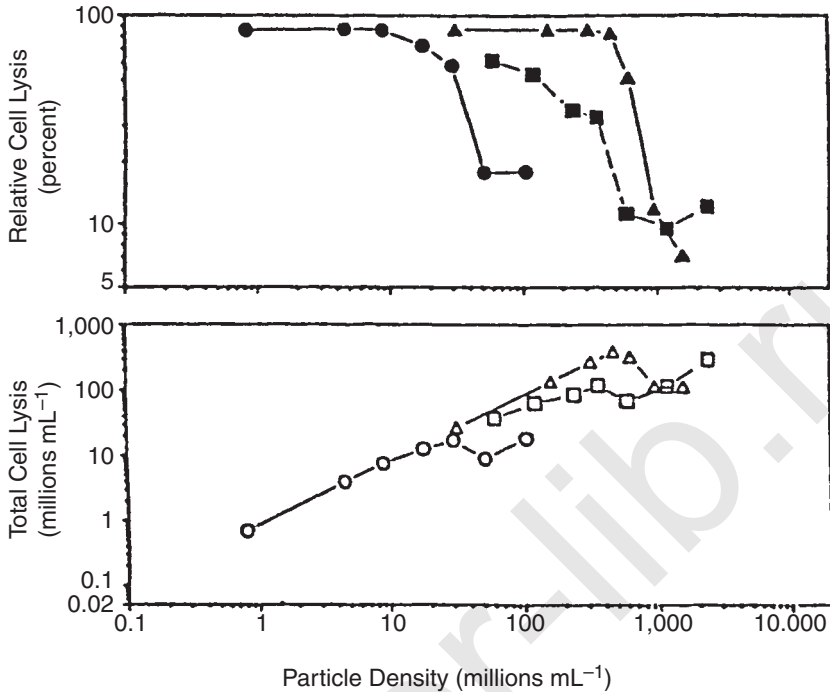


Fig. 7.3. Relative cell lysis (upper panel) and total lysis (lower panel) of murine P388 cells (circles), human erythrocytes (squares), and bovine erythrocytes (triangles) exposed to CW, 1 MHz ultrasound (5 to 8 W cm⁻²) as functions of the cell concentration in the insonated suspensions; from a re-analysis of data in Brayman *et al.* (1992), Miller *et al.* (1995a), and Carstensen *et al.* (1993), respectively.

cavities are lysed (although it has not been established that jets may form as a result of a cell-bubble encounter). Miller *et al.* (1991a) estimated bubble speeds of up to 10 m s⁻¹ for 1.6 MHz ultrasound up to 16 W cm⁻². Carstensen *et al.* (1993) have indicated that bubbles in the range of a few tenths to several micrometers in radius and exposed to CW ultrasound at intensities of about 8 W cm⁻² will achieve terminal velocities of 1 to 5 m s⁻¹. These speeds would place a moving bubble near a 15 μm diameter cell for several acoustic cycles which, according to Flynn and Church (1988), is ample time for a lytic encounter to occur.

7.2.2.4 Free Radicals and Other Sonochemicals. There are reports of bioeffects which appear to relate indirectly to inertial cavitation. For example, Riesz and Kondo (1992) suggest that inertial

cavitation results in the production of free radicals. The physical factors of inertial cavitation which produce these radicals are discussed in detail in Sections 5.10 and 5.11. Given the production of sufficient concentrations of sonochemicals such as hydrogen peroxide (Miller and Thomas, 1994b), cell death and lysis from this mechanism might be expected, in addition to that arising *via* the mechanical mechanisms noted above. Using the estimates of the bubble numbers obtained from cell lysis observations (Section 7.2.2.2), one can estimate that the inertial cavities appeared to produce 93 to 150 fM of H_2O_2 per 10 ms burst of 2.17 MHz ultrasound. This production is actually comparable to the highly bioactive chemical production of phagocytic cells during the respiratory burst response, but in cell suspensions, this sonochemical yield is rapidly diluted throughout the chamber volume, reducing its effectiveness.

Fu *et al.* (1979) noted that the free radical scavenger cysteamine increased cell survival following exposure to 1.1 MHz ultrasound as judged by plating efficiency, although lysis was unaffected. Armour and Corry (1982) found protective effects from cysteamine, which permeates the cells, but not from cysteamine, which does not enter cells. These results were confirmed by Inoue *et al.* (1989). These collective findings might imply that cavitation-induced free radical generation occurs inside the cells. This phenomenon may have an alternative interpretation, however, since penetrating scavengers also protect against the effects of hydrogen peroxide which may be generated in the medium far from the cells, diffuse to and penetrate the cells, and produce intracellular free radicals (Mello Fikho and Menghini, 1984; Miller *et al.*, 1991c).

Kondo *et al.* (1988), in experiments using an ultrasound frequency of 50 kHz, noted that cell lysis was the same for different dissolved gases, which produced a wide range of free radical formation and concentration, and concluded that lysis was primarily a mechanical phenomenon. At 1.6 MHz, Miller and Thomas (1993b) noted that hydrogen peroxide production and hemolysis had about the same ultrasound intensity threshold (presumably the inertial cavitation threshold) but that conditions giving near 100 percent lysis after 1 min ultrasound exposure yielded only about 10 μ M concentrations of H_2O_2 after a 30 min ultrasound exposure. For comparison, cell killing by H_2O_2 exposure, which appears to result from lethal DNA damage rather than direct membrane damage, requires concentrations of the order of 1 mM (Prise *et al.*, 1989). An interesting observation was made by Jeffers *et al.* (1995) that dimethylformamide (DMF), a polar solvent from among a class of drugs with anticancer properties, was shown to enhance cavitation-induced HL-60 cell lysis *in vitro*. The drug did not affect membrane fragility in the absence

of ultrasound, as evidenced by lytic equality among regimens which involved only mechanically generated shear forces and the presence or absence of DMF. It also had no effect on properties of the exposure medium which are known to affect the occurrence of inertial cavitation—*i.e.*, vapor pressure and surface tension. There was also no difference in subharmonic emissions between regimens involving ultrasound plus albumin bubbles and ultrasound plus albumin bubbles plus DMF, except at the highest ultrasound intensity (1 MHz, 2.5 W cm^{-2} spatial peak intensity, 0.3 MPa pressure amplitude), where there was a greater amount of cavitation activity (as indicated by subharmonic emissions) with the latter regimen. A similar enhancement of ultrasound-induced cell lysis was noted for two other similar drugs at the 2.5 W cm^{-2} spatial peak intensity, 0.3 MPa pressure amplitude exposure level. Because the results with DMF suggest a synergistic effect on ultrasound-induced cell lysis (*i.e.*, significantly more lysis than achieved with separate ultrasound and DMF regimens), the authors hypothesize that highly reactive and lytically effective chemical species are formed in the DMF medium during insonation.

To summarize, the presently available information suggests that the free-radical component of the inertial cavitation assault can affect survival of nonlysed cells, but cell lysis appears to be due primarily to mechanical membrane damage, which may be influenced by highly reactive sonochemicals.

7.2.3 *Influence of Various Aspects of Cells and Media*

7.2.3.1 Nucleation. The nucleation process is of critical concern in *in vitro* bioeffects studies (Section 4.2.1). The first step in ultrasound-induced cavitation-related bioeffect induction involves the nucleation and generation of bubbles of appropriate size in the suspending medium, if *they are not already present*. Without the presence of stabilized gas nuclei, it is very difficult to cavitate ultrasonically a solution; *i.e.*, the “cleaner” the medium, the higher the expected threshold for cavitation (Section 4.5.8 in NCRP, 1983). In typical experimental systems, bubbles may already be present due to the presence of microscopic crevices on a vessel wall (Brayman and Miller, 1994; Carstensen *et al.*, 1993; Williams, 1982) or the biological materials themselves may contain microscopic pockets of gas due to the presence of opposing hydrophobic surfaces (Christenson and Claesson, 1988). Furthermore, the number of gas nuclei may increase during insonation of nucleation sites through manipulations of the vessel (Williams, 1982) or to fragmentation of bubbles during

implosion (Apfel, 1986). Under insonation, the bubbles in fluids may (1) be translated by radiation force, (2) undergo oscillations in volume in response to the pressure variations of the sound field, (3) collapse either symmetrically or asymmetrically under appropriate conditions, possibly producing more cavitation nuclei, and/or (4) grow beyond resonance size (by rectified diffusion and/or coalescence) and rise out of the suspending medium. The number of bubbles per unit volume may also decrease with increase in ultrasound exposure duration due to degassing of the medium and/or loss of nucleation sites.

The nature of the nucleation process may be among the differences between stationary and rotating exposure systems (discussed in Section 7.2.1) for inducing bioeffects during insonation. For example, rotation of a vessel exposes more of the vessel surface and nucleation sites than would stationary exposure. Miller *et al.* (1991a) examined the contributions of wall nuclei and medium nuclei to the total population of nuclei by subjecting either or both sites to high pressures, which tend to crush nuclei and dissolve gas. Pressurization of either the medium or vessel alone produced results intermediate between no pressurization and simultaneous pressurization of both components. Thus, it appears that nucleation can occur at the vessel walls or from nuclei in the medium. Additional studies were undertaken with exposure vessels in which a discrete line was scarified (scratched) in the inner vessel wall (Brayman and Miller, 1994). Ultrasound-induced cell lysis was always greater for (1) scarified tubes as opposed to nonscarified tubes and (2) tubes whose scarification was nearest the transducer as opposed to that farthest from the transducer. These and other results suggest that the containment vessel can function as an important site for nucleation and that tube rotation enhances nucleation (Brayman and Miller, 1994; Carstensen *et al.*, 1993; Miller and Williams, 1989; 1992; Miller *et al.*, 1991a; Williams, 1982; Williams and Miller, 1989).

Carstensen *et al.* (1993) undertook qualitative measures of chemiluminescence and found a correspondence between the onset of visible luminescence (2 W cm^{-2}) and cell lysis, and the disappearance of visible luminescence during ultrasound exposure (2 W cm^{-2}) with cessation of tube rotation, thus providing support for the postulate that the rotation of the tube is important in providing nucleation sites for subsequent inertial cavitation. Stationary tubes showed no or minimal chemiluminescence, but rotation of the tube, even slowly, appeared to “trigger” luminescence. Deliberate scratching of the inner walls of the tube or the use of an acoustic reflector to induce standing waves in the tube resulted in intense luminescence during insonation. The correspondence of thresholds for ultrasound-induced

chemiluminescence and cell lysis strongly suggests inertial cavitation as a dominant mechanism whereby cell membranes are ruptured in these experiments.

As noted by many, inertial cavitation is a highly variable phenomenon (Brayman and Miller, 1994; Carstensen *et al.*, 1993; Miller and Williams, 1989; Verrall and Sehgal, 1988). For instance, under insonation conditions which could result in cell lysis, the results were so variable that it has been dubbed an “all or none” phenomenon (Miller and Williams, 1989), or “something or nothing” (Carstensen *et al.*, 1993). It is postulated that as few as one nucleus may be needed to initiate cavitation activity in a rotating tube system (Miller and Williams, 1989; 1992). Whether cavitation occurs at all depends upon the existence of cavitation nuclei, but the effects obtained when nucleation occurs are roughly constant (Miller and Williams, 1992). In two seemingly identical exposures, cavitation may occur if nuclei are present, or fail to occur if none is present. Apparently, the one required nucleus can proliferate within a few rotations to yield the thousands of bubbles needed for the observed cell lysis effects.

In addition to “endogenous” cavitation nuclei (*i.e.*, nuclei that occur naturally), “exogenous” or purposely introduced nuclei (*e.g.*, microbubble ultrasound contrast agents) may also have a pronounced influence on ultrasound-induced cell lysis. This was demonstrated with Nuclepore® membranes containing stabilized “pockets” of gas and immersed in a solution containing cells *in vitro* (Section 6). Williams *et al.* (1991) have shown that for cells *in vitro* exposed to 1 MHz CW ultrasound (3 W cm⁻² intensity, 0.3 MPa pressure amplitude) in a stationary tube, a substantial increase in the amount of cell lysis occurred when the echo-contrast medium, Echovist®, was present. Lysis with Echovist® in a stationary tube was greater than that with a tube rotated at 30 rpm but without added Echovist®. Miller *et al.* (1995a) produced qualitatively similar results using a different cell line and a different echo-contrast medium, Albunex®. The ultrasound contrast agents can serve as nuclei for inertial cavitation: when either Albunex® or Levovist® were added to a noncavitating system (which had been depleted of nuclei by filtration) the sonochemical hydrogen peroxide was detected above 0.41 MPa pressure amplitude at 2.17 MHz (Miller and Thomas, 1995a). Brayman *et al.* (1996b) studied ultrasound-induced (1.07 MHz, 5 to 1,000 μs pulses at spatial-peak temporal peak (SPTP) intensities of 0 to 110 W cm⁻², 0 to 1.8 MPa pressure amplitude) hemolysis of whole human blood *in vitro* supplemented with 3.6 percent volume/volume Albunex® microspheres. The dependence of hemolysis on the peak negative pressure was examined (Figure 7.4). The background-corrected hemolysis using 5, 10, 20 or 30 μs ultrasound pulses

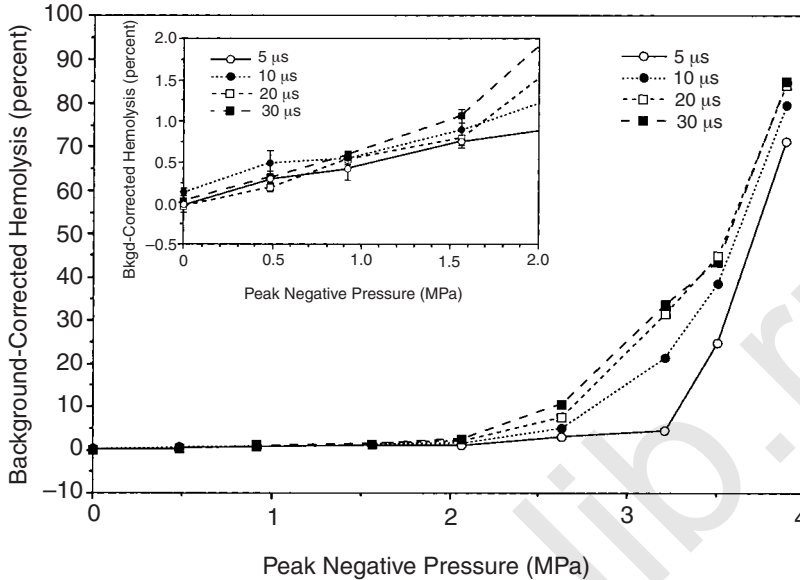


Fig. 7.4. Background-corrected hemolysis produced by 5, 10, 20, or 30 μ s pulses of 1 MHz ultrasound as a function of peak negative acoustic pressure measured at the position of the sample vessel. Each point represents the mean of five donor means; error bars represent the standard error; when not shown, error bars are smaller than the symbol. The inset provides an expanded scale view of the data obtained with peak negative pressures <2 MPa (Brayman *et al.*, 1996b).

revealed four interesting results: (1) there were statistically significant increases in hemolysis at all pulsing regimes, (2) the amount of hemolysis was relatively low at peak negative pressures <2 MPa regardless of pulse duration (see insert of Figure 7.4), (3) the amount of hemolysis was relatively large and increased rapidly for peak negative pressures >2 MPa, and (4) the longer the pulse length the greater the lysis. Alburnex[®] has been shown to reduce cavitation thresholds in whole blood. For example, the threshold for hemolysis in 100 ms exposures to 1.28 MHz ultrasound was reduced from 17.8 to 10 MPa by the addition of one percent Alburnex[®] (Miller and Thomas, 1996a).

Miller *et al.* (1997) undertook a study with canine blood exposed *in vitro* in a stationary tube to pulsed ultrasound (2.25 MHz center frequency) in the presence of Alburnex[®]. Cell lysis was observed to increase at 50 percent hematocrit and 50 percent volume/volume Alburnex[®] with increase in acoustic pressure. Statistically significant hemolysis occurred for 0.28 MPa continuous exposures of 1 s

duration and for 0.58 MPa pulsed exposures of 100 s duration with 10 μ s pulses and 1 ms pulse repetition period. Ultrasound-induced cell lysis increased with increase in pulse duration or Alburnex[®] concentration, and decreased with increasing ultrasound center frequency such that higher acoustic pressures were needed to cause an effect. The data are consistent with an inertial cavitation mechanism and indicate the possibility of ultrasound-induced cell lysis in “whole blood” provided sufficient cavitation nuclei are present.

Deng *et al.* (1996) studied hemolysis of human blood *in vitro* exposed to 4.3 and 2.5 MHz pulsed ultrasound. For the former (4.3 MHz, 0.465 percent duty cycle, 1 kHz *PRF*, 20-cycle pulse duration), the thresholds for 45, 23 and 12 percent hematocrit were >6.2 MPa, but with infused micrometer-sized polystyrene particles the thresholds were >6.2, 5.5 and 5.4 MPa, respectively. Somewhat similar results were obtained with the pulsed 2.5 MHz regimes. The acoustic pressure thresholds without particles for 45, 23 and 12 percent hematocrit were >5.2, 4.1 and 3.9 MPa, respectively, but with particles were >5.2, 4.3 and 2.9 MPa, respectively. The threshold (>5.2 MPa) for whole blood in Deng *et al.* (1996) at 2.5 MHz is considerably greater than that reported by Brayman *et al.* (1997). The difference in acoustic thresholds between the two general sets of results for whole blood supplemented with microparticle suspensions may be related to the fact that experiments of Brayman *et al.* (1997) used pre- and post-insonation procedures for stabilization of the erythrocytes (Azadniv *et al.*, 1996) and controlled for time-dependent increments in autolysis, whereas Deng *et al.* (1996) apparently did not.

The two echo contrast media (Echovist[®] and Alburnex[®]) are suspensions of numerous stable, microscopic bubbles. Bleeker *et al.* (1990) have given an extensive description of the physical and chemical properties of Alburnex[®]. The results of Williams *et al.* (1991) and Miller *et al.* (1995a) strongly indicate that it is not necessary to rotate the tube to achieve ultrasound-induced cell lysis, provided large numbers of cavitation nuclei are present. The use of echo contrast media or hydrophobic particles such as polystyrene spheres (Holland and Apfel, 1990; Holland *et al.*, 1992) or other particles with cells exposed *in vitro* to ultrasound provides a unique opportunity to study biological effects and cavitation.

7.2.3.2 Cell Concentration. Ellwart *et al.* (1988), Lehmann (1953), Loverock and ter Haar (1991), Saad (1983), and Veress and Vincenze (1977) have shown the importance of cell concentration in ultrasound-induced cell lysis *in vitro*. Ultrasound-induced cell lysis, which is easily and unequivocally detectable at low cell concentrations, is

not readily detectable at high cell concentrations. Nyborg and Miller (1982a; 1982b) obtained theoretical and experimental evidence that cells exposed to ultrasound are attracted to air bubbles, leading to the formation of rosettes of cells around the bubbles. The radiation force driving the migration of cells toward oscillating bubbles was found theoretically to be inversely proportional to the fifth power of the distance between cells and an oscillating bubble. Brayman and Miller (1993) tested the hypothesis that at high cell densities, bubble activity is damped by cell aggregation around bubbles, thereby suppressing their oscillatory and translational activities. Manometric analyses of gas evolution from insonated nonviable cell suspensions supported the hypothesis that as cell concentration increased, evolved gas decreased, *i.e.*, the ultrasound became less effective at “degassing” the medium. Nonviable cells were used for the above study since Brayman *et al.* (1992) had shown that vital cells in suspension depress apparent cavitation activity in part *via* respiratory modification of the medium’s dissolved gas composition.

The apparent absence of ultrasound-induced cell lysis with only very modest increase in hematocrit, as noted above, is a very interesting observation. Intuitively, one might expect that the greater the cell concentration, the greater the number of cells potentially affected by an imploding or translating bubble, but a decrease in *relative* cell lysis with increasing hematocrit is observed (Carstensen *et al.*, 1993; Ellwart *et al.*, 1988; Miller, 1988a; Miller *et al.*, 1995a; Veress and Vincenze, 1977; Williams and Miller, 1989). However, the *extent* of ultrasound induced cell lysis actually increases with increasing cell concentration. Figure 7.3 shows the same data sets for three different cell types *in vitro* exposed to sonolytic ultrasound while contained in a rotating (200 rpm) exposure vessel. The top panel shows the usual decline in *relative* cell lysis with increase in cell density for each cell type and the bottom panel shows, for the same cell lines, that the total number of lysed cells actually increases with increase in hematocrit. The apparent reasons for the decrease in relative ultrasound-induced cell lysis with increasing hematocrit are that (1) the extent of cell lysis does not increase in direct proportion to cell concentration and (2) the overall sensitivity of the assay for ultrasound-induced cell lysis diminishes as cell concentration increases. The decrease in relative cell lysis with increasing cell concentration gives the impression that “significant” levels of hemolysis do not occur at high cell densities and therefore that hemolysis in whole blood is unlikely. This impression now appears to be incorrect. Greater total ultrasound-induced cell lysis occurs at high than at low cell concentrations although the relative fraction of cell lysis is substantially lower at high cell concentrations, as discussed more

fully by Brayman *et al.* (1996c). This aspect of ultrasound-induced cell lysis needs considerable additional study. For example, it is clear from visual inspection of the data in Figure 7.3 (top panel) that there is considerable difference in sensitivity of the three cell types to ultrasound (1 MHz, CW, 5 to 8 W cm⁻²) and that total cell lysis (bottom panel) is maximal at cell concentrations at which relative cell lysis is minimal. This latter result suggests that, at least within a cell type, total cell lysis is limited by the distances separating randomly distributed cells and cavitation nuclei, suggesting, in turn, that cell-to-cell separation distance may be a unifying parameter for comparing the results across cell types. The evidence in support of this postulate is indirect, and is based on the observation that for three cell types, with each type having a significantly different average cell volume from that of the other two, the amount of ultrasound-induced cell lysis appears to “level off” once a critical cell concentration is reached. In other words, the ultrasound-induced cell lysis becomes independent of cell concentration, an observation consistent with the formation of cellular aggregates around bubbles and consequent suppression of bubble activity (Nyborg and Miller, 1982a; 1982b). A plot of ultrasound-induced cell lysis data as a function of cell separation distance shows that the former increases as the latter decreases ($r = -0.78$, $p \sim 0.0003$).

7.2.3.3 Ultrasound Contrast Agents. Brayman *et al.* (1995) undertook a series of experiments in which blood (1 to 40 percent hematocrit) was infused with a clinically relevant concentration of Alunex[®] echo contrast medium (35 $\mu\text{L mL}^{-1}$) and exposed for 1 min to 1 MHz ultrasound with a pulse duration of 1 ms and a *PRF* of 20 Hz. Statistically significant cell lysis was observed at all hematocrit values, the fraction of lysed cells diminished with increasing hematocrit, but the total number of cells lysed per sample was nearly constant over the range of 5 to 40 percent hematocrit; a 40 percent hematocrit is approximately equivalent to that of whole blood. These results suggest that with large numbers of cavitation nuclei it may be possible to cause ultrasound-induced effects on cell suspensions even at relatively high cell densities.

Holland and Apfel (1990) have assayed for inertial cavitation thresholds using a “passive” broadband receiver to detect scattered emissions from acoustically activated, encapsulated bubbles (the term “encapsulated” refers to the shell of albumin or other material used to stabilize the gas within the bubble), specifically, Alunex[®], a pulse-echo contrast agent (Bleeker *et al.*, 1990). For cavitation activity in water or in an ethylene glycol mixture, there was a modest increase in the threshold acoustic pressure with increase in

ultrasound frequency from 0.757 to 2.3 MHz. When the water was nucleated with an approximate eight percent solution of Alburnex®, the threshold acoustic pressure for acoustic cavitation was about a third to a half (roughly between 0.5 and 0.6 MPa) of that needed to cavitate water. The addition of 0.6 to 1.6 percent of red blood cells did not affect the cavitation threshold of a saline solution. Holland *et al.* (1992) exposed diluted suspensions of Alburnex® to pulsed ultrasound fields from two diagnostic units, one operating at 2.5 MHz (2.83 kHz *PRF*), the other at 5 MHz (5 kHz *PRF*) with either one (M-mode) or four (Doppler) acoustic cycles per burst. Maximal negative acoustic pressures were 1.3 and 1.2 MPa, respectively. An approximate cavitation threshold was established for the 2.5 MHz exposures at 1.1 MPa, and no cavitation was detected at 5 MHz at a peak negative pressure of 1.2 MPa.

It has been recognized for many years that thresholds for cavitation increase at frequencies above 1 MHz (Section 5) (Flynn and Church, 1988). Hill and Joshi (1970) noted a marked increase in the threshold for cavitation effects with increasing frequency up to about 4 MHz. Miller and Thomas (1993b) used a rotating exposure vessel (60 rpm) to study the effect of 0.745 to 2.95 MHz ultrasound on red blood cell lysis and hydrogen peroxide production. Cell lysis required a relatively brief exposure period (15 s) relative to that for H₂O₂ production (15 min) for detection. Nonetheless, it was found that the ultrasound-pressure threshold for an effect increased “roughly” in approximate proportion to increasing frequency. For example, the acoustic pressure amplitude thresholds for hemolysis at 0.745 and 2.17 MHz were about 0.2 and 0.6 MPa, respectively. This diminishing role for cavitation as frequency is increased represents an important consideration for the safety of diagnostic ultrasound, because many units operate at 3.5 MHz or above, while echocardiography in adults is usually at 1.3 to 2.5 MHz.

7.2.3.4 Viscosity of the Medium. Carstensen *et al.* (1993) reported that ultrasound-induced cell lysis was diminished with increase in viscosity of the suspension medium (produced by adding Ficoll), with all other factors remaining the same. The amount of ultrasound-induced cell lysis was markedly reduced by an increase in viscosity of the medium from 1 to 5×10^{-3} Pa s (1 to 5 cP). This observation supported an inertial cavitation mechanism as causing ultrasound-induced cell lysis since such an increase in viscosity would have only a marginal effect on shear forces associated with bubble translation but a very marked effect on inertial cavitation in that it would markedly increase its threshold.

7.2.3.5 Multicellularity. Multicell spheroids are ball-like aggregates of loosely-associated cells *in vitro*, often with large (relative to that occurring in normal tissue architecture) intercellular spaces between and among the loosely coalesced cells. These spaces may serve as “internal” sites (containing gas nuclei) for ultrasound-induced cavitation damage. Conger *et al.* (1981) noted cell killing and detachment from spheroids exposed to therapeutic, but not diagnostic, ultrasound devices. Sacks *et al.* (1983), using a rotating polystyrene test tube exposure vessel and multicell spheroids, noted that much cellular damage occurred on the periphery of the spheroid, though there were also localized regions of cellular damage inside the spheroid. Since cell damage was noted inside the spheroid, it seems likely that there were stabilized gas bodies within the spheroid which became activated with the application of acoustic waves. The data were interpreted as suggesting the intercellular occurrence of ultrasound-induced damage, probably through a cavitation mechanism.

7.2.3.6 Gas Content of the Medium. Environmental factors within the exposure vessel can greatly affect the occurrence of inertial cavitation. For instance, Kondo and Kano (1987; 1988) reported that bubbles comprised of diatomic gases produce chemical reactions more readily in an ultrasound field than those containing triatomic gases. Kondo and Kano (1988) reported that for 1 MHz CW ultrasound exposures (5.8 W cm^{-2}) the effectiveness of various gases in yielding iodine (an indication of inertial cavitation) from an insolated aqueous medium was $\text{O}_2 > \text{Ar} > \text{N}_2 > \text{N}_2\text{O} \approx 0$, but for cell killing the order was $\text{O}_2 = \text{Ar} = \text{N}_2 > \text{N}_2\text{O} \approx 0$. The results suggest that the different amounts of free radicals produced by the ultrasound are not directly related to cell killing. There were two assays for cell killing: (1) immediate lysis and (2) reduced clonogenicity, *i.e.*, decreased capability of a cell to proliferate and form a colony. The presence of cysteamine, an intracellular scavenger of free radicals, inhibited the decrease in clonogenicity of surviving cells but had no effect on immediate cell lysis. The collective results indicate that ultrasound-induced cell lysis is primarily a result of mechanical stress from cavitation, but the decrease in clonogenicity is due to the effectiveness of ultrasound-generated free radicals.

7.2.3.7 Temperature. Temperature of the medium is another important factor in *in vitro* experiments. Temperature history is particularly important for the gas content of the medium. Armour and Corry (1982) noted that warming to 37°C a previously cooled (3°C) suspension prior to exposure resulted in supersaturation of the medium and enhanced ultrasound-induced cellular effects.

Miller and Williams (1992) confirmed this influence of gas content by gassing or degassing media at constant exposure temperature; supersaturation increased lysis and undersaturation decreased lysis relative to the normal condition of atmospheric air saturation.

Exposure temperature is important in regard to the sensitivity of the cells to ultrasound. Several workers have studied the effect of hyperthermia on cell killing *in vitro* after a report of enhanced effects by Li *et al.* (1977). ter Haar *et al.* (1980; 1988) found a significant nonthermal component to cell killing from heat and ultrasound exposures *in vitro*. It is difficult to ascertain the role of cavitation in all such studies, but Dunn (1985) noted that heating combined with simple bulk acoustic streaming flow for long periods provides an alternative explanation of the synergistic effects (Section 3.3.4). Kondo and Kano (1987) tested the involvement of cavitation in the enhancement of hyperthermic mouse L cell killing *in vitro* by ultrasound and concluded that some nonthermal mechanism other than cavitation was indicated since the effect occurred even with nitrous oxide saturation, which was initially thought to suppress cavitation. Subsequent research showed an equal amount of ultrasound-induced hemolysis whether argon or N₂O was dissolved in the saline solution containing the cells (the effect was attributed to cavitation), but the former resulted in the production of lots of free radicals whereas the latter did not (Kondo *et al.*, 1989). They proposed the use of ultrasound with N₂O for cell disruption without free radical damage; the N₂O cavitation is assumed to involve mechanical stresses without the high transient temperatures obtained with argon. The interaction of the effects of heat and ultrasound are therefore quite complicated, and careful interpretation is required.

7.2.3.8 Superposed Ionizing Radiation or Chemotherapeutic Agents. Several reports deal with the combined action of ionizing radiation or chemotherapeutic agents and ultrasound. This research complements the work on combined ultrasound and hyperthermia regimens in the search for enhanced therapeutic performance by combined treatments. Early work was reviewed in a previous report (NCRP, 1983). A modest enhancement of gamma-ray effects was found for 2.6 MHz ultrasound (Loverock *et al.*, 1990). Recently, several authors have noted an enhancement in the effects of adriamycin by ultrasound. Saad and Hahn (1989) found enhanced cytotoxicity with combined 2 MHz ultrasound exposure in a nonrotating chamber and 1 mg mL⁻¹ adriamycin on CHO cells *in vitro*. Loverock *et al.* (1990) and Harrison *et al.* (1991) found similar effects for some specific conditions and cell lines. Yumita *et al.* (1990) and Umemura *et al.* (1990) reported a synergistic effect of 1.92 MHz ultrasound

and hematoporphyrin on a sarcoma cell line. Sonoluminescence was produced in separate experiments with similar conditions, indicating that free radicals produced by cavitation were involved.

7.3 Effects on Viable Cells

7.3.1 *Structure and Function*

The most thoroughly studied effect of ultrasonic cavitation *in vitro* is cell lysis. However, sublethal effects can also be important from a biological viewpoint. Sublethal effects might occur, for example, from near-misses of bubbles, from released cell lysate or from the action of sonochemicals remote from the cavitation site. Reports of sublethal effects fall into three general categories: (1) changes in morphology, (2) membrane transport effects, and (3) growth rate reductions of cells surviving the initial exposure.

7.3.1.1 *Cell Morphology.* Changes in the surface morphology of BALB/c 3T3 cells were reported by Liebeskind *et al.* (1982). The changes persisted in culture for many days over apparently many cell generations. Liebeskind *et al.* (1982) used an exposure vessel arrangement similar to that shown in Figure 7.1, No. 4, in which the transducer is aligned with the tube's axis, with the ultrasound beamed down into the tube. An Ekoline-20 diagnostic ultrasound unit provided the ultrasound. The exposure parameters were: 2.2 MHz center frequency, 35 W cm⁻² SPTP intensity, 1 MPa p_r, 200 Hz *PRF*, 3 μs pulse length, and 30 min exposure duration. However, more recent work by Miller *et al.* (1990), employing BALB/c 3T3 cells and comparable ultrasound exposure conditions (2.2 MHz, 3 μs pulse duration, 200 Hz *PRF*, 30 min exposure duration) and assayed blindly for cell morphology and motility, failed to confirm this earlier report. In a test of the procedure, a positive control (1 to 4 Gy x rays) yielded significant alterations for cell motility and morphology.

7.3.1.2 *Electrical Excitability and Phagocytic Activity.* The electrical excitability of myelinated frog sciatic nerve *in vitro* was reported to be modified by exposure to 500 μs bursts of ultrasound (Mihran *et al.*, 1990). While some cavitation may have occurred, evidence was given which indicates that a noncavitation mechanism was primarily responsible for the effect (Section 3).

Ultrasound exposure *in vitro* can alter the permeability or transport activity of cell membranes, a class of effects reviewed by Dinno *et al.* (1989a; 1989b). For example, Mortimer and Dyson (1988) exposed chick 3T3 fibroblasts to 1 MHz therapeutic ultrasound (0.25

to 1.5 W cm^{-2} SPPA, with a 2 in 8 ms “on-off” regimen for up to 20 min) which resulted in a maximal 18 percent uptake of calcium after a 5 min exposure for the 0.5 W cm^{-2} SPPA regimen. It appears that this increase occurred in viable cells because the calcium level returned to normal 10 to 20 min post exposure. Some such effects are closely associated with cell lysis caused by cavitation and may represent a sublethal permeability effect (Fahnestock *et al.*, 1989). Young and Dyson (1990) reported that CW, 0.5 W cm^{-2} SATA, 0.75 and 3 MHz ultrasound-exposure of macrophage suspensions resulted in a “conditioned” medium which could stimulate growth of fibroblasts. This finding supports the idea that release of substances from macrophages could promote a therapeutic healing effect of ultrasound.

Frog skin provides a convenient model system for the study of membrane effects from cavitation. Dinno *et al.* (1989a; 1989b) found that electrical parameters were modified and total ion conductance increased by 1 MHz ultrasound. The effects were probably mediated by inertial cavitation, since free radical scavengers such as cysteamine reduced the effects (Al-Karmi *et al.*, 1994; Dinno *et al.*, 1993). Coble and Dunn (1976) observed that the MP and SCC from ultrasound-exposed frog skin *in vitro* responded (1) in opposite directions and with different time courses of response with the interior skin surface facing the transducer, and (2) reversed response when the direction of the ultrasound exposure (1 MHz, 5 to 100 W cm^2 , 0.5 to 3 s exposure duration) was with the exterior skin surface facing the transducer. The ultrasound exposures occurred under steady-state temperatures, thus obviating a thermal mechanism, and the skin bathing medium was degassed, thus mitigating inertial cavitation. However, Coble and Dunn (1976) have given reasons to believe that such effects can be produced in the absence of acoustic cavitation, and hypothesized that mass transport aspects (microstreaming, radiation force, etc.) may be the causative factor.

Studies of phagocytic activity of murine peritoneal macrophages by Prohaska *et al.* (1992a; 1992b) indicate that no effect occurs in surviving cells after exposure to 1 MHz ultrasound (0.28 to 10 W cm^{-2} , 5 to 10 min exposure duration) or to 2.25 MHz pulsed ultrasound (50 percent duty cycle, 10 W cm^{-2} SPPA, 5 to 30 min exposure duration). For treatment, the cells were contained in polystyrene test tubes, oriented vertically and at right angles to the transducer. The tubes were rotated during treatment. There was a decrease in cell viability with increase in ultrasound intensity or exposure duration. However, there was no apparent degradation of the immunologic competence of surviving cells.

7.3.1.3 Growth. The study of ultrasound-induced effects on growth involves two general types of assessments. The first is the ascertainment of whether an apparently viable cell is capable of proliferation, *e.g.*, the production of a colony. For instance, the plating efficiency of a population of cells can be determined by noting the fraction of cells which produce colonies. The second assessment involves determination of whether a test population of cells proliferates at a rate comparable to or different from that of a control population.

A threshold for alteration in plating efficiency of about 1 W cm^{-2} SPTA was reported for V-79, HeLa and mouse L cells by Fu *et al.* (1980), Kaufman and Miller (1978), and Clarke and Hill (1970), respectively, in which the exposure vessel was rotated during ultrasound exposure. Without tube rotation, there was no effect. The decrease in plating efficiency observed by Kaufman *et al.* (1977) was correlated with an increase in cell lysis. Growth rate changes in the ultrasound-exposed cells were apparent only shortly after the ultrasound exposure; the growth rate returned to steady-state control levels by 36 h post exposure (Kaufman and Miller, 1978). A subsequent study showed that the apparent initial growth reduction was partially the result of increased cell lysis (Ciaravino *et al.*, 1981c), *i.e.*, that cell lysis could be immediate or, for some cells, delayed. Additional studies in this area are summarized in NCRP Report No. 74 (Section 8.4 in NCRP, 1983) and generally indicate the close association of inertial cavitation with alterations in survival and growth. For example, Chapman *et al.* (1980) showed that the sensitivity of thymocytes to ultrasound was inversely related to ultrasound frequency, with cell survival and viability altered more by a lower (0.75) than by a higher (3 MHz) ultrasound frequency at comparable acoustic pressure. This result is consistent with an inertial cavitation mechanism (Flynn and Church, 1988). Additionally, the sonochemicals produced as a result of inertial cavitation have been demonstrated to be biologically effective. Armour and Corry (1982) reported that cells exposed to ultrasound in the presence of a radical scavenger which penetrated cells marginally reduced the rate of lethality of intact cells.

Fu *et al.* (1979) showed a similar result, but noted that the scavenger had no effect on cell lysis, a result consistent with the expectation that cell lysis is the result of the purely mechanical action of inertial cavitation.

7.3.2 Effects on Deoxyribonucleic Acid

The evidence for ultrasound-induced genetic, cytogenetic and macromolecular effects is less certain than that for cell lysis. For instance,

reports exist of ultrasound-induced increases in sister chromatid exchanges (Barnett *et al.*, 1988; Liebeskind *et al.*, 1979a; Stella *et al.*, 1984), but the majority of reports are negative (Ciaravino *et al.*, 1986; Miller, 1985b; Miller *et al.*, 1991d). Additionally, specific attempts to replicate certain claimed ultrasound-induced effects have failed [*e.g.*, compare Barnett *et al.* (1983; 1988) and Miller *et al.* (1989c); Liebeskind *et al.* (1979a) and Ciaravino *et al.* (1985); Liebeskind *et al.* (1979b) and Harrison and Balcer-Kubiczek (1989), Zhu *et al.* (1991)]. For example, Liebeskind *et al.* (1979a) exposed human lymphocytes *in vitro* to the ultrasound fields of two different diagnostic ultrasound units, a Reflectoscope or an Ekoline-20, and reported an increase in sister chromatid exchanges with the ultrasound exposure regimens. The former unit's ultrasound parameters were 2 MHz center frequency, 2 μ s burst duration, 700 Hz *PRF*, and 4 W cm⁻² SATP while the latter's were 2.2 MHz center frequency, 2 μ s burst duration, 200 Hz *PRF*, and 49 W cm⁻² SATP. Ciaravino *et al.* (1985) used three blood donors in attempting to replicate the results of Liebeskind *et al.* (1979a), including the same ultrasound equipment as used by Liebeskind *et al.* (1979a). The slides were coded and sent out for independent analyses by three different scorers. None of the evaluations indicated a statistically significant increase in the frequency of sister chromatid exchanges with ultrasound exposure. For genetic effects, it is clear that most reports are negative (Thacker, 1985a; Wegner and Lang, 1986).

It is not easy to understand such disparate results. On the one hand, the positive reports may have resulted from experimental artifacts. On the other hand, because of the high variability in the occurrence of inertial cavitation, it is possible that the negative studies simply did not include those important but apparently subtle conditions conducive to observing an effect. Of course, without a reproducible effect it is very difficult to study a mechanism of action.

More recently, however, mechanistic studies aimed at finding effects have revealed some potential for genetic effects under *in vitro* exposure conditions. Since inertial cavitation is reported to produce long-lived free radicals (Kondo and Kano, 1988; Riesz and Kondo, 1992), it appears that mechanisms are present which can directly and indirectly affect cells. A claim of increased mutation frequency (Kaufman, 1985) in mammalian cells surviving initial ultrasound exposure has been independently confirmed (Doida *et al.*, 1990; 1992b). There are also reports of altered macromolecular synthesis (Dooley *et al.*, 1984; Harvey *et al.*, 1975; Liebeskind *et al.*, 1979b). Induction of single strand breaks in cellular DNA by low level pulsed ultrasound has been reported by Pinamonti *et al.* (1986), but this could not be reproduced (Miller *et al.*, 1989a). However, at higher exposure levels involving cavitation, strand breaks were readily

detected. These breaks appear to reside primarily in nonviable cells (Miller *et al.*, 1991b). Strand breaks could also be produced in viable cells by adding them to medium subjected to prolonged cavitation (Miller *et al.*, 1991c), and this appeared to be mediated by the cavitation-induced production of H_2O_2 . This DNA effect can be revealed in cells surviving direct exposure to ultrasound by sufficiently sensitive methods. Miller *et al.* (1995b) have used the single cell gel electrophoresis assay (also called the “comet assay”) to measure DNA damage in suspensions with two to five percent cell survival after 2.17 MHz ultrasound exposure at 0.82 MPa. The cells could repair some of the breaks, an indication of viability. The effect was correlated with the hydrogen peroxide production (used as a cavitation dosimeter) but was not eliminated with the addition of catalase, which degrades peroxide, indicating that the DNA damage was not due to the action of H_2O_2 alone.

7.3.3 Membrane Permeabilization

There is a variety of mechanical and chemical techniques useful for inserting large molecules into cells; these techniques include direct microinjection, liposome-, detergent- or virus-mediation, the use of scrape loading, cell membrane permeabilization agents, and electroporation (Hersey and Perez, 1990). The purposes of these techniques is to introduce substances into the cell which otherwise would not normally pass through the cell membrane. For example, in direct microinjection, an extremely thin glass needle attached to a micromanipulator is used to puncture the cell membrane and deliver a specific chemical to the cytosol (see, *e.g.*, Graessmann and Graessman, 1976). In scrape loading procedures, cells which are attached to a culture vessel surface are scraped by a “rubber policeman” from the surface while in the presence of a specific chemical marker; the “scraping” results in openings in the cell membrane, which allows for penetration of the marker (see, *e.g.*, Fechheimer *et al.*, 1986). For cells in suspension, electroporation can accomplish the insertion of specific markers into the cell (see, *e.g.*, Bartoletti *et al.*, 1989; Glogauer and McCullogh, 1992; Lambert *et al.*, 1990). The cells are exposed very briefly to an electric field large enough to exceed the dielectric strength of the cell membrane; transient pores are formed, usually at the polar ends of the cells (relative to the direction of the applied electric field), and substances can then pass through these pores and be incorporated into the cytosol. Liposomes have been used to permeabilize intact cell membranes to facilitate the introduction of proteins into living cells (Hall *et al.*,

1979). Lee *et al.* (1996) reported that laser-induced shear waves can be used to permeabilize cell membranes as evidenced by a transient intracellular increase in propidium iodide. The uptake diminished rapidly within 80 s post-laser exposure, thus indicating the transient duration of membrane permeabilization with this procedure. The process of membrane permeabilization holds promise for the direct introduction of specific hereditary-type chemicals (*e.g.*, specific DNA sequences) into cellular genetic materials, a process commonly referred to as “gene therapy” (see, *e.g.*, Delius *et al.*, 1995).

Ultrasound can also be used to insert large molecules into cells. Zhang *et al.* (1991) were among the first to report the use of ultrasound in achieving direct gene transfer to living cells. Leaf segments *in vitro* of tobacco were placed in 3 mL of a buffer containing 20 mg mL⁻¹ pBI121.1 DNA and 40 mg mL⁻¹ salmon sperm DNA. Details of the ultrasound exposure are sparse except for the authors' notation that the ultrasound was pulsed, of 0.5 W cm⁻² intensity and 30 min duration. After insonation, the cells were assayed histochemically for the presence of beta-glucuronidase activity. After one month of culture, in which there was growth on a selective medium containing 100 mg L⁻¹ kanamycin, the controls had no explants with regenerating shoots; the leaf segments exposed to ultrasound in the presence of the extracellular DNA had 60 percent (54 of 90 treated explants) which produced shoots. Joersbo and Brunstedt (1992) used a tapered microtip to expose sugar beet and tobacco protoplasts to 20 kHz ultrasound (0.5 to 15 W cm⁻²; 500 to 900 ms exposure duration) in the presence of plasmid DNA. Cells were then assayed for the expression of the introduced gene coding for the enzyme amphenicol acetyltransferase. In the absence of ultrasound exposure, the percent of cells expressing the gene were 0.03 and 0.02 for tobacco and sugar beet, respectively. In the presence of ultrasound, *e.g.*, 1.6 W cm⁻², 800 ms exposure duration, the expression percentages were 0.13 and 0.21, respectively. The authors hypothesized that ultrasound-induced small breaks in the plasma membrane were responsible for the increased expression.

Permeabilization of the cell membrane can also occur with specific exposures to ultrasound. Gambihler *et al.* (1994) exposed L1210 cells *in vitro* in the presence of fluorescence-labeled dextran (3,900 to 2,000,000 molecular weight) to focused shock waves generated by an XL1 lithotripter (Dornier Medizintechnik, Germany) operated at 25 kV, 60 pulses per minute, for a total of 250 shock waves; the exposure system was as shown in Figure 7.1, No. 2. Cells exposed to the shock waves had a considerable increase in fluorescence over the controls. Confocal laser microscopic analysis indicated for control cells diffuse, vesicular localizations of the dextran, and for lithotripter-

exposed cells an intracellular distribution apparently involving vacuole-like structures but without nuclear involvement. Delius *et al.* (1995) subsequently suggested that lithotripter shock waves could be used for gene therapy of *in vivo* tumors, noting the shock waves can be highly focused to specific intrabody sites, are already an established modality with a low rate of side effects, and are noninvasive. Kim *et al.* (1996) exposed primary rat fibroblasts and chondrocytes *in vitro* to 1 or 3 MHz CW or pulsed wave ultrasound (*PRF* of 25, 50, 100, 150 and 200 Hz), using an exposure system somewhat like that shown in Figure 7.1, No. 7. During the sham/ultrasound exposure period, the cell suspension medium contained two different types of plasmids, one having 6,821 and the other having 3,854 base pairs. Transfection of individual cells was monitored by phase microscopy. The largest number of transfected cells occurred after 20 to 30 s exposures at 0.4 MPa or after 20 to 60 s at 0.3 MPa; the largest number of transfected cells occurred with exposure regimens which killed approximately 50 percent of the initial cell population. Because there were reductions in transfection with the 3 MHz regimens (zero percent) relative to those obtained with 1 MHz (2.4 percent), the authors suggested that the occurrence of acoustic cavitation was essential to the ultrasound-induced transfection process.

Johannes and Obe (1997) exposed CHO cells *in vitro* to the sound field of an ultrasonic cell disruptor (20 kHz, 25 W output) and then noted an increase in chromosomal anomalies in cells permeabilized with two endonucleases, the higher the concentration of bathing endonuclease the higher the frequency of aberrations. Bao *et al.* (1997) exposed CHO cells *in vitro* to 2.25 MHz ultrasound in the presence of Albunex® (to facilitate nucleation of the medium bathing the cells) and noted an increase in cellular uptake of large fluorescent dextran molecules and also a transfection with a reporter plasmid, relative to that obtained with sham-exposed cells. The effects did not occur in the absence of Albunex®, indicating that sonoporation under the conditions of the experiment is related to the occurrence of cavitation. The uptake of the fluorescent dextran was a relatively sensitive test for membrane damage, because of the zero background in sham-exposed suspensions. Statistically significant numbers of cells (about 1.5 percent) were fluorescent after exposure to 0.1 MPa for 1 min with 60 rpm rotation.

7.4 Bioeffects and Lithotriptors

Extracorporeal shock wave lithotripsy has gained acceptance as a treatment for kidney stone diseases. The treatment involves widely

spaced shock waves of high acoustic pressure amplitude, which are capable of causing a variety of nonthermal effects. Coleman and Saunders (1993) have reviewed the physical properties and biological effects of the high amplitude acoustic fields used in lithotripsy.

There are two general classes of lithotriptors, the ESWL and endoscopic lithotriptors. Both produce shock waves with rise times of many nanoseconds and durations of a few microseconds. There can be compressional and rarefactional components to the pressure wave form, and often it is asymmetric. Coleman and Saunders (1993) summarize the pressures (p_+ , p_-) and rise times of the different types of commercial shock wave sources, and Church (1989) provides a theoretical analysis of the response of bubbles to an ESWL-generated asymmetric pressure wave form in which the ratio of the peak positive (p_+) to the peak negative (p_-) pressure is approximately six. The shock waves from lithotriptors generally have most of their energy in the decade below 1 MHz.

Lithotripter exposures have also been used for studies of cell lysis *in vitro*, including those of multicell spheroids. In general, lithotripter studies parallel the ultrasound studies discussed above, and the effects are normally attributable to cavitation. Inertial cavitation is expected to occur if gas nuclei are present because of the very substantial instantaneous pressures associated with the pulse. Coleman *et al.* (1993) undertook contour pressure plots of lithotripter pulses in a tank of water and also made photographic analyses of sonoluminescence. While there was some variability in the results, high pressure regions generally coincided with regions of relatively intense sonoluminescence and the greatest amount of cell lysis *in vitro*. Church (1989) described theoretical transient behaviors of bubbles exposed to lithotripter fields. His investigation indicated that a stabilized bubble undergoes an immediate compression in response to the acoustic pressure of the sound field. The bubble subsequently undergoes rapid expansion, followed by inertial collapse. Bubbles may also pulsate ("ring") several times after the primary event. Because the acoustic pressures are so high during a lithotripter pulse, it is reasonable to expect that nearly all cavitation nuclei would become inertially active. Additionally, Church (1989) hypothesized that the violent collapse of microbubbles in the focal area of an extra corporeal shock wave lithotripter, because of the extremely high temperatures generated during bubble implosion, can generate biologically damaging far ultraviolet and soft x-ray photons. Vona *et al.* (1995) provided partial support for Church's hypothesis by observing: (1) the presence of near-ultraviolet emissions (~ 250 nm) from lithotripter shocks ($p_+ = 43$ MPa, $p_- = 9$ MPa) in water, and (2) the occurrence of photonic emissions from a

lithotripter-exposed scintillation cocktail [a chemically engineered fluid designed to capture the electrons emitted during radioactive decay and to re-emit them (at lower-energy), such that they can be detected by photomultiplier tubes].

Brauner *et al.* (1989) showed that lithotripter fields eroded the periphery of multicell spheroids but that the cellular damage in agar or gelatin, during exposure to ultrasound, resulted in spheroids being comparable to controls. Sacks *et al.* (1983), exposing multicell spheroids to CW 1 MHz ultrasound exposures in aqueous media in tubes which were rotating, noted areas of external and internal damage in spheroids. Brummer *et al.* (1989) reported a relationship between lithotripter shock wave number and cell damage; the higher the number of shocks, the greater the damage. Gambihler *et al.* (1990) showed that higher shock wave amplitudes were more effective than higher shock wave numbers in affecting cell integrity. The gases oxygen and argon enhanced free radical generation, but nitrous oxide and carbon dioxide reduced free radical generation by lithotripter exposure, which is similar to the effects of these gases for ultrasonic cavitation in CW ultrasound fields (Gambihler and Delius, 1992). The lysis of suspended cells was relatively unaffected by the different gases, which indicates that lysis is mostly the result of the physical action of the cavitation bubbles. Some activity of free radicals may be indicated, however, since Vitamin E appears to reduce the lithotripter-induced cellular damage (Suhr *et al.*, 1994). Like ultrasonic cavitation, the effect of shock waves depends on the experimental set-up (Smits *et al.*, 1991), and cells imbedded in gelatin sustained no detectable cytotoxicity.

Lithotripter treatments of up to 2,000 shock waves reduced the viability of cells in suspension (Randazzo *et al.*, 1988). Carcinoma cells appeared to be more sensitive than normal cells. Prat *et al.* (1991; 1993) were able to produce complete inhibition of cell growth with 1,000 shock waves administered together with gelatin-stabilized bubbles. Steinbach *et al.* (1992) exposed human prostate carcinoma cells and multicell spheroids *in vitro* to electromagnetically generated ultrasound shock waves ($p_+ = 20$ to 60 MPa, $p_- = 5$ to 10 MPa, 100 to 400 pulses) and noted a larger fraction of cell lysis in aerated relative to nonaerated medium, and a variety of intracellular damages to spheroids, including cell membrane permeabilization, and altered vimetin structure, mitochondrial MPs and nuclear membranes. Prat *et al.* (1994) were also able to show an enhanced effectiveness of the chemotherapeutic agent fluorouracil with shock wave exposure of suspensions with stabilized bubbles. This beneficial anti-tumor effect was also observed in animals infused during lithotripter treatment with a suspension of stabilized bubbles and tumor cells,

which indicates some applicability of *in vitro* findings to the *in vivo* situation (Prat *et al.*, 1993).

Miller *et al.* (1996) exposed CHO cells to the focal zone of a spark-gap lithotripter and noted significant cell lysis and significant DNA damage in surviving cells. The spark-gap discharge generated a bright flash of light in addition to the shockwaves. When the shock wave was administered in the presence of a sheet of black plastic to mitigate light transmittance to the sample, cell lysis remained high but DNA damage was not present. Thus, the authors were able to show that the DNA damage was caused by the flash of light from the spark gap, not by the shockwaves. The shockwave-induced cavitation produced detectable hydrogen peroxide, but the amount of this sonochemical was insufficient to cause detectable strand breaks in surviving cells (Miller and Thomas, 1996b). A positive control regimen, involving ultraviolet exposure of cells, yielded the expected high amount of DNA damage. In one regimen, simultaneous treatment of lithotripter-exposed cells with novobiocin, an inhibitor of the preincision steps of nucleotide excision repair, resulted in high cell lysis but no DNA damage. In another regimen, simultaneous treatment with aphidicolin, an inhibitor of the enzymes dealing with resynthesis of the excised DNA, increased the amount of ultrasound-induced damage to DNA. The authors cautioned that the ultraviolet light from therapeutic spark-gap lithotripters might be sufficient to cause DNA damage in the skin cells of exposed patients.

7.5 Summary

The possibility for manipulation of the environment of cells *in vitro*, and of their numbers, provides the investigator with much needed tools for studying basic mechanistic principles of interaction between ultrasound and cells. It has been shown that a wide variety of cellular effects can be induced by *in vitro* nonthermal exposures to ultrasound; a major mechanism is cavitation. To be effective, cells and acoustically activated bubbles must generally be brought into close physical proximity. The action may be mechanical or chemical. When inertial cavitation is involved, highly reactive chemicals may be produced that have the potential to affect cells. The sensitivity of cavitation to details of experimental conditions may help to explain the variability of results among different laboratories for biological endpoints such as sister chromatid exchange and cell transformation.

The extent to which the physical and chemical processes that occur in *in vitro* experiments are biologically effective during clinical

exposures is yet to be determined. For many tissues, the activity of any bubbles that might be present would be highly restricted by surrounding structures. However, the volume of bulk fluid present in some *in vivo* environments (e.g., the amniotic sac, bladder and blood vessels) present physical conditions somewhat analogous to those obtainable with *in vitro* systems. While fluids in the body normally appear to possess few gas microbubbles, the emerging use of gas-containing pulse-echo contrast agents as diagnostic tools may change the *in vivo* environment to one with many potential sites for cavitation activity such as occurs in *in vitro* experiments.

akusher-lib.ru

8. Bioeffects of Acoustic Cavitation in Mammalian Tissues

8.1 General Evidence for the Occurrence of Cavitation in Tissues

There is no direct evidence, at present, that cavitation occurs in the tissues of patients during routine diagnostic examinations, but a few studies with laboratory animals demonstrate that cavitation can be produced in mammalian tissues at high pressure amplitudes and relatively long pulses or CW ultrasound. In this Section, cavitation includes the mechanical response of a gaseous cavity in tissue to acoustic stress. All known effects of ultrasound *in vivo* that depend upon the presence of gas bodies in the tissue are discussed here.⁵

8.1.1 Studies of Brain and Liver

Perhaps the first quantitative observation of the effects of ultrasonically induced cavitation *in vivo* in a functioning mammal is that of Fry *et al.* (1970) and Dunn and Fry (1971) in which pulses of 1 MHz ultrasound of a few milliseconds duration were focused transdurally into the brain of a cat, under deep anesthesia. The skull bone in the propagation path had been removed. Threshold lesions had a qualitatively different histological appearance at acoustic intensities above approximately $2,000 \text{ W cm}^{-2}$ (pressure amplitude 8 MPa) than below that level. Whereas, at the lower levels (and longer pulse durations), where heating produced a lesion with a well defined boundary, the lesions observed above 8 MPa, in contrast, showed gross tissue disruption. At lower levels, white matter was found to exhibit the lowest threshold and the lesion exhibited demyelination

⁵When intensities and corresponding acoustic pressures are cited, the relationship assumed is that between the time-averaged intensity and the pressure amplitude in a plane traveling wave in water. For example, pressure amplitudes of 0.1 and 1 MPa correspond to intensities of 0.33 and 33 W cm^{-2} , respectively.

of the axons. Gray matter was found to be more resistant. Glial structures and the blood vessels were found to be most resistant to ultrasound. For threshold lesions, interruption of the blood supply did not occur. Although no formal cavitation detection apparatus was employed, a sharp audible “snap” at the high pressure amplitudes could be correlated with the diffuse nonthermal histological picture. Together with other evidence, this suggests that at high acoustic pressures the dominant mechanism for tissue damage was cavitation. The lesions attributed to cavitation had several distinguishing features. First, the tissue damage appeared immediately after the exposure, in contrast with thermal lesions, where approximately 10 min following ultrasonic exposure were required before histological evidence of the tissue alteration, detected by a variety of light microscopy staining methods, emerged. Second, cavitation lesions were not necessarily found at the transducer focal region, as they were for thermal lesions and as might be expected on the basis of the distribution of the acoustic pressures. Rather, the lesions occurred at interfaces between neural tissue and fluid-filled spaces, such as ventricles and blood vessels. Third, lesions associated with cavitation did not exhibit the tissue selectivity characteristic of the thermal lesions. This suggests that there are few, if any, cavitation nuclei (see Glossary and Section 4.2.1) in neural tissue, and there are more to be found at the boundaries of fluid-filled regions such as in blood vessels or in the ventricular system. The thresholds for lesions associated with cavitation quoted above refer to *focal* pressures associated with the observed damage. However, the damage frequently appeared at some distance from the focus.

Chan and Frizzell (1977) and Frizzell (1988) reported lesions, qualitatively similar to the cavitation lesions described above, in cat liver exposed to 3 MHz ultrasound at levels approximately the same as those used by Fry *et al.* (1970) in cat brain. The lesions exhibited irregular boundaries and homogenization of tissue structures within the lesion, whereas at lesser intensities associated with thermal events, the lesions occurred with well defined ellipsoidal boundaries.

Lele (1977; 1978) sought to correlate the detection of cavitation with histologically observed damage in the cat brain *in vivo* and in the liver *in vitro* by monitoring the harmonic (including subharmonic, a signal with half the frequency of the incident sound) and broadband noise for detecting, respectively, stable and inertial cavitation. The time-averaged energy from subharmonic signals increased monotonically with output levels up to focal intensities of nearly $1,500 \text{ W cm}^{-2}$ (7 MPa) and was observable at the lowest intensities used, *viz*, 100 mW cm^{-2} (0.05 MPa). However, the time-averaged output from the broadband noise detector was erratic

and noise was never observed below approximately $1,000 \text{ W cm}^{-2}$ (5 MPa). The subharmonic emission increased suddenly and markedly with the onset of noise emission, and the noise emission threshold was reduced if similar acoustic emissions had previously been observed. There was good correlation between the noise emission and gross tissue disintegration in the damaged zone, which is consistent with the studies described above. Recall that Fry *et al.* (1970) correlated the observation of an audible click with the occurrence of cavitation lesions. However, Lele found no correlation between subharmonic emission, which was presumed to indicate stable cavitation, and histological evidence of damage. Subharmonic emission was observed at intensities orders of magnitude below the threshold for histological damage. If lesions occurred in the absence of noise emission they were indistinguishable histologically from those produced by heat.

Vykhodtseva *et al.* (1995) reported that the thresholds for subharmonic emission from rabbit brain *in vivo* range from 13 to 9 MPa ($6,000$ to $3,000 \text{ W cm}^{-2}$), for pulse lengths ranging from 1 to $1,000 \text{ ms}$ (1.7 MHz), respectively. By applying multiple pulses at levels above the subharmonic threshold with relatively low pulse repetition rates, the investigators were able to produce nonthermal histological lesions. Furthermore, under exposure conditions above the subharmonic threshold but below the thresholds for histologically detectable lesions, they found evidence for a breakdown in the blood brain barrier, indicating subtle permeability changes from cavitation activity at levels too low to cause major damage to tissue structures.

8.1.2 Muscle

Cavitation in pork muscle *in vivo* was reported to have been detected by subharmonic emission during 75 W cm^{-2} exposure with CW ultrasound (Sommer and Pounds, 1982). Hynynen (1991) reported the sudden onset of subharmonic emission from the focal zone in dog muscle during hyperthermia procedures at intensities of approximately 300 W cm^{-2} (3 MPa) at 0.5 MHz and at approximately 800 W cm^{-2} (5 MPa) at 1 MHz. There was a corresponding marked increase in the rate of heating of the tissue, in the attenuation of sound in transmission measurements, and in the acoustic scattering when this occurred. Thresholds for the occurrence of these phenomena increased with frequency. The most sensitive of the three effects as indicators of cavitation was the abrupt increase in rate of heat generation. Temperature increments of the order of 40 to 60 °C were reported for 1 s exposures. All of the observations are consistent

with the occurrence of cavitation in tissue. A kind of hysteresis was observed in both temperature increments and subharmonic indications for cavitation. That is, cavitation appeared to occur at lower levels when the acoustic pressure was being reduced than when it was being increased.

Evidence of bubble growth *in vivo* during exposure to CW ultrasound at 0.75 MHz and at intensities above 80 mW cm^{-2} have been reported (ter Haar and Daniels, 1981; ter Haar *et al.*, 1982). In those studies, the hind legs of guinea pigs were exposed to ultrasound while an 8 MHz pulse-echo ultrasound system capable of detecting bubbles $10 \text{ }\mu\text{m}$ or larger in diameter was used for imaging. New echoes generated after the beginning of the radiation procedure were interpreted to be bubbles. The number of detected bubbles increased as the intensity was increased from 80 to 680 mW cm^{-2} (0.05 to 0.14 MPa). Equally important may be the observation that the number of bubbles detected in this way was suppressed by increased hydrostatic pressure. The threshold intensity for the formation of bubbles $10 \text{ }\mu\text{m}$ or larger in diameter during 10 min exposures was reported to be approximately 0.08 MPa (240 mW cm^{-2} SATP intensity, 2 ms pulse duration, 50 percent duty cycle) (ter Haar and Daniels, 1981; ter Haar *et al.*, 1982). The theory for rectified diffusion (Crum and Hansen, 1982a) (see also Section 4 of this Report) suggests that small cavitation nuclei (Section 4.2.1), if present, would grow to detectable size under the exposure conditions used in the experiments of ter Haar and Daniels. None of these studies involved tests for biological effects related to the presence of these ultrasonically generated bubbles, but the generation of bubbles large enough to be detected in this way is indirect evidence for the existence of cavitation nuclei in tissues. A recent study (Watmough *et al.*, 1991) demonstrated artifacts arising from bubbles on the specimen's skin that might be interpreted as bubbles within the tissue. The original investigators argue that their experimental design took these sources of artifact fully into account (Daniels and ter Haar, 1992).

A recent study by Leighton *et al.* (1990) failed to detect sonoluminescence *in vivo* in the human cheek exposed to ultrasound, with the ultrasound either directly applied to the cheek or *via* an intervening water-bag path. The source of ultrasound was a therapeutic instrument (Therasonic, Electro Medical Supplies) producing up to 2 W cm^{-2} (0.2 MPa) at 1 MHz CW. The volunteers experienced discomfort above the 2 W cm^{-2} exposure level. When the water bag was placed against the inner surface of the cheek, sonoluminescence was observed in the water, however, showing that absorption of sound by the cheek tissue was not preventing cavitation. The authors concluded that the lack of suitable cavitation nuclei (Section 4.2.1)

centers was the most likely cause for their failure to detect sonoluminescence, which is associated with inertial cavitation. As indicated by the findings of ter Haar and Daniels (1981) discussed above, and others discussed below, it is quite possible that small gas-filled cavities may exist within tissues, and even grow by rectified diffusion in the presence of ultrasound, but that the threshold for inertial cavitation that would be detected by sonoluminescence is somewhat higher in tissues than it would be in water.

Gels may serve, in some ways, to model tissues in studies of cavitation. Daniels *et al.* (1987) reported the appearance of macroscopically visible bubbles in agar gels, after 5 min exposures at 0.7 MHz CW ultrasound at intensities of 3 to 30 mW cm^{-2} (0.01 to 0.03 MPa). The gels had been allowed to equilibrate with atmospheric gas at refrigerator temperatures and, thus, were supersaturated with gas when exposed at room temperature. Formation of bubbles was reduced at high frequencies and with repetitive pulses less than 1 ms in length. The appearance of bubbles alone is an aspect of cavitation. Daniels and Price (1991) demonstrated sonoluminescence, a clear indication of inertial cavitation, in agar gels at acoustic pressure amplitudes of the order of 0.2 MPa with the threshold increasing as the agar concentration increased.

8.1.3 Paraplegia

Frizzell *et al.* (1983) used a functional endpoint for cavitation *in vivo*. Dunn (1958) had shown earlier that ultrasound exposure, under suitable conditions, can produce hind limb paralysis in neonatal mice. Using the same biological model, Frizzell *et al.* (1983) determined the exposure time required to produce hind limb paralysis in 10, 50, and 90 percent of mouse neonate specimens exposed to 1 MHz ultrasound at 10 °C, at 0.1 and 1.6 MPa hydrostatic pressure, in the intensity range 80 to 300 W cm^{-2} . The 50 percent point of the paralysis curve was not affected by exposing the animals under a hydrostatic pressure of 1.6 MPa when the acoustic pressure amplitude was either 1.6 MPa (86 W cm^{-2}) or 2 MPa (144 W cm^{-2}) but, at an intensity of 289 W cm^{-2} (3 MPa), the hydrostatic pressure increased the 50 percent exposure time by a factor of two, suggesting that cavitation may have influenced the production of the hind limb paralysis in the neonate at atmospheric pressure at acoustic pressure amplitudes of 3 MPa.

Earlier, Fry (1953) concluded that neither heating nor cavitation, nor a combination of the two mechanisms could adequately explain ultrasonically induced paralysis in frog hind limbs. Although temperature

increments in his studies ranged from 15 to 25 °C under conditions producing paralysis, he was able to obtain equivalent effects when the animals were cooled to 5 °C before exposure. Exposing the animals under hydrostatic pressures great enough to avoid tensile stresses during negative excursions in the acoustic wave did not alter the functional endpoint. Furthermore, there was no histological evidence of damage to the spinal cord comparable to that described above for "cavitation lesions" in brain tissue (Fry *et al.*, 1970).

The production of paraplegia and hemorrhagic injury in the rat spinal cord by pulsed (10 ms pulses separated by 100 ms) ultrasound at peak intensities of 25 W cm⁻² (0.8 MPa) and 50 W cm⁻² (1.2 MPa) was observed (Taylor and Pond, 1972). It was shown that paraplegia occurred at lesser dosages when the rat was placed under hypoxic conditions. Temperature increments in the cord for the greater exposure level ranged from 5 to 10 °C for frequencies from 0.5 to 6 MHz. Although the heating of the cord increased with frequency, the effectiveness of the exposure in producing paraplegia decreased over that frequency range. The results reported are consistent with cavitation as the mechanism of damage.

Miller *et al.* (1999) found no effect on hind-limb paralysis in mice from exposure to 800 lithotripter shock waves (peak positive pressure 24 MPa, peak negative pressure 5 MPa). However, burst mode 1 MPa, 0.4 and 1 MHz ultrasound (10 ms "on", 100 ms "off") caused reduction in grip strength after exposures of 150 s. These exposures were associated with significant elevation of the temperature of the spine (~12 °C after 200 s). Overall, evidence favors heat as the biophysical mechanism responsible for paralysis.

8.1.4 Intestine

Lehmann and Herrick (1953) showed earlier that petechiae developed in the peritoneal cavity of mice exposed for 2 min to 1 MHz, CW ultrasound from an ultrasonic diathermy instrument (bath temperature, 30 °C). Only one-fifth as many lesions per animal were observed when the experiments were performed under 0.7 MPa hydrostatic pressure. The threshold hydrostatic pressure for reduction in petechiae was between 0.3 and 0.4 MPa for acoustic pressure amplitudes of approximately 0.3 MPa (2.5 W cm⁻²). With the bath temperature of 42 °C, at atmospheric pressure and an acoustic pressure amplitude of approximately 2.5 W cm⁻² (0.3 MPa), the investigators found approximately five times as many petechiae at 0.17 MHz as at 1 MHz. These results are consistent with cavitation, some of

whose effects increase with increasing temperature, as the mechanism of damage.

After replicating and extending the Lehmann and Herrick study, Miller and Thomas (1994b) concluded that heating is the dominant mechanism in intestinal hemorrhage with CW exposures at frequencies near 1 MHz. Heating and cavitation may interact synergistically as noted above (Hynynen, 1991). Using both continuous and pulsed (100 μ s) 400 kHz ultrasound, Miller and Gies (1998b) concluded that heating and cavitation play largely independent roles in intestinal hemorrhage. Lithotripter fields cause intestinal hemorrhage (Dalecki *et al.*, 1995b; Raeman *et al.*, 1994). In that case, heating can be ruled out as the causal mechanism. Similarly, in a study using pulsed ultrasound exposures, Dalecki *et al.* (1995b) demonstrated hemorrhage in murine intestine that could not be explained on the basis of heating.

8.1.5 Blood

The possibility of cavitation in blood is of particular concern in the arterial circulation because any bubbles, platelet aggregates, or thrombi produced by cavitation could lodge in the capillary bed downstream. Wong and Watmough (1983) provided evidence for the occurrence of hemolysis *in vivo* from exposure to 0.75 MHz at 0.25 to 3 W cm⁻² therapeutic ultrasound in the rat. The hypothesis that this effect was the result of cavitation in blood was supported by anomalous spikes attributed to bubbles seen in traces from a Doppler ultrasound device aimed at the aortic arch. As noted below, lithotripter pulses may cause cavitation *in vivo*, including blood (Delius *et al.*, 1990a). Williams *et al.* (1986) confirmed the observation of hemolysis in rats reported by Wong and Watmough (1983), but implicated heating of the liver to hemolytic temperatures as the cause of the hemolysis rather than cavitation. In addition, Williams *et al.* (1986) noted that the position of the rat lung might impede the view of an ultrasound beam aimed at the aortic arch in the rat, thus weakening the support for the cavitation hypothesis afforded by the Doppler device observations of Wong and Watmough (1983).

Improved electronic surveillance techniques were employed by Gross *et al.* (1985) to search for cavitation bubbles in blood. Cavitation was not detectable in heart and aortic blood by means of a resonant-bubble detector located on the abdominal aorta of dogs exposed to 0.5 to 1.6 MHz up to 16 W cm⁻² spatial peak intensity (0.7 MPa), CW ultrasound (Gross *et al.*, 1985). Gross *et al.* (1985) suggested that cavitation nuclei might be removed by the lungs in

a continuous filtering action that could lead to a relatively high cavitation threshold for blood. The resonant bubble detector method also failed to detect cavitation from 0.75 and 1.45 MHz ultrasound up to 1 kW cm^{-2} (5.5 MPa) focused into the left ventricle or from lithotripter pulses delivered to the abdominal aorta (Williams *et al.*, 1989) as discussed below.

Ivey *et al.* (1995) required 23 MPa ($19,000 \text{ W cm}^{-2}$) with a 15 ms pulse of 1.8 MHz ultrasound to obtain an imaginable bolus of bubbles in canine artery. For discussion of hemolysis *in vitro* see Section 7. Hemolysis *in vivo* is discussed in Section 8.3.3 below. Thrombus formation caused by acoustic microstreaming was discussed earlier in Section 3.3.9.

8.1.6 Urine

Fowlkes *et al.* (1991) reported the generation of bubbles of 100 to 140 μm diameter in urinary bladders of dogs by peak standing wave pressures of 1 to 2 MPa, in 10 s exposures to 555 kHz CW ultrasound.

8.1.7 Summary

A substantial body of evidence is consistent with the conclusion that acoustic cavitation can occur in tissues exposed to CW ultrasound or pulses of ultrasound longer than 1 ms if the pressure amplitude is sufficiently great. The required pressures range from less than 1 MPa to greater than 10 MPa depending upon conditions of exposure and the characteristics of the tissues.

8.2 Evidence of Cavitation *In Vivo* from Lithotripsy

Over the past decade, lithotripsy has revolutionized the treatment for kidney stones through the use of acoustic shock waves. In the process, millions of patients have been exposed to pressure levels considerably greater than those used in diagnostic ultrasound. Similar techniques have been used experimentally in the treatment of gallstones. There is evidence from several investigators that cavitation is a factor in the destruction of stones (Phillip *et al.*, 1993; Sass *et al.*, 1992; Vakil and Everbach, 1991; 1993). Cavitation induced by ~ 200 kHz ultrasound has been used experimentally to enhance the chemical dissolution of gallstones (Fry *et al.*, 1995).

8.2.1 *Kidney and Liver*

There is evidence from studies of the side effects of lithotripsy that cavitation-related tissue damage occurs with isolated short pressure pulses. Delius and coworkers obtained indirect evidence of cavitation *in vivo* generated during *electrohydraulic* lithotripsy treatments through damage to the kidney (Delius *et al.*, 1988a; 1988b) and liver (Delius *et al.*, 1990a; 1990b). Recent studies have shown that collateral damage to kidney tissues during routine clinical treatment of kidney stones can be significant (Evan and McAteer, 1996). Typical clinical treatments with electrohydraulic lithotriptors require more than 1,000 shocks at peak positive pressures greater than 30 MPa. However, extravasation of blood cells has been observed in kidneys exposed to 10 spark-generated, spherically diverging shocks at peak positive pressures as low as 3 MPa (Mayer *et al.*, 1990). One possible site for cavitation activity is in the blood. If cavitation occurs there, small holes may be created in the vessel walls which permit leakage of the blood cells into the surrounding tissues (extravasation). This is an extremely sensitive test because extravasation is almost never observed in normal (sham exposed) tissues (Mayer *et al.*, 1990). In these studies, the mouse kidney appears to be more sensitive than the overlying tissues, and the interior of the kidney (medulla) is more sensitive than the outer tissues (cortex). When exposed to the fields of a *piezoelectric* extracorporeal lithotripter with peak positive pressures of the order of 40 MPa (Raeman *et al.*, 1994), some extravasated blood was observed under the capsule, which contains the murine kidney, in 25 percent of the cases, but there was little or no evidence of hemorrhage to the interior of the kidney as seen with spark-generated pulses of lower peak positive pressure (Mayer *et al.*, 1990).

Evidence is accumulating that damage of the kidney resulting from lithotripsy may lead to chronic hypertension (Knapp *et al.*, 1996).

With the exception of lung and intestine, most of the tissues of mice can be exposed to positive acoustic pressures in excess of 30 MPa from a piezoelectric lithotripter without evidence of hemorrhage. However, almost every tissue in the mouse, including the kidneys, becomes susceptible to hemorrhage when exposed to lithotripter fields at pressures less than 2 MPa if the contrast agent, Albunex[®], is added to the blood (Dalecki *et al.*, 1997c). There can be little question that this is the result of acoustic cavitation in the blood vessels of the animal. A comparison of normal animals with those injected with Albunex[®] provides a vivid demonstration (1) that acoustic cavitation can occur *in vivo* at modest acoustic pressures but also (2) that cavitation nuclei are rare in the tissues of most mammals. The

remarkable success of lithotripsy in the treatment of kidney stone disease depends very largely on the fortuitous paucity of gas bodies in tissues. Alburnex[®] ceases to serve as an effective contrast agent within a few minutes after injection. This means that bubbles larger than roughly 1 μm are destroyed quickly in the circulation. Surprisingly, Alburnex[®] continues to provide nuclei for acoustic cavitation *in vivo* as long as 4 h after injection. The evidence comes from a study of hemorrhage in mice exposed to 2 MPa lithotripter fields (Dalecki *et al.*, 1997d). The remnant cavitation nuclei must be very small gas bodies adhering somehow to fragments of the stabilizing shells of Alburnex[®] or be very small, highly stable, Alburnex[®] particles.

Evidence that gaseous nuclei do exist *in vivo* comes from lithotripter exposures in which the focal volume in liver becomes highly echogenic to B-scan ultrasound (Coleman *et al.*, 1995; Delius *et al.*, 1990a). Typically, this increased scattering develops only after many shock waves. Very likely, the extremely high acoustic pressures in lithotripter fields are able to cause a few cavitation events even in mammalian tissues, in which cavitation nuclei are normally sparse. Gaseous fragments formed during these events grow to the point where they become detectable with diagnostic ultrasound and begin to cause significant tissue damage as the lithotripsy exposure continues. It cannot be ruled out, however, that the first action of lithotripter fields does not involve cavitation and that, only after initial tissue damage, does cavitation occur.

8.2.2 Embryos

Chick embryos exposed to three shocks at pressure amplitudes of 10 MPa had significantly elevated rates of early deaths, delayed deaths, and malformations (Hartman *et al.*, 1990a). There were suggestions in the study of possible developmental effects at lower pressure levels.

8.2.3 Lung

One can speculate that the adult mammalian lung, with its richly structured arrangement of gas bodies, should be particularly susceptible to injury by lithotripter fields. The low frequencies included in the spectrum of lithotripter pulses are ideally suited for waves to penetrate the outer tissues. Experimental tests showed monotonically decreasing thresholds for injury from spherically diverging spark-generated shock waves with increasing pulse number leading

to a threshold of 1.5 MPa peak compressional pressure with 20 pulses (Hartman *et al.*, 1990b) in the adult murine lung. A related study showed that predominately positive pressure waves were at least as effective as negative pressures in producing hemorrhage (Bailey *et al.*, 1996). Fetal murine lung, in contrast, did not show signs of damage at 20 MPa (Hartman *et al.*, 1990b). The lower sensitivity of fetal lung is presumably related to its lack of undissolved gas. Threshold levels similar to those for hemorrhage of adult murine lung had been found for killing of the larvae of the fruit fly, *Drosophila melanogaster* as discussed in Section 6 (Carstensen *et al.*, 1990c).

8.2.4 Intestine

Chaussy (1986) reported widely disseminated petechial bleeding in eventrated large intestine after exposure to the fields of an electrohydraulic extracorporeal lithotripter. Mice exposed to the fields of an extracorporeal piezoelectric lithotripter with pressure amplitudes of the order of 25 MPa showed extensive hemorrhaging in the intestine (Raeman *et al.*, 1994). In this study, there was a greater probability of damage to the intestine than to the kidney. Miller and Thomas (1995b) used a focused electrohydraulic shock wave source and acoustic attenuators to control the levels of the fields experienced by their mice. Their threshold for intestinal hemorrhage was between 1.6 to 4 MPa for positive pressure. The frequency of their lithotripter pulses at threshold was in the range from 0.1 to 0.2 MHz. Similar thresholds for hemorrhage in mouse intestine were found for the fields of a piezoelectric lithotripter (Dalecki *et al.*, 1995b). Depending upon the exposure level, intestinal lesions ranged in size from small petechiae near threshold to hemorrhagic regions extending 5 cm or more along the intestine at super threshold levels. At threshold, the lithotripter wave forms were nearly sinusoidal. Damage to the intestine from lithotripter exposures is markedly increased when microbubble contrast agents are employed (Dalecki *et al.*, 1997c; Miller and Gies, 1999).

8.2.5 Heart

Dalecki *et al.* (1991b) showed that lithotripter shock waves with peak positive pressures in excess of 10 MPa can trigger ventricular extrasystoles in frog hearts. Similar effects were demonstrated by Delius *et al.* (1994) in piglets. Their thresholds were found to be of the order of 1 MPa. Subsequently, this investigation was extended

to single bursts of focused, 1 to 4 MHz ultrasound (Dalecki *et al.*, 1993a). Depending upon the amplitude of the pressure pulse and the timing of the pulse within the heart cycle, a single pulse, at high intensity, can produce either a premature ventricular contraction or a reduction in aortic pressure, again with thresholds of the order of 10 MPa. It is also possible to pace the heart with acoustic pressure pulses (Dalecki *et al.*, 1993a). There were two qualitative differences between the effects on the heart of lithotripter exposures and pulsed ultrasound. First, in the case of focused ultrasound, no effect was observed for pulse lengths less than 1 ms. These pulse lengths are greater than those employed in routine echocardiographic procedures (Carstensen *et al.*, 1992). With the piezoelectric lithotripter used in the original study (Dalecki *et al.*, 1991b), the effective pulse length is of the order of 2 μ s. Second, in contrast with pulsed ultrasound, lithotripter fields had no effect on aortic pressure.

From both theory and direct temperature measurements, heating can be ruled out as the mechanism responsible for these cardiac phenomena (Dalecki *et al.*, 1993b). As discussed in Section 3, it appears that reduction in aortic pressure is a response of the heart to the radiation force of the sound field (Dalecki *et al.*, 1997a). However, premature ventricular contraction whether by lithotripter fields or pulsed ultrasound requires direct interaction of the sound field with cardiac tissue (Dalecki *et al.*, 1997a) is affected by the viscosity of the fluid surrounding the heart and is greatly enhanced when the blood contains contrast agents (Dalecki *et al.*, 2000a; van der Wouw *et al.*, 2000), suggesting that the effect is related to the action of cavitation near or in the heart. Similar effects have been observed in mice (MacRobbie *et al.*, 1997).

8.2.6 *Blood*

Williams *et al.* (1989) were unable to detect shock-wave-induced cavitation activity within the intact vascular systems of dogs. However, bubbles were generated when plastic arterio-venous shunts of the canine circulation were exposed to the fields of an electrohydraulic extracorporeal shock waves. Chaussy (1986) failed to find any evidence of hemolysis *in vivo* in animals exposed to an electrohydraulic lithotripter.

8.2.7 *Negative Lithotripter Fields*

As discussed in Section 5, the violence of the inertial collapse of a bubble is related to the extent of its expansion during the negative

phase of the acoustic cycle. This suggests that negative pressures may play a more important role than positive pressures as predictors of the effects of inertial cavitation. Whether *negative* pressures play a unique role when bubbles are limited in their ability to expand by surrounding tissue is open to question. The pressure pulse generated by an isolated spark is largely positive. Bailey *et al.* (1996) compared the biological effects of this pulse with that of its mirror image obtained by its reflection from a pressure release interface. The degree of hemorrhage in murine lung and the killing of *Drosophila* were found to be at least as great with a purely positive pulse as with a purely negative pulse at comparable pressure levels. In contrast, the damage caused by the activity of microbubble contrast agents in fields of high acoustic pressure is much greater when they are exposed to negative pressure than to positive pressure pulses. This information suggests that the physical processes involved in killing of larvae and hemorrhaging of lung are not cavitation-related or that the cavitation acting in these examples differs greatly from the classic response of bubbles in water to fields of high acoustic pressure. To answer this question, Dalecki *et al.* (2000b) compared hemorrhage in abdominal tissues exposed to positive and negative pressure pulses after introducing microbubble contrast agents, in this way making sure that a generous supply of cavitation nuclei were present. In this case, the damage caused by negative pulses was much greater than that from positive pressures. Because, as pointed out earlier, the greater effectiveness of negative pressures is expected when inertial cavitation is involved, the above experiment provides strong evidence that inertial cavitation can occur *in vivo*.

8.2.8 Hemorrhage Near Fetal Bone

Hemorrhage occurs in fetal tissues when late term pregnant mice are exposed to lithotripter fields of relatively low amplitude (Dalecki *et al.*, 1997e). These hemorrhages are always observed in tissues near bone or cartilaginous structures such as the head, limbs and ribs, while soft tissues distant from bone remain relatively free of hemorrhage. This was discovered in studies of pregnant mice which were exposed on the 18 d of gestation to 200 pulses from a piezoelectric lithotripter. Thresholds for hemorrhage to the head, limbs, ribs and lung were all less than 1 MPa. At these pressure levels each pulse approximated one and one-half cycles of a sinusoid with a frequency of 0.1 MHz.

Until this observation, consensus statements had emphasized that low thresholds for damage to tissues are found only in tissues that

are known to contain stabilized gas bodies. Yet, there is no reason to believe that cavitation nuclei are selectively associated with the ends of partially formed bone. More likely, the action of ultrasound in the case of fetal bone is purely mechanical (not involving cavitation) (Section 3.4.5).

This phenomenon has not been found in adult bone nor has it been seen in the embryo/fetus before bone is formed. However, the phenomenon can be demonstrated in neonatal mice. One of the most sensitive sites in the fetus is the head. These observations add a new reason for avoiding lithotripsy of pregnant patients, but it is impossible to extrapolate from a knowledge of the effects of lithotripter fields to recommendations regarding the practice of diagnostic ultrasound.

8.3 Cavitation Effects with Diagnostically Relevant Acoustic Fields

While the results of investigations of the biological effects of lithotripter shock waves and CW ultrasound provide clues for an understanding of cavitation in tissues, it is not possible to draw conclusions with regard to the possible hazards of diagnostic ultrasound simply and directly from these studies. For example, it was noted above that 10 spherically diverging, spark-generated shock waves caused extravasation in murine kidneys at pressure levels of the order of 3 MPa. However, when the same organs were exposed to focused, pulsed ultrasound where NLP transformed each cycle of the incident wave into an acoustic shock with a peak compressional pressure of the order of 10 MPa, no significant extravasation was found even though the total numbers of individual shocks in the exposures exceeded one million (Carstensen *et al.*, 1990a). In contrast, thresholds for lung hemorrhage, discussed below, and killing of *Drosophila* larvae, discussed in Section 6, are quantitatively similar for both piezoelectric and electrohydraulic lithotripsy and for pulsed ultrasound.

8.3.1 Lung

Extension of the study of the effects of lithotripter fields on mouse lung to similar studies involving pulsed ultrasound (Section 8.2.3) gave a qualitatively new picture of the effects of diagnostic levels of ultrasound on mammalian tissues (Child *et al.*, 1990). Thresholds for lung hemorrhage from pulsed ultrasound with carrier frequencies in the range from 0.5 to 5 MHz are of the order of 1 MPa. Thus, in

contrast with the case for kidney hemorrhage (Section 8.2.1), the pressure thresholds for lung damage are of the same order for spark-generated shocks and for pulsed piezoelectrically generated waves. As with fruit-fly larvae (Section 6.3.2), the threshold was only very weakly dependent upon *PRF* (an increase in repetition frequency by a factor of 10 resulted in less than a 30 percent decrease in threshold acoustic pressure), *i.e.*, temporal peak parameters rather than temporal average parameters of the sound field are predictors of this biological effect. In particular, the authors suggest that the best predictor of lung hemorrhage is the temporal peak amplitude of the fundamental frequency⁶ component of the pressure pulse (Child *et al.*, 1990). As might be anticipated for a highly localized event such as cavitation, thresholds for lung hemorrhage (expressed in terms of spatial-peak pressures) are the same for focused or unfocused fields. Morphological studies of ultrasonically treated lung tissue support the conclusion that the thresholds for damage of blood vessels and other tissues are approximately the same (Penney *et al.*, 1993).

The limited data available at the present time show only minor differences in threshold for lung hemorrhage among species or ages of laboratory animals. Using a commercial diagnostic scanner, Holland *et al.* (1996) found the threshold for lung hemorrhage in rats to be approximately 2 MPa at 4 MHz using a 1 μ s pulse length. This is essentially identical to the threshold for mice under the same exposure conditions (Child *et al.*, 1990). At 2 MHz, adult mice and neonatal and juvenile swine have approximately the same values for lung hemorrhage threshold (Baggs *et al.*, 1996; Dalecki *et al.*, 1996). No statistically significant differences were found in the thresholds for lung hemorrhage in neonatal, juvenile or adult mice (Dalecki *et al.*, 1997b). Lung hemorrhage has been demonstrated with a commercial diagnostic ultrasound unit in monkeys (Tarantal and Canfield, 1994) and in rabbits (Zachary and O'Brien, 1995), but these studies were not designed to determine thresholds for hemorrhage.

The threshold for lung hemorrhage depends weakly upon the duration of the pressure pulse. As the pulse duration increases by 10-fold from 1 to 10 μ s (*PRF*, 100 Hz), the acoustic pressure thresholds for hemorrhage of murine lung decrease by approximately one-half (Child *et al.*, 1990). Similar pulse duration effects have been reported for killing of *Drosophila* larvae (Carstensen *et al.*, 1992). This should be considered in evaluating possible hazard with pulsed-

⁶As used here the fundamental frequency is the frequency of the wave stripped of harmonics generated by NLP.

Doppler devices which may have pulse durations an order of magnitude greater than those of scanning systems.

The threshold acoustic pressures for effects in tissues with stabilized populations of bubbles depend only weakly upon the pulse repetition rate and hence the temporal average intensity. This has been shown in systems as different as mouse lung (Child *et al.*, 1990; Raeman *et al.*, 1996) and *Drosophila* larvae (Child *et al.*, 1981).

Raeman *et al.* (1993) explored the influence of timing in the exposure of adult mouse lung and showed that, even with the same total on-time, the threshold was higher when the total exposure was delivered in a shorter time. The explanation may lie in a time-dependent change in the acoustic properties of the lung resulting from irreversible changes in tissue structure that favor penetration of the sound wave. That is, the initial acoustic insult to the tissue may initiate pooling of fluid near the point of entry of the sound beam (Raeman *et al.*, 1993). This may account for the time dependent penetration of lesions into the lung. Normal lung has a very high attenuation for ultrasound (Bauld and Schwan, 1974; Dunn, 1974, 1986; Dunn and Fry, 1961; Pedersen and Ozcan, 1986). Yet, exposures only a little above threshold extending over a period of 3 min have been shown to penetrate the mouse lung. When ultrasound with the same total "on-time" is delivered to the lung in 0.3 min, however, the threshold pressure for penetration doubles (Raeman *et al.*, 1993).

As bioeffects information continues to accumulate, it becomes less and less obvious that inertial cavitation is responsible for lung hemorrhage. (The physics of inertial cavitation is described in Section 5 and its biological effects in suspensions are described in Section 7.) Negative pressures cause no greater effect than positive pressures (Bailey *et al.*, 1996) in contrast with expectations for classical inertial cavitation and with observations of hemorrhage in other tissues after infusion with microbubbles. Adding nuclei to the blood has no apparent effect on the severity of lung hemorrhage (Raeman *et al.*, 1997). A plot of acoustic pressure thresholds for bioeffects produced by pulsed ultrasound of low time-averaged intensity in various tissues containing stabilized gas bodies is shown in Figure 8.1. The frequency dependence of bioeffects that are more clearly related to inertial cavitation *in vivo*, *e.g.*, hemolysis and intestinal hemorrhage, is stronger than the frequency dependence of lung hemorrhage (Section 8.3.4). For lung hemorrhage, a log-log plot of the pressure threshold as a function of frequency has a slope of 0.54 ± 0.39 (Fowlkes and Holland, 2000). Similar plots of thresholds for cell lysis in the presence of contrast agents, where cavitation is probably the mechanism, have slopes ≥ 1 (Brayman *et al.*, 1997; Dalecki *et al.*, 1997b;

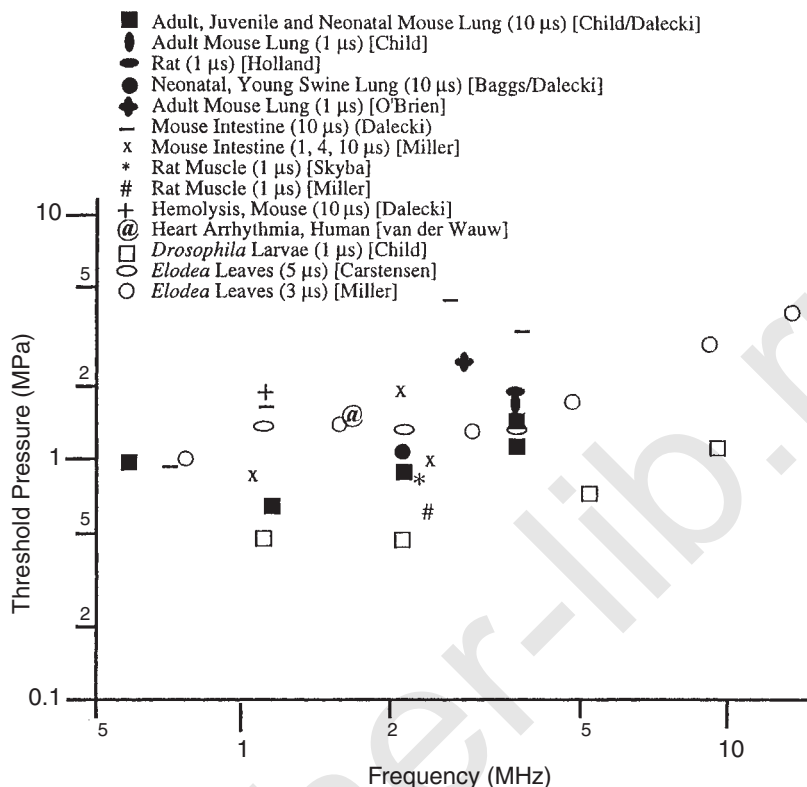


Fig. 8.1. Threshold, *in situ*, negative pressures for biological effects *in vivo* of low temporal-average intensity, pulsed ultrasound. Pulse durations are shown in parenthesis in the legend. In all cases, the tissues contain identifiable, small, stabilized gas bodies. As in diagnostic ultrasound, all exposures consisted of repetitive pulses ($\leq 10 \mu$ s). Total exposure times were less than 5 min. Sources: Murine lung hemorrhage (Child *et al.*, 1990; Dalecki *et al.*, 1997b; O'Brien *et al.*, 2000; Raeman *et al.*, 1993; 1996); rat lung (Holland *et al.*, 1996); swine lung (Baggs *et al.*, 1996; Dalecki *et al.*, 1997f); murine intestine (Dalecki *et al.*, 1995c); murine intestine with microbubbles (Miller and Gies, 2000); rat muscle with microbubbles (Skyba *et al.*, 1998); hemolysis *in vivo* when contrast agents are added to the blood (Dalecki *et al.*, 1997g); and human heart arrhythmia with contrast agents (van der Wouw *et al.*, 2000). For comparison, open symbols show killing of insect larvae (Berg *et al.*, 1983; Child *et al.*, 1981) and lysis of cells in leaves of aquatic plants (Carstensen *et al.*, 1990b; Miller and Thomas, 1993c).

Fowlkes and Miller, 2000). Mice are as sensitive to pulsed ultrasound when exposed under hyperbaric conditions (1.1 MPa) as they are at atmospheric pressure (0.1 MPa) (O'Brien *et al.*, 2000). None of these characteristics of lung hemorrhage are consistent with classical inertial cavitation.

Conceptually, we have to ask what is meant by cavitation in an organ like the lung. The obvious gas bodies in the lung, the air in the alveoli, are so large and closely packed that they are far from ideal nuclei for inertial cavitation. The fluid layers lining the alveoli are much too thin to accommodate cavitation. Bubbles at the site (since they are surrounded mostly by gas) would be more akin to soap bubbles than cavitation bubbles. Many of the septa that divide the alveoli are so thin that, if cavitation were to occur within the septa (including the blood vessels in the septa), the environment for the bubble would be far different than the infinite fluid that is assumed in most cavitation theories, such as that discussed in Sections 4 and 5, to surround a bubble engaged in the kind of activity discussed there. This leaves the relatively thick connective tissues distributed about the lung as potential sites of cavitation. However, hemorrhage is almost entirely confined to the alveolar capillaries, the most fragile part of the vascular system, not the thick connective tissues (Carstensen *et al.*, 2000). Despite the uncertainties regarding the mechanism of lung hemorrhage, enough is known phenomenologically about the bioeffect—the nature of the damage and its long term prognosis, similarity of thresholds among species and for different ages within species—to provide a reasonable basis for the formulation of recommendations for safety in the use of diagnostic ultrasound.

8.3.2 Intestine

The intestine contains bubbles in a wide range of sizes that are potential nuclei for acoustic cavitation. Negative pressure thresholds for hemorrhage in murine intestine have been found to be in the range of 1 to 2 MPa in the frequency range from 1 to 4 MHz (10 μ s pulses) (Dalecki *et al.*, 1995c). Perhaps the best evidence that cavitation is involved in damage to the intestine is the observation that fetal intestine which is presumed to contain no bubbles is essentially immune to damage under the same exposure conditions that produces intestinal hemorrhage in 100 percent of the dams (Dalecki *et al.*, 1996).

8.3.3 Heart

Diagnostic ultrasound does not appear to have either transient or long term effects on the heart in normal applications. However, when contrast agents are present in the blood, ultrasound has been shown to cause premature ventricular contractions in patients (van der Wouw *et al.*, 2000) and in mice (Dalecki *et al.*, 2000a). The general subject of effects of ultrasound on the heart is discussed in greater detail in Section 8.2.5.

8.3.4 Blood

There is no direct evidence that hemolysis occurs in normal mammalian subjects under diagnostically relevant exposure conditions. Hemolysis can occur, however, if appropriate cavitation nuclei are present in the blood. Dalecki *et al.* (1997g) exposed murine hearts for 5 min at either 1.1 or 2.4 MHz with a pulse length of 10 μs and *PRF* of 100 Hz. During the exposure period, Albunex[®] was injected into a tail vein. With Albunex[®] present in the blood, the threshold for hemolysis at 1.1 MHz was 3 MPa peak positive pressure (~ 2 MPa negative pressure, $\sim 180 \text{ W cm}^{-2}$ pulse average intensity).

No statistically significant hemolysis was observed at 2.4 MHz at the highest pressures available with the experimental procedure (10 MPa peak positive pressure and 4 MPa maximal negative pressure), indicating a very strong dependence of the negative-pressure thresholds for hemolysis on frequency (Dalecki *et al.*, 1997b). This relation is consistent with the results of studies of hemolysis *in vitro* by Brayman *et al.* (1997) who found a stronger than first-power dependence of the same threshold on frequency. The strong dependence of the threshold for hemolysis upon frequency is similar to the frequency dependence of the threshold for hemorrhage in intestine (Dalecki *et al.*, 1995b). In both sites, the biological effects depend upon the presence of microbubbles and thus the most likely candidate for a physical mechanism at each site is inertial cavitation.

As discussed in Section 7, Brayman *et al.* (1996a) report a “pseudo-threshold” for hemolysis in whole human blood *in vitro* of approximately 3 MPa peak positive pressure with a 10 μs pulse after addition of Albunex[®]. This level is remarkably similar to that for hemolysis *in vivo* considering the great differences in the environment for cavitation in the two studies. The exposure itself was almost identical in the two experimental protocols. Only the duty cycle differed: 0.01 in Brayman *et al.* compared with 0.001 in Dalecki *et al.* (1997g). In view of this similarity of threshold values, an important finding from

Brayman *et al.* should be mentioned. They used the term “pseudo-threshold” because they observed small, but statistically significant, levels of hemolysis below the “pseudo-threshold” pressure level. Thus, it must be acknowledged that a small level of hemolysis may occur even *in vivo* below the threshold levels reported above.

The observation of hemolysis with the addition of microbubbles to the blood demonstrates that cavitation can occur *in vivo* if appropriate nuclei are present. The absence of hemolysis without microbubbles suggests that nuclei are relatively rare in mammals.

8.3.5 Hemorrhage Near Fetal Bone

The hemorrhage near fetal bone, originally discovered in exposures to lithotripter fields (Section 8.2.8), can also be produced with pulsed ultrasound (Dalecki *et al.*, 1999). With a 1 MHz carrier, 10 μ s pulses at a repetition frequency of 100 Hz, the threshold, negative acoustic pressure for hemorrhage of the murine fetal head was found to be ~ 2.5 MPa. The positive pressure in the wave was 4 MPa. At 3 MHz, the negative threshold pressure was approximately 5 MPa.

8.3.6 Synergism

As the temperature of the medium increases, its gas solubility decreases, and the availability of cavitation nuclei and their rate of growth in the acoustic field should increase. As discussed in Section 11, ultrasound as used in diagnosis has a potential for increasing tissue temperature through absorption. This provides an additional mechanism by which exposure of tissues to ultrasound modifies the tissue in such a way that the probability of cavitation is increased.

In addition, the ultrasound absorption cross section for a bubble may be many times greater than its physical cross section. Thus, even a small concentration of resonant bubbles in tissue can greatly increase the effective absorption coefficient of the medium. An example of this kind of interaction has been reported by Hynynen (1991). The extent to which this synergism is important in diagnostic applications of ultrasound has not been investigated.

8.3.7 Summary

To relate directly to the question of hazards associated with cavitation produced by pulsed diagnostic ultrasound, exposures used in

studies of biological effects should be applied in repeated short pulses with temporal average intensities low enough to make it possible to eliminate heating as the primary mechanism of the effect. Whether cavitation-related effects occur depends critically upon the presence of nuclei in the tissues. Since the population of nuclei may be much different *in vitro* and *in vivo*, it is essential that direct conclusions be based on studies of effects in laboratory mammals. Figure 8.1 summarizes the threshold data currently available on bioeffects observed in tissues under these conditions. It is interesting that, in each case, the tissue target contains a rich collection of stabilized gas bodies.

8.4 Related Reports of Biological Effects

In addition to the biological effects that have been cited above as evidence for the occurrence of cavitation *in vivo*, there are other reports whose relevance to the subject is only speculative at the present time.

8.4.1 Endothelial Damage to Blood Vessels

The phenomenon of banding of blood cells exposed to standing wave ultrasonic fields and accompanying stasis is discussed in Section 3. Thresholds for the effect may be lower than 0.5 W cm^{-2} at 3 MHz. Dyson *et al.* (1974) reported bands of endothelial cell damage in the vessels of chick embryos in which stasis occurred. ter Haar *et al.* (1979) noted a variety of ultrastructural changes in mouse uteri that had been subjected to standing wave fields at 2 W cm^{-2} . However, they did not find bands of damage as Dyson *et al.* (1974) found for chick embryos. There is no clear evidence that inertial cavitation occurs in whole blood under the exposure conditions used in these experiments. There is evidence, however, that inertial cavitation may occur in plasma *in vitro* at levels of the order of 1 W cm^{-2} (Carstensen *et al.*, 1993). Thus, when cell stasis occurs in a standing wave field, it is reasonable to assume that the probability of the occurrence of cavitation in the cell-free pressure antinodes increases. Whether this explains the bands of endothelial cell damage in the chick blood vessels is only conjecture in the absence of further experimental studies.

In clinical applications, standing waves might occur near tissue-bone or tissue-air interfaces, as in the lung or intestine. The threshold levels for red cell stasis observed experimentally by Dyson *et al.*

(1974) were in the therapeutic range. In ultrasonic diathermy, continuous movement of transducers is standard procedure for uniform distribution of heat. Dyson *et al.* (1974) noted that cell stasis is unlikely to occur if the applicator is in continuous motion.

The likelihood that cell stasis will occur in diagnostic applications of ultrasound is remote. Furthermore, for a given temporal average intensity, the lytic effectiveness of ultrasound is markedly reduced by pulsing even though the pulse average intensities may go well above 100 W cm^{-2} (Brayman *et al.*, 1994; Carstensen *et al.*, 1993). Therefore, if cavitation is involved in the damage reported by Dyson *et al.* (1974) and ter Haar *et al.* (1979), it appears very unlikely that the endothelial damage will occur under diagnostic pulsed ultrasound exposure conditions in the absence of contrast agents even if cell banding takes place.

8.4.2 Ultrasonic Enhancement of Thrombolysis and Perfusion

Ultrasound at frequencies in the tens of kilohertz has been used to disrupt blood clots *in vitro* (Hong *et al.*, 1990) and to accelerate reperfusion when applied *via* vascular catheters to thrombi in dogs (Ariani *et al.*, 1991; Rosenschein *et al.*, 1990; Stumpff, 1979; Trubestein *et al.*, 1976). The mechanism of action presumably involves acoustic cavitation. The effect can be enhanced through the infusion of microbubbles and accomplished with extracorporeal sound sources (Birnbaum *et al.*, 1998).

There is a growing body of evidence from several laboratories that ultrasound accelerates the rate of enzymatic lysis of blood clots *in vitro* and *in vivo* (Blinc *et al.*, 1993; Francis *et al.*, 1992; Hamano, 1991; Kudo, 1989; Schlansky-Goldberg *et al.*, 1991; Tachibana, 1985; 1992; Tachibana and Koga, 1981). Although enzymatic activity increases with temperature, ultrasonic heating is not an adequate explanation of the phenomenon (Blinc *et al.*, 1993). Ultrasound appears to accelerate the penetration of the enzymes into the clot, but the physical mechanisms responsible for the action have not been identified. One possibility is that bubbles in the plasma near the surface of the clot, or within the clot, may be involved. Tachibana and Tachibana (1995) reported that addition of the echo contrast agent Alburnex® to the fluid outside the clot significantly improved the ultrasonic enhancement of clot dissolution by urokinase. Low frequencies of ultrasound (<1 MHz) may be more effective than high frequencies (>4 MHz) (Blinc *et al.*, 1993). There does not appear to be a sharp threshold, but rather a gradual increase in effectiveness of ultrasound as the intensity increases from 1 to 4 W cm^{-2} at 1 MHz.

There is evidence that mid-kilohertz frequencies may be even more effective than 1 MHz (Olsson *et al.*, 1994; Sehgal *et al.*, 1993; Suchkova *et al.*, 1998; Tachibana, 1992; Tachibana and Tachibana, 1995). Interpretation of studies of ultrasound-enhanced thrombolysis in animals has been compromised by the possibility that the invasive introduction of clots includes air, which may not be present in naturally occurring clots in the vessels of patients. Suchkova *et al.* (2000) produced clots in the femoral arteries of rabbits noninvasively (by application of ferric chloride to the vessel wall). Using this model, 40 kHz ultrasound (0.75 W cm^{-2}) together with streptokinase produced 5 to 10 times the flow rate of either streptokinase or ultrasound alone.

Ultrasound enhances transport of tissue plasminogen activator (t-PA) into thrombi (Francis *et al.*, 1995), accelerates hydrostatic pressure-mediated flow through fibrin (Siddiqi *et al.*, 1995a) and reversibly fragments fibrin fibers (Braaten *et al.*, 1997). It also alters the interaction of t-PA with fibrin, accelerating binding and increasing the maximal t-PA binding to fibrin (Siddiqi *et al.*, 1998).

Because the intensities required for ultrasonic enhancement of thrombolysis are within the therapeutic range, the technique has promise as a clinical tool for the treatment of peripheral vascular thrombi. Applications of ultrasound in the treatment of myocardial infarction and stroke are being explored currently. There is at least one problem that must be explored, however. Kornowski *et al.* (1994) treated blood clots in rabbit femoral artery segments with tissue-type plasminogen activator and found that 1 MHz ultrasound at 6 W cm^{-2} accelerated reflow in the artery, but that reocclusion was more common in vessels treated by ultrasound than those treated by the enzyme alone.

Using a laser-Doppler flowmeter, capillary perfusion in ischemic muscle tissue was monitored during application of 40 kHz ultrasound (0.75 W cm^{-2}) (Suchkova *et al.*, 2000). Over a period of 1 h, blood flow in the muscle gradually increased to nearly normal levels and declined again as soon as the ultrasound was turned off. There was a corresponding increase in pH of the tissues as blood flow increased.

8.4.3 Contrast Agents

The use of radio-opaque materials as contrast agents has played a central role in radiology for many years (Section 4.3). The last decade has seen a parallel development with regard to diagnostic ultrasound (Nanda *et al.*, 1997). Techniques have progressed to the point that ultrasound contrast agents are now commercially available.

Most ultrasound contrast media use small stabilized gas bubbles because they have very high scattering cross sections in comparison with liquid or solid materials (Section 4.3). As discussed in Sections 4.3, 7.2.3, 8.2.1, 8.2.4 and 8.3.3, it appears that these bubbles may also act as nuclei for cavitation. Caution should be exercised in the use of contrast agents in conjunction with and prior to lithotripsy procedures.

One of the striking generalizations from studies of the effects of lithotripter fields on laboratory animals (Section 8.2) is that most normal tissues are relatively immune to shock wave insult even at levels used to fragment kidney stones (>20 MPa positive pressures and up to 10 MPa negative pressures). Yet, after administration of contrast agents, these same tissues become vulnerable to relatively low pressures (~ 1 to 2 MPa). From this, it is reasonable to infer that cavitation nuclei are rare in mammals under normal conditions (Carstensen *et al.*, 2000). From the point of view of safety, ultrasound examinations that are conducted with and without the use of contrast agents differ almost qualitatively. Most tissues that are not known to contain stabilized gas bodies can be exposed to the highest levels used in diagnostic ultrasound with no apparent nonthermal effects. Yet after infusion with contrast agents, it is necessary to consider the likelihood of hemorrhage in the risk/benefit analysis.

Recent reports document this conclusion under diagnostic conditions. Skyba *et al.* (1998) reported thresholds for rupture of microvessels in rat muscle tissue at less than 1 MPa with a source operating at 2.3 MHz. The contrast agent in these studies was Optison[®]. The observations have been confirmed quantitatively by Miller and Quddus (2000b). Higher, but still diagnostically relevant, thresholds have been reported for contrast-agent-mediated hemorrhage in mouse intestine (Miller and Gies, 1998b; 2000).

Many investigators have taken advantage of cavitation to increase the permeability of cells in suspension. Section 7.3.3 summarizes much of this work. Cavitation appears to create relatively large transient holes in cell membranes allowing large molecules in the external environment, which normally are excluded, to enter the cell. Under suitable conditions, the cell membrane is repaired and a sufficient number of viable, modified cells survive to make the use of ultrasound (including lithotripsy fields) promising in applications such as gene modification.

Analogous techniques have been used in mammals to increase the permeability of blood vessels. The extravasation of blood cells under diagnostically relevant conditions mentioned above demonstrates that, when contrast agents are present, cavitation occurs and produces relatively large transient holes in vessels. Price *et al.* (1998),

for example, used a diagnostic imaging system operating at 2.3 MHz. The acoustic pressures used were not directly reported but can be inferred to be of the order of 2 MPa. A single sweep of the sound field was administered to muscle tissue following administration of the microbubble contrast agent, Optison®. A quantitative study of the exposed tissue by optical viewing identified fluorescent red blood cells and polymer microspheres, which had passed through the vessel wall. The authors state that the damage to blood vessels appears to be transient and readily repaired.

Several investigators have devised techniques for drug delivery by using contrast agents with drugs bound to their protective shells. This specialized product is injected in the same manner as with other contrast agents. By exposing the target tissue with ultrasound at this time, the agents are disrupted and the drug is deposited selectively in the target tissue. Whether the vessel wall rupture described above is necessary for delivery of the bound drugs to tissues outside the vessel has not been thoroughly investigated. Clearly, it is not needed for delivery of the drug to clots within vessels. It appears that frequencies in the tens of kilohertz are particularly effective for this application of ultrasound. Porter *et al.* (2001) used a frequency of 20 kHz and acoustic pressures of the order of 0.1 MPa in this technique to deliver a drug selectively to coronary arteries of pigs that had experienced experimental balloon injury during angioplasty. The treatment reduced the stenosis of vessels that frequently occurs following this kind of injury. Other investigators have used similar techniques to facilitate sonothrombolysis (Wu *et al.*, 1998) and chemotherapy (Unger *et al.*, 1998).

Thus, bioeffects studies using contrast agents have demonstrated that cavitation can occur *in vivo*. If an appropriate cavitation nucleus is present, regardless of source, then, in principle, cavitation can occur under diagnostic conditions.

8.4.4 Sonochemical Tumor Treatment

Certain antitumor agents appear to be more effective if chemotherapy is accompanied by irradiation of the tumor with ultrasound. Hematophophyrin, as an example, which is relatively nontoxic when used alone, can be activated selectively within a tumor by focused ultrasound (Umemura, 1994). Typical exposures employed a 0.75 MHz source at $\sim 300 \text{ W cm}^{-2}$ in 0.1 s pulses. Studies of these phenomena *in vitro* suggest that acoustic cavitation may account for the effect (Section 7.2.3.8).

8.5 Summary

It appears that bioeffects can result from cavitation *in vivo* during diagnostic examinations. The possibility of nonthermal bioeffects during diagnostic examinations is greatest when ultrasound interacts with (postnatal) lung, with bubbles in the gastrointestinal tract or with cells and tissues infused with contrast agents. However, it is also true that the minor risks of cavitation bioeffects may be acceptable when compared to the benefits to be obtained from the use of diagnostic ultrasound. Although cavitation, in principle, may be destructive, cavitation events are highly localized phenomena. Rare, destructive effects on one or a very few cells may be difficult to detect in a mammal and may not be important to the overall well being of the organism were they to occur. Moreover, there is evidence to suggest that cavitation may have a higher threshold in tissues than in liquids such as water where it is commonly studied, and, if it occurs in mammalian tissues, it may be less violent than it would be under comparable exposure conditions in water. Thus, extrapolations from classical theory for inertial cavitation may be overly alarming because the assumptions upon which the theories are based are not directly applicable to tissues.

Derated focal outputs of many diagnostic units (Section 10) exceed the thresholds for lung hemorrhage shown in Figure 8.1. In a number of specialized applications, the focus of the sound field may occur at the surface of the lung for several minutes for which these derated values may be appropriate (AIUM, 1993a). Examples include cases where lung tissue is exposed to ultrasound through the heart. Perhaps, the greatest concern might be the inadvertent use of a Doppler instrument with a standoff for the examination of the neonatal heart. During pulsed, color-Doppler sampling of flow through the pulmonary valve, the surface of the lung moves through the focus of the beam as the patient respire. In transesophageal echocardiography, the focus of the transducer commonly intersects the surface of the lung as the transducer is manipulated to attain optimal positioning for image acquisition. Meltzer *et al.* (1998) looked for possible lung hemorrhage from transesophageal ultrasound during surgical procedures. The maximal estimated exposures of the surface of the lung in those procedures were approximately equal to the threshold for lung hemorrhage that has been determined in laboratory animals. The results were negative. Doppler sampling of pulmonary venous flow and subclavian artery/vein flow also puts the focus of the beam on the surface of the lung. However, derated focal pressures have little meaning for the common case in which the transducer is in contact with the chest wall over the lung. Because the attenuation

of the lung tissue is far greater than the value used in standard derating formulations, derated focal fields may greatly overestimate the true focal fields of the modestly-focused scanheads used in echocardiography when these transducers are directed into the lung. In that case, the acoustic pressures near the source (Duck, 1999a) are more likely to give information relevant to lung damage than pressures at the focus. Other situations where the acoustic pressure near the source is the quantity of concern are discussed in Sections 9.4 and 9.6.2. With that in mind, it appears that the largest outputs from currently available commercial instruments approach levels necessary to cause macroscopic hemorrhaging of lung tissue in standard diagnostic procedures (Carstensen *et al.*, 1992). For these reasons, the possibility of lung hemorrhage should be included in the broad assessment of potential hazards of diagnostic ultrasound.

Other tissues containing gas such as the intestine are vulnerable as well. Observations available at the present time suggest that the threshold for intestinal hemorrhage is near the upper limit of the outputs that are available in current commercially available diagnostic ultrasound systems. The use of microbubble ultrasound contrast agents increases the numbers of cavitation nuclei in the blood by orders of magnitude and thresholds for hemorrhage then are well within the range of the outputs of diagnostic equipment in use today.

9. Models for Exposure Estimation in Human Beings

9.1 Introduction

During diagnostic ultrasound examinations, the tissues are exposed to the ultrasound as it passes through them. The extent to which biological changes are produced depends on characteristics of the ultrasound field, called the *exposure quantities*, and on the characteristics of the tissues. One of the former is the acoustic pressure (p) values of which vary in space and time. Another, the intensity, also varies spatially and temporally; its temporal average over a designated interval is often a quantity of particular interest. The time-averaged total power (W) in the beam, equal to the integral of the time-averaged intensity over the beam area, is also a significant exposure quantity. Except in rare experiments, which will be noted, the pressure, intensity and power are not measured *in situ*, *i.e.*, at sites of interest in the body. Instead, during a clinical procedure, the *in situ* values are estimated from quantities measured in water at another time and place.

The estimated *in situ* values of the relevant exposure quantities are important factors in evaluating potential risk from ultrasound. In making such estimates, it is necessary to model the attenuation of the ultrasound beam by “overlying tissues” (*i.e.*, by tissues lying between the ultrasound source, or sources, and the target tissues) as well as the acoustic absorption characteristics of the target organs. Also very important is the potential of these organs to contain gas bodies, either naturally or by intervention, as when contrast agents are injected.

Many of the characteristics of tissue models developed for evaluating risk of thermal bioeffects (NCRP, 1992) are also relevant to assessing the potential of mechanical effects. Overlying-tissue considerations are similar for thermal and nonthermal mechanisms. In evaluating reasonable worst-case situations, there is primary concern for propagation paths traversing a region of low attenuation preceding a target region of interest, thus causing the acoustic

amplitudes there to be relatively high. For cavitation events and related mechanisms, however, the tissues and environments of interest are often different from those for heating. Exposure sites particularly significant for cavitation effects are those in which cavitation nuclei or macroscopic gas bodies are most likely to exist or can be created. Bubbles and large air interfaces in the respiratory and digestive tracts, and, possibly, blood vessels in which contrast agents have been introduced, are the most obvious sources of bioeffects from cavitation and from stresses near tissue-to-air boundaries. Propagation-path models specific to those areas deserve more attention; they will receive more emphasis in the present report than in the previous report (NCRP, 1992), which was concerned only with thermal mechanisms.

The attenuation along propagation paths for general and obstetrical cases has been the topic of numerous studies in recent years; these studies have been summarized in several reports (AIUM, 1992; EHD, 1989; NCRP, 1992; WFUMB, 1992). Values of the attenuation coefficient (a) or the frequency-specific attenuation coefficient [attenuation coefficient divided by frequency (a/f)] for models of propagation-path attenuation that were considered in NCRP Report No. 113 (NCRP, 1992) are summarized in Table 9.1. Included was a general case for homogeneous overlying tissues of frequency-specific attenuation coefficient (a/f) and frequency-specific absorption coefficient

TABLE 9.1—*Propagation-path models from Table 5.1 of NCRP Report No. 113 (NCRP, 1992).*

Name	Model	Frequency-Specific Attenuation Coefficient or Frequency-Specific Attenuation	Application
H ₄ ^a	Homogeneous-medium	0.05 Np cm ⁻¹ MHz ⁻¹ 0.43 dB cm ⁻¹ MHz ⁻¹	Soft tissue
H ₃ ^a	Homogeneous-medium	0.035 Np cm ⁻¹ MHz ⁻¹ 0.30 dB cm ⁻¹ MHz ⁻¹	Soft tissue
F1	Fixed-path	1.0 dB MHz ⁻¹	Obstetrics—first trimester
F2	Fixed-path	0.75 dB MHz ⁻¹	Obstetrics—second trimester
F3	Fixed-path	0.5 dB MHz ⁻¹	Obstetrics—third trimester

^aThe terms “H₃” and “H₄” come from the numerical portion of the specific attenuation coefficient in units of dB cm⁻¹ MHz⁻¹.

(α/f) everywhere equal to either $0.05 \text{ Np cm}^{-1} \text{ MHz}^{-1}$ (Model H₄) or to $0.035 \text{ Np cm}^{-1} \text{ MHz}^{-1}$ (Model H₃). The former is representative of attenuation in normal liver and brain, the latter is an approximate average over a range of attenuation coefficients for soft tissues. For the attenuation coefficient (α) the H₃ model assumes the values $\alpha = 0.035 f \text{ Np cm}^{-1}$ or $\alpha = 0.3 f \text{ dB cm}^{-1}$, where f is the ultrasonic frequency in megahertz. The neper (Np) and decibel (dB) are discussed in Appendix C. Exposure quantities whose values *in vivo* are estimated by applying the known path length and assumed frequency-specific attenuation coefficient are referred to as *derated* quantities (Appendix B). In Model H₃, the derated pressure amplitude (p_d) would be calculated as:

$$p_d(z) = p_w(z)e^{-0.035zf}, \quad (9.1)$$

where p_w is the pressure amplitude measured in water at the same distance, z , from the source (in centimeters). For broadband, pulsed ultrasound, use of a single frequency in this equation is an approximation in which f is chosen as the center frequency. Obstetrical data and models are discussed at length in Section 9.3.

The homogeneous attenuation Model H₃, has been used by the FDA (1985) for regulation of diagnostic ultrasound systems. In this model, the assumed attenuation is a conservative estimate that lies between that for soft tissues and for the very small values applicable to most body fluids. For a path that is entirely through soft tissue, the H₃ ($0.3 \text{ dB cm}^{-1} \text{ MHz}^{-1}$) homogeneous attenuation model is regarded as *conservative*, in that calculations based on it would generally lead to an underestimate of the attenuation and thus an overestimate of *in situ* exposure quantities. However, cases where a significant part of the ultrasound propagation path consists of weakly attenuating fluid are common. In transcutaneous obstetrical imaging in the first and second trimesters, the propagation path typically passes through the bladder, and the H₃ homogeneous attenuation model can lead to an underestimation of exposure quantities. Under these conditions the model could be regarded as *aggressive*. As discussed in Section 9.3.4 for transcutaneous obstetrical examinations, NCRP (1992) recommended a fixed-path model to approximate the attenuation of a reasonable minimum thickness of overlying tissues. Fixed-path models F1 of 1 dB MHz^{-1} , F2 of 0.75 dB MHz^{-1} , and F3 of 0.5 dB MHz^{-1} were recommended for first-, second- and third-trimester obstetrical imaging, respectively. While they are not used generally in existing standards, the NCRP fixed-path models are valid, conservative descriptors of attenuation in obstetrical examinations through the bladder.

Table 9.2 shows a recently developed extensive set of tissue models, largely for obstetrical applications directed primarily toward thermal effects of ultrasound (WFUMB, 1992). In the second column, the “Target Tissue” is that tissue in which the possibility of damage is being considered. A major consideration in selection of models is the wide variability that exists for the propagation-path attenuation between different patients and different conditions, such as full or empty bladder (Ramnarine *et al.*, 1993) and bowel locations and gas contents. One might ask, “What is an allowable fraction of the patients in which the attenuation would be underestimated?” Two common choices are (1) reasonable-worst-case and (2) typical-exposure assumptions. These considerations are discussed more extensively in Section 9.3 in relation to obstetrical examination models.

The thermal index (TI) was developed in NCRP (1992) as an estimate of the maximum temperature rise possible in the body with a given ultrasound beam exposure. This index is the ratio of total acoustic power to the acoustic power estimated to be required to increase tissue temperature by a maximum of 1 °C under specific assumptions. A standard for real-time display of bioeffect-related indices was developed to make safety information conveniently available to users of clinical diagnostic instruments (AIUM/NEMA, 1992; 1998). This standard is referred to in this Report as ODS and is discussed in Section 10 and in Appendix B (see also Abbott, 1999). Three TIs are defined and called for in ODS: TIS for a soft tissue target, TIB for bone at the focus or other deep point of greatest anticipated heating, and TIC for bone at or near the surface of the body as in transcranial examinations.

MI was developed as an indicator of the potential for nonthermal damage during examination of a patient with pulsed ultrasound. It is expressed in terms of (1) a quantity [$p_{r.3}(z_{sp})$] which is characteristic of the estimated *in situ* acoustic pressure during a pulse, and (2) the center frequency (f_c) of the acoustic spectrum of the pulse. Specifically, MI is $p_{r.3}(z_{sp})$, the temporal peak rarefactional pressure derated by 0.3 dB cm⁻¹ MHz⁻¹, and measured at the point z_{sp} of maximal pulse intensity integral (Appendix B), divided by the square root of the center frequency, *i.e.*:

$$MI = \frac{p_{r.3}(z_{sp})}{f_c^{0.5}}. \quad (9.2)$$

To make MI unitless, it is referred to the frequency of 1 MHz and the acoustic pressure of 1 MPa. Many believe that these TIs and MIs are such simple approximations as to be valid only as guidance

TABLE 9.2—Specialized tissue models (WFUMB, 1992).

Clinical Application	Target Tissue and Frequency-Specific Absorption Coefficient (α/f) or Percent Energy Absorbed at Boundary	Tissue Along Propagation Path and Frequency-Specific Attenuation (A/f) or Frequency-Specific Attenuation Coefficient (a/f)
Obstetrics		
<i>Embryo</i> Transvaginal ^a	Soft tissue $\alpha/f = 0.44 \text{ dB cm}^{-1} \text{ MHz}^{-1 \text{ b,c}}$	Soft tissue $a/f = 0.3 \text{ dB cm}^{-1} \text{ MHz}^{-1 \text{ b}}$ (minimum thickness 1 cm)
Transcutaneous	Soft tissue $\alpha/f = 0.44 \text{ dB cm}^{-1} \text{ MHz}^{-1}$	Soft tissue $A/f = 1 \text{ dB MHz}^{-1 \text{ b}}$
<i>Second trimester</i> Transvaginal ^a	Soft tissue/bone energy <50%	Soft tissue $a/f = 0.3 \text{ dB cm}^{-1} \text{ MHz}^{-1 \text{ b}}$ (minimum thickness 1 cm)
Transcutaneous	Soft tissue/bone energy <50%	Soft tissue $A/f = 0.75 \text{ dB MHz}^{-1 \text{ b,d}}$
<i>Third trimester</i> Transvaginal	Soft tissue/bone energy = 50%	Soft tissue $a/f = 0.3 \text{ dB cm}^{-1} \text{ MHz}^{-1 \text{ b}}$ (minimum thickness 1 cm)
Transcutaneous	Soft tissue/bone energy = 50% ^b	Soft tissue $A/f = 0.5 \text{ dB MHz}^{-1 \text{ b,d}}$

*AIUM/NEMA Model^e for Transvaginal and Transcutaneous***Embryo**

Soft tissue

$\alpha/f = 0.44 \text{ dB cm}^{-1} \text{ MHz}^{-1}$

Second and third trimester

Soft tissue

$\alpha/f = 0.3 \text{ dB cm}^{-1} \text{ MHz}^{-1}$

Intraoperative^a

(fluid path prior to sensitive tissues)

Soft tissue

$\alpha/f = 0.44 \text{ dB cm}^{-1} \text{ MHz}^{-1 \text{ b}}$

Soft tissue/bone energy = 50%

Neonatal Head

Soft tissue

$\alpha/f = 0.25 \text{ dB cm}^{-1} \text{ MHz}^{-1 \text{ g}}$

Soft tissue/bone energy = 50%

**General Imaging
Echocardiography**

Soft tissue

$\alpha/f = 0.44 \text{ dB cm}^{-1} \text{ MHz}^{-1 \text{ b}}$

Soft tissue

$\alpha/f = 0.25 \text{ dB cm}^{-1} \text{ MHz}^{-1 \text{ g}}$

Soft tissue

$\alpha/f = 0.25 \text{ dB cm}^{-1} \text{ MHz}^{-1 \text{ g}}$

Soft tissue

$\alpha/f = 0.44 \text{ dB cm}^{-1} \text{ MHz}^{-1 \text{ b}}$

^aIn these and other intracavity applications, self-heating of transducers may be important.^bNCRP (1992)^cMay be reduced once additional reliable data are available.^dAlternatively, if the overlying thickness of tissue is known or can be estimated, use an appropriate attenuation coefficient.^eAIUM/NEMA (1992).^fNon-zero attenuation might be considered in the future for frequencies >10 MHz.^gBased on the best estimate from currently available data.

for users in controlling outputs to minimize true pressures and temperature increases.

ODS (AIUM/NEMA, 1992) discussed above was developed by AIUM and NEMA along with representatives of FDA, the Canadian Health Protection Branch, NCRP, and 14 other medical ultrasound organizations. The homogenous attenuation path Model H_3 , which assumes the specific attenuation coefficient to be $0.3 \text{ dB cm}^{-1} \text{ MHz}^{-1}$ (Table 9.1), was adopted for the standard for real-time display of MIs and TIs on ultrasound systems in which the indices MI or TI exceed certain levels. To help judge whether the current models are overly, or insufficiently, conservative in specific cases, ODS, and certain international models, are reviewed below. Specific numerical models are presented along with examples of unusual situations in which any exposure quantities might be higher than expected. Attention also is given specifically to anatomical situations in which the homogeneous attenuation model (H_3), may overestimate the attenuations and, hence, underestimate the exposure to certain tissues that might be particularly vulnerable. It was noted before, however, that in most cases, the exposure quantities are significantly *overestimated* by the H_3 and other models.

Prior to incorporation in ODS, the homogeneous attenuation model (H_3), was in use for manufacturer's responses to requirements on output disclosures as part of the 510(k) procedure used by FDA for approval of marketing medical ultrasound devices (FDA, 1985). An alternative to exclusive use of the H_3 model, considered in Section 9.3.4, is its use only for certain situations and the use of the F2 model in others. Specifically, H_3 has been proposed only for use with MI and TIS indices computed for soft tissue heating, and for use with the F2 model TIB computed for heating of a bone interface lying at the depth for maximal heating. This use of the F2 model, involving "reasonable-worst-case" estimates (Section 9.3.1) for both the attenuation along the propagation path and for the absorption at the target (bone), would give a "high-worst-case" estimate for TIB. Then, TIS also could be considered as a high average value. These and other *obstetrical* exposure considerations will be discussed in subsequent sections, because it is important for those concerned with ultrasound safety and diagnostic capabilities to be able to estimate as accurately as possible the exposure to the fetus and other potentially critical tissues. As estimated outputs approach relevant bioeffects thresholds, it is important to understand the general relations between the *best practical* models for TIs and MIs that can be provided by equipment in real time.

The World Federation of Ultrasound in Medicine and Biology (WFUMB, 1992) developed models for several critical applications

as summarized in Table 9.2. Refinements and additions to this list of examination-specific or body-part-specific models are presented below, with emphasis on potential mechanical effects. Most notably, attention is paid to sites in the body where ultrasound can be incident on boundaries between air spaces and tissues, *i.e.*, sites where exposure quantities may be increased by reflections, or in which cavitation effects may occur. Attenuation properties of tissues relevant to these additional models are summarized in WFUMB (1992) and listed with minor modifications in Table 9.3. These values are generally consistent with those listed previously by NCRP (1983; 1992).

Recent *in vivo* measurements of insertion loss between fetal sites and the maternal abdominal skin (Siddiqi *et al.*, 1992; 1995b) are discussed in Section 9.3.3. They indicate higher average attenuation coefficients per unit frequency for abdominal wall than those listed in Table 9.3 for typical water-bearing soft tissues. The mean value of the frequency-specific attenuation coefficient for the full bladder group is $0.4 \text{ dB cm}^{-1} \text{ MHz}^{-1}$ with a range of 0.14 to 0.9. However, the distribution of insertion losses was wide and highly asymmetric such that the median insertion losses were somewhat lower than the quoted mean values. As discussed below, underestimation of attenuation by average insertion loss measurement is essentially impossible and overestimation is quite likely. The insertion loss regression lines indicate uterine-muscle attenuations at or below those listed in Table 9.3, but also indicate anomalously high attenuation coefficients for urine and amniotic fluid. The latter may be due in part to reflection and attenuation losses in and at the bladder wall and artifactual refraction losses.

9.2 General Diagnostic Considerations

9.2.1 *Patient-Specific Adjustment of the Homogeneous Attenuation Model*

In many cases where the tissue path is presumed to consist of acoustically homogeneous tissues, it is appropriate to utilize the homogeneous attenuation model H_3 ($0.3 \text{ dB cm}^{-1} \text{ MHz}^{-1}$), adopted by FDA (1991) and in ODS (AIUM/NEMA, 1992; 1998). While more conservative than Model H_4 , Model H_3 is appropriate for calculations providing generally conservative, real-time feedback to the medical imaging specialist during diagnostic examinations. In general cases where a most-likely attenuation estimate is required, without utilizing knowledge of fluid path lengths in specific exams or exam types,

TABLE 9.3—Most relevant acoustic properties of tissues at 37 °C (Duck, 1990; NCRP, 1983; 1992; WFUMB, 1989).

Tissue Types	Speed of Sound (m s ⁻¹)	Frequency-Specific Attenuation Coefficient dB cm ⁻¹ MHz ⁻¹	Frequency (f) Dependency of Attenuation Coefficient ^g	Nonlinearity Parameter B/A ^b
Adult Tissues				
Typical water-bearing soft tissues	1,540–1,580	0.3–0.8 ^c	f ^d	
Amniotic fluid, urine	1,540 ^e	0.002–0.004 ^f	f ²	6.1 ^{g,h}
Bone, cortical	3,000–4,200 ^{i,j,k}	13–26 ^l	f	
Bone, trabecular	1,700–2,100 ⁱ	25–45 ^l	f	
Brain	~1,560 ^m	0.3–0.5 ^{m,n}	f	
Fat	1,410–1,490 ^{m,n,o,p,q,r}	0.5–1.8 ^{o,p,q}	f ^a	10.3 ^r
Liver	1,580–1,610 ^{t,u,v,w}	0.4–0.7 ^{t,x,y}	f ^d	6.8 ^z
Skin ^{aa}		2.0	f ^d	
Skeletal muscle normal to fibers		0.55 ^{bb,cc}		
Smooth muscle (uterus)		0.2–0.6 ^{c,dd,ee}	f	
Tendon (low water content)	1,600–2,000 ^{ff}	~1.0	f ^d	

Testes (high water content)	1,595 ^{eg}	~0.13 ^{hh}	f^d
Lung		42 ⁱⁱ	
Conceptus to Infant Tissues			
Bone	2,100 (vs. 2,410 adult) ^{jj}	kk	f
Brain (fetal)	1,520-1,540	~0.16 ^{ll}	f^d
Brain (infant)		0.16 ^{aa}	
Embryo	~1,550	mm	f
Liver	~1,540 ^z	0.43 at 25 wk to 0.55 at 46 wk ^{oo}	f^d
Lung		0.5 at 25 wk to 0.35 at 46 wk ^{pp,qq}	f^d
Skeletal muscle			
Skin			
Water ^{aa}	1,523	0.0022	f^2

^aWhen the attenuation coefficient does not vary linearly with frequency, it still varies with frequency to some other power of frequency. The values given in Column 3 of the specific attenuation coefficient are convenient approximations that have been used.

^bThe data are from page 98 in Duck (1990). The coefficient of nonlinearity $\beta = 1 + B/2A$ (see Appendix D for definitions and discussion).

TABLE 9.3—Most relevant acoustic properties of tissue at 37 °C (continued)

^c NCRP (1983).
^d f^n where n is 1 to 1.3. For simplicity, assumed to be $n = 1$.
^e Carpenter, D.A. (1991). "Variation in sound propagation velocity from 1529 to 1549 m/s in human urine depending on patient hydration," personal communication (CSIRO - Telecommunications and Industrial Physics, Lindfield, NSW, Australia).
^f Zana and Lang (1974).
^g Sun <i>et al.</i> (1985).
^h Measured at less than 30 °C. For water-dominated tissues below 37 °C, B/A tends to increase with increasing temperature. B/A for 3.3 percent saline increases from 5.21 to 5.37 between 20 and 30 °C (page 99 of Duck, 1990). The temperature coefficient for B/A for human liver between 20 to 37 °C is reported as 0.026 °C (Sehgal <i>et al.</i> , 1986).
ⁱ McKelvie and Palmer (1987).
^j Lees <i>et al.</i> (1983).
^k Yoon and Katz (1979).
^l Fry and Barger (1978).
^m Kremkau <i>et al.</i> (1981).
ⁿ Lyons and Parker (1988).
^o Gammel <i>et al.</i> (1979).
^p Lehmann and Johnson (1958).
^q Schwan <i>et al.</i> (1953).
^r Errabolu <i>et al.</i> (1988).
^s f^n where n is 1 to 1.4. For simplicity, assumed to be $n = 1$.
^t Wilson <i>et al.</i> (1987).
^u Rajagopalan <i>et al.</i> (1979).
^v Bamber and Hill (1979).
^w Chen <i>et al.</i> (1987).
^x Lin <i>et al.</i> (1987).
^y Foster and Hunt (1979).
^z Sehgal <i>et al.</i> (1986).

- ^{aa}Duck (1990).
- ^{bb}Goss *et al.* (1978).
- ^{cc}Goss *et al.* (1980).
- ^{ddd}Masaoka *et al.* (1987).
- ^{ee}Hussain *et al.* (1992).
- ^{ff}Daft and Briggs (1989).
- ^{gg}Jellins and Barraclough (1978).
- ^{hh}Bamber (1981).
- ⁱⁱDunn and Fry (1961).
- ^{jj}Fredfeldt (1986).
- ^{kk}Progresses from soft tissue to nearly adult values from 9 to 40 weeks post conception (Dubowitz *et al.*, 1970).
- ^{ll}Wladimiroff *et al.* (1975).
- ^{mmm}Sun *et al.* (1986).
- ⁿⁿHigh water content (Wladimiroff *et al.*, 1975) (after the embryo is not adhering directly to the endometrium) gives a lower than average soft tissue specific attenuation coefficient, as yet not well specified, most probably less than $0.3 \text{ dB cm}^{-1} \text{ MHz}^{-1}$.
- ^{oo}Carson *et al.* (1990).
- ^{pp}Thieme *et al.* (1993).
- ^{qq}Meyer *et al.* (1984).

a homogeneous attenuation model with an average specific attenuation coefficient of 0.4 or 0.5 dB cm⁻¹ MHz⁻¹ would be more appropriate. Then, if additional knowledge of overlying tissue identities or thicknesses is available, the best available estimate of attenuation coefficients and thicknesses should be employed in the models. These patient-specific calculations are discussed in Section 9.3 in relation to transcutaneous obstetrical examinations.

9.2.2 *Nonlinear Propagation and Other Effects Limiting the Accuracy of Tissue Models for Exposure Estimates*

Errors resulting from NLP of ultrasound, which become significant at relatively high levels of the acoustic pressure, have not been explicitly corrected for in existing standards (AIUM, 1992; AIUM/NEMA, 1992; IEC, 1992). Because of nonlinear behavior, the energy originally emitted at the transducer fundamental frequency is transferred to higher harmonics during propagation, and the waveform becomes distorted. Also, with nonlinearity in the propagation path, the peak pressure at the transducer focus does not increase as rapidly as the applied transducer voltage. Because such effects are much more pronounced in a medium where the attenuation is small than in one where it is large, several errors arise in derating procedures, *i.e.*, in estimating acoustic field quantities in the attenuating tissues of the body from field quantities measured in relatively unattenuating water (Appendix D). In many diagnostic systems operating at maximum output, there can be significant nonlinear distortion of the ultrasound wave (Duck and Martin, 1991), particularly when it propagates in media of low attenuation, such as water and body fluids. In fact, the pressure levels generated in water by many diagnostic instruments are near "saturation," meaning that the peak pressure amplitude does not increase for increases in output power at the transducer. Such saturation effects do not occur as significantly where the attenuation is higher. Therefore, applying derating calculations to the saturated values measured in water might be expected to underestimate the peak pressure and intensity in soft tissues.

Use of water measurements at low applied transducer voltages and linear extrapolation to the highest applied voltages, followed by linear derating, tends to produce the opposite effect, *viz.*, overestimation of the actual pressures that would be achieved in water or tissue. This use, however, is a more conservative approach and has been recommended in reports by WFUMB (1992; 1998) and at least one of the ultrasound-system manufacturers partially follows this approach in its MI calculations. A more correct result than is obtained with

either of the two approaches could be obtained by computation with the appropriate NLP equations (Christopher and Parker, 1991) and extrapolation from data measured in water at low output voltages (Appendix D). This latter approach has not been implemented for real-time-display standards to date because of the extensive computations or computer look-up tables, required for the ultrasound system. However, such computational abilities are becoming more feasible (Cahill and Humphrey, 2000; Carson, 1999; Christopher, 1999; Fowlkes and Holland, 2000).

Derating problems could be avoided if the output pressure waveforms were measured in a medium having attenuation and sound-speed characteristics corresponding to that of the subject tissue model, and having a nonlinearity parameter similar to that of tissue; then, the measured pressures and derived intensities would be the correct values for that model. It is possible that liquids with such attenuating properties and suitable for acoustic field measurements will be available soon.

Another factor limiting the accuracy of simple derating of field parameters for attenuation considerations is that the effect of bandwidth on attenuation is usually ignored. Preferential attenuation of higher frequency components of pulsed waveforms results in a downward shift of the center frequency of the spectrum with increasing depth in the medium (Zagzebski *et al.*, 1982). Most applications of models simply assume that the ultrasound beam is attenuated at the center frequency of the pulse; for broad bandwidth pulses, the actual pulse-beam attenuation could be lower than that assumed by application of the model. This phenomenon would be more important in B-mode imaging than in the narrower-bandwidth Doppler modes.

Another effect limiting the accuracy of estimates occurs when sound beams undergo beam distortion. Usually the dominant forms of distortion are defocusing and abnormally high attenuation in soft tissues because of refraction and scattering (Banjavic *et al.*, 1979). These factors are not included in derating models because of the attempt to be conservative in the calculations and because of the relative unpredictability of these effects.

Some important work has been performed (Bly *et al.*, 1992; Jago *et al.*, 1999; Patton *et al.*, 1994) to evaluate outputs from existing pre-amendment ultrasound equipment with published fixed-path obstetrical models (NCRP, 1992) and the H_3 homogeneous attenuation model ($0.3 \text{ dB cm}^{-1} \text{ MHz}^{-1}$). These evaluations have some bearing on the adequacy of the tissue models as well, particularly as they relate to the effects of nonlinear acoustic propagation.

9.2.3 Considerations with Use of Microbubble Contrast Agents

Contrast agents, composed of small particles with gaseous content, are now widely used in diagnostic ultrasound. Their physical behavior in an ultrasound field, discussed in Section 4.3, is similar to that of small bubbles. It is shown in Sections 6, 7 and 8 that their presence can sometimes significantly affect the biological effects produced by ultrasound in cell suspensions and in mammalian tissues. The presence of microbubble contrast agents in blood and tissues increases the attenuation coefficient, but also decreases the threshold for inertial and other cavitation effects relative to that of pure blood.

Several contrast agents are rather selective to specific organs. Some are stable enough that time can be allowed for them to become concentrated into groups around the reticulo-endothelial cells in the liver and spleen and are primarily of interest for those organs. The particles are small enough and administered diffusely enough that they are likely to be imaged only in those organs and in pathology with concentrations of macrophages. Unless severe cavitation activity causes significant damage to the vascular wall or the chorionic plate in the placenta, the micron-size-bubble contrast agents are not likely to move in large quantities from the vasculature to the tissues supplied. However, it is an open question as to whether some intravenously injected microbubble contrast agents are likely to pass through these vascular barriers and affect cavitation thresholds significantly in or adjacent to critical cells in the patient or the fetus.

GI contrast agents are designed primarily to reduce bubbles in the GI tract, particularly in the stomach. In that role, they are likely to reduce somewhat the incidence of cavitation.

9.3 Obstetrics

9.3.1 Introduction

When the very highest outputs now available from some diagnostic systems are required, the need will arise for estimates of exposure to the fetus, based on the best information available, including individual patient data such as maternal weight and minimum thickness of overlying tissues. When these patient-specific estimates are not feasible but rather high exposures are expected, estimates might best be based on *reasonable-worst-case* assumptions regarding factors that vary from one patient to another. Such assumptions are,

ideally, those in which it is expected that (for given settings of the ultrasound equipment) a critical exposure quantity will not be exceeded in more than some percentage of the particular class of patients being considered. It has been found useful to define, for any exposure quantity (q) its reasonable-worst-case value, say, $q_{2.5}$, for a given class of exposures: the latter is a value such that no more than 2.5 percent of the actual q values will exceed $q_{2.5}$. In a normal distribution of any observed quantity, 2.5 percent of the observations exceed the mean by, at least, twice the standard deviation (Carson *et al.*, 1989a; WFUMB, 1992).

In addition to $q_{2.5}$, physicians may want to know a quantity closer to the mean value; *i.e.*, they may want to know an anticipated exposure quantity that will not be exceeded in some higher percentage of the patients in a given class; this might be labeled a “typical value of the quantity,” say, q_{typ} . Typical exposure estimates are a less conservative alternative to reasonable-worst-case estimates. For example, a percentage of individuals for which the exposure quantity is greater than q_{typ} might be 33 or 50 percent of the cases, but the term q_{typ} has not been defined precisely. Typical exposure estimates are particularly useful in estimating risk levels to an entire class of patients, or to individuals when the individual risks are small and are proportional to total exposure. For example, in typical diagnostic x-ray imaging, where the risk from radiation is exceedingly low but thought to exist at even the lowest exposures, it is sensible to quote an average or typical exposure (NCRP, 1977). An exception is made to this when the embryo/fetus is exposed to a sufficiently high dose that there is more than usual concern for its safety. In that case, a patient-specific dose estimate is made.

Biological effects of ultrasound are typically viewed as showing thresholds even though the latter may not always be well defined. The goal might well be to choose exposures in which the user can be fairly sure that the thresholds are not exceeded. This might be particularly true in first-trimester obstetrical examinations in which damage to a few cells can have major effects. In the increasingly rare trans-abdominal first-trimester obstetrical examinations, the occasional large, minimally attenuating, fluid path can be a source of significant underestimates of exposure with the dominant models for attenuation by overlying tissues. If general exposure estimates are high for given settings, and these settings may be needed for obtaining the necessary diagnostic information, then more examination-specific or patient-specific estimates ought to be made.

Because attenuation by overlying tissues (*i.e.*, tissues between source and target) is probably the dominant source of uncertainty in estimates of fetal exposure, one simple approach for defining limiting

conditions is to require that this attenuation not be overestimated in more of the patients than the percentages defined for reasonable-worst-case and typical estimates. Other sources of uncertainty include errors in measurements of the actual field quantities, such as acoustic pressure, in the ultrasound beam. For calculating TI, assumptions about transducer self-heating, tissue absorption coefficients, tissue perfusion, and acoustic quantities along the entire beam path are important. It has been argued that the errors in possibly underestimating the heating in any obstetrical case using the homogeneous-attenuation model H_3 ($0.3 \text{ dB cm}^{-1} \text{ MHz}^{-1}$) are relatively small and will be quite infrequent in actual practice. Further, it can be argued that an attenuation-path estimate only moderately more conservative than the average expected attenuation would be more valuable in clinical use than a worst-case model. There might well be concern that the accumulation of conservative assumptions, taken in series over the several stages of calculations to arrive at MIs and TIs, would produce such high, unrealistic pressure and temperature estimates that users would tend to discount them. However, if users are aware of the fraction of cases in which the attenuation is greater than that assumed and of the fraction in which other beam intensity effects and target effects might be overestimated, appropriate interpretations can be assigned to high values of those indices based on direct observation of the subject and knowledge of the examination.

In more complex estimates of exposure, using significantly more information than is now available, the probabilities of the various variables affecting the estimate might be combined in such a way that the final worst-case estimate of exposure is not actually exceeded in over a certain percent of the cases. A percentage of 2.5 has frequently been used as the number of underestimates of exposures in reasonable-worst-case estimates (*e.g.*, Carson *et al.*, 1989a). However, because the quantitative combination of uncertainties has not yet been attempted, it is reasonable to apply the reasonable-worst-case assumption to the largest source of uncertainty, *viz*, the overlying attenuation model. In a fully analyzed system, any easily identified class of patients (such as obstetrical examinations with a full bladder) would not be unknowingly exposed in a higher percentage of cases than the accepted reasonable-worst-case level.

9.3.2 *Measurements of Path Lengths in Individual Tissues Overlying the Fetus*

A series of studies of overlying tissue path lengths was reported with progressively increasing attention to worst-case (shortest soft

tissue and longest fluid) path lengths and to phase-independent attenuation measurements (Carson *et al.*, 1989a; Duck and Perkins, 1988; Hall, 1975; Smith *et al.*, 1985). The data do suggest that the attenuation along overlying-tissue paths throughout gestation is somewhat less than that in model F2 (Table 9.1), but not by more than a factor of 2 dB. Duck and Perkins (1988) studied tissue path lengths in procedures involving scanning through the bladder to the gestational sac. In 74 randomly chosen obstetric ultrasound scans, the investigators measured a least tissue thickness overlying the bladder of 0.7 to 6 cm with a mean of 2.1 cm and a standard deviation of 0.8 cm. The greatest bladder depth (presumably greatest path length to the distal internal border of the bladder) ranged from 3 to 10.5 cm with a mean of 7.5 cm.

A tissue-thickness study (Ramnarine *et al.*, 1993), which included most types of common obstetrical examinations, provided data independent from, but consistent with, the most recent data available for NCRP Report No. 113 (NCRP, 1992). It was estimated from the Ramnarine study that the beam traverses the bladder in 30 percent of transcutaneous, first-trimester examinations. Data in their Figure 1 for cases with the beam traversing the bladder are redrawn in Figure 9.1, along with data from the AIUM report (AIUM, 1993a).⁷ These data are discussed below.

For the *reasonable-worst-case* in first-trimester examinations, a different model than H_3 (Table 9.1) is warranted by the data and analysis represented in Figures 9.1, 9.2 and 9.3. The fixed-path model at 1 dB MHz⁻¹ (F1 in Table 9.1) would be a reasonable-worst-case model for first-trimester examinations through the distended bladder. Another such model that appears appropriate for the data of Figure 9.1 is [(0.3 d - 1) dB MHz⁻¹], where d is the thickness (in centimeters) of the overlying tissues. Only the fixed path model is justifiable as a reasonable-worst-case for the full bladder first-trimester data combined from Ramnarine *et al.* (1993) and from Zagzebski *et al.*⁷ as analyzed in Figures 9.2 and 9.3. In Figure 9.1, the lower Curve C marks the level at which 97.5 percent of future individual points would be expected to lie above the line.

9.3.3 Insertion-Loss Measurement In Vivo

The attenuation estimates described above were based both on measured tissue thicknesses and measured attenuations. These

⁷Zagzebski, J., Curmally, S. and Purath, L. (1991). Unpublished data compiled at the University of Wisconsin, School of Ultrasound, distributed at the Output Display Committee Meeting, 1991, New Orleans, Louisiana and later included in an AIUM conference report (AIUM, 1993a).

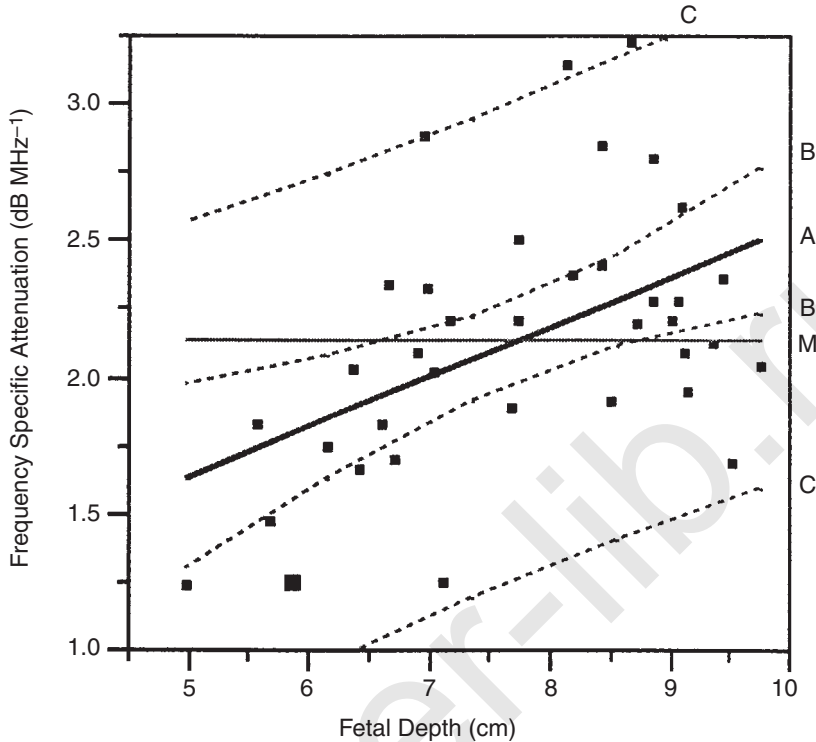


Fig. 9.1. Frequency-specific attenuation versus fetal depth (adapted from Ramnarine *et al.*, 1993). Shown are the data points for each subject studied, for which the ultrasound passed through the distended bladder. The solid line (M) shows the mean frequency-specific attenuation of 2.14 dB MHz^{-1} , while line (A) gives the least-squares fit of $(0.18 d + 0.7) \text{ dB MHz}^{-1}$, with d in centimeters. Also, the dotted lines show the 95 percent CI for the regression line (B) and for the data points (C). The slope of the best-fit line, $(0.18 \pm 0.05) \text{ dB cm}^{-1} \text{ MHz}^{-1}$, is significantly different from that of Model H₃, which falls outside the 95 percent CI.

separately measured attenuation coefficients utilized modern phase-insensitive techniques (NCRP, 1983), which usually indicate how rapidly power is attenuated in the beam as a function of distance traveled. Tissue-attenuation estimates based on these phase-insensitive measures are probably best for estimating heating effects of ultrasound beams (NCRP, 1992) and may be the most practical, certainly the most conservative, estimates for mechanical effects, which depend primarily on pressure amplitude.

Attenuation coefficients reported in the literature often have been measured *in vitro* both by phase-sensitive and phase-insensitive

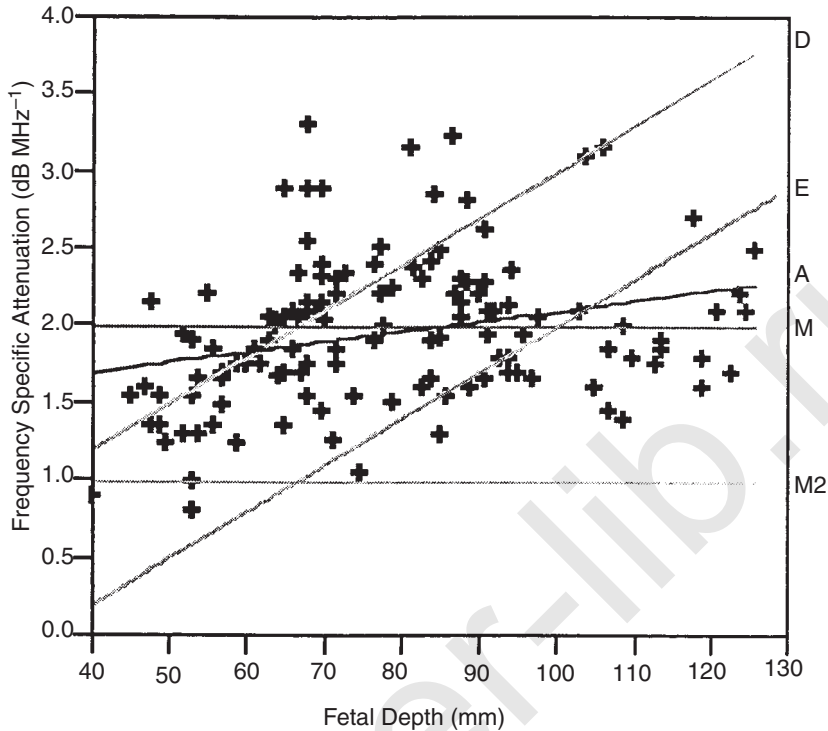


Fig. 9.2. Frequency-specific attenuation versus fetal depth (d). Here the data from Figure 9.1 are combined with the Zagzebski *et al.* data (Figure 5.3, AIUM, 1993a); the latter data include one point from a transverse and a longitudinal scan of each subject. (A) indicates the line of linear regression, $(0.07 d + 1.4)$ dB MHz⁻¹; (M) is the mean attenuation, 2 dB MHz⁻¹, (M2) gives the mean M minus twice the standard deviation; finally, lines (D) and (E) represent, respectively, $0.3 d$ and $(0.3 d - 1)$ in dB MHz⁻¹ where d is in centimeters.

methods [Duck (1990) and Table 2.3 of NCRP Report No. 74 (NCRP, 1983)]. When attenuation coefficients have been measured *in vivo*, by modern backscatter tissue-characterization methods (Kuc and Schwartz, 1979; Meyer *et al.*, 1984; Ophir and Mehta, 1988), the values obtained have usually been relatively low, like those from the phase-insensitive measurements (Bamber, 1981; Goss *et al.*, 1978; 1980; NCRP, 1983). However, with few exceptions, the *in vivo* backscatter-based measurements and phase-insensitive measurements have not included the highly heterogeneous and rather highly attenuating mixtures of skin, fat, muscle and connective tissue that comprise the abdominal wall. The earliest measures of the average

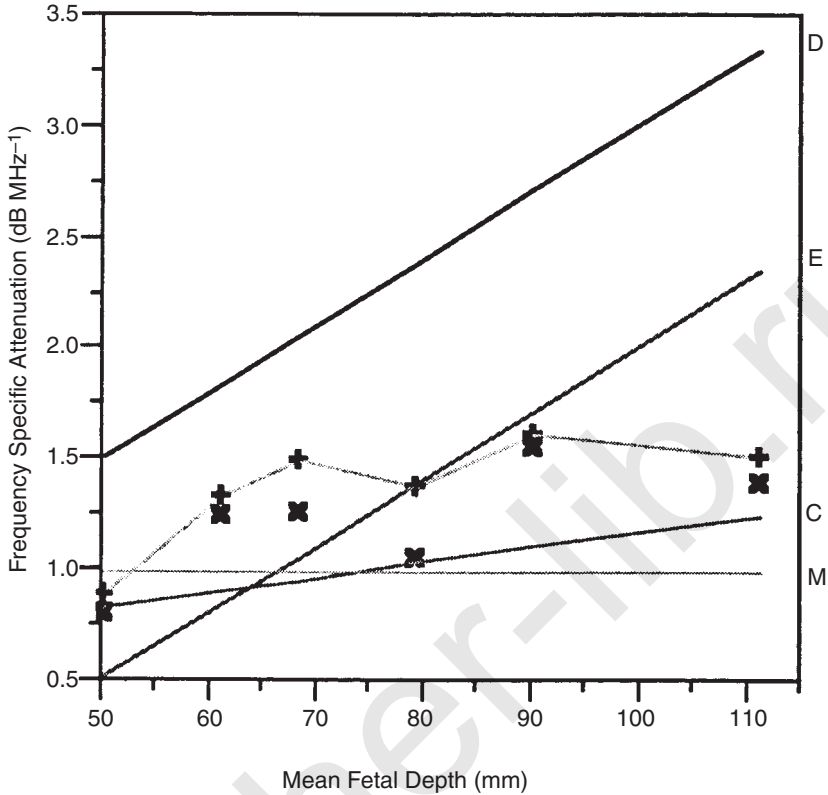


Fig. 9.3. Re-analysis of the data in Figure 9.2, using a generalized additive model that accounts for possible non-Gaussian distributions. Curves D, E and M have the same meanings as in Figure 9.2 and Curve C is the lower 95 percent limit for the data, as in Figure 9.1. The 2.5 percent quantile (+) and 10 percent quantile (x) of the data are shown for comparison.

attenuation coefficient between transducers on the skin and small receiver in the uterus (Bang, 1972) were difficult to obtain because the receiver was not small enough to mitigate against phase-cancellation effects due to coherent summation of pressures over a region in which they would be varying. Phase aberration, caused by beam passage through nonplanar tissue inhomogeneities, can produce interference of the beam with itself or refraction of the beam. If the wave pressure is measured with a piezoelectric (pressure sensitive) transducer, bending or distortion of the wavefront can cause the pressure peaks from different parts of the wave to arrive at the receiving transducer face at different times; this can result in a lower recorded peak pressure amplitude than might exist and be measured

for a slightly different scanhead position or angle. Furthermore, if the beam is defocused in any way by the overlying tissues, the peak pressure and pressure-squared integral will not yield accurate estimates of the *in situ* power, which is an important determinant of local heating. These errors would tend to cause underestimates of expected exposures and, therefore, would be considered aggressive, rather than conservative. (Phase-insensitive attenuation measurements would be preferred because they should be accurate or should underestimate the attenuation, leading to a correct estimate or an overestimate of pressure amplitudes).

Direct measurements of pressure *in situ* are extremely difficult to perform with accuracy. If a small piezoelectric transducer is employed, the beam pattern for reception is broadened, but not as much as expected from simple theory (Shombert *et al.*, 1982). However, the small receiver transducer must be scanned extremely carefully in three dimensions with the transducer in fixed orientation and in less detail in two other orientations to find the true peak pressure for a given entrance beam path into the uterine cavity through tissues that cause phase aberration. The possibility would still always exist that the beam would not be nearly as distorted passing through a slightly different path of the tissues. Therefore, to measure the maximum possible pressure transmission through tissues overlying the fetus, the transmitting transducer must be moved around over the skin. For each transmitter location, the small detecting transducer in the uterus or other detection point would have to be scanned in three dimensions. These measurements and that of *in situ* total power should be improved greatly when relatively large, high-quality, dense, 2D array hydrophones are developed.

Siddiqi *et al.* (1991; 1992; 1995b) manually manipulated an array of small transducer elements (Daft *et al.*, 1990) to help locate the peak pressure transmitted into the uterus or vaginal fornix. Such hand-scanning procedures are probably the best practically achievable for estimating peak acoustic pressures without dense 2D arrays. From these values (as explained below) values of the insertion loss were obtained. Careful search procedures for maximum peak pressures (minimum insertion loss) apparently were performed. However, almost any error in the search for maximum pressure amplitude will cause an overestimation of the insertion loss. In Siddiqi's work (*e.g.*, Siddiqi *et al.*, 1995b), mean values were emphasized rather than reasonable-worst-case values. Five measurements were made in each uterus, but the value analyzed was of the *mean* of those pressures and intensities, rather than the peak of the five. For estimating the potential for bioeffects, one is most interested in

whether damage might occur. While the mean is a useful quantity, information on the peak values is needed for safety considerations.

Results similar to those from tissue-path-length-measurements (Figures 9.1, 9.2 and 9.3) were obtained from actual transmission insertion-loss measurements and are plotted in Figure 9.4a.⁸ In making these measurements, a hydrophone array that had been inserted into the vaginal fornix of a nonpregnant woman volunteer received the signal from a 3 MHz imaging transducer applied to the abdomen. The signal level was compared with that received when the same transducer and hydrophone array were placed in a 37 °C water bath and operated in the same configuration as before. From the ratio of signal amplitudes for the two situations the insertion loss was determined. Those results are analyzed more extensively in Siddiqi *et al.* (1992), but without presentation of the raw data. Another significant study (Siddiqi *et al.*, 1995b) provided insertion loss measurements for first- and second-trimester transcutaneous ultrasound with a hydrophone array in the uterus among the products of conception (Figure 9.4b). All but one of the full bladder studies are from the first trimester, as are 60 percent of the empty-bladder studies. The insertion loss per unit frequency is referred to here as the specific insertion loss. Table 9.4 presents values of the mean and standard deviation reported by Siddiqi *et al.* (1995b), assuming three different models: F as the fixed path (dB MHz^{-1}), H as the homogeneous attenuation ($\text{dB cm}^{-1} \text{MHz}^{-1}$), and O as a model of specific attenuation coefficient for each centimeter of overlying soft tissue not counting fluids ($\text{dB cm}^{-1} \text{MHz}^{-1}$).

9.3.4 Obstetrical Attenuation Models

Data up to 1991 (NCRP, 1992) suggested the desirability of fixed path models F2 and F3, for second- and third-trimester transcutaneous examinations, which are relatively conservative compared with the first-trimester model, F1. The reduction in estimated minimum attenuation with increasing gestational age, or trimester, was based on image data and the stretching and thinning of the abdominal wall which typically occurs as pregnancy progresses. For second- and third-trimester examinations for the fetal-abdominal cross section and the biparietal diameter, Ramnarine *et al.* (1993) found that worst-case conditions could be met by a fixed-path model with attenuation of 0.8 dB MHz^{-1} . (They also observed, however, that only

⁸O'Brien, W.D., Jr. (1991). Data analyzed in Siddiqi *et al.* (1992). Presented at Output Display Committee Meeting, 1991, New Orleans, Louisiana.

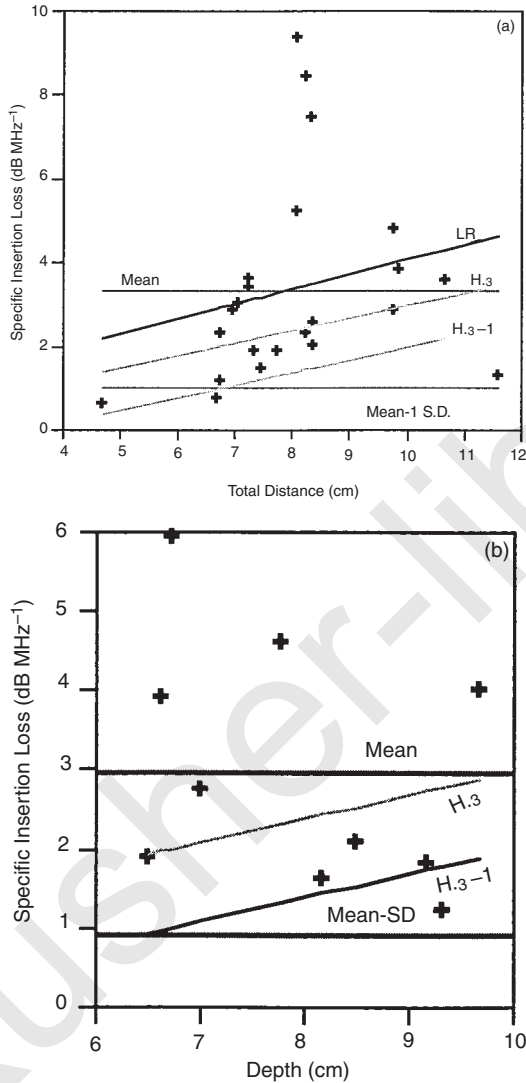


Fig. 9.4. Plots of insertion loss per unit frequency in transabdominal scans as a function of skin to hydrophone depth (d). Plotted are the mean, the Model $H_{3, 1}$ dB MHz^{-1} less than $H_{3, 3}$, and the mean minus one standard deviation (SD). (a) The receiver probe in the vaginal fornix during ovarian scans with a full (or nonempty) bladder (data analyzed in Siddiqi *et al.*, 1992). (b) First-trimester (and a small number of second-trimester) insertion-loss measurements with the hydrophone array in the uterus (Siddiqi *et al.*, 1995b). The linear regression (LR) line is plotted in (a), but the linear regression slopes and intercepts are not significant in (a) or (b) and the lower 95 percent CI are negative.

TABLE 9.4—*In vivo* insertion-loss data expressed in resulting frequency-specific values of the attenuation or attenuation coefficient (Siddiqi *et al.*, 1995b).

Bladder	Parameter	Attenuation Model		
		F = Fixed Path (dB MHz ⁻¹)	H = Homogeneous (dB cm ⁻¹ MHz ⁻¹)	O = Overlying (dB cm ⁻¹ MHz ⁻¹)
Empty	Mean and standard deviation	3.9 ± 2.3	0.56 ± 0.36	0.82 ± 0.55
	Range	1.1 to 9.6	0.16 to 1.4	0.19 to 2.1
Full	Mean and standard deviation	3.0 ± 1.5	0.40 ± 0.23	0.83 ± 0.54
	Range	1.3 to 5.9	0.14 to 0.89	0.28 to 1.8

negligible error would be made with the 0.3 dB cm⁻¹ MHz⁻¹ homogeneous attenuation model.) In the second-trimester examinations studied by Carson *et al.* (1989a; 1989b), acoustic viewing directions passing through significant amniotic fluid spaces were sought in analyses of the recorded photographs and, in many of the cases, during the examination. Thus, a *larger fraction of cases* than in the study by Ramnarine *et al.* (1993) were observed to have a calculated attenuation which is low compared to average values and low compared with the total length of the acoustic path. Kamel (1994) showed similar results in 52 third-trimester transcutaneous examinations; these were consistent with a reasonable-worst-case, fixed-path model of 1 dB MHz⁻¹ or a homogeneous attenuation for the entire path length of 0.24 dB cm⁻¹ MHz⁻¹.

In transvaginal scans, the first-trimester data of Ramnarine *et al.* (1993) supported the conclusions of the WFUMB symposium summarized in Table 9.2 (WFUMB, 1992); the latter were based on data published later by Hussain *et al.* (1992) and Kossoff *et al.* (1993). Thus, the data are consistent with the H₃ homogeneous attenuation model with a minimum path length of 1 cm. In the data of Ramnarine *et al.* (1993) that model would lead to an overestimate of attenuation in two cases out of 96 (*i.e.*, approximately two percent) by 0.45 dB MHz⁻¹. The data are also consistent with a fixed-path model of 0.6 dB MHz⁻¹.

An attenuation model specifically for obstetrical cases is not included in the dominant standard for informing users of the relative potential for thermal and mechanical effects. That standard, ODS (AIUM/NEMA, 1992), calls for TIs and MIs that are provided by the

displays on an increasingly large fraction of ultrasound systems worldwide. This standard employs only the $0.3 \text{ dB cm}^{-1} \text{ MHz}^{-1}$ homogeneous attenuation model, H_3 (Appendix B). In the decision to include, or not to include, a separate tissue model for obstetrics in ODS, data were available from several publications and some unpublished sources,⁹ *e.g.*, Carson *et al.* (1989b), Duck and Perkins (1988), Hall (1975), and Smith *et al.* (1985). In these publications, exposures were estimated from measurements on ultrasound images in a significant number of obstetrical cases. Pressure waveforms measured *in situ* with a hydrophone (Daft *et al.*, 1990) were also considered. In a reasonable-worst-case analysis, illustrated in Figure 9.1, those sets of data agree rather well with the fixed path attenuation models (NCRP, 1992) $F1 = 1 \text{ dB MHz}^{-1}$, $F2 = 0.75 \text{ dB MHz}^{-1}$, and $F3 = 0.5 \text{ dB MHz}^{-1}$ in the first, second and third trimesters, respectively. Significantly less attenuation than that predicted by the $0.3 \text{ dB cm}^{-1} \text{ MHz}^{-1}$ homogeneous attenuation model, was estimated or measured in over five percent of the cases.

The extensive tissue thickness study (Ramnarine *et al.*, 1993), which included most of the common obstetrical examination types, provided data in addition to those available discussions of ODS (AIUM/NEMA 1992). The greatest impact of their data is in first-trimester examinations, where they estimated, from actual images [for crown rump length measurement and chorionic villus sampling (biopsy)], that 70 percent of cases with a beam path through the bladder had a mean-path, specific-attenuation coefficient less than Model H_3 (the $0.3 \text{ dB cm}^{-1} \text{ MHz}^{-1}$ homogeneous attenuation model utilized for FDA approvals and the ODS). Model H_3 overestimated attenuation in 78 percent of the images studied through the bladder and overestimated attenuation in nine percent of all the transcutaneous cases by 0.9 to 1.2 dB MHz^{-1} , or more than a factor of four in intensity and two in pressure at 7 MHz.

Based on the foregoing discussions, a correction is possible that uses the H_3 homogeneous-attenuation model but with subtraction of 1 dB MHz^{-1} from the overlying attenuation assumed by the Model H_3 . The line 0.3 dB MHz^{-1} , with and without subtraction of 1 dB MHz^{-1} , is shown in Figures 9.1 to 9.4 for comparison with the measured first-trimester (and some second-trimester) data. For all first-trimester

⁹Hottinger, C. (1991). Personal communication, and subsequent presentation at the Output Display Committee Meeting, New Orleans, Louisiana (Saratoga, California).

Carson, P.L. and Kamel, I.R. (1991). Personnel communication and subsequent presentation at the Output Display Committee Meeting, New Orleans, Louisiana (University of Michigan Medical Center, Ann Arbor, Michigan), data analyzed in Kamel (1994).

distended bladder examinations in which MI was of concern, the 1 dB MHz^{-1} correction could be applied by multiplying the displayed MI by 1.12^f , where f is the displayed frequency in megahertz [$1 \text{ dB f}^{-1} (20 f^{-1}) \log(p p_0^{-1})$, therefore, $p p_0^{-1} = 10^{(f/20)} = 1.12^f$]. For similarly correcting TI, the displayed TI would be multiplied by the factor 1.26^f . This model can be thought of as a two-component model, *i.e.*, 3 cm of unattenuating fluid followed by tissue attenuating at the usual $0.3 d \text{ dB cm}^{-1} \text{ MHz}^{-1}$. This two compartment model with the fluid at the surface is somewhat nonphysical and would be a little more conservative than necessary for very short path lengths to the fetus. However, such short path lengths do not occur when the first-trimester embryo/fetus is scanned through the full bladder. Furthermore, it is primarily at high-amplitude ultrasound exposures where the exposure estimates make a significant difference, and high exposures generally should not be needed for very short transabdominal path lengths.

For practical implementation of this model ($0.3 d - 1$) by ultrasound users with ultrasound systems displaying MI and TI as defined by ODS (AIUM/NEMA, 1992; 1998), the displayed MI could be multiplied by 1.12^f (or C_{MI} from Table 9.5) for full bladder examinations in which MI is of concern. Here f is the displayed frequency in megahertz. A multiplicative correction for the displayed TI would be 1.26^f (or C_{TI} from Table 9.5).

This relationship for 3 cm fluid path preceding homogenous tissue also fits well other first trimester data (AIUM, 1993a) and the non-gravid insertion loss measurements (Siddiqi *et al.*, 1992). Those data, also shown in Figure 9.1, fit a fixed path attenuation model of 1.2 dB MHz^{-1} quite well. Subtraction of 1 dB MHz^{-1} from the displayed MI and TI, as plotted in Figure 9.1 and proposed here, would still result in some underestimation of the actual peak negative

TABLE 9.5—Possible correction factors by which to multiply displayed MI and TI in obstetrical examinations performed transcutaneously through the bladder when MI and TI approach levels of concern.

Frequency	C_{MI}^a	C_{TI}^a
3.5 MHz	1.5	2
5 MHz	2	3
7.5 MHz	2	6

^aThe corrections apply only to fetal or maternal uterine artery depths greater than 3 cm.

pressure for four of the eight full-bladder cases presented in Figure 9.1 with fetal depths of 9 cm or more. However, the error in the worst case at the 10.5 cm depth would only be 0.5 dB MHz⁻¹.

In the skin to vaginal fornix insertion loss measurements of Figure 9.1, the Model H₃ (0.3 *d*) underestimates attenuation in 43 percent of the 23 full-bladder measurements and in two of the 21 empty-bladder measurements. It can be seen from the skin to intrauterine insertion-loss measurements in Figure 9.4b that exposure would be underestimated in four (40 percent) of the 10 full-bladder cases and four (16 percent) of the 25 empty-bladder cases by the homogeneous attenuation model (0.3 dB cm⁻¹ MHz⁻¹) and in one each (10 and 4 percent, respectively) by a modified Model H₃ minus 1 dB MHz⁻¹. The 0.3 dB cm⁻¹ MHz⁻¹ - 1 dB MHz⁻¹ model underestimates exposure in only 4 and 18 percent of the cases in Figures 9.1 and 9.2, respectively, making this model a much better reasonable-worst-case model than H₃ itself.

In all the studies represented in Figures 9.1 to 9.4, the data on transabdominal, first-trimester scans with an empty bladder were consistent with the overlying attenuation model H₃ employed in the current TI and MI. For second- and third-trimester examinations for fetal-abdominal cross section and biparietal diameter (Figure 9.5),

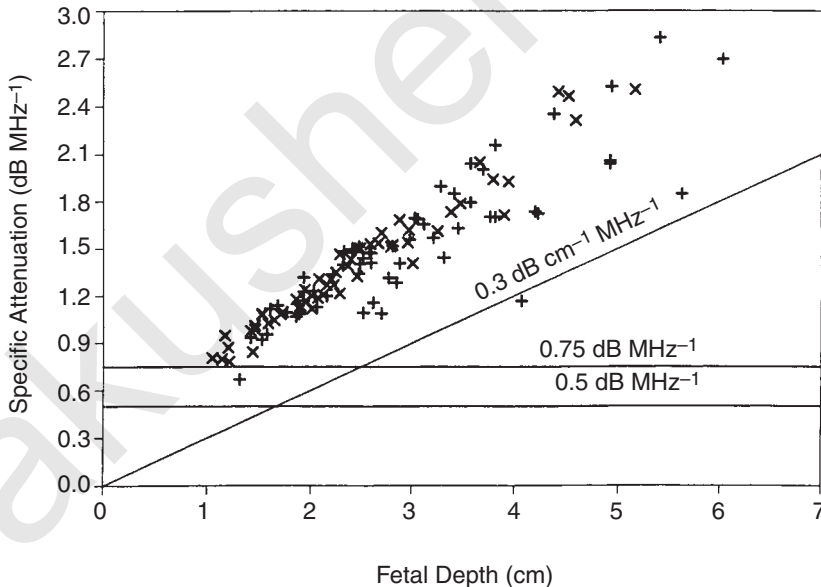


Fig. 9.5. Plot of calculated specific attenuation of overlying tissues as a function of fetal depth for second- and third-trimester transabdominal scans of the fetal abdomen (+) and biparietal diameter (×) (Ramnarine *et al.*, 1993).

Ramnarine *et al.* (1993) found that worst-case conditions could be met by a fixed-path model (F2) with attenuation of 0.8 dB MHz^{-1} , thereby being essentially consistent with the second- and third-trimester recommendations of NCRP (1992). They also observed, however, that almost no error would be made with the $0.3 \text{ dB cm}^{-1} \text{ MHz}^{-1}$ homogeneous attenuation model. This latter observation was based on there not usually being a significant amniotic fluid path between the fetal head or abdomen and the transducer in late second and in the third trimester. This observation indicates a somewhat higher attenuation than that reported in Carson *et al.* (1989a) in which an effort was made to find acoustic viewing directions passing through significant amniotic fluid spaces in analyses of the recorded photographs of second-trimester examinations for amniocentesis. One second- or third-trimester examination in which the fetus is less likely to be pressed against the proximal uterine wall (providing a long amniotic fluid path) is the Doppler study of maternal uterine arteries. Ramnarine *et al.* (1993) showed that in 44 left and 45 right maternal uterine artery measurements, the $0.3 \text{ dB cm}^{-1} \text{ MHz}^{-1}$ homogeneous attenuation model would overestimate attenuation in one measurement by 0.8 dB MHz^{-1} , and in three measurements by 0.4 dB MHz^{-1} .

In summary, the most analyzable published literature relevant to these models that depend only on examination type, and do not depend on specific patient conditions such as maternal weight, are evaluated in Table 9.6. It may be seen that the most conservative model, the fixed path model at 1 dB MHz^{-1} is the only one that is appropriate or conservative for all the studies at approximately the 95 percent prediction level. The next most conservative model, $(0.3 d - 1) \text{ dB MHz}^{-1}$ is appropriate for most of the obstetrical examination types studied, or for all of the examinations types if the prediction limits are relaxed from 95 percent to approximately 80 percent. The $0.3 d$ (dB MHz^{-1}) model (H_3) can be used for studies in which there are no very lengthy fluid paths or in which occasional, large overestimates of attenuation can be accepted. For example, the largest apparent error for TI in the obstetrically relevant Figure 9.2 is 2 dB MHz^{-1} . This value represents an apparent underestimate in the tissue model part of the exposure computation of a factor of 6.3 in TI at 4 MHz, the frequency used to obtain the B-mode images in the Zagzebski *et al.*¹⁰ study. If all other aspects of MI calculation were correct, MI in that case would have underestimated p by a factor

¹⁰Zagzebski, J., Curmally, S. and Purath, L. (1991). Unpublished data compiled at the University of Wisconsin, School of Ultrasound, distributed at the Output Display Committee Meeting, 1991, New Orleans, Louisiana and later included in an AIUM conference report (AIUM, 1993a).

TABLE 9.6—Summary of interpretations of measurements relevant to obstetrical models.

Reference and Condition	Attenuation Model ^a		
	1 dB MHz ⁻¹	0.3 d dB MHz ⁻¹	(0.3 d - 1) dB MHz ⁻¹
Ramnarine <i>et al.</i> (1993) first trimester, not through bladder		X	
Ramnarine <i>et al.</i> (1993) second and third trimester, abdominal and cranial size studies		X	
Ramnarine <i>et al.</i> (1993) second and third trimester, Doppler, fetal umbilical cord		X	X
Ramnarine <i>et al.</i> (1993) second and third trimester, Doppler, uterine arteries	◇		X
Hottinger, ^b umbilical vessel, Doppler	◇		X
Several transvaginal studies (Ramnarine <i>et al.</i> , 1993; Siddiqi <i>et al.</i> , 1995b)	X	X	◇
Ramnarine <i>et al.</i> (1993) first trimester, through bladder	◇		X
Carson <i>et al.</i> (1989a) second trimester	X		
Zagzebski <i>et al.</i> ^c through bladder	X		
O'Brien, ^d skin to vaginal fornix, nongravid	X		◇
Siddiqi <i>et al.</i> (1995b) skin to conceptus parts, through bladder, first and few second trimester	X		◇
Siddiqi <i>et al.</i> (1995b) skin to conceptus parts, not through bladder, first and few second trimester		X	◇
Siddiqi <i>et al.</i> (1991) transcutaneous exams ^d	X		◇
Kossoff <i>et al.</i> (1993), transvaginal, all trimesters, 0.3 dB MHz ⁻¹	◇		◇

^a An "X" is used to indicate that the model fits the data in the left column quite well or is the best available model, ideally, at approximately the 95 percent in the source cited prediction level. An ◇ indicates that the model is a modestly good, second-best fit to the data, either somewhat too conservative or aggressive. For many of the studies these are not the conclusions of the authors of the publications.

^b Hottinger, C. (1991). Presentation and handout at Output Display Committee Meeting New Orleans, Louisiana.

^c Zagzebski, J., Curmally, S. and Purath, L. (1991). Unpublished data compiled at the University of Wisconsin, School of Ultrasound, distributed at the Output Display Committee Meeting, 1991, New Orleans, Louisiana and later included in an AIUM conference report (AIUM, 1993a).

^d O'Brien, W.D., Jr. (1991). Data analyzed in Siddiqi *et al.* (1992). Presented at the Output Display Committee Meeting, New Or-

of 2.5. Since other aspects of TI and MI calculations are generally conservative, the chances that such large underestimates of exposure would occur in a given case are rather small.

As its name suggests, the fixed-path model is more suitable for reasonable-worst-case estimates than one which assumes homogeneous tissue for those examination types offering a minimum thickness of soft tissues (in thin patients) and a variable fluid path length. A fixed-path model also is a good fit for the data of Figure 9.2b. In the "fixed-path model," Equation 20 of Siddiqi *et al.* (1995b), the constant term in the multivariate analysis, the true fixed-path term, was highly significant ($p < 0.008$).

The 0.3 d (dB MHz^{-1}) model gives essentially the same results and allows for simpler user estimates based on MI's from existing ultrasound systems. This model also allows for increased abdominal wall thickness in larger patients as suggested in Figure 9.1b.

Reservations have been expressed above regarding the cases in which the 0.3 $\text{dB cm}^{-1} \text{MHz}^{-1}$ homogeneous attenuation model (H_3) overestimates the attenuation by tissues overlying the fetus. Some believe ODS indices MI and TI should not be taken as approximate indicators of acoustic pressure and temperature rise, but only as monotonically increasing functions of those biophysically relevant quantities, analogous to an automobile speedometer (AIUM, 1994a). However, the overall ODS, with its use of the 0.3 $\text{dB cm}^{-1} \text{MHz}^{-1}$ homogeneous attenuation model, contributes to calculations of MI and TI that can be thought of qualitatively as reasonable-worst-case for most examinations, including several obstetrical situations (Bly *et al.*, 1992; Ellis and O'Brien, 1992; Patton *et al.*, 1994). For the remaining obstetrical examinations (through long fluid paths to the focus) and other classes of examinations, more specific models can be employed to be certain that MIs and TIs are not significant underestimates of patient exposures. Fortunately, when attenuation by overlying tissues is low due to significant fluid paths, it is rarely necessary to use high outputs; the output can be reduced while still obtaining the desired image brightness at nearly the full gain setting. In general, because diagnostic information is rarely reduced by such practices, it is better to decrease output than receiver gain unless electronic noise from full-gain settings is obscuring the echo signals.

9.3.5 Patient-Specific Models

For practical implementation by ultrasound users, an examination-specific, rather than a patient-specific, correction could be made to MI and TI as defined by ODS (AIUM/NEMA, 1992; NEMA, 1992).

Fixed-attenuation path models also have been proposed in which the attenuation per unit frequency is a function of maternal weight (Carson *et al.*, 1989a; 1989b; Kamel, 1994). Other models have been proposed in which the abdominal-wall thickness or all overlying-tissue thicknesses are measured from the ultrasound images (Carson *et al.*, 1989a; Siddiqi *et al.*, 1995b). In the latter, estimated specific attenuation coefficients of the type A_i [or specific attenuation coefficients per unit path length (A_i/d_i)] were obtained by multiple regression for the various tissues in the beam path. The best fit was obtained in a plot applicable to the *overlying tissue*, *i.e.*, to all tissue along the path from transducer to fetus except the bladder and the amniotic fluid. Representing the specific attenuation through this tissue as A_{ov} (in dB MHz⁻¹) and the distance through it as d_{ov} (in centimeters), the relevant relationship was found to be:

$$A_{ov} = -0.13 d_{ov}^2 + 1.5 d_{ov}, \quad (9.3)$$

with a p value of 0.001. From Equation 9.3 one finds that the minimum value of A_{ov} occurs when d_{ov} equals 0.7 cm and is equal to 1.1 dB MHz⁻¹. Because d_{ov} can be measured on images of individual patients, a film with soft tissue path length that minimizes A_{ov} can be selected and used for the most-accurate, patient-specific, worst-case-exposure estimates available. For patients similar to those in the study of Siddiqi *et al.* (1995b), the predicted A_{ov} would be minimized by choosing $d_{ov} = 0.7$ cm, or the largest value of d_{ov} if this is less than 0.7 cm.

The negative coefficient in Equation 9.3 might have physical bases that would apply generally. For example, an increased path length due to the urine, amniotic fluid, and even myometrium might produce pressure that flattens abdominal wall fat and, therefore, reduces beam dispersion. Increases in volume in these three relatively non-distorting fluids and tissues might also provide larger acoustic apertures for transmitting ultrasound to the conceptus, thus allowing selection of a better transducer position on the skin for minimizing attenuation.

If ultrasound examinations were suspected of causing abnormalities in a given case, patient-specific calculations could be employed in the retrospective risk estimate, as is currently done after a large x-ray exposure to the developing fetus. For such calculations, it would be necessary to select an appropriate soft-tissue attenuation coefficient. Either one of those employed in developing the fixed-path attenuation models (NCRP, 1983) or a value from the insertion-loss measurements of Siddiqi *et al.* (1995b) may be appropriate.

9.4 Scanning Sensitive Tissues Through Saline During Surgery and Other Cases of Minimally Attenuating Fluid Paths

Interoperative ultrasound at high amplitudes merits special attention for two reasons. First, as mentioned in the discussion of thermal effects, the negligible attenuation through saline, or other coupling fluid paths, is less than that of typical imaging paths and even that of the modest attenuation assumed in the homogeneous-attenuation model of ODS for evaluating TIs and MIs. Second, cavitation nuclei may exist in the coupling fluid and offer the potential of microscopic damage, particularly if the fluid is saturated with gas at room temperature or below and warmed just before use.

In cases such as ultrasonically guided surgery, where very sensitive or damage-intolerant tissues, such as the spinal cord, are in direct contact with the coupling fluid which is usually gas-saturated, particular attention should be directed toward keeping the acoustic fields at the tissue boundary below those that could cause inertial cavitation in the coupling fluid (Section 5). Because it is possible with many ultrasound-imaging systems to generate peak negative pressures greater than 2 MPa both at the transducer face and towards the focus (Duck, 1999a; Duck and Martin, 1991), it is important that interoperative sonography not be performed at such maximal output settings without awareness of the potential problems. Normally, the highest outputs would not be necessary in interoperative imaging, because the low-attenuation fluid path allows relatively high signal levels at low output. In unusual situations where very high sensitivity and resolution are desired, as in Doppler imaging of small vasculature, it may be worth considering use of filtered and degassed coupling fluid to avoid cavitation. However, the possibility of biological effects from anoxic saline in contact with the tissue should be considered.

Fluid-path coupling to sensitive tissues has been used extensively in ophthalmologic ultrasound, without observed adverse effects (see Section 9.9 for further discussion).

9.5 Lung and Other Respiratory Tract

9.5.1 *Indirect Lung Exposure During Echocardiography*

Overlying attenuation models for echocardiography deserve special attention. As discussed in the summary of Section 8, Carstensen *et al.*

(1992) have addressed the issue. However, a more thorough study of reasonable-worst-case attenuation paths should be undertaken for comparison with the $0.3 \text{ dB cm}^{-1} \text{ MHz}^{-1}$ homogeneous-attenuation model H_3 , in pathological as well as normal circumstances. The lung lies alongside and behind the heart in many echocardiographic views. The lung also overlies the heart, but it is not likely to be exposed for long durations in that position, because lung in the beam would produce ultrasound reverberations between the lung and the transducer or overlying tissue that, in turn, would obscure much of the heart structures being imaged. In adults, the chest wall and heart muscle are more highly attenuating than the H_3 model; hence, the latter model would appear to provide a safety margin. However, the combination of chest and heart wall, along with a long acoustic path through blood to the focus might, in some cases, provide lower attenuation than the currently employed H_3 model, particularly with neonatal echocardiography, where the parasternal ribs are not well calcified, as well as with substernal examinations.

9.5.2 Other Indirect Lung Exposures and Direct Lung Studies

The lung is exposed in many breast examinations, in relatively rare chest wall examinations, and in an increasing number of superficial musculoskeletal examinations. The diaphragm and lung are also exposed in the most cephalic views in upper abdominal examinations. Attenuation in most of those examinations is probably treated conservatively (underestimated) by the $0.3 \text{ dB cm}^{-1} \text{ MHz}^{-1}$ homogeneous-attenuation model, although water standoff imaging of the breast and superficial tissues was common in the past and could again become popular. A linearly scanned annular array with water standoff has gained some acceptance worldwide in the last few years. Higher exposures than estimated might occur in pathologic cases of abdominal fluid collections and in examination of the distal stomach wall.

The lung itself is examined with ultrasound, usually when fluid collection is expected. It is unlikely that deeper lung tissues are more susceptible to serious damage than the tissues directly under the pleura. However, a long path of fluid-filled lung may exist. Data are limited on the specific-attenuation coefficient of such fluid-filled lung tissue, but, it might well be at least as high as that assumed in the $0.3 \text{ dB cm}^{-1} \text{ MHz}^{-1}$ homogeneous attenuation model. A report of the attenuation coefficient in a pneumonitis of dog lung suggests only a 25 percent reduction at 1 MHz, compared with normal lung inflated with residual air (Dunn and Fry, 1961). *In vivo* estimates of the attenuation coefficient of fetal lung (Meyer *et al.*, 1984; Thieme *et al.*, 1983) have been on the order of $0.4 \text{ dB cm}^{-1} \text{ MHz}^{-1}$. Fetal lung tissue

consists of a low density of alveoli or alveolar buds. This low density also raises the question of whether mechanically weaker, fluid-filled lung tissue might be more susceptible to mechanical damage from ultrasound. However, this and other questions of effects on pathological tissue have not been addressed. It might well be that most ultrasound damage, if it occurs at all in human beings, is less severe than the existing pathology (Section 8 for more extensive discussion of bioeffects to the lung).

9.5.3 *Thyroid and Other Organs Near the Respiratory Tract*

In imaging the neck, including thyroid and carotid imaging and Doppler studies, the trachea is often exposed directly at various distances from the transducer. Although there are no known data on tracheal damage from exposure to diagnostic ultrasound, the tracheal epithelium, lying at a tissue-air boundary, might be more susceptible to damage than tissues surrounded by other soft tissues. Essentially, only in pathological cases, and with transducer-to-tissue standoffs of low-attenuation gel or fluid, might this exposure be performed with significantly less overlying tissue attenuation than that anticipated by the $0.3 \text{ dB cm}^{-1} \text{ MHz}^{-1}$ homogeneous-attenuation model.

9.6 Digestive Tract

9.6.1 *Air Cavities*

As discussed in Section 8, the intestines can experience ultrasound-induced damage at relatively low acoustic pressure thresholds. As with the lungs, this is probably due to gas bodies, but the measured thresholds are somewhat higher in the intestines than in the lung. It might happen in some cases that the air-filled digestive tract would be exposed to higher than expected pressure amplitudes through normal fluid-filled spaces, such as the urinary bladder, stomach and intestines, as well as through pathological abnormal fluid collections. No studies have been published on the frequency and extent of such exposure conditions.

9.6.2 *Esophageal and Other Intracavitary and Intraoperative Probes (with Bubbles Possibly Trapped in the Coupling Fluid)*

Air bubbles can be trapped in coupling gels and fluids between the transducer and the contacted body part. While acoustic pressure amplitudes are generally not as great at the transducer face as at the beam focal plane, peak negative pressures at the scanhead surface routinely exceed 2 MPa (Duck, 1999a). Furthermore, cavitation nuclei may exist at the transducer surface. The possibility of cavitation occurring near the transducer would be particularly important in any case of direct coupling to unusually important or sensitive tissues. The higher the viscosity of the coupling medium, the higher will be the threshold for cavitation. However, in viscous gels, entrapped gas bubbles are more difficult to remove in a clinical setting and may serve as a source of cavitation damage or localized heating. For suppression of cavitation, for less-distorted sound transmission for therapeutic ultrasound and for some diagnostic applications, utilization of prepackaged, partially degassed coupling gels might be considered. Recent acoustic-pressure information should be compared with information on cavitation thresholds in coupling gels, as that information becomes available. Duck (1987) estimated a mean acoustic pressure at the source from commercial diagnostic ultrasound systems of approximately 550 kPa and maximal rarefactional (negative) pressure of 1.5 MPa (Duck *et al.*, 1985) from studies through 1987. These values can be compared with values at which cavitation effects can be significant, as discussed in Sections 4 to 8.

Self heating from intracavitary and intraoperative probes deserves special attention (Wu *et al.*, 1995), as does self heating in relation to transcranial imaging. A thermal trigger for system shutdown is required (IEC, 1988) actuated at a probe temperature exceeding 41 °C. However, the specified measurement conditions are inappropriate for ultrasound and the standard is not applied with an *ad hoc* procedure of temperature measurement while the scanhead is in coupling gel. At a probe temperature of 42 to 44 °C, the temperature rise *in situ* can be twice that estimated by ODS (AIUM/NEMA, 1992). Efforts are ongoing to make this standard more relevant to diagnostic ultrasound. Increased temperature is expected to reduce the cavitation threshold, or increase the severity of cavitation by increasing the gas saturation of the heated tissues. This topic is treated in Section 11, where transducer self-heating and its implications are discussed.

9.7 The Neonatal Head

A model for the neonatal head has been proposed that uses a minimal distance of 3 cm between the scan-head face and the neonatal head. This arrangement results in an overall reasonable-worst-case (minimal) transmission loss of 0.56 dB MHz^{-1} (WFUMB, 1992). The minimal 3 cm distance is based on the typical minimal focal length employed and on the possibility of increased heating when the focal point is incident on the cranial bone. For any additional distance through the neonatal brain, the recommended incremental specific-attenuation coefficient is $0.16 \text{ dB cm}^{-1} \text{ MHz}^{-1}$. This WFUMB concept of minimal propagation path may underestimate exposures in some cases of short focal lengths, as would use of the common H_3 model ($0.3 \text{ dB cm}^{-1} \text{ MHz}^{-1}$) in scanning through the anterior fontanel and neonatal brain. The neonatal brain has a specific attenuation coefficient of $0.16 \text{ dB cm}^{-1} \text{ MHz}^{-1}$ (Table 9.3). In the WFUMB model, the critical target tissue is considered to be a soft-tissue-to-bone interface, with specific-absorption coefficients of 0.44 and $16 \text{ dB cm}^{-1} \text{ MHz}^{-1}$ for soft tissue and bone, respectively.

9.8 Transcranial Doppler

For adult transcranial imaging and transcranial Doppler, the main concern has been thermal effects in the brain at the bone-brain interface adjacent to the scan head (see Section 11.7). Other sites are probably more important for mechanical effects. There is a reasonable amount of sound reverberation between the scan head and the proximal skull that could lead to some local, extracranial increase in pressure amplitude and possible petechia formation on the skin. If significant damage were to occur in that way, however, it should be detected fairly easily by patients with normal feeling. As mentioned above, the highest rarefactional (negative) pressure observed in two surveys in the 1980s (Duck, 1987; Duck *et al.*, 1985), as well as in Duck (1999a), that reported pressures near the transducer surface, was 1.5 MPa, with a mean peak pressure of approximately 550 kPa. These values are high enough to produce cavitation in some situations (Sections 4 to 8). They are at least comparable to the peak pressures observed at the focus in water, *e.g.*, a peak rarefactional (negative) pressure of 4.3 MPa and a mean of 2.1 MPa for pulse-echo-imaging systems (Duck and Martin, 1993). Whittingham (2000) has measured somewhat higher peak pressures in the beam, *e.g.*, 4.9 MPa in color Doppler and 5.5 MPa for spectral Doppler.

An unlikely, and highly speculative, possibility for mechanical effects in the adult and neonatal brain is inadvertent focusing of a relatively unfocused beam by the skull geometry. In rare circumstances, this focusing could produce peak pressures and intensities well beyond the rated values for a given transducer. Such infrequent, body-produced focusing effects have not been considered seriously to date, as the skull usually defocuses the beam and attenuates it by scatter and absorption.

9.9 Ophthalmic Ultrasound

In safety considerations for applications of ultrasound to the eye, heating of the lens (Carson, 1988), blanching of the retina (Purnell *et al.*, 1964a; 1964b) and cavitation at the cornea in water path scanning have been suggested as effects of potential concern. FDA 510(k) guidelines (*e.g.*, FDA, 1991), set limits on ophthalmic ultrasound intensities that were lower than those for most other application classes. These lower guideline levels were based primarily on historical, pre-1976, ophthalmic scanner outputs. In the newer FDA guidelines (FDA, 1997), limits on all equipment systems, except ophthalmic systems, that meet the requirements of ODS (AIUM/NEMA, 1992) were raised to the highest previous limits, *viz* those of cardiovascular systems. Acoustic properties of several tissues of the eye were listed in Table 2.3 of NCRP Report No. 74 (NCRP, 1983) and were provided in more detail *in vitro* (De Korte *et al.*, 1994), and *in vivo* (Trier *et al.*, 1984).¹¹ Herman and Harris (1999) considered two cases of circular ultrasound apertures, through the lens and around the lens.

9.10 Summary

Attenuation estimates for human tissues have been summarized, as have proposed and implemented models for attenuation by tissues overlying the ultrasound focal point and critical organs. Advantages of applying many different examination-specific models as in WFUMB (1992) (Table 9.2) have not been demonstrated or analyzed, but a few such specific models may become appropriate as more is learned.

¹¹Pessel, M. and Trier, H.G. (1996). Private communication (Schering AG, Berlin).

The currently employed Model H₃ is convenient, and it does not overestimate attenuation for most applications. However, as further exposure information and understanding of the need for more accurate estimates become available, examination-specific models can be developed for any large identifiable classes of patients that might have sensitive tissues exposed to significantly higher fields than are estimated by the general model. As developed and accepted, the models may be implemented on the equipment displays or estimated by users from nomograms and other simple rules.

Relatively little attention has been paid to attenuation paths and other exposure conditions in applications other than obstetrical examinations. If more studies were performed, published in the various specialty literature and emphasized in training, they would help assure appropriate interpretation of general guidelines that are presently available.

Certain obstetrical and ovarian examinations are examples of studies in which special models are needed. In particular, the fixed-path model at 1 dB MHz⁻¹ is appropriate for conservatively predicting attenuation by overlying tissues for all types of obstetrical studies. Available experimental data indicate that the attenuation from the overlying tissues in first-trimester and, possibly, second-trimester examinations is lower than the predictions of this model in 90 to 97.5 percent of the examinations through the full bladder.

This previously recommended fixed-path model (NCRP, 1992) is still considered superior to the homogeneous-attenuation model for transcutaneous obstetrical examinations, particularly for scanning through the full bladder. Use of separate models by trimester may not be necessary, as little error from underestimation of exposure would be produced by use of a single, fixed path of 1 dB MHz⁻¹. In fact, for scanning through the full bladder, the attenuation is usually less for first-trimester than for second and less for second trimester than for third. In such cases of long fluid paths, the user should be aware that MI and TIB provided by present ultrasound systems may understate the exposure to the fetus.

Model H₃ [(0.3 d dB MHz⁻¹), where d is the overlying-tissue thickness in centimeters] is probably applicable in several large classes of obstetrical examinations. It can be used best for studies in which there are no lengthy fluid paths or in modest output situations in which occasional, large underestimates of exposure can be accepted. For example, an underestimate of the attenuation by 2 dB MHz⁻¹ would result in large errors in TIs and MIs; TI would be lowered by a factor of six and MI by a factor of 2.5 at a frequency of 4 MHz. These errors might be acceptable if the indices are small. The MI

in that model would be three times lower than would be obtained with the best available attenuation data.

A model of $(0.3 d - 1)$ dB MHz⁻¹ is reasonable for the several obstetrical examination types, such as empty-bladder imaging. If used for all of the examination types, the model would over predict values for TIs and MIs in a few cases. Specifically, in five percent of the full bladder, first-trimester examination cases, the model would predict TIs and MIs that are 2 and 1.4 times, respectively, lower than those based on the best individual estimate for each of those cases.

As exposure estimates made with accepted general models approach critical values for obstetrical examinations, more detailed exposure estimates can be made using attenuation information based on properties such as measured minimal overlying tissues or maternal weight. The same process could be used for other examinations with low-attenuation propagation paths in specific cases. Examples of nonobstetrical, low-attenuation paths include interoperative or other scanning through water or other fluid as a coupling medium and scanning through a fluid-filled stomach or bladder to the intestines and other tissues containing gas bodies (Carson *et al.*, 1989a; Ramnarine *et al.*, 1993; Siddiqi *et al.*, 1995b). These patient-specific attenuation estimates may be applied to the displayed MIs and TIs and, if need be, used with measured acoustic pressures, powers and intensities produced by the ultrasound system under the conditions of the patient's examination.

In the future, it may be possible for the operator of equipment to estimate the attenuation in each individual case rather closely and easily when high outputs appear to be required. So called "tissue-characterization algorithms" have been studied for some time to calculate attenuation coefficients of tissues based on the change in magnitudes of returned echoes with depth (Kuc and Schwartz, 1979; Meyer *et al.*, 1984; Ophir and Mehta, 1988). These and related methods have been investigated for imaging the tissue backscatter with correction for attenuation (Yao *et al.*, 1990). However, the accuracy of these algorithms is limited, at present, particularly for inhomogeneous tissues.

The highest outputs are not normally required with cases of low or even average attenuation. However, when high-attenuation paths necessitate the highest outputs, that higher attenuation usually provides a degree of protection.

10. Employed and Needed Sound Pressure Waveforms

10.1 Introduction

This Section begins with examples of known outputs of existing diagnostic ultrasound systems. Included are discussions of standardized reporting of output information. Actual outputs for different types of systems are reviewed for different types of scanheads and applications, as are historical trends in these outputs. Reviews of that nature are published frequently. In the various engineering/scientific literature there are also many detailed developments of methods to improve the quality of ultrasound images and other signals. Much less common, however, are meaningful studies that compare the outputs at which risks are significant with the outputs needed for image quality or other diagnostic information.

What are the tradeoffs between safety and efficacy and how can balances be achieved? A major goal of this Section is to expand the relatively limited earlier discussion of these questions in NCRP Report No. 113 (NCRP, 1992). In many applications, it is possible to improve safety with no loss in diagnostic information simply by informed use of the equipment. However, when output levels needed to obtain desired information are great enough to cause biological effects, a choice must be made between risk and benefit. That choice must be based on a knowledge of the nature of possible biological effects and a basis in experience to predict the benefits of increased outputs. Equipment design and features for adjusting the combination of safety and efficacy are addressed primarily in this Section. Some of the “win-win” approaches may involve increased development and production costs. But, as discussed here and in other literature, users can greatly change this safety/efficacy balance by use of high outputs only as needed.

The general principles relating acoustic exposures and image quality or other information content were discussed in Section 9 of NCRP Report No. 113 (NCRP, 1992) for pulse-echo and Doppler diagnostic ultrasound. The topic of that report was thermal mechanisms for

biological effects of ultrasound; thus, the emphasis was on temporal-average exposure quantities, such as the time-averaged output power (W_0) and the spatial-peak, temporal-average intensity (I_{SPTA}). It was also argued (NCRP, 1992) that, under conditions for most diagnostic-ultrasound examinations, information is degraded by random processes (signal noise), which is often dominated by electronic noise. Further, the contrast-to-noise ratio for detection of various lesions or other tissue targets is proportional to the signal-to-noise ratio and often is not large. The relation of needed acoustic pressures to estimated temperature rises (Appendix B) will not be discussed significantly in this Section; the subject was discussed extensively in the previous report (NCRP, 1992). In this Section, the relationship between needed acoustic pressures and nonthermal biological effects will be discussed.

In Section 8 of the previous report (NCRP, 1992), it was stressed that, in theory, for a given pulse repetition rate, the product of pulse duration and pulse-average intensity, *i.e.*, the energy fluence per pulse, controls ultrasound diagnostic performance. In the traveling waves employed in diagnostic ultrasound, the pulse-average intensity is proportional to the pulse average of the acoustic pressure squared. Known nonthermal biological effects, especially cavitation-related effects, depend much more strongly on acoustic pressure than on pulse length (τ). In some applications, therefore, it may be possible to reduce the probability of bioeffects with no loss in system performance through tradeoffs between pulse length and pressure. Adjustments can be made in such a way as to keep constant the risk of, or safety margin for, thermal bioeffects. It may be possible to gain safety by increasing τ and reducing acoustic pressure. In addition, it may be difficult to obtain high-acoustic-pressure levels at large propagation distance because of acoustic saturation, a characteristic of NLP. Under saturation conditions, the best possibility of increasing image quality is by increasing pulse length rather than by increasing the output of the source. With available medical-imaging technology, however, there have been limits on the pulse length that can be used without significant loss of axial resolution and image contrast. Coded excitation was recently implemented in a commercial system to improve maximal imaging depth without equivalent increases in peak pressure [Logiq 700, April 1998, General Electric (GE) Medical Systems, Waukesha, Wisconsin].

In Section 8 of NCRP Report No. 113 (NCRP, 1992), it was also observed that there was almost no correlation between acoustic-output quantities of different scanheads in earlier ultrasound systems and relative needed magnitudes of those quantities for each scanhead as calculated by an elementary theory. In some more recent

systems from the late 1980s, the outputs from the different scan-heads seem to be designed more closely to FDA limits and, to a lesser extent, to the relative needed output as calculated by the theory in that previous NCRP Report No. 113. For example, after FDA guideline limits were raised in 1985 to incorporate effects of acoustic attenuation by the body tissues, the outputs in many systems also tended to increase.

10.2 Outputs from Existing Diagnostic Systems and Historical Trends

10.2.1 General Comments

Recent summaries of ultrasound-system outputs include those of the AIUM (1993a; 1993b), Duck and Martin (1993), and Patton *et al.* (1994). Little has been published on acoustic-output levels required to obtain a given level of performance, the latter not being well defined other than by the state of the art; an exception is the publication of Harris *et al.* (1989). Most of the diagnostic-imaging literature consists of investigations of methods of improving performance. Those improvements are pursued vigorously in a market that has been very competitive in terms of attempts to achieve the best-possible performance with rather broad cost constraints. In the last 15 y, ultrasound-system output in the United States has been limited in practice by the FDA 510(k) guidelines used to obtain approval to market the system (FDA, 1997). These guidelines are based on historical precedent, specifically, on outputs of equipment existing before 1976 and are among the best available indicators of output levels that were considered at the time to be needed for satisfactory performance. However, there were some systems in which the outputs may have been higher than would have been necessary had better (and more expensive) receiving and signal-processing components been employed.

10.2.2 Output-Labeling Guidance and Requirements

10.2.2.1 FDA 510(k) Guidance. FDA released its 510(k) guidance (FDA, 1991), for diagnostic-ultrasound systems, according to which systems could be cleared for marketing by the “510(k)” process, rather than by the more involved “premarket-approval” process. The guidance established maximal levels for selected acoustical quantities

(Table 10.1) based on known maximal outputs of all systems commercially available before 1976, rather than on known levels for thermal and nonthermal effects. These outputs were based partly on several output surveys (Carson *et al.*, 1978) and partly on measurements on commercial devices at the FDA acoustic laboratory (Harris, 2000). New systems began to be designed to utilize only the highest intensities when focused at the greatest depths, where the highest output might often be needed. Systems were then allowed (FDA, 1985) to meet the output guidelines of Table 10.1 for focal intensities and pressures after derating to values estimated *in situ* by Model H₃ (Section 9), rather than in water. The 510(k) process evolved steadily; a major change occurred when ODS (AIUM/NEMA, 1992) was adopted (this standard is discussed in Appendix B). For systems complying with ODS (regulatory Track 3), maximal output levels were increased (FDA, 1991) for ultrasound systems directed at obstetrical and general purpose applications as well as for cardiac. Measurements are made in water at the point where the maximal pulse-intensity integral (*PII*) (Appendix B) would be if the medium

TABLE 10.1—FDA 510(k) Track 3 application specific guidance, pre-ODS (Track 1) and post-ODS (Track 3) (FDA, 1997).^a

Application	Intensity ^b			
	Pre-ODS		Post-ODS	
	$I_{SPTA,3}^c$ (mW cm ⁻²)	$I_{SPPA,3}^c$ (W cm ⁻²)	$I_{SPTA,3}^c$ (mW cm ⁻²)	MI ^{c,d}
Fetal imaging, neonatal, pediatric and other (general purpose)	94	190	720	1.9
Cardiac	430	190	720	1.9
Peripheral vascular	720	190	720	1.9
Ophthalmic	17	28	50	0.23

^aTrack 2 was an interim track and was discontinued.

^bPost-ODS guidelines (Track 3) are 720 mW cm⁻² I_{SPTA} for all applications with a maximal MI of 1.9, except for Ophthalmic, which has an MI limit of 0.23.

^cAll values are attenuated (derated) according to Model H₃.

^dThe post-ODS limit was based on $I_{SPPA,3}$ from 1991 until 1994 at which time an MI-based limit was introduced. Then, the manufacturers were given the choice of maintaining either MI or $I_{SPPA,3}$ below its respective limiting value. There is a TI limit for ophthalmology of one and an advisory requirement for other models if TI exceeds six.

were homogeneous with attenuation as in H_3 . For those ODS-compliant systems, general purpose and all specialty diagnostic systems, except those solely for ophthalmology or for fetal heart rate monitoring, limits were increased to the highest previous values, those of peripheral-vascular systems; thus, for most applications, the limit on $I_{SPTA,3}$, the derated value of I_{SPTA} , was established as 720 mW cm^{-2} .

There was a more modest change allowed in the guideline levels for peak acoustic amplitude, which is more clearly related to mechanical effects than is the time-averaged intensity. The guidance $p_{r,3}f^{-0.5} \leq 1.9$ (with pressure in megapascal and frequency in megahertz) replaced the $I_{SPPA} \leq 190 \text{ Wm}^{-2}$ limit in 1994. Above 1.6 MHz, this allowed higher acoustic pressures, elevated in proportion to $f^{0.5}$.

It should be noted that the outputs of the ultrasound systems and their labeling may be revised modestly from the output levels provided to the FDA in the 510(k) process. Information provided in the user's manual should be more up-to-date than that of the FDA submission. Symbols commonly used in the United States supplied output information are described in Table 10.2 and discussed in Appendix B. Most important among those to the user are ODS indices. The MI is related to the estimated potential for nonthermal bioeffects and is calculated as the derated *in situ* peak rarefactional pressure divided by the square root of the ultrasound frequency (Equations 9.2 and B.7). The TIs are very simplified estimates of the maximal steady-state temperature rise in the body. Different versions, TIS, TIB, and TIC are calculated for different body parts, *viz*, soft tissue, bone surface, and cranium, respectively (Equations B.1, B.3 and B.6). Table 10.3 is an example of information provided in a user's manual (ATL, 1996) by a manufacturer for a single, small parts scanhead, in accord with Track 3 of the FDA 510(k) guidelines (AIUM, 1998; FDA, 1997). The amount of data required for understanding the conditions producing maximal values of these most important acoustic-field quantities and biophysical indices is quite large. Simplified forms, in addition to these tables, might be helpful to show the peak-index values possible from a given scanhead.

10.2.2.2 AIUM Output Measurement and Labeling Standard and Corresponding NEMA Standard. The AIUM Output Measurement and Labeling Standard (AIUM, 1992) and the NEMA Output Measurement Standard (NEMA, 1992) call for an extensive set of measurements obtained at the locations of the peak values in water. These standards also call for measurements in water, but are calculated for modeled *in situ* conditions (FDA, 1985). That is, the exposure quantities are calculated to be those that would occur in material with a specific attenuation coefficient of $0.3 \text{ dB cm}^{-1} \text{ MHz}^{-1}$

TABLE 10.2—Description of quantities currently required for labeling in the newest track (Track 3) allowed for 510(k) approval of diagnostic ultrasound systems (FDA, 1997).^{a,b}

Symbol	Units	Description
Intensity, Power and Pressure Quantities:		
$I_{SPTA,3}$	$mW\ cm^{-2}$	Spatial-peak temporal-average intensity, obtained by reducing (derating) water-measured values of I_{SPTA} to what they would be in material attenuating at $0.3\ dB\ cm^{-1}\ MHz^{-1}$
$I_{TA,3}$	$mW\ cm^{-2}$	Time average intensity, derated to $0.3\ dB\ cm^{-1}\ MHz^{-1}$
PII_{max}	$J\ cm^{-2}$	Maximal free-field pulse-intensity integral
W_0	mW	Ultrasonic power
$W_3(z_1)$	mW	Derated ultrasonic power at axial distance (z_1)
$P_r(P_-)$	MPa	Peak rarefactional (negative) pressure
$P_{r,3}$	MPa	Peak rarefactional (negative) pressure, derated to $0.3\ dB\ cm^{-1}\ MHz^{-1}$
Transmit Parameters:		
f_c	MHz	Center frequency
PD	μs	Pulse duration
PRF	kHz	Pulse repetition frequency
Output Display Indices:		
MI	unitless	Mechanical index
TIS_{scan}	unitless	Soft tissue thermal index (scanning mode)
$TIS_{nonscan}$	unitless	Soft tissue thermal index (nonscanning mode)
TIB	unitless	Bone thermal index
TIC	unitless	Cranial thermal index

TABLE 10.2—Description of quantities currently required for labeling in the newest track (Track 3) allowed for 510(k) approval of diagnostic ultrasound systems (FDA, 1997).^{a,b} (continued)

Symbol	Units	Description
Distance/Depth and Area Parameters:		
$d_{eq}(z)$	cm	Equivalent beam diameter as a function of $z = [(4/\pi) W_0 I_{TA}(z)]^{1/2}$, where $I_{TA}(z)$ is the temporal-average intensity in water at axial distance (z)
z_{sp} (under MI column)	cm	Axial distance to spatial peak of $P_{r,3}$
z_{sp} (under TIB)	cm	Axial distance to spatial peak of $[W_3(z)I_{TA,3}(z)]$ (equal to $z_{B,3}$)
z_1	cm	Axial distance to the location of $\max\{ \min[W_3(z), I_{TA}(z) \times 1 \text{ cm}^2] \}$ where $z \geq z_{bp}$
z_{bp}	cm	Break point depth, $h = 1.69 (A_{aprt})^{1/2}$
FL	cm	Focal length
A_{aprt}	cm ²	Area of active aperture
D_{eq}	cm	Equivalent aperture diameter = $[(4/\pi)(A_{aprt})]^{1/2}$

^aAdapted from GE users manual (GE, 1996).

^bSee example of Acoustic Output Reporting Table in Table 10.3. Track 3 is the FDA approved track for systems reporting the Output Display indices in compliance with ODS (AIUM/NEMA, 1992).

TABLE 10.3—Example of acoustic output reporting table.^{a,b,c}

Transducer Model: L7-4. Operating Mode: 2D + Color & Triple Mode

Index Label		MI	TIS			TIB	TIC ^d	
			Scan	nonscan		Nonscan		
				A _{aprt} ≤ 1	A _{aprt} > 1			
Maximal Index Value		1.88	1.60	1.50	N/A ^e	2.90		
Associated Acoustic Parameter	P _{r,3} (MPa)	3.73						
	W ₀ (mW)		87.5	80.0		80.0		
	min of [W ₃ (z ₁), I _{TA,3} (z ₁)] (mW)					N/A		
	z ₁ (cm)					N/A		
	z _{bp} (cm)					N/A		
	z _{sp} (cm)		1.10				1.50	
	d _{eq} (z _{sp}) (cm)						0.41	
	f _c (MHz)		3.95	Col: 4.5 ^f PD: 4.0 ^f 2D: 4.0 ^f	4.00	N/A	4.00	
Dimensions of A _{aprt}	X (cm)		Col: 3.80 ^f PD: 1.30 ^f 2D: 2.30 ^f	1.30	N/A	1.30		
	Y (cm)		0.66	0.66	N/A	0.66		
Other Information	PD (μs)		1.20					
	PRF (Hz)		40.4 ^g					
	P _{@PII_{max}} (MPa)		4.28					
	d _{eq} @PII _{max} (cm)						0.32	
	Focal length (FL)	FL _x (cm)		7.00	7.00	N/A		
FL _y (cm)			1.70	1.70	N/A			
I _{pa,3} @MI _{max} (W cm ⁻²)		557						
Operating Control Conditions	Control 1 ^h		MI					
	Control 2 ⁱ		TIS _{as} ^j	TIS _{asU} ^j		TIS _{bs} ^j		

^aAdapted with permission from Advanced Technologies Laboratory (ATL, 1996).

^bContains information on one scanhead provided in compliance to the newest track, Track 3 of the 510(k) approval process (FDA, 1997).

^cSymbols are described in Table 10.2.

^dThis probe is not intended for transcranial or neonatal cephalic uses.

^eN/A = not applicable.

^fCol, PD, and 2D refer, respectively, to frequency - shift plus color-flow imaging, power-Doppler, and gray-scale B-mode imaging.

^gIf MI comes from a scanning pulse, PRF listed is the average per second for the “worst-case” scan line.

^hControl settings #1—Triple mode, FZ \$1, max voltage, Doppler PRF 1250, 2D PRF 617, color-box width min, sample volume = 15.

ⁱControl settings #2—Triple mode, FZ \$7, max voltage, Doppler PRF 1250, 2D PRF 941, color-box width min, sample volume = 15. FDA requirements since those are measurements actually included in system operator’s or reference manuals in the United States. Some manuals include both the United States guideline data (modeled *in situ*) as well as the European-required peak values in water of Table 10.4.

^jCode by the manufactures.

at the point where those calculated quantities would reach their maximal values. These modeled *in situ* values are obtained by “derating” (reducing) water-measured values to what they would be in the H_3 model and are represented symbolically by adding a “0.3” subscript to the derated quantity (Appendix B). These standards call for a large amount of data, which provide useful and necessary information for assessing ultrasound system safety. In 1997, the required data were simplified (FDA, 1997) and in 1998, the AIUM published an output labeling standard consistent with the acoustic output reporting tables in the FDA guidance (AIUM, 1998). Some manuals include not only these values, but also European-required data; the latter are based on measurements in water according to IEC Standard 61157 (IEC, 1992) (Section 10.2.2.5).

10.2.2.3 Thermal- and Mechanical-Index Data. Most of the data referred to in Table 10.3 are for points of expected maximal derated pulse-intensity integral ($PII_{0.3}$) (Appendix B, Equation B.5) in a medium of homogeneous attenuation of $0.3 \text{ dB cm}^{-1} \text{ MHz}^{-1}$. Those measurements were performed according to the *in situ* sections of the Acoustic Output Measurement and Labeling Standards (AOMLS) (AIUM, 1992) and Acoustic Output Measurement Standard (NEMA, 1992), which have been maintained to remain consistent with ODS (AIUM/NEMA, 1992), discussed in Section 9.1. Recently, AOMLS was divided into two separate standards, one for labeling (AIUM, 1998) and the other for measurements (AIUM/NEMA, 1998). Only limited summaries of TI and MI data are available from systems displaying the indices. Some MI related data have been available somewhat longer because MI is relatively simple to calculate if peak rarefactional pressure is measured in the proper location. Actually, most of the early available data are at the point of maximal measured p_+ or p_- rather than at ODS-specified location of maximal $PII_{0.3}$. Considerable MI and TI data were calculated and simulated for existing systems in evaluation of ODS (Curley, 1993; Thomenius, 1993; Wu *et al.*, 1992). Availability of real-time display of the indices in systems exceeding certain minimal values of these quantities represents a major breakthrough in maintaining the safety and efficacy of diagnostic ultrasound. There is no comparably sophisticated display of biophysically relevant data on x-ray systems. Individualized calculations of exposure are made (normally retrospectively) by professional radiation physicists when unusually high exposures to critical structures such as the embryo/fetus are suspected.

A major rationale for ODS was that it would significantly help individual users make judgments on their output levels in specific cases, based on their currently displayed values of the indices and

on the need for higher outputs and the importance of the expected diagnostic data to clinical management in terms of benefit and risk. Concomitant with the introduction of ODS there has been an effort to educate user physicians and technologists in the interpretation of the indices in specific clinical studies. That educational effort had a slow start, but is now beginning to receive more attention (AIUM, 1994a; 1997a; 1997b; EFSUMB, 1996; Lopez, 1998). A constant effort must be maintained to develop user awareness and use of the indices.

Calculation of TIs and MIs is explained in Appendix B. The accuracy of these indices as indicators of potential temperature rises and acoustic pressures has not been fully described in the literature, and many developers of the standard did not consider the indices to be actual indicators of these quantities. In many cases, it is not expected that TI values can estimate temperature increase to within a factor of two. The topic is discussed in Appendix B.4; an example of very useful information has been given by Jago *et al.* (1999). All indices are generally calculated conservatively, *i.e.*, such that the output will actually be overstated. However, there are cases where the great simplifications employed in the calculations allow for the potential heating and rarefactional pressure to be underestimated when they are reported for deep focal zones. Probably the largest uncertainty is in the assumed model of propagation in the tissues. Table 9.4 shows examples of potential underestimates in the case of long fluid paths prior to the focal point. In extreme cases, such as long fluid paths and high diagnostic ultrasound frequency, the inaccuracy can increase to a factor of six under the present ODS regulations and procedures.

10.2.2.4 Acoustic Data Provided in Compliance with the Output Display Standard. Basic data on the acoustic output of diagnostic-ultrasound equipment approved for marketing by the FDA, according to ODS, is made available to purchasers of equipment in operators' manuals, and to the general public upon requests made through the Freedom of Information Act. Labeling requirements for compliance with ODS include Acoustic Output Tables, of which an example is given in Table 10.3. Tables of this kind are supplied with every transducer (scanhead) employed with a given system for each mode in which any of the safety indices TIS, TIB, TIC or MI can exceed one. Table 10.3 applies to Transducer L7-4 operated with the ATL 3000 System (Advanced Technology Laboratories, Bothell, Washington) in the modes: 2D + Color & Triple Mode. The quantities specified are identified in Table 10.2 and discussed further in Appendix B.

The "associated quantities" listed in Table 10.2, for which values are given in Table 10.3, are needed in calculating the safety indices,

according to equations specified by ODS (Appendix B). Thus, $p_{r,3}$ (evaluated at z_{sp}), the maximal derated value of the peak negative (rarefactional) pressure, is used in calculating MI (Equation B.7).

The ultrasonic power (W_0) is used directly in calculating TIC and, also, (for the smaller apertures) TIS, according to Equations B.1 and B.6. Its derated value as a function of distance $W_3(z)$ (Equation B.2) is used in calculating TIB (Equation B.3).

The center frequency (f_c) appears explicitly in expressions for TIS and MI in Equations B.6 and B.7; also f_c affects all the indices through the derating factors (defined in Equation B.2).

The active aperture area (A_{aprt}) is required for calculating the equivalent aperture diameter (D_{eq}) the latter being given by $\sqrt{4 A_{\text{aprt}}/\pi}$; from D_{eq} and the power W_0 , one obtains TIC according to Equation B.1. Also, the calculation of TIS for a nonscan mode depends on whether or not A_{aprt} is greater than 1 cm^2 .

The equivalent beam diameter (d_{eq}) (defined by Equation B.4) does not appear in general equations for the indices (Equations B.1, B.3, B.6, and B.7) but is a factor in equations (Equation B.9, etc.) for the maximal FDA-allowed values for TIs. The appearance of d_{eq} in the latter equations comes from the fact that ODS limits are applied to the SPTA intensity, specifically to the derated spatial-peak temporal-average intensity ($I_{\text{SPTA},3}$) rather than to TIs themselves.

According to Equation B.9, the maximal value of TIB that is allowed under Track 3 requirements of ODS (AIUM/NEMA, 1992) and the related FDA guidance (FDA, 1991) is given by $12 d_{\text{eq}}$, the diameter (d_{eq}) being expressed in centimeters. The relationship is shown by Curve A on Figures 10.1a and 10.1b. These figures show data for two commercial diagnostic ultrasound systems, made available by the manufacturer. Each point shows the maximal possible TIB for a specific transducer operated in a specific mode within either of the two systems. In applications to fetal imaging, TIB is to be displayed and considered when the fetus is being examined in the second or third trimester. For such applications, the maximal TIB allowed by FDA for equipment to be marketed in the United States is given by the above-mentioned Curve A in Figure 10.1. For the same applications, the maximal TIB allowed before 1991 is given by Curve C in Figure 10.1a. The allowed TIB after adoption of ODS was, therefore, increased by a factor of $720/94$, *i.e.*, 7.7. The large number of representative points above Line C in Figure 10.1a represent operating conditions available in the United States for fetal scanning after a change in rules, but not before. Data from Acoustic Output Reporting Tables for other manufacturers also show that much of the latest equipment for fetal scanning operates at higher

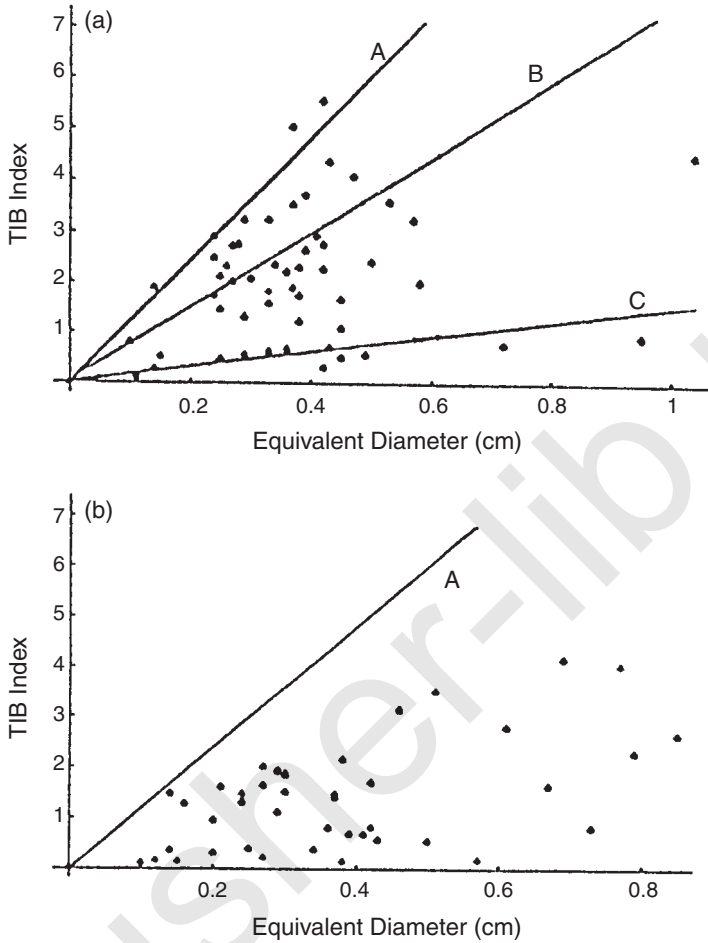


Fig. 10.1. TIB for two widely used commercial diagnostic-ultrasound systems. Each point is for a specific transducer (scanhead) driven by the system console in a specified mode. For the point representing a particular transducer-mode combination, the ordinate gives the maximal TIB that can be produced within that combination; the abscissa is the equivalent diameter (d_{eq}) of the beam at the axial position where the maximum occurs. (a) ATL 3000 System (Advanced Technology Laboratories, Bothell, Washington). Curve A is a plot from Equation B.7; it shows TIB corresponding to a value of 720 mW cm^{-2} for the SPTA intensity. Similarly, Curves B and C show TIB corresponding to values of 430 mW cm^{-2} and 94 mW cm^{-2} , respectively, for the SPTA intensity. Thus, Curve A shows maximal values of TIB allowed by ODS (AIUM/NEMA, 1992) or the related guidance (FDA, 1991) for diagnostic-ultrasound equipment approved under the rules for Track 3, for all applications except ophthalmology. Curves A, B and C show the corresponding maximal application-dependent TIB values for equipment approved prior to 1991, and for equipment approved after that date under the rules for Track 1; under the latter rules, Curve A applies to “Peripheral Vascular,” Curve B to “Cardiac,” and Curve C to “Fetal Imaging and Other” (FDA, 1997). (b) Same as (a) except that the System is ATL HDI 5000; Curve A has the same meaning as in (a).

levels of TIs than before 1991. For example, data for the B & K 2002 Ultrasound Scanner (obtained from archives of AIUM) show that for the 65 transducer/mode combinations, 58 percent of the maximal possible TIBs are higher than pre-1992 levels, 37 percent are more than three times higher and 18 percent are more than six times higher. In the latter group, TIBs range up to 10. Evidently, manufacturers and users have responded to the change in rules by taking advantage of the permitted increase in SPTA intensity. For cardiac applications, the increase in allowed SPTA intensity after 1992 is 720/430, *i.e.*, 1.7.

The increase in SPTA intensity after 1992 leads to improved imaging capabilities, as explained in Section 10. It also leads to increased potential for thermal damage, as pointed out in Section 11. Hence, users obviously have increased responsibility for weighing advantages against disadvantages of the available options.

10.2.2.5 IEC 61157 Data and Requirements. IEC Standard 61157 (IEC, 1992) for declaration of acoustic-output quantities took the approach of requiring measurements of acoustic quantities at the point of maximal pulse-intensity integral (*PII*) (pulse pressure squared integral) at the location where it would occur in water, rather than where it would occur in a more attenuating medium. Examples of a labeling form in accord with IEC Standard 61157 is given as Table 10.4. Some of the important parameters and variables are described here and the remaining are in the standard (IEC, 1992). Measurement methods are specified in IEC Standard 61102 (IEC, 1991). The mode symbols B, M and rD refer to B-mode, gray-scale, M-mode, and range-gated Doppler. Subscripts I and P refer to imaging and pulsed-spectral Doppler, respectively. System settings include depth of the measurement or range gate and sample length (sample volume). The dimension W_{pb6} is the 6 dB pulse-echo beam width, both parallel and normal to the scan plane. Pulse-repetition rate and scan-repetition rate are symbolized prr and srr, respectively. The elevational (perpendicular) output beam width is 5 mm in this case and the lateral dimensions are given in the table. The acoustic working frequency (f_{awf}) is similar to center frequency and acoustic power up fraction (percent) is the fraction of maximal acoustic-power output at the time of turning on the ultrasound system. Acoustic initialization (percent) refers to the fraction of maximal power after changing to a new patient. The intensity I_{ob} is I_{SPTA} when the system is set for obstetrical applications. In the United States, it is recommended that measurements be made of acoustic quantities both at peaks in water and (by derating) at peaks in tissue; the latter

TABLE 10.4—Quantities now required for labeling according to IEC Standard 61157 (IEC, 1992).^{a,b}

Parameter	Mode			
	B _I	B + M _I	B + rD _p	B + rD _I
P_- (MPa)			3.6	
I_{SPTA} (mW cm ⁻²)	206.4	1,682.4		1,264.9
System settings				
Depth (mm)	21.0	20.0	29.9	59.9
Frequency mode	0.0	0.0	0.0	0.0
Sample-volume gate (mm)	N/A	N/A	N/A	N/A
I_p (mm)	2.4	2.3	2.0	2.5
W_{pb6}				
(∥) (mm)	0.8	0.8	4.0	14.0
(⊥) (mm)	1.6	1.7	1.7	1.7
prr (kHz)	N/A	10.6	N/A	N/A
srr (Hz)	62.3	49.5	23.0	17.0
Output beam dimensions				
5 mm elevational width	1.7	2.6	1.0	2.0
× _____ mm				
f_{awf} (MHz)	6.7	6.4	7.1	5.0
Acoustic power up fraction (%)	user defined			
AI (%) (acoustic initialization)	user defined			
Maximal power (mW)	55.1	88.5	224.5	224.5
Power system settings				
Depth (cm)	63.0	63.0	79.9	79.9
Frequency mode	2.0	2.0	0.0	0.0
Sample-volume gate (mm)	N/A	N/A	N/A	N/A
I_{ob} (mW cm ⁻²)	42.4	68.0	172.6	172.6
Power up mode	N/A			
Initialization mode	N/A			
Acoustic output freeze	N/A			
I_{tt} (mm)	0.66 mm			
I_{ts} (mm)	contact			
Inclusive modes	—	None	None	None
Notes				

^aThis Table is an example of information provided in one manufacturer's recent user's manual (GE, 1996) for a single, small parts scanhead (adapted with permission from GE Medical Systems).

^bSee symbols explanations in Section 10.2.2.5. Columns for 4 of the 14 modes and combination modes are given here.

derated quantities are estimated on the assumption of homogeneous tissue attenuation (AIUM/NEMA, 1992). However, in essence, only the derated quantities are required (FDA, 1991). As indicated above, the IEC requires measurements at the locations of maxima in water. Thus, compliance with both IEC Standard 61157 and the FDA 510(k) processes requires manufacturers who wish to sell equipment in the major world markets to perform extensive search procedures for two different peak quantities. While the cost of this redundancy may be excessive for typical, lower-system outputs, it provides significantly more safety-related information, particularly for use of the ultrasound application in locations where the path to the focus is predominantly in low-attenuation liquids. Extensive output information is required by professional engineers, scientists and physicians involved in technological assessment of safety and performance of ultrasound systems. Agreement has not been reached in various standards bodies to provide a more limited and interpretable set of parameters in users' manuals.

10.2.2.6 *Other Current Sources of Output Data Provided in Operators' Manuals and Reference Manuals.* NCRP Report No. 113 provided evidence that, for the several ultrasound systems analyzed, the spatial peak intensities were highest, or at least not reduced, in those scanheads in which the least intensity was needed, according to the calculations of needed intensity (NCRP, 1992). Since then, some manufacturers, apparently, have adjusted the output power to be higher for the deeper transmitted focal depths where more power is generally needed. One company, in particular, apparently adjusted its system, at least in pulsed-Doppler mode, to stay reasonably close to the FDA 510(k) maximal intensity guidelines assuming homogeneous attenuation by tissue of $0.3 \text{ dB cm}^{-1} \text{ MHz}^{-1}$. The derated I_{SPPA} and p_{-} were more constant than the values measured in water.

The AIUM, through its Manufacturer's Commendation Panel, has solicited system and scanhead-output data from manufacturers that are more up-to-date than those provided in the 510(k) applications. Those data have been published fairly regularly by AIUM (1985; 1987; 1993b). In the 1993 publication, the data were provided on computer disk (in both PC and Mac formats) for simple reanalysis and display. The availability of these digital data facilitate analysis such as those in Figures 10.2 and 10.3. One can look at relations between variables within all scanheads of a given system, as in Figure 10.2, where I_{SPTA} as a function of maximal intensity (I_{max}) is plotted for all scanheads described in one system's 1989 operator manual (128 XP, Acuson Corporation, Mountain View, California).

All intensities are measured in water. The maximal intensity (I_{\max}), the time-averaged intensity over the largest of any positive or negative half cycles of the pulse at its spatial peak, is approximately equal to $p_+^2/2 \rho c$, where p_+ is the temporal-peak-positive pressure measured at the position of its spatial maximum in water. The curved lines in Figure 10.2 are representations of the log/linear plots of linear regression (straight) lines obtained by applying linear analysis to the same data. On this log/linear plot, the two intensities track approximately monotonically in B-mode and M-mode, with I_{SPTA} much lower in B-mode than M-mode; the latter is as expected from distributing the transmitted beams over the B-mode image plane. In a linear plot the two intensities track rather linearly in B-mode and M-mode. The linear fit for M-mode is $r^2 = 0.71$; $I_{\text{SPTA}} = -(30 \pm 23) + (0.23 \pm 0.04) I_{\max}$. In B-mode, $r^2 = 0.43$; $I_{\text{SPTA}} = -(0.39 \pm 10) + (0.5 \pm 0.016) I_{\max}$. Increased information content in the presence of electronic noise at deeper imaging depths can result from the increased signal power, often allowed by the increase in I_{SPTA} . This increase in I_{SPTA} is often achieved in the system by increased peak signal (increased I_{\max}), rather than by increased pulse duration or *PRF*.

In Figure 10.2, the I_{SPTA} values are derated; they were calculated from measurements in water at 700 to 2,000 mW cm^{-2} for pulse

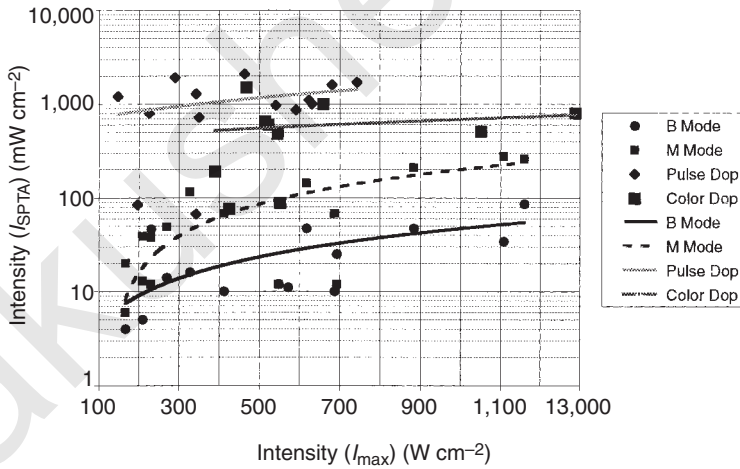


Fig. 10.2. Reported I_{SPTA} as a function of the reported average intensity during the largest half-cycle of the pulse (I_{\max}) for all scanheads and frequencies of a given system, but separated by system operating mode. All intensities were measured in water (see text).

Doppler. They were obtained by applying the $0.3 \text{ dB cm}^{-1} \text{ MHz}^{-1}$ assumed specific attenuation coefficient. It is the derated values that are subject to the FDA limits (Track 1 or pre-1992) of 720 mW cm^{-2} for peripheral vascular or 430 mW cm^{-2} for cardiac applications. Pulsed-Doppler (spectral) mode and, to some extent, color Doppler seem to be limited at or near the maximal I_{SPTA} values in water, but with widely ranging I_{max} . With a more focused or more efficient transducer, where the temporal-peak intensity is higher with the same pulsar voltage, the pulse duration or PRF is reduced relative to that for the less focused scanheads to stay within the allowed I_{SPTA} . This all suggests that the pulsed-Doppler system performance was more restrained by the FDA limit than was pulse-echo, B-mode, and M-mode quality. At that point in the evolution of the ultrasound system analyzed in Figures 10.2 and 10.3, the effort was made only in the Doppler system signal to keep I_{SPTA} (corresponding to Doppler or image signal-to-noise) as high as allowed by the FDA limit. The two pulse-Doppler points (diamonds) in Figure 10.2 at low I_{SPTA} ($< 100 \text{ mW cm}^{-2}$) were for very short focal lengths (considering the low frequencies), suggesting less need for high intensities. There are two such outlying points in the color-Doppler mode.

Following the hypothesis that I_{max} exhibits a pattern of theoretically needed peak intensity, Figure 10.3 is plotted showing reported intensity as a function of calculated, needed intensity, derived from Equation 9.8 of NCRP Report No. 113 (NCRP, 1992) as follows. This Equation, now 10.1, is, after correction of the sign in the exponent:

$$I_{\text{calc}} \propto K \frac{F^2}{d^2 f^2} e^{4aFf}, \quad (10.1)$$

where I_{calc} is the calculated needed intensity as measured in water, K is a constant, F is the focal length, d the beam diameter, f the frequency, and a the assumed attenuation coefficient. For constant f-number (focal length divided by active transducer aperture length), as employed in this particular system, $d^2 f^2$ is constant so that in this special case:

$$I_{\text{calc}} \propto F^2 e^{4aFf}. \quad (10.2)$$

The data points in Figure 10.3 are widely spread, showing that practical considerations are more important than simple theoretical considerations in system designs. Clearly, the reported maximal values of I_{max} cover a much narrower range of peak intensities, *viz*, an order of magnitude, than the calculated “needed” values, *viz*, five orders of magnitude. This large difference may arise from complications in the focused fields of linear arrays, because the focal lengths reported for these arrays do not necessarily represent well the

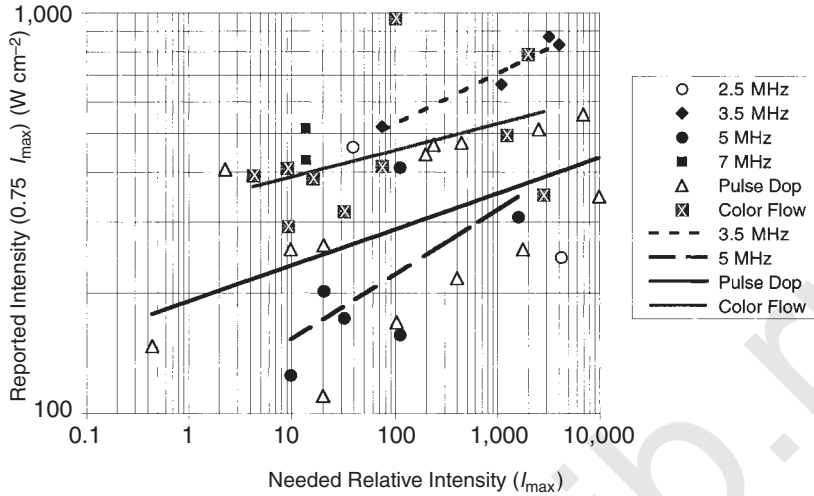


Fig. 10.3. Reported I_{\max} versus calculated (or “needed”) relative I_{\max} . All points and lines labeled by a frequency are for pulse-echo mode. Reported I_{\max} is scaled by 0.75 to set all the data in one decade of the ordinate. The term “Needed I_{\max} ” represents the intensity calculated as needed to achieve a given ratio of signal power to preamplifier-noise power at the focal planes of the scanheads (see text).

combined longitudinal focal length and elevational (slice thickness) focal length.

In any case, Figure 10.3 shows a general trend toward increasing reported I_{\max} as a function of the calculated relative “needed” I_{\max} . The recent system analyzed in Figure 10.3 shows a better correlation between “needed” and reported values of I_{\max} than was found in NCRP Report No. 113 (NCRP, 1992). It will be informative to study even more modern systems to evaluate whether they are designed and adjusted according to needed signal-to-noise ratio, or merely staying below the maximal allowed MI. The existence of a general positive slope to the data in Figure 10.3 is demonstrated by the power law regressions (plotted as visual guides) in a linear, least squares fit of all the data of I_{\max} as a function of the log of the calculated I_{\max} . The r^2 values of the regression are not good, but the intercept and slope are significant ($p < 0.002$ for each). The slope and intercept are significant for reported I_{\max} plotted either against the calculated value or the log of the calculated value, as shown in Figure 10.3. The fit is not improved much by eliminating the outlier point in Figure 10.3 at an I_{\max} of 1,290 W cm^2 . That high I_{\max} was

in color flow for a 3.5 MHz sector scanhead designed for cardiac imaging.

For the pulsed-Doppler mode alone, the intercept and slope of the regression curves are also significant ($p \ll 0.02$ for each). For the B mode, there is a modest, but not statistically significant trend of increasing I_{\max} with calculated needed I_{\max} . For the 3.5 MHz B-mode scanheads, the linear fit is particularly good, $r^2 = 0.98$, but there are only four points. The color-flow symbol, boxed x (at ordinate ~ 340 and abscissa $\sim 2,900$), appears to be a low outlier. Perhaps the 2.5 MHz transducer producing this point provided enough penetration for nearly all practical applications, particularly the cardiac applications, for which it probably was originally designed and which did not require imaging at depths much greater than its 7.5 cm focal length. The two relatively separate points at 3.5 MHz, in the upper right, had very short focal lengths of 0.5 and 1.3 cm.

10.2.3 *Recent Independently-Measured Output Data and Comparisons with Manufacturer-Reported Data*

10.2.3.1 *Recent Independently-Measured Output Data and Historical Trends in System Output.* National, state and other governments and individual hospitals have not supported the rather time-consuming-measurement procedures of medical-ultrasound systems. In the United States, most measurements have been conducted by experienced laboratories, under contract with manufacturers and the data have not been published. However, such measurements have been reported more regularly elsewhere, particularly in the United Kingdom. Duck and Martin (1993) have observed an increase in ultrasound-system outputs. For example, Figure 10.4 gives their recorded pulse-echo peak-positive and peak-negative pressures over most of the history of clinical diagnostic-ultrasound imaging. Henderson *et al.* (1995) reported a six-fold increase in I_{SPTA} values from 1991 to 1994 and a threefold increase in color-Doppler mode intensities.

10.2.3.2 *Comparison of Manufacturer-Supplied and Independently-Measured Output Data.* Jago *et al.* (1995) and Henderson *et al.* (1995) reported very significant differences between the overall peak intensities measured on three ultrasound systems in their laboratories and those reported in the user's manuals of three different manufacturers, all measured in water. Despite this, much of the difference apparently arose from the particular maximal amplitudes observed. The manufacturer-reported intensities were measured at

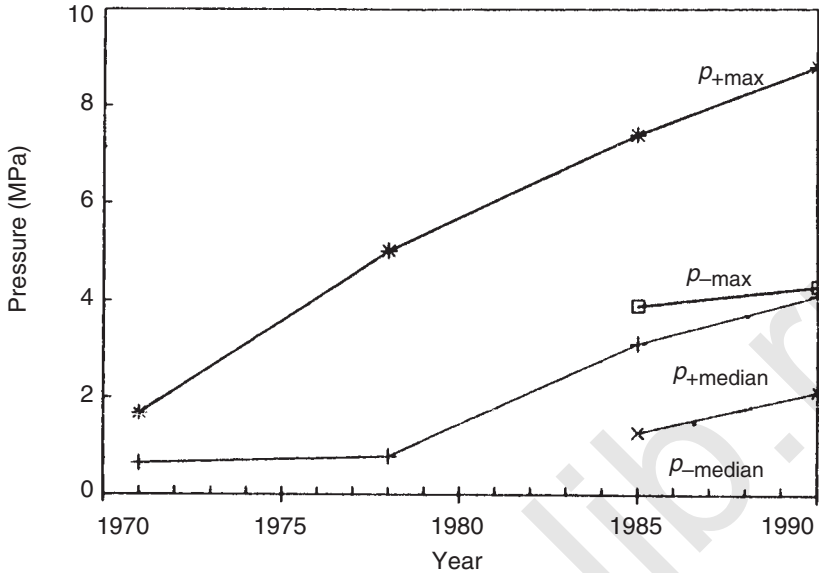


Fig. 10.4. The change in peak pressures recorded from pulse-echo equipment from 1970 to 1990 (Duck and Martin, 1993). The quantities, p_{+max} , $p_{+median}$, are respectively maximal and median values of the peak positive pressure (p_{+}) reported by manufacturers in a given year; and the quantities, p_{-max} , $p_{-median}$, are similarly defined values of the peak negative pressure (p_{-}).

the location of the peak derated intensity, as specified in ODS (AIUM/NEMA, 1992), rather than at the location of the peak in water, as specified by IEC (1992). Notably, after using the same procedure, two of the manufacturers confirmed the independent measurements (Henderson *et al.*, 1995).

Another source of differences between measurements can come from the large effective spot sizes of available hydrophones in comparison with modern beam focal dimensions. Different effective spot sizes provide different spatial averaging, particularly of the peak signals (Smith, 1989). Henderson *et al.* (1995) reported one case of disagreement in which the problem arose from the manufacturer not taking sufficient account of multiple transmit focal zones when using a zoomed field of view. This result points out the difficulties in finding the true peak quantities in the versatile, modern ultrasound systems and the potential value of having some independent laboratories measuring acoustic outputs.

10.2.4 Other Exposure Quantities

10.2.4.1 Frequencies.

The frequency range of diagnostic-ultrasound systems has been increasing slowly. The frequencies normally

employed for general purpose and “small parts” B-mode imaging have increased from 2 to 3.5 MHz in 1971 to 2 to 12 MHz in 1996. This illustrates that the greatest improvement in image quality allowed by lower-system noise, wider-dynamic range, and possibly higher MIs and TIs can be realized by increasing the frequency, as discussed in Section 10.4. Special-purpose systems for superficial applications and operating at 20 to 35 MHz are available commercially and some research systems use frequencies as high as 40 to 70 MHz (Ryan and Foster, 1997). Such applications include corneal thickness imaging, skin imaging, intravascular imaging, and spectral-Doppler imaging of peripheral vessels such as those in the fingers.

A most important change affecting the quality of ultrasound is the development of transducers that are sensitive over a wide frequency bandwidth. These scanheads may be employed at any of a number of center frequencies. This option allows imaging of superficial structures at high frequencies, and deeper structures at much lower frequencies. An alternative method for imaging at greater depths is by transmitting a broadband pulse and sweeping the receiver-frequency band down as echoes are returning from increasingly greater depths. These different approaches affect the needed-peak pressures and intensities, as well as image quality, and are often built into the hardware design of the systems (Goldstein, 1993). Broadband transmission with broadband beamforming, for example, should allow good suppression of speckle noise, *i.e.*, improved low-contrast resolution. This method may, however, include transmission of energy into frequency bands that may not be used over all of a given focal zone. Generally, frequencies employed in color-flow-Doppler imaging are somewhat lower than the center frequencies employed for pulse-echo regimes with the same scanhead.

10.2.4.2 Pulse Durations and Repetition Rates. Pulse-repetition frequencies and pulse lengths have been included in several surveys (Carson *et al.*, 1978; Duck, 1987; Duck *et al.*, 1985). As shown in Table 10.5, the pulse durations of diagnostic systems are generally shortest for B-mode imaging and M mode and longest for pulsed Doppler. Information on color-flow imaging (CFI) is not provided in the table, but intermediate pulse durations are employed to give moderate Doppler frequency resolution and spatial resolution. Pulse-repetition frequencies are generally highest for Doppler modes. In color-Doppler modes, as many as 16 or 32 pulses are transmitted sequentially along the same path to detect and measure the frequency shift between pulses by averaging techniques. The number of pulses averaged is referred to as the ensemble length. In pulsed

TABLE 10.5—*Ranges of pulse durations and repetition frequencies (Duck and Martin, 1993).*

Mode	Pulse Duration	PRF
Pulse echo	0.15 – 1.2 μs	0.5 – 4.0 kHz
Pulsed Doppler	0.35 – 90 μs	1.5 – 50 kHz
Pulsed therapy	1 – 3 ms	50 – 250 Hz
Lithotripsy	0.3 – 10 μs	1 – 100 Hz

Doppler, these ensemble lengths are even longer in order to obtain spectra of high-frequency resolution. Very long pulses may be used for some fetal-heart monitors, in which pulse durations up to 90 μs may be used. Ranges of pulsing regimes used in therapeutic systems are given in Table 10.5 for comparison. CFI consists of real-time display of gray-scale images and a region or window in which blood flow in color is superimposed on the gray-scale image. In nearly all cases, the color-flow part of the image is produced by a separate set of transmitted pulses. Groups of gray-scale and color-flow pulses are usually interlaced to form the composite image. Transmission of all these pulses and the interval for their return prior to the next pulse requires considerable time, reducing the achievable image repetition rate (acoustic frame rate). A minimal image-frame rate from 5 to 60 s^{-1} is usually required to provide real-time feedback to the operator, or to track physiologic motions. Both CFI and Duplex Mode (B-mode image along with a Doppler spectrogram of a single sample volume) are coming into more frequent general use.

10.2.4.3 Beam Dimensions and Focal Gain. Focal gain is the ratio of spatial-average intensity at the focus to that at the transmitting aperture; thus, focal gain equals the ratio of the areas of the active aperture and the focus. The beam dimensions at the focus have been included in some surveys (AIUM, 1985; 1987; 1993b; Duck *et al.*, 1985), and ranged from 0.4 to 32 mm^2 . Smaller focal dimensions are generally associated with higher-frequency beams as the focal-beam dimensions are inversely proportional to frequency for the same aperture and focal length. The beamwidth of the positive-pressure amplitude is always smaller than that of the negative pressure (Duck *et al.*, 1985). For circular, spherically focusing transducers operating in a piston mode, the -6 dB beamwidth of the primary maximum of the focal pressure is $1.4 \lambda F d^{-1}$, where λ is the wavelength (cf^{-1}), F is the focal length, and d the source diameter. The focal beamwidth is not much different for rectangular or ellipsoidal apertures where

the diameter (d) is replaced in the beamwidth formula by the aperture width in the direction of measuring the focal beamwidth.

10.2.4.4 Nonlinear Propagation. Nonlinear-acoustic propagation has been discussed. It is important to include this topic here because (1) the achievable pressure amplitude is significantly reduced, particularly the negative pressure amplitudes, and (2) increased particle acceleration and other related phenomena are produced at the shock wavefront. Implications of the latter effect are not well understood. NLP effects also might become usable as a method of tissue imaging and identification of particular tissues based on their nonlinearity parameter (B/A). Table 9.3 gives some measured values of B/A . As shown there, the nonlinearity parameter is larger in fat than in other soft tissues. Certain commercially available diagnostic systems now use NLP phenomena for second-harmonic imaging. To develop harmonic contrast of sufficient amplitude for imaging, these “tissue harmonic” imaging techniques usually require pressure amplitudes near the highest levels presently allowed. Because pressure amplitude and accumulation of harmonic wave content depend on axial distance from the scanhead, even higher amplitude might be desired for significant harmonic content over the entire field of interest.

One method of quantifying the degree of nonlinear distortion employs the shock parameter (σ_s) (NCRP, 1992, Appendix A). The value of σ_s increases linearly with the frequency and with the pressure amplitude of the wave. When $\sigma_s < 1$, the wave has not reached shock conditions and no significant loss of energy is associated with its propagation through a medium such as water. Formation of a fully developed shock wave occurs for $\sigma_s > 3$ and implies substantial loss of energy due to the absorption of the higher frequency harmonics produced.

Measurements of σ_s have been reported by Starritt and Duck (1992) for 37 pulsed diagnostic beams generated in water by commercial scanning equipment. The range of σ_s reported for Doppler and pulse-echo systems was 0.1 to 6.9. In 30 percent of the beams, the value of σ_s exceeded three.

For a given focused aperture and drive voltage there are greater nonlinearity effects in water than would normally occur in tissue or in the hypothetical homogeneously attenuating tissue assumed in ODS (AIUM/NEMA, 1992). Because the measurements were done in water, and because of its assumption of linear propagation in derating, the ODS calculation tends to underestimate the actual pressures and intensities in tissues (see Appendix D for further discussion).

10.3 Bioeffects Particularly Relevant to Possible Changes in Diagnostic Equipment Design

The following is not an exhaustive summary of the information and conclusions elsewhere in this Report, but rather a discussion of certain issues of particular relevance to equipment design.

10.3.1 *General Wave Shape and Polarity Observations*

For several types of cavitation bioeffects, the pulse polarity, or actual wave shape, has been shown to affect thresholds or magnitudes of the effects (Umemura and Kawabata, 1993). However, results obtained in water are quite different from those found in tissue. Ayme and Carstensen (1989a) studied relative effects of sinusoidal and distorted pulses and found a surprisingly small difference. Also, Bailey *et al.* (1996) found no significant difference in effects on *Drosophila* larvae between single positive and negative pulses of the same amplitude. Later, Bailey *et al.* (1999) observed a large increase in the erosion produced by cavitation in water using time-reversed lithotripter pulses compared with the erosion produced by a positive-leading pulse. Umemura *et al.* (1997) reported enhancement of sonochemical effects with superposition of second harmonic at the correct phase to the fundamental, and Chapelon *et al.* (1997) showed reduction of cavitation in ultrasound therapy using pseudo-random CW rather than single-frequency CW insonification. Lewin *et al.* (1990) described techniques of controlling the ratio of peak-positive to peak-negative pressures at high amplitudes. This topic deserves further research as an area in which diagnostic benefit/risk ratios might be improved or specific therapeutic ratios might be enhanced.

10.3.2 *General Observations Related to Pulse Duration*

The possible dependence of nonthermal bioeffects on pulse duration and pulse-repetition rate merits further investigation. Because of the implications for ultrasound system design, and the possibilities of various compromises between safety margins and system performance, the topic deserves considerable attention as nonthermal bioeffects begin to limit peak pressures in diagnostic systems. Some relevant bioeffect observations regarding pulse duration are:

1. Elsewhere in this Report (Section 8) and in conference conclusions (WFUMB, 1992), it has been stated that the exposure-

time dependence of cavitation thresholds is only weakly dependent on ultrasonic pulse duration. This statement is reasonably true for the important case of inertial-cavitation thresholds for existing bubbles of optimal size on which MI is primarily based (Apfel and Holland, 1991). Child *et al.* (1990) observed a 50 percent reduction in acoustic-pressure threshold for murine lung hemorrhage given a factor of 10 increase in pulse duration at constant *PRF* (Section 8). Fowlkes and Crum (1988) suggested a pulse-duration-dependence effect on the threshold for cavitation as detected by sonoluminescence that is qualitatively similar to that seen in bioeffects data.

2. The occurrence rate of low-probability effects involving the chance of a cavitation nucleus passing through the beam or even a statistical fluctuation in a pure, homogeneous liquid (Herbertz, 1988) or inhomogeneous liquid depends linearly on duty factor (pulse duration times *PRF*).
3. Requirements for relatively long durations of single pulses for extensive cell lysis at reasonably low pressures were recognized early and have been studied extensively (Section 8).

10.3.3 *Effects of Repetition Rate, Duty Factor, and Dwell Time*

Effects of pulse-repetition rate, duty factor, and dwell time along a single beam path are usually primarily associated with thermal effects. Under nonthermal conditions, the threshold for bioeffects of ultrasound increase only weakly with *PRF* and dwell time, but the occurrence rate and extent of damage depend strongly on the *PRF* and dwell time. The threshold for murine lung hemorrhage, for example, decreased only 30 percent for a factor of 10 increase in *PRF* (Child *et al.*, 1990) and was essentially constant with exposure time from 20 s to 3 min (Raeman *et al.*, 1996). Holland *et al.* (1996) observed with a commercial ultrasound scanner approximately the same threshold for rat lung hemorrhage with 4 MHz pulsed Doppler (*PRF* = 1,250 Hz, pulse duration $\sim 1.3 \mu\text{s}$) as with 4 MHz color-flow Doppler (*PRF* = 400 Hz, pulse duration $\sim 5 \mu\text{s}$). The small effects of *PRF* and pulse duration which may have existed could have canceled each other.

The situation was found to be more complex with other pulse regimes (Raeman *et al.*, 1993). When 10 μs pulses, all with the same total on time of 0.03 s, were spread over 3 min rather than 3 s, the threshold was lower and the extent of damage was greater. It was suggested that the response of the tissue to the initial damage increased the effect. Delius *et al.* (1990b) compared effects of 1,500

lithotripsy pulses directed at dog liver and gall bladder either at 1 s^{-1} or, in a faster mode, as bursts of 10 pulses fired 10 ms apart repeated once per second. In the liver, free plasma hemoglobin was statistically significantly greater in portal veins with burst exposures. The increased hemolysis in the burst mode was compatible with cavitation damage, apparently from subsequent pulses sustaining and growing any nuclei produced. However, other effects on the liver or gall bladder were about the same for the two modes delivering the pulses.

The strong dependence of nonthermal bioeffects of diagnostically relevant, pulsed ultrasound on acoustic pressure leads to the concept of a threshold pressure. The threshold itself depends only weakly on dwell time. However, at suprathreshold pressures, each of these factors is positively correlated with the severity of damage.

10.3.4 *Summary of Effects of Pulse Duration, Repetition Rate, and Dwell Time*

It is desirable to remain below the pressure thresholds for damage to lung, intestines and other gas-body containing tissues. Current knowledge shows that thresholds for damage depend much more strongly on the acoustic pressure than on pulse duration, repetition rate, and dwell time. However, if suprathreshold acoustic pressures are required in some applications, it would be wise to minimize the other exposure quantities. Time-average power and intensities are linearly dependent on pulse duration and pulse repetition rate. Dwell time is the exposure time in one location, which is a simple concept as long as the beam or image plane are held steady in one place; holding the beam steady generally results in the highest temperature rise.

10.4 Dependence of Information Content on Acoustic Pressure

10.4.1 *General Factors Relating Pressure and Diagnostic Information*

CFI and duplex mode (B-mode image along with a Doppler spectrogram of a single sample volume) are coming into more frequent general use. The speed of ultrasound propagation places strong restrictions on the achievable information content and image quality

in Doppler and pulse-echo diagnostic ultrasound when a minimal image frame rate is required to provide real-time feedback to the operator or to track physiologic motions. These restrictions are expressed in the number of acoustic beam lines across the image, the number of transmit focal zones per beam line, and the number of acoustic samples in the time allowed to form an image over a specified depth of imaging. There are incentives to reduce the number of samples averaged from a given beam line and increase the pulse amplitude in that these changes can allow increased image-frame-rate frequencies and depth of imaging.

Lateral resolution (in the image plane) and elevational resolution (scan-plane thickness) are inversely correlated with the level of the lower frequencies in the pulse and axial resolution is improved with shorter pulse lengths that, in turn, require greater bandwidth. These image quality considerations are described well by Wells *et al.* (1992). In principle, with systems optimally designed for signal-to-noise ratio, contrast-to-noise ratio, and spatial-resolution considerations, it is not the peak amplitude in the pulse that is the ultimate determining factor, but the product of pulse-average intensity and bandwidth. Acoustic contrast (C) is the ratio of received waveform power (usually expressed in decibels) from two tissues to be distinguished; $C = 10 \log_{10} (W_2/W_1)$. One index of image quality is Q , defined by:

$$Q = \frac{C}{\eta VF}, \quad (10.3)$$

where η is the electronic-noise power per unit frequency, V is the sample volume, and F is the frame repetition rate.

A brief analysis of the advantages and disadvantages of increased output was presented by Kremkau (1989). He included the following conclusions, while noting that, in the simplest analysis, the increase in penetration resulting from increased acoustic output was small, ~ 5 percent for a doubling of the intensity (or a 41 percent increase in peak pressure). Advantages listed for increased output were: improved resolution, increased imaging depth, increased dynamic range, and increased sensitivity. Disadvantages or counterbalancing effects listed were: NLP reduces depth improvement, no dynamic range or sensitivity improvement is achieved if the lower signal limit is controlled by acoustic noise, there is a possible increase in risk. These are discussed in more detail below.

Image quality is represented largely by the volumetric resolution and, hence, can be improved dramatically by using an increase in peak pressure to allow an increase in frequency. Another advantage of the increased frequency is an effective reduction in acoustic multiple-scattering noise in relation to the signal from small reflectors (part

of Kremkau's increased dynamic range). The counterbalancing effect of limited improvements in the presence of acoustic noise refers primarily to noise caused by phase aberration (beam dispersion), and not multiple scattering. The issue might be summarized, as was done by Insana (1995), that "The ideal output intensity (and pressure) can be determined only by balancing many issues related to instrumentation, sound-tissue interactions, and the risk of bioeffects. The results could vary widely in the diverse clinical environment."

10.4.2 *Effects of Increased Output on Effective Penetration*

NCRP Report No. 113 (NCRP, 1992) addressed this issue in some detail. It was derived there that the effective penetration depth of imaging or Doppler signal acquisition is given by z_m in the expression:

$$z_m = (R_G + D + N + S_r) / (2 af). \quad (10.4)$$

Here, a is the specific attenuation coefficient in $\text{dB cm}^{-1} \text{MHz}^{-1}$ and f is the center frequency; thus, the quantity $2afz_m$ is the round-trip attenuation in decibel between a sending-receiving transducer and a target at a distance of z_m . Also, R_G is the global-system dynamic range in decibel and N , D and S_r are negative numbers in decibel, as follows:

- R_G is the ratio of the maximal unsaturated signal to the minimal signal above noise that can be detected from the focal plane at the maximal power setting in a nonattenuating medium, *i.e.*, the global dynamic range for that power setting. The minimal signal is that signal which is 3 dB above the system electronic noise.
- D is the ratio of the signal level from a sample of tissue in water at the distance of interest compared with the signal when the sample is at the focal point in water.
- N is the ratio of the minimal detectable signal level, under ideal conditions, to the signal level necessary to visualize the tissue or to obtain other defined information, such as a Doppler spectrum, in the presence of typical or minimally diffuse scattering or reverberation. N does not deal with reduction of speckle noise nor does it resolve two tissues of similar backscattering.
- S_r is the backscatter factor of the most weakly scattering tissues of interest, the ones producing the weakest gray-scale texture that can be seen above the electronic and reverberation noise at the greatest depths, but does not include effects of attenuation, transducer focusing, reverberation noise, etc.

Backscatter from tissues is often reported as the backscatter coefficient (S) ($\text{cm}^{-1} \text{sr}^{-1}$), which is the backscatter cross section per unit sample volume per steradian and should be transducer-independent (Dickinson, 1986). A three-parameter power-law fit for the frequency dependence of S as $c_1 + c_2 f^n$, allows separation of the scatter from large frequency-independent scattering surfaces in the organ from that of the smaller scatterers. In that case, it can be seen in Table 10.6 that soft tissues approach Rayleigh scatters (f^3 to f^4) except for the large, frequency-independent surface term. For estimating contrast between different tissues at various frequencies, it may be informative to compare the frequency dependence of S from a two-parameter fit to the data of the form af^b , in which case b varies from 1.2 to 1.4 for brain, liver and spleen.

The backscatter factor (S_r) is easier to work with for some experimental situations. This is the backscatter signal from a tissue (in decibel) relative to that from a perfectly reflecting flat surface in water at the same axial distance. At the focal point at axial distance

TABLE 10.6—*Backscatter coefficients (S) and related quantities for four human tissues.*

Quantity	Tissue ^a			
	Blood	Brain	Liver	Spleen
S^b ($\text{cm}^{-1} \text{sr}^{-1}$)	1.8×10^{-6}	7.2×10^{-5}	8.7×10^{-4}	6.6×10^{-4}
c_1	0	0.23×10^{-4}	3.3×10^{-4}	1.2×10^{-4}
c_2	2.2×10^{-8}	0.6×10^{-6}	0.2×10^{-4}	0.2×10^{-4}
n	4.0	4.0	3.0	3.0
S_r (dB)	-81	-65	-54	-55
z_m^c (cm)	9	12	15	14
D^d (dB)	0	-6	-10	-10

^a Values for blood are from Yuan and Shung (1988) and the others are from Nicholas (1982).

^b Backscatter coefficient (S) for 3 MHz using a 19 mm diameter, 8 cm focal length transducer. The constants are given for a three-parameter power-law fit to the tissue data of the form $S = c_1 + c_2 f^n$.

^c Values of effective penetration (z_m) for imaging organ parenchyma are also given as calculated by Equation 10.3 with the attenuation coefficient by overlying tissues $a = 0.5 \text{ dB cm}^{-1} \text{ MHz}^{-1}$ assumed global dynamic range $R_G = 120 \text{ dB}$, $N = -12 \text{ dB}$ and the estimated diffraction corrections D as indicated.

^d For blood, D is estimated as zero because one is not likely to image blood at a range greater than the focal point.

(L_s) and a transducer solid angle (Ω) about the focus, S_r (decibel) is equal to $10 \log (S L_s \Omega)$ (Section 10.4.3.).

Equation 10.3 was used to calculate z_m in Table 10.6 for the example of $R_G = 120$ dB. The value of D was only estimated. For imaging liver at 3 MHz and other conditions listed in the table, the calculated maximal effective penetration is:

$$z_m = (120 - 10 - 12 - 54)/(2 \times 0.5 \times 3) = 15 \text{ cm.} \quad (10.5)$$

This calculated 15 cm effective penetration is reasonably representative of experience with normal liver, which suggests consistency between the measured dynamic range and the measured scattering and attenuation characteristics of liver. Some recently produced high-end ultrasound systems with high-focal gains on transmission and reception exhibit R_G significantly higher than 120 dB. Some comparison with Equation 10.3 is possible from measured maximal depths of CFI in a $0.5 \text{ dB cm}^{-1} \text{ MHz}^{-1}$ tissue-mimicking test object with well simulated blood (Boote and Zagzebski, 1988). These measured Doppler results are summarized in Table 10.7, along with experimental data from Carson (1986) on maximal depths of imaging with 13 pulse-echo systems and 35 transducers. The pulse-echo measurements were in an approximately liver-equivalent scattering

TABLE 10.7—*Measured effective penetration for Doppler and from pulse-echo ultrasound scanners (Boote and Zagzebski, 1988; Carson, 1986).*

Frequency ^a (MHz)	Effective Penetration Depth ^b (z_m , cm)	
	Doppler	Pulse Echo
2.5	14.0 – 15.5	11.5 – 16.5
3	9.7 – 12.0	12.8 – 13.5
3.5	—	11.0 – 14.0
5 high	7.3 – 10.0	6.0 – 11.5
5 low	4.3 – 6.5	—
7.5	—	3.6 – 4.7

^aFrequencies listed are specified, rather than measured. Results for high and low power settings are given for 5 MHz transducers of three scanners, although the change in output power was not reported. In one of the three Doppler systems, the increase in effective penetration at 5 MHz was 2 cm, 47 percent, for an approximate power change of 15 dB.

^bWide variations in output power and transducer aperture and focusing are primarily responsible for the large ranges of penetration. The phantom backscatter was unquantified and the specific attenuation coefficients were 0.5 and $0.7 \text{ dB cm}^{-1} \text{ MHz}^{-1}$ for Doppler and pulse echo, respectively.

material (Radiation Measurements, Inc., Middleton, Wisconsin), with a nominal one-way-attenuation coefficient of $0.7 \text{ dB cm}^{-1} \text{ MHz}^{-1}$, which mimics the more attenuating paths in some ultrasonically important patient anatomy such as liver cirrhosis.

A key question from the standpoint of bioeffects: Given a specific increase in peak pressure, what is the possible change in *effective penetration* (the maximal depth of imaging or other signal acquisition above incoherent noise)? If the system's maximal power is increased by a factor W_2/W_1 symbolized by Ψ_p (decibel), then R_G (the global dynamic range in decibels) becomes $R_G \Psi_p$ under conditions of linear acoustic propagation in the tissue. The effective penetration is then increased by the increment:

$$\Delta z_m = \Psi_p / 2 \text{ af}. \quad (10.6)$$

For $0.5 \text{ dB cm}^{-1} \text{ MHz}^{-1}$ one-way-liver attenuation, 3 MHz frequency and a 41 percent increase in pressure amplitude (3 dB increase):

$$\begin{aligned} \Delta z_m &= 3 \text{ (dB)} / [2 \times 0.5 \text{ (dB cm}^{-1} \text{ MHz}^{-1}) \\ &\quad \times 3 \text{ (MHz)}] = 1 \text{ cm}. \end{aligned} \quad (10.7)$$

For a maximal imaging depth of 18 cm, the percent change in imaging depth is:

$$100 \times \Delta z_m / z_m = 6\%. \quad (10.8)$$

This is a relatively small percentage change in imaging depth from a 41 percent increase in pressure. However, that change, or the larger change from, say, a five-fold increase in acoustic-pressure amplitude, might be critical in cases where the anatomy of interest lies within the lowest part of the field of view and a particular frequency is required. These changes in maximal imaging depth are not realized fully in the case of NLP, which can occur at the highest diagnostic amplitudes and only modest focal gains.

10.4.3 *Effects of Increased Output on Other Image and Signal Quality Measures*

For a given effective penetration, increasing the transmitted power or acoustic pressure makes it possible to increase resolution by increasing frequency. As shown in NCRP Report No. 113 (NCRP, 1992), the global dynamic range (R) is increased by raising the maximal pressure by a ratio of Ψ_p so that $R = R_G + \Psi_p$. With z_m fixed, the additional dynamic range can then be used to increase the

frequency to $f + \Delta f$. Then the backscattering from the weaker, small scatterers is increased by Ψ_{Sr} to $S_r + \Psi_{Sr}$, according to the frequency dependence as given in Footnote a of Table 10.6. Adding the changes in those quantities to Equation 10.4 gives:

$$z_m = (R_G + \Psi_p + D + N + S_r + \Psi_{Sr}) / 2 a(f + \Delta f). \quad (10.9)$$

Subtracting Equation 10.4 from the above expression for z_m gives:

$$2 a \Delta f z_m = \Psi_p + \Psi_{Sr}. \quad (10.10)$$

S_r is related to the backscatter coefficient [S ($\text{cm}^{-1} \text{sr}^{-1}$)], which is the backscatter cross section per unit sample volume (Dickinson, 1986). For efficient computations with a given transducer, S can be expressed as the backscatter factor (S_r) but in decibels relative to the signal from a perfectly reflecting flat surface in water. Thus, if we assume for simplicity that both the tissue and the planar reflector are at the transducer focal point and that the axial length of the sample volume in tissue is L , then:

$$S_r(\text{dB}) = 10 \log(S L \Omega), \quad (10.11)$$

where Ω is the solid angle subtended by the transducer about the focus. For L equal to a typical pulse length of approximately two wavelengths, 0.103 cm for a 3 MHz transducer, and $\Omega = 0.044$ steradians for a 19 mm diameter transducer focused at 8 cm:

$$S_r(\text{dB}) = 10 \log(0.0045 S). \quad (10.12)$$

Using Equation 10.11 and the frequency dependence of backscattering, obtainable from Table 10.6, gives:

$$\Psi_{Sr} = 10 \log \{L \Omega [c_1 + c_2(f + \Delta f)^n]\} - S_r \quad (10.13)$$

This can be arranged as the transcendental equation:

$$(2 a z_m) \Delta f - (\Psi_p - S_r) = 10 \log \{L \Omega [c_1 + c_2(f + \Delta f)^n]\}. \quad (10.14)$$

Because all quantities are known, we can solve this for Δf , corresponding to a given Ψ_p .

Taking values from Table 10.6 for the 3 MHz case in liver, and assuming a 3 dB increase (equivalent to a ratio of 1.41) in transmitted pressure and $a_1 = 0.5 \text{ dB cm}^{-1} \text{ MHz}^{-1}$, Equation 10.14 gives $\Delta f = 0.24 \text{ MHz}$. Thus, the frequency is increased by eight percent, *i.e.*, to 3.24 MHz, if the effective penetration in liver is kept constant. For 3 MHz in blood, the frequency dependence of scattering is greater than in liver, allowing a much larger 0.79 MHz value for Δf , *i.e.*, a 26 percent increase in frequency with a 41 percent increase in the output pressure for a fixed penetration.

For ultrasound imaging in homogeneous tissues, the achievable beam width in both lateral directions and the axial response length (in millimeters) are inversely proportional to the frequency. The resolution in cycles per millimeter is proportional to the frequency. For imaging blood to the fixed depth (or effective penetration) in the above example the increase of $\sqrt{2}$ in output pressure allowed an improvement in resolution by 26 percent in each direction. The improvement in image or other signal quality is described much better by the volumetric resolution than by any single linear resolution such as lateral, axial or elevational resolution. The volumetric resolution in the example for blood is thus improved by a factor of $(1.26)^3 = 2$ by increasing the output acoustic pressure 41 percent. In the example for liver that shows the linear resolution of 1.08, the volumetric resolution is increased by $(1.08)^3$ or 26 percent for the same increase in acoustic pressure.

One does not always have tissue paths of uniform speed of sound, so the beam is often spread to greater than an ideal width, and this dispersal can be more significant at higher frequencies. However, there do appear to be important cases in the human body in which achievable increases in frequency result in approximately the expected resolution improvement. This is supported by continued increase in commonly utilized diagnostic-ultrasound frequencies. The number of situations in which beam dispersal is the limitation some day may become dramatically reduced as progress is made with application of the various compensation methods for beam dispersal (Fink, 1992; Liu and Waag, 1997; Nock and Trahey, 1989; O'Donnell and Flax, 1988). In addition to improved resolution, increased frequency can provide increased contrast among many tissues because of the enhancement of diagnostically useful attenuation shadows and because of the strong frequency dependence of scattering. Back-scattering from weakly scattering tissues such as brain, blood and fat lobules in the breast makes these tissues visible and distinguishable from hypoechoic lesions therein.

As an alternative to increasing frequency with a concomitant increase in acoustic pressure and power, an increase in temporal-average-output power can be utilized to increase the frame-repetition rate or the number of pulses averaged over a scan line or the number of transmitted focal zones. All three are directly proportional to output power, or p^2 for constant waveforms. Increased frame-repetition rate may result in shorter exam times, capture of faster motions, or improved averaging of speckle and other noise. An increased number of transmit focal zones allows high resolution in the image over a wider range of distances from the transducer. Increased signal

averaging from pulses in the same location should increase the signal-to-noise ratio in proportion to the square root of the temporal-average transmitted power.

10.4.4 *Experimental Studies: Dependence of Image Quality on Output*

Many considerations regarding the effect of peak acoustic-pressure amplitude on image quality were presented in Sections 10.3 and 10.4. In Section 9.4 of NCRP Report No. 113 (NCRP, 1992), several experimental studies were referenced and discussed. A useful publication on this subject is Harris *et al.* (1989). Most notable for demonstrated effects of increased output were Boote and Zagzebski (1988) for Doppler systems, and Carson and Zagzebski (1980) for pulse-echo systems.

The number of publications of careful clinical studies regarding the effect of output on successful performance of difficult examinations is small. Transcranial Doppler (TCD) is one application in which detection of basic structures has been strongly limited by available outputs. There are several studies of TCD-ultrasound success rates. Yagita *et al.* (1996) studied the rate of successful recording of intracranial blood-velocity signals as a function of intensity (I_{SPTA}) from 76 to 532 mW cm⁻². In males, success rates were 46 and 81 percent, respectively, at the lowest and highest intensities, and in females rates were 30 and 61 percent. Success rates at the highest intensity were only 54 percent in women over 50 y of age. The authors concluded it should be possible to increase TCD usefulness significantly in an aging Japanese population by increases of available intensity in TCD, within safety limitations.

Two unpublished reports addressed the relation of image quality to intensities *in vivo*. In the first, it was stated that most or all of the obstetrical examinations in one particular facility could be performed at Doppler-output and pulse-echo output settings well below the maximal available values (Taylor, 1986). The second study (Larsen, 1986) indicated that the intensity does not consistently affect image quality until depths are reached at which the penetration is nearly inadequate, although some possible counter examples were shown. Basically, very little has been published on how much information is lost or how much the examination time is increased due to specific limits on output pressures and intensities of a specific or generic ultrasound system.

10.5 Pulse Compression as a Possible Tool for Reduction of Peak Pressure

In systems in which there is an apparent need to approach, or exceed, the threshold for inertial cavitation *in vivo*, there is reason for reducing the peak-acoustic pressure by increasing the pulse duration. It has been thought that this could be done without loss of image, or other diagnostic information content, by implementing *pulse-compression* techniques, *i.e.*, signal processing, such as matched filtering with pseudo-random and other code systems, to produce a short signal from a target insonified with a long pulse (Haider *et al.*, 1998; Newhouse, 1988; Shen and Ebbini, 1994). Pulse compression has recently been implemented commercially to extend maximal imaging depth without increasing MI (Logiq 700, GE Medical Systems, Milwaukee, Wisconsin).

Pulse compression also potentially allows for simultaneous acquisition of a large number of image lines because distinguishing features can be coded into the individual pulses. This could be helpful in increasing Doppler-sampling rates, frame rates, and focal zones for 2D imaging systems or allowing for real-time implementation of three-dimensional (3D) imaging systems. The need for real-time 3D in echocardiography may induce acceptance of some drop in quality of individual images to achieve the third dimension at reasonable rates.

Performance criteria are less understood for Doppler than for pulse-echo systems (AIUM, 1993c); however, there are basic principles critical to the tradeoff of system performance and output. The pulse-echo system sensitivity and Doppler-information content, as measured by the signal-to-noise ratio, are proportional to the time-averaged power and intensity (Baker *et al.*, 1978; Shannon, 1948). For a constant bandwidth, these time averages can be kept constant by maintaining a constant product of the pulse duration and the average intensity during the pulse. Therefore, the signal-to-noise ratio should be independent of the pulse intensity if the frequency spectrum and pulse duration are appropriately adjusted and the detection and processing system is optimized for that waveform.

Whether this flexibility can be realized is an important question. Experience with radar, in which peak intensities are limited, indicates that a longer pulse can be used to obtain a larger product of time, bandwidth and intensity (Skolnik, 1990). Pulse-compression signal processing is then employed to obtain high axial resolution, providing good imaging results in accord with theory.

With gray-scale pulse-echo ultrasound, the weakest signals that are to be displayed are usually only 50 to 70 dB weaker than the strongest signals expected at the same distance from the transducer.

This local dynamic range of ultrasound systems is limited by the poor lateral resolution and contrast resolution that result if one attempts to display signals that are much weaker than those that arise from the sides of the ultrasound beams, *i.e.*, in the side lobes and clutter. Occasionally, when the gain is set high to see weak signals in hypoechoic regions, the summation of signals from strong reflectors, lying above, below, and to the sides of the image area of interest, will saturate the ultrasound-system electronics so that the signal does not increase correctly with increasing echo amplitude. The strong echoes will merge together as a single bright blob. When the pulse length is extended beyond the usual few half cycles to allow reduction of the peak intensity, the incorrect system processing of those echoes will extend over a larger region of the image, a region equal in area to that of the pulse sample volume before compression. Multiple scattering, nonlinearity, or other artifacts of propagation in tissue can produce similar effects. All these artifacts will be most noticeable in those weak-echo regions underlying or overlying the very strong echoes that exceed the system dynamic range.

In Doppler imaging of the weak signals from blood flow, compression techniques are less likely to be adequate because of the high dynamic range required of the ultrasound system for it to recover the weaker signals in the presence of strong signals arriving at the same time from other surrounding tissues. It has been speculated (Reid, 1992)¹² that Doppler demodulators might be designed with much greater dynamic range, much as is done at high cost for the demodulator in MRI systems. In general, however, there is considerable skepticism that the dynamic-range problem can be overcome to achieve as good a signal-to-noise ratio and resolution as could be achieved with shorter pulses while retaining the same product of pulse duration, intensity and bandwidth.

In CFI, the number of usable transmitter focal zones is limited by the difficulties in maintaining a reasonable frame rate. Until very recently, only a single, long, transmit focal zone was used for the color-flow part of the image. Furthermore, there is rarely excess signal power from the Doppler signals except from the large vessels. Therefore, improvements in image quality may result from maintaining full transmitted power, even when the beam has a substantial low-attenuation path to the image region. The higher-intensity portions of the beam may undergo substantial NLP losses before reaching the region of interest (Starritt *et al.*, 1985). NLP losses may be at the point, in many high-output, pulse-echo situations, where

¹²Reid, J.M. (1992). Personal communication (Biomedical Engineering and Science Institute, Drexel University, Philadelphia).

increasing the output does not result in comparably increased received signal. Also, as mentioned elsewhere, beam distortion by tissues in the propagation path (*e.g.*, peritoneal fat) can be so great that increased output does not improve imaginable depth and image quality. However, increased output usually will result in some increase in the received signal, and may be required when the tissues overlying the beam focus are too highly attenuating (Insana, 1995).

Because nonlinear effects in tissue propagation could be reduced by use of longer pulses and reduced peak pressures, it is possible that the reduction of unnecessary energy in the longer pulses could result in improved image quality, though this is unproved at current levels of system operation. In pulse-echo ultrasound, there are often several, up to 10, sharp focal zones in the transmitted beam. NLP techniques have also been proposed as a means of improving pulse-echo-image resolution (Bjorno and Lewin, 1982; Christopher, 1997; Ward *et al.*, 1997).

10.6 Equipment Features for Reducing Acoustic Pressures

10.6.1 *General*

At least with pulse-echo systems, output amplitude has been limited largely by the cost of high voltage electronics as well as a professional concern by designers that the units be perceived as safe at the highest output levels. Often, systems have then been used as though they were known to be entirely safe despite many official admonishments to minimize the output consistent with obtaining the desired diagnostic, training or research objectives. Given inevitable uncertainties about acoustic outputs and bioeffects, the apparent relative safety of diagnostic-ultrasound systems should be emphasized, but should be accompanied by a dedication to utilize the systems in the safest practical ways. Two techniques of particular note have been proposed to reduce power and intensity, but have not been employed extensively, *viz*, single-knob-output control and multiple-receive lines.

10.6.2 *Single-Knob Output Control*

For most ultrasound systems, overall sensitivity is controlled by two or more separate controls, *i.e.*, a transmitter power control and a series of controls for system gain. If any one of these controls is fixed, it usually is power. Even when a power control is available, it is relatively easy and fairly common to leave the power at its

maximal value and adjust the overall gain to obtain an image of the desired gray level. There would be little or no additional imaging time, or cost of system construction and design, to have a single control for overall system sensitivity that would automatically keep the exposures to the patient as low as practical. One implementation would be as follows: At low sensitivity settings the power would be 20 or more decibels below the maximal available and the knob would control only the receiver gain until it was raised to near maximal gain. After that, the system power (and peak pressure) would be increased as far as available or prudent. Finally, the gain might be increased up to the level where electronic noise is displayed because, under some circumstances, the weakest imaginable echoes might be discerned in the noise.

In some cases, this one-knob implementation should actually simplify operation and improve image quality, because the maximal signal-to-noise ratio of the amplifiers is generally near the maximal gain, where the system would nearly always be operated. The combination of output power and receiver gain in a single control was recommended by NCRP (1992), and has been implemented by one manufacturer (HDI 1000, ATL, Inc., Bothel, Washington). An important addition would be to design the system to make the time-gain compensation achieve maximal gain at a depth no greater than the maximal imaginable depth or the maximal displayed depth, whichever is the shorter. Short of design changes, with all systems capable of high MI and TIs, the operators would need to be trained in this method of setting the time-gain compensation. This one-knob recommendation might not be as simple, or even applicable, in imaging of contrast agents or in tissue harmonic imaging.

10.6.3 *Multiple-Receive Lines on a Single-Transmit Pulse (Explososcan Techniques)*

The “explososcan techniques” of Von Ramm and Smith (1987)¹³ allow one to obtain numerous partially independent echo lines from a single transmit pulse by aiming different receiver apertures in a single-transmit focal zone. This is a technique for clearly reducing speckle and random electronic noise by averaging, yielding an improvement in low-contrast delectability and possibly even a net increase in resolution, though costs for the electronics and an adequate number of transducer channels are relatively high for this

¹³Von Ramm, O.T. and Smith, S.W. (1987). *Three-Dimensional Imaging System*, U.S. Patent No. 4,694,434.

array imaging technique. It has been implemented in a full-featured CFI system, initially for echocardiography¹⁴ and subsequently for general purpose use. Most of the newest full-featured, general-purpose systems utilize two receive beams for each transmit line *via* a simple phase-shifting method (O'Donnell, 1990), and one apparently extracts four receive lines per transmission.¹⁵

10.7 Summary and Conclusions

In early diagnostic ultrasound systems, there was little correlation between actual and calculated “needed” output levels (NCRP, 1992). An analysis of 1989 data for a full-featured ultrasound model showed that manufacturers were beginning to use fields that reflected the levels needed in many applications. Very few independent and periodic checks of ultrasound-system outputs are performed in the United States. Most laboratories capable of performing those tests lack the support or mandate to do so.

For a 41 percent increase in peak pressure, the increased imaging depth (penetration) is small, on the order of six percent. However, for the same increase in output pressure and a fixed penetration, a 26 percent increase in acoustic frequency is possible for recording signals from blood, resulting in a 26 percent increase in linear resolution in each dimension. This corresponds to a factor of two for improvements in volumetric resolution in the absence of nonlinear and phase-aberration effects.

Strong consideration should be given to design of ultrasound systems to maintain and improve image quality (and other diagnostic information) in ways that minimize the acoustic power and pressures, particularly in applications where maximal peak-acoustic pressures are not required. For example, to minimize outputs a single control for overall system sensitivity is recommended in Section 10.6.2 that would automatically keep the exposures to the patient close to the lowest practical.

A major effort to educate user physicians and technologists in the interpretation of the indices in specific clinical studies was to be concomitant with the introduction of ODS. That educational effort has not had the desired practical effect. A constant effort must be maintained to develop user awareness and use of MI and TI.

¹⁴Toshiba (Tustin, California) PowerVision Ultrasound System, shown in the United States in 1995.

¹⁵Acuson (Mountain View, California) Sequoia Ultrasound System, 1996.

11. Temperature Elevation and Its Biological Effects

11.1 Introduction

This Section represents an effort to update an earlier NCRP report (NCRP, 1992). As stated in Section 2, that report reviewed existing knowledge on heat production by ultrasound in biological media and its consequences. On the basis of this knowledge, exposure criteria were developed, defining conditions under which ultrasound can be used without concern for any thermal hazard. In the interim, a significant amount of research has addressed these issues. The findings and recommendations of the NCRP and other organizations and individuals have been examined, extended and utilized. Although the present report deals primarily with nonthermal mechanisms, it is important to update the knowledge base on thermal mechanisms, so that overall exposure criteria can be developed from the best information available on all mechanisms.

Since NCRP Report No. 113 (NCRP, 1992) was prepared, many publications relevant to its topic have appeared. Some of these, presented in Section 11.2, treat the response of organisms to temperature elevation produced by nonacoustic as well as acoustic means; recent findings are described. Topics treated include the nature and function of heat-shock proteins (HSPs), the role of heat as a teratogen (re-evaluated in Section 11.3), and the importance of considering potential fetal/maternal temperature differences in determining an allowable thermal increment to the fetus from ultrasound exposure. Section 11.4 deals with bioeffects attributed to temperature rise in which ultrasound is the source of heat. In Section 11.5, theory is presented for computing the temperature rise expected when ultrasound passes through media of specified characteristics, and in Section 11.6 results are reported of actual measurements that have been made in laboratory models; of special interest is the extent to which measured values of the temperature rise agree with theoretical predictions. In Section 11.7, experiments with laboratory animals are discussed, in which measurements are made of the temperature rise resulting from ultrasound exposure, and compared with computed

values, when possible. Section 11.8 deals with clinical applications of ultrasound hyperthermia; attention is given to the accuracy with which temperature increases can be computed and, related to this, the extent to which tissue damage can be controlled. Conclusions based on the new findings are presented in Section 11.9.

11.2 Biological Responses to Temperature Change

11.2.1 General Conclusions

Section 2 of NCRP Report No. 113 (NCRP, 1992) indicated that both “natural” and “induced” body temperature fluctuations occur throughout nearly every organism’s lifetime, and summarized relevant information on this topic. The human body has remarkable abilities to sense heat. In 1932, Bazett and McGlone (1932) showed that the skin can detect a 0.3 °C rise in temperature produced at a rate of 0.2 °C s⁻¹. Hardy and Opiel (1937) subsequently reported a greater sensitivity depending on the location and size of the area exposed. The forehead was found to be highly and uniformly sensitive to thermal sensation, being twice as sensitive as the forearm and hand. The anterior surface of the body was able to detect a temperature elevation produced at a rate of 0.001 °C s⁻¹ for 3 s. Human cells *in vitro* grow normally at a temperature of about 37 °C but can be frozen in liquid nitrogen (-210 °C) and will remain viable if the freezing and subsequent thawing processes are appropriately controlled. However, human cells *in vitro* generally have limited tolerance to temperatures above 37 °C and appear universally to have mechanisms for dealing with minor temperature elevations.

There is a modest range of normal rectal temperatures among various species of animals such as human beings (37 °C, see below), cat (39 °C) and sparrow (40 to 44 °C) [see Table 2.2 of NCRP Report No. 113 (NCRP, 1992)]. Above these normal temperatures, there appear to be time-temperature relations that pertain to thermal-induction of deleterious effects. For example, for human cells, a 30 min treatment at 44 °C is roughly equivalent in effectiveness in causing a hyperthermic effect to a 60 min treatment at 43 °C.

All organisms (prokaryotes, eukaryotes) appear to have comparable macromolecular responses to short-term exposures of elevated, nonlethal temperatures. Examples among prokaryotes include blue-green algae (Bhagwat and Apte, 1989) and bacteria (Herman *et al.*, 1995); examples among eukaryotes include algae (Lai *et al.*, 1988), plants (Howarth and Ougham, 1993), fruit flies (Storti *et al.*, 1980),

rats (Walsh *et al.*, 1987), mice (Hahnel *et al.*, 1986), and human beings (Honda *et al.*, 1992). At several degrees above “normal” temperature, cells will quickly form heat specific proteins (HSPs), and the presence of these proteins correlates with the organism’s ability to withstand the higher temperatures (hyperthermia) or to tolerate a subsequent “spike” in temperature, as elaborated in Section 2.4.2 of NCRP Report No. 113 (NCRP, 1992). The mechanisms, however, by which thermotolerance is achieved are not known.

11.2.2 Maternal and Fetal Core-Temperature Relations

NCRP Report No. 113 (NCRP, 1992) presents a number of “normal” core temperatures for human beings, citing (1) Dickson and Calderwood (1980) for 37 °C, (2) Hardy (1982) for 37 °C but within a normal range of approximately ± 0.8 °C, and (3) Mellette *et al.* (1951) for ~ 37 °C plus or minus the diurnal temperature variation of not more than 1 °C. These collective data have typically been derived from a small number of subjects; *e.g.*, Mellette *et al.* (1951) used 22 subjects (11 men, 11 women). For purposes of this Report, it is accepted that 37 °C is the normal core temperature of the human body, and that it may generally vary by about ± 0.5 °C throughout a normal 24 h period.

It should be noted that more recent data, involving a large population base and modern equipment, suggest a slightly lower average temperature for the population. For each of 148 subjects (aged 18 to 40) the oral temperature was determined four times per day throughout each day over a 2.5 d measurement period (Mackowiak *et al.*, 1992) using relatively fast equilibrating modern electronic thermometers with digital displays and an audio alert of thermal equilibrium. The overall mean temperature was 36.8 °C [± 0.4 ; 95 percent confidence interval (CI)]; the subject mean varied diurnally, with a low at ~ 6 a.m. (~ 36.4 °C) and a high at ~ 4 to 6 p.m. (~ 36.9 °C). Only eight percent of the 700 oral temperatures were as high as 37 °C. Whether or not the “old” standard of 37 °C for the normal temperature of human beings is abandoned in favor of 36.8 °C remains to be seen.

The near-term human fetus is normally warmer than its mother by up to about 0.5 °C (Alexeef, 1876; Macaulay *et al.*, 1992a; 1992b; Mann, 1968; Muller, 1851; Randall *et al.*, 1991; Walker *et al.*, 1969; Wood and Beard, 1964; Ziliani *et al.*, 1983) as determined by comparative and simultaneous temperature measurements of fetuses *in utero* and related maternal structures. A similar temperature differential between near-term fetuses and their mothers has been reported for

sheep (+0.4 to 0.8 °C) by Joelsson *et al.* (1970), Abrams *et al.* (1969), and Schroder *et al.* (1988); baboons (+0.47 °C) by Morishima *et al.* (1975; 1977); and rabbits (+0.25 °C) by Hart and Faber (1965). These temperature differentials have been corroborated by measures of heat flux between fetal and maternal structures. For example, Rudelstorfer *et al.* (1981) measured a heat flux of between 9.8 and 12.6 W m⁻² from the fetal scalp somewhat before delivery, with heat flux often increasing by 1 to 3 W m⁻² during contractions. Rudelstorfer *et al.* (1987) further noted a correlative rise ($r = 0.736$) in fetal-scalp heat flux with decrease in fetal blood pH. "For each 0.1 decrease of scalp blood pH, scalp heat flux decreased approximately 5 W m⁻² within the range of pH 7.15 to 7.35." They concluded that fetal-scalp heat flux is related to fetal metabolism.

During labor, the temperature of the mother can rise by as much as 1 °C and the fetal temperature has also been observed to rise. Three mechanisms appear to be responsible for the increase in fetal temperature. Firstly, the labor of the mother can represent prolonged physical exertion, with concomitant heat production. Macaulay *et al.* (1992b) showed a correlation between maternal contractions and uterine temperatures, with an overall additional fetal temperature rise of about 0.1 °C. Secondly, the labor of the mother can result in diminished umbilical flow due to constriction from the contraction (Ramsey and Donner, 1980). Heat produced by the fetus is transferred to the mother by two routes; about 85 percent of fetal heat is transferred across the placenta *via* umbilical flow, and about 15 percent exits across the fetal skin to the amniotic fluid and uterine wall (Gilbert *et al.*, 1985). Thus, a restriction in umbilical flow would compromise the major mechanism for fetal cooling. Furthermore, a restriction in umbilical flow could be manifested by a fetus with intrauterine growth restriction who would, therefore, be scanned with diagnostic ultrasound more often than a normal fetus, thereby possibly increasing the risk even more. Thirdly, certain analgesic procedures have been reported to increase maternal temperatures during labor. Fusi *et al.* (1989) reported an approximate 1 °C increase in temperature of mothers in labor for more than 6 h when administered an epidural analgesic; those mothers who received only a pethidine hydrochloride analgesic for comparable labor periods did not show a rise in vaginal temperature ($p < 0.001$). Similar results were reported by Macaulay *et al.* (1992a) and Camann *et al.* (1991) for separate groups of mothers in labor treated with either epidural or nonepidural analgesics.

The mechanism by which epidural analgesics cause a temperature rise is not clear. Macaulay *et al.* (1992a) briefly summarizes clinical observations pertinent to women given epidural analgesics and those

not. For the former, there is a concomitant increase in skin temperature, and an absence of sweating and hyperventilation. Heat is conserved. Because the epidural analgesic impairs maternal heat loss, fetal ability to dissipate heat is diminished.

Once delivered, the neonate's temperature rapidly declines. Most delivery rooms have ambient temperatures of between 23 to 27 °C (e.g., Rudelstorfer *et al.*, 1983) but can be higher (27 to 33 °C) to achieve environmental thermal neutrality for the naked neonate (e.g., Du and Oliver, 1969; Harper *et al.*, 1991; Macaulay *et al.*, 1992a; Mann, 1968; Smales and Kime, 1978). Thus, at birth, the neonate is normally exposed immediately to a temperature considerably less than that of its mother, and the newborn's temperature falls by as much as 2 to 3 °C (Adamsons and Towell, 1965). The decrease in temperature is related to the fact that the neonate's "core" temperature is about 0.5 °C and the skin temperature about 2.5 °C higher than that normal to subsequent extrauterine life. Immediately upon birth, evaporation of amniotic fluid from the neonatal skin reduces the neonatal heat content, as does the onset of respiratory ventilation. The neonate's temperature may fall to 35 °C. Bruck (1978) writes that "Soon after the infant is transferred into a heated crib, his O₂ uptake diminishes to the minimum, although it may take the colon temperature several hours to reach 36 to 37 °C."

It is not known when the temperature differential develops between the fetus and its mother. Presumably, at conception the mother's core temperature is also the temperature of the conceptus. Hart and Faber (1965) studied the relationship between maternal and fetal temperatures and gestational age in rabbits. Fetal temperature appeared to exceed maternal temperature after days gestational age (dga) 26 (normal term is 29 to 31 d). At that time (dga 26), the fetal rabbits had grown to about one-third their term weight. The authors cautioned against extrapolating their results to other species because fetal size and number, insulation (fur bearing, non-fur bearing) and other factors (metabolism, umbilical flow, and placental functions) can affect the relationship.

Some insights into human-fetal-thermal control are offered by premature infants, which, because of their reduced body mass, large ratios of surface area to body weight, and a thin layer of subcutaneous fat have less thermal stability than mature infants (Adamsons and Towell, 1965). The thermoneutral zone (TNZ) is defined by Bruck (1978) as an ambient temperature within which the metabolic rate is at a minimum, sweat gland activity is zero, and the core-body temperature is at a level for that species. By way of reference, TNZ for an unclothed resting adult human is 26 to 28 °C. For normal weight newborn infants, TNZ is 32 to 34 °C. For premature infants

(e.g., 1 kg), the *lower* (emphasis added) limit of TNZ may be as high as 35 °C (Bruck, 1978). Dodman (1987) indicates that the premature infant often needs air temperatures between 35 and 37 °C. Hey (1969) reports that for a human newborn with a birthweight 1 to 2 kg, the oxygen consumption for the first 12 h is about 6 mL kg⁻¹ min⁻¹ at TNZ of >35 °C, rising to about 9 mL kg⁻¹ min⁻¹ at the TNZ of >32 °C by 30 to 35 d of age.

The neonate is capable of heat production beyond normal metabolic processes through three mechanisms: (1) voluntary muscle activity, (2) shivering, and (3) chemical thermogenesis (summarized from Brueggemeyer, 1993). Shivering is the most efficient method in adults, but the pre-term infant has “virtually no ability to generate heat using this method.” Voluntary muscle activity is also nearly absent in pre-term infants, and the fact that the pre-term infant must be maintained at an environmental temperature that is very near or at “normal” body temperature (37 °C) indicates a near absence of thermogenic competence.

The normal human gestational period is approximately 40 weeks; this period has been divided into three phases (trimesters), with each lasting approximately 13 weeks. There are three general categories of newborn infants by weight and gestational age. These are illustrated in Figure 11.1 and include pre-term, term, and post-term infants (summarized from Endo and Nishioka, 1993). It can be seen that pre-term infants are usually those delivered during (approximately) 24 to 37 weeks of gestation, when the weight of “small” infants ranges from about 500 to 2,100 g, respectively (Battaglia and Lubchenco, 1967).

Delivery of these “small” pre-term infants, which have limited to nonexistent thermoregulatory competence, occurs in the early part of the third trimester. Thus, it seems likely that for the initial two-thirds of the *in utero* infant’s existence (*i.e.*, the first and second trimesters), the core temperature of the mother is also that of the infant. The “normal” term fetus does have some thermoregulatory capabilities, part of which is related to the presence and metabolism of brown fat, which has a much higher thermogenic capability than white fat. It seems reasonable to expect that *in situ* fetal mechanisms for close regulation of fetal temperature begin operating some time in the third trimester, possibly midway for “normal” fetuses and considerably later (*i.e.*, post-term) for pre-term infants.

11.2.3 *Thermally Induced Teratogenesis*

Two anonymous independent editorials in 1978 questioned whether hyperthermia is a human teratogen. The British Medical Journal (Anonymous, 1978a) suggested that “There is . . . still no

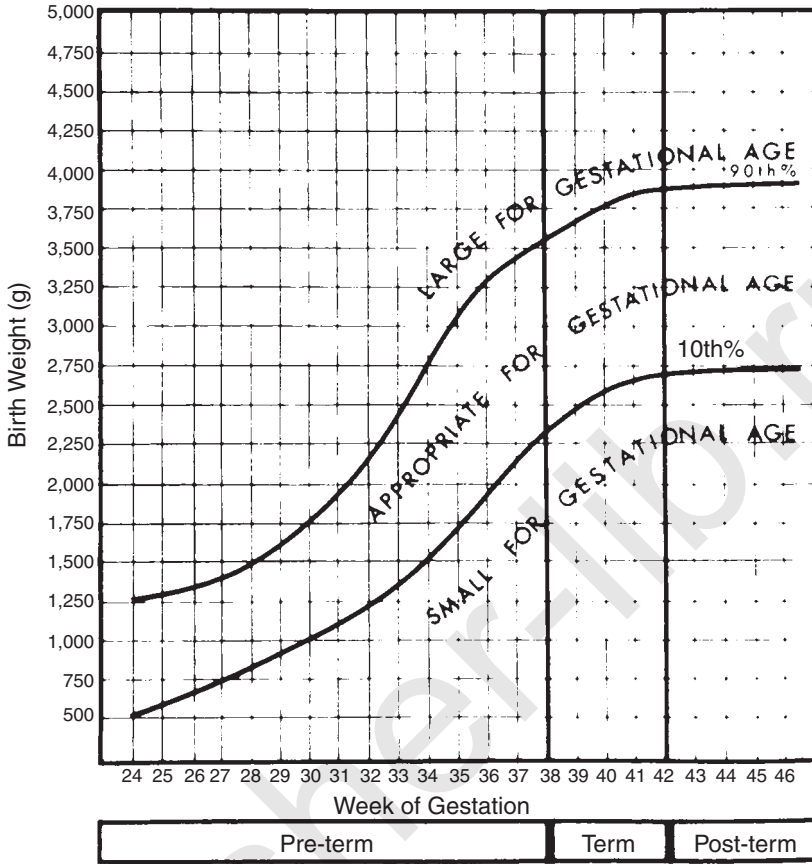


Fig. 11.1. University of Colorado Medical Center classification of newborns by birthweight and gestational age (Battaglia and Lubchenco, 1967).

convincing evidence to implicate hyperthermia *per se* as a human teratogen,” and Anonymous (1978b) indicated that “The evidence incriminating hyperthermia is so far very tenuous.” The direct evidence from human studies is still equivocal, but, as indicated in NCRP Report No. 113 (NCRP, 1992) and below, the observations of teratogenic effects in nonprimates and primates from exposure to hyperthermia coupled with emerging evidence from macromolecular, cytochemical and genetic investigative approaches provide support for the claim that hyperthermia is teratogenic to human beings.

Sasaki *et al.* (1995) undertook a study of rats which were induced to engage in strenuous exercise during pregnancy; a sharp increase in core temperature was observed, and also a concomitant increase

in the number of fetal anomalies. At dga 9, rats were divided into four groups. They were then (1) forced to swim for 30 min in a water bath at 40.5 °C, (2) forced to swim as in Group 1, but at 36 °C, (3) maintained at 40.5 °C without exercising, or (4) maintained as cage controls. The core temperature for the rats in group one sharply increased in 10 to 15 min to 42 °C and remained at that temperature; for group two, there was a gradual increase (over 15 to 20 min) to the same plateau temperature (~42 °C). Overall, there were significantly increased durations at elevated temperatures for group one relative to those for group two. There were no changes in core temperatures for the other two groups. On dga 18, the dams were sacrificed and the fetuses examined for anomalies and weight. Only group one had a statistically significant increase in numbers of fetal anomalies ($p < 0.001$), which included but were not limited to microphthalmia, encephalocele, and mandibular hypoplasia; there was also a statistically significant decrease in weight of live fetuses. The authors note that "The ninth day of gestation in rats corresponds to the fourth week of gestation in humans." The numbers of dams in this study were small, being six per regimen.

Kimmel *et al.* (1993a) confirmed and extended the results of Arora *et al.* (1979); both studies showed that mainly skeletal anomalies are induced by maternal hyperthermia at dga 10 in the rat. In the report of Kimmel *et al.* (1993b), unanesthetized or anesthetized pregnant rats were exposed to an air temperature of 43 °C until the core temperatures of the animals became 39.2 to 40.4, 40.5 to 40.9, 41 to 41.9 or ≥ 42 °C; a heating period of about 30 min was required to achieve the 39.2 to 40.4 °C core temperature range and ~60 min to achieve the 41.9 to 42 °C range. The dams were then allowed to come to term and the pups were examined at postnatal day three. There was a temperature-dependent increase above sham-exposed levels in pup anomalies over the core temperature ranges, with no obvious effect of the presence or absence of anesthesia. Maternal mortality occurred with core temperatures of 42 °C (unanesthetized) and no dam survived a core temperature of 43 °C (unanesthetized). The authors suggest that "the differences between a nonteratogenic, a teratogenic, and a maternal lethal body temperature appear to be small, probably no more than 1 °C in each case." Arora *et al.* (1979) also showed that an approximate 3 °C rise in core temperature was associated with increased placental weight, with the placenta having noticeable areas of necrosis, when heat was applied at dga 6, 8 or 10.

The embryonic development *in vitro* and *in vivo* of rat somites was further investigated in two complementary studies. Rat embryos were exposed *in vitro* at dga 10 to 42 or 43 °C for 10 to 25 min and examined 24 h later (Kimmel *et al.*, 1993b). Time and temperature

relations were observed for the incidence of growth effects and fetal anomalies. The 10 min 42 °C exposure regimen induced a reduction in crown-rump length; the 15 min regimen resulted in decreased total protein and somite number, and for the 10 min 43 °C regimen, all parameters, of which there were many, were affected. A follow-up study involved comparable hyperthermic exposures of fetal rats *in vivo* at dga 10 and evaluated 24 h later (Cuff *et al.*, 1993). There was a very good correlation between the results of the two studies for teratogenic effectiveness of the comparable hyperthermic treatments.

Edwards (1993) asserted that hyperthermia is a “confirmed” teratogen in guinea pigs, rats, mice, hamsters, rabbits, sheep, pigs, monkeys and human beings. Some of his research is summarized in NCRP Report No. 113 (NCRP, 1992). Many of the experimentally induced defects appeared to be related to the central nervous system, and his subsequent studies have focused on this aspect (*e.g.*, microencephaly, microphthalmia) with certain early fetal stages apparently more sensitive to heat than others.

Three recent reports provide partial support for the hypothesis that hyperthermia is teratogenic in human beings. Erickson (1991) undertook an analysis of conditions surrounding 4,900 babies born with major birth defects, compared with 3,000 babies born without defects. Telephone interviews were conducted so that the first of two independent interviewers established reproductive outcomes and the second interviewer (without knowledge of the outcome information) asked “the rest of the questions.” Thus, the first interviewer was not blinded with respect to outcome, but the second was. There were 92 defect categories and 105 exposure/factor variables, yielding 9,660 comparisons. At an acceptance level of $p < 0.05$, there would be 483 “significant” chance observations; there were 1.5 times that number of statistically significant observations among the various comparisons. Similar results were apparent at the $p < 0.01$ (97 expected, 348 observed) and $p < 0.001$ (10 expected, 154 observed) levels of statistical significance. The authors felt that the data suggested a nonrandom association between the exposure variables (which included but were not limited to chronic disease, fever, flu, illicit drug use, parental age, etc.) and the birth defects, but it was not possible to establish causality between any of the variables and the outcomes. Fever was found to be associated with statistically significant increases in cleft lip, pseudohermaphroditism and diaphragmatic hernia; the respective odds ratios were 2.54, 5.25 and 3.20 and the 95 percent CI were 1.7 to 3.8, 2.1 to 13.4 and 1.7 to 5.9, respectively. There were also strong associations between maternal fever and birth defects, including anencephaly, spina bifida, and anomalies in the ventricular system and heart valves.

Milunsky *et al.* (1992), in a prospective follow-up study, attempted to determine from a cohort of 23,941 women if there was any correlation between maternal heat during pregnancy and fetal neural tube defects (NTDs). Maternal heat was associated with exposure to hot tub, sauna, fever and/or electric blankets during early pregnancy. Two types of analyses were undertaken. There was a statistically significant increase in NTDs for women who took hot baths [relative risk (RR) = 2.8; 95 percent CI = 1.2 to 6.5]; there were no statistically significant associations between NTDs and maternal fever or use of saunas or electric blankets. The data were then grouped and re-analyzed for exposure to zero of three, one of three, two of three, and three of three heat sources (sauna, hot tub and fever); there was a statistically significant RR for NTD production from exposure to two of the three heat sources (n = 3 NTDs of 265 neonates; RR = 6.2; 95 percent CI = 2.2 to 17.2) but not for exposure to one (n = 10 NTDs of 2,890 neonates) or three (n = 0 NTDs of 22 neonates) heat sources. The fact that the NTD frequency was significantly associated with maternal/fetal exposure to two but not to three of the heat sources detracts from their conclusion of “an increased risk for NTDs among offspring of women exposed to heat in the form of hot tub, sauna, or fever during early pregnancy.” However, the small sample size (n = 22 neonates) for the three heat sources’ outcome may have precluded detection of an NTD. No measures of body temperature from any of the regimens were available.

Chambers *et al.* (1997) undertook a prospective cohort study involving 546 pregnant women; 273 experienced fever during their pregnancy, 273 did not. The women in the fever category were divided into two groups: (1) fever ≥ 38.9 °C for at least 24 h (high fever) and (2) fever < 38.9 °C for any duration, or fever ≥ 38.9 °C for < 24 h. There was no evidence of increased fetal loss, prenatal growth deficiency, or prematurity between the two groups (fever versus non-fever). However, for women in the high fever group who experienced fever during the first four weeks of pregnancy (n = 25), the rate of major malformations was statistically significantly increased (p < 0.002) and included one transposition of the great vessels with ventricular septal defects, and two cases of anencephaly.

Shepard, in his book *Catalog of Teratogenic Agents* (Shepard, 1989), lists hyperthermia as a teratogenic agent in human beings (see Table 2 of Shepard, 1989). He summarizes the data pertaining to maternal fever and congenital defects, including anterior neural tube closure, microphthalmia, spina bifida, CNS malformations, and anencephaly. Shepard notes that in terms of animal studies, a “moderately large literature exists on hyperthermia . . . [and] . . . congenital defects.” The animal models have been useful in testing this

postulated association because the experimentation can involve heat alone, absent any other potentially confounding associations, as, for instance, in human beings where fever usually is associated with infections. Shepard also noted that there was no apparent association between sauna bathing and teratogenic outcomes.

In an earlier, related study, Harvey *et al.* (1981) had reported that of 20 nonpregnant women placed in hot tubs set at either 39 or 41.1 °C, the highest body temperature tolerated before all the women had voluntarily left the bath, due to discomfort, was 38.9 °C, with the majority of participants already having left the water before reaching that core temperature. The duration of the stay in the tub was inversely related to the water temperature, being about 15 min at 39 °C and 10 min at 41 °C. Ridge and Budd (1990) obtained results somewhat different from those of Harvey *et al.* (1981). Ridge and Budd (1990) asked 24 Australian nonpregnant young women to remain in a spa pool set at 40 °C until any one of the temperatures recorded in the ear canal, rectum or mouth reached 39 °C, or they became too uncomfortable to continue. None of the subjects left the pool before their core temperature had reached 39 °C, and 54 percent indicated they were not uncomfortably hot. A possible explanation for the differences in heat tolerance between the Harvey *et al.* (1981) findings, involving Canadian subjects, and those of Ridge and Budd (1990), involving Australian subjects, is that the former may not be as heat tolerant as the latter, who would probably be exposed to higher environmental temperatures in summer and winter. In support of this hypothesis, Spraggett and Fraser (1982) showed that of 50 Canadian female subjects (ages 16 to 45), only 20 remained in a sauna bath long enough to elevate body temperature to 38.9 °C without undue comfort. The editorial in the *Lancet* noted “. . . in Finland, the home of the sauna, the incidence of anencephaly is 0.32 per 1,000 births, and in Sweden it is 0.37 per 1,000. These are amongst the lowest reliable rates in the world.” Of course, it is always possible that with human beings there are specific periods of fetal development in which the fetus is extremely sensitive, and that the sensitivity of this population has a statistical distribution, with some fetuses more sensitive than others to the combined relationship of time, temperature duration, and thermal burdens. Harvey *et al.* (1981), while noting that their data do not contraindicate the use of hot tubs or saunas during pregnancy, recommend that pregnant women avoid lengthy periods of hot-tub or sauna use.

The low prevalence rate of neonates with NTD in the Scandinavian countries appears not to take into account any abortifacient effects of heat or surgical intervention. For the former, Morishima *et al.*

(1975) showed with pregnant baboons (dga 147 to 174), that at a maternal-core-temperature elevation of about 4 °C (normal core temperature is 38 °C), there was a two-fold increase in spontaneous labor in the hyperthermia group, plus a significant rise in heart rate, a fall in blood pressure, an increased metabolic acidosis, cardiac arrhythmia and hypoxia. There were also additional fetal complications: one became mildly alkalotic due to maternal hypocardia; maternal heat prostration with shock and convulsions occurred twice, as did fetal cardiac arrest; fetal asphyxiation occurred twice. Harvey *et al.* (1981) had shown a mean vaginal temperature of 38 °C following 20 min of sauna bathing, and Sohar *et al.* (1976) indicated about a fifth of the subjects had temperatures greater than 39 °C, with the highest at 40.2 °C. Spraggett and Fraser (1982) also reported that “in half the women exposed to the heat of the sauna for 20 min, the oral temperature was found to be at least 39 °C, and in one case reached 39.9 °C.” The duration of the sauna bathing period and the temperature of the sauna environment are known to vary (*e.g.*, Lipson and Edwards, 1993; Saxen *et al.*, 1982); additionally, some bathers undertake more than one heating cycle per sauna episode (*i.e.*, do “innings”), interspersing a cool shower between heatings. In the Sohar *et al.* (1976) report, pathophysiological effects that developed in the sauna bathers included a substantially increased heart rate, syncope in three of the 60 subjects, an anginal attack in another, and electrocardiogram changes suggestive of coronary insufficiency.

Saxen *et al.* (1982) tested the hypothesis of a causal relationship between sauna-induced hyperthermia in pregnant women and congenital defects in their offspring. A retrospective, matched-pair, case-controlled study included 302 cases of a child with a congenital anomaly (100 cases of central nervous system defects and 202 cases of oral clefts) and a similar number of referent mothers who delivered apparently healthy children. Each referent mother’s delivery occurred in the same geographic area as its match case mother. The sauna bathing habits of case and referent mothers were compared and found not to be distinguishable, thereby suggesting that the difference in birth outcome between the two classes of mothers was not related to sauna bathing. Saxen *et al.* (1982) argue that the high core temperatures that demonstrably result in congenital defects in laboratory animals “have never been reported in human subjects during or after a sauna bath” and that during a “typical sauna” (20 to 25 min at 70 to 80 °C) “the rectal temperature rises 0.5 to 1.5 °C.” In Sohar *et al.* (1976), some sauna bathers’ core temperatures rose 2 to 3 °C.

If (as shown later in Figure 11.5) the lowest-reported temperature increment above core is 1.8 °C for teratogenic effects in laboratory rats (Kimmel *et al.*, 1993b), if there is a common mechanism for hyperthermia-induced teratogenicity, and if the threshold for this effect in Kimmel *et al.* (1993b) is less than 1.8 °C above core, then there is reason to continue to be cautious. Timing of the hyperthermic event has been demonstrated to be very crucial for induction of NTDs. A comparison of birth outcomes among case and referent mothers whose sauna bathing occurred on a weekly or monthly basis, as was done by Saxen *et al.* (1982) could easily miss delineation of stage sensitivity.

There are regional and time-dependent variations for the prevalence rates of various congenital defects. For example, for a 15 y period (1974 to 1988), the prevalence rates for anencephaly in the United States and Mexico were 3.4 and 18.4 per 10,000 infants. For the United States, the rate was highest in 1974 (4.4 per 10,000) and lowest in 1988 (2.1 per 10,000), with the data displaying a time-dependent decrease in rate ($r = 0.98$; $p < 0.001$) (WHO, 1991). Limb and Holmes (1994) and Sellar and Hancock (1985) have noted sharp declines in the birth prevalence of NTD in Boston and the United Kingdom over the past decade. Limb and Holmes (1994) speculate that the decline in birth prevalence is related to increased prenatal detection of anomalous fetuses and subsequent elective abortion, but suggest, as do Sellar and Hancock (1985), that vitamin supplementation during pregnancy has also somewhat mitigated against the birth incidence of NTD. Zimmer *et al.* (1997) showed for a 5 y period (1989 to 1993) that the voluntary termination of pregnancy after ultrasound detection of fetal abnormalities had a statistically significant impact ($p < 0.01$) on the prevalence of abnormalities in newborns.

For most of gestation, the fetal temperature is approximately equal to the maternal core temperature. However, at some point during the latter part of the gestational period, the fetus becomes somewhat warmer (about 0.5 °C) than its mother. After birth, the fetal temperature rapidly adjusts to 37 °C. Because this Report is focused on exposure criteria for diagnostic ultrasound, it is important that the temperature of the fetus be used in deriving recommendations pertinent to possible temperature elevations of ultrasound-interrogated fetuses.

It is not clear if one should use actual or relative temperatures as reported in the literature for estimating the potential for hyperthermic, teratogenic effects in human beings. As shown in NCRP Report No. 113 (see Figure 2.8 of NCRP 1992) and also Miller and Ziskin (see Figure 9 of Miller and Ziskin, 1989), there are no experimentally induced thermal bioeffects in a wide spectrum of animals (*e.g.*, rat,

monkey, guinea pig, mouse, Chinese hamster, chicken, etc.) below 39 °C. Thus, on an actual temperature basis it is tempting to suggest, as do Barnett *et al.* (1994), that a “diagnostic exposure which produces a maximum temperature rise of no more than 1.5 °C above normal physiological levels (37 °C) may be used without reservation in clinical examinations.” In contrast to the above suggestion is that of the International Non-Ionizing Radiation Committee of the International Radiation Protection Association’s (IRPA/INIRC, 1991) Guidelines, *Protection of the Patient Undergoing a Magnetic Resonance Examination*, which indicates “For whole-body exposures or exposures of the head and trunk, no adverse health effects are expected if the increase in body temperature does not exceed 1 °C. In the case of infants, pregnant women, and persons with cardiocirculatory impairment, it is desirable to limit temperature increases to 0.5 °C.”

In determining an acceptable level of ultrasound-induced temperature increase in the fetus, Edwards (1986) has suggested that a 1.5 °C increase in fetal temperature should be viewed as a “universal threshold” for induction of teratogenic effects—*i.e.*, it is the *relative* (emphasis added) temperature increase which is critical. Edwards had shown that this threshold temperature differential (+ 1.5 °C) is applicable to a wide variety of mammals and argued that it would seem appropriate for human beings as well. Edwards writes “In a number of species with varying normal body temperatures it has been found that the threshold-temperature elevation for heat teratogenesis is about 1.5 to 2.5 °C, but there is some doubt whether the threshold is determined by a given elevation over the normal, or by the absolute temperature reached. A number of studies indicate that it is probably the elevation over the normal . . . The species known to be affected include birds, all the common laboratory animals, farm animals, and primates. It would be remarkable if it were not also a human teratogen.” Kimmel *et al.* (1993a), studying fetal skeletal development in rats following heat exposure, notes that “the differences between a nonteratogenic, a teratogenic, and a maternal lethal body temperature appear to be small, probably no more than 1 °C in each case.”

11.2.4 Heat-Shock Proteins

An excellent review of the literature on gene expression under thermal stress (Howarth and Ougham, 1993) has its foundation in the observation that the “heat-shock response” is nearly ubiquitous among eukaryotic systems and is characterized by: (1) a decrease in

normal cellular protein synthesis, as occurs at translational and transcriptional levels, and a sudden induction of HSP, and (2) a correlation between the production of HSP and induced thermotolerance. HSP are derived from newly synthesized messenger ribonucleic acid and fall into several categories of large molecules (MW > 80 kDa; 70 kDa; 14 to 30 kDa). The fact that HSP of all organisms appear to be of comparable size and variety and that many also appear when the organism is exposed to other types of stressors (*e.g.*, cold, heavy metals, etc.) suggest that HSP are functionally important and first appeared early in phylogeny. For example, Borbely *et al.* (1985) showed that exposure of the blue green alga *Synechococcus* to a heat shock resulted in the nearly immediate synthesis of a series of polypeptides ranging from 11.4 to 91 kDa. Bhagwat and Apte (1989) subsequently showed that exposure of another blue green alga (*Anabena*) to several different types of stressors (heat, salinity and osmotic stress) resulted in the production of a large number of polypeptides. A few were unique to heat treatment and others to the other stressors, but many were common to all stressors. Fisher *et al.* (1995) showed, with heat-treated rat embryos, that the accumulation of HSP 72 preceded the development of aberrant somite morphology, that HSP was transcriptionally regulated as evidenced by its suppression with actinomycin D, and that HSP accumulated in the embryonic neuroectodermal tissues and was not found in the somite mesoderm—an observation that may explain the sensitivity of this tissue to heat. Walsh *et al.* (1987; 1989) report that it takes about 10 to 15 min for a heated organism such as an embryo or fetus to switch from its normal synthetic pathways to ones that produce HSP.

The mechanism by which HSPs confer some degree of tolerance to hyperthermia is not yet certain, but one strongly supported hypothesis is that HSPs bond to critical protein molecules and thereby stabilize them against thermal denaturation. A second hypothesis is that HSPs assist in the repair of thermally damaged macromolecules. The synthesis of HSPs is attended by a rapid decrease in translational and transcriptional activities, and thus follows closely the repression of “normal” gene expression. Westwood *et al.* (1991) have identified in the giant salivary chromosomes of *Drosophila* a heat-stressed oligomerization and chromosomal localization of heat-shock factor (HSF), the transcriptional activator which interacts with a heat-shock element, a conserved DNA sequence. HSF was shown by immunofluorescence microscopy to be localized to highly specific bands across the many chromatids composing the giant chromosome, suggesting a genetic association of the heat-shock response. Herman *et al.* (1995), showed that an

allele in *Escherichia coli*, which confers temperature-sensitive growth at 42 °C, can be suppressed by the loss of another specific allelic factor and by anaerobic growth.

11.2.5 *Investigations Involving Ultrasound Exposures of Mammalian Embryos or Fetuses In Vivo and In Vitro*

There are a number of reports (Lele, 1975; Carstensen and Gates, 1984; 1985) in which investigators sought to determine whether or not ultrasound could cause teratogenic effects. Many, but not all, of these studies, conducted during the 1970s and 1980s, appeared to focus on nonthermal mechanisms. Some of the studies have involved mice. Kimmel *et al.* (1983; 1989) undertook two studies with anesthetized pregnant mice insonated (1 MHz, 0.05, 0.5 and 1 W cm⁻², CW, 1.7 mm -3 dB beam width) for 2 min on day eight of gestation (period of organogenesis) while contained in a water bath at 30 °C. The first trial (Kimmel *et al.*, 1983) resulted in no statistically significant effects of insonation on all the comparative measures (*e.g.*, early resorptions, dead fetuses/litter, sex ratios, fetal weight) but a slight increase in teratogenic effects with increase in ultrasound intensity. The second study (Kimmel *et al.*, 1989) was conducted much the same as the initial one but used pulsed ultrasound (1 MHz center frequency, 0.05, 0.5 and 1 W cm⁻² SATA, 6.5 μs pulse duration, 90 W cm⁻² SPPA, 1.6 cm -6 dB beam width) but there was no detectable effect on the subsequent development of the *in utero* fetuses. Because these investigators used a broad, unfocused transducer and a 1 MHz ultrasound frequency, there appeared to be good grounds for expecting that the uterine horns were exposed since some of the animals developed what is described as “hind limb paralysis” (due most likely to overheating of the maternal spinal column). However, the animals were immersed in water at 30 °C. Hence, the core temperatures were probably depressed relative to an unanesthetized mouse’s normal core temperature, which is about 37.5 °C (see Table 2.2 of NCRP, 1992). It is, therefore, possible that the insonated uterine horns experienced some ultrasound-induced temperature elevation, but that it was insufficient to cause an effect due to the abnormally low body temperature of the dam. No core temperature measures were made before, during or immediately after the insonation.

Child *et al.* (1988) exposed anesthetized pregnant mice at day eight of gestation to 2 MHz pulsed ultrasound (pulse length 10 μs; pulse repetition frequencies of 1,000 or 200 Hz; SATA 0.6 and 0.1 W cm⁻², respectively) for 5 min while suspended in a 37 °C water bath. Under

these insonation conditions, the ultrasound-induced temperature increase in the uterine-horn area was about 1 °C as determined by implanted thermocouples. The dams were sacrificed at day 18 of gestation and the fetuses examined. There were no growth, viability or teratogenic effects; these results contrasted with an earlier report by Takabayashi *et al.* (1981), who, using comparable exposure conditions and about a third the number of fetuses, reported a modest increase (nine percent) in malformed fetuses. Kim *et al.* (1983) exposed pregnant mice (dga 8) to 1 MHz, 2.5 W cm⁻² CW ultrasound for 20 s and analyzed the fetuses at dga 18. Some of the mice were fed a normal diet, others received a restricted protein diet. There were adverse growth effects of the restricted diet on the fetuses, but no statistically significant effects were attributable to the ultrasound, although the authors thought there was a tendency toward decreases in fetal weight, and in DNA and RNA contents (each measured in milligrams per fetus), as determined by standard chemical analytical techniques.

There are also reports in which embryos or fetuses *in utero* or *in vitro* were heated preferentially, as can be done with focused ultrasound. Earlier, as reported in NCRP Report No. 113 (NCRP, 1992), Abraham *et al.* (1989) showed that rat fetuses *in utero* could be heated with an ultrasound exposure (1 MHz) and that induced temperatures were higher on the interior of the fetus than on its outer surface. Barnett and colleagues (Angles *et al.*, 1990; Barnett *et al.*, 1990) exposed 9.5 d old rat embryos in culture to pulsed ultrasound (3.14 MHz center frequency, 2 kHz *PRF*, 1.2 W cm⁻² SPTA, up to 30 min exposure duration) and noted the subsequent presence of neural plate damage, delayed development, a reduction in somite number, and an induction of HSPs. Stolzenberg *et al.* (1980) exposed pregnant mice at five stages of gestation to 2 MHz ultrasound (CW, 1 W cm⁻², for up to 2 min; dorsal application) and noted a decrease in fetal weight, and an increase in maternal and fetal mortality at the longer exposure durations. The authors also noted fetal exencephaly at necropsy, especially in the group exposed for 80 s on day eight of gestation. All effects were attributed to sonically produced heat, the temperature rise being as much as 6 °C.

Shoji *et al.* (1975) exposed two lines of anesthetized pregnant mice on day eight of gestation to 2.25 MHz, 40 mW cm⁻² intensity ultrasound for 5 h using glycerin as a coupling medium. Some animals were bound but not insonated; another group served as a control (not bound, not insonated). For the A/HeMk strain of mice, a statistically significant increase in malformed fetuses was observed for the insonated group; this difference did not occur with the similarly treated DHS strain of mice. The authors cautioned that binding of the mice

may have been a contributing factor to the observed results as a statistically significant decrease in A/HeMk mean fetal weight was observed for the bound and insonated groups relative to the unbound, not insonated (control) group. A commercially available diagnostic ultrasound device (Doppler Fetal Detector) was used for the insonations. No temperature measurements of the insonated tissue were reported.

Similar types of experiments have been done with rats. Takeuchi *et al.* (1970) exposed pregnant rats on days three and four of gestation to 2.25 MHz, 150 mW cm⁻² CW ultrasound for 20 min but did not observe any effects on the fetuses. The timing of the ultrasound exposures would be somewhat before the organogenesis stage in fetal development, which in rats is around day nine of gestation. McClain *et al.* (1972) used a diagnostic ultrasound device emitting an unfocused beam (2.25 MHz, 9.1 mW cm⁻² averaged output) to expose or sham-expose anesthetized pregnant rats suspended in a heated water bath at 37 °C at days 8 to 10 or 11 to 13 for either 0.5 or 2 h d⁻¹ (e.g., once per day on days 8, 9 and 10). No skeletal or soft-tissue morphological effects were noted. No temperature measures were made of the insonated tissues. Child *et al.* (1984) exteriorized the right uterine horn of pregnant rats at day three or six of pregnancy and exposed it to ultrasound (2.25 MHz, 1 μs pulse duration, pulse repetition rate of 500 Hz, temporal spatial-average intensities of 1.2 or 12 mW cm⁻²) using a continuous flow of 37 °C saline as a coupling agent. After exposure or sham exposure, the uterine horn was placed back into the abdominal cavity and the animals sacrificed on day 17 of gestation. There was no effect on fetal weight, numbers of living fetuses or resorptions. These results contrasted with those of Pizzarello *et al.* (1978) who reported fetal growth reduction and abortions for similar exposures. Sikov and Hildebrand (1976) exteriorized the uterine horns of pregnant rats at 9 d of pregnancy, exposed them to ultrasound (3.25 MHz, 0 to 32.4 W cm⁻² CW for 5 or 15 min exposures), replaced the uterine horns, and allowed the pregnancy to continue until day 20 of gestation. There was an "apparent threshold" for prenatal mortality at 3 W cm⁻² but fetal size was unaffected. There were a few malformations, occurring at intensities of 10.5 W cm⁻² or higher. There were no temperature measures of the insonated tissues, and no indication that the exteriorized uterine horns were maintained at normal core temperature during insonation. Lele (1975) has commented on some of this literature and suggested that some of the reported effects may be due to ultrasound-induced thermal burdens.

Carstensen and Gates (1984) subsequently reviewed the literature dealing with the effects of pulsed ultrasound on the fetus and noted

negative (*i.e.*, no effect) and positive (*i.e.*, an effect claimed) reports. Among the 25 studies reviewed by Carstensen and Gates (1985), 15 lacked any published attempt at independent confirmation, five failed to confirm the initial observation, and five had a mix of positive and negative results with attempted verification. The report with the highest (temporal) peak intensities did not yield positive results, suggesting that inertial cavitation was not the mechanism of action. Because several of the positive studies involved quite large temporal average intensities, it was not possible "to unequivocally eliminate heating as a contributing factor." Indeed, it appears likely that heat was a contributing factor.

There have been two reports dealing with an investigation of prenatal ultrasound exposure of monkeys (Tarantal and Hendrickx, 1989). An ATL MK 600 diagnostic ultrasound sector scanner (7.5 MHz center frequency, SPTA 12 mW cm^{-2} , SPPA 98 W cm^{-2}) was used five times weekly to scan *in utero* each pregnant animal's fetus. The schedule for the ultrasound examinations was as follows: dga 21 to 35, five times weekly at 10 min per examination, dga 36 to 60, three times weekly at 10 min per exam, and dga 61 to 150, once per week at 20 min per exam. There were 16 exposed and 14 control animals. A large number of different measures was made of the neonates, including Apgar scores, heart rate, respiratory performance, temperature, weight, length, morphometric measures, and hematologic assessments over a period ranging up to six months post delivery. Some differences between control and exposed animals were noted, such as statistically higher Apgar scores for the ultrasound-exposed infants, lower birth weight, and lower white-blood-cell counts. These differences tended to disappear with increasing neonatal age such that by 1 y the two groups were virtually indistinguishable. No gross abnormalities, abortions or still births were observed in any of the neonates.

11.3 Re-evaluation of Data on Thermally Induced Teratogenicity

In the earlier NCRP report, data were presented on the relationship between temperature elevation and time duration at that temperature (see Table 2.5 and Figure 2.8 in NCRP, 1992). Figure 11.2 is a reproduction of Figure 2.8, with the data points derived from the various reports listed in Table 2.5 of NCRP Report No. 113 (NCRP, 1992).

For example, Edwards and colleagues did a large number of experiments with guinea pigs in which they were placed for an hour in a

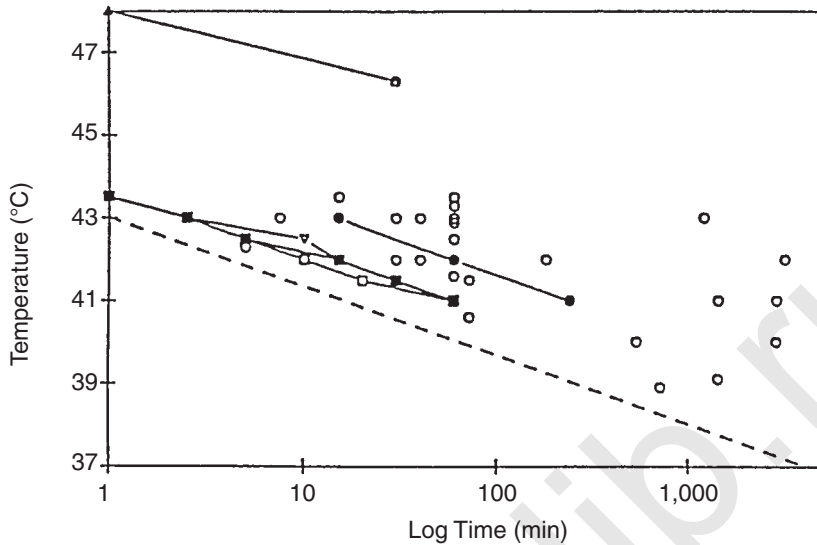


Fig. 11.2. A plot of temperature-time conditions under which teratogenic effects occur based on the results listed in Table 2.5 of NCRP Report No. 113 (NCRP, 1992) that have been reported in the literature in which the temperature elevation and exposure durations are provided. Each point of the data represents either the lowest temperature reported for any duration or the shortest time at a given temperature for the occurrence of a given effect. In the experiments, some investigators found the same effect with differing combinations of temperature elevation and duration reported for a given effect. The solid lines represent multiple data points relating to a single effect; the dashed line is a plot of Equation 11.1a and represents a lower boundary for observed thermally induced biological effects (Figure 2.8 in NCRP, 1992). As explained in the text, the time plotted is the exposure time for the pregnant animal; the effective time of exposure for the fetus at the indicated temperature is shorter.

convection oven set at 43 °C (see Table 2.5 in NCRP, 1992); thus, the results of these experiments are plotted at the intersection of 60 min and 43 °C in the Figure 11.2. Similarly, Webster *et al.* (1985) warmed rats to 43.5 °C in two heating cycles, separated by 6 h, in a water bath at 43.5 °C; the total time duration of the two heating cycles was about 60 min. Thus, these latter data are plotted at the intersection of 60 min and 43.5 °C on the figure. In general, what is plotted in the figure is the temperature of the medium that warmed the animal and the total exposure time in that heated medium. Additionally, a “boundary curve” was also imposed on the figure; this dashed line is a plot of the equation:

$$t = t_{43} 4^{(43-T)}, \quad (11.1)$$

where t is the time (in minutes) corresponding to the threshold for a specific bioeffect that results from exposure to a temperature (T) (in degrees Celsius) and t_{43} is the value of t when $T = 43$ °C. This line served as a convenient boundary below which there were no observed biological effects and was intended to serve as a “guide for determining whether or not a biological effect due to hyperthermia would be likely. Combinations of temperature elevation and exposure durations falling below this boundary would be considered unlikely to produce any harm; exposure conditions falling above this boundary would have a significant possibility of damage” (page 32 in NCRP, 1992).

An inspection of the data plotted in the figure, with a general aim of extrapolating to safety considerations for human hyperthermia, suggests that “changes occur at a temperature which is at least 2 °C above the core temperature for humans” and that it would take a very lengthy exposure period (~1,000 min) at that temperature to cause an effect.

A reanalysis of the literature presented in Figure 11.2 was undertaken. There were two central concerns that appeared reasonable for suggesting an alternate presentation of that data. Firstly, the data in Figure 11.2 were derived from laboratory animals whose core temperatures varied widely (see Table 2.2 of NCRP, 1992). For instance, the core temperatures of guinea pigs, rats and mice are about 39.5, 38.5 and 38 °C, respectively. Thus, for example, a guinea pig core temperature (39.5 °C) is about equal to that of an average human fever (Table 2.1 of NCRP, 1992). Secondly, the tabulated information (Table 2.5 of NCRP, 1992) and associated plotted data (Figure 2.8 in NCRP, 1992) generally present only the temperature of the heating medium and the time during which the pregnant mammal is exposed to that medium, but do not address the temporal course of temperature at the core of the organism being heated.

The reanalysis deals with the time course of the core temperature during a heating experiment. Consider the heating profile reported by Edwards (1969) for a large number of studies with guinea pigs, using a hot-air convection oven set at 43 °C and exposing the guinea pigs for 1 h; the heating profile (core temperature versus time) of the guinea pig is depicted in Figure 11.3. It is apparent that the initial core temperature of the mother is about 39.3 °C, and that it takes a 60 min heating period to raise the core temperature of the mother to about 43 °C, after which the animal is removed from the oven and begins to cool. Thus, the maternal core temperature is at 43 °C for a short period of time (say, 1 min), and is at increasing

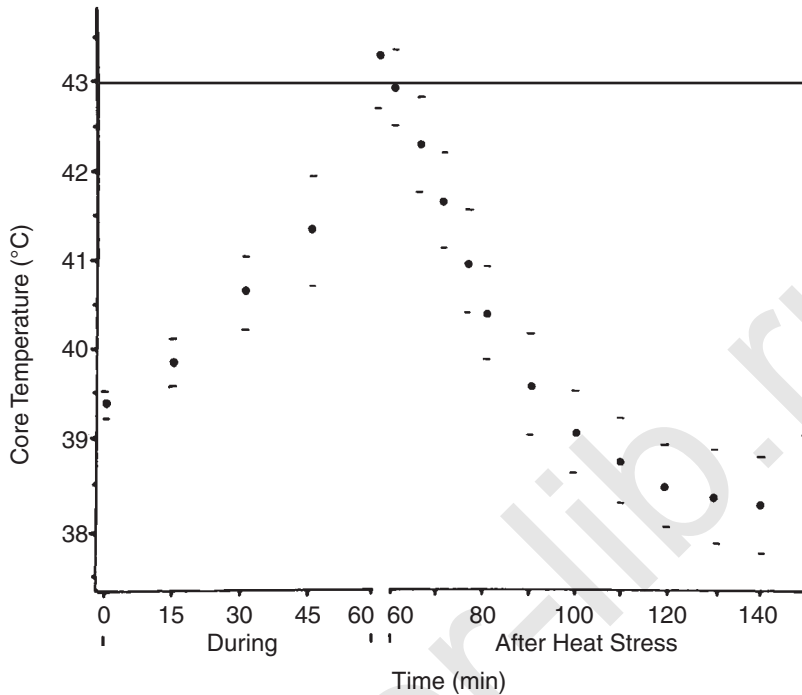


Fig. 11.3. Pattern of core-temperature elevation as determined by a rectal thermometer in guinea pigs during heat treatment (0 to 60 min) in an air convection oven at 43 °C (shown by the horizontal line), and subsequent recovery after heat treatment (60 to 150 min). Error bars are ± 1 standard deviation (adapted from Edwards, 1969).

time durations at other lower temperatures for both the heating and cooling phases of the regimen. Because the fetal temperature is approximately that of the core, the fetus also is exposed to a variable-temperature regime.

In evaluating a variable-temperature exposure, it is useful to compare it with a (hypothetical) exposure in which the temperature is held constant, using an analysis similar to that on which Equation 11.1 is based. For this comparison, the time (t_6) is estimated for an equivalent exposure in which temperature rise is held constant at 6 °C. An example is shown in Table 11.1, based on the data of Figure 11.3. The temperature range of the experiment is divided into 0.5 °C intervals centered at 43 °C, 42.5 °C, etc. From each of these intervals is subtracted the core temperature 39.5 °C to obtain ΔT_c shown in the second column as 3.5, 3, 2.5 °C, etc. The time (t) during which ΔT_c was in the 0.5 °C range centered at 3.6 °C was estimated and entered

TABLE 11.1—An illustrative calculation of a “ t_6 ” value based on: (1) the heating profile depicted in Figure 11.3 and (2) a procedure modified from one used by Sapareto and Dewey (1984).

T^a (°C)	ΔT_c^b (°C)	t^c (min)	ΔT^d (6 - ΔT_c)	$\Delta t_6 = tR^{(6-\Delta T_c)^e}$ (min)
43.0	3.5	1	2.5	0.03
42.5	3.0	6	3.0	0.09
42.0	2.5	8	3.5	0.06
41.5	2.0	8	4.0	0.03
41.0	1.5	12	4.5	0.02
40.5	1.0	12	5.0	0.01
40.0	0.5	14	5.5	0.01

$t_6 = \Sigma \Delta t_6 = 0.25 \text{ min}^f$

^a T is a specific heating profile temperature centered in a 0.5 °C interval.

^b $\Delta T_c = T - T_c$, where T_c is the body core temperature.

^c t is the time in minutes spent at the temperature interval.

^d $\Delta T = 6 - \Delta T_c$.

^e Δt_6 is the contribution to t_6 from the exposure in an individual temperature interval. The value of 0.25 is used for R .

^fThus, when $t_6 = 0.25 \text{ min}$, t_5, t_4, t_3 , and $t_2 = 1, 4, 16$ and 32 min , respectively.

in the third column as 1 min, and similar estimates centered for the other intervals. The equivalent time (Δt_6) for the interval is set equal to t multiplied by the indicated weighting factor. Finally, all Δt_6 contributions are added to give 0.25 min as t_6 , the exposure time at a constant value of $\Delta T_c = 6 \text{ °C}$ that would be equivalent to the actual variable-temperature exposure to which Figure 11.3 applies. More generally, one might define t_n as the duration for an equivalent exposure at a constant core temperature elevation of $n \text{ °C}$. Then, because, according to Equation 11.1, the time t_n increases by a factor of four for each decrease in temperature by 1 °C, one obtains $t_5 = 1 \text{ min}$, $t_4 = 4 \text{ min}$, etc.

A similar type of analysis is possible for any study reporting a heating profile (Cockroft and New, 1978; Edwards, 1968; 1969; Germain *et al.*, 1985; Kimmel *et al.*, 1993a; Kreshover and Clough, 1952; Pennycuik, 1965; Shiota, 1988; Webster and Edwards, 1984; Webster *et al.*, 1985). From these publications, data were obtained from 34 experiments in which core temperatures were measured as a function of time during exposure of pregnant animals to heated environments. Then, calculations were made (analogous to the calculation of t_6 in Table 11.1) of the time (t) that would be required to

produce the observed effect in hypothetical exposures during each of which the core temperature rise is held constant at a selected value ΔT ; an equation similar to the one in the heading of the fifth column in Table 11.1 was assumed to apply, with $R = 0.25$. Then, using a different form of the equation, a calculation was made for each experiment of the equivalent 10 min temperature rise (T_{10}); here T_{10} is the increase in core temperature that would produce the same teratological effects in a hypothetical exposure where this increase is maintained constant for 10 min. The equation used was:

$$T_{10} = x + 1.67 \log (y/10), \quad (11.2)$$

where x and y are the previously selected and calculated values of ΔT and t for the same experiment. For the set of 34 experiments, the values of T_{10} , obtained in this way, varied from 3.1 to 5.2 °C. The mean value of T_{10} was 4.15 °C and the standard deviation ± 0.52 °C. The distribution is shown in Table 11.2.

The 34 experiments to which these results apply were obtained by subjecting pregnant rats, mice and guinea pigs to heated environments in air chambers or water baths at or around the period of embryonic organogenesis. The emphasis was on observation of craniofacial abnormalities, partly because of their importance, and partly because they occur relatively infrequently in sham exposures, thus reducing requirements for large numbers of test animals. The temperatures and exposure times used were values found to produce significant effects with reasonable numbers of animals; the percentage of abnormalities observed varied over a very wide range, from 15.2 to 100 percent in the experiments Kimmel *et al.* (1993a), Shiota (1988), and Edwards (1968).

The paper by Kimmel *et al.* (1993a) reports effects occurring at the lowest temperature elevation in mammals, results characterized by the original investigators as "minimal." Unanesthetized pregnant rats (dga 10) were used for this study. There were three categories

TABLE 11.2—*Distribution of T_{10} values.*

T_{10} range (°C)	Number of Experiments (N) ^a
3.0 – 3.49	5
3.5 – 3.99	7
4.0 – 4.49	12
4.5 – 4.99	8
5.0 – 5.49	2

^a N gives the number of experiments (in a total of 34) for which T_{10} lie in the indicated range.

of treatment: (1) cage controls, in which the animals were maintained in their respective cages, (2) sham-exposed in which the animals were placed in the exposure chamber at room temperature (20 °C) for 60 min, and (3) heat-exposed, in which the animals were placed in the exposure chamber at 43 °C and maintained there until their core temperature reached the “minimal-effect” level, or longer for a “maximal-effect” level. Core body temperatures were measured for the course of these two heating regimens; they are shown in Figure 11.4.

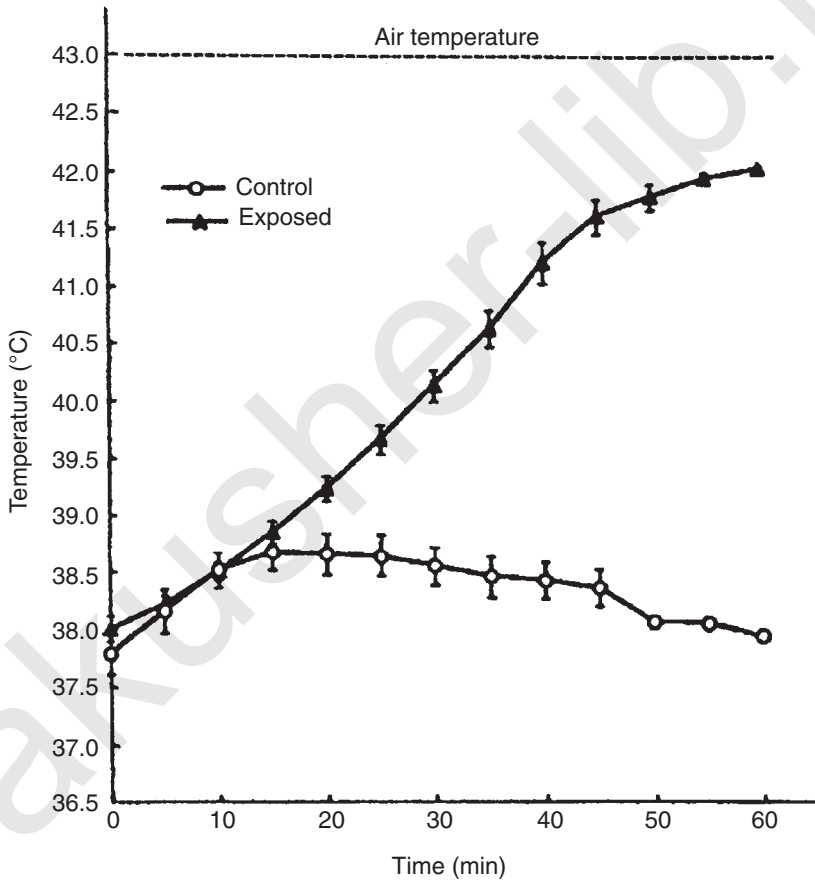


Fig. 11.4. Core-body temperatures of pregnant rats as a function of time in response to controlled air temperatures. For test animals, the air temperature was 43 °C (indicated by the horizontal line); for sham controls, the temperature was 20 °C (adapted from Kimmel *et al.*, 1993a).

Malformations resulting from the thermal exposures were primarily to the axial skeleton but did include some associated with organogenesis. Effects characterized by the authors as “maximal” were obtained when the animals were exposed until the core temperatures reached values in the range of 41 to 41.9 (mean 41.5) °C, corresponding to increases (ΔT) of 3 to 3.9 (mean 3.5) °C above the core value (38 °C). Under these conditions, 93 percent of the pups per litter were malformed; the effect was reported as statistically significant ($p < 0.05$).

The “minimal-effect” results were obtained following exposures in which the core temperatures reached values of 39.2 to 40.4 (mean 39.8) °C, corresponding to $\Delta T = 1.2$ to 2.4 (mean 1.8) °C above the core value (38 °C). Under these conditions, the types of malformations were similar to those observed at the higher temperature, but the numbers were less; specifically, the percentages of malformed fetuses were 12.3, 9.1 and 26.4 percent for the cage control, sham-exposed, and heated regimens, respectively. In evaluating these data, the authors claimed a “minimal effect” but noted that, when the cage-control value was compared to that of the heat-treated value, the result was not significantly different. Because the authors claim an effect for this “minimal” group, a retrospective analysis was undertaken. From the data in the paper, it was ascertained that the control values did not differ from those of (1) the heat-treated-regimen or the sham-exposed values ($p > 0.074$). However, when the data from the heat-treated regimen were compared to that of (1) the sham-exposed regimen or (2) a combination of the cage-control and sham-exposed regimens, statistically significant elevations for the heat-treated regimen ($p < 0.05$) were observed. Thus, there is a reasonable basis for concluding that a “minimal effect” was observed, as claimed by the authors. However, the overall result is unconfirmed by independent investigation.

The effects reported by Kimmel *et al.* (1993a) are interesting in that they represent apparently very low time durations for the “minimal” and “maximal” effects. A Sapareto and Dewey-type analysis (Sapareto and Dewey, 1984) yields a $t_{1.8} = 12.6$ min for the “minimal effect,” which translates to $t_{3.5} = 6$ min, which translate to t_2 and t_6 values of 48 and 0.2 min, respectively. From Equation 11.2 the corresponding value of T_{10} for the maximal effect (3.14 °C) is one of the set included in Table 11.2. For the “minimal effect,” T_{10} is found to be 1.96 °C, approximately 1 °C lower than the lowest of the set of values to which Table 11.2 applies; if the results were confirmed, they would indicate that vertebral transformations require less thermal exposure for their production than do the craniofacial deformities to which Table 11.2 applies. Li and Shiota (1999) have

provided evidence for a basic difference in the mechanisms for producing the two kinds of abnormalities.

The fact that the hyperthermia and teratogenicity literature is generally derived from experiments in which a pregnant animal is placed in a heated convection oven or water bath means that the rate of heating of the uterine contents is generally much slower than that which would occur with ultrasound. For example, on the one hand, it takes about an hour of heating from a convection oven set at 43.5 °C for a pregnant guinea pig to have its core temperature raised about 3.6 °C (Figure 11.3). On the other hand, it takes only about 1 min for ultrasound (in the frequency range appropriate for diagnostic ultrasound) to heat bone nearly to its maximum temperature (NCRP, 1992). Because the heating rates are relatively slow in the animals associated with the hyperthermia and teratogenicity literature, it is possible that HSPs would be synthesized during the lengthy heating of the outer tissues, and thus provide some degree of protection against thermal insult (Howarth and Ougham, 1993; Li and Lazlo, 1985; Lindquist and Craig, 1988) (Section 11.2.4). It takes about 10 to 15 min for a heated organism such as an embryo or fetus to switch from its normal synthetic pathways to ones that involve HSPs (Walsh *et al.*, 1987; 1989). With tissue under insonation, the conversion of acoustic energy to thermal energy is rapid and well short of the time needed for the formation of HSPs. Thus, tissue heated by ultrasound would not have sufficient time to generate HSPs before reaching the maximum temperature, and thus might be somewhat more sensitive to the heat than were the tissue heated slowly.

Another difference between situations where heat is administered to a pregnant animal in a heated chamber and those in which ultrasound is focused on the fetus, is in the extent to which maternal stress occurs. The whole-body heating characteristic of much of the hyperthermia-teratogenicity literature can involve heat-induced maternal effects, which may affect fetal well-being. As an example, Kimmel *et al.* (1993a) reported a number of “maternal effects,” including heat exhaustion or death, when the rectal temperatures reached the range 41 to 41.9 °C, or exceeded 42 °C, respectively.

As shown in Figure 10.1, computations indicate that under some conditions diagnostic ultrasound is capable of raising the temperatures of exposed tissues, especially bone, to levels which are well within and beyond the levels needed to cause teratogenic effects. Figure 10.1 shows the maximal TIBs for a set of 54 transducer-output mode combinations provided with a leading manufacturer’s diagnostic ultrasound equipment. The highest maximum TIB for this data set is about six, corresponding to a temperature rise

estimated as 6 °C. This value would be well above the level shown in Figure 11.3 to cause deleterious effects in laboratory animals, if applied too long. For another set of data on 118 transducer applications submitted to the FDA by another manufacturer of diagnostic ultrasound equipment, TIBs ranged from 0.1 to 10.

There are, of course, imponderables for which there presently is little or no information. First, there is very little experimental information about the effectiveness or potential of modern diagnostic ultrasound to heat tissues to teratogenic levels (Section 11.2.5). In terms of the hyperthermia and teratogenicity literature, experiments generally involved experimental protocols in which the whole pregnant animal is immersed in a heated water bath or is in a convection oven. Under these circumstances, the entire animal is heated, including its *in utero* contents; the pregnant animal's peripheral nervous system would recognize the heating and possibly cause certain physiological changes to mitigate, potentiate or offset somewhat the heating of the uterine contents. For diagnostic ultrasound exposures, however, the ultrasonic beam is highly focused and generally only a part of the fetus is examined within the beam of a specific transducer. Thus, heating would be confined to that area of the fetus exposed to the ultrasound; the area might be small since beam diameters are typically in the millimeter range. Additionally, the transducers are typically moved during an examination, thereby mitigating against the possibility of tissue heating, and the normal respiratory movements of the patient's body are often sufficient to continuously offset an ultrasonic beam from a specific target, thereby reducing further the possibility of ultrasound-induced heating.

Second, there appear to be no published data on the effectiveness of elevated temperatures on hematopoiesis and bone development. Third, there is an indication that short- and relatively long-term temperature increases are associated with increased background mutation frequencies for a wide spectrum of organisms, ranging from fungi to human foreskin cultures *in vitro*. For example, heat-adapted mice had significantly more univalent (single, unpaired) X and Y chromosomes than cool-adapted mice (cage temperature 21 °C) that were transferred for 5 d to a hotter (33 °C) environment; also, rats whose testes were heated by immersion into a water bath at 42 °C for 20 min had a statistically significant increase in X and Y univalents at the 12 d but not the 5 d post-immersion sampling interval (van Zelst *et al.*, 1995). Simons (1982) showed a temperature-dependent rise in mutation frequency of the HGPRT locus per cell generation of human foreskin cells *in vitro* to be 1.36×10^{-8} at 30.7 °C, 1.17×10^{-7} at 34 °C, and 7.30×10^{-7} at 36.8 °C. These results support a long-standing claim of an association between gonadal-

temperature increase (due to clothing) and an increase in spontaneous-mutation rates in human beings (Ehrenberg *et al.*, 1957). Lindgren (1972) has provided a literature review of the influence of temperature on spontaneous-mutation rates in plants, fruit flies and fungi, the analysis generally showing "that high temperatures increase the mutation rate."

As noted elsewhere in this Section, there has been some conjecture whether hyperthermic effects are associated with an actual temperature or to a temperature elevation above the normal value. The former seems less likely because some organisms, *e.g.*, guinea pig, have normal temperatures that would represent "average-fever" temperatures in human beings (Table 2.1 in NCRP, 1992).

Recently, Sarge *et al.* (1995) provided additional support for relative temperature as the governing quantity. The responses of mouse testicular and liver cells were tested for the presence of a heat-shock-factor (equivalent to a HSP). The temperature of mouse testicular cells *in vivo* is 30 °C, or about 7 °C lower than the body cavity (which includes the liver). The experiment sought to determine whether the "temperature profile of HSF activation in mouse testis cells is identical to that in liver cells. . ." Testicular and liver cells were obtained from adult mice, and subjected to potential heat-shock treatments. For the liver, treatment with a temperature of 42 °C or higher induced HSFs whereas similar results were obtained with testis cells at 36 °C or higher. In other words, the testicular cells responded to a heat treatment that was less than that normally associated with the body cavity; *i.e.*, the effect on a particular cell depended on the temperature increase above the normal temperature for the same cell.

The literature dealing with microwave-induced hyperthermia is not included in the present reanalysis, mainly because temperature measures of animals during exposure is precluded since the thermistors act as antennae and greatly affect the animal; however, some investigators used an RF-insensitive thermistor (*e.g.*, Lary *et al.*, 1982; 1986). Nonetheless, substantial literature exists in this field, with reports usually choosing the specific absorption rate (*SAR*) as the quantity related to hyperthermic effects. For example, Berman *et al.* (1984) exposed pregnant mice on dga 6 through 17 (100 min daily exposure period; 2,450 MHz RF radiation; $SAR = 16.5 \text{ W kg}^{-1}$) and subsequently noted significantly reduced neonatal body and brain weights; the effects were attributed to a thermal mechanism. In another study, Lary *et al.* (1982; 1986), pregnant rats were exposed in a pilot study to 27.12 MHz RF fields ($SAR = 10.8 \text{ W kg}^{-1}$) until their core temperatures reached 41, 41.5, 42, 42.5 or 43 °C. No malformations were noted if the core temperature remained below 41.9 °C.

However, the core temperatures of the control animals rose from 38.6 to 39.1 °C (due to the irritation caused by the rectal implant of the thermistor and the fact that the rats were restrained within a holder during sham exposure). The number of animals used in the pilot study is not specified. In a larger study, in which the colonic temperature is raised to 43 °C for 30 min on dga 1, 3, 5, 7, 9, 11, 13 or 15, there was a 19 percent reduction in fetal weight and an 83 percent increase in litters with major skeletal abnormalities when exposures occurred on dga 7, with fetuses displaying many cranial anomalies including micropthalmia and exencephaly. O'Connor (1980) and Brent (1983) reviewed much of the literature in this area and concluded that a thermal mechanism of action was primarily responsible for the production of effects. Michaelson (1982) noted that for studies that report an effect from microwave exposures for which there appears to be no significant rise in colonic temperature, a thermal mechanism could still be operating due to resonant absorption and focusing within the body. Overall, the results pertaining to laboratory fetuses *in utero* exposed to microwaves exposures appear to be consistent with those induced by direct heating with an air convection oven or hot water bath.

There are reasons to suspect that the temperature elevation of the fetus required to produce a teratogenic effect is somewhat less than that indicated in Figure 11.2. First, the temperatures measured in these reports are maternal rectal temperatures. Edwards (1969) provided some indication that the fetal temperatures during a heating cycle, as measured for guinea pigs, are a little less than those of the rectal temperature. Edwards (1982), in describing a large number of hyperthermia studies on brain growth in guinea pigs, writes "the threshold elevation of maternal temperature above which growth retardation can be detected is 2 °C. This represents an elevation of embryonic temperature of about 1.5 to 1.7 °C." Second, there are typically a small number of fetuses analyzed and the background prevalence of congenital anomalies is generally quite low. For instance, in mice, the normal incidence of microencephaly is about 1 in 500. Thus, if one were attempting to demonstrate the temperature-time duration needed to cause the incidence to rise (statistically significantly) to two or three times above the background (a level of concern that would appear to be relevant to human exposures) it would take a very large number of animals, including appropriate independent trials to insure reproducibility of results. For example, NCRP Report No. 74 (Equation 5.1 in NCRP, 1983) provides a relationship for determining the number of subjects (N) required in a study to conclude that an observed increase in incidence is significant:

$$N = \frac{Z_{\alpha}^2 P_0 (1 - P_0)}{(P - P_0)^2}, \quad (11.3)$$

where Z_{α} is the standard normal variate at a specified level of significance (α), P_0 is the proportion of cases in which the event occurs naturally, and P is the proportion of cases in which the event occurs following treatment.

For the above instance, Z_{α} is 1.65, assuming a choice of five percent for the required level of significance. Assuming $P = 3 P_0$ and that $P_0 \ll 1$, Equation 11.3 reduces to:

$$N = 0.68/P_0. \quad (11.4)$$

For $P_0 = 1/500 = 0.002$, one obtains $N = 340$ subjects per regimen (*i.e.*, 340 for central, 340 for exposed). If P_0 is 10/500 subjects (*i.e.*, the background rate is increased 10-fold), then N becomes 34 subjects per regimen.

The possibility of embryonic or fetal-tissue heating by diagnostic ultrasound deserves special commentary. Since the adoption of FDA (1991), there has been increasing use of diagnostic ultrasound devices with capabilities of heating tissues to temperatures (as estimated by TIs) known to be teratogenic (Section 9). Under some circumstances, when the ultrasound focus is held fixed on a fetal part for a time interval, that part may be heated to a temperature higher than that of the maternal peripheral tissues. There appear to have been no published studies of teratology under such circumstances, *i.e.*, circumstances in which the embryo or fetus *in utero* is heated preferentially (see, *e.g.*, NCRP, 1992). Such an exposure is quite different from that, say, of a sauna or hot water bath in which the maternal tissues are heated first, thus possibly eliciting corrective maternal responses including increased blood flow; also, in the sauna situation the mother might voluntarily leave before the fetal temperatures have been significantly elevated. During an ultrasound examination, when the focus is held at a fixed site for an interval, the temperature at the focus will rise relatively quickly, and the temperature of the mother's peripheral system might not be raised significantly during the interval of fetal exposure; hence, there might be significant heating of the fetus without eliciting corrective maternal responses, and without the mother being aware of it.

11.4 Role of Temperature in Biological Effects of Ultrasound

In undertaking an experiment in which a biological specimen is selected for testing a specific hypothesis, the choice of the mode of

application of ultrasound often reflects a desire to maximize one physical mechanism of action over that of another. For instance, to maximize a thermal mechanism, an application involving a continuous ultrasound wave of relatively large area and high time-averaged intensity might be selected; under these conditions the average acoustic field might be sufficient to induce an increase in temperature. To maximize a nonthermal mechanism, a pulsed field of small area, with a very high peak pressures and a low duty factor (*i.e.*, with relatively long “off” periods between pulses) might be selected. Under these latter conditions, the temporal average ultrasound intensity might be very low; such conditions might induce inertial cavitation activity but not produce a significant temperature increase in the exposed specimen. There are, obviously, situations in which it is possible to have contributions from both mechanisms (thermal, nonthermal) impacting the results. Following are several examples of recent studies in which the investigators evaluated thermal contributions to observed effects.

Brayman and Miller (1993) studied the cell-density dependence of ultrasonic degassing of gluteraldehyde-fixed erythrocyte suspensions. The general mechanistic hypothesis tested was that the majority of the cell-density dependence of ultrasonic cell lysis *in vitro* can be explained on the basis of bubble activity being damped by aggregates of cells that restrict the oscillatory and translational movement of the bubbles. Fixed cells were used to obviate the potentially confounding effects of cellular gas exchange. Cells were insonated or sham-insonated in phosphate buffered saline (1 MHz, CW, 5 W cm^{-2}), and the total manometrically determined pressure change of the air above the insonated cells (which were contained in a polypropylene tube) and the temperature of the cell suspension were measured. The results showed a rapid rise in pressure (indicating degassing of the solution) and a temperature increase, both in proportion to insonation duration. When the temperature was changed in the absence of ultrasound, the pressure changes produced were smaller than those produced (for the same temperatures) with the ultrasound present. Thus, ultrasonic degassing of the fluids in excess of that attributable to thermal effects was observed. It was suppressed by the presence of fixed erythrocytes when the cell density was greater than $5 \times 10^6 \text{ cells mL}^{-1}$. At higher cell densities, the inhibition of ultrasonic degassing by fixed cells increased monotonically with increasing the cell density, attaining complete suppression at a cell density of $5 \times 10^8 \text{ cells mL}^{-1}$. Thus, when corrected for thermal effects, the data supported the hypothesis that the major portion of the cell-density effect arises as a consequence of the cell-

density dependence of cellular aggregation around oscillating bubbles in an ultrasound field (Nyborg and Miller, 1982a; 1982b).

Dalecki *et al.* (1993a) investigated the possible role of thermal mechanisms in the reduction in aortic pressure produced by exposing frog heart to a single ultrasound pulse. They were able to separate the localized heating near the thermocouple from the direct ultrasound-induced heating of the tissues, and the excess heating caused by NLP was assessed theoretically. Two exposures for which the estimated heating rates were approximately equal produced qualitatively different results. The authors concluded therefore that “heat can be ruled out as the primary physical mechanism responsible for the effects.”

Muscarella *et al.* (1991) used a laser-Doppler flowmeter to investigate the effect of ultrasound (1 MHz, 2 W cm⁻², 5 min exposures) on regional cerebral blood flow (rCBF) in neonatal rats. With application of the ultrasound there was an immediate augmentation in rCBF, which increased by a factor of 2.7 during the 5 min ultrasound exposure and then decreased post-ultrasound exposure to original pre-exposure values. A thermocouple was used to monitor cerebral temperature. The augmentation and return to “normal” rCBF values correlated with the temperature rise and decline, respectively. The ultrasound-induced effect on rCBF was attributed to “direct heating of the brain’s cortex by ultrasound as well as the conduction of heat from the skull to the underlying cortex.” There is further discussion of this work in Section 11.6.

11.5 Computations of Temperature Rise

Theory based on a linear bioheat-transfer equation (BHTE) was presented in NCRP Report No. 113 (Equation 4.1 in NCRP, 1992) for calculating temperature fields produced in perfused media by ultrasound fields; aspects of the theory are presented briefly here for convenience in later discussion. BHTE can be written in the form:

$$\frac{\partial T}{\partial t} = \kappa \nabla^2 T - \frac{\Delta T}{\tau} + \frac{q_v}{c_v}, \quad (11.5)$$

where $\partial T/\partial t$ is the rate of temperature rise at a point; κ is the thermal diffusivity; ∇^2 is the Laplacian operator; T is the temperature; ΔT is the temperature elevation above the ambient level; τ is the time constant for perfusion; q_v is the heat-source function, rate of heat production per unit volume; and c_v is the heat capacity per unit volume.

The heat-source function q_v at any point is assumed to be equal to:

$$q_v = \alpha p_0^2 / \rho c, \quad (11.6)$$

where α is the absorption coefficient (in nepers per unit length) and p_0 is the pressure amplitude, while ρ and c are, respectively, the density and speed of sound. The expression in Equation 11.6 had been shown previously to be valid for a Newtonian fluid in which the absorption is from volume relaxation alone. However, it does not always apply if the absorption arises from other mechanisms, such as shear viscosity (Nyborg, 1986). If the local acoustic field is similar to a traveling plane wave, the local intensity (I) is equal to $p_0^2 / 2\rho c$ and one has, simply:

$$q_v = 2 \alpha I. \quad (11.7)$$

It is often true that the temperature rise ΔT within a region of interest is mostly a result of sonically-produced heat within that region; that is, there is little or no contribution to ΔT from nonacoustic sources within the region or from heat flow across the boundary. Then calculations of the temperature rise $\Delta T(r, t)$ at any point r in the medium and at time (t) after the sound field is established can be made by performing numerical integrations of the type:

$$\Delta T(r, t) = \int q_v(r_1) H(s, t) dv, \quad (11.8)$$

where $q_v(r_1)$ is the local value of the heat-source function at any position (r_1) in the sound field and $H(s, t)$ is a solution of BHTE for a point source that has been generating heat at a constant rate for time (t) (Appendix A of NCRP, 1992; Nyborg and Wu, 1994) and $s = |r - r_1|$; the volume integral is carried out over the entire heated region. Solutions of the general type represented by Equation 11.8 have been applied successfully to predicting the temperature rise produced by ultrasound in absorbing media, especially in focused fields where the region of interest is near the focus. When the region of interest (in a focused or unfocused field) is near the source transducer, it may be necessary to add a term to the right-hand side of Equation 11.8, to account for heat produced *within* the transducer, and transported into the outer medium. This term has been approximated as a surface integral (analogous to the volume integral in Equation 11.8) that gives the temperature rise produced by a given (known or assumed) surface distribution of heat sources. Nyborg (1988) and Wu *et al.* (1995) describe applications in which this surface-integral approximation has been used.

In NCRP Report No. 113 (NCRP, 1992) solutions of BHTE were discussed, and methods described for estimating the temperature

rise in clinical situations. Since that time, advances have been made in theoretical development and in applications.

A special situation arises when a beam of ultrasound passes from a tissue possessing a small or moderate absorption coefficient into bone or other tissue which is highly absorbing. As the ultrasound travels in bone, most of its acoustic energy is converted into heat in a short distance. If the beam has circular symmetry and impinges on a flat area of bone perpendicularly, the energy conversion occurs primarily in a thin disc whose diameter (d_6) can be equated to a characteristic dimension of the beam, such as its -6 dB diameter. Theory was developed by Carstensen *et al.* (1990d) and discussed further by NCRP (1992) for the temperature field produced by such a heated disc, assumed to be in a homogeneous perfused tissue. A simplified form of the result gives a convenient estimate of the steady-state temperature rise (ΔT) on the surface of the disc at its center:

$$\Delta T = W/4 d_6, \quad (11.9)$$

where W is the total acoustic power in the beam as it impinges on the bone and d_6 is the corresponding -6 dB diameter of the beam; in this equation W is in milliwatt, d_6 in millimeter, and ΔT in degrees Celsius (kelvins). It is assumed that half of the acoustic power incident on the bone is converted into heat (NCRP, 1992). From Equation 11.9, if the power is 100 mW and the beam diameter is 2 mm, the estimated temperature rise is 12.5 °C. The simple expression in Equation 11.9 is convenient for determining an upper limit to the temperature rise in an exposure of bone to ultrasound. It is based on a solution of BHTe adapted to fit experimental results of Carstensen *et al.* (1990d). It applies when effects of perfusion are rather small, as is true when the beam diameter is small compared to the perfusion length parameter; when this is not true, a more general expression is required (Carstensen *et al.*, 1990d; NCRP, 1992).

Since 1992, several articles have appeared which contain information that was originally discussed in NCRP Report No. 113 (NCRP, 1992). These articles include an analysis by Bly *et al.* (1992) who applied formulae developed in NCRP (1992) and AIUM (1992) to estimate maximal temperatures generated by 236 commercial diagnostic ultrasound systems, for which acoustical data had been supplied to the Bureau of Radiation and Medical Devices in Canada. Another such publication is that by Curley (1993) in which a computational method is described for approximating the maximal temperature rise produced in soft tissue by scanned diagnostic ultrasound. After computing results for 1,400 transducers with a range of differing characteristics, the author found, as a working approximation,

that an acoustic power of 210 mW cm^{-1} of scan length per megahertz can generate a maximal temperature rise of 1°C in soft tissue.

Also referenced in NCRP Report No. 113 (NCRP, 1992), but not discussed, is a publication (Wu and Nyborg, 1992) in which calculations are made for an unscanned beam that passes through nonattenuating liquid before entering soft tissue, and is focused in the soft tissue near the entry site. The temperature maximum then occurs near the focus. Calculations based on Equations 11.5 and 11.6 were made, employing each of two approximations for the beam: (1) a concave-piston model used in NCRP (1992) and (2) a Gaussian model that had been used by Wu and Du (1990) for convenience. Results of the calculations for the two models proved to be in good agreement.

As anticipated by NCRP (1992), ODS was developed in the United States, according to which diagnostic ultrasound equipment have features that make safety-related data available to users on a real-time basis during patient examinations (AIUM/NEMA, 1992). In ODS, use is made of algorithms for estimating the maximal temperature rise produced by ultrasound under various conditions. For diagnostic ultrasound equipment in compliance with ODS, a TI representing a standardized temperature-rise estimate is available for display, unless it is known to be negligibly small (*i.e.*, less than one) under all possible operating conditions. (MI, discussed in Section 9 and Appendix B, may also be displayed.) FDA has adopted ODS as an option available to manufacturers wishing to obtain approval for marketing in the United States (FDA, 1991). As of 1996, many manufacturers have elected this option and are providing real-time displays of the relevant TIs and MIs on their diagnostic ultrasound equipment. An educational brochure was produced by AIUM (1994a) to assist users in applying safety-related information supplied by manufacturers of diagnostic ultrasound equipment, with emphasis on TIs and MIs. A summary of such information for commercial equipment has been published (Patton *et al.*, 1994) based on data submitted to FDA during the 2 y period 1990 to 1991.

A report published by the AIUM Bioeffects Committee (AIUM, 1993a) contains, among other information, consensus statements on the accuracy of temperature estimates represented by ODS-defined TIs. These statements were reached by carrying out detailed and computationally intensive calculations based on Equations 11.5, 11.6 and 11.8 for numerous situations of clinical importance. Among the conclusions is the following:

“Calculations of the maximum temperature increase resulting from ultrasound exposure *in vivo* should not be assumed to be exact because of the uncertainties and approximations

associated with the thermal, acoustic and structural characteristics of the tissues involved. However, experimental evidence shows that calculations are capable of predicting measured values within a factor of two. Thus, it appears reasonable to use calculations to obtain safety guidelines for clinical exposures where temperature measurements are not feasible. To provide a display of real-time estimates of tissue temperature increases as part of a diagnostic system, simplifying approximations are used to yield values called TIs. Under most clinically relevant conditions, TIS and TIB, either overestimate or closely approximate the best available estimate of the maximal temperature increase (ΔT_{\max}). For example, if $TIS = 2$, then $\Delta T_{\max} \leq 2^\circ\text{C}$."

Values of TIs reported for present-day equipment range up to at least six (see Figure 10.1 and associated discussion).

Several authors have described computations of temperature rise based on solutions of BHTE. Vyas and Rustgi (1992) employed a Green's-function solution of the equation to calculate temperature fields produced in tissue by lasers; their solution applies to fields with cylindrical symmetry and thus differs from a more general one employed by Carnes *et al.* (1991) in studies discussed in Section 11.6. Nyborg and Wu (1994) discuss mathematical features of a solution given earlier by Nyborg (1988) of the type represented by $H(s, t)$ in Equation 11.8; partial differentiation of this solution with respect to time yields the Green's function used by Carnes *et al.* (1991). In another publication, Nyborg (1992) derives a simple formula for estimating the temperature rise produced in a femur or other approximately cylindrical bone. Also, Drewniak and Dunn (1996) propose a method to be used in some situations where the heat-source function (q_v) cannot be obtained from either of Equations 11.6 or 11.7.

Ellis and O'Brien (1996) performed detailed calculations of heating produced by ultrasound beams in tissue-like media, using the general approach represented by Equation 11.8, but assuming steady-state conditions. After computing the acoustic pressure distribution by complete three-dimensional integration for the source configuration, they determined q_v from Equation 11.6; they then performed integrations according to Equation 11.8 to determine spatial distributions of the temperature rise (ΔT). For a focused beam produced by a uniform source with circular aperture, they compared results obtained by the above detailed method with those obtained by a simplified "heated disc" approach, which has sometimes been used (NCRP, 1992). They found that differences were small in the region near the source, but were larger in the focal region. The general approach involving detailed integration based on Equation 11.8,

while demanding of computer capabilities, allows treatment of problems, such as are presented by arbitrary source configurations, which are otherwise difficult to solve.

Shaw (1994) obtained solutions of BHTE by performing integrations as in Equation 11.8; Equation 11.7 was used for q_v . His calculations differed from others in that *measured* values of the intensity were used for the several ultrasound beams, rather than values from approximate models of the beams. For the absorption coefficient (α), he considered several tissue models used in NCRP (1992) and AIUM/NEMA (1992). Calculations for each model were made of the temperature rise after 180 s as a function of axial distance for each transducer. Comparison of the maximal temperature rise so calculated was made with calculations from simple formulas used in NCRP (1992) and AIUM/NEMA (1992) for worst-case estimates. [These simple conservative formulas had been offered as a convenient way to identify situations where thermal damage is very unlikely. According to advice given in NCRP (1992), if a simple formula suggests a possibility of harm, a more accurate calculation should be done.] It was concluded by Shaw (1994) that the simple formulas, as intended, give values that are usually conservative; more specifically, he found them to give values for the temperature rise that are equal to, or in excess of, the more accurately calculated values, under some conditions by a factor of two or more.

Perfusion tends to reduce the temperature rise produced by exposure of mammalian tissue to ultrasound. Under some conditions, this effect can cause significant uncertainty in calculations of the temperature rise because of inadequate knowledge of perfusion coefficients and, also, because of inadequacies in BHTE itself. However, perfusion effects are negligible if the exposure time is short. BHTE (Equation 11.5) then reduces to the classical equation for heat diffusion in a homogeneous isotropic solid, namely:

$$\frac{\partial T}{\partial t} = \kappa \nabla^2 T + \frac{q_v}{c_v}, \quad (11.10)$$

and, if the exposure time is so short that even the diffusion term can be neglected, one has, simply:

$$\frac{\partial T}{\partial t} = \frac{q_v}{c_v}. \quad (11.11)$$

Filipczynski and Wojcik (1991) realized that, in calculating the temperature elevation (ΔT) produced by a single lithotripter pulse, one can neglect both heat diffusion and perfusion so that Equation 11.11 is applicable, and the temperature rise (ΔT) is equal to $q_v t/c_v$, where t is the duration of exposure; q_v (based on Equation 11.7) was

calculated by superposing contributions from the entire frequency spectrum for the pulse. In other work, Filipczynski *et al.* (1993) showed how an estimate of the temperature rise produced by a focused ultrasound beam in soft tissue could be obtained, without high demands on computer time, as a function of exposure duration, for short durations (up to a few minutes) by neglecting perfusion and obtaining approximate solutions of Equation 11.10; for this purpose the authors used Equation 11.7 and assumed the beam to be Gaussian. Drawing upon results for a series of examples, they show that the maximal temperature rise produced in soft tissue can be significantly less in exposures of 5 min or less than are predicted by computational methods that assume steady-state conditions (which would require exposures of much longer duration).

It is recognized by investigators of heat transfer in mammalian tissues that BHTE has limitations in representing the effects of blood flow in real tissues. In recent publications by Creezey *et al.* (1994) and by Kolios *et al.* (1995), the authors use BHTE and other models in evaluating procedures for obtaining uniform temperature fields in applications of hyperthermia. They conclude that BHTE should be supplemented with other models under some conditions, especially, where large blood vessels are involved (Arkin *et al.*, 1994).

In NCRP Report No. 113 (Appendix C of NCRP, 1992) it is shown that diagnostic ultrasound fields can be affected significantly by the distortion which occurs because of nonlinearity in the medium. Christopher and Carstensen (1996; 1998) utilized a computer program specifically developed to investigate further the consequences of nonlinearity, including its effects on the ultrasonically produced temperature rise. In water, because of its low attenuation coefficient and high nonlinearity parameter, a diagnostic pulse can become very distorted. However, in mammalian tissues such as liver or brain, the same pulse is affected much less than in water; also, values of the computed steady-state temperature rise in such tissues are not greatly different from values that would apply if the medium were linear. The implications of these findings for estimating human exposure are discussed in Section 9 and Appendix D.

When an ultrasound beam impinges on bone at an oblique angle, shear waves will be produced in the bone and will contribute to the heat generated to an extent that depends on the angle. Wu and Cubberley (1997) have provided information needed for determining the rate of heat production by measuring the phase velocity and attenuation of 4 to 10 MHz shear waves in compact bone from bovine femur.

11.6 Measurements of Temperature Rise in Models

Phantoms constructed of materials that mimic ultrasonic characteristics of tissues have been employed by investigators in studies

of temperature fields produced by ultrasound beams; in such studies, measurements can be made under well-defined conditions, and it is possible to test experimentally algorithms that have been developed for calculating or estimating the temperature rise produced by an ultrasound beam. TMM is usually a gel in which material has been included to provide absorption, but does not include a feature to mimic effects of blood flow, *i.e.*, perfusion, on heat transport. An exception is the phantom described by Chin *et al.* (1990); here the TMM consists of closely packed agar spheres whose interstitial space is filled with fluid that can be caused to flow by a pressure gradient.

Chin *et al.* (1991) used a phantom whose TMM was constructed from agar spheres embedded with powdered talc to give tissue-like attenuation. While the interstitial space was fluid-filled, no flow was induced, so the heat transport was by conduction alone. A 525 kHz continuous, focused ultrasound beam with 3.9 W total power was projected into the phantom and the temperature measured as a function of time at several points. The heat-source function (q_v) was obtained from Equation 11.6, using values of the pressure amplitude (p_0) based on measurements in water (found to be in good agreement with theory) and calculated in the phantom by taking the attenuation into account. In calculating the temperature rise produced by the ultrasound, Equation 11.10 was solved by using a finite-difference method, and found to be in good agreement with measured values.

Wu *et al.* (1992) measured the temperature rise generated in a (nonperfusing) TMM phantom by continuous, focused and unfocused, ultrasound beams at frequencies of 1 and 3.5 MHz, and compared results with calculations based on several models. TMM was a gel containing droplets of oil to produce absorption; the measured absorption coefficient was $0.08 \text{ Np cm}^{-1} \text{ MHz}^{-1}$. Each transducer used in the experiments was positioned so that the associated ultrasound beam propagated into the phantom with its axis along a line of thermocouples imbedded in TMM. Calculations of the temperature rise were made by performing numerical integrations of the type represented by Equation 11.8, the solution $H(s, t)$ being for a nonperfused medium. For $q_v(r_1)$, Equation 11.7 was used with the beam intensity given by any one of three models: (1) a simple "geometric" model used by Nyborg and Steele (1983), (2) a concave disc model taking diffraction into account in an approximate way, similar to that used in NCRP Report No. 113 (NCRP, 1992), and (3) a Gaussian model previously used by Wu and Du (1990). The temperature rise, calculated for exposure times up to 20 min, was found to result partly from heat generated within the transducer itself, *i.e.*, from transducer self-heating; this contribution to $\Delta T(r, t)$ was particularly significant at points near the transducer. The authors concluded

that the other contribution to the temperature rise, that caused by absorption in the medium, was given reasonably well by all three models in the near field of the unfocused beams and near the radii of curvature of the focusing transducers.

Bacon and Shaw (1993) describe a measurement system, developed at the United Kingdom's National Physical Laboratory, for estimating the temperature elevation produced in an application of diagnostic ultrasound. A TMM phantom is employed in which TMM is a gel similar to that described by Madsen *et al.* (1982), having an attenuation coefficient of about $0.044 \text{ Np cm}^{-1} \text{ MHz}^{-1}$. The authors made measurements on nine focused transducers covering frequencies from 2 to 10 MHz and -6 dB focal diameters from 1 to 3 mm. Temperature measurements were made at the focus with thin-film thermocouples embedded in the gel. Each transducer was positioned in a water bath above the phantom; the emitted ultrasound beam passed, in order, through (1) water, (2) 7 mm of gel, (3) the thermocouple (at the focal maximum), (4) 30 to 40 mm of gel, and (5) low-reflection absorbers. Under these conditions the temperature maximum occurred near the focus (*i.e.*, the position of maximal pressure amplitude). Observations were made of the temperature rise versus time in the first few minutes of exposure, with emphasis on the temperature rise that occurred after 180 s. In making calculations of the temperature rise for comparison with experimental results, several methods were used. The first was based on a solution of the type represented by Equation 11.8 but with zero perfusion (thus, a solution of Equation 11.10). The second was like the first, except that the sound field in the region of interest, a relatively small region near the focus, was approximated with a Gaussian function and an analytical solution was obtained for the temperature rise:

$$\Delta T(t) = \frac{\alpha I_0 a^2}{2K} \ln \left(1 + \frac{4 \kappa t}{a^2} \right), \quad (11.12)$$

where I_0 is the axial intensity at the focus, a the -8.7 dB focal beam radius, and K the thermal conductivity of the medium ($K = \kappa c_v$). The first method, based on Equations 11.6 and 11.8 using actual measurements of the ultrasound field, predicted values of ΔT in 180 s that averaged five percent higher than measured values, while predictions from the second method, based on Equation 11.12, averaged seven percent higher than measured values. It was concluded that, for both methods, predictions agreed with experimental values of the temperature rise within the limits of experimental error. It is noted by the authors that, in fitting a Gaussian model to a beam, better results are obtained by matching the axial intensity than by matching the total power. A third method of calculation involved an

expression used by ODS and listed as an estimate by NCRP (Equation 5.25 in NCRP, 1992); this gave good agreement with experiment for beams with “Gaussian-like” profiles but tended to overestimate the temperature rises, by as much as a factor of two, for beams differing greatly from the Gaussian. Shaw *et al.* (1996) have proceeded further by deriving theory, based on Equation 11.5, for calculating the temperature rise produced by ultrasound in a perfused medium, given the temperature rise (whether obtained from theory or experiment) in an unperfused medium.

As part of a series of experiments with ultrasound TMM phantoms, Wu *et al.* (1994) used an arrangement in which a beam of focused 3.5 MHz CW ultrasound passed, in order, through (1) low-attenuation fluid, (2) a thin layer of TMM gel, and (3) a specimen of human postmortem femur. The purpose was to model a “worst-case” situation for obstetrical ultrasound. The temperature was monitored at the bone surface where the ultrasound impinged by means of an attached fine thermocouple. Among other results was the finding that acoustic streaming in the fluid caused significant cooling at the bone surface, especially when the TMM layer was absent, or very thin. For example, for a beam of 180 mW total acoustic power, the bone temperature rose about 14 °C after 100 s when the TMM thickness was 5 mm, but only 4 °C when the layer was absent.

O’Neill *et al.* (1994) developed and tested an improved TMM phantom and used it in experimental determination of the temperature rise produced by focused 3.2 or 5 MHz ultrasound beams at the surface of an excised femur (bovine or human) imbedded in TMM gel, the latter having acoustic absorption coefficient of 0.3 dB cm⁻¹ MHz⁻¹. Although exposures were continued for 1,200 s, it was found that after 60 s the bone surface temperature had reached 80 percent of its final value. Comparison of the results was made with the simple “ $W/4d_0$ ” expression of Equation 11.9. Measured values of the temperature rise were found to be about 75 percent of the values calculated from this equation. The authors note that the compact bone used in the experiments is less absorbing than cancellous bone and thus probably does not represent a “worst-case.”

In other experiments, Wu *et al.* (1995) measured the temperature rise generated at the surfaces of bone, using commercial diagnostic ultrasound equipment and a two-layered phantom representing transcranial applications. One layer of this phantom was a thin slab of bone and the other consisted of a TMM representing soft tissue. In these experiments, the phantom was oriented with the bone layer uppermost so that the ultrasound was directed from above downward through bone into the TMM. Measurements were made at the upper and lower surfaces of bone for each of several operating modes of

Hewlett Packard Sonos 1000 equipment; results were compared with the relevant thermal index (TIC), defined by the AIUM/NEMA standard (AIUM, 1992) and displayed on the equipment. It was found consistently that the measured temperature rise was much in excess of that expected from TIC. Tests showed that the excess was from heat generated within the transducers, *i.e.*, from self-heating. Experimental tests were done to determine the extent of this contribution to the temperature rise, and a theoretical procedure was developed for estimating it (Section 11.7). When the self-heating contribution was subtracted, the remainder was attributed to absorption of ultrasound in the medium. For example, in a typical result, the observed temperature rise at the upper surface of bone after 1,200 s was 11 °C; of this, 6.1 °C was found to be caused by self-heating and the remainder, 4.9 °C, by absorption in the bone and in the TMM. TIC was 4.3, a value which the authors suggest might be appropriate in a living animal, because perfusion would cause cooling. At the lower surface of the bone, the temperature was less than that at the top, by a factor of about 0.7. The results on self-heating indicate that consideration should be given to this effect in temperature estimates.

Duck and Starritt (1994) describe an arrangement designed to provide a convenient means of examining the heating capabilities of diagnostic ultrasound systems and investigating the effects of system parameters on temperatures produced. In this arrangement, a transducer of interest is positioned so that its ultrasound beam is projected downward into water in a cylindrical polyethylene container, passes through its base (a 1 mm thick polyethylene sheet) and is reflected at its lower surface which is bounded below by air. (Little reflection occurs at the water-polyethylene boundary.) The polyethylene base absorbs a large fraction of the energy in the ultrasound beam, and the resulting temperature rise is monitored by a thermocouple attached to its lower surface. With this arrangement, the authors found that the ultrasound beam produced by diagnostic equipment, when focused on or near the thermocouple, would cause the temperature to rise rapidly, essentially reaching its steady-state value in about 60 s. For commercial systems, the observed maximal temperature rise was over 20 °C for Doppler systems under some conditions, but did not exceed 2 °C for imaging systems. Effects of saturation associated with NLP (Appendix D) were seen when the pressure amplitude was high and the water path was long; the temperature then decreased when the amplitude was further increased. While the arrangement has proved valuable for obtaining insight on the effects of system variables, the authors point out that it is not intended as an accurate model for any actual clinical situation.

It was shown by Watmough *et al.* (1993) that when small gas-filled bubbles are present in tissue-mimicking gels, the temperature rise produced by ultrasound can be greatly enhanced. In one kind of experiment, a small sheet of (hydrophobic) Astralux® printing paper, 200 μm in thickness, was imbedded in a TMM gel, then exposed to 0.75 MHz CW unfocused ultrasound from a therapy device. The Astralux® sheet is a paper product that contains a large number of pores whose sizes range from 1 to 6 μm (Shiran *et al.*, 1990). In other experiments, a thin layer of gel-based foam (made by stirring the gel in a food mixer) replaced the Astralux® sheet as the source of bubbles in the gel. The temperature rise near the bubbly layer was monitored with a small thermocouple that had been inserted into the gel. In a series of tests with four phantoms, the mean temperature rise observed after 60 s exposure to ultrasound of spatially-averaged intensity 1 W cm^{-2} was 40°C , about 20 times the temperature rise in the same gel when no bubbles had been introduced. The temperature rise dropped quickly at the end of the exposure and was localized to a region in the immediate vicinity of the bubbly layer.

11.7 Measurements of Temperature Rise in Mammalian Tissues

In this Section, six reports are discussed that have appeared since the publication of NCRP Report No. 113 (NCRP, 1992) and that deal specifically with ultrasonic heating of particular tissues and organs; some studies involved *in vivo* examinations, and others were *in vitro* or *ex vivo* (manipulated outside the living body but still attached to it). The results of these experiments provide additional insights into biological and physical factors that affect heat generation and temperature elevation produced by ultrasound in tissues. Four of the reports dealt with fetal brain, a fifth with other fetal soft tissue, and the sixth with neonatal cerebral blood flow.

Bosward *et al.* (1993) studied ultrasound-induced heating of brains of fetal guinea pigs; they were either freshly euthanized or, following euthanasia, histologically fixed, or the brains were excised. Some brains were left within the cranium, thus allowing for investigation of the effect of bone on tissue heating. Timed pregnancies were used to obtain fetuses of dga 30 to 60; hence, there were differences among the fetuses in the biparietal diameters and in the extent of mineralization of the cranium. Inserted thermocouples were used to monitor temperatures. A bowl-shaped transducer with radius of curvature

100 mm, center frequency 3.2 MHz and aperture-diameter 19 mm, was used for all experiments, the pulsing parameters (6.25 μ s pulse duration, 4 kHz repetition frequency) being similar to those used in some pulsed-Doppler clinical examinations. Exposures were for durations in the range 0 to 300 s. Of particular interest are the results obtained using a time-averaged acoustical power of 260 mW; at this power level, the focal length was measured to be 6.9 cm. When the experimenters exposed the guinea-pig head to ultrasound at different distances between transducer and the point on the skull where the ultrasound impinged, they found that the resulting temperature rise was maximal when the distance was 6 cm, and subsequent experiments were done at this distance. The distribution of intensity in the beam at the same distance, as measured in water under free-field conditions, resembled a Gaussian function with -6 dB width of 2.7 mm; the corresponding pulse-average and overall temporal-average intensities at the center of the beam were 112 and 2.8 W cm^{-2} , respectively. The results of this study in terms of heating were as follows: for *in situ* brain tissues (fresh or fixed) there was a consistently higher increase in temperature of the tissue adjacent to proximal bone relative to that observed in the middle of the cerebral hemisphere, where the temperature increase was also somewhat less than that of the brain tissue adjacent to the distal parietal bone. The mean ultrasound-induced temperature rise correlated with gestational age; for example, in exposures for 120 s, the temperature adjacent to proximal bone rose by 1.6 $^{\circ}\text{C}$ for dga 40 and by 5.2 $^{\circ}\text{C}$ for dga 60. Correspondingly, the bone thickness increased from 0.17 to 0.30 mm and the ash content from 18 to 30 percent as the gestational age increased from dga 40 to 60. There was no difference between temperature increments for fresh or fixed brain. When the exposures were made with the highly absorbing skull removed, the 120 s temperature rise, measured in the middle of the cerebral hemisphere, was greater by about a factor of three. Although this study used nonperfused brain tissue, which will obviously accumulate more thermal energy than well-perfused brains, it is useful for providing some indication of a "worst-case" magnitude of tissue heating. The finding that the temperature rise in brain is greatest near bone interfaces is consistent with results discussed in NCRP Report No. 113 (NCRP, 1992); in this reference it is proposed that an upper limit to the steady-state temperature rise (in degrees Celsius) produced by exposure of bone to ultrasound focused normally upon it can be obtained by use of Equation 11.9. Applying this formula to the above experiment gives $[260/(4 \times 2.7)]$ or 24 $^{\circ}\text{C}$ for the predicted upper limit. This is 4.6 times the largest measured value of temperature rise. The authors suggest that the thermocouple may not have

read the maximum value of the temperature because of heat conduction along the thermocouple needle. Also, a reduced reading of the temperature would be expected if the thermocouple junction were not flat against the insonated bone; calculations show marked diminution of the temperature in a short distance from a small heated disc (Figure B.1 in NCRP, 1992). In addition, it is probable that Equation 11.9 overpredicts the temperature rise when applied to the temperature rise that occurs within the skull when the latter is exposed to ultrasound externally. In the measurements of Wu *et al.* (1995), the temperature rise produced at a bone surface on which the sound is incident is greater than that produced in tissue on the other side of the bone; in one example, the factor is about 1.4.

A study of ultrasound-induced temperature increases in guinea pig fetal brains *in vitro* and *in vivo* has recently been reported by Horder *et al.* (1998a; 1998b; 1998c). The same insonation and temperature measurement procedures were generally comparable among the studies. A pulsed ultrasound beam was focused on the brain through a water bath. Temperature was measured by a 26-gauge thermocouple implanted directly under the parietal bone, or at some distance away from the bone and into the brain. In their *in vitro* studies, Horder *et al.* (1998a) observed temperature increase of 5.1 °C at the underside of the parietal bone of formalin-fixed brains of dga 57 to 66 (full term = 68 d) with a $2.8 \text{ W cm}^{-2} I_{\text{SPTA}}$ exposure; when the scalp was removed, the ultrasound-induced temperature increment was 3.3 °C, indicating a 35 percent reduction of the tissue temperature, resulting from cooling of the bone by acoustic streaming in the water bath. The temperature increment measured at the midbrain was only 1.2 °C; with the scalp and parietal bones intact; when the latter were removed, the ultrasound-induced temperature increment was 2.8 °C, indicating a substantial attenuation of the beam by the parietal bone. Further results, using the same intensity, were obtained with live or dead fetuses insonated *in utero* at dga 57 to 61 (Horder *et al.*, 1998b). Temperature increases of 4.9 and 1.2 °C, respectively, in brain close to parietal bone and midbrain were observed in living, *in utero* fetuses. The measures were repeated at the same sites in the fetuses after death (including euthanasia of the dam) were 4.9 and 1.3 °C, respectively. It was evident that cerebral blood perfusion had little effect on ultrasound-induced heating in the guinea pig. A significant cooling effect of vascular perfusion was observed when the guinea pigs obtained near-term status (dga 62 to 66) (Horder *et al.* 1998b). At this stage, the temperature increases were 4.3 and 1.1 °C, respectively, in brain close to parietal bone and in midbrain. For each of these studies (Horder *et al.* 1998a; 1998b; 1998c), a modified thermal index for cranium (TICm) was

found to approximate the measured ultrasound-induced temperature increment. The modification was deemed appropriate since the usual TIB algorithm includes tissue attenuation factors that do not apply, whereas a TIC (modified) approximates the situation in which the bone is close to the surface of the tissue being insonated and the beam is unscanned. The TIC calculation was modified to include the power at the inner table of the parietal bone and the beam diameter at that site. The TIC_m calculation yielded a 7.7 °C increment for the insonation; the measured increment was 5.1 °C (e.g., Horder *et al.* 1998a); thermocouple transfer of some heating away from the biological site was thought to account for at least some of the difference between calculated and observed values.

Duggan *et al.* (1995) measured ultrasonic heating of the brains of fetal sheep *in utero* under *in vivo* and *ex vivo* conditions. A special device was fabricated that positioned the transducer 1 cm from the fetal skull and held it within the amniotic cavity. The transducer operated at 3.5 MHz, with 5.8 μs pulse durations and pulse repetition rates of either 6 or 10 kHz. Of special interest are the results for a power output of 0.6 W for which the -6 dB beam width was 17 mm, while the SPPA and SPTA intensities were 8.9 and 0.3 W cm⁻², respectively, with an exposure duration of 120 s. Thermocouples were mounted just inside the skull at either the beam center or the beam periphery. All ultrasound regimens resulted in temperature increases that correlated with exposure duration (to 120 s); the peripheral antemortem temperatures were less than the beam center antemortem temperatures. Temperatures decreased with time post-insonation over the next ~280 s but did not achieve baseline values. The temperatures produced in antemortem exposures were considerably lower than those from postmortem exposures, reflecting the effects of vascular perfusion on temperature mitigation. For example, the maximal antemortem and postmortem beam-center measures for ultrasound-induced temperature increases were ~1.5 and 3 °C, respectively, at 120 s of exposure. These studies corroborate the conclusions reached in other studies; *i.e.*, that the most likely areas for ultrasound-induced temperature increases in brain tissue are near skull surfaces in the propagation path. The temperature rise observed (maximum of 1.5 °C antemortem) was considerably less than would be calculated from Equation 11.9, namely, 8.8 °C for $W = 600$ mW and $d_6 = 17$ mm. There are several plausible explanations for the discrepancy. First, the beam diameter was relatively large; it is expected from theory based on Equation 11.5 that in a wide-beam exposure, perfusion significantly reduces the steady-state temperature rise, and the time required to reach the steady-state temperature is increased (NCRP, 1992). Second, the authors indicate

that for the thermocouple placed inside the scalp and dura mater, there was a 0 to 1 mm variation in distance from the latter; this may have caused some reduction in the temperature rise. Third, the temperature rise produced inside the skull is expected to be less than that produced directly on the outer side where the ultrasound impinges.

Muscarella *et al.* (1991) studied the effect of a specific ultrasonic regimen on cerebral-blood flow in 2 to 6 d old neonatal rats *in vivo*. A laser-Doppler blood perfusion device was used to measure blood flow with its probe placed on each neonate's head where a small circular portion of the scalp had been partially removed to provide a "window" for measuring regional cerebral-blood flow. An unfocused 1 MHz transducer with a conical water-filled tip extension provided focusing of the beam to a -6 dB beam area of 0.28 cm^2 ; the total power in the beam was 0.56 W and the (time averaged) intensity at the spatial peak was 6.7 W cm^{-2} . Exposure durations were for 5 min. A thermocouple was inserted mid-beam atop the insonated cranial section. Both temperature and blood flow rose with increase in ultrasound exposure duration over the 5 min treatment period. There was an approximate 2.7-fold increase in cerebral-blood flow and a concomitant $1.3 \text{ }^\circ\text{C}$ rise in skull temperature. The results suggest that modest ultrasound-induced heating may cause increased perfusion, resulting in turn from a vasodilatory response. The temperature rise of $1.3 \text{ }^\circ\text{C}$ is very small compared to the $28 \text{ }^\circ\text{C}$ value calculated from Equation 11.9 with $W = 560 \text{ mW}$ and $d_b = 5 \text{ mm}$. This suggests that the absorption of ultrasound in the neonate skull may have been much smaller than assumed in the derivation of Equation 11.9. Also, acoustic streaming probably occurred in the coupling fluid, thus reducing the temperature of the heated skull (Wu *et al.*, 1994).

Tarantal *et al.* (1993) measured temperature *in utero* long-tailed macaque monkeys, exposed at dga 70 to 150 to ultrasound from an ATL MK 600 Ultrasound Imaging System. In the scan mode, the center frequency was 7.5 MHz and the acoustic power was 12 mW while the SPTA and SPPA intensities were 27 mW cm^{-2} and 85 W cm^{-2} , respectively. In the pulsed-Doppler mode, the center frequency was 5 MHz and the acoustic power was 68 mW while the SPTA and SPPA intensities were 54 mW cm^{-2} and 1.5 W cm^{-2} , respectively. Thermocouples were placed in the fetus, either intracranially or at the muscle-long-bone interface (humerus or femur). There were 68 temperature measurements in 22 pregnant macaques; 30 in the scan mode, 32 in pulsed Doppler, and six for sham controls. Ultrasound exposure durations were up to 30 min in the scan mode and 15 min in the pulsed-Doppler mode. Temperature increments up to $0.6 \text{ }^\circ\text{C}$ were measured; the highest values were somewhat in

excess of values the authors computed (up to 0.4 °C) using equations specified in ODS (AIUM/NEMA, 1992). These equations do not include effects of transducer self-heating, and it is not known whether this source of heat may have contributed to the small excess temperature.

Doody *et al.* (1999) undertook measurements of ultrasound-induced heat in post-mortem sections of fixed human fetal thoracic vertebrae ranging in gestational age from 14 to 39 weeks; the vertebrae were insonated *in vitro* (single-element 3.5 MHz transducer, I_{SPTA} 0.53 W cm⁻² pulse length 4.4 μs, PRF 6.8 kHz) and temperature was measured with a 50 mm thermocouple, attached to the bone surface. Each sample, consisting of the bone and thermocouple, was embedded in agar, was insonated for 295 s. There was an increase in temperature with initiation of insonation, a factor of three increase with older bone relative to that obtained with younger bone. About 70 percent of the temperature rise occurred with the first minute of insonation.

Carnes *et al.* (1991) measured the temperature rise produced by 1 MHz unfocused CW ultrasound in the murine fetus *in vivo* and compared results with values computed from solutions of Equation 11.5. In their experiments, the anesthetized pregnant mouse was positioned in a tank of 37 °C degassed Ringer's solution with abdomen facing the source transducer. During exposure to ultrasound, the beam impinged directly on the uterus, the overlying tissues having been surgically removed. The temperature was monitored during exposures by means of fine thermocouples which had been inserted into selected fetuses. The transducer was positioned so that the uterus was in the far field of the beam, which was assumed to be Gaussian, and the intensity was nearly uniform over the fetal sites. Measured values of the absorption coefficient were used in the calculations. Exposures were at incident SPTA intensities varying from 0.5 to 10 W cm⁻² and for durations from 30 to 400 s. Results are shown in Table 11.3.

Computations were based on an integration process that is equivalent to that indicated in Equation 11.8, the quantity (q_s) being estimated by approximating the beam shape as Gaussian and using Equation 11.7. The low-intensity absorption coefficient was chosen as 0.035 Np cm⁻¹ for the dam and as smaller values, increasing with gestational age, for the fetus. At the higher intensities, increased values were used for the absorption coefficient, as determined by separate experiments. In the absence of independent information on perfusion in the mouse, values of the perfusion time constant were chosen for agreement of temperature predictions with the data in Table 11.3. The time constants decreased (indicating increased

TABLE 11.3—Measured and calculated temperature elevation in murine fetus of dga 9, 12 and 15 produced by exposure to ultrasound for particular intensities and durations.^a

It ($J\text{ cm}^{-2}$)	I ($W\text{ cm}^{-2}$)	t (s)	τ^b (s^{-1})	Temperature Elevation ^c (ΔT) at		
				Day 9 [$\Delta T(^{\circ}C) \pm SD$] ^d	Day 12 [$\Delta T(^{\circ}C) \pm SD$] ^d	Day 15 [$\Delta T(^{\circ}C) \pm SD$] ^d
200	0.5	400	2,000	2.0 \pm 0.7 [1.4]	2.1 \pm 0.6 [1.3]	1.5 \pm 0.5 [1.3]
200	1.0	200	2,000	1.9 \pm 0.4 [1.9]	2.4 \pm 0.7 [1.9]	2.2 \pm 0.8 [1.8]
300	2.5	120	500	2.9 \pm 1.2 [3.2]	3.1 \pm 0.8 [3.0]	2.0 \pm 0.9 [3.0]
300	10.0	30	100	3.4 \pm 1.3 [3.6]	3.2 \pm 1.0 [3.4]	2.1 \pm 1.7 [3.5]
450	5.0	90	100	4.0 \pm 1.2 [3.8]	3.9 \pm 0.8 [3.6]	2.8 \pm 0.6 [3.6]

^aData are from Carnes *et al.* (1991).

^b τ is the perfusion time constant assumed for computed values.

^cEach experimental value of ΔT is the average of measurements made in at least 10 different specimens.

^dSD is the standard deviation. Computed values shown in brackets [].

perfusion) as the time increased. Values of the temperature elevation obtained from the computations are given in Table 11.3 for comparison with experimental values. As the authors point out, the computed temperature elevation is nearly equal to or greater than the measured value at the higher intensities, but at the lower intensities and longer times and for the younger gestational ages, the computed values are lower than measured. The authors advised that exposure criteria for such conditions be conservative.

11.8 Ultrasonic Hyperthermia and Temperature-Related Surgery

NCRP Report No. 113 (NCRP, 1992) summarized the clinical uses and outcomes of ultrasound-induced hyperthermia. This report also gives extensive treatment of the responses of cells and tissues to temperature elevations over varying exposure periods; for example, a nomograph developed by Sapareto and Dewey (1984) is included that shows that equivalent hyperthermic responses were produced by a 60 min exposure at 43 °C, a 30 min treatment at 44 °C, and a 15 min treatment at 45 °C. In general, the higher the temperature of the tissue, the shorter the exposure duration at that temperature to cause a hyperthermic response. For example, "the critical dose to kill tissue is 43 °C for 240 minutes and the time needed decreases by a factor of two for each 1 °C rise in temperature . . . it would take only one second to kill tissue at 57 °C" (Cline *et al.*, 1994). The facts that cell killing can occur with very high temperatures for very brief exposure periods and that an ultrasonic beam can be highly focused to deposit a large fraction of its power into a prescribed volume to achieve sharply elevated temperatures locally have led to the development of ultrasound focal-beam surgery. Section 7 of NCRP Report No. 113 (NCRP, 1992) deals with the use of focused ultrasound to produce small thermal lesions, and methods are discussed that have proven successful in predicting the temperatures generated. Since the NCRP (1992) report was written, the subject has advanced considerably. The potential uses of this technology include neurosurgical, ophthalmological, urological and oncological applications. At present, ultrasound focal-beam surgery is used in ophthalmology and urology. The results of a recent feasibility study using focused ultrasound-induced tissue hyperthermia to treat cardiac arrhythmia are encouraging (Zimmer *et al.*, 1995).

A recent review of thermal ultrasound surgery has been undertaken by ter Haar (1995). She notes that for conditions commonly

employed, “the primary mechanism for cell killing is thermal.” At present, commercial focused-ultrasound surgery units are used extracorporeally in a number of applications, and transrectally for treatment of the prostate. For both use categories, the ultrasonic intensities are sufficient to destroy the tissue within the focal volume. Because the spatial-average intensity is relatively low in the region between transducer and target volume, the tissue lying in this region tends to be subjected to lower temperatures than at the focus of a strongly focused beam. The ultrasound parameters used for surgical purposes must be “appropriate” to the clinical setting. The best choice of ultrasound frequency depends on the amount of tissue intervening between the transducer and the target volume; the higher the ultrasound frequency, the greater the beam attenuation at constant tissue depth. Thus, the clinician must use an ultrasound frequency that allows sufficient energy to reach the target and to achieve a temperature rise sufficient to ablate the tissue.

While heating is the primary mechanism involved in producing focal lesions under common conditions, it is not the only one operating with ultrasound surgery in general (see NCRP, 1992 and Section 8 of this Report). Where the primary mechanism is thermal, the ablated tissue mass resembles coagulated or “cooked” tissue. However, when the intensity is well above that needed for a thermal lesion, some parts of the treated material contain “holes,” or cavities, which are thought, possibly, to arise from cavitation or boiling. Ultrasound-induced thermal lesions are sharply defined. ter Haar (1995) notes the ubiquity of the term “island and moat” (initially used by Barnard *et al.*, 1956) to describe the histological appearance of these lesions. The “island,” or lesion center, is a coagulated necrosed tissue that is identified easily through appropriate histological staining techniques, and the “moat” is a well-defined narrow border between the “island” and the surrounding apparently unaffected tissue, and is “a border of cells that takes up stain less than normal cells.”

Prionas *et al.* (1991) evaluated thermal profiles produced in isolated, *ex vivo* perfused canine kidneys as a result of exposure to unfocused ultrasound at 2 MHz. Thermocouples were used to determine two dimensional temperature profiles in the kidney as the rate of perfusate flow was varied. As expected, there was a general perfusion-dependent relation for ultrasound-induced hyperthermia; *i.e.*, the slower the perfusion rate, the higher the induced temperature and the greater the area of increased thermal burden. There was scatter or “heterogeneity” in the data at low perfusion rates, which the authors attribute to the inherent heterogeneity of the tissue or to other factors associated with the conduct of the experiment; *e.g.*, local changes in perfusion patterns, the presence of small

gas bubbles, tissue damage, etc. Computations based on BHTE were performed (by finite-element analysis) and used to indicate trends in the dependence of temperature distributions on perfusion. By observing the temperature decrease after exposure ended, time constants were obtained; the shortest perfusion times were about 100 s, roughly equal to values cited in NCRP Report No. 113 (NCRP, 1992) for brain and liver, but larger than that cited for kidney (about 15 s).

Harari *et al.* (1991) used implanted thermocouples to monitor the temperature in tumors of patients to be treated with a specially designed scanned focused ultrasound system, involving a modified clinical diagnostic-imaging device (an Octoson, Ausonics Ltd., Australia) and an array of therapeutic 1 or 3.95 MHz transducers (Figure 11.5). The diagnostic imaging system consisted of eight transducers mounted in an arc so that there could be three-way positioning of the beams to a common focus. The four therapeutic transducers were high power, were individually focused to a common focal area, and operated at either 1 or 3.95 MHz; the former are used for relatively "deep" tumors, the latter for superficial or peripheral tumors. The general goal was to produce controlled intratumoral temperatures of $>42.5^{\circ}\text{C}$ over the entire tumor for 30 min. Seventy-one patients were treated for whom conventional therapies had been exhausted or were considered highly unlikely to provide benefits; of these, 83 tumors in 67 patients were available for evaluation. The tumors included areas of the pelvis, chest, head and neck, groin, axilla and extremities; following hyperthermia treatment, the patients also underwent radiation therapy regimens. The response was encouraging; 22 percent of the treated tumors demonstrated complete disappearance, and 40 percent displayed >50 percent reduction in volume. Substantial pain reduction was obtained in 42 percent of the treated patients. Several patients whose tumors were very deeply seated made dramatic responses.

Damianou and Hynynen (1993) showed that for a single element transducer with a sharply focused beam, multiple sonications were needed to expose a target larger than the beam diameter. To avoid excessive heating in front of the focal zone, it was necessary to have time intervals between pulses greater than 20 s. Shorter pulse durations and reduced numbers of pulses also mitigated against temperature increments in front of the focal zone. Damianou *et al.* (1995) attempted to correlate the size of ultrasound-induced hyperthermic lesions with calculated estimates of the thermal dose, the latter as presented by Dewey *et al.* (1977). Solutions of BHTE, obtained by finite-element methods, were used to estimate temperature elevation in an insonated tissue volume exposed to calibrated 1.7, 2.7 and 3 MHz ultrasonic beams. There were three biological

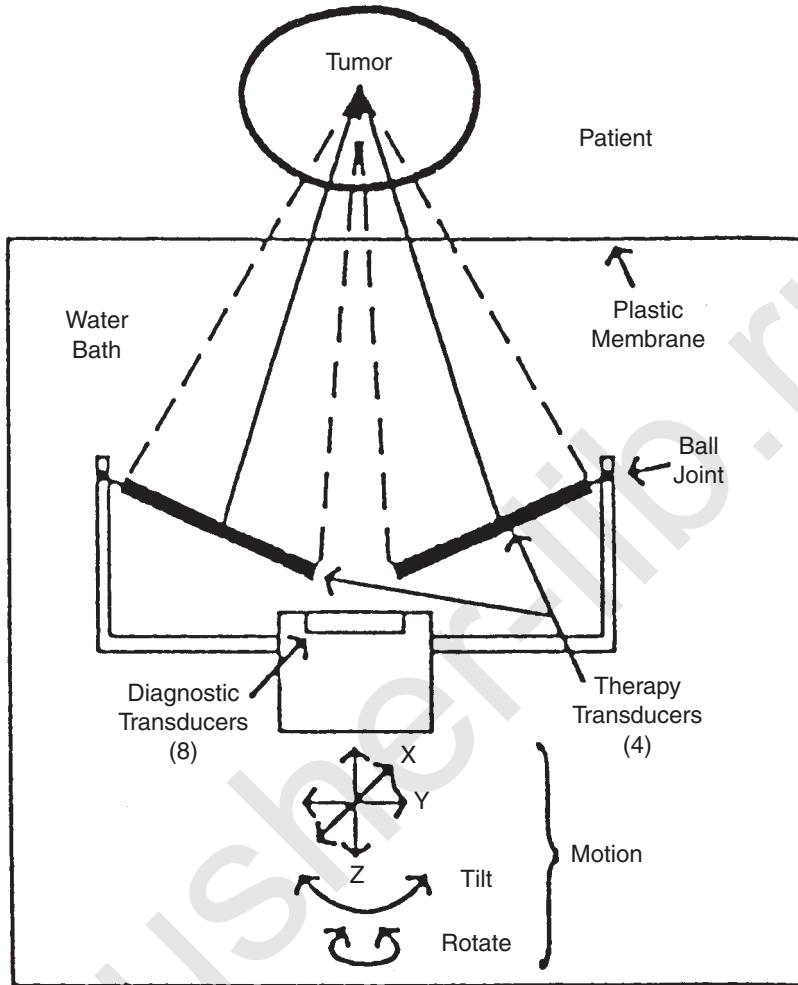


Fig. 11.5. Schematic representation of the Octoson® diagnostic ultrasound imaging system modified for ultrasound hyperthermia treatment (Shimm *et al.*, 1988).

specimens used in the test: (1) rabbit thigh muscle, (2) cat brain, and (3) rat brain. In general, there was good agreement between the predicted and the observed lesion size. In terms of depth of tissue, the authors concluded that the important variable for lesion development was ultrasound center frequency; *i.e.*, the deeper the area to be insonated, the lower the required ultrasound frequency. Earlier, Damianou and Hynynen (1993) had shown, using similar analytic

constructs and empirical observations, a good agreement between predicted and observed lesion size; the latter was found to be nearly independent of tissue perfusion with pulse lengths < 5 s. Lesion size increased with increasing pulse duration, acoustic power, and number of pulses. These tumors would have been considered difficult to heat by other procedures (excepting whole-body hyperthermia) and illustrate the potential of focused ultrasound for treating deep-seated tumors.

Vykhodtseva *et al.* (1994) produced lesions in rabbit brains *in vivo* with focused ultrasound beams (1 to 1.7 MHz; 0.5 to 10 s exposure durations, and intensities up to $\sim 3,700$ W cm^{-2}); there was a decrease in threshold ultrasound intensity with increase in pulse duration for lesion induction but only modest agreement between lesion size and predicted lesion size based on calculations of equivalent thermal dose for tissue-volume heating. There was less agreement between predicted and observed lesion sizes with longer exposure durations, which the authors attribute to tissue perfusion. At the very high ultrasound intensities, there was also evidence of the occurrence of cavitation as evidenced by extensive damage to the tissue vasculature. By using similar theoretical formulations for estimating lesion size, Fan and Hynynen (1995) showed that relatively large tumor volumes could be treated successfully with a hyperthermic ultrasound surgical procedure using a 16 element phased array. The maximal necrosed tissue volume induced by the array was very much larger than that induced by a similar spherical transducer, thereby holding forth the prospect of reducing patient-exposure duration for hyperthermic surgery.

More recently, Fan and Hynynen (1996) used both a single-element transducer and a 16 element phased-array transducer to compare the abilities of these transducers to induce necrosis of large tumors. A single-element, focused 1.48 MHz transducer was mounted on a three-way positioner such that it could be moved in any combination of x, y and z coordinates so that its focal area could expose, through a series of sequential transducer positions, a volume of material (*e.g.*, tumor) that was larger than the focal zone. There were, however, inherent problems with use of a single transducer in achieving hyperthermic exposures of large tumors: (1) multiple sonications, involving sequential repositionings of the transducer entail lengthy overall treatment times. (2) While avoidance of normal tissue damage can be achieved by the use of time intervals between consecutive pulses, this again engenders lengthy overall treatment times. (3) To increase size of overall necrosed tissue volume, increased acoustic power and/or pulse duration can be used, but increasing the pulse duration brings into play effects of vascular perfusion on ultrasound-induced

temperature elevations. Tissue temperature elevations were kept below 100 °C to avoid boiling and gas-body formation. The 16 element phased array mitigated several problems inherent with a single-element transducer by facilitating the near simultaneous exposure of a large tumor volume while achieving a more evenly distributed tumor temperature elevation. Hynynen (1993) had earlier cautioned that because of potential variability among what would appear to be comparable transducer arrays, it is essential to measure the acoustic power output from each element before clinical use to assure appropriateness of beam pattern and power density.

Hill *et al.* (1994) developed simplified analytical theory for the production of thermal lesions with focused ultrasound. Using the common assumption that the lesion boundary is the surface on which the tissue reaches a threshold temperature, they described approximate expressions for the width and length of the region of damaged tissue as a function of time. In comparing the influence of perfusion and thermal diffusion on lesion dimensions, they found that for a focal beam width of 2.2 mm and exposure times up to 30 s, diffusion dominates and perfusion plays a minor role. General agreement is found with experimental data from several laboratories on focal lesions produced with exposure durations of 0.1 to 30 s and *in situ* intensities (spatially averaged over the focal area) up to 1,800 W cm⁻² at 1.7 MHz. This theory was used by Hill (1994), together with other information, in discussing optimum conditions for surgical applications of focused ultrasound.

Watkin *et al.* (1996) studied the shape and position of lesions produced in ox liver as a result of 2 s *in vitro* exposures to 1.69 MHz focused ultrasound, the distance from focal point to transducer being 150 mm. Examining histological sections of the liver exposed to different intensities, they found that, as the (free-field) spatial peak intensity increased from 1,220 to 4,200 W cm⁻², the lesion midpoint moved progressively from 146 to 128 mm; *i.e.*, it moved toward the transducer. The lesion also changed in shape. This displacement and change in shape were attributed mostly to increase in attenuation of the ultrasound in the liver caused by formation of cavities (through acoustic cavitation processes or by boiling) at the higher intensities.

Lizzi *et al.* (1992) describe methods for computing and displaying temperature distributions produced by ultrasound in ocular tumors. These methods were developed to facilitate effective use of ultrasound in treating tumors by hyperthermia or ablation. For applications to hyperthermia, where the intensity is relatively low and the duration of exposure relatively long, steady-state solutions of Equation 11.5 are obtained by an integration process, as indicated in Equation 11.8, but with the function $H(s, t)$ reduced to a constant

multiplied by $e^{-(s/L)/s}$, where L is the perfusion length constant for the medium; the “H” function then gives the limiting temperature field produced by a steady point source of heat after a long time. For application to ablation, where short pulses of high-intensity ultrasound are applied at a focal point, Equation 11.5 still governs but reduces to the classical equation for heat conduction by omitting the perfusion term ($\Delta T/\tau$). Computations of the temperature elevation during ablation also follow an integration process, as indicated in Equation 11.8, except that the “H” function is chosen to give the temperature field from a point heat source in a conducting medium activated for an infinitesimal time period, and the integration is then necessarily over time as well as space; here the increased computational burden is dealt with by use of supercomputers. The heat generation quantity (q_v) (Equation 11.5) in the tumor is obtained from knowledge of the pressure amplitude in the ultrasound field and application of Equation 11.7 with the absorption coefficient chosen to be $0.08 \text{ Np cm}^{-1} \text{ MHz}^{-1}$. For the hyperthermia calculations, the perfusion length (L) is estimated as 11 mm. Boundaries of the tumor are defined by B-mode imaging, and display of the computed temperature distribution allows interactive adjustments in order to optimize treatment conditions.

Damianou *et al.* (1995) reviewed results of their experiments and those of others in which thermal lesions were produced in animal tissue, and compared the results with computations based on BHTE (Equation 11.5), using finite-element analysis. Also, they examined the influence of attenuation coefficients and other parameters on computed lesion dimensions. Computed values for the length and diameter of lesions were found to be in good agreement with results for lesions produced in cat brain at a frequency of 2.7 MHz and a total acoustic power of 10 W. For lesions in rabbit muscle produced with a frequency of 1.7 MHz, there was good agreement when the total acoustic power was 100 W or less; however, at higher powers the lesion diameter produced experimentally was much larger than computed, apparently because of the occurrence of cavitation.

Seip and Ebbini (1995) describe a novel ultrasonic method for measuring temperature distributions in tissues produced by therapeutic ultrasound. Their approach is based on use of diagnostic ultrasound together with theory for ultrasound scattering in which it is assumed that biological tissues can be treated as “semi-regular” scattering lattices. In experiments exposing dog thighs *in vivo* and exposing a rubber phantom with the therapeutic ultrasound field, it was found that the results on temperature rise obtained by the ultrasonic method compared well with those obtained by use of a thermocouple.

11.9 Summary

A re-evaluation of the data on thermally induced teratogenicity was undertaken in consideration of the fact that different species of higher animals can have different basal ("core") temperatures and to take into account, where possible, a temperature/time analysis more appropriate to *in utero* fetuses. Emphasis in the re-evaluation is given to the temperature increment of the core as being the important factor, as opposed to the temperature of the heated environment, in ascertaining the potential for inducing a teratologic effect. In an earlier discussion of this topic (NCRP, 1992), the emphasis was placed on the duration of a particular heating regimen and the temperature of the air in the chamber or water in the bath used to heat the animals; *e.g.*, for Edwards (1969), the duration (t_{43}) was 60 min. In the re-evaluation, the same heating regimen yielded an effective duration ($t_{3.5}$) of about 8 min. The latter figure, derived from an analysis of the heating and cooling profile of the core of the heated animal, reflects a temperature-increment/time exposure parameter, which can easily be extended to other temperature increments or time intervals to arrive at an exposure that would yield the same effect (an "isoeffect"); *e.g.*, when $t_{3.5} = 8$ min, then $t_{2.5} = 32$ min (because a decrease of temperature by 1 °C during an exposure is assumed equivalent to an increase in duration by a factor of four). Such an analysis aids in assessing the potential risk when a TI is known, because TI is intended to reflect an ultrasound-induced temperature increment in the target tissue.

In the interim since NCRP Report No. 113 (NCRP, 1992) was published, there has been continued progress in understanding the response of biological systems to temperature change and in knowledge of temperature increases that occur when systems are exposed to ultrasound. Further evidence has been found that HSPs are produced as a response to stressors of various kinds (not only to hyperthermia), and more has been learned about genetic and biochemical mechanisms by which HSP appear to confer protection. Additional evidence has been found for hyperthermia as a teratogen in laboratory animals, although the existing evidence on teratogenicity of hyperthermia for human beings is contradictory.

Recent studies in which biological systems were exposed to ultrasound have provided new insights into effects caused either by hyperthermia alone or by a combination of thermal and nonthermal mechanisms. Temperature rise is implicated in the production by CW ultrasound of petechial hemorrhages in murine intestine (Section 8.1.4) and increased cerebral blood flow in neonatal rat. However, heat was ruled out as the primary cause of the reduced aortic

pressure in frog heart which results from exposure to a single pulse of ultrasound. Also, while heat production accompanied the degassing that occurred during *in vitro* exposures of fixed erythrocyte suspensions to CW ultrasound, the dependence of the rate of degassing on cell density was explained in terms of nonthermal mechanisms.

In NCRP Report No. 113 (NCRP, 1992), basic equations were presented for predicting the temperature rise produced by ultrasound, and solutions were discussed for special situations relevant to applications of diagnostic ultrasound; also, TI was defined and proposed as an indicator of safety from thermal injury. Since that report was published, there has been further development of theory and of its application to medical ultrasound. Alternative approaches have been offered that may lead to reduced computational time or higher accuracy. Special approximate equations developed for ODS have been accepted by FDA for regulatory purposes. Many manufacturers now provide real-time display of TIs that are computed from standardized algorithms. ODS algorithms are often conservative, predicting temperature elevations that are higher than are likely to occur clinically. However, there are situations where the reverse is true, for example, (1) when there is a significant length of low-attenuation path in tissues, (2) when there is a significant contribution from transducer self-heating, or (3) when the measurements in water, made as required for ODS algorithms, are affected by saturation associated with NLP.

In the last few years, numerous investigations have involved measurements of temperature rise produced by ultrasound in TMM. These are gels designed to have acoustical and thermal characteristics similar to those of mammalian tissues (except that perfusion is usually absent). It can be concluded from this work that the temperature field produced by a well-defined ultrasound beam in a nonperfused homogeneous medium of known characteristics similar to those of soft mammalian tissue can be predicted well by computations based on solutions of Equation 11.10. Even for the ultrasound fields of transducers actually used in applications of diagnostic ultrasound, approximate methods have been found to be satisfactory for predicting temperature distributions in tissue-mimicking homogeneous media. In an exposure of bone to ultrasound, the simple formula in Equation 11.9 was found to predict reasonably well the temperature rise. In some situations, the temperature rise is affected significantly by factors not included in most calculations; these include: (1) extra heating arising from the transducer itself, (2) cooling produced by acoustic streaming, (3) extra absorption when gas-filled cavities are in the field, (4) shear waves set up in mineralized tissues, and (5) NLP in water or other media of similar acoustical characteristics.

Investigations have also been made into the increase of temperature produced *in vivo* by ultrasound in mammalian systems, such as fetal brain, fetal soft tissue, and neonatal brain. In the studies involving brain within the skull, it was found, as expected, that the temperature rise was greatest near the skull. However, it appears that measured values of the maximal temperature rise within the skull were much smaller than would be calculated from Equation 11.9; several reasons were suggested for this. In the neonatal study it was found that ultrasound caused a considerable increase in cerebral blood flow although the measured rise in temperature was only 1.3 °C. In two studies designed specifically to allow comparison between measured and computed values of the temperature rise produced by ultrasound in the fetus, reasonable agreement was found with theory based on solutions of Equation 11.5, although measured values sometimes exceeded those predicted.

The normal near-term human fetus can be slightly warmer (approximately 0.5 °C) than its mother's core temperature. Indirect evidence suggests that this temperature differential develops during the third trimester of pregnancy. A recognition of this temperature differential is important for situations in which a temperature increment is anticipated in relation to the diagnostic ultrasound exposure of a third-trimester fetus.

Medical applications to hyperthermia and surgery have advanced in the last several years, in which tissues are heated in a controlled manner by pulsed and focused ultrasound. Theory based on solutions of Equation 11.5 or 11.10 has been found to be very useful in optimizing treatment design. Uniform temperature over a tumor has been achieved by using arrays to shorten the total treatment time, thus minimizing uncertainties caused by perfusion.

12. Epidemiology of Ultrasound Exposure

12.1 Introduction

A review of the epidemiology of human exposure to ultrasound appeared in NCRP Report No. 74 (NCRP, 1983). Since the publication of that report there have been numerous epidemiological studies on the effectiveness and safety of diagnostic ultrasound. The current review is an update of the previous report. Although the epidemiological studies present in NCRP Report No. 74 have been included, the emphasis in the present section is placed on the critical analysis of more recent studies. Particular attention is given to the potential risks of fetal exposure to diagnostic ultrasound.

The use of diagnostic ultrasound in medicine has gained ever-increasing popularity over the past 30 y. Many millions of patients have had diagnostic ultrasound examinations, and the number of such examinations increases each year. A large fraction of the children born in the United States (over three million annually) is examined one or more times with ultrasound before birth (Nyborg, 1996). This implies that in the near future, if this trend continues, the majority of our entire population will have been exposed to ultrasound prior to birth. Reports from other countries make it clear that most fetuses in developed countries are now exposed to diagnostic ultrasound examination. Four European countries, Germany, Norway, Iceland and Austria, employ ultrasound screening for all pregnant women (Salvesen *et al.*, 1994).

Because of the vast exposure of the general population to ultrasound, any question of the possibility of adverse effects or harm becomes very important. This has certainly been a major concern of physicians ever since they began using ultrasound; and in spite of the fact that no adverse effects arising from ultrasound examinations have been identified, clinical safety is and will always remain a concern. This is especially true for exposures to the fetus.

The study of the effects of ultrasound exposure on human populations is the province of epidemiology. Even if laboratory studies of ultrasound bioeffects are reassuring, it is still necessary to study

directly the effect of ultrasound in human populations before making definitive statements with regard to risk. Fortunately, a number of epidemiological investigations of the use of ultrasound in diagnosis is available at the present time (Brent *et al.*, 1991; Naumburg *et al.*, 2000; Salvesen and Eik-Nes, 1995; 1999a; 1999b).

Unfortunately, most of the epidemiology reports do not provide an adequate description of the ultrasound exposure; and, in fetal studies, many do not give the gestational ages when the exposures took place. If there were adverse effects arising from diagnostic ultrasound, one would presume that the effects would become more severe with increasing exposure. While contrasting data for persons exposed *in utero* to ultrasound to those for persons not so exposed is valuable, the lack of exposure dosimetry precludes the ability to show any quantitative dose-response relationship, which is important in establishing a satisfactory causal relationship between ultrasound and adverse effects.

There is another important concern relating to dosimetry. As discussed in Section 9, the acoustic output levels of diagnostic ultrasound machines have increased significantly over the past 10 to 15 y. The most important change occurred in 1991 when FDA developed Tract III of the 510(k) process by which manufacturers obtain approval for their ultrasound machines. This change has permitted maximal output levels in fetal examinations to increase from 94 to 720 mW cm⁻² (see Section 10 and Appendix B). Because all of the exposures to diagnostic ultrasound in the existing epidemiology literature occurred before October 1991, the results and conclusions were based on ultrasound exposures that were smaller than those typical of current practice. This fact should be remembered when interpreting the significance of negative findings in epidemiological studies of fetal exposures.

12.2 Epidemiologic Methodology

Epidemiology is concerned with the patterns of the occurrence of disease or injury in human populations and of the factors that influence these patterns. With regard to the safety of ultrasound, the aim of an epidemiological study is to assess possible associations between exposure and disease. Epidemiological studies have been classified by MacMahon and Pugh (1970) into observational and experimental studies. The observational studies are subdivided into descriptive and analytical studies. The descriptive studies (surveys, cross-sectional, and longitudinal) are suitable for generating new

hypotheses of associations between exposure and disease, whereas the analytical studies (cohort and case-control) are designed to test such hypotheses. Surveys gather population information using questionnaires, cross-sectional studies investigate conditions at a single instant in time, and longitudinal studies explore how conditions change over time. In cohort studies, subjects and controls are selected according to whether or not they received a given ultrasound exposure, and then observed for the development of disease. In case-control studies, subjects and controls are selected according to whether or not they have a given disease, and then compared with respect to the degree of ultrasound exposure.

Cohort studies generally provide a more complete picture of the association between a disease and the exposure than a case-control study, because they are less susceptible to biases associated with selection or response. However, cohort studies are economical only when the disease under investigation is relatively frequent. For infrequent diseases, very large cohorts are required to obtain firm estimates of disease rates. This is certainly the case in searching for effects due to exposure to ultrasound.

A limitation of case-control studies is that information of the supposed cause must be retained either in the memories of persons or in written documents until after a subject is identified as having the disease. Written documentation is often lacking for many important details of epidemiologic variables. This is especially true for ultrasonic dosimetry.

Experimental epidemiologic studies can be employed to test a cause-effect hypothesis. They are characterized by the deliberate application or withholding of the supposed cause, and the observation for the subsequent appearance or lack of appearance of the effect. Randomized clinical studies are the most rigorous method for assessing the potential adverse effects of diagnostic ultrasound. Ethical considerations usually restrict such experiments to those that involve the addition of things presumed to be beneficial or the removal of things presumed to be harmful. Furthermore, if benefit from the procedure appears very likely, the withholding of it to obtain additional evidence may be unethical. However, when experimental studies can be performed, they can provide valuable evidence.

In all epidemiologic studies, it is important to avoid any subject selection bias that might interfere with the proper interpretation of the results. Another major problem is the presence of confounding factors. These factors are variables that are associated with both the disease and the ultrasound exposure. Unless matched for in the selection of controls, or controlled for in the analysis, the results may be skewed and lead to incorrect conclusions.

12.3 Causality

Epidemiological studies reveal associations between exposures and diseases. These associations may be statistically significant or nonsignificant, weak or strong, and causally related or a random coincidence. The likelihood of an association being due to a random chance can be assessed statistically. Epidemiologists normally choose the 0.05 level of significance for this purpose. However strong an association, epidemiological studies do not determine causality. That is, epidemiological studies do not provide conclusions that a particular exposure caused a particular disease, merely that a disease is associated with a particular exposure. Hill (1965) has provided a list of criteria to be used in judging causality as follows:

1. *Strength of the association.* The stronger the association, the more likely is an association causal.
2. *Consistency.* Are the results consistent with previous research findings? Are the research findings reproducible?
3. *Specificity.* Is exposure linked to a specific disease or to a particular site?
4. *Relationship in time.* To be causal, exposure must precede outcome.
5. *Biological gradient.* The finding of a graded dose-response relationship strengthens confidence in the association being causal.
6. *Biological plausibility.* Does the relationship make sense?
7. *Experimental evidence.* Are observations supported by laboratory studies?

The more criteria that are satisfied for any given association and the greater the degree of satisfaction, the greater is our confidence the two factors are related casually. Rarely, are all criteria satisfied in any epidemiological study. The requirement that the exposure must precede the outcome is the only *sine qua non*.

12.4 Clinical Surveys

The simplest and most rudimentary form of epidemiological study is a clinical survey, of which several have been performed. These surveys dealt with routine clinical examinations of patients in which commercial diagnostic ultrasonic instruments were used; acoustic output data and exposure durations were not specified.

Ziskin (1972) reported on an international survey of clinical users of diagnostic ultrasound. He reported that no adverse effects attributed

to examination by ultrasound had been identified by any of the 68 respondents to the survey in over 121,000 patient examinations. The report represented a combined total of 292 institute-years of experience in the clinical use of diagnostic ultrasound. A national survey of clinical users was carried out by the Environmental Health Directorate of Canada (EHD, 1980). From the replies, it was estimated that 340,000 patients were examined with diagnostic ultrasound in 1977 for a total of 1.2 million examinations. Only one adverse effect on a patient was reported by the 111 respondents, and its nature was not identified. It can be shown from statistical considerations that these large surveys give strong evidence against ultrasound producing obvious abnormalities, which, in the absence of any exposure, are rare (NCRP, 1983). However, even large surveys are not well suited for detecting small changes in the rate of more common occurrences (see Section 12.4.6 for more details).

While it is reassuring that these two surveys of clinical users of ultrasound found no clear example of an adverse effect, it must be pointed out that it is not known how diligently these users were looking for adverse effects or what kinds of effects they were looking for. Perhaps, the fairest statement to be made is that, based on 461,000 patient examinations, 179 clinical users overwhelmingly believed that their usage of ultrasound had been safe.

Three studies have been conducted to investigate specific biological endpoints on exposure to diagnostic ultrasound. These include the following: Ford (1974) examined the brains at autopsy of 24 neurological and neurosurgical patients who had multiple ultrasonic pulse-echo examinations at up to 120 d prior to death. He could not detect any changes attributable to the ultrasound. Kohorn *et al.* (1967) examined 20 normal babies during the first 3 d of life. The output from a diagnostic pulse-echo instrument was applied to the head for a 10 min exposure. No alterations in the electroencephalogram (EEG) tracings were detected. Timmermans (1973) exposed the urological tract of 300 patients to the output of a 2.25 MHz pulsed diagnostic instrument and found no detectable disorders.

12.4.1 *Studies of Fetal Exposure*

A number of attempts has been made to determine whether diagnostic ultrasound affects the human fetus. A good review has been prepared by Scheidt and Lundin (1977). The largest completed study considered in their review was conducted by Hellman *et al.* (1970). It consisted of a retrospective, but not case-control, study of 1,114 apparently normal pregnant women examined by ultrasound in the

United States, Sweden and Scotland. A 2.7 percent incidence of congenital abnormalities was found by physical examination of the newborns in this group as compared with a figure of 4.8 percent reported in a separate and unmatched survey of women who had not been examined with ultrasound. Hellman *et al.* concluded that neither the ultrasound examination frequency nor the time of the first examination seemed to adversely affect the overall incidence of fetal abnormality and abortion, and also that abnormalities among patients receiving ultrasound were no more common than in the general population. According to statistical analysis based on a sample size of 1,114 patients, a decrease in fetal abnormality from 4.8 to 2.7 percent is significant ($p < 0.01$) (NCRP, 1983). It is not known how to interpret this finding, because the exposed and unexposed groups were not matched. For example, it is possible that information derived from ultrasound examinations was used as an indicator for therapeutic abortions; if so, fewer abnormalities would have been expected among full-term births.

Other studies have been performed that show no significant change produced by diagnostic ultrasound. Bernstine (1969) exposed 720 fetuses *in utero* to 6 MHz CW Doppler ultrasound at an intensity (spatial average at the transducer face) of 20 to 30 mW cm⁻². He was unable to detect any difference in the incidence of obstetric complications resulting from exposure to ultrasound. The statistical significance of these findings is discussed in Section 12.4.6.

Scheidt *et al.* (1978) studied 1,907 infants with respect to 123 variables including those concerned with pregnancy, delivery, and the neonatal period. Intensity data for the ultrasound equipment were apparently not available. While 297 infants were exposed to ultrasound *in utero* and had amniocentesis, 661 had amniocentesis only, and 949 had neither. Clinical follow-up at 1 y of age included a history, physical examination, and the Denver Development Screening Test (Frankenburg and Dobbs, 1967). There were more grasp and tonic neck reflex abnormalities in the group with both ultrasound and amniocentesis than in the group with neither, but no such difference existed between the group with both ultrasound and amniocentesis and the group with amniocentesis alone. There were no other statistically significant findings.

Falus *et al.* (1972) and Koranyi *et al.* (1972) examined 171 children aged 6 months to 3 y who had been exposed to ultrasound *in utero*. Physical examinations and histories led the investigators to conclude that bodily and mental development was average or better. Karyotype analysis of 10 exposed children and 10 control children failed to reveal any differences.

Other studies resulting in negative findings were performed by Serr *et al.* (1971) on 150 exposed fetuses, by Watts and Stewart (1972) on 10 mothers at term, by Ikeuchi *et al.* (1973) on 98 first-trimester fetuses, and by Abdulla *et al.* (1971) on 35 second-trimester fetuses.

Using data from a larger long-term study of children exposed to ultrasound *in utero*, Moore *et al.* (1982) analyzed a subset of previously accumulated records of 2,135 single births (half of them exposed) for the possibility of a reduction in birth weight due to the ultrasound. Upon finding a crude association that was statistically significant ($p < 0.01$), they limited their attention to 527 single births for more detailed analysis in which they adjusted for demographic characteristics, previous pregnancy history, and some events during pregnancy. Then using a multiple logistic regression analysis, they were still able to show an association between ultrasound exposure and low birth weight ($p < 0.05$). Finally, using a multiple linear regression analysis, they found again a small but statistically significant ($p < 0.05$) lower mean birth weight between the exposed and nonexposed infants.

The report by Moore *et al.* (1982) is important because of its positive findings. However, it must be noted that the data were analyzed several years after they had been collected and that the reasons for which pregnant women did and did not receive the ultrasound are not known. The possibility that a problem pregnancy would be more likely to receive the ultrasound than a normal one cannot be discounted even with the adjustments made in the analysis. Furthermore, no adjustments were made for the physical size of the parents or whether the mother smoked. The failure to take these factors into account introduces a possible bias and weakens the conclusions reached. Nevertheless, this report cannot be disregarded.

Using a subset of cases from the same data base as that used in the above study, Stark *et al.* (1984) analyzed the records of 425 children exposed to diagnostic ultrasound and 381 matched controls. They compared 17 different outcome variables, 10 at the time of birth and seven at 7 to 12 y of age, and found no biologically or statistically significant differences between the exposed and unexposed children. The measurements at birth included Apgar scores, gestational age, head circumference, birth weight, length, congenital abnormalities, neonatal infection, and congenital infection. Measurements at ages 7 to 12 included hearing, visual acuity, color vision, complete neurological examination, cognitive function, and behavior.

An ambitious study was performed in Canada (Lyons *et al.*, 1980). It was planned that 10,000 pregnancies exposed to ultrasound would be identified and matched with 500 controls. Data extracted from

medical records and long-term follow-up evaluations of the offspring were studied. In a preliminary report, Lyons and Coggrave-Toms (1979) followed 2,428 children. They reported no evidence for increased incidence of congenital malformations, chromosome abnormalities, neoplasms, speech or hearing disorders, or developmental problems. In a later study, Lyons *et al.* (1988) found no statistically significant differences at age six in height, weight or head circumference in 149 sibling pairs of the same sex, and in which one of whom had been exposed to ultrasound *in utero*.

Salvesen *et al.* (1992a; 1992b; 1993a; 1993b) carried out a long-term follow-up of 2,161 children from two Norwegian randomized trials (Bakketeig *et al.*, 1984; Eik-Nes *et al.*, 1984). They wished to determine if there are any neurologic developmental problems associated with *in utero* exposure to diagnostic ultrasound. Routine ultrasonography offered in weeks 19 and 32 of pregnancy did not lower school performance, and did not cause an increased incidence of dyslexia, sensory deficits, or other impaired neurological development. However, 19 percent of the exposed children were classified as non-right handed compared to 15 percent of control children (odds ratio = 1.32; 95 percent CI = 1.02 to 1.71).

An excellent review of birthweight, childhood malignancies and neurological development in relation to ultrasound exposure *in utero* was provided by Salvesen and Eik-Nes (1999a). They reviewed more than 100 papers on ultrasound safety, including 11 studies with birthweight data, four case-control studies on childhood malignancies, and several studies containing more than 1,000 children. Three of the 11 studies with birthweight data found a small, but statistically significant, association between ultrasound exposure and birthweight. Of these three, two found a decrease in birthweight, and one found an increase. Also, there was no association between *in utero* ultrasound and childhood leukemia or solid tumors in any of the studies. A meta-analysis, including neurological outcomes such as handedness, speech development, motor development, hearing and vision, resulted in the conclusion that there was no association between diagnostic ultrasound exposure and reduced birthweight, childhood malignancies or neurological maldevelopment; however, the possible association between ultrasound and non-right handedness was evaluated further by the same investigators (Salvesen and Eik-Nes, 1999b). They performed a meta-analysis of one Swedish and two Norwegian studies providing a total of 4,715 children at the age of 8 to 9 y. Handedness was assessed through a questionnaire to the parents. They found that there was no significance in the prevalence of non-right handedness between the ultrasound-exposed children and the controls. However, there was a small, but

statistically significant, difference in a subgroup analysis among the boys. The authors concluded that a conservative, analytical approach indicates no association between ultrasound *in utero* and subsequent non-right handedness.

A number of studies has been made to determine whether chromosome damage has occurred in the mother and/or fetus following ultrasound examinations. Serr *et al.* (1971) suggested (although the results were not statistically significant) that damage to the chromosomes of fetal cells obtained by amniocentesis, may occur following a 10 h exposure to 6 MHz ultrasound of intensity 22 mW cm^{-2} (probably I_{SATA}). This suggestion is in contrast to Ikeuchi *et al.* (1973) who found no chromosome damage in 98 first-trimester fetuses exposed for 5 min to 20 MHz CW ultrasound at 40 mW cm^{-2} (probably I_{SATA}). Abdulla *et al.* (1971), studying maternal and fetal lymphocytes following exposure to 1.5 MHz pulsed ultrasound (intensity 0.8 mW cm^{-2} , I_{SATA}) or to continuous ultrasound from either of two devices (frequency 2 MHz for both; spatial-average intensity 22 mW cm^{-2} for one, and 0.8 mW cm^{-2} for the other, both measured at 10 cm from the transducer) did not find any increase in chromosome abnormalities.

In a case-control study, Kinnier Wilson and Waterhouse (1984) examined 1,731 children who had been exposed to ultrasound *in utero* and had died of cancer in the United Kingdom between 1972 and 1981, and an equal number of matched controls. Exposure to ultrasound *in utero* did not differ between the children who had cancer and the control children, and they concluded that ultrasound is safe with regard to the risk of cancer and leukemia. Another study by Cartwright *et al.* (1984) yielded similar results. In a review article, Salvesen and Eik-Nes (1995) conclude that there is no association between ultrasound exposure *in utero* and childhood cancer, and that there is no urgent need for more epidemiological studies on this subject.

In a very recent study, Naumburg *et al.* (2000) reported on the results of a nationwide case-control study in Sweden. Prospectively assembled data on prenatal exposure to ultrasound were used in the analysis. The case consisted of all children born and diagnosed as having leukemia between 1973 and 1989, yielding a total of 752 cases. One control was randomly selected for each child with leukemia, and matched by sex, year of birth, and month of birth. They found that the risk of lymphatic leukemia was not influenced by either the number of ultrasound examinations or the times when the examinations were performed. Myeloid leukemia was found not to be influenced by the number of examinations. Exposures occurring in the second trimester showed a slightly greater, but not statistically

significant, risk (odds ratio = 1.42; 95 percent CI = 0.88 to 2.29). The authors concluded that single or repeated intrauterine exposure to ultrasound, early or late in the pregnancy, does not influence the risk of subsequent development of lymphatic or myeloid childhood leukemias.

In addition to fetal exposures, one report, unconfirmed, suggested that premature ovulation may occur following the use of certain ovulation-inducing medications when ultrasonic scanning (intensities unspecified) is used in the late follicular phase (Testart *et al.*, 1982). A study of the effect of ultrasound on ovulation in mice (Heyner *et al.*, 1989) showed that 5 min exposures of CW 2.2 MHz ultrasound at intensities up to 1.5 W cm^{-2} produced no effects. However, at 3 W cm^{-2} (SATA) there was a statistically significant reduction in the number of oocytes recovered 10 d following ultrasound exposure.

12.4.2 *Effect on Fetal Activity*

In 1975, David *et al.* (1975) reported a 90 percent increase in fetal activity during a 15 min exposure of CW Doppler ultrasound following a 15 min control period. This was considered to be of general medical interest and not an indication of harmful effect. Fetal activity was determined by the number of times a mother reported the subjective sensation of fetal movement. This study, performed on 36 mothers, had a number of serious design flaws, such as the sequence of test period always following control period, and the subjective nature of test variable.

Another study of fetal activity was reported in 1979 by Powell-Phillips and Towel (1979). They used an objective strain-gauge measurement for defining fetal movement. They were unable to show any increase in fetal activity during ultrasound exposure thus casting doubt on the previous study. However, it is also possible that the strain gauges were not as sensitive as the mother. The major limitation of the latter study was that only 25 patients were evaluated.

Hertz *et al.* (1979) also studied the possibility of fetal activity being increased during CW ultrasonic examination. They also obtained negative results. However, their study was even smaller, with only 13 patients.

Arulkumaran *et al.* (1991) reported studies involving patients scheduled for induction of labor. A hydrophone placed near a fetal ear detected a clicking noise when imaged by an ultrasound beam. The clicking sound had the same 10 Hz repetition frequency as the commercial scanner. The authors suggested that ultrasound scanning of the fetal head might generate sound within the head that

would be audible to the fetus and might stimulate increased fetal activity (Section 3.2.2.4).

12.4.3 *The RADIUS Study*

There have been several recent studies involving fetal exposure that have been particularly important because of the quality of the research methodology and because of their potential impact on clinical practice. These include the routine antenatal diagnostic imaging with ultrasound (RADIUS) study performed in the United States (Ewigman *et al.*, 1993), the study by Newnham *et al.* (1993) performed in Australia, and the study by Campbell *et al.* (1993) performed in Canada. These studies will be reviewed in detail in this and the following two sections.

The RADIUS trial was a practice-based, multicenter study of pregnant women at low risk for adverse outcomes of pregnancy (Ewigman *et al.*, 1993). AIUM has published a review of this trial (AIUM, 1994a). The study was designed to test the hypothesis that routine screening with standardized ultrasonography on two occasions (between 15 to 22 weeks gestation and 31 to 35 weeks gestation, respectively) would reduce the primary outcome variable of perinatal morbidity and mortality. Perinatal mortality was defined as fetal death or neonatal death up to 28 d of age. Perinatal morbidity was categorized as severe or moderate depending upon the type and/or severity of known neonatal complications. Each ultrasound examination was performed in one of 28 ultrasound laboratories staffed by 91 physician-sonologists and 60 sonographers using either Acuson (Model 128 or 128 XP) or ATL Ultramark (Model 4 or 8) scanning equipment. The standardized ultrasonography examination included the assessment of placental location, amniotic-fluid volume, uterine and adnexal pathology, the number of fetuses, and sonographic biometry of the fetus as well as a detailed anatomical survey. A single experienced investigator provided in-service training and reviewed the first 25 sonograms obtained by each participating sonographer and sonologist.

Subjects were recruited from 92 obstetrical and 17 family practices in six states (81 private, 15 academic, and 13 health-maintenance-organization sites). Of the 55,744 women who registered for prenatal care at the participating practices between November 1, 1987 and May 31, 1991, 21,050 (37.8 percent) fulfilled the eligibility criteria for low risk, spoke English, were >17 y of age, and presented for care prior to 18 weeks gestation. Of these, 15,530 (27.9 percent of the original 55,744) were actually randomized to the ultrasound

screening (7,812) or control (7,718) groups. The mean number of sonograms per woman in the ultrasound screening group was 2.2 compared to 0.6 per woman in the control group. The rate of adverse perinatal outcome was 5 versus 4.9 percent among the infants of the women in the ultrasound screening and control groups, respectively. There were no significant differences between the groups in the rates of preterm delivery or the distribution of birth weights. Comparisons between the subgroups of women with post-date pregnancies, multiple-gestation pregnancies, or infants who were small for gestational age, also did not show any significant differences.

This was a well-designed and rigorously conducted, randomized clinical trial with an *a priori* statistical power analysis to ensure an adequate sample size to test the study hypothesis. The investigators made every effort to ensure adherence to a standardized protocol at each of the collaborating practices with appropriate instruction and quality assurance mechanisms. Uniform data collection procedures were instituted and all records of pregnancies with an adverse perinatal outcome were reviewed in detail for accuracy and completeness. Based on these data from a select, low risk population, the authors concluded that "screening ultrasonography did not improve perinatal outcome as compared with the selective use of ultrasonography on the basis of clinician judgment" and "the adoption of routine ultrasound screening in the United States would add considerably to the cost of care in pregnancy, with no improvement in perinatal outcome." The results and conclusions of this study may have a major impact on the health care debate in this country. It is for this reason that this study has been critically reviewed by several authorities in the field (Goncalves and Romero, 1993), and is being presented here.

At the completion of the study, statistical analysis of the data did not support the hypothesis that "routine screening with standardized ultrasonography on two occasions (between 15 to 22 weeks gestation and 31 to 35 weeks gestation, respectively) would reduce the primary outcome variable of perinatal morbidity and mortality." The conclusions and inferences drawn from the results of this study "that the adoption of routine ultrasound screening in the United States would add considerably to the cost of care in pregnancy, with no improvement in perinatal outcome" are, however, subject to significant criticism, especially if there is an attempt made to extrapolate indiscriminately these findings to the entire population of pregnant women in the United States.

The subjects enrolled in the RADIUS study by design comprise a very select and truly low risk population in that 95 percent of the women were between the ages of 20 to 35 y, 93 percent were white,

71 percent had some college education, 90 percent had ideal body weight, and 87 percent denied tobacco abuse. Sixty-five percent were multiparous of whom approximately 23 percent had a history of a previous miscarriage or induced abortion. All subjects were screened for 19 listed exclusion criteria in the categories of known conditions or suspected problems in addition to meeting the eligibility criteria of age >17 y, English-speaking, last menstrual period known within one week, gestational age <18 weeks, and no plans to change providers. Whether conclusions drawn from such a sample of low-risk pregnant women should be indiscriminately applied to all women who give birth in the United States annually remains doubtful.

The results of the RADIUS study are in marked contrast to the previously published meta-analysis of three randomized clinical trials to evaluate the efficacy of routine ultrasound screening in pregnancy (Thacker, 1985b). A total of 15,935 pregnancies was included in the analysis (7,992 with routine ultrasound screening versus 7,943 controls). Although the live birth rate was identical in both groups, perinatal mortality was significantly lower in the routine ultrasound screening group while there was no detectable group difference in perinatal morbidity (defined as newborn babies with Apgar score <7 at 1 min). The decrease in perinatal mortality was primarily due to a high rate of induced abortion of malformed fetuses in the Helsinki trial (Saari-Kemppainen *et al.*, 1990). In the RADIUS study, only 16.6 percent of congenital abnormalities were detected prior to 24 weeks gestation in the routine ultrasound screening group versus over 50 percent in European trials. Of these, the rate of pregnancy termination was 33 percent in the RADIUS study versus 61 percent in the Helsinki trial. It is difficult to ascertain the reasons for the very low detection rate of congenital anomalies in the RADIUS study and the population preference to continue with pregnancies with known malformed fetuses. Presumably, the latter issue represents local cultural and social attitudes. It is difficult to ascertain from the data provided whether the low-anomaly detection rate was a result of the types of anomalies present or the expertise of the individuals producing or interpreting the sonograms.

Finally, there exist nonquantifiable variables that may be very important for parents and obstetricians, but were not evaluated. Reassurance with respect to the normality of a fetus, the option for therapeutic abortion for severe fetal anomalies, and the avoidance of medico-legal liability by accurate prenatal diagnosis of congenital anomalies, are appropriate and desirable endpoints that should be included in the consideration of whether or not routine ultrasound screening during pregnancy is warranted (CMA, 1992).

Although not specifically designed to evaluate the safety of diagnostic ultrasound, the RADIUS study provides a very well-controlled, large-scale population study with much attention given to the health of the infants who had been exposed *in utero*. Had there been any increase in the number or severity of congenital abnormalities, this would surely have been reported. The fact that none were reported is reassuring.

12.4.4 *The Newnham Study*

In the study by Newnham *et al.* (1993), 2,834 women with single pregnancies were selected to be studied at 16 to 18 weeks of gestation. 1,415 were selected at random to receive ultrasound imaging and CW Doppler flow studies at 18, 24, 28, 34 and 38 weeks of gestation (the intensive group) and 1,419 to receive single ultrasound imaging at 18 weeks (the regular group). Outcome data were obtained from 99 percent of the women who entered the study. The only difference claimed by the authors between these two groups was significantly higher intrauterine growth restriction in the intensive group when expressed both as a birthweight less than the tenth centile (RR = 1.35; 95 percent CI = 1.09 to 1.67; $p = 0.006$) and birthweight less than the third centile (RR = 1.65; 95 percent CI = 1.09 to 2.49; $p = 0.020$). The mean birthweight in the intensive group was 25 g less than that in the regular group, but this difference was not significant.

This appears to be a well-designed and carefully conducted study. The underlying hypothesis in this study was that intrauterine ultrasound and Doppler would improve pregnancy outcome as expressed in the reduction in the number of neonatal days and in the decrease in prematurity rate. Gestational age was determined by ultrasonic biometry at 18 weeks, or if history was certain, by menstrual history. Measurements included fetal biparietal diameter, occipitofrontal diameter, head circumference, abdominal circumference, and femur length. Amniotic fluid was analyzed as well as the placental location and morphology. The groups were well matched with respect to maternal and obstetrical factors.

This is an important study primarily because it is a randomized clinical trial with relatively few inherent biases. The purpose of this study was to test the hypothesis that intensive use of ultrasound imaging and Doppler flow studies would improve pregnancy outcome. The results did not support the authors' hypothesis. As they themselves have indicated, their finding of diminished growth was not specifically studied and can well be a chance finding. Another

major flaw in this study is that both the intensive and the regular groups had a significant number of ultrasound exposures, although the intensive group had many more. However, if one looks at the number of imaging studies, one will see that 54 women in the intensive group had more than six scans, while only three in the regular group did; however, only 57 in the intensive group had more than three scans as compared to 130 in the regular group. Although the findings of the study cannot be discounted, it is important to note that both groups were exposed to repeated ultrasound examinations.

Another important issue is the use of infant weight as a measure of prenatal insult. The weight of the fetus can be very variable and can be influenced by a number of factors, not the least of which could be genetics, *in utero* exposure to various agents, or nutrition. For example, it has been shown that low-birth-weight infants occur among well nourished, female physicians, particularly residents. This would be an unlikely group in which to expect this outcome, but this finding is thought to be due to their hard-work lifestyle. This has also been shown in athletes, and the hypothesis is that there is diversion of blood toward the extremities and from the uteroplacental bed. In any event, use of birth weight as an outcome variable is a very complicated issue, and, when coupled with both study groups receiving ultrasound, casts a shadow of doubt on the interpretation of the results of this study.

Given the randomized nature of the study, the findings of differences in delivery at a low percentile of birth weight for gestational age cannot be dismissed as a statistical artifact. There is no overall support in the literature for a causal relationship between diagnostic ultrasound and fetal growth. The most likely alternative explanation for this finding is that enhanced pre-partum diagnosis of growth retardation led to obstetrical interventions that were themselves detrimental to growth or that caused early delivery. Evidence for this proposition comes from the observation that "obstetric intervention" was a very strong predictor of low weight for gestational age (RR = 2.65; 95 percent CI = 1.69 to 4.17). Unfortunately, the authors of the article do not define what "obstetric intervention" encompasses. Thus, even though this variable was included in the multivariate analysis examining the association of allocation to the intensive group with delivery at a low percentile of birth weight for gestational age, it is impossible to judge the adequacy of statistical control for all of the various interventions that might have occurred as a result of enhanced pre-partum diagnosis of fetal growth retardation. Furthermore, though the authors state that gestational age at birth was "similar" in the two groups, they did not state exactly what the mean

gestational age was in the two groups, and they did not show the results of a statistical test of this difference.

Even if the observation of a higher rate of delivery at a low percentile of weight for gestational age is shown to be a result of interventions made on the basis of a diagnosis of pre-partum growth retardation, there is an important lesson to be learned. One must not be sanguine about interventions during pregnancy, even interventions that appear to be benign. Newnham *et al.* (1993) make a strong case for continued use of randomized trials to evaluate rigorously what is done during all phases of pregnancy care.

In providing a balance, it should be noted that there were 10 neonatal deaths in the regular group and only three in the intensive group. Of the deaths due to congenital abnormalities, five were in the regular group and only one was in the intensive group. Similarly, of the deaths due to premature birth between 22 and 29 weeks of gestation, five were in the regular group and only one was in the intensive group. In addition, there was one death in the intensive group due to a motor vehicle accident. Although not presented as being statistically significant, this does represent in the regular group a five-fold increase in neonatal deaths due to congenital abnormalities and a five-fold increase in neonatal deaths due to premature birth between 22 and 29 weeks of gestation. This statistically nonsignificant finding may be more important than the statistically significant reduction in birth weight found in the intensive group. It is interesting to note that the birth weight was determined at less than the tenth centile and less than the third centile. There is no rationale for why these centiles were utilized or if other centiles were also tested. Although statistically not significant, there were fewer spontaneous abortions less than 20 weeks, fewer pregnancy terminations less than 20 weeks, and fewer stillborns in the intensive group as compared to the regular group. Finally, there was no difference in the duration of neonatal stay. The authors' conclusion that "repeated prenatal ultrasound imaging and Doppler flow examinations should be restricted to those women to whom the information is likely to be of clinical benefit," although probably true, is a judgment and is not a valid conclusion from this study.

Four other randomized controlled studies have evaluated Doppler ultrasound examinations in pregnancy (McParland and Pearce, 1988; Omtzigt, 1990; Trudinger *et al.*, 1987; Tyrrell *et al.*, 1990). A meta-analysis of these studies showed a decrease in perinatal mortality of normally formed infants. There were no significant differences on other obstetric or perinatal-outcome measures (Neilson, 1991).

In a more recent study (Mason *et al.*, 1993), 2,025 low-risk primigravid women underwent Doppler analysis of umbilical-artery

waveforms. No significant differences could be demonstrated between control and study women in birth weight, gestational age at delivery, Apgar scores, or any of the other outcomes measured.

Further evidence that ultrasound exposure *in utero* does not cause a reduction in birth weight is provided by the Oxford Database of Perinatal Trials, in which was published a series of meta-analyses of five studies of prenatal exposure to ultrasound (Neilson, 1991). The only outcomes that reached conventional levels of significance were a decreased rate of admission to special care units for singleton babies and a decreased incidence of low birth weight in the exposed group.

12.4.5 *The Campbell Study*

The objective of the study by Campbell *et al.* (1993) was to determine whether there is an association between prenatal ultrasound exposure and delayed speech in children. This study reviewed the clinical records of 72 children aged 24 to 100 months who had undergone a formal speech-language evaluation and were found to have a delayed speech of unknown cause. For each case subject, two control subjects were matched for sex, date of birth, sibling birth order, and associated health problems. The 72 children with delayed speech were found to have a higher rate of ultrasound exposure than the 144 control subjects (odds ratio = 2.8; 95 percent CI = 1.5 to 5.3; $p = 0.001$). There was no dose-response effect nor any relationship to timing of exposure. The investigators concluded that despite the inherent limitations of case-control studies, there does seem to be an association between prenatal ultrasound exposure and delayed speech in children, and they recommended caution in the use of *in utero* ultrasound if there is no clinical indication for same.

This study was a case-control study involving medical records, many of which were greater than 5 y old. This always makes the study more difficult and is not as scientifically reliable as a randomized prospective study. There was no identification of the ultrasonic exposure levels or durations of exposure. Furthermore, there was no relationship to the timing of exposures, and only four out of the 72 cases had more than one exposure.

The main problem with any nonexperimental study of the association between ultrasound and delayed speech, as well as other measures of child development, is the problem of confounding. We know very little about the effect of complications of pregnancy and delayed speech. It is possible that ultrasound is done because of conditions during pregnancy that affect the likelihood of delayed speech. Not all of these conditions may affect birth weight and gestational age.

Furthermore, and probably most importantly, it was not made clear why patients received ultrasound examinations, how many ultrasound examinations they received, and whether they received additional ultrasound-related studies such as Doppler, continuous fetal heart-rate monitoring, or other studies. In addition, because in the 1980s experts in Canada concluded that routine ultrasound is unwarranted unless there is clinical suspicion of a prenatal problem or abnormality (Nesheim *et al.*, 1987), it would seem as if patients who are receiving multiple ultrasound examinations may in fact have a clinical problem. These patients may have also received several other types of ultrasound studies. Therefore, we are left to assume that the reasons for the ultrasound examinations might, in fact, influence the outcome, and not necessarily that the diagnostic modality *per se* was causally related or associated with the outcome.

There is also a problem in the analysis. In the study, 8.5 percent of cases and five percent of controls had a birth weight less than 2,500 g. Thirteen percent of cases and 11.4 percent of controls had a gestational age less than or equal to 37 weeks. Although neither of these differences is statistically significant using a conventional criterion ($p < 0.05$), an analysis adjusting for low birth weight and for being pre-term should have been done. It also would be of interest to know the percentage of cases and controls who were small for gestational age, the percentage who weighed less than 1,500 g, and the percentage who were born at less than 34 weeks of gestation. If there were any differences between cases and controls on any of these measures, even statistically nonsignificant differences, they should have been adjusted in a multivariate analysis.

Delayed speech is viewed not as a pathological or organic syndrome, but rather as a developmentally defined symptom complex that may have several different causal factors. Therefore, the association with ultrasound exposure may be a consequence of some confounding factor in the population studied.

This study was motivated by an observation of an apparent increase in prevalence of delayed speech in the practice of an otolaryngologist. This case-control study was set up to see if there was an increased exposure to ultrasound in children who had delayed speech. The endpoint and the hypothesis were formulated before the study was undertaken, whereas many of the positive results in existing publications came from after-the-fact manipulation of the data. A statistically significant increase in the number of ultrasound exposures prenatally was found in the children with delayed speech. This finding deserves to be taken more seriously than a chance finding in a multiple endpoint type of epidemiological search.

In a later study, Salvesen *et al.* (1994) compared the incidence of delayed speech in 1,107 children who had been exposed to ultrasound *in utero* with 1,033 controls. They found no significant differences in delayed speech, limited vocabulary, or stuttering. According to health center records, children who were exposed *in utero* were less likely to be referred to a speech therapist (odds ratio 0.51). The authors concluded that routine ultrasonography *in utero* is not associated with delayed speech in children.

12.4.6 Statistical Considerations

The ability to detect an adverse effect depends on a number of things. Perhaps the two most important factors are: (1) the visibility or conspicuousness of the effect if it does occur, and (2) whether it constitutes a new event or merely an increase in the incidence of a naturally occurring event.

For adverse effects that are characterized by an increased incidence of a spontaneously occurring abnormality, statistical methods must be employed to detect their existence. As will be shown, the most important factor for the detectability of this type of effect is the resulting relative increase in its incidence. The smaller the relative increase in incidence, the larger the number of subjects required in the study. It makes a difference whether one is considering the significance of an observed increased incidence in a previously published report or if one is planning a future study to determine if there is an increased incidence.

It can be shown (Choi, 1978; Feinstein, 1977) that the minimal number of subjects (N) required in a study in order to conclude that an observed increase in incidence is significant is given in the equation (repeated from Equation 11.3):

$$N = \frac{Z_{\alpha}^2 P_0 (1 - P_0)}{(P - P_0)^2}, \quad (12.1)$$

where Z_{α} is the the standard normal variate at a specified level of significance (α), P_0 is the proportion of cases in which the event occurs naturally, and P is the proportion of cases in which the event occurs following ultrasound.

Equation 12.1 is less general than equations often used in statistics, but it is satisfactory for the present illustrative purposes. Consider its application to the evaluation of a clinical study the aim of which was to determine whether ultrasound applied during pregnancy increases the rate of incidence of congenital abnormalities. The natural rate is 4.3 percent of all births (Trimble and Doughty,

1974), and it was desired to test the hypothesis that ultrasound increases the rate by at least one percentage point, that is to 5.3 percent or more. Then in Equation 12.1 the quantities P_0 and P are equated to 0.043 and 0.053, respectively. A numerical value for Z_α is arrived at by specifying the *level of significance* which is accepted as meaningful. Usually taken as five percent, the level of significance (α) is defined for the present example as the probability that by chance the study will produce a false positive result; that is, a rate higher than 5.3 percent in the test group if, in fact, the ultrasound has no effect. (More generally, α is defined as the probability of rejecting a null hypothesis, given that the null hypothesis is true.) For a choice of five percent for α , the variate (Z_α) is known from tables to be 1.65. Then, from Equation 12.1, one obtains for the minimal sample size:

$$N = \frac{(1.65)^2 (0.043) (0.957)}{(0.053 - 0.043)^2} = 1,120. \quad (12.2)$$

If the observed increase in incidence had been 0.5 percent instead of one percent, that is, if the observed incidence had been 4.8 percent instead of 5.3 percent, the sample size would have had to be four times larger to establish the presence of an adverse effect. In this case, the sample size would have had to be at least 4,480. Very few of the studies reported in this Section have had sample sizes this large.

Equation 12.1, upon rearrangement, can also be used to determine, for a given sample size, how large a detected increase in incidence must be in order to be statistically significant. For example, in a study by Bernstine (1969) of 720 pregnancies, the United States Navy-wide incidence of prematurity was 7.9 percent. For any observed increase to be statistically significant, the observed incidence would have had to exceed 9.5 percent (a relative increase of over 20 percent). This points out that what might appear as a reasonably large study is quite limited in its ability to detect small changes in incidence if the frequency is appreciable in the general population.

The statistical considerations so far have involved α , the probability that a study will yield by chance a false positive result (an observed rate above 5.3 percent even though ultrasound actually had no effect). In planning a future study, it is obviously just as important to consider the probability that a true effect will be detected if it occurs. This probability is represented by another parameter, $1 - \beta$, the "statistical power" of the study. Statistical power is the probability of detecting a true effect (*i.e.*, rejecting the

null hypothesis when the null hypothesis is, in fact, incorrect). The larger the power demanded, the larger the sample size required.

Furthermore, in the previous example it was assumed that the naturally occurring rate of congenital abnormalities was known. However, for any given population, this information is rarely known, and a control group equal in size to the test group will also be required. The minimal number of subjects required in a study being planned is given in the following equation (Fleiss, 1981):

$$N = \frac{(Z_\alpha \sqrt{2 \bar{P}\bar{Q}} - Z_{(1-\beta)} \sqrt{P_1 Q_1 + P_2 Q_2})^2}{(P_2 - P_1)} + \frac{2}{|P_2 - P_1|} \quad (12.3)$$

where P_1 is an estimate of the proportion of cases in which the event occurs spontaneously; $P_2 = P_1 + \delta$, where δ is the smallest increment considered medically significant and is desired to be able to be detected; $\bar{P} = \frac{P_1 + P_2}{2}$; $\bar{Q} = 1 - \bar{P}$; $Q_1 = 1 - P_1$; and $Q_2 = 1 - P_2$. The Z values are the appropriate ordinates of the normal distribution. The term $\frac{2}{|P_2 - P_1|}$ is a correction for continuity (that is, an adjustment to compensate for the use of the normal distribution, a continuous distribution, to approximate the distribution of proportions in a population, a discrete distribution). The one-sided Z_α is used because one would normally be concerned only with possible increases in the rate of congenital abnormalities. However, if one were interested in both increases and decreases in the rate of congenital abnormalities, the two-sided $Z_{\alpha/2}$ should be used.

As in the previous example, if we suspect that the naturally occurring rate of congenital abnormalities is 4.3 percent, and wished to be able to detect an one percentage point increase in a future study, we could use Equation 12.3 to determine the minimal sample size required to obtain a 95 percent CI ($Z_\alpha = 1.65$) and a statistical power of 80 percent [$Z_{(1-\beta)} = -0.0842$]. Thus:

$$N = \frac{[(1.65)\sqrt{2(0.048)(0.952)} - (-0.0842)\sqrt{(0.043)(0.957) + (0.053)(0.947)}]^2}{(0.053 - 0.043)^2} + \frac{2}{|0.053 - 0.043|} = 2,948, \quad (12.4)$$

which shows that the sample size required is 2,948 for the test cases and an equal number of control cases, requiring a total of 5,896 subjects. If we wished to be able to detect a 0.5 percentage point increase with the same statistical power, the sample size would need to be nearly quadrupled. It should also be noted that even with a sample size as large as 2,688, we would fail to detect a true one percentage point increase 50 percent of the time.

The purpose of this discussion has been to demonstrate (1) the importance of considering the statistical power of a study and (2) the very large sample sizes necessary to achieve any reasonable likelihood of detecting a small increase in incidence of a naturally occurring event.

For events that do not occur naturally, the situation is different. Statistical theory permits one to make quantitative the significance of nonobservance for these events, provided that they can be detected if they occur. That is, based on the number of patient examination studies, we can state that the probability of such an event is less than some amount (with 95 percent CI). The exact relationship is given by:

$$p \leq 1 - (0.05)^{1/N}, \quad (12.5)$$

where p is the probability of the event under consideration and N is the number of patient examinations studied.

For example, suppose that there have been no cases of a missing right thumb in 10,000 live births of infants who received ultrasound *in utero*. In this case:

$$p \leq 1 - (0.05)^{1/10,000} \leq 0.0003. \quad (12.6)$$

Thus, we can be 95 percent confident that the true occurrence of this effect is less than 0.03 percent. If we had wished to be more conservative and demanded to be 99 percent confident, 0.01 would have been substituted for 0.05 in the above equation, and we would have obtained a maximal occurrence rate of 0.046 percent.

Equation 12.3 can be used to show the importance of sample sizing in providing meaningful results of a clinical survey in which there were no observed abnormalities. For example, consider a study by Kohorn *et al.* (1967) who found no EEG tracing alterations in 20 infants. Even though no abnormalities were observed, the true incidence of EEG alterations following ultrasound exposure could be as high as 14 percent of all infants.

Equation 12.3 may also be applied to large clinical surveys with negative findings, such as the one by Ziskin (1972) and another by EHD (1980). For example, in the Ziskin survey of 121,000 patient examinations, there were no positive responses to a question as to whether any adverse effects had been observed that were caused by the ultrasound. If one substitutes 121,000 for N in Equation 12.3, one obtains: $p < 0.000025$. This very small value for p might be considered an upper limit to the probability that ultrasound caused any adverse effects in the patients examined. However, this sanguine interpretation must be tempered by the fact that some abnormalities

might not be detected and that even if detected might not be attributed to the ultrasound.

The implication of these qualifications can be seen by considering how a typical respondent, Dr. A., would reply to a questionnaire by considering patient records, which include observations of abnormalities in infants, some of whom were exposed to diagnostic ultrasound prenatally, and some not. The physician would necessarily report “no adverse effects attributed to ultrasound” even though abnormalities were observed among the exposed population unless their number significantly exceeds the number expected in an equal population of unexposed infants. Consider the case of an obstetrician who performs 300 deliveries a year from patients who are examined with ultrasound. Table 12.1 illustrates the number of abnormalities that would have to be observed before the physician would have reason to be suspicious that ultrasound may be causing any harm.

In this Table, it is assumed that the exact value of the naturally occurring rate of an abnormality is known to the physician. In reality, this will rarely, if ever, be the case. Therefore, the physician’s estimate of the expected number of abnormalities will be uncertain, and this will cause him to be more reluctant to decide that the number of instances of abnormalities he observed is truly in excess of the expected number. Of course, even this assumes that the abnormality is readily detectable, and that the physician is really looking for and counting the abnormalities that occur. The above discussion points out that it is extremely unlikely that an individual physician would conclude that ultrasound caused an observed adverse effect unless

TABLE 12.1—*Minimal number of abnormalities to implicate ultrasound in a 300 deliveries-per-year obstetrical practice.*

P_0^a	$P - P_0^b$	X_0^c	X^d
0.50	0.0475	150	165
0.05	0.0207	15	22
0.005	0.0067	1.5	4
0.0005	0.0021	0.15	1

^a P_0 is the presumed naturally occurring rate of an abnormality.

^b $P - P_0$ is the minimal increment to be declared significant (as determined by Equation 12.1).

^c X_0 is the expected number of abnormalities if there is no effect of ultrasound.

^d X is the minimal number of abnormalities in order to implicate ultrasound.

the magnitude of the effect is very large and obvious, or that the abnormality is so rare that its occurrence draws suspicion.

12.4.7 *Commentary on Results from Human Epidemiology*

Any analysis of ultrasound epidemiological studies must recognize that the diagnostic exposures have occurred as part of the medical care of the population. Although teratogenic and reproductive toxic effects can be studied in the offspring of these exposed populations, the gestational stages at the times of exposure in many studies did not include the most sensitive period of embryonic development (early organogenesis). However, most studies did include exposure during gestational periods that would affect subsequent growth and neurobehavioral development. Animal studies can be helpful in providing substantiating data for the human studies. Combining the epidemiological studies with the animal studies does permit us to draw reasonable conclusions about the effects or lack of effects of diagnostic ultrasound.

It appears from findings reviewed in this Section that epidemiological studies and surveys of clinical experience have yielded no firm evidence of any adverse effects from diagnostic ultrasound, in spite of large clinical usage. This apparent safety is of paramount importance to the physician. While recognizing the limitations of clinical trials, these still represent, to the physician, the most sensitive and ultimate tests of any drug or agent. Experience shows that even when all laboratory tests have been free of adverse effects, unexpected reactions will frequently be seen when any given agent is administered to a large number of patients.

The inability to find convincing proof of an effect, either from epidemiology or from the physician's experience, does not preclude the possibility of its happening. As Equation 12.1 shows, it is difficult to identify a small increase in rate of a commonly occurring event, even if each event is easily seen. Also, subtle effects (such as minor chemical changes and minor behavioral changes), long-term delayed effects, and certain genetic effects could escape detection. Overall, the results of epidemiological studies have been reassuring. However, most studies were performed using smaller acoustic outputs than those in current diagnostic use. How much effect the increased exposures will have on future epidemiological studies is unknown. Furthermore, if we are eventually to identify subtle effects, if any, it will probably be necessary to rely on studies of the effects of ultrasound on laboratory animals and extrapolate from these results

to the clinical situation. When a clear hypothesis can be generated in this manner, it may be possible to design an epidemiological study that will have the statistical power to determine the extent of the effect and its implication in the human population. Conditions to be evaluated when considering the advisability of an epidemiological study on safety of diagnostic ultrasound were discussed in a previous report (NCRP, 1983, Section 10.2.2).

akusher-lib.ru

13. Summary and Conclusions

13.1 Introduction

This Section brings together in one location the summaries and conclusions for each of Sections 3 to 12. Each summary presents the salient points of its corresponding section and provides background for the related conclusions; the reader is to refer back to the section itself for more detailed discussion. The identification of the sections in the previous text is by reference to the number of the first subsection; for example, Subsection 13.3 with Subsections 13.3.1 and 13.3.2 provide the summary and conclusions for Section 3, and Subsection 13.4 provides them for Section 4. To allow this correspondence, Subsection 13.2 has been omitted.

In addition, this Section includes Subsection 13.13 that contains conclusions on the thermal and mechanical indexes that are now displayed on diagnostic ultrasound equipment in the United States. These provide information relating to safety which is otherwise not readily available.

13.3 Nonthermal Mechanisms for Bioeffects in the Absence of Cavitation

13.3.1 *Summary*

Examples are discussed in Section 3 of changes in biological systems that are produced by ultrasound in the apparent absence of significant temperature elevation or cavitation activity. When the mechanisms have been identified, they have been found to involve nonlinear aspects of the sound field, specifically, the time-averaged quantities known as acoustic radiation force, acoustic radiation pressure, acoustic radiation torque, and acoustic streaming.

Radiation force can be localized, as in applications where focused ultrasound is used to exert a force on part of the retina. By modulating the acoustic power, the radiation force can be made to vary with

time. Localized pulsed radiation force applied to nerve can alter its response to electric excitation. When applied to the middle ear, time-varying radiation force can give rise to an auditory response; when applied to the skin it can elicit a tactile response; when applied to the heart it can affect the cardiac function. Ultrasound fields can be designed to redistribute cells in suspension, or to manipulate small biological objects, by the action of radiation force.

Large-scale acoustic streaming can occur in any fluid-filled region through which a beam of ultrasound passes; it can affect transport of heat or matter, or affect cells. Microstreaming, of small scale, occurs near small obstacles to the sound field; in a blood vessel exposed to ultrasound, the shearing stresses can lead to thrombogenesis if a small obstacle is present.

Also, under some conditions ultrasound causes biological effects for which the mechanism does not appear to involve significant temperature elevation or cavitation, but is unknown.

13.3.2 Conclusions

1. Pulses of ultrasound can be sensed by human beings *via* radiation force under some conditions. Under special conditions, diagnostic ultrasound might produce hearing sensations.
2. Several experiments have shown that a burst of ultrasound can produce biological effects on eye (such as reversible blanching) and heart (reduction in ventricular contraction) *via* radiation force. These findings are relevant to present or potential therapeutic applications of ultrasound in medicine, but the effects have not been shown to occur under conditions of current practice in diagnostic ultrasound.
3. An ultrasound field can produce redistribution and reorientation of particles in suspension, to an extent that depends on the nature of the field, of the particles, and of the particles' environment. These findings may be relevant to present or potential applications of ultrasound in medicine, but the effects have not been shown to occur under conditions of current practice in diagnostic ultrasound.
4. Acoustic streaming is to be expected whenever an ultrasound beam passes through a fluid-filled region of the body. Observations of the induced particle motions may prove useful for diagnostic purposes. When the dimensions of the region are larger than the beam diameter, gentle stirring and weak shearing stresses can be produced that cause biological effects *in vitro* at elevated temperatures; the significance of these effects for

safety or therapy has not been explored. When small solid objects lie in the path of an ultrasound beam, acoustic microstreaming and much higher shearing stresses can be produced under some circumstances. Experiments to date have not been adequate for determining whether such effects are important in medical practice.

5. Ultrasound at temporal average intensities well below the maximal levels used in diagnosis has been reported to produce effects on membranes, muscles and bone that have not been explained by temperature elevation, cavitation or radiation force. Some of these effects, such as accelerated bone healing, are beneficial. There is no evidence, at present, that any of these phenomena cause adverse effects in the normal practice of diagnostic ultrasound.

13.4 Noninertial Cavitation; Gas-Body Activation

13.4.1 Summary

Low-pressure-amplitude ultrasound can interact with a bubble or gas body to produce a nearly sinusoidal oscillation of small amplitude. In this context, "small amplitude" refers to a balance in the equations of motion, leading to a mass and spring type oscillation, in contrast to the dominance of the inertial terms at higher amplitudes, leading to inertial cavitation. The small amplitudes of oscillation can take on many forms, including the radial pulsation of spherical gas bodies in ultrasound contrast agents, the drumhead-like motion of the air-water interface of gas trapped in a pore, or transverse oscillation of plant cell walls around a gas-filled intercellular channel. In each case, the oscillation concentrates acoustic energy and enhances the operation of physical mechanisms in the vicinity of the oscillation, potentially by orders-of-magnitude above that expected in the absence of the localized oscillation. An ultrasonically activated gas body can act to attract small particles by the radiation-force mechanism and to stir the liquid in its vicinity by the acoustic-microstreaming mechanism.

The importance of these phenomena to the consideration of biomedical ultrasound arises from the initiation of the activity at any non-zero level of exposure, provided that bubbles or gas bodies are present in the ultrasonic field. The thresholds for adverse biological effects in this case are related to the biological thresholds for mechanical damage. For example, cells can be attracted to an oscillating

gas body and may tend to gather near the body at very low levels; when caught up in the local microstreaming flow, the cells can be lysed if the time-averaged shear stress exceeds the threshold for membrane rupture. Other perturbations relate directly to the instantaneous pulsation of the gas bodies, as has been noted in the fruit-fly larvae.

These physical mechanisms can operate during diagnostic ultrasound examinations when suitable gas bodies are present. This may occur for gas-bearing tissues of lung and intestine, although these tissues are not common targets of diagnostic ultrasound. The situation most pertinent to clinical medicine occurs with the use of gas-body-based contrast agents, which are specifically designed to be suitable for strong activation by diagnostic ultrasound, as described in Section 4, and this interaction represents GBA or cavitation. The gas-body or bubble activity creates secondary points sources, which gives strong echos that enhance diagnostic images in various ways, and generate mechanical perturbations in their local vicinity. That is, the enhancement of the image-contrast and of nonthermal bioeffects mechanisms originate from the same phenomena. Because the contrast effect and the bioeffects mechanisms are linked, improvements in delivery, persistence and response not only improve the diagnostic effectiveness of gas-body-based contrast agents but also tend to increase the potential for bioeffects. The effectiveness of gas-body agents for enhancing biological effects has led to their use in therapeutic applications of ultrasound.

13.4.2 *Conclusions*

1. Activation of stabilized gas bodies, and other forms of noninertial cavitation, can occur at any level of ultrasound exposure when suitable bubbles or gas bodies are present, and they greatly increase the mechanical stresses in the vicinity of the activated gas bodies.
2. Activation of stabilized gas bodies has potential for causing bioeffects in examinations where the lung or intestines are exposed to diagnostic ultrasound (Section 8).
3. Diagnostic ultrasound can destabilize gas bodies in contrast agents, thus generating effective cavitation nuclei, and can then produce inertial cavitation.

4. Bioeffects are linked to contrast-aided diagnostic ultrasound because the strong response of the gas bodies is responsible for both the contrast effect and the enhancement of local bioeffects mechanisms.

13.5 Nonlinear Bubble Response; Inertial Cavitation

13.5.1 *Summary*

When free bubbles of gas are exposed to ultrasound at the acoustic pressure levels used in most applications of diagnostic ultrasound, the bubble response is nonlinear. Resonance characteristics are modified or absent. The spectrum of ultrasound scattered from the bubbles contains components that are integral and nonintegral multiples and submultiples of the incident frequency. Often the motion is chaotic and the spectrum contains noise. Under specialized conditions, a free bubble maintains a spherical shape during nonlinear oscillations, but more often the surface becomes severely contorted. Under the latter conditions, small microbubbles of gas are created at the interface; also, jets of liquid are formed that project inward.

When the pressure amplitude of the field driving the bubble exceeds a critical value, inertial cavitation occurs; then, the phase of motion during which the radius is decreasing is dominated by an implosion, or collapse, as the surrounding liquid rushes inward. The bubble decreases to a minimal volume which is a small fraction of its original value. This highly compressed state persists for a very short time, after which the fate of the bubble varies; it may rebound or it may disintegrate into very small fragments, some of which dissolve and some of which may become active bubbles. During the state of greatest compression, the pressure and temperature of the gas are very high. If the bubble is near a boundary when it collapses, a liquid jet may form that impinges on the boundary at high speed. The term inertial cavitation is given to the activity described above, because the vigor of the collapse comes from inertia (or momentum) of the inward rushing liquid (Section 5).

All of the above characteristics of inertial cavitation are expected from physical theory in the form of nonlinear differential equations; these are solved numerically for conditions of interest by using special computational programs. The model chosen for most computations is a single spherical bubble that contains a gas of known properties; it exists in a Newtonian fluid well away from boundaries and maintains a spherical shape as it oscillates. Such theory has

been shown to agree well with important features of the observed oscillatory motion of single bubbles in special arrangements. However, in a typical experiment where ultrasound is applied to a liquid in a test tube or other container, it is difficult to compare results with predictions from theory. This difficulty arises primarily because cavitation activity is strongly dependent on the number, size and location of cavitation nuclei, and information on these is not known unless special steps are taken. The use of contrast agents consisting of small stabilized gas bodies of controlled size as cavitation nuclei has made it possible to make more specific predictions of cavitation activity in liquids.

When ultrasound is applied to a liquid which has not been “prepared” by adding cavitation nuclei, the onset of cavitation requires the occurrence of such nuclei accidentally on vessel walls or on small impurity particles, the latter being ubiquitous unless the liquid has been very thoroughly filtered. These accidental nuclei are typically small, and the acoustic-pressure levels required to activate them are also high enough to produce inertial cavitation. Hence, when cavitation activity is produced in an unprepared liquid, inertial cavitation is likely to dominate, although noninertial cavitation may be present also. If stabilized gas bodies of suitable size are added to a liquid, cavitation activity of a noninertial type can occur at levels of the acoustic pressure too low for the production of inertial cavitation (Section 4).

It is known from many experiments that chemical reactions of widely varying nature are accelerated by exposure of liquids to ultrasound. These chemical effects often can be attributed to free radicals produced during the short pulses of high temperature expected when inertial cavitation occurs. Some of these reactions are accompanied by sonoluminescence, *i.e.*, by the production of light. Techniques for detecting and measuring chemical reaction products, or the light output when sonoluminescence occurs, have proven useful for assessing the extent to which inertial cavitation occurs in a liquid.

An approximate theoretical result has proven convenient for predicting the lowest acoustic-pressure level at which inertial cavitation can be produced in a liquid when cavitation nuclei of optimal size are present; according to this result, for frequencies in the range 1 to 10 MHz, the threshold value of the peak negative pressure (p_-) is proportional to the square root of the frequency. This relationship was found to agree with experiments in which water, containing contrast agents or other cavitation nuclei, was exposed to pulsed ultrasound; an ultrasonic method was used to detect cavitation events. In other experiments, sonoluminescence and, hence, inertial cavitation was found to occur in water exposed to ultrasound pulses comparable to those used in medical diagnostic ultrasound.

13.5.2 *Conclusions*

1. Much of what is known about inertial cavitation has been obtained from theoretical models and from recent experiments for a single free bubble in a homogeneous liquid.
2. Inertial cavitation is capable of producing severe chemical and/or mechanical damage to physical and biological structures.
3. Inertial cavitation can be produced in water and aqueous solutions by short pulses of ultrasound similar to those used in diagnostic medicine, provided that suitable cavitation nuclei (such as contrast agents) are present.
4. The production of inertial cavitation is inhibited if the only cavitation nuclei available are bounded by structures that limit their ability to expand.
5. A good index for the production of inertial cavitation by pulsed ultrasound in water at a given frequency is the peak negative pressure p_- [rarefactional pressure (p_r)].

13.6 Bioeffects of Noninertial Cavitation Involving Free and Stabilized Gas Bodies in Non-Mammalian Systems

13.6.1 *Summary*

Research on ultrasonic activation of stable bodies of gas *in vitro* and *in vivo* has generated basic information on potential bioeffects. The primary experimental subjects are gas-filled micropores and contrast-agent gas-bodies *in vitro*, and gas-filled channels in plants and insects *in vivo*. In many cases, the physical oscillation of the gas bodies can be described theoretically (Section 4), which is a critical step in generalization beyond the immediate experiment. Biophysical analysis has yielded an understanding of some pertinent mechanisms, including radiation forces and acoustic microstreaming. The predominant cause of cell death appears to be membrane rupture in regions of high hydrodynamic shear stress. However, additional mechanisms may be involved in producing damage to other systems, such as insect larvae.

The recent emergence of gas-body-based contrast agents for diagnostic ultrasound has been of special interest for nonthermal bioeffects research. These agents can introduce a potential for nonthermal bioeffects of ultrasound into situations, such as sterile culture media

or blood samples, for which cavitation phenomena are normally absent, due to the lack of cavitation nuclei. Reports of research concerning the potential of these agents to mediate bioeffects of ultrasound are beginning to appear in the literature. Observed effects appear to be related to destabilization of contrast agent gas bodies and can be enhanced by improvements in the agents that enhance, for example, persistence between pulses. The effects also appear to be correlated to some extent with acoustic emissions from the gas bodies, such as the second harmonic or subharmonic, which suggests a possible correlation of bioeffects potential with contrast-associated features in images formed from received emissions. The microscale effects would likely be clinically subtle, and their medical significance remains to be determined. As information accumulates, the possibilities for bioeffects, such as hemolysis, sonoporation, lysis, and erosion of monolayers, can be related to potential clinical risks and weighed against the clinical benefits contrast agents provide to the diagnostic process.

The basic knowledge gained from research on activation of stabilized gas bodies in plant and insect tissue is highly relevant to the problem of defining the potential for bioeffects of medical ultrasound. Many effects are readily produced by pulsed ultrasound, even with short pulses and low duty cycles characteristic of diagnostic applications. The frequencies of maximal oscillation for some gas bodies are near or within the range of medically relevant frequencies. The frequency dependence of most observed effects of GBA in tissue are similar, with threshold intensities roughly proportional to frequency (pressure amplitudes roughly proportional to the square root of frequency). This frequency dependence and some selected thresholds are summarized in Figure 8.1. It may be noted that data for mammalian lung are included in this figure, along with those for plant and insect subjects. The presence of gas bodies is crucial in producing the effects observed for all of these situations. However, the specific mechanism for the action probably varies from one situation to another.

13.6.2 Conclusions

1. Biological effects, such as membrane damage and cell death, can be produced *in vitro* and in plant tissues by ultrasonic activation of stabilized gas bodies at pressure amplitudes below the thresholds for inertial cavitation.
2. If suitable gas bodies are present, bioeffects, such as sonoporation, cell lysis and erosion of monolayers, are possible under

conditions of pressure amplitude, frequency, pulse mode, pulse waveform, and cell density that are relevant to medical applications of ultrasound.

3. Biological effects from activation of stabilized gas bodies have been demonstrated *in vitro* for gas-filled micropores and contrast-agent gas bodies, and *in vivo* for plants, insects and mammalian lung (Section 8).
4. The findings with gas-body-based contrast agents are particularly relevant for diagnostic ultrasound; bioeffects, which might be subtle clinically, have been reported in *in vitro* studies using diagnostic instruments.
5. For therapeutic ultrasound applications, such as lithotripsy or high-intensity focused ultrasound, vigorous inertial cavitation activity may be initiated in the presence of gas-body-based contrast agents. This potential remains for hours after the loss of the contrast agent because of cavitation nuclei stabilized by remnants of the agents.

13.7 Bioeffects of Inertial Cavitation *In Vitro*

13.7.1 Summary

A large variety of exposure vessels is available for undertaking ultrasound exposure of cells *in vitro*. The vessels can influence the ultrasonic field, and their choice can facilitate the study of mechanisms of action. Additionally, the rotation of the vessel and/or the infusion of gas-containing microbubbles in the cell exposures can facilitate or mitigate the inertial cavitation induction of bioeffects.

Cell lysis has been the most frequently studied parameter for ultrasound-induced cellular effects in vitro. The lysis occurs (1) from shear forces in the hydrodynamic fields associated with bubbles driven by radiation force through the medium, and (2) from forces present during implosions of the bubbles. Examples of nonlytic effects for which results have been confirmed include: reversible modification of electrical activity, production of single-strand breaks in DNA within cells, mutation and reversible changes in cell permeability to large molecules.

The value of studies employing *in vitro* systems is that they afford excellent control over many biological (*e.g.*, cell number and size), physical (*e.g.*, precise dosimetry), and chemical (*e.g.*, nucleation, medium viscosity) factors, thereby facilitating the study of mechanisms of action. The relevance of the results from studies employing

in vitro systems to *in vivo* situations is often unclear, but those studies whose *in vitro* conditions approximate those *in vivo* have a greater chance for reasonable extrapolation.

13.7.2 Conclusions

1. Studies of ultrasound-induced biological effects *in vitro* have provided insights into the nonthermal mechanisms by which cells are affected by ultrasound. Such studies may suggest hypotheses that can be tested in laboratory animals. In some cases, there has been good agreement between results of *in vitro* experiments and those of *in vivo* experiments with mammals. The more closely the *in vitro* conditions approach those of living mammals *in vivo*, the greater is the potential for relevance of the *in vitro* findings to questions of health and safety.
2. Generalized heating is usually minimal during *in vitro* investigations of effects produced by ultrasound in cell suspensions, and observed effects are usually associated with cavitation mechanisms.
3. The exposure system for studying ultrasound-induced bioeffects *in vitro* can have a substantial effect on the results. When the exposure vessel is in the form of a tube, its rotation is commonly used to enhance the probability of inducing a bioeffect *in vitro* with ultrasound exposure.
4. In the presence of gas bodies, there is an association between ultrasound-induced cell lysis and cell density *in vitro*; as the cell density increases, the percentage lysed decreases, but the total number of cells lysed may actually increase.
5. Sonochemicals generated during inertial cavitation can affect cells *in vitro*, for example, by production of single-strand breaks in DNA.
6. Ultrasound contrast agents increase the nucleation of the exposure medium *in vitro* and can enhance lytic effectiveness of the ultrasound exposure.
7. Effects observed on cells that have been exposed to ultrasound *in vitro* and survived the exposures include reversible changes in electrical activity, single-strand breaks in intracellular DNA, mutation, and reversible permeability of cells to large molecules.
8. *In vitro* experimental research has demonstrated DNA damage in viable cells from CW exposure under special conditions, with contrast agents present, above a threshold of about 0.5 MPa for a frequency of 2.2 MHz. This is in close agreement with the

theoretically predicted threshold for inertial cavitation, thus suggesting that the DNA damage resulted from the action of cavitation-produced free radicals.

13.8 Bioeffects of Acoustic Cavitation in Mammalian Tissues

13.8.1 Summary

A substantial body of evidence is consistent with the conclusion that acoustic cavitation can occur in tissues exposed to CW ultrasound or pulses of ultrasound longer than 1 μ s if the pressure amplitude is sufficiently great. The required pressures range from less than 1 MPa to greater than 10 MPa depending on conditions of exposure and the characteristics of the tissues.

To relate directly to the question of hazards associated with cavitation produced by pulsed diagnostic ultrasound, exposures used in studies of biological effects should be applied in repeated short pulses with temporal-average intensities low enough to make it possible to eliminate heating as the primary mechanism of the effect. Whether cavitation-related effects occur depends critically on the extent to which cavitation nuclei exist, which may be much different *in vitro* than *in vivo*. Figure 8.1 summarizes the threshold data currently available on biological effects observed in tissues after exposure to pulsed ultrasound. At frequencies commonly used in diagnosis (2 to 10 MHz), thresholds for relevant biological effects in mammalian tissues are above 1 MPa.

The threshold acoustic pressures for effects in tissues with stabilized populations of bubbles depend only weakly on the pulse-repetition rate and, hence, only weakly on the temporal-average intensity. This has been shown in systems as different as mouse lung and *Drosophila* larvae.

A study was devoted to exploring the influence of timing on penetration of hemorrhage through adult murine lung. It showed that, even with the same total on-time, the threshold was higher when the total exposure was delivered in a shorter time. The explanation may lie in a time-dependent change in the acoustic properties of the lung resulting from irreversible changes in tissue structure that favor penetration of the sound wave; *i.e.*, the initial acoustic insult to the tissue may initiate pooling of fluid near the point of entry of the sound beam. This may account for the time-dependent penetration of lesions into the lung. Normal lung has been shown, by several groups,

to have a very high attenuation for ultrasound. Yet, exposures only a little above threshold extending over a period of 3 min have been shown to penetrate the mouse lung. When ultrasound with the same total *on-time* is delivered to the lung in 0.3 min, however, the threshold pressure for penetration was shown to double.

It appears that bioeffects *in vivo* from diagnostic examinations cannot be completely ruled out. Thresholds for damage to lung are well within the capabilities of diagnostic-ultrasound systems in current use. Thresholds for hemorrhage related to bubbles in the gastrointestinal tract or in blood vessels with contrast agents are near the upper limits of modern diagnostic systems. These bioeffects are sometimes minor and may be acceptable under some conditions when compared to the diagnostic benefits derived. Although cavitation may be destructive, cavitation events are highly localized phenomena. Rare, destructive effects on a small number of cells may be difficult to detect in a mammal and may not be important to the overall well being of the organism were they to occur. Moreover, there is evidence that cavitation has a higher threshold in tissues than in liquids such as water where it is commonly studied, and, that, if it occurs in mammalian tissues, it may be less violent than it would be under comparable exposure conditions in water. Thus, extrapolations from classical theory for inertial cavitation may be overly alarming because the assumptions upon which the theories are based are not directly applicable to tissues.

Derated focal outputs of many diagnostic units (Section 10) exceed the thresholds for lung hemorrhage shown in Figure 8.1. There are a number of specialized applications in which the focus of the sound field may occur at the surface of the lung. Examples include cases where lung tissue is exposed to ultrasound through the heart. Perhaps, the greatest concern might be the inadvertent use of a Doppler instrument with a standoff for the examination of the neonatal heart. During pulsed, color-Doppler sampling of flow through the pulmonary valve, the surface of the lung moves through the focus of the beam as the patient respire. In transesophageal echocardiography, the focus of the transducer commonly intersects the surface of the lung as the transducer is manipulated to attain optimal positioning for image acquisition. Doppler sampling of pulmonary venous flow and subclavian artery/vein flow also puts the focus of the beam on the surface of the lung. However, the derated focal pressures have little meaning if the lung is exposed directly and if the focus is much deeper than the surface of the lung, as would be the case when the transducer is in contact with the chest wall over the lung. In that case, acoustic pressures near the source are more likely to give information relevant to lung damage than acoustic pressures at the focus.

It appears that the largest source pressures from currently available commercial instruments approach levels necessary to cause macroscopic hemorrhaging of lung tissue in standard diagnostic procedures. For these reasons, the possibility of lung hemorrhage should be included in the broad assessment of potential hazards of diagnostic ultrasound.

Other structures containing gas, such as the intestine, are vulnerable as well. Observations available at the present time suggest that the threshold for intestinal hemorrhage is near the upper limit of the outputs that are available in current commercially available diagnostic-ultrasound systems. The use of microbubble ultrasound contrast agents increases the number of cavitation nuclei in the blood by orders of magnitude. The (very few) studies available at the present time, however, suggest that the acoustic pressures required for destructive cavitation activity in animals at frequencies above 2 MHz may be greater than exist in the fields currently used in diagnostic procedures.

13.8.2 Conclusions

1. Tissues containing stabilized gas bodies are more at risk in terms of a nonthermal mechanism of action from diagnostic ultrasound exposures than tissues lacking these inclusions.
2. For a given tissue, the threshold of known, potentially adverse, biological effects from diagnostically relevant pulsed ultrasound depends strongly on *in situ* values of the acoustic pressure (during the pulses) at a given frequency but only weakly on other acoustic parameters such as the temporal average intensity, pulse duration, and repetition rate, the exposed volume of tissue and the total exposure time.
3. Threshold acoustic pressures for many known nonthermally mediated biological effects (for example, hemolysis, lung and intestinal hemorrhage) increase as the frequency of the ultrasound increases.
4. Once the acoustic pressure exceeds threshold level for an adverse nonthermally mediated biological effect at a given frequency, the extent of damage depends strongly upon the acoustic pressure, as well as on the exposed volume of tissue and the total exposure time; it also depends, to some degree, on such parameters as the pulse duration and repetition rate.
5. Threshold pressure amplitudes for potentially adverse nonthermally induced biological effects that have been confirmed in animal studies employing diagnostically relevant pulsed

ultrasound are above 0.5 MPa *in situ* at 2.5 MHz. The outputs of commercially available diagnostic-ultrasound systems can exceed this pressure.

6. Pulmonary capillary bleeding has been observed in neonatal, young and adult mice and swine, and adult rats, rabbits and monkeys, after exposure to diagnostically relevant, pulsed ultrasound at threshold pressure amplitudes of about 1 MPa *in situ* at 2.5 MHz. The outputs of commercially available diagnostic-ultrasound systems can exceed this pressure.
7. Pulsed ultrasound can cause bleeding in normal murine intestine. The threshold pressure amplitude for intestinal hemorrhage in mice is about 3 MPa *in situ* at 2.5 MHz; this is close to the highest estimated *in situ* exposure levels from commercially available diagnostic-ultrasound systems.
8. The induction of extravasation and petechial hemorrhage and hemolysis have been reported in mammalian tissues exposed to diagnostic ultrasound when gas-body-based ultrasound contrast agents are present.
9. There are no confirmed adverse nonthermal effects *in vivo* from ultrasound exposures in which the value of $pf^{-0.5}$ *in situ* is less than 0.5 MPa MHz^{-0.5}.

13.9 Models for Exposure Estimation in Human Beings

13.9.1 Summary

Models of human tissue have been adopted to assist in estimating acoustic fields in the human body during diagnostic procedures (NCRP, 1992). These models are based on measured values of the attenuation in tissue. Summaries can be found in NCRP (1992) and WFUMB (1992). For a homogeneous soft-tissue path between source and site of interest, the NCRP (1992) recommended using an attenuation coefficient of 0.05 Np cm⁻¹ MHz⁻¹ (~0.4 dB cm⁻¹ MHz⁻¹). ODS (AIUM/NEMA, 1992) uses 0.3 dB cm⁻¹ MHz⁻¹ for all applications (Model H₃). The latter model has the advantage of convenience; it does not underestimate the attenuation in most applications.

As further exposure information becomes available and the need is recognized for more accurate estimates, exam-specific models should be developed for identified large classes of patients who might have sensitive tissues exposed to significantly higher fields than are estimated by the general model. As developed and accepted, the models may be implemented on the equipment displays or estimated

by users from nomograms and other simple rules. Relatively little attention has been paid to attenuation paths and other exposure conditions in applications other than obstetrical examinations. More studies should be performed, published in the literature for various specialties, and emphasized in training, to help assure appropriate interpretation of the tissue model used in calculating TIs and MIs in specific applications.

Certain obstetrical and ovarian examinations are examples of studies in which special models are needed. In particular:

The fixed-path model at 1 dB MHz^{-1} is the only one that is appropriate for conservatively predicting attenuation by overlying tissues for all types of obstetrical studies. Available experimental data indicate that the attenuation from the overlying tissues in first-trimester and, possibly, second-trimester examinations, is higher than the predictions of this model in 90 to 97.5 percent of the examinations through the full bladder.

This previously recommended fixed-path model (NCRP, 1992) is superior to the homogeneous-attenuation model for transcutaneous obstetrical examinations, particularly for scanning through the full bladder and amniotic sac. Use of separate models by trimester may not be necessary, as little error from underestimation of exposure would be produced by use of a single, fixed-path model of 1 dB MHz^{-1} . In fact, for scanning through the full bladder and amniotic sac, the attenuation probably is usually less for first trimester than second and less for second trimester than for third. In such cases of long fluid paths, the user should be aware that ODS indices MI and TIB (see Section 10 and Appendix B) provided by present ultrasound systems may understate the exposure to the fetus.

Model H_3 (which assumes homogeneous tissue with an attenuation coefficient of $0.3 \text{ dB cm}^{-1} \text{ MHz}^{-1}$) is probably applicable in several large classes of obstetrical examinations. It can be used for studies in which there are no lengthy fluid paths or in modest output situations in which occasional, large underestimates of exposure can be accepted. However, with a large fluid component in the path, the underestimation can be as large as 2 dB MHz^{-1} in the attenuation along the path preceding the target tissue; at a frequency of 4 MHz this would lead to underestimates of TIs and MIs by factors of six and three, respectively.

A model of $0.3 \text{ dB cm}^{-1} \text{ MHz}^{-1}$ is reasonable for the several obstetrical examination types, such as empty-bladder imaging. If used for all of the examination types, the model would predict TIs and MIs which are two times and 1.4 times lower, respectively, than those

based on the best individual estimates, in over five percent of the full-bladder, first-trimester examination cases.

As exposure estimates *via* accepted general models approach critical values for obstetrical examinations, more detailed exposure estimates can be made using attenuation estimates based on properties such as measured minimal overlying tissues or maternal weight. The same might be true for other examinations with low-attenuation-propagation paths in specific cases. Examples of nonobstetrical, low-attenuation paths arise during (1) interoperative or other scanning through water or other fluid used as a couplant, and (2) during scanning through a fluid-filled stomach or bladder to the intestines and other tissues containing gas bodies. These patient-specific attenuation estimates may be applied to the displayed MIs and TIs and, if need be, on the measured acoustic pressures, powers and intensities produced by the ultrasound system under the conditions of the patient's examination.

In the future, it may be possible for the operator of equipment to estimate rather closely and easily the attenuation in each individual case when high outputs appear to be required. So called "tissue-characterization algorithms" have been studied for some time to calculate the attenuation coefficient of tissues based on the change in returned echoes with depth; these and related approaches have been investigated for imaging the tissue backscatter coefficient with correction for attenuation. However, the accuracy of these algorithms is limited, at present, particularly for inhomogeneous tissues. The highest outputs should not normally be required in cases of low or even average attenuation.

13.9.2 Conclusions

1. The derating model (H_3) used by ODS, which assumes homogeneous tissue with an attenuation coefficient of $0.3 \text{ dB cm}^{-1} \text{ MHz}^{-1}$, is conservative (underestimates the attenuation) in nearly all examinations, including several large classes of obstetrical examinations. However, where lengthy fluid paths are involved, the use of this model may result in occasional large overestimates of the attenuation.
2. The attenuation by overlying tissues for all types of obstetrical examinations is greater than 1 dB MHz^{-1} . Therefore, as opposed to the H_3 model, the fixed-path model at 1 dB MHz^{-1} , does not overestimate the attenuation. Compared with other models considered, it is the best reasonable-worst-case estimate of

attenuation in obstetrical and ovarian examinations performed through the fluid-filled bladder and other long fluid paths.

3. If greater accuracy is desired than is obtainable from general attenuation models, more accurate estimates can be made for specific cases, based on properties measured in the patient being examined, such as the overlying tissue thickness.
4. Among nonobstetrical low-attenuation paths are those encountered in (a) interoperative scanning, (b) scanning through water or other couplant fluid, and (c) scanning through a fluid-filled stomach or bladder. When scanning the fluid-filled anatomical structures, such tissues as gas-filled intestines or lung may receive increased exposure.
5. Relatively little attention has been paid to attenuation paths and other exposure conditions in applications other than transcranial and obstetrical examinations.

13.10 Employed and Needed Sound Pressure Waveforms

In early diagnostic ultrasound systems, there was little correlation between actual levels and those needed in theory to achieve adequate signal-to-noise ratios. An analysis of 1989 data for a full-featured ultrasound model showed that manufacturers were beginning to use fields that reflected the levels needed in many applications. Very few independent and periodic checks of ultrasound-system outputs are performed in the United States. Most laboratories capable of performing those tests lack the support or mandate to do so.

13.10.1 Summary

Increased output of an ultrasound system can often result in increased image quality. However, an increase can also have little effect on or, in rare cases, can actually reduce the image quality. For a 41 percent increase in peak pressure, the increased imaging depth (effective penetration) is small, on the order of six percent. However, for the same increase in output pressure and a fixed penetration, a 26 percent increase in acoustic frequency, resulting in a 59 percent reduction in the area of the focal spot, is possible for recording signals from blood. This translates to a 106 percent improvement in overall (volumetric) spatial resolution in the absence of nonlinear and phase-aberration effects.

13.10.2 Conclusions

1. While few experiments have been performed to conclusively demonstrate the following conclusions, signal detection theory, and the simple analyses presented here, illustrate some of the advantages and disadvantages of an increase in peak-output acoustic pressure. It should be noted that the physics of acoustic saturation places upper limits on attainable fields at large depths and high frequencies. Advantages from increased output (acoustic pressure as well as intensity) involve probable increases in the available ultrasonic information (*e.g.*, image quality) and/or reduced examination time. Specific advantages and disadvantages are listed below.

Potential health-benefit advantages of increased acoustic output include some combinations of:

- a. increased imaging depth
- b. improved resolution
- c. increased signal-to-noise ratio
- d. the possibility of second-harmonic imaging in which the signal-to-noise ratio is often increased in difficult imaging situations
- e. during harmonic imaging of contrast agents, increased sensitivity for slower-moving or smaller concentrations of agent-containing blood or tissues

Potential disadvantages or counterbalancing effects of increased output include:

- a. no dynamic-range or sensitivity improvement if the lower-signal limit is controlled by phase-aberration effects
- b. an increase in risk of occurrence, or in the extent or severity, of adverse biological effects when the output is above relevant threshold levels
- c. during imaging of contrast agents, increased rate of destruction of the agent; although this leads to the release of free bubbles, which is desired for achieving effective contrast, it also causes a decrease in the duration of contrast enhancement

2. In 1991, FDA increased the limiting-guidelines spatial peak, time-averaged intensity levels for nearly all applications to the levels previously allowed only for peripheral vascular studies (FDA, 1991). For general and obstetrical examinations, these intensities were allowed to increase by a factor of almost eight. The clear improvement since that time, in frame rate and quality of both CFIs and multiple-focal-zone gray-scale images, has been made possible largely by the change in allowed output

intensity. Improvements were also made possible, particularly at higher diagnostic frequencies, by a change in the peak acoustic output guideline from 190 W cm^{-2} for the derated SPPA intensity to 1.9 for MI.

3. In some diagnostic applications, use of outputs above damage thresholds may be justified when it is determined that there is net health benefit. In the risk/benefit analysis that must be made, there is no substitute for the judgment of a user who knows the patient's needs and is informed about the level of exposure and the potential for adverse biological effects at the site of investigation under those exposure conditions.

13.11 Temperature Elevation and Its Biological Effects

13.11.1 Summary

In the interim since NCRP Report No. 113 (NCRP, 1992) was published, there has been continued progress in understanding the response of biological systems to temperature change, and in knowledge of temperature increases that occur during exposure to ultrasound. Further, evidence has been found that HSPs are produced as a response to stressors of various kinds (not only to hyperthermia), and more has been learned about genetic and biochemical mechanisms by which HSP appear to confer protection. Additional evidence has been found for hyperthermia as a teratogen in laboratory animals, and it has been advised that women be cautious about exposure to elevated temperature during pregnancy, although the existing evidence on teratogenicity of hyperthermia for human beings is less certain.

Examination of existing literature on teratological effects of exposing pregnant animals to heated environments indicates that results depend strongly on the time course of the core temperature elevation. Re-analysis of available data was done (Section 11.3) to determine equivalent times (t_x) for producing the same effects in hypothetical exposures during which the temperature elevation was constant at selected values (x), as well as corresponding temperature elevations (T_{10}) for which the observed effects would occur in 10 min.

Recent studies in which biological systems were exposed to ultrasound have provided new insights into effects caused either by hyperthermia alone or by a combination of thermal and nonthermal mechanisms. Temperature rise is implicated in the production by CW ultrasound of petechial hemorrhages in murine intestine and

increased cerebral blood flow in neonatal rat. However, heat was ruled out as the primary cause of the reduced aortic pressure in frog heart that results from exposure to a single pulse of ultrasound. Also, while heat production accompanied the degassing that occurred during *in vitro* exposures of fixed erythrocyte suspensions to CW ultrasound, the dependence of the rate of degassing on cell density was explained in terms of nonthermal mechanisms.

In NCRP Report No. 113 (NCRP, 1992), basic equations were presented for predicting the temperature rise produced by ultrasound, and solutions were discussed for special situations relevant to applications of diagnostic ultrasound; also, TI was defined, and proposed as an indicator of safety from thermal injury. Since that report was published, there has been further development of theory and of its application to medical ultrasound. Alternative approaches have been offered that may lead to reduced computational time or higher accuracy. Special approximate formulae developed for ODS have been accepted by the FDA for regulatory purposes. Many manufacturers now provide real-time display of TIs that are computed from standardized algorithms. ODS algorithms are often conservative, predicting temperature elevations that are higher than are likely to occur clinically. However, there are situations where the reverse is true, for example, when the measurements in water, made as required for ODS algorithms, are affected by saturation associated with NLP.

In the last few years, numerous investigations have involved measurements of temperature rise produced by ultrasound in TMM; these are gels designed to have acoustical and thermal characteristics similar to those of mammalian tissues except that perfusion is usually absent. It can be concluded from this work that the temperature field produced by a well defined ultrasound beam in a homogeneous medium of known characteristics similar to those of soft mammalian tissue can be predicted well by computations based on solutions of Equations 11.1, 11.7 or 11.8. Even for the ultrasound fields of transducers actually used in applications of diagnostic ultrasound, approximate methods have been found to be satisfactory for predicting temperature distributions in tissue-mimicking homogeneous media. In an exposure of bone to ultrasound, the simple formula in Equation 11.6 was found to predict reasonably well the temperature rise. In some situations, the temperature rise is affected significantly by (1) extra heating arising from the transducer itself, (2) cooling produced by acoustic streaming, (3) extra absorption when gas-filled cavities are in the field, (4) shear waves set up in mineralized tissues, and (5) NLP in water or other media of similar acoustical characteristics.

Investigations have also been made into the increase of temperature produced *in vivo* by ultrasound in mammalian systems, such as fetal brain, fetal soft tissue, and neonatal brain. In the studies involving brain within the skull, it was found, as expected, that the temperature rise was greatest near the skull. However, it appears that measured values of the maximal temperature rise within the skull were much smaller than would be calculated from Equation 11.6; several reasons were suggested for this. In the neonatal study, it was found that ultrasound caused a considerable increase in cerebral blood flow although the measured rise in temperature was only 1.3 °C. In two studies designed specifically to allow comparison between measured and computed values of the temperature rise produced by ultrasound in the fetus, reasonable agreement was found with theory based on solutions of Equation 11.1, although measured values sometimes exceeded those predicted.

The normal near-term human fetus can be slightly warmer (about 0.5 °C) than its mother's core temperature. Indirect evidence suggests that this temperature differential develops during the third trimester of pregnancy. A recognition of this temperature differential may be important for situations in which a temperature increment is anticipated in relation to the diagnostic-ultrasound exposure of a third-trimester fetus.

Medical applications to hyperthermia and surgery, in which tissues are heated in a controlled manner by pulsed and focused ultrasound, have advanced in the last several years. Theory based on solutions of Equation 11.1 or 11.7 has been found to be very useful in optimizing treatment design. Uniform temperature over a tumor has been achieved by using arrays to shorten the total treatment time, thus minimizing uncertainties caused by perfusion.

13.11.2 *Conclusions*

1. Hyperthermia has been found to be teratogenic in laboratory animals; it is presumed to be true also for human beings.
2. By using available theory based on classical equations for conductivity of heat, it is possible to compute accurately the temperature rise produced by a well-defined ultrasound field in a nonperfused homogeneous medium of known acoustical and thermal properties. When high accuracy is not required, relatively simple algorithms can be used for estimating the temperature rise.
3. Prediction of the temperature rise produced by ultrasound in a mammalian system *in vivo* is more difficult because the

propagation path is more complex and perfusion affects heat transport. Nevertheless, reasonably accurate estimates can be made. Excellent progress in temperature predictions has been made in medical applications of ultrasonically induced hyperthermia applied to specific situations in ophthalmology and cancer therapy.

4. Prediction of the temperature rise produced during examinations with diagnostic ultrasound is especially difficult because of the complex modes of operation utilized by modern equipment. Here predictions are usually not capable of high accuracy, although the maximal temperature rise is often predicted within a factor of two. TIs, such as those defined in NCRP Report No. 113 (NCRP, 1992) and ODS, are capable of providing users with better information on safety from thermal damage than any single directly measurable acoustical parameter such as acoustic power or intensity.
5. Present federal guidelines in the United States [for compliance with Track 3 of the 510(k)] allow an SPTA intensity of 720 mW cm^{-2} for all applications of diagnostic ultrasound, except those to ophthalmology; previously, the corresponding level was 94 mW cm^{-2} for applications to fetal imaging. This change corresponds, for the latter applications, to a possible 7.7-fold increase in all TIs since 1991.
6. Under some conditions, transducer self-heating can be an important factor, and its contribution can result in a significant increase in temperature near the transducer surface during a diagnostic examination.
7. An analysis (Section 11.3) of available information from 34 carefully performed and well documented experiments in which pregnant animals were exposed to heated environments while the core temperatures were monitored shows a distribution of values for the equivalent constant core temperature rise (T_{10}) which produced craniofacial abnormalities in 10 min: the mean value of T_{10} was $4.1 \text{ }^\circ\text{C}$, the standard deviation was $0.52 \text{ }^\circ\text{C}$, and the lowest value was $3.1 \text{ }^\circ\text{C}$.

13.12 Epidemiology of Ultrasound Exposure

13.12.1 Summary

It appears from findings reviewed in this Section, that epidemiological studies and surveys of clinical experience have yielded no firm

evidence of any adverse effects from diagnostic ultrasound, in spite of large clinical usage. This apparent safety is of paramount importance to the physician. While recognizing the limitations of clinical trials, these still represent, to the physician, the ultimate tests of any drug or agent. Experience shows that, even when all laboratory tests have been free of adverse effects, unexpected untoward reactions will frequently be seen when any given agent is administered to a large number of patients.

The inability to find convincing proof of an effect, either from epidemiology or from the physician's experience, does not preclude the possibility of it happening. As Equation 12.1 shows, it is difficult to identify a small increase in rate of a commonly occurring event, even if each event is easily seen. Also, subtle effects (such as minor chemical changes and minor behavioral changes), long-term delayed effects, and certain genetic effects could easily escape detection. Overall, the results of epidemiological studies have been reassuring. However, if we are eventually to identify subtle effects, if any, it will probably be necessary to rely on studies of the effects of ultrasound on laboratory animals and extrapolate from these results to the clinical situation. When a clear hypothesis can be generated in this manner, it may be possible to design an epidemiological study that will have the statistical power to determine the extent of the effect and its implication in the human population.

13.12.2 *Conclusion*

A number of epidemiological studies of the use of ultrasound in pregnancy, including several case-control and randomized-control studies, have been performed over the past 20 y. In some studies, there was identified an association of diagnostic ultrasound with one or another bioeffect, such as low birth weight, dyslexia, or delayed speech development. However, the majority of studies have been negative for association with any bioeffect, including low birth weight. Based on the epidemiological evidence to date, there is insufficient justification to warrant a conclusion there is a causal relationship between diagnostic ultrasound and any adverse effect.

It is necessary, however, to realize that the entire database of the epidemiological evidence of human exposure to diagnostic ultrasound is limited to the time prior to 1991, when the FDA relaxed the permissible upper limit of acoustic outputs. Current exposures to the fetus, for example, could be considerably greater than those occurring before 1991. Also, other important changes in the practice of diagnostic ultrasound have been introduced during the past

decade, such as the widespread use of contrast agents. Furthermore, it must be recognized that very large sample sizes would be required in order for epidemiological studies to reveal a small increment in the occurrence of an adverse effect.

Therefore, the comfort obtained from the absence to date of any harm based on epidemiological evidence must be tempered by the fact that there are no epidemiological studies appropriate and adequate for current clinical practice.

13.13 The Thermal and Mechanical Indices

13.13.1 Introduction

Since 1992, manufacturers of equipment for medical diagnostic ultrasound have been able to obtain approval for marketing in the United States by complying with requirements under Track 3 of ODS (see Sections 9 and 10, and Appendix B). According to these requirements, the equipment must include features for real-time display of selected data in the form of indices relating to patient safety. TIs (TIB, TIC and TIS) assist users in assessing the possibility of harm from excessive temperature elevation, while MI relates to the possibility of mechanical damage. When the Track 3 requirements are met, the restrictions on output are relaxed; for example, in applications to fetal scanning the limits on SPTA intensity are raised from 94 to 720 mW cm⁻², an increase by a factor of 7.7.

Equipment is now widely available with features for displaying these indices, and experience is being gained in their use. As concluded earlier (NCRP, 1992) “this [provision of features for display of safety information] is an encouraging development, since it helps users to make the required decisions. The data will be increasingly useful as their accuracy and completeness increase.”

The next subsection deals with discriminating use of ODS indices. When understood, these indices can be of considerable value in making safety decisions. However, they should not be interpreted in an oversimplistic fashion. Table 13.1 briefly lists conditions that should be recognized by the user, under which the indices may either underestimate the potential for risk or overestimate it. These conditions are discussed further in Appendix B.4. Some of the problems can be dealt with by the knowledgeable user, and others may be reduced in the future by improvements in the ways safety information is obtained and presented. In Sections 13 and 14, some of the conclusions and recommendations relate to improvements of this latter kind.

TABLE 13.1—*Conditions for which TIs and MIs may be inaccurate.*^a

A. Conditions for which the true values of the acoustic pressure or the temperature rise may be underestimated by the indices (making the estimates overly aggressive)

1. Long fluid path

This affects accuracy of TIB, TIS and MI, and may occur under the following conditions:

- a. Full urinary bladder and amniotic sac
- b. Ascites
- c. Hydrocephalus
- d. Polyhydramnios
- e. Intraoperative examination using saline coupling

2. Transducer surface heating

The temperature rise may be higher than indicated by a TI for any tissue in contact with a heated transducer, especially, if the tissue is not highly perfused.

3. High amplitude ultrasound pulses

As explained in Section B.4, MI, TIB and TIS may be underestimated because, in present procedures, they are based on measurements of the acoustic pressure in water where acoustic saturation may occur.

B. Conditions for which the true or relevant values of the acoustic pressure or the temperature rise may be overestimated by the indices (making the estimates overly conservative)

1. Path through soft tissue

TIB and MI will be overestimated if there is a long sound path through soft tissue before reaching the structure of interest, as will occur under these conditions:

- a. Obese patients
- b. Large muscular patients
- c. Very deep structures (distal to the focal zone)

2. Site of interest is not at the location where the index applies

This can be true for TIS, TIB and/or MI for any of the following:

a. Lung surface

The MI typically overstates the true value when applied to lung exposure, because the ultrasound is seldom focused on the lung.

b. Any structure not located at the site of maximal temperature rise or maximal acoustic pressure.

This includes fetal examinations because TIB does not always apply at the focus and TIS usually does not apply there.

3. Conditions where the time required to reach the steady-state

temperature predicted by TI is much greater than the *dwelt time* (see Glossary) in a typical examination, as is often true for TIS

^aSee Appendix B.4 for further details.

13.13.2 Conclusions

1. TIs and MIs of ODS (AIUM, 1994b; AIUM/NEMA, 1992) provide indications of the relative potential for bioeffects; these are helpful to users who are knowledgeable in their application.
2. The values of these indices that are displayed on medical ultrasound equipment are based on specific distance and attenuation assumptions in ODS intended for application to clinical conditions. In bioeffects research where such equipment is used, the exposure conditions may vary significantly from those assumed in calculating the displayed TI or MI. In particular, *in vitro* or small animal *in vivo* exposures typically involve short tissue paths and long water paths. Therefore, in such experiments the output indices displayed may differ significantly from the actual values of the physical exposure parameters at the site of interest.
3. The TI proposed in NCRP (1992), and its variants (TIB, TIC and TIS) adopted by ODS (AIUM/NEMA, 1992; FDA, 1997) (see Appendix B), provide useful estimates of tissue temperature increments that result from exposure to ultrasound, though subject to errors described in Table 13.1. In the absence of significant effects from transducer self-heating and long fluid paths to critical structures, examinations of afebrile patients can be considered free from producing thermal bioeffects, if the relevant TI is less than one.
4. The MI adopted by ODS (AIUM/NEMA, 1992; FDA, 1997) (see Appendix B) is useful for safety considerations, though subject to errors described in Table 13.1. For example, adverse, non-thermal, biological effects would not usually be expected when MI is less than approximately 0.5, even for the fetus and for tissues with stabilized gas bodies.
5. Decreasing the acoustic output in order to reduce MIs and TIs considerably below their thresholds for bioeffects level 0.5 would probably do little to improve safety and could compromise the quality of the diagnostic information.
6. Commercial equipment which has become available in the United States since 1992 allows fetal scanning under conditions for which the maximal possible TIBs (for different systems and transducers) range from about 0.1 to 10. Use of conditions corresponding to the highest TIBs may be hazardous if the temperature rise is maintained for more than a few seconds.
7. There is no experimental evidence indicating that adverse non-thermal effects would occur during examination of any nonfetal tissues without stabilized gas bodies, even if the highest outputs of diagnostic-ultrasound equipment now commercially available in the United States were employed.

14. Recommendations

14.1 Introduction

During the past decade the diagnostic capabilities and applications of ultrasound have increased dramatically. The increased diagnostic power comes partly from improved design, availability of new materials and computational aids, and employment of new procedures. Among the latter is the use of gas-body-based contrast agents. The diagnostic improvements also come partly from the use of higher acoustic intensities. In the United States, the relaxation of federal controls, which occurred in 1992, allowed an increase in SPTA intensity for applications to fetal scanning by nearly a factor of eight.

Along with the improvements in capabilities has come increased understanding of biological effects that can be produced by present-day diagnostic ultrasound under some conditions. These effects are partly of thermal and partly of nonthermal origin. Important steps have been taken to convey safety information to users so that risks can be considered along with benefits of various procedures and operating conditions. The need for continuing improvement of this information is recognized as the medical community assumes increasing responsibility for maintaining the excellent safety record that diagnostic ultrasound enjoys.

A user could select the operating conditions for an optimum ratio of benefit to risk, if it were possible to know, quantitatively, how both of these depend on the many variables that characterize exposures to ultrasound, biological responses to these exposures, and patient needs. Of course, this ideal situation does not exist, and it is necessary to exercise judgment based on the best available knowledge. To evaluate the risk, the user must (1) be able to estimate the exposure level at the location of the tissue under study, and (2) understand the possible biological effects that may occur in those tissues under the anticipated exposure conditions. The following recommendations relate to these needs; they are addressed partly to manufacturers and others who must provide accurate data on relevant characteristics of the ultrasound fields produced by their equipment, and present them to users in a convenient form. They are also addressed partly to users

and educators, as well as to regulating agencies and professional organizations.

14.2 Exposure Quantities

1. The acoustic-pressure amplitude (Section 5.11) at the point of interest for a given frequency should be used as a primary predictor of the threshold for adverse, nonthermal biological effects of an ultrasound exposure. For biological effects resulting from a thermal mechanism, the acoustic power and acoustic intensity are important quantities.
2. Ordinarily, it is necessary to infer the *in situ* field from measurements in water. The practice, now required of manufacturers by ODS, of estimating acoustic quantities in the body of a patient by derating measurements made in water (Appendix B) at high amplitudes should be discontinued, because of errors associated with NLP in water.
3. To estimate acoustic quantities in the body of a patient, these quantities (if measured in water) should be determined under small-signal conditions, derated and extrapolated as linear functions of the output levels. This procedure results in conservatively large values for the acoustic quantity in most applications, though its use can sometimes lead to underestimation of the temperature rise (Appendix D). When greater accuracy is desired, corrections for effects of NLP in tissue can be made either theoretically or experimentally.
4. In derating acoustic field measurements made in water to obtain estimates of fields that will be present in tissues, one must consider the acoustic characteristics of, and path lengths through, the tissues in the sound path. For a path consisting largely of soft tissues such as liver or kidney, NCRP reaffirms its previous recommendation that the specific attenuation coefficient for such tissues be approximated by $0.05 \text{ Np cm}^{-1} \text{ MHz}^{-1}$ ($0.44 \text{ dB cm}^{-1} \text{ MHz}^{-1}$) (NCRP, 1992).
For transcutaneous obstetrical examinations where aqueous media, such as the full bladder, constitute a significant part of the sound path, NCRP reaffirms its previous recommendation (NCRP, 1992) that a fixed-path model with an attenuation of 1 dB MHz^{-1} be used in derating.
5. The exposure parameters that give rise to a biological effect in an experimental investigation should be reported in terms of the local acoustic or thermal parameters measured at the site

(see Recommendation 1 of this Section). If a clinical ultrasound system is used in the investigation, there may be some justification for reporting the displayed TIs or MIs corresponding to conditions under which bioeffects are observed, but these should not substitute for measurements at the site of interest. Furthermore, clinicians should be cautious in interpreting on-screen display MI or TI values specified in research reports as exposure parameters for conditions that may differ greatly from the conditions presumed in the calculation of the indices as defined in ODS.

14.3 Safety Criteria

1. Safety evaluations must consider the characteristics of the tissue being exposed. Thresholds for nonthermal biological effects are lowest in (a) tissues which naturally contain gas bodies, for example, postnatal (including adult) lung and intestine, and (b) all tissues in the presence of introduced gas bodies, such as gaseous ultrasound contrast agents.
2. A risk-benefit decision is especially important if the anticipated acoustic-pressure amplitude at the surface of aerated lung tissue exceeds 1 MPa.
3. A risk-benefit decision may be important if MI exceeds 0.5. The acoustic pressure at the site of interest may be either underestimated or overestimated by MI, and it is necessary to consider the nature of the clinical situation in order to make an informed judgment (Table 13.1).
4. A risk-benefit decision is especially important if the anticipated temperature rise of an embryo or fetus exceeds 3 °C for a duration of 10 min.
5. The duration expected to be important in risk management depends strongly on expected temperature. The duration should be decreased by one-half for each 0.5 °C by which the rise is above 3 °C and, if the temperature rise exceeds 1 °C, may be doubled for each 0.5 °C by which the rise is less than 3 °C. (No adverse thermal effects have been observed in which the temperature rise was 1 °C or less from exposures of duration up to more than 1,000 min.)
6. A risk-benefit decision may be important if TIB, TIC or TIS exceeds one. The temperature rise at the site of interest may be either underestimated or overestimated by a TI, and it is necessary to consider the nature of the clinical situation in order to make an informed judgment (Table 13.1).

14.4 Equipment Features; Output and Product Information

1. Ultrasound systems should be designed to improve image quality and diagnostic information in general by using only those acoustic-wave amplitudes that are needed for the application.
2. Diagnostic systems should be designed where possible to keep exposures to the patient close to those required for a given examination (Section 10.6.2).
3. Information on output levels should be provided to the user for guidance in risk-assessment considerations. This includes labeling on screen or in documentation accompanying the systems that include the information currently required for 510(k) applications and for compliance with IEC (1992).
4. While output information is apparently reported responsibly by manufacturers, spot checks of system outputs should be performed by independent laboratories.
5. The data in the Acoustic Output Tables prepared by manufacturers in obtaining approval for marketing in the United States and the updates of those tables published in the users' reference manuals are in the public domain, and contain valuable information relevant to safety. They should be stored in archives by a professional organization, and made conveniently available to the medical community.
6. Presently available methods have proven valuable for estimating the temperature rise produced by diagnostic ultrasound, though they can and should be improved. Development and testing of theoretical and experimental methods for temperature-rise predictions should be continued.
7. The Output Display process, with its on-screen display of TIs and MIs, is the best source of safety information available to users of medical diagnostic-ultrasound equipment. However, there should be continuous efforts to encourage users to utilize this information, and also efforts to develop methods to make the information more accurate and more complete (see Table 13.1 and Appendix B).
8. Diagnostic ultrasound equipment should be provided with the capability for on-screen display of MI if it can exceed 0.5.
9. Manufacturers of gas-body-based ultrasound contrast agents should inform purchasers (*e.g.*, in product package inserts and other methods) that acoustic cavitation will occur during interaction of diagnostic ultrasound with the agents.

14.5 Responsibilities of Users

1. ODS indices provide crude measures of the risk of adverse effects arising from an ultrasound examination and provide better indications of the change in risk as controls are adjusted. The final benefit/risk assessment should be performed by a user who is knowledgeable in ultrasound dosimetry and biological effects, and who takes into account the index values and the particular details of the patient being examined. Users should be helped and encouraged by development of educational materials designed, specifically, for evaluating benefits and risks of diagnostic ultrasound procedures. Laboratory guidelines for making these decisions and training in these decisions should be documented as part of the accreditation process.
2. For each application, a default setting for the diagnostic-ultrasound system employed should be set, or reviewed, and documented, by the user. The MI and all TIs should be assigned values based on the best available information on bioeffects and, also, on knowledge of the lowest values at which the system employed will yield the required diagnostic information. For example, operation when MI is less than 0.5 and all TIs are less than one poses negligible risk under most conditions (but see Section 14.3). For some situations, the desired diagnostic information can be obtained with settings of the indices in these ranges, while for others, higher outputs should be used when justified by consideration of risk and benefit to the patient. The user may find it helpful to employ a feature of the equipment that provides a reminder signal when a user-selected value of a relevant index is exceeded.

Appendix A

Mechanical Equilibrium of Free Bubbles

It was shown in Section 4 that a sound field can cause growth of a bubble in a liquid by either of two processes: (1) rectified diffusion, *i.e.*, net diffusion into a bubble of gas dissolved in the surrounding liquid (Section 4.1.4); or (2) coalescence of smaller bubbles that are brought together by acoustic-radiation force (Section 4.4.2). It was noted by Blake (1949) that, under some circumstances, bubbles can become unstable and will grow, even if no diffusion or coalescence occurs. This result can be understood by considering the condition for mechanical equilibrium of a single bubble in a liquid, under the assumption that no gas exchange occurs across the bubble surface. For a bubble of momentary radius (R_0) in which the vapor pressure is p_v and the momentary gas pressure is p_{g0} , surrounded by liquid under hydrostatic pressure (P_0), the condition for mechanical equilibrium is:

$$p_v + p_{g0} = P_0 + \frac{2 \sigma}{R_0}, \quad (\text{A.1})$$

where σ is the surface tension at the bubble surface. Suppose a bubble is in equilibrium under these conditions and that the external pressure is then decreased by a positive amount P_A . If a new equilibrium state is possible, the radius will now increase, say, to R and, assuming an isothermal process, the gas pressure will decrease to $p_{g0} (R_0/R)^3$ satisfying the new equilibrium condition:

$$p_v + p_{g0} \left(\frac{R_0}{R} \right)^3 = P_0 - P_A + \frac{2 \sigma}{R}. \quad (\text{A.2})$$

From Equation A.1, the original gas pressure (p_{g0}) can be written as :

$$p_{g0} = P_0 + \frac{2\sigma}{R_0} - p_v. \quad (\text{A.3})$$

Letting y equal the ratio R_0/R , Equation A.2 can be put in the form of a reduced cubic:

$$y^3 + ay + b = 0, \quad (\text{A.4})$$

where $a = -2\sigma/(R_0 p_{g0})$ and $b = (p_v + P_A - P_0)/p_{g0}$. Decrease of the external hydrostatic pressure from P_0 to $P_0 - P_A$ leads to a new equilibrium situation only if Equation A.4 has one or more real positive roots, *i.e.*, if one or more real positive values of $y = R_0/R$ exist that satisfy Equation A.4. Standard methods exist for finding roots of the cubic equation. Insight on possibilities can be gained by referring to Equation A.2 and considering an example.

Figure A.1 shows the hydrostatic pressure $(P_0 - P_A) = [p_v + p_{g0}y^3 - (2\sigma/R_0)y]$ plotted against y when the parameters have the values: $\sigma = 0.08$ Pa m, $R_0 = 2 \times 10^{-6}$ m, $P_0 = 10^5$ Pa, and $p_v = 4 \times 10^3$ Pa. It can be seen that there is a single real positive value of y for which Equation A.4 is satisfied when the hydrostatic pressure $(P_0 - P_A)$ is reduced, provided that it remains greater than $p_v = 4,000$ Pa; however, there are two positive real roots when $(P_0 - P_A)$ is reduced to values lying between $-16,700$ Pa and $4,000$ Pa, and there are none for lower

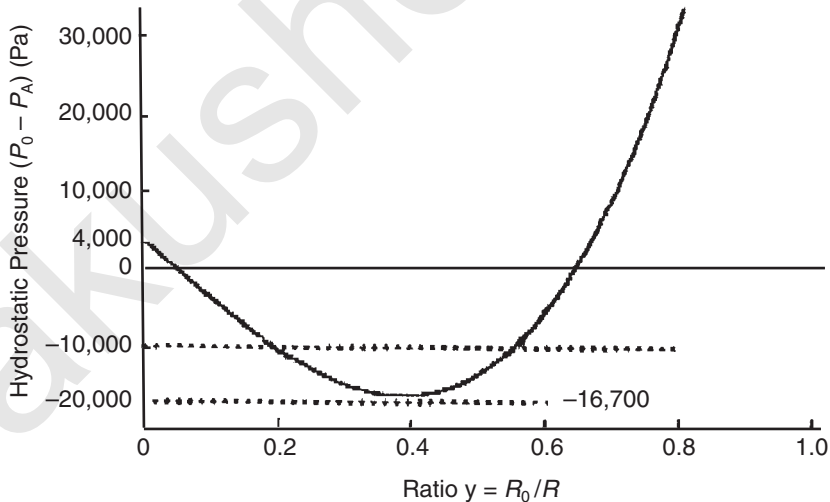


Fig. A.1. Equilibrium relation between the hydrostatic pressure ($P_0 - P_A$) and the ratio $y = R_0/R$ for a spherical bubble initially of radius $R_0 = 2 \mu\text{m}$ in a liquid under a hydrostatic pressure P_0 of 10^5 Pa (see text).

values of $(P_0 - P_A)$. Figure A.2 shows a plot of $(P_0 - P_A)$ similar to that in Figure A.1, except that the abscissa is now $y^{-1} = R/R_0$, the relative radius. Although these figures show that under some conditions there are two equilibrium values of the radius to which a bubble can expand when the hydrostatic pressure is reduced, the equilibrium is stable only at the smaller of these values. For example, one sees from Figure A.2, that, when the hydrostatic pressure is $-10,000$ Pa, the bubble under consideration [whose radius (R_0) is $2 \mu\text{m}$ when the hydrostatic pressure is 10^5 Pa] will be at equilibrium at a normalized radius (R/R_0) of either 1.8 or 5.3. These equilibrium values can be tested for stability by using Equation A.2, whose left side gives the pressure inside the bubble tending to cause expansion, and whose right side gives the pressure tending to cause contraction. At equilibrium the two sides are equal. By calculating values of the two sides of Equation A.2 at, for a hydrostatic pressure of $-10,000$ Pa, values of R/R_0 in the vicinity of each of the two equilibrium values, it is found that deviations from equilibrium near $R/R_0 = 1.8$ tend to bring the bubble back to the equilibrium size, while deviations from $R/R_0 = 5.3$ do the opposite. Thus, an increase

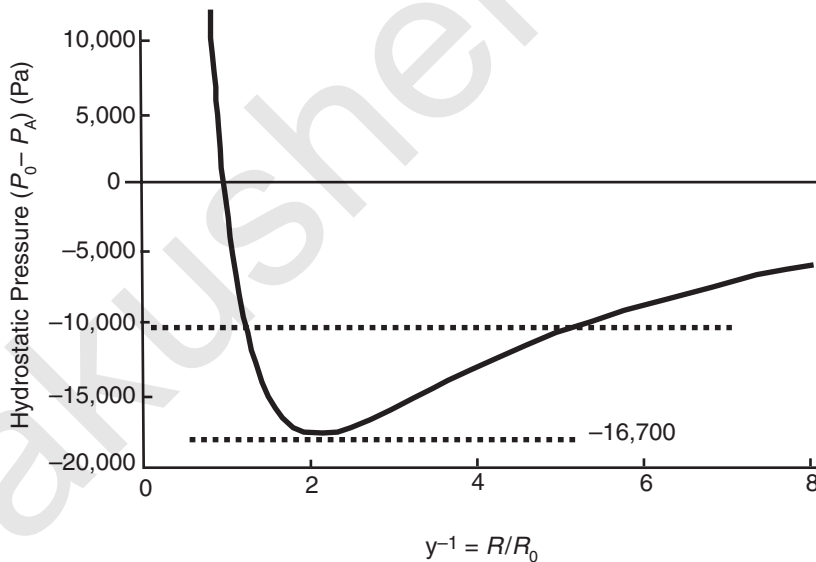


Fig. A.2. Same as Figure A.1 except that here the abscissa is $y^{-1} = R/R_0$. Equilibrium relation between the hydrostatic pressure ($P_0 - P_A$) and the ratio $y = R_0/R$ for a spherical bubble initially of radius $R_0 = 2 \mu\text{m}$ in a liquid under a hydrostatic pressure P_0 of 10^5 Pa (see text).

of the bubble radius beyond the higher equilibrium value causes an imbalance such that the bubble tends to expand even further.

At hydrostatic pressures ($P_0 - P_A$) less than a critical value, *viz.*, $-16,700$ Pa, there are no real positive roots of Equation A.4; *i.e.*, there are no values of the radius (R) at which the bubble under consideration is in equilibrium. This critical value of ($P_0 - P_A$) can be calculated by first determining the value of R at which the minimum occurs. This is done easily by solving for b in Equation A.4 and setting equal to zero the derivative of the resulting expression with respect to y ; from this one finds that the critical value of y is $(-a/3)^{0.5}$ so that the corresponding critical value of R is $R_0 (-a/3)^{-0.5}$. Substituting this value for y into Equation A.4 one obtains the value cited above for the critical value of the hydrostatic pressure, $(P_0 - P_A) = -16,700$ Pa.

The corresponding critical value of P_A , the amount by which the hydrostatic pressure is decreased, is commonly called the *Blake threshold* (Blake, 1949) and given the symbol P_B . For the example being considered, this threshold is $P_B = 116,700$ Pa. In general, the threshold P_B is given by:

$$\frac{P_B}{P_0} = 1 - \frac{p_v}{P_0} + 0.385 s \left(\frac{s}{1 + s} \right)^{0.5}, \quad (\text{A.5})$$

where $s = 2 \sigma/R_0 P_0$.

Appendix B

Output Display Standard

B.1 Introduction

In 1992, a significant document was published jointly by AIUM and NEMA (AIUM/NEMA, 1992; 1998). This document, commonly called the “Output Display Standard” (ODS) established, for the first time in the history of diagnostic ultrasound, procedures for making quantitative safety-related information available to users of diagnostic equipment, in real-time displays. In this Appendix, principal features of ODS are described, for the convenience of readers; those requiring more information are referred to the original document (AIUM/NEMA, 1992; 1998), to a later publication (FDA, 1997), and to a valuable review by Abbott (1999).

Four indices were defined by ODS: three TIs and one MI. TIs (TIB, TIC, and TIS), defined below, are reasonable-worst-case estimates of the temperature rise that will result from exposure to ultrasound and can be used to assess the potential of harm to a patient *via* a thermal mechanism. (They are considered dimensionless, though numerically equal to the estimated temperature rise in degrees Celsius.) Also defined is a MI which analogously allows assessments of the likelihood that harm will result from mechanical activity (especially, some form of cavitation). All such estimates are highly dependent on various assumptions, including the assumption that the patient’s soft tissues have a homogeneous, moderately low, attenuation coefficient.

The distinction among the three TIs depends on whether the ultrasound impinges on bone (the most highly absorbing tissue in the body) and, if it does, on whether the bone is encountered near the transducer, as in a cranial examination, or in the interior of the body, as in an examination of a fetus after the first trimester. Specifically:

- TIS applies when the ultrasound beam passes primarily through soft tissue and does not impinge on bone. It provides an estimate

of the maximal temperature along the path, which may occur near the source. It is appropriately displayed during examination of a fetus in the first trimester.

- TIB applies when the ultrasound impinges on bone at or near the focus of the beam after it has passed through soft tissue. This index provides an estimate of the temperature rise that occurs at the surface of the bone. It should be displayed when the fetus is being examined during its second or third trimester.
- TIC applies when the transducer is very close to bone and gives an estimate of the temperature rise produced at the surface of the bone during transcranial examinations.

The calculated value of any TI or MI varies with the equipment settings chosen by the operator. In order to alert a sonographer that an index is approaching the critical value of one, ODS requires that the index be displayed whenever it equals or exceeds the value of 0.4. This requirement applies to all ultrasound equipment capable of exceeding an index value of one under any condition.

No display capability is required for a particular item of equipment if none of the indices exceeds one for any choice of settings. At a given time, only one index need be displayed. For real-time modes (B-modes), it is typically true that TIs do not exceed one, while MI can exceed this value (Patton *et al.*, 1994). Hence, for equipment operating in this mode, MI can be displayed, but no display of TIs is required in ODS. For other modes, if the equipment is able to exceed one for either TIB or TIS, then it must be provided with the capability of displaying the indices, but it need not display them simultaneously.

B.2 Equations for the Indices

The indices are computed from measured quantities, according to algorithms based on a combination of theory and experiment. The expression for TIC is particularly simple; this expression, which applies to a cranial examination during which the transducer is placed in near-contact with part of the head, is:

$$\text{TIC} = \frac{W_0}{40 D_{\text{eq}}}, \quad (\text{B.1})$$

where W_0 is the (time-averaged) acoustic power (in milliwatt) produced by the transducer and D_{eq} is the diameter (in centimeters) of its effective transmitting area. If W_0 is 100 mW and D_{eq} is 1 cm, TIC is 2.5. Equation B.1 is based on theory for the temperature produced

on the surface of a heated absorbing disc in the presence of modest perfusion, which was found to be in agreement with experiments in which focused ultrasound was applied to the skulls of living animals (Section 11.5). If D_{eq} is equated to d_6 , the two Equations B.1 and 11.9 are identical (except for the length units). An experimental test of TIC is discussed in Section 11.6.

The expression for TIB applicable to an unscanned beam is also based on theory for a heated disc, but is complicated by the fact that the bone of concern (the heated portion of which is represented by the disc) lies within the patient's body. Because of this, it is necessary to use an estimated (rather than measured) value of the acoustic power in the beam at the bone surface. This estimate must take into account the attenuating characteristics of the tissues along the acoustic path between transducer and bone. The tissues are assumed to constitute a homogeneous medium with an attenuation coefficient of $0.3 \text{ dB cm}^{-1} \text{ MHz}^{-1}$ ($0.035 \text{ Np cm}^{-1} \text{ MHz}^{-1}$) (the Model H₃ discussed in Section 9); the tissue is also absorbing, but the heat generated within this medium is neglected in calculating TIB. The expression for TIB must then differ from that for TIC in that W_0 is replaced by the *derated* value $W_{.3}(z)$; this value is calculated at a distance z from the source by the expression:

$$W_{.3}(z) = W_0 10^{-0.03Z} = W_0 e^{-0.069Z}, \quad (\text{B.2})$$

where $Z = zf_c$. The quantity $10^{-0.03Z} = e^{-0.069Z}$ is the derating factor for the power or intensity in the ODS model.

Another difference between the unscanned TIB and TIC is in the lateral intensity distribution assumed to exist in the ultrasound beam where it intercepts the bone. For TIC situation, the transducer is in near-contact with the bone and the intensity is considered to be constant over a circular area of diameter (D_{eq}); for TIB, it is in the focal region where the beam intercepts bone and the intensity distribution is assumed to be approximately Gaussian. When a Gaussian distribution applies, the steady-state-temperature rise is given by an expression analogous to that in Equation B.1; ΔT is equal to the acoustic power divided by $38.5 d_6$, where d_6 is the -6 dB width of the beam (NCRP, 1992). For the purposes of ODS, it was found convenient to eliminate d_6 from the expression by using the fact that the acoustic power in a Gaussian distribution is equal to $0.569 I_{\text{TA}} d_6^2$, where I_{TA} is the time-averaged intensity on the axis. The result is approximated as the ODS expression:

$$\text{TIB} = \frac{\sqrt{W_{.3}(z) I_{\text{TA}.3}(z)}}{50}, \quad (\text{B.3})$$

in which the derated quantities $W_{.3}(z)$ and $I_{TA.3}(z)$ are to be evaluated at the distance ($z_{B.3}$) where the product of the two quantities is maximal. Again, the subscript “0.3” on a quantity means that the quantity is calculated as it would be in a hypothetical medium where the attenuation coefficient is $0.3 \text{ dB cm}^{-1} \text{ MHz}^{-1}$, relative to measurements made in water (Section 9). In the Acoustic Output Reporting Tables (see, *e.g.*, Table 10.3 in Section 10), the quantity (z_{sp}) given in TIB column is identical to $z_{B.3}$.

In practice, the lateral distribution of the intensity only approximates the Gaussian and varies somewhat from one beam to another. An equivalent beam diameter (d_{eq}) is defined, such that the power in the beam is equal to the time-averaged axial intensity multiplied by $\pi d_{eq}^2/4$. In terms of the derated power and intensity, the expression for d_{eq} becomes:

$$d_{eq} = \sqrt{\frac{4W_{.3}}{\pi I_{TA.3}}} \quad (\text{B.4})$$

It is assumed in ODS that d_{eq} is approximately equal to $1.1 d_6$. (For a Gaussian beam, d_{eq} would be equal to $1.17 d_6$.)

To determine $z_{B.3} = z_{sp}$ and the corresponding value of $I_{TA.3}$, measurements are made in water of the acoustic pressure (p) as a function of time and of distance (z) along the axis, by means of a suitable small hydrophone. The local instantaneous intensity is defined as the quantity $p^2/\rho c$, where ρ and c are, respectively, the density and speed of sound for the medium. At each point, the pulse-intensity integral (PII) is determined; the latter is defined as the integral:

$$PII = \int \frac{p^2}{\rho c} dt, \quad (\text{B.5})$$

where the integration is over the acoustic pulse waveform. The time-averaged intensity (I_{TA}) is equated to PII multiplied by PRF ; its derated value $I_{TA.3}$ is obtained by multiplying I_{TA} with the derating factor $e^{-0.069zf}$. In the procedure for determining TIB for a given ultrasound beam, the quantity I_{TA} and the product $W_{.3}(z) I_{TA.3}(z)$ are determined at various distances (z). The distance $z_{B.3} = z_{sp}$ at which the product is maximal is determined and the quantity on the right hand of Equation B.3 is calculated for this value of z .

Equation B.3 applies if the focal beam diameter is not too small. Body motions would be expected to prevent the exposed area from being smaller than one with a diameter of about 0.1 cm. In ODS, the condition that d_{eq} should not be considered to be less than 0.1 cm is imposed by requiring that TIB should be given by $W_{.3}(z_{B.3})/4.4$, if this is less than the value given in Equation B.3.

When an ultrasound beam propagates entirely through homogeneous soft tissue, the generation of heat, and the consequent temperature rise, are no longer confined primarily to a small region, as is true when the beam impinges on bone or other highly absorbing tissue. Instead, if the absorption coefficient is the same everywhere, the rate at which heat is generated at any point (in a traveling plane wave) is proportional to the local value of the acoustic intensity. Several methods have been derived for calculating the temperature rise produced by a focused beam passing through perfused homogeneous tissue by obtaining solutions to a BHTE (AIUM, 1993a; NCRP, 1992). In ODS, simple expressions were obtained empirically for the applicable TIS, which fit reasonably well to the derived equations. For apertures (A_{aprt}) less than 1 cm^2 in area, the empirical equation is:

$$\text{TIS} = \frac{W_0 f_c}{210}. \quad (\text{B.6})$$

Here, as before, W_0 is the acoustic power (in milliwatt) generated by the source and f_c is the center frequency in megahertz. If W_0 is 100 mW and f_c is 3 MHz, one obtains 1.4 for TIS.

When the aperture area (A_{aprt}) is greater than 1 cm^2 , Equation B.6 still applies, except that W_0 is replaced by a “power parameter,” equal to the maximum with respect to distance (z) of a local power parameter (LPP); the latter is the lesser of two local quantities, the derated power [$W_{.3}(z)$] in milliwatt or the derated time-averaged axial intensity [$I_{\text{TA},.3}(z)$] in mW cm^{-2} . These two quantities are equal at the position $z = z_1$, where the “equivalent beam area” (equal to $\pi d_{\text{eq}}^2/4$) is 1 cm^2 . In determining $LPP(z)$, the distance z should equal or exceed the “break point” value $z_{\text{bp}} = 1.5 D_{\text{eq}}$ in order to avoid near-field complications.

In homogeneous soft tissue, the maximal temperature rise (of which TIS is an estimate) typically occurs near the surface where the beam enters the tissue. The exceptions are usually for stationary highly focused beams, characterized by large apertures and short focal lengths. The temperature rise at the focus is usually significantly less than the maximum (NCRP, 1992). Cases in which the temperature rise near the surface is probably not greater than at the focus are discussed in Section 9.

MI was developed from a theoretical expression for the lowest value of the peak negative (rarefactional) pressure in an ultrasound pulse that can produce inertial cavitation in water (Section 5). In ODS procedures, a required step for determining MI for an ultrasound beam is to determine $p_r(z)$ and the pulse-intensity integral [$PII(z)$] at various distances (z) along the axis of the beam. At each value of z the integral $PII(z)$ is multiplied by the derating factor

$e^{-0.069zf_c}$, to obtain the derated quantity $PII_{.3}(z)$, and the distance $z = z_{sp}$ is determined for which $PII_{.3}(z)$ is maximal. MI is defined as:

$$MI = \frac{p_{r.3}(z_{sp})}{f_c^{0.5}}, \quad (\text{B.7})$$

where $p_{r.3}(z_{sp})$ is the product of $p_r(z_{sp})$ and the pressure derating factor $e^{-0.035z_{sp}f_c}$ (Equation 9.1); here the pressure ($p_{r.3}$) is in megapascals and the frequency (f_c) in megahertz. If $p_{r.3}$ is 3 MPa and f_c is 4 MHz, one obtains $MI = 1.5$.

B.3 Maximal Values of the Thermal Indices

Manufacturers meeting the requirements of FDA for marketing diagnostic ultrasound equipment can do so by following either Track 1 or Track 3. Those who comply with ODS requirements for displaying TIs and MIs can follow Track 3; others must follow Track 1 (FDA, 1997). For Track 1 the upper limits to the intensity and to MI vary with the application as shown in Table B.1. These are the limits that applied before adoption of ODS in 1992.

For those who follow Track 3, which has been an option since 1992, the limit on the derated SPTA intensity and MI are, respectively, 720 mW cm^{-2} and 1.9 for all applications except ophthalmic, which has lower limits (Table 10.1). For purposes of determining the largest allowed values of TIB and TIS (under Track 3), for nonophthalmic applications, the equations are rewritten below in terms of the intensity $(I_{\text{SPTA.3}})_{\text{lim}} = 720 \text{ mW cm}^{-2}$.

For TIB, reference is made to Equation B.3, recalling that in deriving this equation the derated power ($W_{.3}$) is equated to $0.569 d_g^2$ multiplied by the time-averaged axial intensity; hence, the maximal value of TIB allowed in Track 3 is:

TABLE B.1—Upper limits on $I_{\text{SPTA.3}}$ and MI under Track 1 of ODS (FDA, 1997).^a

Application	$I_{\text{SPTA.3}}$ (mW cm ⁻²)	MI
Peripheral vessel	720	1.9
Cardiac	430	1.9
Fetal imaging and other	94	1.9
Ophthalmic	17	0.23

^aThe same limits applied to $I_{\text{SPTA.3}}$ before 1991.

$$\text{TIB}_{\max} = 0.015 d_6 \times (I_{\text{SPTA},3})_{\text{lim}} = 0.015 d_6 \times 720. \quad (\text{B.8})$$

Then, setting d_6 equal to $1.1 d_{\text{eq}}$, one obtains:

$$\text{TIB}_{\max} = 12 d_{\text{eq}}. \quad (\text{B.9})$$

For the (small aperture) TIS, reference is made to Equations B.2 and B.6; here W_0 is equated to $W_{.3}$, $e^{0.069z_{\text{F}}/f_c}$ where z_{F} is the focal distance (assumed to be the distance at which the $I_{\text{SPTA},3}$ is to be limited to 720 mW cm^{-2}) and $W_{.3}$ is equated to $(\pi/4)d_{\text{eq}}^2 (720)$; hence, the maximal value of the (small aperture) TIS allowed in Track 3 is:

$$\begin{aligned} \text{TIS}_{\max} &= (0.785) f_c d_{\text{eq}}^2 e^{0.069z_{\text{F}}/f_c} / (210) 720 \\ &= 2.69 f_c d_{\text{eq}}^2 e^{0.07z_{\text{F}}/f_c}. \end{aligned} \quad (\text{B.10})$$

For TIC (Equation B.1), W_0 is evaluated as for TIS. Hence, the maximal value of TIC allowed in Track 3 can be written as:

$$\text{TIC}_{\max} = (0.785 d_{\text{eq}}^2 e^{0.069z_{\text{F}}/f_c} / 40 D_{\text{eq}}) 720, \quad (\text{B.11a})$$

or, using Equation B.10:

$$\text{TIC}_{\max} = 5.3 f_c^{-1} D_{\text{eq}}^{-1} \times (\text{small aperture}) \text{TIS}_{\max}. \quad (\text{B.11b})$$

An example for the three TIs is as follows:

- if d_{eq} is 0.3 cm, $\text{TIB}_{\max} = 3.6$
- if, further, f_c is 3 MHz and z_{F} is 6 cm, the (small aperture) $\text{TIS}_{\max} = 2.6$
- if, further, D_{eq} is 1 cm, $\text{TIC}_{\max} = 4.6$

B.4 Accuracy of the Output Display Standard Indices

B.4.1 Nonlinear Propagation

The accuracy of the indices depends on several factors. Fundamental to all indices are the algorithms employed in estimating *in situ* values of the acoustic pressure, intensity and power. Present procedures required by ODS have, as a first step, characterization of the source by determining the acoustic field in water with equipment operated with the same settings as are used in clinical practice. As pointed out in Appendix D and in Section 9, propagation through water at typical output levels leads to distortion and added attenuation of the propagated wave. Because the added attenuation is much less in propagation through tissues (excepting aqueous fluids), significant errors can arise from procedures in which such water-

measured values are used as the basis for estimating *in situ* values in tissues by simple linear derating. Christopher and Carstensen (1996) show that such procedures can lead to underestimation of the acoustic pressure in tissue by a factor of two or more. These procedures can cause MI to be underestimated by the same factor, because the latter is proportional to the derated acoustic pressure (Equation B.7).

Also, the same procedures cause underestimation of the unscanned TIB and TIS. The former is proportional to the maximal value of the square root of the product of the power W_3 and the intensity $I_{TA,3}$ (Equation B.3); of these two quantities, the derated power W_3 is not affected by the measurements of acoustic pressure in water (because it is given in terms of the source power output, by Equation B.2), but the intensity is assumed proportional to the integrated square of the acoustic pressure (Equation B.5). Hence, the unscanned TIB is roughly proportional to the derated acoustic pressure and, like MI, is affected by underestimates of this quantity. However, if NLP in tissue causes appreciable extra attenuation of the power, the error in the unscanned TIB will be somewhat reduced, because the power will then be overestimated by linear derating according to Equation B.2. The unscanned TIS also can be affected by underestimation of the acoustic pressure if the beam is wide because, under some conditions, this index is then proportional to the maximal derated axial time-averaged intensity.

Alternative methods for characterizing the source are described in Appendix D and recommended in Section 14; if these are followed in future versions of ODS, errors resulting from measurements in water under conditions of NLP will be reduced.

B.4.2 *Estimation of Attenuation*

Once the source is well characterized, the accuracy of estimated *in situ* values of the acoustic quantities depends on assumptions made about acoustical properties of tissues in paths along which the ultrasound beam propagates. These paths are mostly through soft tissues and, as pointed out in Section 9, the Model H_3 used by ODS is usually conservative in that use of this model (which assumes the attenuation coefficient to be $0.3 \text{ dB cm}^{-1} \text{ MHz}^{-1}$) usually leads to underestimation of the attenuation along such paths by $0.1 \text{ dB cm}^{-1} \text{ MHz}^{-1}$ or more. However, paths relevant to fetal scanning, as well as other paths, sometimes (in two to five percent of cases) pass through an appreciable amount of weakly attenuating fluid, for which the H_3 model overestimates the attenuation by as much as $0.3 \text{ dB cm}^{-1} \text{ MHz}^{-1}$. A “fixed-

path model” is described in Section 9, and recommended in Section 14, which is shown to provide a suitable conservative means of estimating the attenuation for obstetrical applications.

B.4.3 *The Cranial Thermal Index and the Bone Thermal Index*

TIs are estimates (usually conservative) of the temperature rise produced during an ultrasound examination, and are calculated from approximate equations derived for simplified theoretical models. The simplest is TIC which applies when the ultrasound transducer is in near-contact with bone, as in a cranial examination; it is an estimate of the temperature produced at the exposed bone surface. The equation for calculating TIC (Equation B.1) is based on the fact that mature bone is the most highly absorbing tissue in the body; it is assumed that, when an ultrasound beam impinges on mineralized bone, about half of its energy is converted into heat within the bone in a thin layer near its surface. TIC is proportional to the ratio of the ultrasonic power output of the source to its equivalent diameter.

Equation B.1 has been tested by experiments in which the temperature of a bone specimen is measured with an imbedded thermocouple during exposure to ultrasound. Good agreement was obtained between theory and experiment for *in vivo* exposure of living mouse (Carstensen *et al.*, 1990d; NCRP, 1992). In other studies, it is shown that when a transducer is in near contact with bone, self-heating from the transducer can cause the temperature to rise much more than expected from Equation B.1. However, if there is a significant water path immediately preceding the bone, the temperature rise is less, because heat is transported away by acoustic streaming set up by the ultrasound in the water (O'Neill *et al.*, 1994; Shaw *et al.*, 1998; Wu *et al.*, 1994, 1995) (Sections 11.6 and 11.7).

A related index is TIB which applies when focused ultrasound impinges on bone in the interior of the body, as in a fetus whose skeletal tissue has become mineralized. This index is relevant when a fetus is being examined during the second or third trimester. For the (unscanned) TIB, the equation is like that for TIC (although it is expressed differently, for convenience), except that here the *local* value of the power in the ultrasound beam is divided by the *local* value of the equivalent beam diameter. A problem arises, because TIB is determined for equipment without knowing where bony structures may be encountered during an examination. A conservative value is obtained by estimating the temperature rise that would occur at any axial position where the bone might be; the maximum is then determined and equated to TIB. This quantity and its axial

position (z_{sp}) are specified (the latter in the column under “TIB”) in an Acoustic Output Table supplied by the manufacturer (Table 10.3). It is found that, depending on the transducer, z_{sp} varies from small values (indicating positions near the transducer) to values nearly equal to the elevational focal length. If bone is encountered at some position other than z_{sp} , the temperature rise will be less than indicated by the maximal TIB.

An example can be obtained by using the information given in Table 10.3 for a specific transducer, mode and system. Here the listed TIB is 2.90; it applies in focal zone FZ #7 at a distance $z_{sp} = 1.5$ cm. For this focal zone, the azimuthal and elevational focal distances FL_x and FL_y are 7 and 1.7 cm, respectively. At the larger focal distance (7 cm), the temperature rise (being approximately proportional to the local ratio of the power to the equivalent-beam diameter, as in Equation B.1) is likely to be much less than at 1.5 cm because of attenuation. The latter can be estimated as the product of $0.3 \text{ dB cm}^{-1} \text{ MHz}^{-1}$ with the distance 7 to 1.5 cm and the frequency 3.95 MHz; *i.e.*, the attenuation is about 6.5 dB. The equivalent beam diameter is not given in Table 10.3, but is larger at 7 cm than at 1.5 cm; hence, the expected temperature rise at 7 cm is less than the listed TIB by a factor of four or more, according to the model being employed. Information is not given for other focal zones, except that TIB will not exceed the value (2.90) listed. In the future, the operator will be able to make better judgments about the approximate temperature rise for actual conditions employed, if information is made conveniently available for all of the relevant focal zones.

B.4.4 *The Soft Tissue Thermal Index*

A third TI, TIS, provides an estimate of the maximal temperature rise produced by an ultrasound beam as it passes through soft tissue. Its calculation is based on a model in which the actual beam is replaced by a cylinder heated at a uniform rate by the ultrasound. It is shown by more accurate (and more lengthy) calculations for homogeneous media that, when a weakly focused beam traverses a homogeneous medium, the maximal (steady-state) temperature rise does not occur at the focus but, instead, occurs at or near the transducer. In an example treated by NCRP (1992), the ratio between the temperature rise where the maximum occurs and that at the focus is about two. For this reason, TIS displayed during use of a weakly focused beam to scan an embryo, or a fetus during the first trimester, usually overestimates the temperature rise of these objects, assuming

that these lie at the focus. However, when short focal lengths are used the principal spatial maximum of the temperature rise may occur at or near the focus and TIS may approximate the actual temperature rise of the object being examined (Thomenius, 1993).

Another reason TIS can suggest temperature rises higher than those that actually occur is that it is based on an estimate of the steady-state temperature, *i.e.*, the ultimate temperature reached after an exposure of long duration. The time required to approach the steady-state value is small when the beam is narrow and the tissue well perfused, but can be 5 min or more in a wide beam if the perfusion is modest (NCRP, 1983; 1992; Wu *et al.*, 1995). Because of this, when TIS applies near the transducer where the beam is relatively wide, the temperature rise that occurs there during the duration of a typical ultrasound examination is usually appreciably less than suggested by TIS. This consideration is less important for TIC and TIB; when ultrasound impinges on bone, the temperature rise reaches its steady-state value relatively quickly (NCRP, 1992).

B.4.5 *Frequency Dependence of the Threshold for Nonthermal Damage*

Exposure criteria for damage to tissue when ultrasound interacts with gas bodies are directly expressible in terms of the *in situ* acoustic pressure, as can be seen in the Conclusions and Recommendations in Sections 13 and 14. The extensive data on lung damage, shown in Figure 8.1 together with data for other tissues containing stabilized gas bodies, exhibit a tendency for the threshold to increase with frequency, a trend given approximately by the dependence in the expression (Equation B.7) for MI. However, existing data (still very limited) on damage produced when gaseous contrast agents in the circulatory system are exposed to ultrasound suggest that the threshold for such damage increases more rapidly with frequency.

B.4.6 *Spatial Distribution of Acoustic Pressure*

There is another important source of error for MI, with its derating factor, if used to indicate potential for lung damage, because the derating factor applies to the distance (given as z_{sp} in the column under "MI" in Acoustic Output Tables; see Table 10.3.) at which PII_3 is maximal (Equation B.7). Knowledge of the acoustic pressure at this maximum is desired for some applications, but, in assessing lung exposure, MI as defined would usually suggest greater exposure

than actually exists because the acoustic pressure at the surface of lung would be less (often, much less) than the maximum during typical clinical procedures. An adequate assessment of lung exposure would require a more complete knowledge of the spatial distribution of acoustic pressure.

B.4.7 *Recent Tests of the Accuracy of the Output Display Standard Thermal Indices*

Evaluations of the accuracy of ODS thermal calculations and displayed TIs were reported recently (Shaw *et al.*, 1998). Tests of actual temperature rises from diagnostic systems were performed with test objects consisting of thermal sensors sandwiched between layers of TMM (Bacon and Shaw, 1993). Attenuation simulating that assumed in ODS was included by inserting acoustical attenuators (Preston *et al.*, 1991) in the propagation path. Simulation of worst-case measures were performed with a path through water, except for some TMM (0.35 dB MHz⁻¹ attenuation) that surrounded the sensors. It was concluded that an on-screen TIB or TIS value should not be regarded as an upper limit to the possible temperature rise. The displayed TIB varied from 9 to 144 percent of the measured worst-case maximum and the displayed TIS varied from 40 to 130 percent of the measured worst-case maximum. The displayed TIB and TIS varied, respectively, from 20 to 150 percent and 60 to 210 percent of the maximum measured with 0.3 dB cm⁻¹ MHz⁻¹ attenuation. However, the average ratios of displayed values to measured temperatures with attenuation were quite good, 1.3 for TIS and one for TIB.

Shaw *et al.* (1998) concluded further that measured temperature rises showed reasonably good agreement with calculations according to the ODS formula. However, the displayed TIB and TIS varied, respectively, from 20 to 150 percent and from 40 to 180 percent of the values calculated by the investigators using ODS equations and measured acoustic quantities. While the test conditions did not include perfusion, the exposure time of 3 min was short enough to overcompensate for this effect on the average.

Tests of the algorithms used in ODS calculations were made by Jago *et al.* (1999). They considered a “worst-case” model representing a third-trimester pregnancy, in which the ultrasound beam traversed a water path before impinging on bone. Detailed measurements were made of 3D acoustic pressure distributions (in water) in the fields of probes from two commercial diagnostic ultrasound scanners, operating in B, pulsed-Doppler (PD) or CFI modes, set for maximal output. Using these data, calculations were made of the maximal

steady-state temperature rise in the model, by obtaining solutions of BHTE (Equation 11.5). Also, for the same equipment settings, determinations were made of the relevant ODS TIs, using prescribed procedures. Considering the latter nondimensional quantities to be numerically equal to simplified estimates of the maximal temperature rise (in degrees Celsius), ratios were determined of the calculated temperature rise to that obtained from the corresponding ODS index. For PD modes, ratios were found to vary from 1.46 to 2.92, indicating that the calculated value significantly exceeded that obtained from TI. The difference was attributed to the fact that ODS assumes a homogeneous medium, while the model considered here included a path of low attenuation. Similarly, for CFI modes, the calculated values exceeded those obtained from ODS indices, the ratios varying from 1.26 to 2.45. For B-modes, the difference is smaller and the ratios are sometimes less than unity, varying from 0.62 to 1.25.

Appendix C

Nepers and Decibels

In Section 9 and elsewhere in this Report, reference is made to the attenuation experienced by an ultrasound beam in propagation through tissue. The acoustical quantity considered may be the pressure amplitude (p), the intensity (I), or the power (W) and the attenuation is expressed in terms of either nepers (Np) or decibels (dB). The neper and the decibel are each equal, or proportional, to the logarithm of a ratio. Suppose the attenuation in question is that experienced by a beam in passing from Point a to Point b and that the acoustical quantity applicable at these points is identified by the subscript a or b, respectively. Then the following relationships hold:

$$\text{Attenuation in Np} = \ln\left(\frac{p_b}{p_a}\right) = 0.5 \ln\left(\frac{I_b}{I_a}\right) = 0.5 \ln\left(\frac{W_b}{W_a}\right) \quad (\text{C.1})$$

and

$$\text{Attenuation in dB} = 20 \log\left(\frac{p_b}{p_a}\right) = 10 \log\left(\frac{I_b}{I_a}\right) = 10 \log\left(\frac{W_b}{W_a}\right). \quad (\text{C.2})$$

Here “ln” and “log” designate logarithm base “e” and “10,” respectively. Because $\log x = 0.434 \ln x$ for any real x , the attenuation in decibels is 8.7 times the attenuation in nepers. Thus, an attenuation coefficient for Model H₄ (Table 9.1) is either 0.05 Np cm⁻¹ MHz⁻¹ or 0.44 dB cm⁻¹ MHz⁻¹.

Table C.1 shows ratios of acoustic amplitude and power corresponding to selected values of the attenuation in decibels and nepers.

TABLE C.1—*Decibel and neper relationships.*

Attenuation		Ratio	
Decibels (dB)	Nepers (Np)	Amplitude	Power
0	0	1	1
3	0.35	1.41	2
6	0.69	2	4
10	1.15	3.16	10
20	2.30	10	100
40	4.60	100	10,000

The ratios for intensity are the same as for power. An increase of 3 dB corresponds to an increase in amplitude by a factor of $\sqrt{2}$, or 1.4, and to an increase in power by a factor of two. A 10 dB increase means that the amplitude and power increase by factors of $\sqrt{10}$ and 10, respectively, and for 20 dB the corresponding factors are 10 and 100.

akusher-lib.ru

Appendix D

Nonlinear Propagation: An Update

D.1 Introduction: Conclusions of NCRP Report No. 113 on Nonlinear Propagation

The discussion, in Appendix C of NCRP Report No. 113 (NCRP, 1992), of the implications that NLP has for the thermal effects of ultrasound was based on weak shock theory (Blackstock, 1966), which assumes that the small-signal absorption coefficient of the propagating medium is negligibly small. Even though that assumption is unrealistic for tissue, it was possible with the help of weak-shock theory to explain the basic physical processes at work in the propagation of high-amplitude acoustic waves and to make a number of qualitative and quantitative predictions that are relevant to applications in diagnostic ultrasound.

The usual small-signal analyses of acoustic wave propagation fail to take into consideration the fact that the speed of sound increases as the local pressure increases. In reality, because the pressure maxima in a sound wave travel faster than the pressure minima, a wave of finite amplitude is gradually distorted as it propagates. The distortion of the wave from its original sinusoidal form means that harmonics, integral multiples of the source frequency, are generated. If this process continues, at a critical combination of distance, frequency and amplitude, a pressure discontinuity, *i.e.*, a shock wave, begins to develop. Losses occur as a result of strong irreversible processes generally resulting from accentuated effects of viscosity, heat conduction, and relaxation at the discontinuity, and these losses depend on the strength of the shock and the shape of the waveform on either side of the shock. The process of shock formation and decay

continues as the wave progresses. Although a shock is not truly discontinuous (its rise time is always finite), its approximation as a discontinuity is often quite good particularly in poorly absorbing materials such as water.

Because the absorption of sound increases with increasing frequency, the harmonics generated by NLP enhance losses. With NLP, the absorption coefficient of linear acoustics, which is solely a property of the medium, must be replaced, at high amplitudes, by a *finite-amplitude absorption parameter*,¹⁶ which is a function of the source amplitude and frequency, the amplitude dependence of the sound speed, the geometrical configuration of the sound field, and the length of the propagation path. Surprisingly, in poorly attenuating materials such as water, the absorption parameter is essentially independent of the small-signal absorption coefficient of the medium (Dalecki *et al.*, 1991a). Under realistic conditions encountered in diagnostic ultrasound, the finite-amplitude absorption parameter for water can become as large as the small-signal absorption coefficient of tissues such as liver. Momentum lost from the sound field through nonlinear absorption is transferred to the propagating medium resulting in macroscopic acoustic streaming in liquids or, in solids, a strain proportional to the product of the finite-amplitude absorption parameter and the intensity (Carstensen *et al.*, 1980; Starritt *et al.*, 1989).

A corollary of the enhanced loss associated with NLP is the fact that levels achievable at distant points in the sound field are limited. In the extreme case, field amplitudes become independent of source amplitudes, a phenomenon known as *acoustic saturation*.

For perspective, when amplitudes of acoustic fields are great enough to produce the potentially adverse biological effects cited in Section 8, it is highly probable that the influence of NLP will become apparent in the waveform of the acoustic signal, and it may become important to consider NLP in estimating the exposures experienced by target tissues.

From weak-shock theory, it is apparent that, as the amplitude of the field increases, excess losses occur on the axis and, as a result, beam patterns are broadened by NLP. These same losses, however, result in the narrowing of heating patterns as shock waves begin to develop (Dalecki *et al.*, 1991a).

¹⁶As in NCRP Report No. 113 (NCRP, 1992), the *finite-amplitude absorption parameter* is defined as the thermal power per unit volume delivered to the medium by the sound field (the negative divergence of the intensity) divided by twice the intensity. At small signal levels, the finite-amplitude absorption parameter approaches the classical absorption coefficient of the medium.

Nonlinear enhancement of absorption can be greater in focused than unfocused fields. The shorter the focal length, the greater the potential absorption parameter. The explanation lies in the fact that converging waves travel over most of their path at low levels where finite-amplitude losses are negligible. However, only as the wave nears the focus are finite-amplitude processes involved, and, because of this, greater source and focal amplitudes are necessary to achieve maximal enhancement of the absorption parameter with short focal distances (Dalecki *et al.*, 1991a).

D.2 Nonlinear Propagation in Tissue

While the general physical processes involved in NLP were evident from extensions of weak shock theory at the time of the preparation of NCRP Report No. 113 (NCRP, 1992), it was not possible at that time to deal quantitatively with propagation at high-pressure amplitudes in media with losses as great as those of tissue. A numerical approach to this problem has now been developed that accurately describes the effects of absorption, diffraction, dispersion, nonlinearity and planar-(fluid)-boundary transmission of axially symmetric acoustic beams (Christopher, 1993; Christopher and Parker, 1991). This model has been used to explore the derating problem for realistic applications of ultrasound propagation in diagnostic ultrasound (Christopher and Carstensen, 1996; 1998).

D.2.1 Intensity

The salient results of this investigation are contained in Figure D.1 which plots the focal intensities as a function of source intensity for three propagating media, water, liver and fat. In these computations, a 3 MHz source with a radius of 1 cm and a focal length of 8 cm is assumed. Realistic assumptions are made for tissue properties but their primary differences are in their absorption coefficients, 0.0023, 0.12, 0.26 Np cm⁻¹ for water, liver and fat, respectively. Dotted lines show the linear extrapolation of small signal focal intensities for each of the three media. In each case, focal fields depart from linear predictions at high amplitudes. The effects of NLP are seen at lower source levels in water than in tissue because intensities along the propagation path are smaller in highly absorbing media than in water.

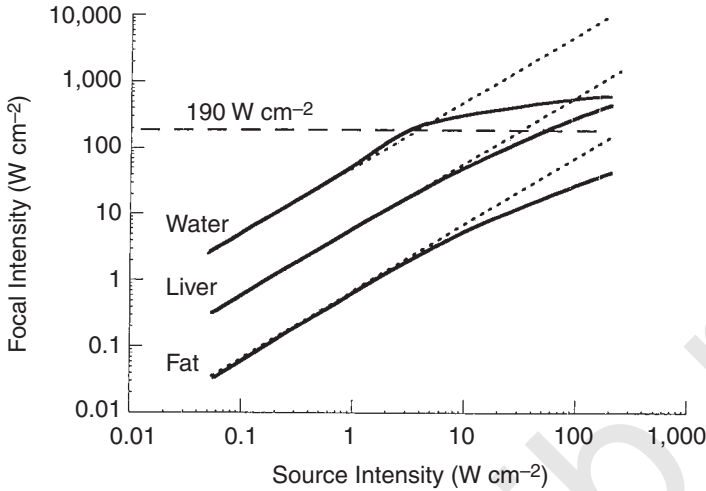


Fig. D.1. Focal intensities for the core example. Conditions: 3 MHz, 1 cm radius nonapodized source, 8 cm focal length. To give perspective to the intensities, the dashed horizontal line is at 190 W cm^{-2} , the pulse average intensity formerly used by FDA in the 510(k) regulatory process (Christopher and Carstensen, 1996; 1998).

For perspective, Figure D.1 has a dashed line at 190 W cm^{-2} corresponding to the *de facto* upper limit formerly imposed by FDA.¹⁷ When a diagnostic device is compared with this limit, measurements are made in water and “derated” to account for losses in a “typical” tissue. It is possible to see the effect of this derating process by lowering the water curve in Figure D.1 until its linear segment coincides with the data for liver. This shows that virtually all devices with the frequency and geometrical parameters chosen for this example would have derated fields below the 190 W cm^{-2} FDA limit.

Figure D.1 illustrates a serious problem that will occur if NLP is ignored when estimating the maximal derated fields for commercial medical ultrasound 3 MHz devices. Assume that, for this purpose, the device is turned up to its full output and the pulse average intensity at the focus is measured in water and found to be 560 W cm^{-2}

¹⁷At the present time, FDA guidelines are expressed in terms of MI, which is defined in terms of the maximal negative pressure in a pulse, rather than the pulse average intensity. Conversion from MI to pulse average intensity depends on the temporal characteristics of the pulse and the degree of nonlinear distortion of the waveform. For purposes of comparison, however, FDA’s limit of $MI = 1.9$ corresponds to a pulse average intensity of 360 W cm^{-2} at 3 MHz for a long pulse in which the waveform is sinusoidal.

(corresponding to 100 W cm^{-2} on the abscissa in Figure D.1). The waveform, as viewed on an oscilloscope, would be highly distorted and it would be obvious in a qualitative sense that NLP is important. However, if that is ignored and a linear derating of $0.3 \text{ dB cm}^{-1} \text{ MHz}^{-1}$ (ODS) (attenuation coefficient of 0.9 dB cm^{-1} multiplied by a focal distance of $8 \text{ cm} = 7.2 \text{ dB}$) is applied, the derated intensity would be 110 W cm^{-2} instead of $\sim 330 \text{ W cm}^{-2}$, the actual value in Figure D.1, which was calculated for liver by taking NLP into account. This example illustrates the severe problems that can be encountered if high-level measurements in water are used to estimate tissue fields. The closer water fields approach saturation, the more difficult it becomes to use water data to predict fields in any other medium.

Some form of apodization is used in most diagnostic transducers in order to form phased arrays. It should be noted that the results shown in Figure D.1 are for a nonapodized transducer. In general, apodization increases the effects of NLP for given focal intensities. The introduction of apodization would lower the six curves shown and slightly modify the curvature of the three nonlinear curves. For example, a good approximation of the data for a source with Gaussian apodization (sufficient to reduce the one-way, focal-plane, first-side-lobe levels to -35 dB relative to axial intensities) could be obtained by multiplying the intensity for all of the curves in Figure D.1 by 0.2 and labeling the abscissa “*Axial* Source Intensity.” Thus, it is apparent that for such a source it would be difficult to achieve focal intensities as high as 190 W cm^{-2} because of nonlinear saturation. Further discussion of the impact of acoustic saturation on the FDA regulation process has been given by Duck (1999b).

D.2.2 *Derating Intensities*

Linear derating procedures are attractive for their simplicity, but may lead to error. On the one hand, as mentioned above, estimation of tissue fields from high level water measurements can severely underestimate the true tissue fields. On the other hand, simple linear extrapolation of the small-signal derated fields (the dotted curves in Figure D.1), in general, overestimates the true focal fields. The latter is more appropriate in assessing safety, and it is proposed here for this purpose. It is better to overestimate than underestimate tissue fields. In this approach, the fields of each source are determined by hydrophone measurements at levels low enough that it is possible to relate linearly each point in the sound field, including the focus, to the source power. Basing estimates of tissue fields on small-signal-field determinations avoids experimental errors associated with

hydrophone measurements of sound fields at high-output levels and simplifies the theoretical and computational aspects of the derating problem as well. Once the field has been characterized through measurements in water for a given low-source power, it can be derated linearly by an appropriate attenuation factor for the tissue path. The intensities in these derated fields are assumed to be linearly related to source power. Because, for almost all diagnostic systems, the source acoustic power is linearly related to the electrical input power to the transducer, it is relatively simple to provide an indication of source power and, in this way, give the linearly derated field values for any operating condition. Of course, these are not the true fields in tissues at high output levels, but the linearly derated estimates of tissue fields can be the baseline for possible NLP corrections. The use of this conservative approach to estimation of tissue fields was first recommended by the World Federation of Ultrasound in Medicine (WFUMB, 1992). It should be noted that the NCRP (1992) TI for homogeneous tissues is currently formulated in terms of the source power.

D.2.3 Heating Rates

NLP affects the temperature elevation that takes place when mechanical energy in the sound beam is converted into thermal energy in the tissues by two different processes (Dalecki *et al.*, 1991a). First and most fundamental is the modification of the heating rate (*i.e.*, q_v , the rate of heat production per unit volume) through the generation of harmonics and by saturation phenomena. Second, the spatial distribution of q_v is changed. Because of these changes, NLP modifies the linear phenomenon of heat diffusion.

Nonlinear absorption results from the cumulative distortion of the wave as it propagates from the source to the site of interest. As the waveform is distorted, the local absorption increases. As the source level increases from zero, the local absorption parameter at a given point in the sound field is at first just equal to the small-signal absorption coefficient of the medium until the wave at the site begins the process of shock formation. A further increase in source amplitude by a factor of two to three results in a sharp increase in the local effective absorption parameter. If the source amplitude is increased further, excess absorption in the path in front of the site of interest becomes so great that the intensity (Figure D.1) and the effective absorption parameter at the site approach constants; then the heating rate at the site levels off and becomes essentially independent of source amplitude (the phenomenon of acoustic saturation). The

progression described here is particularly evident in poorly absorbing materials such as water. But, qualitatively similar phenomena occur in soft tissues such as liver.

This progression from linear absorption through the nonlinear enhancement of heating to saturation as source amplitude increases occurs first on the axis of the sound beam (Dalecki *et al.*, 1991a). Off axis sites go through the same process but require higher-source levels to reach a given degree of enhancement in heating rates. At very low-source levels, the heating pattern (q_v distribution) of the sound field is identical to the beam intensity pattern. When the source level is in the range such that the axial focal-field position is in shock but has not yet reached saturation, the effective heating pattern is narrower than the beam pattern intensity. Above source levels for which the axial position approaches saturation, the effective absorption parameter of off-axis sites still continues to increase giving rise to a heating-rate pattern that is actually broader than the linear intensity beam pattern. If it were not for this secondary change in the heating pattern that accompanies the nonlinear enhancement of heating, the change in steady-state-temperature increase on the axis would be directly proportional to the change in the axial heating rate. Instead, when the heating pattern is narrower than the beam intensity pattern, heat diffusion is increased and the steady-state-temperature increment on axis is less than proportional to the axial heating rates. But, when saturation is approached on axis, the beam broadens, heat diffusion decreases and the axial temperatures are greater than anticipated on the basis of axial heating rates alone (Baker, 1997; Dalecki *et al.*, 1991a).

Heating rates in water, liver and fat corresponding to the numerical example of Figure D.1 (3 MHz, 1 cm radius, nonapodized source focused at 8 cm) are shown in Figure D.2 (Christopher and Carstensen, 1996; 1998). Note that, in the small-signal (essentially linear-propagation) range, the focal heating rates are of comparable magnitude for water and for fat. Linear losses in the intervening 8 cm of fatty tissue reduce the focal intensity so much that the heating rate is low in spite of the high absorption coefficient.

The effects of NLP on heating rates are illustrated dramatically in Figure D.2. The smaller the absorption of the medium, the greater are the nonlinear enhancements of the heating rates. In a medium such as water with a very small linear-absorption coefficient, sound travels with only minor losses most of the pathway to the focus building up its amplitude and developing a strong shock as it progresses. Only as the wave approaches the focus does the finite-amplitude-absorption parameter become great enough to convert significant acoustic power from the beam into heat. Not only are the relative

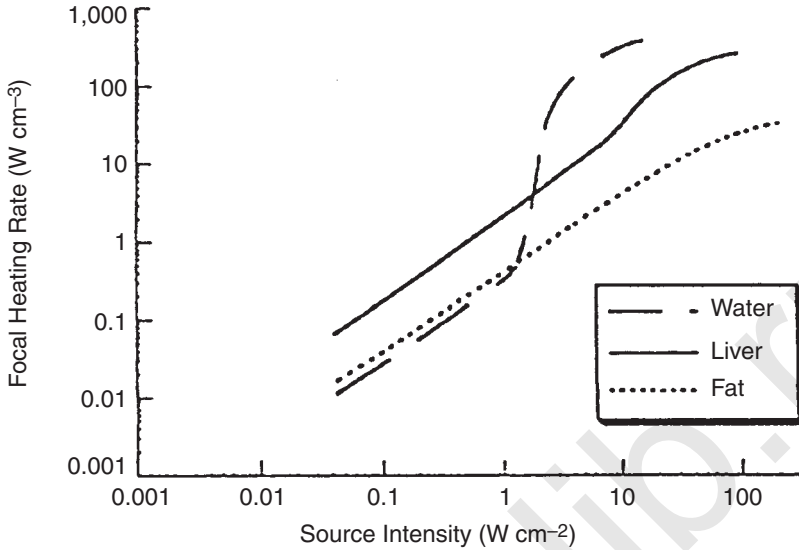


Fig. D.2. Focal heating rate of water, liver and fatty tissues. Conditions: 3 MHz, 1 cm radius, nonapodized source, 8 cm focal length (Christopher and Carstensen, 1996; 1998).

focal heating rates for poorly absorbing materials increased by orders of magnitude in this way, but the absolute heating rates can be very large as well. At high intensities, the heating rate in water actually exceeds that of liver in this example. There is significant enhancement of the focal heating of liver before saturation sets in, but the absorption in fat is so great that the only effect of NLP on its heating, in the example of Figure D.2, is a reduction from the linearly predicted levels at the highest outputs. The discussion thus far has considered only heating at the focus in homogeneous media. For highly absorbing materials, the highest temperatures and even the highest heating rates are found along the path to the focus rather than at the focus itself.

The effects on the steady-state-temperature increments are less dramatic. Enhancement of the axial heating rate makes the heating pattern narrower than the small-signal beam pattern. This increases heat diffusion and significantly reduces the impact of NLP on the steady-state-temperature increment. Figure D.3 illustrates this by comparing the heating rates as a function of distance from the axis for two conditions in which the temporal-average source intensity is the same but the temporal-peak intensities differ by 10^3 . Although the axial heating rate is greater with the higher peak intensities,

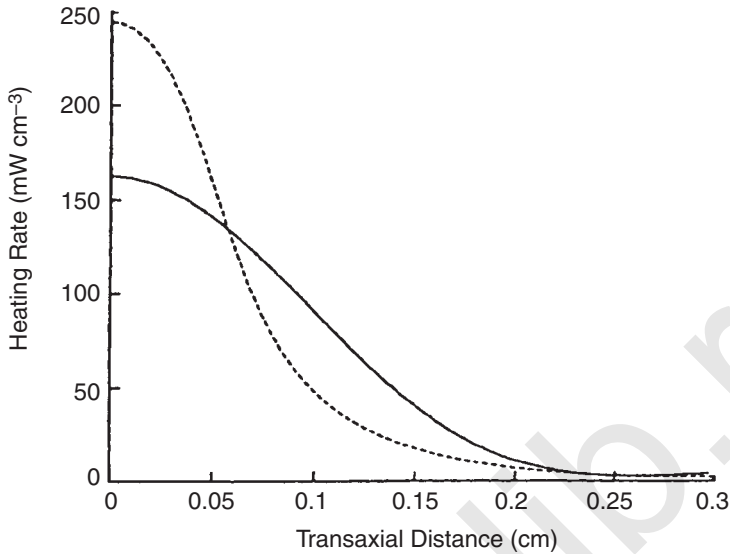


Fig. D.3. Heating patterns (q_v distributions) under linear and NLP conditions. The solid curve gives the heating rate at the focus as a function of distance from the axis for a CW source intensity of 0.1 W cm^{-2} . The dashed curve is the corresponding heating pattern with a temporal maximal source intensity of 100 W cm^{-2} but with a $1/10^3$ duty factor. Source, nonapodized, 3 MHz, 1 cm radius, focal distance = 8 cm, propagation through liver (Christopher and Carstensen, 1996; 1998).

the heat development across the entire beam at the focal distance is actually greater for the linear propagation condition. Of course, in the steady-state when thermal diffusion is dominant, the temperature increment depends more on the total energy converted into heat than on the axial heating rate. It is the steady-state-temperature rise that is used in formulation of TI.

D.2.4 Temperature Increments

Because thermal diffusion tends to compensate for enhanced axial heating rates as illustrated in Figure D.3, NLP has a surprisingly small effect on temperature increments. Figure D.4 shows the steady-state-temperature increment in liver along the axis from the source past the focal region for the 3 MHz source of Figures D.1 and D.2. The solid curve gives the steady-state-temperature increment for a CW source intensity of 0.1 W cm^{-2} that would produce a focal intensity of 0.05 W cm^{-2} after propagating through 8 cm of liver

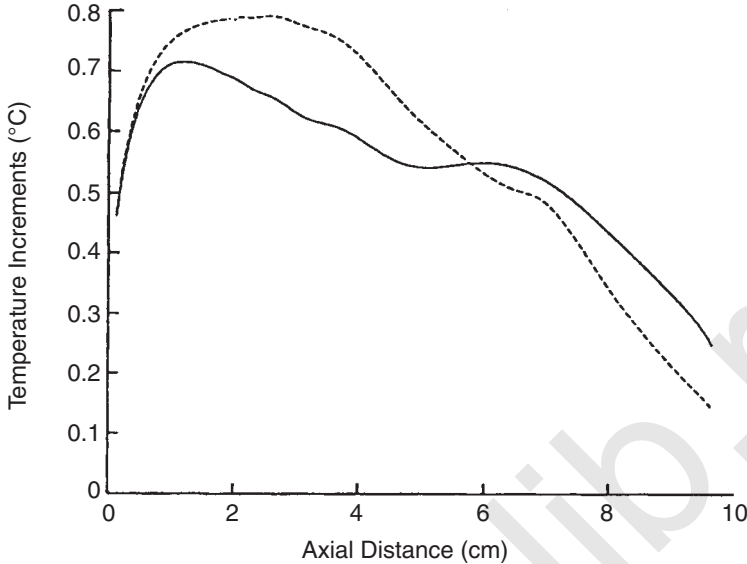


Fig. D.4. Axial steady-state temperature increments (ΔT) under linear and NLP conditions. The solid curve gives the steady-state-temperature increment with a source intensity of 0.1 W cm^{-2} . The temporal-average source intensity is the same for the dashed curve but here the pulse-average intensity is 100 W cm^{-2} . Nonapodized, 3 MHz transducer with a liver propagation path (Christopher and Carstensen, 1996; 1998).

(Figure D.1). The dashed curve gives the steady-state-temperature increment for a source intensity of 100 W cm^{-2} with a duty cycle of $1/10^3$ so that the temporal-average source intensities are the same for the two curves. As is usually the case (NCRP, 1992), the maximal heating occurs in front of the focal region. Note that although the temporal-average axial heating rates are greater for the (pulsed-mode) high-intensity case at the focus (Figure D.2), the steady-state-temperature increment at the focus is actually smaller than it is in the case of linear propagation. The explanation lies in the heating patterns shown in Figure D.3. At the focus, the near-axis gains in heating rate in the high-intensity case are out-weighed by the corresponding off-axis losses. In the near field, where the beam is much broader, there is a small enhancement in temperature increment associated with the higher-heating rate at the higher-peak intensity.

Figure D.2 shows that, for tissues as highly absorbing as fat, NLP has little impact on heating rates except to reduce heating at the

focus over that predicted on a linear basis at the highest-source levels.

There is little practical clinical interest in the heating of water. Even though the heating rate can be made very large by NLP, convection essentially eliminates any temperature rise in the fluid. But, in a general sense, it is clear from Figure D.2 that the effects of NLP on relative heating rates is much stronger for poorly absorbing materials than for liver-like tissues.

Although there are theoretically interesting nonlinear effects in local heating rates, the 10 to 20 percent enhancements in steady-state-temperature increments that are shown in Figure D.4 are small in comparison to the errors inherent (1) in estimating the temperature with the models of heating used for TI calculations and (2) in the uncertainties that are inherent in our knowledge of acoustic properties of the propagation path in any real clinical setting. Thus, it appears that the effects of NLP can be ignored in applications of TI to homogeneous media as defined in NCRP Report No. 113 (NCRP, 1992) and in ODS (Carstensen *et al.*, 1999). Note, however, that, for this conclusion to hold, fields should be specified in terms of the source power or intensity. Fields estimated on the basis of hydrophone measurements at high-signal levels in water as illustrated in Figure D.1, could lead to significant errors in estimation of TI.

The example given above has assumed a uniform source intensity across the piston source. Although this illustrates the general phenomena associated with NLP, individual applications should consider the apodization which is commonly used in clinical devices as noted in the discussion of Figure D.1 above.

D.2.5 Acoustic Pressures

At small signal levels where the waveforms are sinusoidal, the pressure amplitude of the fundamental and the magnitude of the negative pressure are identical. In the case of a plane wave of infinite extent in a poorly attenuating medium such as water, as the source amplitude increases, the wave front steepens as the wave propagates. In the high-intensity limit, harmonics with amplitudes inversely proportional to their number are generated, (*e.g.*, the second harmonic has one-half the amplitude of the fundamental) and the waveform assumes a sawtooth shape. In a medical ultrasound field, diffraction, absorption and dispersion combine the harmonic components to yield an asymmetric wave as shown in Section 5, Figure 5.20, where the magnitude of the negative phase of the wave is smaller than the positive phase. Depending on phase relationships

among the harmonics, the negative pressure can be either greater or smaller than the fundamental component alone but frequently they are of comparable magnitude.

Figure D.5 gives the amplitude of the negative component of the acoustic pressure at the focus of a 3 MHz, 1 cm radius source, nonapodized, 8 cm focal length as in Figure D.1, for homogeneous propagation paths in water and liver as computed by the NLP model (Christopher and Parker, 1991). Liver was chosen as a representative soft tissue. Its absorption coefficient is only a little greater than the $0.3 \text{ dB cm}^{-1} \text{ MHz}^{-1}$ that is used in ODS derating protocol (Parker, 1983). Because of the differences in small-signal absorption coefficients, the focal pressures in liver are less than half those in water for equivalent source intensities. However, finite-amplitude absorption has a greater effect on the high-amplitude water wave than on the wave in liver, and the saturation levels of the fundamental component of the focal pressure in water and liver are comparable. As discussed above, measurements made in water at levels approaching saturation have almost no value in predicting the sound fields that the same source would generate in tissue.

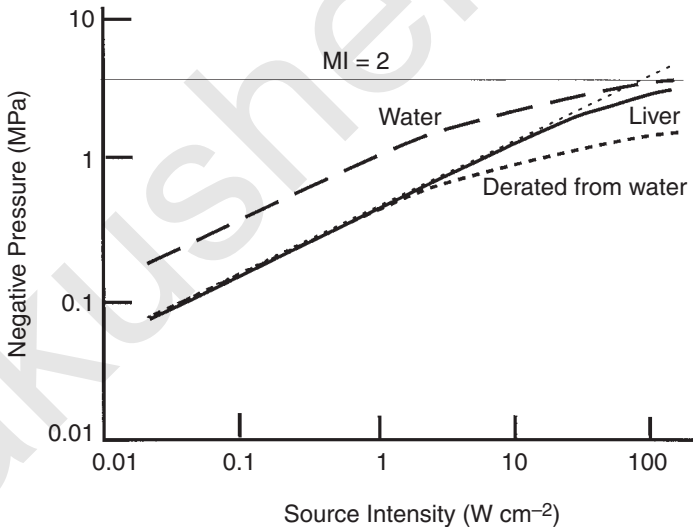


Fig. D.5. Focal acoustic pressures in water and liver for a 3 MHz, 1 cm radius source, nonapodized, with an 8 cm focal length. The dotted curve is derated from the water curve using the linear attenuation coefficient of liver. The light dotted line is a linear extrapolation of the derated pressure (Carstensen *et al.*, 1999).

D.2.6 Derating Pressures

The first requirement for predicting the occurrence of a biological effect in the body from exposure to diagnostic ultrasound is knowledge of the exposure at the site of interest. Of course, acoustic fields are not measured in the body directly. Instead, the traditional method for estimating these fields has been (1) to place the transducer in a water bath where losses are assumed to be zero, (2) to measure its field with a hydrophone under the same operating conditions that will eventually be used in a diagnostic exam, and (3) to reduce mathematically the measured values by an attenuation factor that is thought to represent the characteristics of the tissues encountered in transit of the signal through the body. This process is called *derating*. The primary source of error in estimating tissue fields by this process arises in the choice of the attenuation coefficients used to represent the tissues in the sound path. Several consensus groups have recommended attenuation models for tissues. NCRP (1992) recommended $0.05 \text{ Np cm}^{-1} \text{ MHz}^{-1}$ ($0.44 \text{ dB cm}^{-1} \text{ MHz}^{-1}$). In ODS (AIUM/NEMA, 1992), the attenuation recommended is $0.3 \text{ dB cm}^{-1} \text{ MHz}^{-1}$. Both of these models assume that the propagation path is homogeneous. NCRP (1992) recommends a different model for applications in which a large part of the propagation path is fluid. Both of these models are intended to be conservative, *i.e.*, to overestimate rather than underestimate the tissue fields. In contrast, NLP phenomena can lead to underestimates in the derating process when the output levels of diagnostic systems are very large.

Figure D.5 provides an illustration. The important point demonstrated by Figure D.5 is that saturation is approached at lower source intensities in water than in tissue. As a result, when water values are linearly derated (dashed) as prescribed by consensus models, the tissue field is *underestimated* at high source intensities. The true focal pressures in liver are approximately twice as large as the derated values at the highest output levels in this example.

Note that, at the highest source intensities in Figure D.5, the linearly derated pressures are only a little greater than 1 MPa, well within the limit (3.3 MPa at 3 MHz) for diagnostic equipment set by the FDA Track 3 approval process (see Section 10 and Appendix B). Because the fields in water for this transducer approach saturation at the upper end of this curve, it appears that outputs for this transducer would be limited by physical and engineering considerations rather than by regulatory guidelines.

Although the water fields start to level off at the upper end of the curves in Figure D.5, the effects of finite-amplitude attenuation are only beginning to be seen in liver. Thus, it should be possible to

achieve somewhat higher pressure levels in the tissue by further increases in the source levels before saturation in the tissue becomes limiting—all within FDA limits. This is true only for relatively long propagation distances. Of course, the principal need for high-pressure amplitudes is to achieve greater depths of penetration. In fact, the existence of regulatory limits may actually give a false sense of security to some users.

A simple solution to the problem presented above can be achieved by characterizing the field of the transducer at small-signal levels, derating these values linearly and extrapolating linearly to higher levels as illustrated by the fine dotted line in Figure D.5. The result is a closer approximation of the true fields but with an *overestimate* rather than an underestimate of the tissue fields at the highest-output levels.

This procedure has a number of conceptual and practical advantages. From a safety standpoint, the most important of these is that the field estimates are usually conservatively large. In addition, fields need only be measured at small-signal levels where the waveform is simple and bandwidth requirements of the detection system are modest. Each pulse can be characterized by its pressure amplitude, defined as one-half the maximal peak to peak excursion of the wave. Conceptually then, the *linearly* extrapolated fields would have the same wave shape at all output levels in spite of the fact that the real fields in the tissue may be distorted by NLP. In describing the output of the system, this procedure avoids the question of which characteristic of the nonlinearly distorted wave to use in characterizing pressures.

If for any reason greater accuracy is desired than one achieves through linear extrapolation of small-signal values, either theoretical or experimental procedures may be used to estimate the pressures in tissue taking into account NLP.

In general, no single parameter or combination of parameters that describe the sound field can be used in isolation to predict whether biological effects will occur or whether the exposures used in a given examination are safe. There is no single number that can be displayed on-screen that by itself signals hazard without consideration of the site of exposure. Modern trends in on-screen labeling make field information available, but, risk/benefit decisions must be made in the context of current knowledge of the biological effects which those fields can produce. Because the likelihood of the occurrence of biological effects is site dependent, only an informed user can decide whether the field amplitudes necessary to achieve the desired diagnostic information are warranted in light of the possible occurrence of adverse biological effects. Fortunately, the relevant information

can be summarized succinctly through threshold data for nonthermal biological effects that have been observed in laboratory mammals. This subject is discussed in detail in Section 8.

D.2.7 *Nonlinear Propagation and the Mechanical Index*

MI has served the manufacturers and users of diagnostic ultrasound equipment well since its official adoption in 1992. It provided a rationale for increasing output levels at frequencies above 1.6 MHz within the legal framework that empowers FDA. Having been incorporated in the hardware and software of many modern ultrasound systems, it is likely in the United States to remain the best, readily available indicator of temporal-peak as opposed to temporal-average outputs for some time into the future.

In assessing the probability of the occurrence of bioeffects, one needs to know the acoustic field at the target site. An obstetrician is probably most concerned about exposure of the fetus and is somewhat less troubled by the possibility of effects in the overlying abdominal tissues. The cardiologist needs to know the exposure of the surface of the lung even though that may not be at the focus of the source. MI does not address this general problem. It was designed simply to provide an estimate of the maximal pressure in the field and it was formulated under the tacit assumption that propagation of ultrasound is linear in spite of the fact that NLP effects are clearly evident in the calibration process.

Briefly, the protocol for measuring MI is as follows:

1. *PII* is measured in water under normal operating conditions along the axis of the sound beam of the transducer. The result is a series of maxima along the axis culminating in the largest maximum at the “focus” of the transducer.
2. These measurements are derated by $0.3 \text{ dB cm}^{-1} \text{ MHz}^{-1}$. The derating process tends to shift the position of the maxima closer to the source.
3. The negative pressure is measured at the position of the derated maximal *PII*.
4. This pressure is derated by $0.3 \text{ dB cm}^{-1} \text{ MHz}^{-1}$.
5. Dividing the derated pressure by the square root of the center frequency of the signal gives MI.

If the entire system were linear as assumed in the ODS protocol, field pressure and source pressure would be proportional and MI would simply increase linearly with output level.

The most striking effect of NLP on MI is the way that it moves the position of the maximal *PII* in the course of implementing Step 1

above. This effect is shown in Figure D.6. Instead of water being a “lossless” medium, it’s finite-amplitude attenuation increases as the output level increases. As noted under Step 2 above, even small-signal absorption tends to shift the “focus” toward the source. (At a source intensity of only 5 W cm^{-2} , the maximum of the *derated PII* is closer to 7 than 8 cm from the source.) However, NLP produces a strange kind of absorption parameter that increases in magnitude with distance from the source. As a consequence, the shift of the maximum of *PII* toward the source as the output level increases is significant. At high output levels (about 20 W cm^{-2} in this example), the final maximum in the integral may fall below the penultimate maximum and there is a discontinuous shift in the position of *PII*. By 50 W cm^{-2} , the highest derated *PII* has shifted discontinuously again, this time to 2.7 cm!

If one applies the ODS protocol to determine the pressure to be used in MI, the same qualitative error is made as was pointed out earlier and illustrated in Figure D.5, *i.e.*, MI will be underestimated at large source intensities. However, the effect of NLP on the position of the maximal *PII* tends to minimize the underestimation of the tissue pressures at that position. This can be seen in Figure D.7 which shows the complete axial profile of the negative pressure in tissue and the linearly derated-water pressures for a source intensity

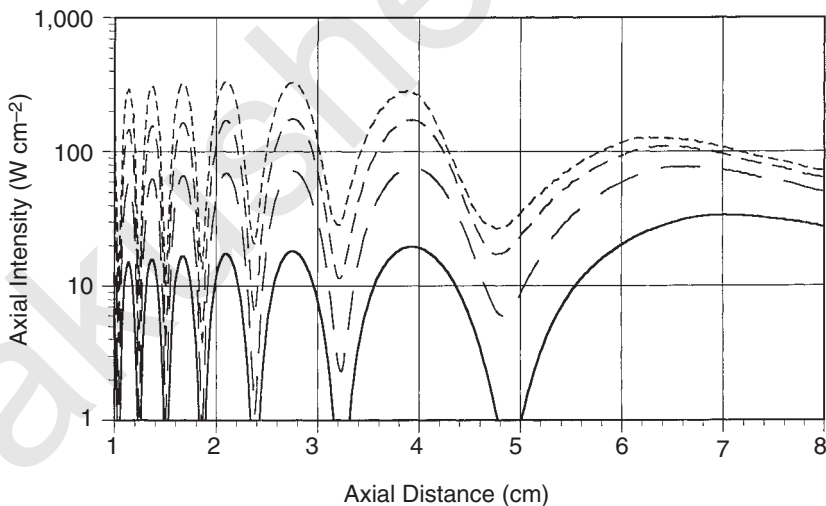


Fig. D.6. Linearly derated axial intensities for the source of Figure D.5. The curves are for source intensities of 5, 20, 50 and 100 W cm^{-2} . Note that the computations assume a “long” pulse, *i.e.*, one for which the rise and decay times do not contribute significantly to *PII* (Carstensen *et al.*, 1999).

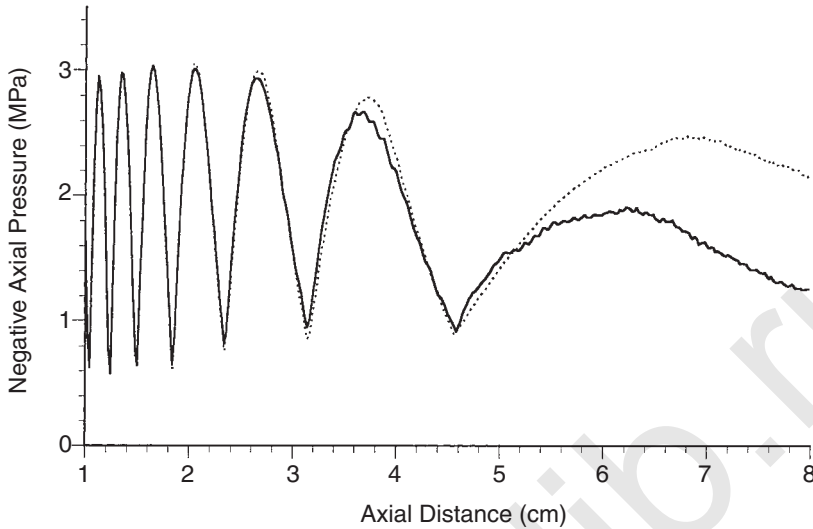


Fig. D.7. Negative axial pressures for the source of Figure D.5. The solid curve is the pressure linearly derived from water measurements and the dotted curve is the computed field propagated through tissue. The source intensity is 100 W cm^{-2} (Carstensen *et al.*, 1999).

of 100 W cm^{-2} . As noted above, the underestimate of tissue fields at 8 cm approaches a factor of two. Yet, the effects of NLP at $\sim 2 \text{ cm}$, where the fields for MI are found, are negligible. In the example being considered (1 cm radius, 3 MHz source), the greatest underestimate of MI is about 20 percent and this occurs at source intensity of $\sim 5 \text{ W cm}^{-2}$ (Carstensen *et al.* 1999). The errors in MI from NLP are actually smaller at higher source intensities. It is impossible with present knowledge to draw general conclusions on the magnitude of errors introduced in MI by NLP. Underestimates as great as a factor of two have been demonstrated in certain experimental configurations. A simple way to avoid underestimating the acoustic fields under the conditions of NLP when there is no fluid in the path is to characterize the fields at low intensities and extrapolate linearly to higher-source intensities.

As currently defined, MI has several severe limitations.

1. As discussed above, the position in the medium at which the field is specified by the index may shift significantly with the output level. That information is not conveyed to the user. Thus, the index is not generally useful in predicting fields at specific sites in the tissues.

2. As an indicator of the maximal negative pressure within the field, MI may understate pressures in tissues at the highest output levels. Although in many cases this error is small, there appear to be transducer-tissue combinations where the effect can be substantial.
3. MI fails to account for poorly attenuating propagation paths as found in scanning the fetus through the bladder and amniotic fluid. The resulting underestimate of tissue fields can be more severe than that associated with NLP.
4. In exposure of lung through the chest wall, MI fails to provide the relevant pressure levels.
5. With the exception of lung hemorrhage, the frequency dependence built into MI does not correspond to the frequency dependence of biological-effects thresholds.
6. As defined, MI ignores positive pressures, which are as effective as negative pressures in producing lung hemorrhage (Bailey *et al.*, 1996).

Limitations 2 and 6 can be solved satisfactorily by linear extrapolation of small-signal levels. On the positive side, the ultrasound industry's on-screen display of MI has provided the first on-line indication of the temporal peak fields to which patients are exposed.

D.3 Summary

1. At high-pressure levels, the positive portion of the sound wave tends to move at higher velocity than the negative portion. So, instead of the wave propagating as the pure sinusoid that was generated by the source, the wave is progressively distorted as it moves through the medium. Under conditions typical for diagnostic ultrasound, diffraction and dispersion phenomena interact with this NLP process in such a way that the wave becomes asymmetric with the positive pressures being somewhat greater than the negative pressures. It appears that neither positive nor negative pressures can be ignored when predicting the occurrence of biological effects in tissues containing bubbles. Furthermore, NLP produces complex changes in the attenuation of the wave that make it very difficult to relate measurements that are made in water at high-ultrasound levels with the levels that would be found if the wave had propagated through tissue.
2. Because the absorption of sound increases with increasing frequency, the harmonics generated by NLP enhance losses. Under

realistic conditions encountered in diagnostic ultrasound, the finite-amplitude-absorption parameter for water can become as large as the small-signal absorption coefficient of tissues such as liver. In the extreme case, field amplitudes become independent of source amplitudes, a phenomenon known as acoustic saturation. Momentum lost from the sound field through nonlinear absorption is transferred to the propagating medium resulting in macroscopic acoustic streaming. With NLP, the absorption coefficient of linear acoustics that is solely a property of the medium, must be replaced, at high amplitudes, by a finite-amplitude-absorption parameter that is a function of the source amplitude and frequency, the amplitude dependence of the sound speed, the geometrical configuration of the sound field and the length of the propagation path. Surprisingly, in poorly attenuating materials such as water, the absorption parameter is essentially independent of the small-signal absorption coefficient of the medium. Under realistic conditions encountered in diagnostic ultrasound, the finite-amplitude-absorption parameter for water can become as large as the small-signal absorption coefficient of tissues such as liver. Beam patterns are broadened at high amplitudes by NLP because of excess losses on the axis. These same losses, however, result in the narrowing of heating patterns as shock waves begin to develop.

3. Although NLP can cause large increases in focal-heating rates in soft tissues compared with those that would be predicted on linear theory, the effect of NLP on the steady-state-temperature rise is small enough that it can be ignored in computation of TI in most applications.
4. The common practice of linear derating from high-level measurements in water is undesirable because it can lead to substantial *underestimates* of acoustic pressures in tissues. This can be avoided if estimates of tissue pressures are based on small-signal characterization of source-field relationships. Once the field has been characterized through measurements in water for a given low source power, it can be derated linearly using an appropriate model and attenuation factor for the tissue path. If these derated fields are linearly extrapolated from the source power, estimates of tissue fields are good approximations of the true fields in tissues for a large range of input values and, at very high field strengths where NLP does modify the field, the linearly derated values are conservatively large. When greater accuracy is desired, corrections for the effects of NLP can be made either theoretically or experimentally.

Glossary

acoustic cavitation: The mechanical response of one or more cavities to a sound field; it may be inertial or noninertial (see Sections 4 and 5).

acoustic pressure: The excess of the instantaneous pressure at a point in a sound field over the pressure in the absence of sound.

acoustic pressure amplitude: For a sound field where the acoustic pressure varies sinusoidally with the time, the maximal value of the acoustic pressure. For a pulsed field of ultrasound, or for nonlinearly distorted waves (see Section 5.4).

acoustic radiation force: Time-averaged force on an object produced by a sound field (see Sections 3 and 4).

acoustic radiation torque: Time-averaged torque on an object produced by a sound field (see Section 3).

acoustic streaming: Time-averaged flow of a liquid or gas produced by a sound field (see Sections 3 and 4).

bubble: A cavity that is nearly, or completely, surrounded by liquid.

cavitation nucleus: A small body, usually a cavity, that can serve as a site for acoustic cavitation.

cavity: A volume filled with gas or vapor, or both.

collapse: Rapid decrease in volume of a cavity that, in an aqueous medium, leads to production of shock waves, free radicals and/or sonoluminescence.

dwell time: The time during which an ultrasound beam is directed to a specific part of a patient's body.

encapsulated bubble: A cavity in which the gas and liquid phases are separated by a thin shell of insoluble solid or liquid material.

fundamental frequency: For a periodic function in general, the repetition frequency. For a function formed by low-frequency periodic modulation of a high-frequency periodic function, the fundamental frequency of the latter; in this case, the (low) frequency of the modulation is the repetition frequency.

gas-body activation (GBA): A sub-category of noninertial cavitation involving the mechanical response of stabilized gas bodies to a sound field (see Section 4).

harmonic: A spectral component whose frequency is n times that of the fundamental where n is a positive non-zero integer.

inertial cavitation: A class of acoustic cavitation involving growth and collapse of one or more cavities (previously called "transient cavitation") (see Section 5).

noninertial cavitation: A class of acoustic cavitation in which collapse does not occur. It includes acoustically induced translational motion of bubbles, bubble growth by rectified diffusion or coalescence, continuous

heat production, radiation forces on neighboring particles and micro-streaming (see Section 4).

polytropic index of a gas: In a small decrease of volume caused by a small increase of pressure, the ratio of the fractional increase in pressure to the fractional decrease in volume.

sonoluminescence: Production of light by inertial cavitation.

stabilized gas body: A gas-filled cavity that is stabilized by structures which partially or completely surround it.

subharmonic: A spectral component whose frequency is $1/n$ times the fundamental frequency, where n is a positive non-zero integer.

akusher-lib.ru

Symbols

This list does not include symbols that are used only locally, *i.e.*, within a single small portion of text.

a	Attenuation coefficient
a/f	Specific attenuation coefficient
A_{aprt}	Area of active aperture
A_i	Estimated specific attenuation coefficient for a particular tissue
A_i/d_i	Estimated specific attenuation coefficient for a particular tissue per unit path length of tissue
A_{ov}	Specific attenuation of overlying tissue
b	Energy-loss constant for bubble
c	Speed of sound
c_0	Value of c under conditions of linear acoustics
c_v	Heat capacity per unit volume
d_6	– 6 dB width of acoustic beam
d_{eq}	equivalent beam diameter
d_{ov}	Distance through overlying tissue
dB	Decibel
D	Diffusion constant
D	Ratio of signal level from tissue sample in water at distance of interest to signal of sample at focal point in water
D_{eq}	Diameter of effective area of transmitting transducer; equivalent aperture diameter
E_k	Kinetic energy density
$\langle E_k \rangle$	Time-averaged kinetic energy density
E_p	Potential energy density
$\langle E_p \rangle$	Time-averaged potential energy density
f	Frequency
f_c	Center frequency of acoustic beam
f_0	Resonance frequency for a bubble
F	Focal length; frame repetition rate
F_{rad}	Acoustic radiation force on an object
F_v	Acoustic radiation force per unit volume; viscous drag
FL	Focal length
H	Enthalpy
I	Acoustic intensity
I_{SPTA}	Spatial-peak temporal-average intensity
$I_{\text{SPTA.3}}$	Spatial-peak temporal-average intensity obtained by reducing (derating) water measured values of I_{SPTA} or the derated value of I_{SPTA}

I_{TA}	Time average intensity
$I_{TA.3}$	I_{TA} derated to $0.3 \text{ dB cm}^{-1} \text{ MHz}^{-1}$
IF	Inertial acceleration function
k	Propagation constant ($k = \omega/c = 2\pi/\lambda$)
k_s	“Effective spring constant” for a bubble
K	Thermal conductivity
ℓ	Acoustic boundary layer thickness
L	Perfusion length constant; pulse length
m	“Effective mass” of a bubble
MI	Mechanical index
N	Ratio of minimal detectable signal level under ideal conditions to signal level necessary to visualize tissue information
N_r	Reynold’s number
ODS	Output Display Standard
p	Acoustic pressure
$p_{0.3}$	Derated pressure amplitude
p_{g0}	Momentary bubble gas pressure
p_0	Pressure amplitude
p_{0c}	Pressure amplitude of center frequency; threshold pressure (in bubble)
$p_{r.3} (z_{sp})$	Derated peak rarefactional pressure at z_{sp}
p_w	Pressure amplitude measured in water
p_+, p_c	Peak positive (compressional) pressure
$p_{+0.3}, p_{c0.3}$	Derated peak positive (compressional) pressure derated to $0.3 \text{ dB cm}^{-1} \text{ MHz}^{-1}$
p_-, p_r	Peak negative (rarefactional) pressure
$p_{-0.3}, p_{r0.3}$	Derated peak negative (rarefactional) pressure derated to $0.3 \text{ dB cm}^{-1} \text{ MHz}^{-1}$
p_{rad}	Acoustic radiation pressure
p_v, P_{v0}	Vapor pressure
P	Proportion of cases in which bioeffect occurs following treatment
P	Total pressure
P_A	Decreased pressure from original P_0
P_0	Hydrostatic pressure
P_0	Proportion of cases in which bioeffect occurs naturally
PD	Pulse duration
PF	Pressure acceleration function
PII	Free-field pulse intensity integral
PRF	Pulse repetition frequency
q	Reasonable-worst-case exposure quantity
q_v	Rate of heat production per unit volume
Q	Image quality
R	Radius of bubble
R_G	Ratio of maximal unsaturated signal to minimal signal above noise

R_{\max}	Largest value of R in an R versus t response for a bubble
R_0	Value of R in the absence of sound
R_t	Blake threshold radius
s	Absorption-scattering cross section of a bubble
s_p	Specific heat
S	Cross-sectional area of target; viscous stress
S_r	Shear stress
S_r	Backscatter factor
SATA	Spatial-average temporal-average
SATP	Spatial-average temporal-peak
SPPA	Spatial-peak pulse-average
SPTA	Spatial-peak temporal-average
SPTP	Spatial-peak temporal-peak
t	Time
T	Temperature
T, T_r	Pulse repetition period
T_c	Core temperature
T_0	Ambient temperature
TI	Thermal index
TIB	Bone thermal index
TIC	Cranial thermal index
TIS	Soft tissue thermal index
u	Component of acoustic particle velocity
U	Acceleration of bubble radius
U_0	Streaming velocity
v	Volume
W	Acoustic power
$W_{.3}(z_1)$	Derated ultrasonic power at axial distance z_1
z_{bp}	Break point depth
z_m	Effective penetration depth
z_{sp}	Axial distance to spacial peak; point of maximal pulse intensity integral
α	Acoustic absorption coefficient
β	Compressibility
β_r	Compressibility ratio
Γ	Polytropic index of a gas
Δ	Acoustic boundary layer thickness
δ	Damping constant for bubble
η	Coefficient of shear viscosity; electronic noise power per unit frequency
θ	Angle between direction of particle-particle axis and direction of oscillatory motion in surrounding fluid

κ	Thermal diffusivity
λ	Acoustic wavelength
ξ	Radial displacement of bubble surface
ξ_0	Displacement amplitude of a bubble
ρ	Density (mass/volume)
ρ_0	Density in the absence of sound
σ	Bubble gas-liquid surface tension
τ	Characteristic time for a bubble; pulse duration; pulse length; time constant for diffusion
ϕ	Duty factor; reciprocal of thermal diffusion layer thickness
χ	Nondimensional displacement amplitude for a bubble
Ψ_p	Ratio of maximal power increase
Ω	Nondimensional frequency ($\Omega = \omega/\omega_0 = f/f_0$)
ω	Angular frequency ($\omega = 2\pi f$)
ω_0	Resonance value of ω for a bubble

References

- ABBOTT, J.G. (1999). "Rationale and derivation of MI and TI—a review," *Ultrasound Med. Biol.* **25**, 431–441.
- ABDULLA, U., DEWHURST, C.J., CAMPBELL, S., TALBERT, D., LUCAS, M. and MULLARKEY, M. (1971). "Effect of diagnostic ultrasound on maternal and fetal chromosomes," *Lancet* **2**, 829–831.
- ABRAHAM, V., ZISKIN, M.C. and HEYNER, S. (1989). "Temperature elevation in the rat fetus due to ultrasound exposure," *Ultrasound Med. Biol.* **15**, 443–449.
- ABRAMOWICZ, J.S. (1997). "Ultrasound contrast media and their use in obstetrics and gynecology," *Ultrasound Med. Biol.* **23**, 1287–1298.
- ABRAMS, R., CATON, D., CURET, L.B., CRENSHAW, C., MANN, L. and BARRON, D.H. (1969). "Fetal brain-maternal aorta temperature differences in sheep," *Am. J. Physiol.* **217**, 1619–1622.
- ADAMSONS, K., JR. and TOWELL, M.E. (1965). "Thermal homeostasis in the fetus and newborn," *Anaesthesiology* **26**, 531–548.
- AIUM (1985). American Institute of Ultrasound in Medicine. *Acoustical Data for Diagnostic Ultrasound Equipment* (American Institute of Ultrasound in Medicine, Laurel, Maryland).
- AIUM (1987). American Institute of Ultrasound in Medicine. *Acoustical Data for Diagnostic Ultrasound Equipment* (American Institute of Ultrasound in Medicine, Laurel, Maryland).
- AIUM (1992). American Institute of Ultrasound in Medicine. *Acoustic Output Measurement and Labeling Standard for Diagnostic Ultrasound Equipment* (American Institute of Ultrasound in Medicine, Laurel, Maryland).
- AIUM (1993a). American Institute of Ultrasound in Medicine. *Bioeffects and Safety of Diagnostic Ultrasound* (American Institute of Ultrasound in Medicine, Laurel, Maryland).
- AIUM (1993b). American Institute of Ultrasound in Medicine. *Acoustical Data for Diagnostic Ultrasound Equipment* (American Institute of Ultrasound in Medicine, Laurel, Maryland).
- AIUM (1993c). American Institute of Ultrasound in Medicine. *Performance Criteria for Doppler Ultrasound Devices. Report of the AIUM Technical Standards Committee* (American Institute of Ultrasound in Medicine, Laurel, Maryland).
- AIUM (1994a). American Institute of Ultrasound in Medicine. *Medical Ultrasound Safety* (American Institute of Ultrasound in Medicine, Laurel, Maryland).
- AIUM (1994b). American Institute of Ultrasound in Medicine. "Bioeffects literature review," *J. Ultrasound Med.* **13**, 917–920.

- AIUM (1997a). American Institute of Ultrasound in Medicine. *Guidelines for the Performance of Pediatric Ultrasound Examinations* (American Institute of Ultrasound in Medicine, Laurel, Maryland).
- AIUM (1997b). American Institute of Ultrasound in Medicine. *Safety Considerations for Diagnostic Ultrasound* (American Institute of Ultrasound, Laurel, Maryland).
- AIUM (1998). American Institute of Ultrasound in Medicine. *Acoustical Output Labeling Standard for Diagnostic Ultrasound Equipment* (American Institute of Ultrasound, Laurel, Maryland).
- AIUM (2000). "Section 6—Mechanical bioeffects in the presence of gas-carrier ultrasound contrast agents," *J. Ultrasound Med.* **19**, 120–142, 154–168.
- AIUM/NEMA (1992). American Institute of Ultrasound in Medicine/National Electrical Manufacturers Association. *Standard for Real-Time Display of Thermal and Mechanical Acoustic Output Indices on Diagnostic Ultrasound Equipment* (American Institute of Ultrasound in Medicine, Laurel, Maryland).
- AIUM/NEMA (1998). American Institute of Ultrasound in Medicine/National Electrical Manufacturers Association. *Acoustic Output Measurement Standard for Diagnostic Ultrasound Equipment* (American Institute of Ultrasound in Medicine, Laurel, Maryland).
- AKULICHEV, V.A. (1971). "Pulsation of cavitation voids in high intensity ultrasonic fields," page 129 in *High-Intensity Ultrasonic Fields*, Rozenberg, L.D., Ed. (Plenum Press, New York).
- ALEXEEF (1876). "Ueber die temperatur des kindes im uterus," *Arch. Gynak.* **10**, 141–144.
- AL-KARMI, A.M., DINNO, M.A., STOLTZ, D.A., CRUM, L.A. and MATTHEWS, J.C. (1994). "Calcium and the effects of ultrasound on frog skin," *Ultrasound Med. Biol.* **20**, 73–81.
- ALLMAN, R. and COAKLEY, W.T. (1994). "Ultrasound enhanced phase partition of microorganisms," *Bioseparation* **4**, 29–38.
- ANGLES, J.M., WALSH, D.A., LI, K., BARNETT, S.B. and EDWARDS, M.J. (1990). "Effects of pulsed ultrasound and temperature on the development of rat embryos in culture," *Teratology* **42**, 285–293.
- ANONYMOUS (1978a). "Editorial: Is hyperthermia a teratogen?" *BMJ* **2**, 1586–1587.
- ANONYMOUS (1978b). "Perinatal body-temperatures," *Lancet* **1**, 964.
- ANSI (1992). American National Standards Institute. *Standard Reference Zero for the Calibration of Pure-Tone Bone-Conduction Audiometers* (Acoustical Society of America, New York).
- APFEL, R.E. (1982). "Acoustic cavitation: A possible consequence of biomedical uses of ultrasound," *Br. J. Cancer (Suppl.)* **45**, 140–146.
- APFEL, R.E. (1986). "Possibility of microcavitation from diagnostic ultrasound," *IEEE Trans. UFFC* **32**, 139–142.
- APFEL, R.E. and HOLLAND, C.K. (1991). "Gauging the likelihood of cavitation from short-pulse, low-duty cycle diagnostic ultrasound," *Ultrasound Med. Biol.* **17**, 179–185.

- ARIANI, M., FISHBEIN, M.C., CHAE, J.S., SADEGHI, H., MICHAEL, A.D., DUBIN, S.B. and SIEGEL, R.J. (1991). "Dissolution of peripheral arterial thrombi by ultrasound," *Circulation* **84**, 1680–1688.
- ARKIN, H., XU, L.X. and HOLMES, K.R. (1994). "Recent developments in modeling heat transfer in blood perfused tissues," *IEEE Trans. Biomed. Eng.* **41**, 97–107.
- ARMOUR, E.P. and CORRY, P.M. (1982). "Cytotoxic effects of ultrasound *in vitro* dependence on gas content, frequency, radical scavengers, and attachment," *Radiat. Res.* **89**, 369–380.
- ARORA, K.L., COHEN, B.J. and BEAUDOIN, A.R. (1979). "Fetal and placental responses to artificially induced hyperthermia in rats," *Teratology* **19**, 251–259.
- ARULKUMARAN, S., TALBERT, D.G., NYMAN, M., WESTGREN, M., HSU, T.S. and RATNAM, S.S. (1991). "Letter: Audible *in utero* sound from ultrasound scanner," *Lancet* **338**, 704–705.
- ATCHLEY, A.A. and PROSPERETTI, A. (1989). "The crevice model of bubble nucleation," *J. Acoust. Soc. Am.* **86**, 1065–1084.
- ATL (1996). Advanced Technology Laboratories. *HDI 3000 Reference Manual*, 4703-0015-05 (Advanced Technology Laboratories, Bothell, Washington).
- AYME, E.J. and CARSTENSEN, E.L. (1989a). "Cavitation induced by asymmetric, distorted pulses of ultrasound: A biological test," *Ultrasound Med. Biol.* **15**, 61–66.
- AYME, E.J. and CARSTENSEN, E.L. (1989b). "Cavitation induced by asymmetric, distorted pulses of ultrasound: Theoretical predictions," *IEEE Trans. UFFC* **36**, 31–48.
- AYME-BELLEGRADA, E.J. (1990). "Collapse and rebound of a gas-filled spherical bubble immersed in a diagnostic ultrasonic field," *J. Acoust. Soc. Am.* **88**, 1054–1060.
- AZADNIV, M., DOIDA, Y., MILLER, M.W., BRAYMAN, A.A. and MELTZER, R.S. (1996). "Temporality in ultrasound-induced cell lysis *in vitro*," *Echocardiography* **13**, 45–56.
- BACHER, R.P. and WILLIAMS, M.C. (1970). "Hemolysis in capillary flow," *J. Lab. Clin. Med.* **76**, 485–496.
- BACON, D.R. and SHAW, A. (1993). "Experimental validation of predicted temperature rises in tissue-mimicking materials," *Phys. Med. Biol.* **38**, 1647–1659.
- BAGGS, R., PENNEY, D.P., COX, C., CHILD, S.Z., RAEMAN, C.H., DALECKI, D. and CARSTENSEN, E.L. (1996). "Thresholds for ultrasonically induced lung hemorrhage in neonatal swine," *Ultrasound Med. Biol.* **22**, 119–128.
- BAILEY, M.R., DALECKI, D., CHILD, S.Z., RAEMAN, C.H., PENNEY, D.P., BLACKSTOCK, D.T. and CARSTENSEN, E.L. (1996). "Bioeffects of positive and negative acoustic pressures *in vivo*," *J. Acoust. Soc. Am.* **100**, 3941–3946.
- BAILEY, M.R., BLACKSTOCK, D.T., CLEVELAND, R.O. and CRUM, L.A. (1999). "Comparison of electrohydraulic lithotripters with rigid and

- pressure-release ellipsoidal reflectors. II. Cavitation fields," *J. Acoust. Soc. Am.* **106**, 1149–1160.
- BAKER, A.C. (1997). "A numerical study of the effect of drive level on the intensity loss from an ultrasonic beam," *Ultrasound Med. Biol.* **23**, 1083–1088.
- BAKER, D., FORSTER, F.K. and DAIGLE, R.E. (1978). "Doppler principles and techniques," pages 161 to 287 in *Ultrasound: Its Applications in Medicine and Biology*, Fry, F.J., Ed. (Elsevier Publishing Company, New York).
- BAKKETEIG, L.S., EIK-NES, S.H., JACOBSEN, G., ULSTEIN, M.K., BRODTKORB, C.J., BALSTAD, P., ERIKSEN, B.C. and JORGENSEN, N.P. (1984). "Randomised controlled trial of ultrasonographic screening in pregnancy," *Lancet* **2**, 207–211.
- BAMBER, J.C. (1981). "Ultrasonic attenuation in fresh human tissues," *Ultrasonics* **19**, 187–188.
- BAMBER, J.C. and HILL, C.R. (1979). "Ultrasonic attenuation and propagation speed in mammalian tissues as a function of temperature," *Ultrasound Med. Biol.* **5**, 149–157.
- BANG, J. (1972). "The intensity of ultrasound in the uterus during examination for diagnostic purposes," *Acta. Pathol. Microbiol. Scand. [A]* **80**, 341–344.
- BANJAVIC, R.A., ZAGZEBSKI, J.A., MADSEN, E.L. and GOODSITT, M.M. (1979). "Distortion of ultrasound beams in attenuating media," *Acoust. Imag. Hologr.* **1**, 165–177.
- BAO, S., THRALL, B.D. and MILLER, D.L. (1997). "Transfection of a reporter plasmid into cultured cells by sonoporation *in vitro*," *Ultrasound Med. Biol.* **23**, 953–959.
- BARBARESE, E., HO, S.Y., D'ARRIGO, J.S. and SIMON, R.H. (1995). "Internalization of microbubbles by tumor cells *in vivo* and *in vitro*," *J. Neurooncol.* **26**, 25–34.
- BARBER, B.P. and PUTTERMAN, S.J. (1992). "Light scattering measurements of the repetitive supersonic implosion of a sonoluminescing bubble," *Phys. Rev. Lett.* **69**, 3839–3842.
- BARDSLEY, D.W., COAKLEY, W.T., JONES, G. and LIDDELL, J.E. (1989). "Electroacoustic fusion of millilitre volumes of cells in physiological medium," *J. Biochem. Biophys. Methods* **19**, 339–348.
- BARNARD, J.W., FRY, W.J. and BRENNAN, J.F. (1956). "Small localized ultrasonic lesions in the white and grey matter of the cat brain," *Arch. Neurol. Pshychia.* **75**, 15–35.
- BARNETT, S.B. and KOSSOFF, G. (1984). "Temporal peak intensity as a critical parameter in ultrasound dosimetry," *J. Ultrasound Med.* **3**, 385–389.
- BARNETT, S.B., BAKER, R.S. and BARNSTABLE, S. (1983). "Is pulsed ultrasound mutagenic?" *Ultrasound Med. Biol. (Suppl.)* **2**, 45–48.
- BARNETT, S.B., MILLER, M.W., COX, C. and CARSTENSEN, E.L. (1988). "Increased sister chromatid exchanges in Chinese hamster ovary cells exposed to high intensity pulsed ultrasound," *Ultrasound Med. Biol.* **14**, 397–403.

- BARNETT, S.B., WALSH, D.A. and ANGLES, J.A. (1990). "Novel approach to evaluate the interaction of pulsed ultrasound with embryonic development," *Ultrasonics* **28**, 166–170.
- BARNETT, S.B., TER HAAR, G.R., ZISKIN, M.C., NYBORG, W.L., MAEDA, K. and BANG, J. (1994). "Current status of research on biophysical effects of ultrasound," *Ultrasound Med. Biol.* **20**, 205–218.
- BARTOLETTI, D.C., HARRISON, G.I. and WEAVER, J.C. (1989). "The number of molecules taken up by electroporated cells: Quantitative determination," *FEBS Lett.* **256**, 4–10.
- BATTAGLIA, F.C. and LUBCHENCO, L.O. (1967). "A practical classification of newborn infants by weight and gestational age," *J. Pediatr.* **71**, 159–163.
- BAULD, T.J. and SCHWAN, H.P. (1974). "Attenuation and reflection of ultrasound in canine lung tissue," *J. Acoust. Soc. Am.* **56**, 1630–1637.
- BAZETT, H.C. and MCGLONE, B. (1932). "Studies in sensation. III. Chemical factor in the stimulation of end-organ giving temperature sensations," *Arch. Neurol. Psychiat.* **28**, 71–91.
- BENES, E., BURGER, W., GROSCHL, M., SCHAFFNER, A., TRAMPLER, F., BOLEK, W., GAIDA, T., DOBLHOFF, O. and HAGER, F. (1993). "Trapping of suspended biological particles by use of ultrasonic resonance fields," pages 515 to 518 in *Ultrasonics International '93 Conference Proceedings* (Butterworth-Heinemann Ltd., Oxford).
- BENJAMIN, T.B. and URSELL, F. (1954). "The stability of the plane free surface of a liquid in vertical periodic motion," *Proc. Roy. Soc. (London)* **A225**, 505–515.
- BERG, R.B., CHILD, S.Z. and CARSTENSEN, E.L. (1983). "Letter: The influence of carrier frequency on the killing of *Drosophila* larvae by microsecond pulses of ultrasound," *Ultrasound Med. Biol.* **9**, L448–L451.
- BERMAN, E., CARTER, H.B. and HOUSE, D. (1984). "Growth and development of mice offspring after irradiation *in utero* with 2,450-MHz microwaves," *Teratology* **30**, 393–402.
- BERNSTEIN, E.F., BLACKSHEAR, P.L., JR. and KELLER, K.H. (1967). "Factors influencing erythrocyte destruction in artificial organs," *Am. J. Surg.* **114**, 126–138.
- BERNSTINE, R.L. (1969). "Safety studies with ultrasonic Doppler technic. A clinical follow-up of patients and tissue culture study," *Obstet. Gynecol.* **34**, 707–709.
- BHAGWAT, A.A. and APTE, S.K. (1989). "Comparative analysis of proteins induced by heat shock, salinity, and osmotic stress in the nitrogen-fixing cyanobacterium *Anabaena* sp. strain L-31," *J. Bacteriol.* **171**, 5187–5189.
- BIRNBAUM, Y., LUO, H., NAGAI, T., FISHBEIN, M.C., PETERSON, T.M., LI, S., KRICSFELD, D., PORTER, T.R. and SIEGEL, R.J. (1998). "Noninvasive *in vivo* clot dissolution without a thrombolytic drug: Recanalization of thrombosed iliofemoral arteries by transcutaneous ultrasound combined with intravenous infusion of microbubbles," *Circulation* **97**, 130–134.
- BJORNO, L. and LEWIN, P.A. (1982). "Nonlinear focusing effects in ultrasonic imaging," *Proceedings of the 1982 IEEE Ultrasonics Symposium* (Institute of Electrical and Electronic Engineers, Piscataway, New Jersey).

- BLACKSHEAR, P.L. and BLACKSHEAR, G.L. (1987). "Mechanical hemolysis," Chapter 15 in *Handbook of Bioengineering*, Skalak, R. and Chien, S., Eds. (McGraw-Hill, New York).
- BLACKSTOCK, D.T. (1966). "Connection between the Fay and Fubini solution for plane sound waves of finite amplitude," *J. Acoust. Soc. Am.* **39**, 1019–1026.
- BLAKE, F.G., JR. (1949). "The onset of cavitation in liquids," Technical memorandum No. 12 (Acoustics Research Laboratory, Harvard University, Cambridge, Massachusetts).
- BLAKE, F.G., JR. (1952). "Spherical wave propagation in solid media," *J. Acoust. Soc. Am.* **24**, 211–215.
- BLEEKER, H., SHUNG, K. and BARNHART, J. (1990). "Ultrasonic characterization of Alunex, a new contrast agent," *J. Acoust. Soc. Am.* **87**, 1792–1797.
- BLINC, A., FRANCIS, C.W., TRUDNOWSKI, J.L. and CARSTENSEN, E.L. (1993). "Characterization of ultrasound-potentiated fibrinolysis *in vitro*," *Blood* **81**, 2636–2643.
- BLOMLEY, M., ALBRECHT, T., COSGROVE, D., JAYARAM, V., BUTLER-BARNES, J. and ECKERSLEY, R. (1998). "Stimulated acoustic emission in liver parenchyma with Levovist," *Lancet* **351**, 568.
- BLOMLEY, M.J.K., ALBRECHT, T., COSGROVE, D.O., ECKERSLEY, R.J., BUTLER-BARNES, J., JAYARAM, V., PATEL, N., HECKEMANN, R.A., BAUER, A. and SCHLIEF, R. (1999a). "Stimulated acoustic emission to image a late liver and spleen-specific phase of Levovist in normal volunteers and patients with and without liver disease," *Ultrasound Med. Biol.* **25**, 1341–1352.
- BLOMLEY, M.J.K., ALBRECHT, T., COSGROVE, D.O., PATEL, N., JAYARAM, V., BUTLER-BARNES, J., ECKERSLEY, R.J., BAUER, A. and SCHLIEF, R. (1999b). "Improved imaging of liver metastases with stimulated acoustic emission in the late phase of enhancement with the U.S. contrast agent SH U 508A: Early experience," *Radiology* **210**, 409–416.
- BLY, S.H., VLAHOVICH, S., MABEE, P.R. and HUSSEY, R.G. (1992). "Computed estimates of maximum temperature elevations in fetal tissues during transabdominal pulsed Doppler examinations," *Ultrasound Med. Biol.* **18**, 389–397.
- BOOTE, E.J. and ZAGZEBSKI, J.A. (1988). "Performance tests of Doppler ultrasound equipment with a tissue and blood-mimicking phantom," *J. Ultrasound Med.* **7**, 137–147.
- BORBELY, G., SURANYI, G. KORCZ, A. and PALFI, Z. (1985). "Computed estimates of maximum temperature elevations in fetal tissues during transabdominal pulsed Doppler examinations," *Ultrasound Med. Biol.* **18**, 389–397.
- BOSWARD, K.L., BARNETT, S.B., WOOD, A.K., EDWARDS, M.J. and KOSSOFF, G. (1993). "Heating of guinea-pig fetal brain during exposure to pulsed ultrasound," *Ultrasound Med. Biol.* **19**, 415–424.
- BOUAKAZ A., DE JONG, N. and CACHARD, C. (1998). "Standard properties of ultrasound contrast agents," *Ultrasound Med. Biol.* **24**, 469–472.

- BOUDJOUK, P. (1988). "Heterogeneous sonochemistry," Chapter 5 in *Ultrasound: Its Chemical, Physical, and Biological Effects*, Suslick, K.S., Ed. (VCH Publishers, New York).
- BRAATEN, J.V., GOSS, R.A. and FRANCIS, C.W. (1997). "Ultrasound reversibly disaggregates fibrin fibers," *Thromb. Haemost.* **78**, 1063–1068.
- BRAUNER, T., BRUMMER, F. and HULSER, D.F. (1989). "Histopathology of shock wave treated tumor cell suspensions and multicell tumor spheroids," *Ultrasound Med. Biol.* **15**, 451–460.
- BRAYMAN, A.A. and MILLER, M.W. (1992). "Bubble cycling and standing waves in ultrasonic cell lysis," *Ultrasound Med. Biol.* **18**, 411–420.
- BRAYMAN, A.A. and MILLER, M.W. (1993). "Cell density dependence of the ultrasonic degassing of fixed erythrocyte suspensions," *Ultrasound Med. Biol.* **19**, 243–252.
- BRAYMAN, A.A. and MILLER, M.W. (1994). "Ultrasonic cell lysis *in vitro* upon fractional, discontinuous exposure vessel rotation," *J. Acoust. Soc. Am.* **95**, 3666–3668.
- BRAYMAN, A.A. and MILLER, M.W. (1997). "Acoustic cavitation nuclei survive the apparent ultrasonic destruction of Alunex microspheres," *Ultrasound Med. Biol.* **23**, 793–796.
- BRAYMAN, A.A. and MILLER, M.W. (1999). "Sonolysis of Alunex-supplemented, 40% hematocrit human erythrocytes by pulsed 1-MHz ultrasound: Pulse number, pulse duration and exposure vessel rotation dependence," *Ultrasound Med. Biol.* **25**, 307–314.
- BRAYMAN, A.A., DOIDA, Y. and MILLER, M.W. (1992). "Apparent contribution of respiratory gas exchange to the *in vitro* 'cell density effect' in ultrasonic cell lysis," *Ultrasound Med. Biol.* **18**, 701–714.
- BRAYMAN, A.A., AZADNIV, M., MILLER, M.W. and CHEN, X. (1994). "Bubble recycling and ultrasonic cell lysis in a stationary exposure vessel," *J. Acoust. Soc. Am.* **96**, 627–633.
- BRAYMAN, A.A., AZADNIV, M., MAKIN, I.R.S., MILLER, M.W., CARSTENSEN, E.L., CHILD, S.Z., RAEMAN, C.H., MELTZER, R.S. and EVERBACH, E.C. (1995). "Effect of a stabilized microbubble echo contrast agent on hemolysis of human erythrocytes exposed to high intensity pulsed ultrasound," *Echocardiography* **12**, 13–21.
- BRAYMAN, A.A., AZADNIV, M., COX, C. and MILLER, M.W. (1996a). "Hemolysis of Alunex-supplemented, 40% hematocrit human erythrocytes *in vitro* by 1-MHz pulsed ultrasound: Acoustic pressure and pulse length dependence," *Ultrasound Med. Biol.* **22**, 927–938.
- BRAYMAN, A.A., CHURCH, C.C. and MILLER, M.W. (1996b). "Re-evaluation of the concept that high cell concentrations 'protect' cells *in vitro* from ultrasonically induced lysis," *Ultrasound Med. Biol.* **22**, 497–514.
- BRAYMAN, A.A., AZADNIV, M., MILLER, M.W. and MELTZER, R.S. (1996c). "Effect of static pressure on acoustic transmittance of Alunex microbubble suspensions," *J. Acoust. Soc. Am.* **99**, 2403–2408.
- BRAYMAN, A.A., STRICKLER, P.L., LUAN, H., BARNED, S.L., RAEMAN, C.H., COX, C. and MILLER, M.W. (1997). "Hemolysis of 40% hematocrit, Alunex-supplemented human erythrocytes by pulsed ultrasound:

- Frequency, acoustic pressure and pulse length dependence," *Ultrasound Med. Biol.* **23**, 1237–1250.
- BRAYMAN, A.A., LIZOTTE, L.M. and MILLER, M.W. (1999). "Erosion of artificial endothelia *in vitro* by pulsed ultrasound: Acoustic pressure, frequency, membrane orientation and microbubble contrast agent dependence," *Ultrasound Med. Biol.* **25**, 1305–1320.
- BRENT, R.L. (1983). "The effects of embryonic and fetal exposure to x-ray, microwaves, and ultrasound," *Clin. Obstet. Gynecol.* **26**, 484–510.
- BRENT, R.L., JENSH, R.P. and BECKMAN, D.A. (1991). "Medical sonography: Reproductive effects and risks," *Teratology* **44**, 123–146.
- BROWN, C.H., III, LEVERETT, L.B., LEWIS, C.W., ALFREY, C.P., JR. and HELLUMS, J.D. (1975). "Morphological, biochemical, and functional changes in human platelets subjected to shear stress," *J. Lab. Clin. Med.* **86**, 462–471.
- BRUCK, K. (1978). "Heat production and temperature regulation," pages 455 to 498 in *Perinatal Physiology*, Stave U. and Weech, A.A., Ed. (Plenum Medical Book Company, New York).
- BRUEGGEMEYER, A. (1993). "Neonatal thermoregulation," pages 247 to 262 in *Comprehensive Neonatal Nursing: A Physiologic Perspective*, Kenner, C., Brueggemeyer, A. and Gunderson, L.P., Eds. (W.B. Saunders Co., Philadelphia).
- BRUMMER, F., BRENNER, J., BRAUNER, T. and HULSER, D.F. (1989). "Effect of shock waves on suspended and immobilized L1210 cells," *Ultrasound Med. Biol.* **15**, 229–239.
- BURNS, P.N. (1998). "Contrast agents for ultrasound imaging and Doppler," page 57 in *Diagnostic Ultrasound*, Volume 1, 2nd ed., Rumack, C.M., Wilson, S.R. and Charboneau, J.W., Eds. (Mosby, St. Louis, Missouri).
- BURNS, P.N., WILSON, S.R. and SIMPSON, D.H. (2000). "Pulse inversion imaging of liver blood flow: Improved method for characterizing focal masses with microbubble contrast," *Invest. Radiol.* **35**, 58–71.
- BURTON, A.C. (1965). "Hemodynamics and the physics of the circulation," pages 523 to 542 in *Physiology and Biophysics*, Ruch, T.C. and Patton, H.D., Eds. (W.B. Saunders, Philadelphia).
- BUTLER, B.D. and HILLS, B.A. (1979). "The lung as a filter for microbubbles," *J. Appl. Physiol.* **47**, 537–543.
- CAHILL, M.D. and HUMPHREY V.F. (2000). "A theoretical investigation of the effect of nonlinear propagation on measurements of mechanical index," *Ultrasound Med. Biol.* **26**, 433–440.
- CAMANN, W.R., HORTVET, L.A., HUGHES, N., BADER, A.M. and DATTA, S. (1991). "Maternal temperature regulation during extradural analgesia for labour," *Br. J. Anaesth.* **67**, 565–568.
- CAMPBELL, J.D., ELFORD, R.W. and BRANT, R.F. (1993). "Case-control study of prenatal ultrasonography exposure in children with delayed speech," *CMAJ* **149**, 1435–1440.
- CARNES, K.I., DREWNIAK, J.L. and DUNN, F. (1991). "*In utero* measurement of ultrasonically induced fetal mouse temperature increases," *Ultrasound Med. Biol.* **17**, 373–382.

- CARROLL, B.A., TURNER, R.J., TICKNER, E.G., BOYLE, D.B. and YOUNG, S.W. (1980). "Gelatin encapsulated nitrogen microbubbles as ultrasonic contrast agents," *Invest. Radiol.* **15**, 260–266.
- CARSON, P.L. (1986). "Abstract: Performance and safety assessments of modern ultrasound equipment, Refresher Course 12," *Med. Phys.* **13**, 626.
- CARSON, P.L. (1988). "Medical ultrasound fields and exposure measurements," pages 287 to 307 in *Nonionizing Electromagnetic Radiation and Ultrasound*, NCRP Annual Meeting Proceedings No. 8 (National Council on Radiation Protection and Measurements, Bethesda, Maryland).
- CARSON, P.L. (1999). "Effects of nonlinear ultrasound propagation on output display indices," *J. Ultrasound Med.* **18**, 27–31.
- CARSON, P.L. and ZAGZEBSKI, J.A. (1980). *Pulse Echo Ultrasound Imaging Systems: Performance Tests and Criteria*, General Medical Physics Committee Ultrasound Task Group, AAPM Report No. 8 (Medical Physics Publishing, Madison, Wisconsin).
- CARSON, P.L., FISHELLA, P.R. and OUGHTON, T.V. (1978). "Ultrasonic power and intensities produced by diagnostic ultrasound equipment," *Ultrasound Med. Biol.* **3**, 341–350.
- CARSON, P.L., RUBIN, J.M. and CHIANG, E.H. (1989a). "Fetal depth and ultrasound path lengths through overlying tissues," *Ultrasound Med. Biol.* **15**, 629–639.
- CARSON, P.L., RUBIN, J.M. and CHIANG, E.H. (1989b). "Constant soft tissue distance model in pregnancy," *Ultrasound Med. Biol. (Suppl.)* **15**, 27–29.
- CARSON, P.L., MEYER, C.R., CHIANG, E.H., FAIX, R.G. and MARKS, T.I. (1990). "Ultrasound attenuation coefficient in the fetal liver as a function of gestational age," *Ultrasound Med. Biol.* **16**, 399–407.
- CARSTENSEN, E.L. and FLYNN, H.G. (1982). "Letter: The potential for transient cavitation with microsecond pulses of ultrasound," *Ultrasound Med. Biol.* **8**, L720–L724.
- CARSTENSEN, E.L. and GATES, A.H. (1984). "The effects of pulsed ultrasound on the fetus," *J. Ultrasound Med.* **3**, 145–147.
- CARSTENSEN, E.L. and GATES, A.H. (1985). "Ultrasound and the fetus," in pages 85 to 95 in *Biological Effects of Ultrasound, Vol. 16, Clinical and Diagnostic Ultrasound*, Nyborg, W.L. and Ziskin, M.C., Eds. (Churchill Livingstone, New York).
- CARSTENSEN, E.L., CHILD, S.Z., LAW, W.K., HOROWITZ, D.R. and MILLER, M.W. (1979). "Cavitation as a mechanism for the biological effects of ultrasound on plants," *J. Acoust. Soc. Am.* **66**, 1285–1291.
- CARSTENSEN, E.L., LAW, W.K., MCKAY, N.D. and MUIR, T.G. (1980). "Demonstration of nonlinear acoustical effects at biomedical frequencies and intensities," *Ultrasound Med. Biol.* **6**, 359–368.
- CARSTENSEN, E.L., CHILD, S.Z., LAM, S., MILLER, D.L. and NYBORG, W.L. (1983a). "Ultrasonic gas-body activation in *Drosophila*," *Ultrasound Med. Biol.* **9**, 473–477.
- CARSTENSEN, E.L., PARKER, K.J. and BARBEE, D.B. (1983b). "Temporal peak intensity," *J. Acoust. Soc. Am.* **74**, 1057–1058.

- CARSTENSEN, E.L., BERG, R.B. and CHILD, S.Z. (1983c). "Letter: Pulse average versus maximum intensity," *Ultrasound Med. Biol.* **9**, L451-L455.
- CARSTENSEN, E.L., HARTMAN, C., CHILD, S.Z., COX, C.A., MAYER, R. and SCHENK, E. (1990a). "Test for kidney hemorrhage following exposure to intense, pulsed ultrasound," *Ultrasound Med. Biol.* **16**, 681-685.
- CARSTENSEN, E.L., CHILD, S.Z., CRANE, C., MILLER, M.W. and PARKER, K.J. (1990b). "Lysis of cells in *Elodea* leaves by pulsed and continuous wave ultrasound," *Ultrasound Med. Biol.* **16**, 167-173.
- CARSTENSEN, E.L., CAMPBELL, D.S., HOFFMAN, D., CHILD, S.Z. and AYME-BELLEGRADA, E.J. (1990c). "Killing of *Drosophila* larvae by the fields of an electrohydraulic lithotripter," *Ultrasound Med. Biol.* **16**, 687-698.
- CARSTENSEN, E.L., CHILD, S.Z., NORTON, S. and NYBORG, W.L. (1990d). "Ultrasonic heating of the skull," *J. Acoust. Soc. Am.* **87**, 1310-1317.
- CARSTENSEN, E.L., DUCK, F.A., MELTZER, R.S., SCHWARZ, K.Q. and KELLER, B. (1992). "Bioeffects in echocardiography," *Echocardiography* **9**, 605-623.
- CARSTENSEN, E.L., KELLY, P., CHURCH, C.C., BRAYMAN, A.A., CHILD, S.Z., RAEMAN, C.H. and SCHERY, L. (1993). "Lysis of erythrocytes by exposure to CW ultrasound," *Ultrasound Med. Biol.* **19**, 147-165.
- CARSTENSEN, E.L., DALECKI, D., GRACEWSKI, S.M. and CHRISTOPHER, T. (1999). "Nonlinear propagation and the output indices," *J. Ultrasound Med.* **18**, 69-80.
- CARSTENSEN, E.L., GRACEWSKI, S. and DALECKI, D. (2000). "The search for cavitation *in vivo*," *Ultrasound Med. Biol.* **26**, 1377-1385.
- CARTWRIGHT, R.A., MCKINNEY, P.A., HOPTON, P.A., BIRCH, J.M., HARTLEY, A.L., MANN, J.R., WATERHOUSE, J.A., JOHNSTON, H.E., DRAPER, G.J. and STILLER, C. (1984). "Ultrasound examinations in pregnancy and childhood cancer," *Lancet* **2**, 999-1000.
- CATHIGNOL, D., CHAPELON, J.Y., NEWHOUSE, V.L. and SHANKAR, P.M. (1990). "Bubble sizing with high spatial resolution," *IEEE Trans. UFFC* **37**, 30-37.
- CHAMBERS, C.D., JOHNSON, K.A., FELIX, R.J., DICK, L.M. and JONES, K.L. (1997). "Hyperthermia in pregnancy: A prospective cohort study," *Teratology* **55**, 45.
- CHAN, S.K. and FRIZZELL, L.A. (1977). "Ultrasonic thresholds for structural changes in mammalian liver," pages 153 to 156 in *Institute of Electrical and Electronic Engineers 1977 Ultrasonics Symposium Proceedings* (Institute of Electrical and Electronic Engineers, Piscataway, New Jersey).
- CHANG, P.H., SHUNG, K.K. and LEVENE, H.B. (1996). "Quantitative measurements of second harmonic Doppler using ultrasound contrast agents," *Ultrasound Med. Biol.* **22**, 1205-1214.
- CHAPELON, J.Y., DUPENLOUP, F., COHEN, H. and LENZ, P. (1997). "Reduction of cavitation in ultrasound therapy," *IEEE Trans. UFFC* (submitted).
- CHAPMAN, I.V., MACNALLY, N.A. and TUCKER, S. (1980). "Ultrasound-induced changes in rates of influx and efflux of potassium ions in rat thymocytes *in vitro*," *Ultrasound Med. Biol.* **6**, 47-58.

- CHAUSSY, C. (1986). *Extracorporeal Shock Wave Lithotripsy* (Karger, Farmington, Connecticut).
- CHEN, C.F., ROBINSON, D.E., WILSON, L.S., GRIFFITHS, K.A., MANOHARAN, A. and DOUST, B.D. (1987). "Clinical sound speed measurement in liver and spleen *in vivo*," *Ultrason. Imaging* **9**, 221–235.
- CHILD, S.Z. and CARSTENSEN, E.L. (1982). "Effects of ultrasound on *Drosophila*—IV. Pulsed exposures of eggs," *Ultrasound Med. Biol.* **8**, 311–312.
- CHILD, S.Z., CARSTENSEN, E.L. and MILLER M.W. (1975). "Growth of pea roots exposed to pulsed ultrasound," *J. Acoust. Soc. Am.* **58**, 1109–1110.
- CHILD, S.Z., CARSTENSEN, E.L. and SMACHLO, K. (1980). "Effects of ultrasound on *Drosophila*—I. Killing of eggs exposed to traveling and standing wave fields," *Ultrasound Med. Biol.* **6**, 127–130.
- CHILD, S.Z., CARSTENSEN, E.L. and LAM, S.K. (1981). "Effects of ultrasound on *Drosophila*: III. Exposure of larvae to low-temporal-average-intensity, pulsed irradiation," *Ultrasound Med. Biol.* **7**, 167–173.
- CHILD, S.Z., CARSTENSEN, E.L. and DAVIS, H. (1984). "A test for the effects of low-temporal-average-intensity pulsed ultrasound on the rat fetus," *Exp. Cell Biol.* **52**, 207–210.
- CHILD, S.Z., CARSTENSEN, E.L., GATES, A.H. and HALL, W.J. (1988). "Testing for the teratogenicity of pulsed ultrasound in mice," *Ultrasound Med. Biol.* **14**, 493–498.
- CHILD, S.Z., HARTMAN, C.L., SCHERY, L.A. and CARSTENSEN, E.L. (1990). "Lung damage from exposure to pulsed ultrasound," *Ultrasound Med. Biol.* **16**, 817–825.
- CHILD, S.Z., RAEMAN, C.H., WALTERS, E. and CARSTENSEN, E.L. (1992). "The sensitivity of *Drosophila* larvae to continuous-wave ultrasound," *Ultrasound Med. Biol.* **18**, 725–728.
- CHIN, R.B., MADSEN, E.L., ZAGZEBSKI, J.A., JADVAR, H., WU, X.K. and FRANK, G.R. (1990). "A reusable perfusion supporting tissue-mimicking material for ultrasound hyperthermia phantoms," *Med. Phys.* **17**, 380–390.
- CHIN, R.B., ZAGZEBSKI, J.A. and MADSEN, E.L. (1991). "Experimental verification of a model for predicting transient temperature distributions by focused ultrasound," *Phys. Med. Biol.* **36**, 1153–1164.
- CHOI, S.C. (1978). *Introductory Applied Statistics in Science* (Prentice-Hall, Inc., Upper Saddle River, New Jersey).
- CHRISTENSON, H.K. and CLAESSION, P.M. (1988). "Cavitation and the interaction between macroscopic hydrophobic surfaces," *Science* **239**, 390–392.
- CHRISTIANSEN, C., KRYVI, H., SONTUM, P.C. and SKOTLAND, T. (1994). "Physical and biochemical characterization of Alunex, a new ultrasound contrast agent consisting of air-filled albumin microspheres suspended in a solution of human albumin," *Biotechnol. Appl. Biochem.* **19**, 307–320.
- CHRISTMAN, C.L., CATRON, P.W., FLYNN, E.T. and WEATHERSBY, P.K. (1986). "*In vivo* microbubble detection in decompression sickness

- using a second harmonic resonant bubble detector," *Undersea Biomed. Res.* **13**, 1–18.
- CHRISTMAN, C.L., CARMICHAEL, A.J., MOSSOBA, M.M. and RIESZ, P. (1987). "Evidence for free radicals produced in aqueous solutions by diagnostic ultrasound," *Ultrasonics* **25**, 31–34.
- CHRISTOPHER, T. (1993). *Modeling Biomedical Ultrasound Wave Propagations*, Ph.D. thesis (University of Rochester, Rochester, New York)
- CHRISTOPHER, T. (1997). "Finite amplitude distortion-based inhomogeneous pulse echo ultrasonic imaging," *IEEE Trans. UFFC* **44**, 125–139.
- CHRISTOPHER, T. (1999). "Computing the mechanical index," *J. Ultrasound Med.* **18**, 63–68.
- CHRISTOPHER, T. and CARSTENSEN, E.L. (1996). "Finite amplitude distortion and its relationship to linear derating formulae for diagnostic ultrasound systems," *Ultrasound Med. Biol.* **22**, 1103–1116.
- CHRISTOPHER, T. and CARSTENSEN, E.L. (1998). "Erratum" to [Christopher and Carstensen (1996). "Finite amplitude distortion and its relationship to linear derating formulae for diagnostic ultrasound systems," *Ultrasound Med. Biol.* **22**, 1103–1116], *Ultrasound Med. Biol.* **24**, 619.
- CHRISTOPHER, P.T. and PARKER, K.J. (1991). "New approaches to non-linear diffractive field propagation," *J. Acoust. Soc. Am.* **90**, 488–499.
- CHURCH, C.C. (1988a). "Prediction of rectified diffusion during nonlinear bubble pulsations at biomedical frequencies," *J. Acoust. Soc. Am.* **83**, 2210–2217.
- CHURCH, C.C. (1988b). "A method to account for acoustic microstreaming when predicting bubble growth rates produced by rectified diffusion," *J. Acoust. Soc. Am.* **84**, 1758–1764.
- CHURCH, C.C. (1989). "A theoretical study of cavitation generated by an extracorporeal shock wave lithotripter," *J. Acoust. Soc. Am.* **86**, 215–227.
- CHURCH, C.C. (1995). "The effects of an elastic solid surface layer on the radial pulsations of gas bubbles," *J. Acoust. Soc. Am.* **97**, 1510–1521.
- CHURCH, C.C. and BRAYMAN, A.A. (1998). "Can the presence of contrast media promote ultrasound bioeffects?" pages 413 to 422 in *Trends in Contrast Media*, Thomsen, H.S., Muller, R.N. and Mattrey, R.F., Eds. (Springer-Verlag, New York).
- CHURCH, C.C. and MILLER, M.W. (1983). "The kinetics and mechanics of ultrasonically-induced cell lysis produced by non-trapped bubbles in a rotating culture tube," *Ultrasound Med. Biol.* **9**, 385–393.
- CHURCH, C.C., FLYNN, H.G., MILLER, M.W. and SACKS, P.G. (1982). "The exposure vessel as a factor in ultrasonically-induced mammalian cell lysis—II. An explanation of the need to rotate exposure tubes," *Ultrasound Med. Biol.* **8**, 299–309.
- CIARAVINO, V. and MILLER, M.W. (1983). "A comparison of two techniques for measured iodine release as an indicator of acoustic cavitation," *J. Acoust. Soc. Am.* **74**, 1813–1816.
- CIARAVINO, V., FLYNN, H.G. and MILLER, M.W. (1981a). "Pulsed enhancement of acoustic cavitation: A postulated model," *Ultrasound Med. Biol.* **7**, 159–166.

- CIARAVINO, V., MILLER, M.W. and CARSTENSEN, E.L. (1981b). "Pressure-mediated reduction of ultrasonically induced cell lysis," *Radiat. Res.* **88**, 209–213.
- CIARAVINO, V., MILLER, M.W. and KAUFMAN, G.E. (1981c). "The effect of 1 MHz ultrasound on the proliferation of synchronized Chinese hamster V-79 cells," *Ultrasound Med. Biol.* **7**, 175–184.
- CIARAVINO, V., BRULFERT, A., MILLER, M.W., JACOBSON-KRAM, D. and MORGAN, W.F. (1985). "Diagnostic ultrasound and sister chromatid exchanges: Failure to reproduce positive findings," *Science* **227**, 1349–1351.
- CIARAVINO, V., MILLER, M.W. and CARSTENSEN, E.L. (1986). "Sister-chromatid exchanges in human lymphocytes exposed *in vitro* to therapeutic ultrasound," *Mutat. Res.* **172**, 185–188.
- CLARKE, P.R. and HILL, C.R. (1970). "Physical and chemical aspects of ultrasonic disruption of cells," *J. Acoust. Soc. Am.* **47**, 649–653.
- CLINE, H.E., HYNYNEN, K., HARDY, C.J., WATKINS, R.D., SCHENCK, J.F. and JOLESZ, F.A. (1994). "MR temperature mapping of focused ultrasound surgery," *Magn. Reson. Med.* **31**, 628–636.
- CMA (1992). Canadian Medical Association. "Periodic health examination, 1992 update: 2. Routine prenatal ultrasound screening. Canadian Task Force on the Periodic Health Examination," *CMAJ* **147**, 627–633.
- COAKLEY, W.T. and NYBORG, W.L. (1978). "Cavitation: Dynamics of gas bubbles; applications," Chapter II in *Ultrasound: Its Applications in Medicine and Biology*, Fry, F.J., Ed. (Elsevier Publishing Co., New York).
- COAKLEY, W.T. and SANDERS, M.F. (1973). "Sonochemical yields of cavitation centres at 1 MHz," *J. Sound Vibrat.* **28**, 73–85.
- COAKLEY, W.T., JAMES, C.J. and MACINTOSH, I.J. (1977). "Haemolysis of human erythrocytes in dextran solutions during rapid flow in capillaries," *Biorheology* **14**, 91–97.
- COBLE, A.J. and DUNN, F. (1976). "Ultrasonic production of reversible changes in the electrical parameters of isolated frog skin," *J. Acoust. Soc. Am.* **60**, 225–229.
- COCKROFT, D.L. and NEW, D.A. (1978). "Abnormalities induced in cultured rat embryos by hyperthermia," *Teratology* **17**, 277–283.
- COLEMAN, A.J. and SAUNDERS, J.E. (1993). "A review of the physical properties and biological effects of the high amplitude acoustic field used in extracorporeal lithotripsy," *Ultrasonics* **31**, 75–89.
- COLEMAN, A.J., SAUNDERS, J.E., CRUM, L.A. and DYSON, M. (1987). "Acoustic cavitation generated by an extracorporeal shockwave lithotripter," *Ultrasound Med. Biol.* **13**, 69–76.
- COLEMAN, A.J., WHITLOCK, M., LEIGHTON, T. and SAUNDERS, J.E. (1993). "The spatial distribution of cavitation induced acoustic emission, sonoluminescence and cell lysis in the field of a shock wave lithotripter," *Phys. Med. Biol.* **38**, 1545–1560.
- COLEMAN, A.J., KODAMA, T., CHOI, M.J., ADAMS, T. and SAUNDERS, J.E. (1995). "The cavitation threshold of human tissue exposed to 0.2-MHz pulsed ultrasound: Preliminary measurements based on a study of clinical lithotripsy," *Ultrasound Med. Biol.* **21**, 405–417.

- CONGER, A.D., ZISKIN, M.C. and WITTELS, H. (1981). "Ultrasonic effects on mammalian multicellular tumor spheroids," *J. Clin. Ultrasound* **9**, 167-174.
- COOK, S.D., RYABY, J.P., MCCABE, J., FREY, J.J., HECKMAN, J.D. and KRISTIANSEN, T.K. (1997). "Acceleration of tibia and distal radius fracture healing in patients who smoke," *Clin. Orthop.* **337**, 198-207.
- CORDAY, E., SHAH, P.M. and MEERBAUM, S. (1984). "Seminar on contrast two-dimensional echocardiography: Applications and new developments. Part I," *J. Am. Coll. Cardiol.* **3**, 1-5.
- CORREAS, J., KESSLER, D., WORAH, D. and QUAY, S.C. (1997). "The first phase shift ultrasound contrast agent: EchoGen," pages 101 to 120 in *Ultrasound Contrast Agents*, Goldberg, B.B., Ed. (Martin Dunitz Ltd., London).
- CREEZEY, J., MOOIBROEK, J., LAGENDIJK, J.J. and VAN LEEUWEN, G.M. (1994). "The theoretical and experimental evaluation of the heat balance in perfused tissue," *Phys. Med. Biol.* **39**, 813-832.
- CRUM, L.A. (1979). "Surface oscillations and jet formation in pulsating air bubbles," *J. Physics* **40**, 131-134.
- CRUM, L.A. (1994). "Sonoluminescence," *Phys. Today* **47**, 22-29.
- CRUM, L.A. and FOWLKES, J.B. (1986). "Acoustic cavitation generated by microsecond pulses of ultrasound," *Nature* **319**, 52-54.
- CRUM, L.A. and HANSEN, G.M. (1982a). "Generalized equations for rectified diffusion," *J. Acoust. Soc. Am.* **72**, 1586-1592.
- CRUM, L.A. and HANSEN, G.M. (1982b). "Growth of air bubbles in tissue by rectified diffusion," *Phys. Med. Biol.* **27**, 413-417.
- CRUM, L.A., DANIELS, S., TER HAAR, G.R. and DYSON, M. (1987). "Ultrasonically induced gas bubble production in agar based gels: Part II. Theoretical analysis," *Ultrasound Med. Biol.* **13**, 541-554.
- CRUM, L.A., ROY, R.A., DINNO, M.A., CHURCH, C.C., APFEL, R.E., HOLLAND, C.K. and MADANSHETTY, S.I. (1992). "Acoustic cavitation produced by microsecond pulses of ultrasound: A discussion of some selected results," *J. Acoust. Soc. Am.* **91**, 1113-1119.
- CUFF, J.M., KIMMEL, G.L., KIMMEL, C.A., HEREDIA, D.J., TUDOR, N. and CHEN, J. (1993). "Relationship between abnormal somite development and axial skeletal defects in rats following heat exposure," *Teratology* **48**, 259-266.
- CURLEY, M.G. (1993). "Soft tissue temperature rise caused by scanned, diagnostic ultrasound," *IEEE Trans. UFFC* **40**, 59-66.
- DAFT, C.M. and BRIGGS, G.A. (1989). "The elastic microstructure of various tissues," *J. Acoust. Soc. Am.* **85**, 416-422.
- DAFT, C.M., SIDDIQI, T.A., FITTING, D.W., MEYER, R.A. and O'BRIEN, W.D., JR. (1990). "In-vivo fetal ultrasound exposimetry," *IEEE Trans. UFFC* **37**, 501-505.
- DALECKI, D., CARSTENSEN, E.L., PARKER, K.J. and BACON, D.R. (1991a). "Absorption of finite amplitude focused ultrasound," *J. Acoust. Soc. Am.* **89**, 2435-2447.
- DALECKI, D., KELLER, B.B., CARSTENSEN, E.L., NEEL, D.S., PALLADINO, J.L. and NOORDERGRAAF, A. (1991b). "Thresholds for premature

- ventricular contractions in frog hearts exposed to lithotripter fields," *Ultrasound Med. Biol.* **17**, 341–346.
- DALECKI, D., KELLER, B.B., RAEMAN, C.H. and CARSTENSEN, E.L. (1993a). "Effects of pulsed ultrasound on the frog heart: I. Thresholds for changes in cardiac rhythm and aortic pressure," *Ultrasound Med. Biol.* **19**, 385–390.
- DALECKI, D., RAEMAN, C.H. and CARSTENSEN, E.L. (1993b). "Effects of pulsed ultrasound on the frog heart: II. An investigation of heating as a potential mechanism," *Ultrasound Med. Biol.* **19**, 391–398.
- DALECKI, D., CHILD, S.Z., RAEMAN, C.H. and CARSTENSEN, E.L. (1995a). "Tactile perception of ultrasound," *J. Acoust. Soc. Am.* **97**, 3165–3170.
- DALECKI, D., RAEMAN, C.H., CHILD, S.Z. and CARSTENSEN, E.L. (1995b). "Thresholds for intestinal hemorrhage in mice exposed to a piezoelectric lithotripter," *Ultrasound Med. Biol.* **21**, 1239–1246.
- DALECKI, D., RAEMAN, C.H., CHILD, S.Z. and CARSTENSEN, E.L. (1995c). "Intestinal hemorrhage from exposure to pulsed ultrasound," *Ultrasound Med. Biol.* **21**, 1067–1072.
- DALECKI, D., RAEMAN, C.H., CHILD, S.Z. and CARSTENSEN, E.L. (1996). "A test for cavitation as a mechanism for intestinal hemorrhage in mice exposed to a piezoelectric lithotripter," *Ultrasound Med. Biol.* **22**, 493–496.
- DALECKI, D., RAEMAN, C.H., CHILD, S.Z. and CARSTENSEN, E.L. (1997a). "Effects of pulsed ultrasound on the frog heart: III. The radiation force mechanism," *Ultrasound Med. Biol.* **23**, 275–285.
- DALECKI, D., CHILD, S.Z., RAEMAN, C.H., COX, C., PENNEY, D.P. and CARSTENSEN, E.L. (1997b). "Age dependence of ultrasonically induced lung hemorrhage in mice," *Ultrasound Med. Biol.* **23**, 767–776.
- DALECKI, D., RAEMAN, C.H., CHILD, S.Z., PENNEY, D.P., MAYER, R. and CARSTENSEN, E.L. (1997c). "The influence of contrast agents on hemorrhage produced by lithotripter fields," *Ultrasound Med. Biol.* **23**, 1435–1439.
- DALECKI, D., RAEMAN, C.H., CHILD, S.Z., PENNEY, D.P. and CARSTENSEN, E.L. (1997d). "Remnants of Alburnex nucleate acoustic cavitation," *Ultrasound Med. Biol.* **23**, 1405–1412.
- DALECKI, D., CHILD, S.Z., RAEMAN, C.H., PENNEY, D.P., MAYER, R., COX, C. and CARSTENSEN, E.L. (1997e). "Thresholds for fetal hemorrhages produced by a piezoelectric lithotripter," *Ultrasound Med. Biol.* **23**, 287–297.
- DALECKI, D., CHILD, S.Z., RAEMAN, C.H., COX, C. and CARSTENSEN, E.L. (1997f). "Ultrasonically induced lung hemorrhage in young swine," *Ultrasound Med. Biol.* **23**, 777–781.
- DALECKI, D., RAEMAN, C.H., CHILD, S.Z., COX, C., FRANCIS, C.W., MELTZER, R.S. and CARSTENSEN, E.L. (1997g). "Hemolysis *in vivo* from exposure to pulsed ultrasound," *Ultrasound Med. Biol.* **23**, 307–313.
- DALECKI, D., CHILD, S.Z., RAEMAN, C.H. and COX, C. (1999). "Hemorrhage in murine fetuses exposed to pulsed ultrasound," *Ultrasound Med. Biol.* **25**, 1139–1144.

- DALECKI, D., CHILD, S.Z., RAEMAN, C.H. and GILDNER, C.D. (2000a). "Premature cardiac contractions produced by ultrasound contrast agents," *J. Ultrasound Med.* **19**, No. 4.S32.
- DALECKI, D., CHILD, S.Z., RAEMAN, C.H., XING, C., GRACEWSKI, S. and CARSTENSEN, E.L. (2000b). "Bioeffects of positive and negative pressures in mice infused with microbubbles," *Ultrasound Med. Biol.* **26**, 1327–1332.
- DAMIANOU, C. and HYNYNEN, K. (1993). "Focal spacing and near-field heating during pulsed high temperature ultrasound therapy," *Ultrasound Med. Biol.* **19**, 777–787.
- DAMIANOU, C.A., HYNYNEN, K. and FAN, X. (1995). "Evaluation of accuracy of a theoretical model for predicting the necrosed tissue volume during focused ultrasound surgery," *IEEE Trans. UFFC* **42**, 182–187.
- DANIELS, S. and PRICE, D.J. (1991). "Sonoluminescence in water and agar gels during irradiation with 0.75 MHz continuous-wave ultrasound," *Ultrasound Med. Biol.* **17**, 297–308.
- DANIELS, S. and TER HAAR, G.R. (1986). "Bubble formation in guinea pigs and agar gels during ultrasonic irradiation," *Proc. Inst. Acoust.* **8**, 142–154.
- DANIELS, S. and TER HAAR, G.R. (1992). "Letter: Formation of bubbles in guinea-pig leg *in vivo*," *Ultrasonics* **30**, 197.
- DANIELS, S., PATON, W.D. and SMITH, E.B. (1979). "Ultrasonic imaging system for the study of decompression-induced gas bubbles," *Undersea Biomed. Res.* **6**, 197–207.
- DANIELS, S., BLONDEL, D., CRUM, L.A., TER HAAR, G.R. and DYSON, M. (1987). "Ultrasonically induced gas bubble production in agar based gels: Part I. Experimental investigation," *Ultrasound Med. Biol.* **13**, 527–539.
- DANIELS, S., KODAMA, T. and PRICE, D.J. (1995). "Damage to red blood cells induced by acoustic cavitation," *Ultrasound Med. Biol.* **21**, 105–111.
- DAVID, H., WEAVER, J.B. and PEARSON, J.F. (1975). "Doppler ultrasound and fetal activity," *BMJ* **2**, 62–64.
- DE JONG, N. (1996). "Improvements in ultrasound contrast agents," *IEEE Eng. Med. Biol.* **15**, 72–82.
- DE JONG, N. and HOFF, L. (1993). "Ultrasound scattering properties of Albunex microspheres," *Ultrasonics* **31**, 175–181.
- DE JONG, N., CORNET, R. and LANCEE, C.T. (1994a). "Higher harmonics of vibrating gas-filled microspheres. Part one: Simulations," *Ultrasonics* **32**, 447–453.
- DE JONG, N., CORNET, R. and LANCEE, C.T. (1994b). "Higher harmonics of vibrating gas-filled microspheres. Part two: Measurements," *Ultrasonics* **32**, 455–459.
- DE KORTE, C.L., VAN DER STEEN, A.F. and THIJSEN, J.M. (1994). "Acoustic velocity and attenuation of eye tissues at 20 MHz," *Ultrasound Med. Biol.* **20**, 471–480.
- DELIUS, M., ENDERS, G., HEINE, G., STARK, J., REMBERGER, K. and BRENDEL, W. (1987). "Biological effects of shock waves: Lung hemorrhage

- by shock waves in dogs—pressure dependence,” *Ultrasound Med. Biol.* **13**, 61–67.
- DELIUS, M., JORDAN, M., EIZENHOEFER, H., MARLINGHAUS, E., HEINE, G., LIEBICH, H.G. and BRENDEL, W. (1988a). “Biological effects of shock waves: Kidney haemorrhage by shock waves in dogs—administration rate dependence,” *Ultrasound Med. Biol.* **14**, 689–694.
- DELIUS, M., ENDERS, G., XUAN, Z.R., LIEBICH, H.G. and BRENDEL, W. (1988b). “Biological effects of shock waves: Kidney damage by shock waves in dogs—dose dependence,” *Ultrasound Med. Biol.* **14**, 117–122.
- DELIUS, M., DENK, R., BERDING, C., LIEBICH, H.G., JORDAN, M. and BRENDEL, W. (1990a). “Biological effects of shock waves: Cavitation by shock waves in piglet liver,” *Ultrasound Med. Biol.* **16**, 467–472.
- DELIUS, M., JORDAN, M., LIEBICH, H.G. and BRENDEL, W. (1990b). “Biological effects of shock waves: Effect of shock waves on the liver and gallbladder wall of dogs—administration rate dependence,” *Ultrasound Med. Biol.* **16**, 459–466.
- DELIUS, M., HOFFMANN, E., STEINBECK, G. and CONZEN, P. (1994). “Biological effects of shock waves: Induction of arrhythmia in piglet hearts,” *Ultrasound Med. Biol.* **20**, 279–285.
- DELIUS, M., HOFSCHEIDER, P.H., LAUER, U. and MESSMER, K. (1995). “Extracorporeal shock waves for gene therapy,” *Lancet* **345**, 1377.
- DENG, C.X., XU, Q., APFEL, R.E. and HOLLAND, C.K. (1996). “*In vitro* measurements of inertial cavitation thresholds in human blood,” *Ultrasound Med. Biol.* **22**, 939–948.
- DEVIN, C., JR. (1959). “Survey of thermal, radiation, and viscous damping of pulsating air bubbles in water,” *J. Acoust. Soc. Am.* **31**, 1654–1667.
- DEWEY, W.C., HOPWOOD, L.E., SAPARETO, S.A. and GERWECK, L.E. (1977). “Cellular responses to combinations of hyperthermia and radiation,” *Radiology* **123**, 463–474.
- DICKINSON, R.J. (1986). “Reflection and scattering,” pages 225 to 260 in *Physical Principles of Medical Ultrasonics*, Hill, C.R., Ed. (John Wiley & Sons, New York).
- DICKSON, J.A. and CALDERWOOD, S.K. (1980). “Temperature range and selective sensitivity of tumors to hyperthermia: A critical review,” *Ann. NY Acad. Sci.* **335**, 180–205.
- DING, Z. and GRACEWSKI, S.M. (1994). “Response of constrained and unconstrained bubbles to lithotripter shock wave pulses,” *J. Acoust. Soc. Am.* **96**, 3636–3644.
- DINNO, M.A., CRUM, L.A. and WU, J. (1989a). “The effect of therapeutic ultrasound on electrophysiological parameters of frog skin,” *Ultrasound Med. Biol.* **15**, 461–470.
- DINNO, M.A., DYSON, M., YOUNG, S.R., MORTIMER, A.J., HART, J. and CRUM, L.A. (1989b). “The significance of membrane changes in the safe and effective use of therapeutic and diagnostic ultrasound,” *Phys. Med. Biol.* **34**, 1543–1552.
- DINNO, M.A., AL-KARMI, A.M., STOLTZ, D.A., MATTHEWS, J.C. and CRUM, L.A. (1993). “Effect of free radical scavengers on changes in ion

- conductance during exposure to therapeutic ultrasound," *Membr. Biochem.* **10**, 237–247.
- DODMAN, N. (1987). "Newborn temperature control," *Neonatal Netw.* **5**, 19–23.
- DOIDA, Y., MILLER, M.W., COX, C. and CHURCH, C.C. (1990). "Confirmation of an ultrasound-induced mutation in two *in vitro* mammalian cell lines," *Ultrasound Med. Biol.* **16**, 699–705.
- DOIDA, Y., BRAYMAN, A.A. and MILLER, M.W. (1992a). "Ultrasonically induced *in vitro* cell lysis: Node-antinode interactions," *J. Ultrasound Med.* **11**, 413–417.
- DOIDA, Y., BRAYMAN, A.A. and MILLER, M.W. (1992b). "Modest enhancement of ultrasound-induced mutations in V79 cells *in-vitro*," *Ultrasound Med. Biol.* **18**, 465–469.
- DOINIKOV, A.A. (1996). "On the radiation pressure on small spheres," *J. Acoust. Soc. Am.* **100**, 1231–1233.
- DOINIKOV, A.A. (1997a). "Acoustic radiation force on a spherical particle in a viscous heat-conducting fluid. I. General formula," *J. Acoust. Soc. Am.* **101**, 713–721.
- DOINIKOV, A.A. (1997b). "Acoustic radiation force on a spherical particle in a viscous heat-conducting fluid. II. Force on a rigid sphere," *J. Acoust. Soc. Am.* **101**, 722–730.
- DOINIKOV, A.A. (1997c). "Acoustic radiation force on a spherical particle in a viscous heat-conducting fluid. III. Force on a liquid drop," *J. Acoust. Soc. Am.* **101**, 731–740.
- DOODY, C., PORTER, H., DUCK, F.A. and HUMPHREY, V.F. (1999). "*In vitro* heating of human fetal vertebra by pulsed diagnostic ultrasound," *Ultrasound Med. Biol.* **25**, 1289–1294.
- DOOLEY, D.A., CHILD, S.Z., CARSTENSEN, E.L. and MILLER, M.W. (1983). "The effects of continuous wave and pulsed ultrasound on rat thymocytes *in vitro*," *Ultrasound Med. Biol.* **9**, 379–384.
- DOOLEY, D.A., SACKS, P.G. and MILLER, M.W. (1984). "Production of thymine base damage in ultrasound-exposed EMT6 mouse mammary sarcoma cells," *Radiat. Res.* **97**, 71–86.
- DRAGANIC, I.G. and DRAGANIC, Z.D. (1971). *The Radiation Chemistry of Water* (Academic Press, New York).
- DREWNIAK, J.L. and DUNN, F. (1996). "Letter: An experimentally obtainable heat source due to absorption of ultrasound in biological media," *J. Acoust. Soc. Am.* **100**, 1250–1253.
- DU, J.N. and OLIVER, T.K., JR. (1969). "The baby in the delivery room. A suitable microenvironment," *JAMA* **207**, 1502–1504.
- DUBOWITZ, L.M., DUBOWITZ, V. and GOLDBERG, C. (1970). "Clinical assessment of gestational age in the newborn infant," *J. Pediatr.* **77**, 1–10.
- DUCK, F.A. (1987). "The measurement of exposure to ultrasound and its application to estimates of ultrasound 'dose'," *Phys. Med. Biol.* **32**, 303–325.
- DUCK, F.A. (1990). *Physical Properties of Tissues: A Complete Reference Book* (Academic Press, New York).

- DUCK, F.A. (1999a). "Estimating *in situ* exposure in the presence of acoustic nonlinearity," *J. Ultrasound Med.* **18**, 43–53.
- DUCK, F.A. (1999b). "Acoustic saturation and output regulation," *Ultrasound Med. Biol.* **25**, 1009–1018.
- DUCK, F.A. and MARTIN, K. (1991). "Trends in diagnostic ultrasound exposure," *Phys. Med. Biol.* **36**, 1423–1432.
- DUCK, F.A. and MARTIN, K. (1993). "Exposure values for medical devices," pages 315 to 344 in *Ultrasonic Exposimetry*, Ziskin, M.C. and Lewin, P.A., Eds. (CRC Press, Boca Raton, Florida).
- DUCK, F.A. and PERKINS, M.A. (1988). "Amplitude-dependent losses in ultrasound exposure measurements," *IEEE Trans. UFFC* **35**, 232–241.
- DUCK, F.A. and STARRITT, H.C. (1994). "A study of the heating capabilities of diagnostic ultrasound beams," *Ultrasound Med. Biol.* **20**, 481–492.
- DUCK, F.A., STARRITT, H.C., AINDOW, J.D., PERKINS, M.A. and HAWKINS, A.J. (1985). "The output of pulse-echo ultrasound equipment: A survey of powers, pressures and intensities," *Br. J. Radiol.* **58**, 989–1001.
- DUGGAN, P.M., LIGGINS, G.C. and BARNETT, S.B. (1995). "Ultrasonic heating of the brain of the fetal sheep *in utero*," *Ultrasound Med. Biol.* **21**, 553–560.
- DUNN, F. (1958). "Physical mechanisms of the action of intense ultrasound on tissue," *Am. J. Phys. Med.* **37**, 152–156.
- DUNN, F. (1974). "Attenuation and speed of ultrasound in lung," *J. Acoust. Soc. Am.* **56**, 1638–1639.
- DUNN, F. (1985). "Cellular inactivation by heat and shear," *Radiat. Environ. Biophys.* **24**, 131–139.
- DUNN, F. (1986). "Letter: Attenuation and speed of ultrasound in lung: Dependence upon frequency and inflation," *J. Acoust. Soc. Am.* **80**, 1248–1250.
- DUNN, F. and FRY, W.J. (1961). "Ultrasonic absorption and reflection by lung tissue," *Phys. Med. Biol.* **5**, 401–410.
- DUNN, F. and FRY, F.J. (1971). "Ultrasonic threshold dosages for the mammalian central nervous system," *IEEE Trans. Biomed. Eng.* **18**, 253–256.
- DYSON, M. and BROOKES, M. (1983). "Stimulation of bone repair by ultrasound," pages 61 to 66 in *Ultrasound '82*, Lerski, A. and Morley, P., Eds. (Pergamon Press, Elmsford, New York).
- DYSON, M., WOODWARD, B. and POND, J.B. (1971). "Flow of red blood cells stopped by ultrasound," *Nature* **232**, 572–573.
- DYSON, M., POND, J.B., WOODWARD, B. and BROADBENT, J. (1974). "The production of blood cell stasis and endothelial damage in the blood vessels of chick embryos treated with ultrasound in a stationary wave field," *Ultrasound Med. Biol.* **1**, 133–148.
- EAMES, F.A., CARSTENSEN, E.L., MILLER, M.W. and LI, M. (1975). "Ultrasonic heating of *Vicia faba* roots," *J. Acoust. Soc. Am.* **57**, 1192–1194.
- ECKART, C. (1948). "Vortices and streams caused by sound waves," *Phys. Rev.* **73**, 68–76.
- ECMUS (1999). European Committee for Medical Ultrasound Safety. "Safety of ultrasonic contrast agents," *Europ. J. Ultrasound* **9**, 195–197.

- EDMONDS, P.D. and SANCIER, K.M. (1983). "Evidence for free radical production by ultrasonic cavitation in biological media," *Ultrasound Med. Biol.* **9**, 635-639.
- EDWARDS, M.J. (1968). "Congenital malformations in the rat following induced hyperthermia during gestation," *Teratology* **1**, 173-177.
- EDWARDS, M.J. (1969). "Congenital defects in guinea pigs: Fetal resorptions, abortions, and malformations following induced hyperthermia during early gestation," *Teratology* **2**, 313-328.
- EDWARDS, M.J. (1982). "The effects of hyperthermia on brain development," *Birth Defects Orig. Arctic. Ser.* **18**, 3-11.
- EDWARDS, M.J. (1986). "Hyperthermia as a teratogen: A review of experimental studies and their clinical significance," *Teratog. Carcinog. Mutagen.* **6**, 563-582.
- EDWARDS, M.J. (1993). "Editorial: Hyperthermia and birth defects," *Cornell Vet.* **83**, 1-7.
- EFSUMB (1996). European Federation of Societies for Ultrasound in Medicine and Biology. "Thermal and mechanical indices: EFSUMB safety tutorial," *Europ. J. Ultrasound* **4**, 145-150.
- EHD (1980). Environmental Health Directorate. *Canada-Wide Survey of Non-Ionizing Radiation Emitting Medical Devices. Part II. Ultrasound Devices* (Environmental Health Directorate, Health Protection Branch, Ottawa).
- EHD (1989). Environmental Health Directorate. *Guidelines for the Safe Use of Ultrasound. Part I. Medical and Paramedical Applications* (Canadian Government Publishing Center, Ottawa).
- EHRENBERG, L., EHRENSTEIN, G.V. and HEDGRAN, A. (1957). "Gonad temperature and spontaneous mutation-rate in man," *Nature* **180**, 1433-1434.
- EIK-NES, S.H., OKLAND, O., AURE, J.C. and ULSTEIN, M. (1984). "Letter: Ultrasound screening in pregnancy: A randomised controlled trial," *Lancet* **1**, 1347.
- ELLER, A.I. (1969). "Growth of bubbles by rectified diffusion," *J. Acoust. Soc. Am.* **46**, 1246-1250.
- ELLER, A.I. (1972). "Bubble growth by diffusion in an 11 kHz sound field," *J. Acoust. Soc. Am.* **52**, 1447-1449.
- ELLER, A.I. and FLYNN, H.G. (1965). "Rectified diffusion during nonlinear pulsations of cavitation bubbles," *J. Acoust. Soc. Am.* **37**, 493-503.
- ELLIS, D.S. and O'BRIEN, W.D., JR. (1992). "Evaluation of the soft tissue thermal index and the maximum temperature increase for homogeneous and layered tissues," pages 1271 to 1285 in *1992 IEEE Ultrasonics Symposium Proceedings*, McAvoy, B.R., Ed. (Institute of Electrical and Electronics Engineers, Piscataway, New Jersey).
- ELLIS, D.S. and O'BRIEN, W.D., JR. (1996). "The monopole-source solution for estimating tissue temperature increases for focused ultrasound fields," *IEEE Trans. UFFC* **43**, 88-97.
- ELLWART, J.W., BRETTTEL, H. and KOBER, L.O. (1988). "Cell membrane damage by ultrasound at different cell concentrations," *Ultrasound Med. Biol.* **14**, 43-50.

- ENDO, A.S. and NISHIOKA, E. (1993). "Neonatal assessment," pages 265 to 293 in *Comprehensive Neonatal Nursing: A Physiologic Perspective* (W.B. Saunders Co., Philadelphia).
- EPSTEIN, P.S. and PLESSET, M.S. (1950). "On the stability of gas bubbles in liquid-gas solutions," *J. Chem. Phys.* **18**, 1505–1509.
- ERICKSON, J.D. (1991). "Risk factors for birth defects: Data from the Atlanta Birth Defects Case-Control Study," *Teratology* **43**, 41–51.
- ERRABOLU, R.L., SEHGAL, C.M., BAHN, R.C. and GREENLEAF, J.F. (1988). "Measurement of ultrasonic nonlinear parameter in excised fat tissues," *Ultrasound Med. Biol.* **14**, 137–146.
- EVAN, A.P. and MCATEER, J.A. (1996). "Q-effects of shock wave lithotripsy," pages 549 to 570 in *Kidney Stones: Medical and Surgical Management*, Coe, F.L., Favus, M.J., Pak, C.Y., Parks, J.H. and Preminger, G.M., Eds. (Lippincott-Raven, Philadelphia).
- EVANS, A. and WALDER, D.N. (1970). "Detection of circulating bubbles in the intact mammal," *Ultrasonics* **8**, 216–217.
- EWIGMAN, B.G., CRANE, J.P., FRIGOLETTO, F.D., LEFEVRE, M.L., BAIN, R.P. and MCNELLIS, D. (1993). "Effect of prenatal ultrasound screening on perinatal outcome. RADIUS Study Group," *N. Engl. J. Med.* **329**, 821–827.
- FAHNESTOCK, M., RIMER, V.G., YAMAWAKI, R.M., ROSS, P. and EDMONDS, P.D. (1989). "Effects of ultrasound exposure *in vitro* on neuroblastoma cell membranes," *Ultrasound Med. Biol.* **15**, 133–144.
- FAIRBANK, W.M., JR. and SCULLY, M.O. (1977). "A new noninvasive technique for cardiac pressure measurement: Resonant scattering of ultrasound from bubbles," *IEEE Trans. Biomed. Eng.* **24**, 107–110.
- FALUS, M., KORANYI, G., SOBEL, M., PESTI, E. and TRINH, V.B. (1972). "Follow-up studies on infants examined by ultrasound during fetal age," *Orv. Hetil.* **113**, 2119–2121.
- FAN, X. and HYNYNEN, K. (1995). "Control of the necrosed tissue volume during noninvasive ultrasound surgery using a 16-element phased array," *Med. Phys.* **22**, 297–306.
- FAN, X. and HYNYNEN, K. (1996). "Ultrasound surgery using multiple sonications—treatment time considerations," *Ultrasound Med. Biol.* **22**, 471–482.
- FATEMI, M., OGBURN, P.L., JR. and GREENLEAF, J.F. (2001). "Fetal stimulation by pulsed diagnostic ultrasound," *J. Ultrasound Med.* **20**, 883–889.
- FDA (1985). U.S. Food and Drug Administration. *510(k) Guide for Measuring and Reporting Output of Diagnostic Ultrasound Medical Devices* (Center for Devices and Radiological Health, U.S. Food and Drug Administration, Rockville, Maryland).
- FDA (1991). U.S. Food and Drug Administration. *510(k) Diagnostic Ultrasound Guidance Update of 1991* (Center for Devices and Radiological Health, U.S. Food and Drug Administration, Rockville, Maryland).
- FDA (1997). U.S. Food and Drug Administration. *Information for Manufacturers Seeking Marketing Clearance of Diagnostic Ultrasound Systems*

- and Transducers (Center for Devices and Radiological Health, U.S. Food and Drug Administration, Rockville, Maryland).
- FECHHEIMER, M., DENNY, C., MURPHY, R.F. and TAYLOR, D.L. (1986). "Measurement of cytoplasmic pH in *Dictyostelium discoideum* by using a new method for introducing macromolecules into living cells," *Eur. J. Cell Biol.* **40**, 242–247.
- FEINSTEIN, A.R. (1977). *Clinical Biostatistics* (C.V. Mosby Co., St. Louis, Missouri).
- FILIPCZYNSKI, L. and WOJCIK, J. (1991). "Estimation of transient temperature elevation in lithotripsy and in ultrasonography," *Ultrasound Med. Biol.* **17**, 715–721.
- FILIPCZYNSKI, L., KUJAWSKA, T. and WOJCIK, J. (1993). "Temperature elevation in focused Gaussian ultrasonic beams at various insonation times," *Ultrasound Med. Biol.* **19**, 667–679.
- FINK, M. (1992). "Time reversal of ultrasonic fields. Part I: Basic principles," *IEEE Trans. UFFC* **39**, 555–566.
- FISHER, B.R., HEREDIA, D.J. and BROWN, K.M. (1995). "Induction of HSP72 in heat-treated rat embryos: A tissue-specific response," *Teratology* **52**, 90–100.
- FLEISS, J.L. (1981). *Statistical Methods for Rates and Proportions*, 2nd ed. (John Wiley & Sons, New York).
- FLYNN, H.G. (1964). "Physics of acoustic cavitation in liquids," pages 57 to 172 in *Physical Acoustics: Principles and Methods, Volume 1*, Mason, W.P., Ed. (Academic Press, New York).
- FLYNN, H.G. (1975a). "Cavitation dynamics. I. A mathematical formulation," *J. Acoust. Soc. Am.* **57**, 1379–1396.
- FLYNN, H.G. (1975b). "Cavitation dynamics. II. Free pulsations and models for cavitation bubbles," *J. Acoust. Soc. Am.* **58**, 1160–1170.
- FLYNN, H.G. (1982). "Generation of transient cavities in liquids by micro-second pulses of ultrasound," *J. Acoust. Soc. Am.* **72**, 1926–1932.
- FLYNN, H.G. and CHURCH, C.C. (1984). "A mechanism for the generation of cavitation maxima by pulsed ultrasound," *J. Acoust. Soc. Am.* **76**, 505–512.
- FLYNN, H.G. and CHURCH, C.C. (1988). "Erratum: Transient pulsations of small gas bubbles in water," *J. Acoust. Soc. Am.* **84**, 1863–1876.
- FOGLER, H.S. and GODDARD, J.D. (1970). "Collapse of spherical cavities in viscoelastic fluids," *Phys. Fluids* **13**, 1135–1141.
- FORD, R.M. (1974). "Clinical-pathological studies on brain tissue response to ultrasonic radiation: Preliminary results," page 85 to 88 in *World Congress on Ultrasonics in Medicine*, de Vlieger, M., White, D.N. and McCready, V.R., Eds. (Elsevier, New York).
- FORSBERG, F., LIU, J.B., BURNS, P.N., MERTON, D.A. and GOLDBERG, B.B. (1994). "Artifacts in ultrasonic contrast agent studies," *J. Ultrasound Med.* **13**, 357–365.
- FORSBERG, F., MERTON, D.A., LIU, J.B., NEEDLEMAN, L. and GOLDBERG, B.B. (1998a). "Clinical applications of ultrasound contrast agents," *Ultrasonics* **36**, 695–701.

- FORSBERG, F., ROY, R., MERTON, D.A., RAWOOL, N.M., LIU, J.B., HUANG, M., KESSLER, D. and GOLDBERG, B.B. (1998b). "Conventional and hypobaric activation of an ultrasound contrast agent," *Ultrasound Med. Biol.* **24**, 1143–1150.
- FORSBERG, F., BASUDE, R., LIU, J.B., ALESSANDRO, J., SHI, W.T., RAWOOL, N.M., GOLDBERG, B.B. and WHEATLEY, M.A. (1999a). "Effect of filling gases on the backscatter from contrast microbubbles: Theory and *in vivo* measurements," *Ultrasound Med. Biol.* **25**, 1203–1211.
- FORSBERG, F., GOLDBERG, B.B., LIU, J.B., MERTON, D.A., RAWOOL, N.M. and SHI, W.T. (1999b). "Tissue-specific US contrast agent for evaluation of hepatic and splenic parenchyma," *Radiology* **210**, 125–132.
- FOSTER, F.S. and HUNT, J.W. (1979). "Transmission of ultrasound beams through human tissue—focusing and attenuation studies," *Ultrasound Med. Biol.* **5**, 257–268.
- FOSTER, K.R. and WIEDERHOLD, M.L. (1978). "Auditory responses in cats produced by pulsed ultrasound," *J. Acoust. Soc. Am.* **63**, 1199–1205.
- FOWLKES, J.B. and CRUM, L.A. (1988). "Cavitation threshold measurements for microsecond length pulses of ultrasound," *J. Acoust. Soc. Am.* **83**, 2190–2201.
- FOWLKES, J.B. and HOLLAND, C.K. (2000). "Mechanical bioeffects from diagnostic ultrasound: AIUM consensus statements," *J. Ultrasound Med.* **19**, 69–168.
- FOWLKES, J.B. and HWANG, E.Y. (1998). "Echo-contrast agents: What are the risks?" pages 73 to 85 in *Safety of Diagnostic Ultrasound*, Barnett, S.B. and Kossoff, G., Eds. (Parthenon Publishing Group, New York).
- FOWLKES, J.B. and MILLER, D.L. (2000). "*In vivo* measurements of bioeffects," Chapter 14 in *Ultrasound Contrast Agents: Basic Principles and Clinical Applications*, 2nd ed., Goldberg, B.B., Raichlen, J.S. and Forsberg, F., Eds. (Martin Dunitz, Ltd., London).
- FOWLKES, J.B., CARSON, P.L., CHIANG, E.H. and RUBIN, J.M. (1991). "Acoustic generation of bubbles in excised canine urinary bladders," *J. Acoust. Soc. Am.* **89**, 2740–2744.
- FOWLKES, J.B., TAN, J.X. and CARSON, P.L. (1992a). "Acoustic enhancement of echocontrast agents: Experimental results," *J. Ultras. Med.* **11**, S56.
- FOWLKES, J.B., TAN, J.X., CARSON, P.L. and RUBIN, J.M. (1992b). "An examination of echocontrast enhancement by frequency-modulated acoustic pulses," *J. Acoust. Soc. Am.* **91**, 2431.
- FOWLKES, J.B., SIRKIN, D.W., IVEY, J.A., GARDNER, E.A., RHEE, R.T., RUBIN, J.M. and CARSON, P.L. (1998). "Transcutaneous interruption of ultrasound contrast agents for blood flow evaluation," *Invest. Radiol.* **33**, 893–901.
- FOX, F.E. and HERZFELD, K.F. (1954). "Gas bubbles with organic skin as cavitation nuclei," *J. Acoust. Soc. Am.* **26**, 984–989.
- FRANCIS, C.W., ONUNDARSON, P.T., CARSTENSEN, E.L., BLINC, A., MELTZER, R.S., SCHWARZ, K. and MARDER, V.J. (1992). "Enhancement of fibrinolysis *in vitro* by ultrasound," *J. Clin. Invest.* **90**, 2063–2068.

- FRANCIS, C.W., BLINC, A., LEE, S. and COX, C. (1995). "Ultrasound accelerates transport of recombinant tissue plasminogen activator into clots," *Ultrasound Med. Biol.* **21**, 419–424.
- FRANKENBURG, W.K. and DODDS, J.B. (1967). "The Denver developmental screening test," *J. Pediatr.* **71**, 181–191.
- FREDFELDT, K.E. (1986). "Sound velocity in the middle phalanges of the human hand," *Acta. Radiol. [Diagn.] (Stockh.)* **27**, 95–96.
- FRINKING, P.J.A. and DE JONG, N. (1998). "Acoustic modeling of shell-encapsulated gas bubbles," *Ultrasound Med. Biol.* **24**, 523–533.
- FRINKING, P.J.A., DE JONG, N. and CESPEDES, E.I. (1999). "Scattering properties of encapsulated gas bubbles at high ultrasound pressures," *J. Acoust. Soc. Am.* **105**, 1989–1996.
- FRITZ-NIGGLI, H. and BONI, A. (1950). "Biological experiments on *Drosophila melanogaster* with supersonic vibrations," *Science* **112**, 120–122.
- FRITZSCH, T., HELDMANN, D. and REINHARDT, M. (1997). "The potential of a novel ultrasound contrast medium," pages 169 to 176 in *Ultrasound Contrast Agents*, Goldberg, B.B., Ed. (Martin Dunitz Ltd., London).
- FRIZZELL, L.A. (1988). "Threshold dosages for damage to mammalian liver by high intensity focused ultrasound," *IEEE Trans. UFFC* **35**, 578–581.
- FRIZZELL, L.A., LEE, C.S., ASCHENBACH, P.D., BORRELLI, M.J., MORIMOTO, R.S. and DUNN, F. (1983). "Involvement of ultrasonically induced cavitation in the production of hind limb paralysis of the mouse neonate," *J. Acoust. Soc. Am.* **74**, 1062–1065.
- FRIZZELL, L.A., MILLER, D.L. and NYBORG, W.L. (1986). "Ultrasonically induced intravascular streaming and thrombus formation adjacent to a micropipette," *Ultrasound Med. Biol.* **12**, 217–221.
- FRY, W.J. (1953). "Action of ultrasound on nerve tissue—a review," *J. Acoust. Soc. Am.* **25**, 1–5.
- FRY, F.J. and BARGER, J.E. (1978). "Acoustical properties of the human skull," *J. Acoust. Soc. Am.* **63**, 1576–1590.
- FRY, F.J., KOSSOFF, G., EGGLETON, R.C. and DUNN, F. (1970). "Threshold ultrasonic dosages for structural changes in the mammalian brain," *J. Acoust. Soc. Am. (Suppl.)* **48**, 1413–1417.
- FRY, F.J., SANGHVI, N.T., FOSTER, R.S., BIHRLE, R. and HENNIGE, C. (1995). "Ultrasound and microbubbles: Their generation, detection and potential utilization in tissue and organ therapy—experimental," *Ultrasound Med. Biol.* **21**, 1227–1237.
- FU, Y.K., KAUFMAN, G.E., MILLER, M.W., GRIFFITHS, T.D. and LANGE, C.S. (1979). "Modification by cysteamine of ultrasound lethality to Chinese hamster V-79 cells," *Radiat. Res.* **80**, 575–580.
- FU, Y.K., MILLER, M.W., LANGE, C.S., GRIFFITHS, T.D. and KAUFMAN, G.E. (1980). "Ultrasound lethality to synchronous and asynchronous Chinese hamster V-79 cells," *Ultrasound Med. Biol.* **6**, 39–46.
- FUSI, L., STEER, P.J., MARESH, M.J. and BEARD, R.W. (1989). "Maternal pyrexia associated with the use of epidural analgesia in labour," *Lancet* **1**, 1250–1252.
- GAITAN, D.F. and CRUM, L.A. (1990). "Observation of sonoluminescence from a single, stable cavitation bubble in a water/glycerine mixture,"

- pages 459 to 463 in *Frontiers of Nonlinear Acoustics: Proceedings of 12th International Symposium on Nonlinear Acoustics*, Hamilton, M.F. and Blackstock, D.T., Eds. (Elsevier Applied Science, New York).
- GAITAN, D.F., CRUM, L.A., CHURCH, C.C. and ROY, R.A. (1992). "Sonoluminescence and bubble dynamics for a single, stable cavitation bubble," *J. Acoust. Soc. Am.* **91**, 3166–3183.
- GAMBIHLER, S. and DELIUS, M. (1992). "Influence of dissolved and free gases on iodine release and cell killing by shock waves *in vitro*," *Ultrasound Med. Biol.* **18**, 617–623.
- GAMBIHLER, S., DELIUS, M. and BRENDEL, W. (1990). "Biological effects of shock waves: Cell disruption, viability, and proliferation of L1210 cells exposed to shock waves *in vitro*," *Ultrasound Med. Biol.* **16**, 587–594.
- GAMBIHLER, S., DELIUS, M. and ELLWART, J.W. (1994). "Permeabilization of the plasma membrane of L1210 mouse leukemia cells using lithotripter shock waves," *J. Membr. Biol.* **141**, 267–275.
- GAMMELL, P.M., LE CROISSETTE, D.H. and HEYSER, R.C. (1979). "Temperature and frequency dependence of ultrasonic attenuation in selected tissues," *Ultrasound Med. Biol.* **5**, 269–277.
- GAUNAURD, G.C. and UBERALL, H. (1978). "Theory of resonant scattering from spherical cavities in elastic and viscoelastic media," *J. Acoust. Soc. Am.* **63**, 1699–1712.
- GAVRILOV, L.R. (1984a). "Use of focused ultrasound for stimulation of nerve structures," *Ultrasonics* **22**, 132–138.
- GAVRILOV, L.R. (1984b). "Focused ultrasound as a stimulator of the nerve structures. Archives of acoustics," *Archives Acoust.* **9**, 67–74.
- GAVRILOV, L.R., GERSUNI, G.V., ILYINSKI, O.B., TSIRULNIKOV, E.M. and SHCHEKANOV, E.E. (1977a). "A study of reception with the use of focused ultrasound. I. Effects on the skin and deep receptor structures in man," *Brain Res.* **135**, 265–277.
- GAVRILOV, L.R., GERSUNI, G.V., ILYINSKI, O.B., TSIRULNIKOV, E.M. and SHCHEKANOV, E.E. (1977b). "A study of reception with the use of focused ultrasound. II. Effects on the animal receptor structures," *Brain Res.* **135**, 279–285.
- GAVRILOV, L.R., TSIRULNIKOV, E.M. and DAVIES, I.A. (1996). "Application of focused ultrasound for the stimulation of neural structures," *Ultrasound Med. Biol.* **22**, 179–192.
- GE (1996). General Electric. *LOGIQ[®] 700 User Manual*, 2153273-100 Rev. 1 (General Electric Medical Systems, Milwaukee, Wisconsin).
- GERMAIN, M.A., WEBSTER, W.S. and EDWARDS, M.J. (1985). "Hyperthermia as a teratogen: Parameters determining hyperthermia-induced head defects in the rat," *Teratology* **31**, 265–272.
- GERSHOY, A., MILLER, D.L. and NYBORG W.L. (1976). "Intercellular gas: Its role in sonated plant tissue," pages 501 to 511 in *Ultrasound in Medicine 2*, White, D. and Barnes, R., Eds. (Plenum Press, New York).
- GILBERT, R.D., SCHRODER, H., KAWAMURA, T., DALE, P.S. and POWER, G.G. (1985). "Heat transfer pathways between fetal lamb and ewe," *J. Appl. Physiol.* **59**, 634–638.

- GILMORE, F.R. (1952). *The Growth or Collapse of a Spherical Bubble in a Viscous Compressible Liquid* (California Institute of Technology, Pasadena, California).
- GLAZMAN, R.E. (1983). "Effects of adsorbed films on gas bubble radial oscillations," *J. Acoust. Soc. Am.* **74**, 980–986.
- GLAZMAN, R.E. (1984). "Damping of bubble oscillations induced by transport of surfactants between the adsorbed film and the bulk solution," *J. Acoust. Soc. Am.* **76**, 890–896.
- GLOGAUER, M. and MCCULLOCH, C.A.G. (1992). "Introduction of large molecules into viable fibroblasts by electroporation: Optimization of loading and identification of labeled cellular compartments," *Exp. Cell. Res.* **200**, 227–234.
- GOLDBERG, B.B., LIU, J.B. and FORSBERG, F. (1994). "Ultrasound contrast agents: A review," *Ultrasound Med. Biol.* **20**, 319–333.
- GOLDSTEIN, A. (1993). "Broadband transducers improve image quality," *Diagn. Imaging* **15**, 89–93, 100.
- GONCALVES, L.F. and ROMERO, R.A. (1993). "A critical appraisal of the RADIUS study," *Fetus* **3**, 6–18.
- GORKOV, L.P. (1962). "On the forces acting on a small particle in an acoustic field in an ideal fluid," *Sov. Phys. Dokl.* **6**, 773–775 [translated from *Dok. Akad. Nauk. SSSR* **140**, 88–91 (1961)].
- GOSS, S.A., JOHNSTON, R.L. and DUNN, F. (1978). "Comprehensive compilation of empirical ultrasonic properties of mammalian tissues," *J. Acoust. Soc. Am.* **64**, 423–457.
- GOSS, S.A., JOHNSTON, R.L. and DUNN, F. (1980). "Compilation of empirical ultrasonic properties of mammalian tissues: II," *J. Acoust. Soc. Am.* **68**, 93–108.
- GOTTLIEB, S., ERNST, A. and MELTZER, R.S. (1995). "Effect of pressure on echocardiographic videodensity from sonicated albumin: An *in vitro* model," *J. Ultrasound Med.* **14**, 109–116.
- GOULD, R.K. (1966). "Heat transfer across a solid-liquid interface in the presence of acoustic streaming," *J. Acoust. Soc. Am.* **40**, 219–225.
- GOULD, R.K. (1974). "Rectified diffusion in the presence of, and absence of, acoustic streaming," *J. Acoust. Soc. Am.* **56**, 1740–1746.
- GRAESSMANN, M. and GRAESSMAN, A. (1976). "‘Early’ simian-virus-40-specific RNA contains information for tumor antigen formation and chromatin replication," *Proc. Natl. Acad. Sci. USA* **73**, 366–370.
- GRAHAM, E., HEDGES, M., LEEMAN, S. and VAUGHAN, P. (1980). "Cavitation bio-effects of 1.5 MHz," *Ultrasonics* **18**, 224–228.
- GRAMIAK, R., SHAH, P.M. and KRAMER, D.H. (1969). "Ultrasound cardiography: Contrast studies in anatomy and function," *Radiology* **92**, 939–948.
- GREGORY, W.D., MILLER, M.W., CARSTENSEN, E.L., CATALDO, F.L. and REDDY, M.M. (1974). "Non-thermal effects of 2 MHz ultrasound on the growth and cytology of *Vicia faba* roots," *Br. J. Radiol.* **47**, 122–129.
- GROSS, D.R., MILLER, D.L. and WILLIAMS, A.R. (1985). "A search for ultrasonic cavitation within the canine cardiovascular system," *Ultrasound Med. Biol.* **11**, 85–97.

- GRUNDY, M.A., BARNES, R.A. and COAKLEY, W.T. (1995). "Highly sensitive detection of fungal antigens by ultrasound-enhanced latex agglutination," *J. Med. Vet. Mycol.* **33**, 201–203.
- GUHARAY, F. and SACHS, F. (1984). "Stretch-activated single ion channel currents in tissue-cultured embryonic chick skeletal muscle," *J. Physiol. (Lond.)* **352**, 685–701.
- HAHNEL, A.C., GIFFORD, D.J., HEIKKILA, J.J. and SCHULTZ, G.A. (1986). "Expression of the major heat shock protein (HSP 70) family during early mouse embryo development," *Teratog. Carcinog. Mutagen.* **6**, 493–510.
- HAIDER, B., LEWIN, P.A. and THOMENIUS, K.E. (1998). "Pulse elongation and deconvolution filtering for medical ultrasonic imaging," *IEEE Trans. UFFC* **45**, 98–113.
- HALL, A.J. (1975). *An Investigation Into Certain Aspects of the Safety of Ultrasound*, M.Sc. thesis (University of Glasgow, Scotland).
- HALL, P.F., CHARPPONNIER, C., NAKAMURA, M. and GABBIANI, G. (1979). "The role of microfilaments in the response of adrenal tumor cells to adrenocorticotrophic hormone," *J. Biol. Chem.* **254**, 9080–9084.
- HAMANO, K. (1991). "Thrombolysis enhanced by transcutaneous ultrasonic irradiation," *Tokyo Jikelkai Med. J.* **106**, 533–542.
- HANSEN, G.M. (1984). *Mie Scattering as a Technique for the Sizing of Air Bubbles*, Ph.D. dissertation (University of Mississippi, University, Mississippi).
- HAPPEL, J. and BRENNER, H. (1983). *Low Reynolds Number Hydrodynamics*, Sections 4 to 21 (Kluwer Academic Publishers, New York).
- HARARI, P.M., HYNYNEN, K.H., ROEMER, R.B., ANHALT, D.P., SHIMM, D.S., STEA, B. and CASSADY, J.R. (1991). "Development of scanned focussed ultrasound hyperthermia: Clinical response evaluation," *Int. J. Radiat. Oncol. Biol. Phys.* **21**, 831–840.
- HARDY, J.D. (1982). "Temperature regulation, exposure to heat and cold, and affects of hypothermia," pages 172 to 198 in *Therapeutic Heat and Cold*, 3rd ed., Lehmann, J.F., Ed. (Williams & Wilkins, Baltimore, Maryland).
- HARDY, J.D. and OPPEL, T.W. (1937). "Studies in temperature sensation. III. The sensitivity of the body to heat and the spatial summation of the end organ responses," *J. Clin. Invest.* **16**, 533–540.
- HARPER, R.G., QUINTIN, A., KREYNIN, I., BROOKS, G.Z., FARAHANI, G. and LESSER, M. (1991). "Observations on the postpartum shivering phenomenon," *J. Reprod. Med.* **36**, 803–807.
- HARRIS, G.R. (2000). "Early hydrophone work and measurement of output exposure limits at the U.S. Food and Drug Administration," in "Biological effects of ultrasound: Development of safety guidelines, Part 1: Personal histories," Nyborg, N.L., Ed., *Ultrasound Med. Biol.* **26**, 930–932.
- HARRIS, G.R., STEWART, H.F., LEO, F.P. and SAUNDERS, R.C. (1989). "Relationship between image quality and ultrasound exposure level in diagnostic US devices," *Radiology* **173**, 313–317.
- HARRISON, G.H. and BALCER-KUBICZEK, E.K. (1989). "Continuous-wave ultrasound and neoplastic transformation *in vitro*," *Ultrasound Med. Biol.* **15**, 335–340.

- HARRISON, G.H., BALCER-KUBICZEK, E.K. and EDDY, H.A. (1991). "Potentiation of chemotherapy by low-level ultrasound," *Int. J. Radiat. Biol.* **59**, 1453–1466.
- HART, F.M. and FABER, J.J. (1965). "Fetal and maternal temperatures in rabbits," *J. Appl. Physiol.* **20**, 737–741.
- HARTLEY, C.J. (1997). "Characteristics of acoustic streaming created and measured by pulsed Doppler ultrasound," *IEEE Trans. UFFC* **44**, 1278–1285.
- HARTMAN, C., COX, C.A., BREWER, L., CHILD, S.Z., COX, C.F. and CARSTENSEN, E.L. (1990a). "Effects of lithotripter fields on development of chick embryos," *Ultrasound Med. Biol.* **16**, 581–585.
- HARTMAN, C., CHILD, S.Z., MAYER, R., SCHENK, E. and CARSTENSEN, E.L. (1990b). "Lung damage from exposure to the fields of an electrohydraulic lithotripter," *Ultrasound Med. Biol.* **16**, 675–679.
- HARVEY, E.N. (1930). "Biological aspects of ultrasonic waves: A general survey," *Biol. Bull.* **59**, 306–325.
- HARVEY, E.N. and LOOMIS, A.L. (1928). "High frequency sound waves of small intensity and their biological effects," *Nature* **121**, 622–624.
- HARVEY, W., DYSON, M., POND, J.B. and GRAHAM, E.R. (1975). "The *in-vitro* stimulation of protein synthesis in human fibroblasts by therapeutic levels of ultrasound," pages 10 to 21 in *Proceedings of the Second European Congress Ultrasonics in Medicine*, Kazner, E., de Vlieger, M., Muller, H.R. and McCready, V.R., Eds., International Congress Series No. 363 (Excerpta Medica, Amsterdam).
- HARVEY, M.A., MCRORIE, M.M. and SMITH, D.W. (1981). "Suggested limits to the use of the hot tub and sauna by pregnant women," *CMAJ* **125**, 50–53.
- HARVEY, C.J., BLOMLEY, M.J., ECKERSLEY, R.J., HECKEMANN, R.A., BUTLER-BARNES, J. and COSGROVE, D.O. (2000). "Pulse-inversion mode imaging of liver specific microbubbles: Improved detection of subcentimetre metastases," *Lancet* **355**, 807–808.
- HAUFF, P., FRITZSCH, T., REINHARDT, M., WEITSCHIES, W., LUDERS, F., UHLENDORF, V. and HELDMANN, D. (1997). "Delineation of experimental liver tumors in rabbits by a new ultrasound contrast agent and stimulated acoustic emission," *Invest. Radiol.* **32**, 94–99.
- HAWKES, J.J. and COAKLEY, W.T. (1996). "A continuous flow ultrasonic cell-filtering method," *Enzyme Microbiol. Tech.* **19**, 57–62.
- HAWLEY, S.A. and DUNN, F. (1964). "UHF acoustic interaction with biological media," *Naturwissenschaften* **51**, 555–556.
- HAYES, C.F., CHINGON, H.T., MCMURDO, M.B., IKEDA, M.B., SANDERSON, S.L. and DEEVER, J. (1983). "Ultrasonic effects on *Dacus dorsalis*," *Ultrasound Med. Biol.* **9**, 185–189.
- HECKMAN, J.D., RYABY, J.P., MCCABE, J., FREY, J.J. and KILCOYNE, R.F. (1994). "Acceleration of tibial fracture-healing by non-invasive, low-intensity pulsed ultrasound," *J. Bone Joint Surg. Am.* **76**, 26–34.
- HELLEBUST, H., CHRISTIANSEN, C. and SKOTLAND, T. (1993). "Biochemical characterization of air-filled albumin microspheres," *Biotechnol. Appl. Biochem.* **18**, 227–237.

- HELLMAN, L.M., DUFFUS, G.M., DONALD, I. and SUNDEN, B. (1970). "Safety of diagnostic ultrasound in obstetrics," *Lancet* **1**, 1133–1134.
- HENDERSON, J., WILLSON, K., JAGO, J.R. and WHITTINGHAM, T.A. (1995). "A survey of the acoustic outputs of diagnostic ultrasound equipment in current clinical use," *Ultrasound Med. Biol.* **21**, 699–705.
- HENGLEIN, A. (1987). "Sonochemistry: Historical developments and modern aspects," *Ultrasonics* **25**, 6–16.
- HENGLEIN, A. and KORMANN, C. (1985). "Scavenging of OH radicals produced in the sonolysis of water," *Int. J. Radiat. Biol. Relat. Stud. Phys. Chem. Med.* **48**, 251–258.
- HERBERTZ, J. (1988). *Spontaneous Cavitation in Liquids Free of Nuclei*, Fortschritte Akustik DAGA '88.
- HERMAN, B.A. and HARRIS, G.R. (1999). "Theoretical study of steady-state temperature rise within the eye due to ultrasound insonation," *IEEE Trans. UFFC* **46**, 1556–1574.
- HERMAN, C., LECAT, S., D'ARI, R. and BOULOC, P. (1995). "Regulation of the heat-shock response depends on divalent metal ions in an hflB mutant of *Escherichia coli*," *Mol. Microbiol.* **18**, 247–255.
- HERRICK, J.F. (1958). "Pearl chain formation," in *Proceedings of the Second Tri-Service Conference on Biological Effects of Microwave Energy*, Pattishall, E.G. and Banghart, F.W., Eds., Astia document No. AD 131 477 (University of Virginia, Charlottesville, Virginia).
- HERRING, C. (1941). "Theory of the pulsations of gas bubbles produced by an underwater explosion," Office of Scientific Research and Development Report No. 236 (U.S. Government Printing Office, Washington).
- HERSEY, S.J. and PEREZ, A. (1990). "Permeable cell models in stimulus-secretion coupling," *Ann. Rev. Physiol.* **52**, 345–361.
- HERTZ, R.H., TIMOR-TRITSCH, I., DIERKER, L.J., JR., CHIK, L. and ROSEN, M.G. (1979). "Continuous ultrasound and fetal movement," *Am. J. Obstet. Gynecol.* **135**, 152–154.
- HERZFELD, K.F. and LITOVITZ, T.A. (1959). *Absorption and Dispersion of Ultrasonic Waves* (Academic Press, New York).
- HEY, E.N. (1969). "The relation between environmental temperature and oxygen consumption in the new-born baby," *J. Physiol. (Lond.)* **200**, 589–603.
- HEYNER, S., ABRAHAM, V., WIKARCZUK, M.L. and ZISKIN, M.C. (1989). "Effects of ultrasound on ovulation in the mouse," *Gamete Res.* **22**, 333–338.
- HILGENFELDT, S., LOHSE, D. and ZOMACK, M. (2000). "Sound scattering and localized heat deposition of pulse-driven microbubbles," *J. Acoust. Soc. Am.* **107**, 3530–3539.
- HILL, A.B. (1965). "The environment and disease: Association or causation?" *Proc. Royal Soc. Med.* **58**, 295–300.
- HILL, C.R. (1994). "Optimum acoustic frequency for focused ultrasound surgery," *Ultrasound Med. Biol.* **20**, 271–277.
- HILL, C.R. and JOSHI, G.P. (1970). "The significance of cavitation in interpreting the biological effects of ultrasound," pages 125 to 131 in *Proceedings*

- of the Conference on Ultrasonics in Biology and Medicine, UBIOMED-70 (Polish Academy of Sciences, Warsaw, Poland).
- HILL, C.R., RIVENS, I., VAUGHAN, M.G. and TER HAAR, G.R. (1994). "Lesion development in focused ultrasound surgery: A general model," *Ultrasound Med. Biol.* **20**, 259–269.
- HILLER, R., PUTTERMAN, S.J. and BARBER, B.P. (1992). "Spectrum of synchronous picosecond sonoluminescence," *Phys. Rev. Lett.* **69**, 1182–1184.
- HILLER, R., WENINGER, K., PUTTERMAN, S.J. and BARBER, B.P. (1994). "Effect of noble gas doping in single-bubble sonoluminescence," *Science* **266**, 248–250.
- HOLLAND, C.K. and APFEL, R.E. (1989). "An improved theory for the prediction of microcavitation thresholds," *IEEE Trans. UFFC* **36**, 204–208.
- HOLLAND, C.K. and APFEL, R.E. (1990). "Thresholds for transient cavitation produced by pulsed ultrasound in a controlled nuclei environment," *J. Acoust. Soc. Am.* **88**, 2059–2069.
- HOLLAND, C.K., ROY, R.A., APFEL, R.E. and CRUM, L.A. (1992). "In vitro detection of cavitation induced by a diagnostic ultrasound system," *IEEE Trans. UFFC* **39**, 95–101.
- HOLLAND, C.K., DENG, C.X., APFEL, R.E., ALDERMAN, J.L., FERNANDEZ, L.A. and TAYLOR, K.J. (1996). "Direct evidence of cavitation in vivo from diagnostic ultrasound," *Ultrasound Med. Biol.* **22**, 917–925.
- HOLMER, N.G., JOHNSSON, A. and JOSEFSSON, J.O. (1975). "Effects of ultrasonic irradiation upon *Amoeba proteus*," *Z. Naturforsch.* **28c**, 607–609.
- HOLT, R.G. (1988). *Experimental Observations of the Nonlinear Response of Single Bubbles to an Applied Acoustic Field*, Ph.D. dissertation (University of Mississippi, University, Mississippi).
- HONDA, K., HATAYAMA, T., TAKAHASHI, K. and YUKIOKA, M. (1992). "Heat shock proteins in human and mouse embryonic cells after exposure to heat shock or teratogenic agents," *Teratog. Carcinog. Mutag.* **11**, 235–244.
- HONG, A.S., CHAE, J.S., DUBIN, S.B., LEE, S., FISHBEIN, M.C. and SIEGEL, R.J. (1990). "Ultrasonic clot disruption: An in vitro study," *Am. Heart J.* **120**, 418–422.
- HORDER, M.M., BARNETT, S.B., VELLA, G.J., EDWARDS, M.J. and WOOD, A.K. (1998a). "Ultrasound-induced temperature increase in the guinea-pig fetal brain in vitro," *Ultrasound Med. Biol.* **24**, 697–704.
- HORDER, M.M., BARNETT, S.B., VELLA, G.J. and EDWARDS, M.J. (1998b). "In vivo heating of the guinea-pig fetal brain by pulsed ultrasound and estimates of thermal index," *Ultrasound Med. Biol.* **24**, 1467–1474.
- HORDER, M.M., BARNETT, S.B., VELLA, G.J. and EDWARDS, M.J. and WOOD, A.K.K. (1998c). "Ultrasound-induced temperature increase in guinea-pig fetal brain in utero: Third-trimester gestation," *Ultrasound Med. Biol.* **24**, 1501–1510.
- HORSBURGH, S.D. (1990). *Radial Instabilities of a Pulsating Air Bubble in Water*, Ph.D. dissertation (University of Mississippi, University, Mississippi).

- HOWARD, D. and STURTEVANT, B. (1997). "In vitro study of the mechanical effects of shock-wave lithotripsy," *Ultrasound Med. Biol.* **23**, 1107–1122.
- HOWARTH, C.J. and OUGHAM, H.J. (1993). "Tansley Review No. 51. Gene expression under temperature stress," *New Phytol.* **125**, 1–26.
- HOWRY, D.H. and BLISS, W.R. (1952). "Ultrasonic visualization of soft tissue structures of the body," *J. Lab. Clin. Med.* **40**, 579–592.
- HSIEH, D.Y. and PLESSET, M.S. (1961). "Theory of rectified diffusion of mass into gas bubbles," *J. Acoust. Soc. Am.* **33**, 206–215.
- HUGHES, D.E. and NYBORG, W.L. (1962). "Cell disruption by ultrasound," *Science* **138**, 108–114.
- HUSSAIN, R., KIMME-SMITH, C., TESSLER, F.N., PERRELLA, R.R., GRANT, E.G. and SANDSTROM, K. (1992). "Fetal exposure from endovaginal ultrasound examinations in the first trimester," *Ultrasound Med. Biol.* **18**, 675–679.
- HWANG, E.Y., FOWLKES, J.B. and CARSON, P.L. (1998). "Variables controlling contrast generation in a urinary bladder model," *J. Acoust. Soc. Am.* **103**, 3706–3716.
- HYNYNEN, K. (1991). "The threshold for thermally significant cavitation in dog's thigh muscle *in vivo*," *Ultrasound Med. Biol.* **17**, 157–169.
- HYNYNEN, K. (1993). "Acoustic power calibrations of cylindrical intracavitary ultrasound hyperthermia applicators," *Med. Phys.* **20**, 129–134.
- IEC (1988). International Electrochemical Commission. *Medical Electrical Equipment—Part 1: General Requirements for Safety*, IEC Publication 60601-1 (International Electrotechnical Commission, Geneva).
- IEC (1991). International Electrochemical Commission. *Measurement and Characterization of Ultrasonic Fields Using Hydrophones in the Frequency Range 0.5 MHz to 15 MHz*, IEC Publication 61102 (International Electrotechnical Commission, Geneva).
- IEC (1992). International Electrochemical Commission. *Requirements for the Declaration of the Acoustic Output of Medical Diagnostic Ultrasonic Equipment*, IEC Publication 61157 (International Electrotechnical Commission, Geneva).
- IKEUCHI, T., SASAKI, M., OSHIMAURA, M., OZUMI, J., TSUJI, K. and SHIMIZU, T. (1973). "Ultrasound and embryonic chromosomes," *BMJ* **1**, 112.
- INOUE, M., CHURCH, C.C., BRAYMAN, A., MILLER, M.W. and MALCUI, M.S. (1989). "Confirmation of the protective effect of cysteamine in *in vitro* ultrasound exposures," *Ultrasonics* **27**, 362–369.
- INSANA, M.F. (1995). "Sound attenuation in tissue," pages 35 to 48 in *Medical CT and Ultrasound: Current Technology and Applications*, Goldman, L.W. and Fowlkes, J.B., Eds. (American Association of Physicists in Medicine, College Park, Maryland).
- IRPA/INIRC (1991). International Radiation Protection Association/International Non-ionizing Radiation Committee. "Protection of the patient undergoing a magnetic resonance examination," *Health Phys.* **61**, 923–928.

- IVEY, J.A., GARDNER, E.A., FOWLKES, J.B., RUBIN, J.M. and CARSON, P.L. (1995). "Acoustic generation of intra-arterial contrast boluses," *Ultrasound Med. Biol.* **21**, 757–767.
- JAGO, J.R., HENDERSON, J., WHITTINGHAM, T.A. and WILLSON, K. (1995). "How reliable are manufacturer's reported acoustic output data?" *Ultrasound Med. Biol.* **21**, 135–136.
- JAGO, J.R., HENDERSON, J., WHITTINGHAM, T.A. and MITCHELL, G. (1999). "A comparison of AIUM/NEMA thermal indices with calculated temperature rises for a simple third-trimester pregnancy tissue model," *Ultrasound Med. Biol.* **25**, 623–628.
- JEFFERS, R.J., FENG, R.Q., FOWLKES, J.B., HUNT, J.W., KESSEL, D. and CAIN, C.A. (1995). "Dimethylformamide as an enhancer of cavitation-induced cell lysis *in vitro*," *J. Acoust. Soc. Am.* **97**, 669–676.
- JELLINS, J. and BARRACLOUGH, B.H. (1978). "Ultrasonic imaging of the scrotum," *J. Ultrasound Med.* **4**, 151.
- JOELSSON, I., BARTON, M.D., DANIEL, S., JAMES, L.S. and ADAMSONS, K. (1970). "A method for prolonged monitoring of physiologic functions during fetal life," *Am. J. Obstet. Gynecol.* **107**, 445–452.
- JOERSBO, M. and BRUNSTEDT, J. (1992). "Sonication: A new method for gene transfer to plants," *Physiologia Plantarum* **85**, 230–234.
- JOHANNES, C. and OBE, G. (1997). "Ultrasound permeabilizes CHO cells for the endonucleases AluI and benzon nuclease," *Mutat. Res.* **374**, 245–251.
- JOHNSON, R.E. and DETTRE, R.H. (1969). "Wettability and contact angles," pages 85 to 153 in *Surface and Colloid Science*, Matijevic, E., Ed. (Plenum Press, New York).
- KAMATH, V., PROSPERETTI, A. and EGOLFOPOULOS, F.N. (1993). "A theoretical study of sonoluminescence," *J. Acoustic Soc. Am.* **94**, 248–260.
- KAMEL, I.R. (1994). "An evaluation of overlying tissues to determine fetal exposure to ultrasound during the third trimester," *Ultrasound Med. Biol.* **20**, 41–51.
- KAMIYAMA, N., MORIYASU, F., MINE, Y. and GOTO, Y. (1999). "Analysis of flash echo from contrast agent for designing optimal ultrasound diagnostic systems," *Ultrasound Med. Biol.* **25**, 411–420.
- KASHKOOLI, H.A. (1977). *Effects of Ultrasonically Produced Shearing Stresses on Selected Enzymes*, M.S. thesis (University of Maine, Orono, Maine).
- KASPRZAK, J.D., VLETTER W.B., VAN MEEGEN, J.R., NOSIR, Y.F.M., JOHNSON, R., TEN CATE, F.J. and ROELANDT, J.R.T.C. (1998). "Improved quantification of myocardial mass by three-dimensional echocardiography using a deposit contrast agent," *Ultrasound Med. Biol.* **24**, 647–653.
- KATZ, J.I. (1992). "Comments on 'Particle gathering and microstreaming near ultrasonically activated gas-filled micropores'," *J. Acoust. Soc. Am.* **91**, 505–506.
- KAUFMAN, G.E. (1985). "Mutagenicity of ultrasound in cultured mammalian cells," *Ultrasound Med. Biol.* **11**, 497–501.

- KAUFMAN, G.E. and MILLER, M.W. (1978). "Growth retardation in Chinese hamster V-79 cells exposed to 1 MHz ultrasound," *Ultrasound Med. Biol.* **4**, 139–144.
- KAUFMAN, G.E., MILLER, M.W., GRIFFITHS, T.D., CIARAVINO, V. and CARSTENSEN, E.L. (1977). "Lysis and viability of cultured mammalian cells exposed to 1 MHz ultrasound," *Ultrasound Med. Biol.* **3**, 21–25.
- KAUL, S. (1997). "Mycocardial contrast echocardiography: 15 years of research and development," *Circulation* **96**, 3745–3760.
- KILLAM, A. and DITTRICH, H.C. (1997). "Cardiac applications of Albunex and FS069," pages 43 to 55 in *Ultrasound Contrast Agents*, Goldberg, B.B., Ed. (Martin Dunitz Ltd., London).
- KIM, H.L., PICCIANO, M.F. and O'BRIEN, W.D., JR. (1983). "The combined effect of ultrasonic exposure and protein restriction on maternal and fetal mice," *Ultrasound Med. Biol.* **9**, 165–175.
- KIM, H.J., GREENLEAF, J.F., KINNICK, R.R., BRONK, J.T. and BOLANDER, M.E. (1996). "Ultrasound-mediated transfection of mammalian cells," *Hum. Gene Ther.* **7**, 1339–1346.
- KIMMEL, C.A., STRATMEYER, M.E., GALLOWAY, W.D., LABORDE, J.B., BROWN, N. and PINKAVITCH, F. (1983). "The embryotoxic effects of ultrasound exposure on pregnant ICR mice," *Teratology* **27**, 245–251.
- KIMMEL, C.A., STRATMEYER, M.E., GALLOWAY, W.D., BROWN, N.T., LABORDE, J.B. and BATES, H.K. (1989). "Developmental exposure of mice to pulsed ultrasound," *Teratology* **40**, 387–393.
- KIMMEL, C.A., CUFF, J.M., KIMMEL, G.L., HEREDIA, D.J., TUDOR, N., SILVERMAN, P.M. and CHEN, J. (1993a). "Skeletal development following heat exposure in the rat," *Teratology* **47**, 229–242.
- KIMMEL, G.L., CUFF, J.M., KIMMEL, C.A., HEREDIA, D.J., TUDOR, N. and SILVERMAN, P.M. (1993b). "Embryonic development *in vitro* following short-duration exposure to heat," *Teratology* **47**, 243–251.
- KINNIER WILSON, L.M. and WATERHOUSE, J.A.H. (1984). "Obstetric ultrasound and childhood malignancies," *Lancet* **2**, 997–999.
- KLIBANOV, A.L., HUGHES, M.S., WOJDYLA, J.K., MARSH, J.N., HALL, C.S., MILLER, J.G., WIBLE, J.H., JR. and BRANDENBURGER G.H. (1998). "Targeting of ultrasound contrast material: Selective imaging of microbubbles *in vitro*," *Acad. Radiol. (Suppl.)* **5**, S243–S246.
- KNAPP, R.T., DAILY, J.W. and HAMMITT, F.G. (1970). *Cavitation* (McGraw-Hill, New York).
- KNAPP, R., FRAUSCHER, F., HELWEG, G., JUDMAIER, W., STRASSER, H., BARTSCH, G. and ZUR NEDDEN, D. (1996). "Blood pressure changes after extracorporeal shock wave nephrolithotripsy: Prediction by intrarenal resistive index," *Eur. Radiol.* **6**, 665–669.
- KOBER, L.O., ELLWART, J.W. and BRETTEL, H. (1989). "Effect of the pulse length of ultrasound on cell membrane damage *in vitro*," *J. Acoust. Soc. Am.* **86**, 6–7.
- KOHORN, E.I., PRITCHARD, J.W. and HOBBS, J.C. (1967). "The safety of clinical ultrasonic examination. Electroencephalographic examination of the neonate subjected to pulsed ultrasound," *Obstet. Gynecol.* **29**, 272–274.

- KOLIOS, M.C., SHERAR, M.D. and HUNT, J.W. (1995). "Large blood vessel cooling in heated tissues: A numerical study," *Phys. Med. Biol.* **40**, 477-494.
- KONDO, T. and KANO, E. (1987). "Enhancement of hyperthermic cell killing by non-thermal effect of ultrasound," *Int. J. Radiat. Biol. Relat. Stud. Phys. Chem. Med.* **51**, 157-166.
- KONDO, T. and KANO, E. (1988). "Effect of free radicals induced by ultrasonic cavitation on cell killing," *Int. J. Radiat. Biol.* **54**, 475-486.
- KONDO, T., GAMSON, J., MITCHELL, J.B. and RIESZ, P. (1988). "Free radical formation and cell lysis induced by ultrasound in the presence of different rare gases," *Int. J. Radiat. Biol.* **54**, 955-962.
- KONDO, T., FUKUSHIMA, Y., KON, H. and RIESZ, P. (1989). "Effect of shear stress and free radicals induced by ultrasound on erythrocytes," *Arch. Biochem. Biophys.* **269**, 381-389.
- KORANYI, G., FALUS, M., SOBEL, M., PESTI, E. and VAN BAO, T. (1972). "Follow-up examination of children exposed to ultrasound *in utero*," *Acta Paediatr. Acad. Sci. Hung.* **13**, 231-238.
- KORNOWSKI, R., MELTZER, R.S., CHERNINE, A., VERED, Z. and BATTLER, A. (1994). "Does external ultrasound accelerate thrombolysis? Results from a rabbit model," *Circulation* **89**, 339-344.
- KOSSOFF, G., GRIFFITHS, K.A., GARRETT, W.J., WARREN, P.S., ROBERTS, A.B. and MITCHELL, J.M. (1993). "Thickness of tissues intervening between the transducer and fetus and models for fetal exposure calculations in transvaginal sonography," *Ultrasound Med. Biol.* **19**, 59-65.
- KREMKAU, F.W. (1989). "Clinical benefit of higher acoustic output levels," *Ultrasound Med. Biol. (Suppl.)* **15**, 69-70.
- KREMKAU, F.W., GRAMIAK, R., CARSTENSEN, E.L., SHAH, P.M. and KRAMER, D.H. (1970). "Ultrasonic detection of cavitation at catheter tips," *Am. J. Roentgenol. Radium Ther. Nucl. Med.* **110**, 177-183.
- KREMKAU, F.W., BARNES, R.W. and MCGRAW, C.P. (1981). "Ultrasonic attenuation and propagation speed in normal human brain," *J. Acoust. Soc. Am.* **70**, 29-38.
- KRESHOVER, S.J. and CLOUGH, O.W. (1952). "Prenatal influences on tooth development. II. Artificially induced fever in rats," *J. Dental. Res.* **32**, 565-577.
- KRISHNA, P.D. and NEWHOUSE, V.L. (1997). "Second harmonic characteristics of the ultrasound contrast agents Albunex and FS069," *Ultrasound Med. Biol.* **23**, 453-459.
- KRISTIANSEN, T.K., RYABY, J.P., MCCABE, J., FREY J.J. and ROE, L.R. (1997). "Accelerated healing of distal radial fractures with the use of specific, low-intensity ultrasound. A multicenter, prospective, randomized, double-blind, placebo-controlled study," *J. Bone Joint Surg. Am.* **79**, 961-973.
- KRIZAN, J.R. and WILLIAMS, A.R. (1973). "Biological membrane rupture and a phase transition model," *Nat. New Biol.* **246**, 121-123.
- KRIZAN, J.E. and WILLIAMS, A.R. (1977). "Non-equilibrium cooperative model for a membrane under hydrodynamic shear," *Collective Phenomena* **2**, 229-234.

- KUC, R. and SCHWARTZ, M. (1979). "Estimating the acoustic attenuation coefficient slope for liver from reflected ultrasound signals," *IEEE Trans. Sonics Ultras.* **26**, 353–362.
- KUDO, S. (1989). "Thrombolysis with ultrasound effect," *Tokyo Jikeikai Med. J.* **104**, 1005–1012.
- LAI, Y.K., LI, C.W., HU, C.H. and LEE, M.L. (1988). "Quantitative and qualitative analyses of protein synthesis during heat shock in the marine diatom *Nitzschia alba* (Bacillariophyceae)," *J. Phycol.* **24**, 509–514.
- LAMB, H. (1879). *Hydrodynamics* (Cambridge University Press, London).
- LAMB, H. (1945). *Hydrodynamics* (Dover Publications, Inc., New York).
- LAMBERT, H., PANKOV, R., GAUTHIER, J. and HANCOCK, R. (1990). "Electroporation-mediated uptake of proteins into mammalian cells," *Biochem. Cell Biol.* **68**, 729–734.
- LANCET (1978). "Editorial: Hyperthermia and the neural tube," *Lancet* **2**, 560–561.
- LARSEN, H. (1986). "The role of ultrasonic intensity in image quality," in presentation and panel discussion by Carson, P., Larsen, H., Stewart, H. and Taylor, K. (American Institute of Ultrasound in Medicine, Laurel, Maryland).
- LARY, J.M., CONOVER, D.L., FOLEY, E.D. and HANSER, P.L. (1982). "Teratogenic effects of 27.12 MHz radiofrequency radiation in rats," *Teratol.* **26**, 299–309.
- LARY, J.M., CONOVER, D.C., JOHNSON, P.H. and HORNUNG, R.W. (1986). "Dose-response relationship between body temperature and birth defects in radiofrequency-irradiated rats," *Bioelectromagnetics* **7**, 141–149.
- LASTMAN, G.J. and WENTZELL, R.A. (1981). "Comparison of five models of spherical bubble response in an inviscid compressible liquid," *J. Acoust. Soc. Am.* **69**, 638–641.
- LAUTERBORN, W. (1976). "Numerical investigation of nonlinear oscillations of gas bubbles in liquids," *J. Acoust. Soc. Am.* **59**, 283–293.
- LAUTERBORN, W. (1991). "Akustische kavitation: Ein typische, nichtlineares dynamisches system," *Acustica* **75**, 145–153.
- LAUTERBORN, W. and PARLITZ, U. (1988). "Methods of chaos physics and their application to acoustics," *J. Acoust. Soc. Am.* **84**, 1975–1993.
- LEE, S., ANDERSON, T., ZHANG, H., FLOTTE, T.J. and DOUKAS, A.G. (1996). "Alteration of cell membrane by stress waves *in vitro*," *Ultrasound Med. Biol.* **22**, 1285–1293.
- LEEMAN, S. and HARRISON, G.H. (1982). "Ultrasound interaction with plant roots," *Br. J. Cancer (Suppl.)* **45**, 196–198.
- LEES, S., AHERN, J.M. and LEONARD, M. (1983). "Parameters influencing the sonic velocity in compact calcified tissues of various species," *J. Acoust. Soc. Am.* **74**, 28–33.
- LEHMANN, J.F. (1953). "The biophysical mode of action of biologic and therapeutic ultrasonic reactions," *J. Acoust. Soc. Am.* **25**, 17–25.
- LEHMANN, J.F., Ed. (1990). *Therapeutic Heat and Cold*, 4th ed. (William and Wilkins, Baltimore).

- LEHMANN, J.F. and BIEGLER, R. (1954). "Changes of potentials and temperature gradients in membranes caused by ultrasound," *Arch. Phys. Med.* **35**, 287–295.
- LEHMANN, J.F. and HERRICK, J.F. (1953). "Biologic reaction to cavitation, a consideration for ultrasonic therapy," *Arch. Phys. Med. Rehab.* **34**, 86–98.
- LEHMANN, J.F. and JOHNSON, E.W. (1958). "Some factors influencing the temperature distribution in thighs exposed to ultrasound," *Arch. Phys. Med. Rehab.* **39**, 347–356.
- LEIGHTON, T.G. (1996). *The Acoustic Bubble* (Academic Press, San Diego, California).
- LEIGHTON, T.G., PICKWORTH, M.J., TUDOR, J. and DENDY, P.P. (1990). "A search for sonoluminescence *in vivo* in the human cheek," *Ultrasonics* **28**, 181–184.
- LELE, P.R. (1975). "Ultrasonic teratology in mouse and man," in *Second Congress, European Congress on Ultrasonics in Medicine*, International Congress Series, Excerpta Medica **363**, 22–27.
- LELE, P.P. (1977). "Thresholds and mechanisms of ultrasonic damage to 'organized' animal tissues," pages 224 to 239 in *Biological Effects and Characterization of Ultrasound Sources: Symposium Proceedings*, Hazard, D.G., Ed. (U.S. Government Printing Office, Washington).
- LELE, P.P. (1978). "Cavitation and its effects on organized mammalian tissues: A summary," pages 737 to 741 in *Ultrasound: Its Application in Medicine and Biology*, Fry, F.J., Ed. (Elsevier, New York).
- LEVERETT, L.B., HELLUMS, J.D., ALFREY, C.P. and LYNCH, E.C. (1972). "Red blood cell damage by shear stress," *Biophys. J.* **12**, 257–273.
- LEWIN, P.A. and BJORNO, L. (1982). "Thresholds for rectified diffusion and acoustic microstreaming by bubbles in biological media," pages 25 to 35 in *The Mechanics and Physics of Bubbles in Liquids*, van Wijngaarden, L., Ed. (Kluwer, New York).
- LEWIN, P.A., CHAPELON, J.Y., MESTAS, J.L., BIRER, A. and CATHIGNOL, D. (1990). "A novel method to control P+/P- ratio of the shock wave pulses used in the extracorporeal piezoelectric lithotripsy (EPL)," *Ultrasound Med. Biol.* **16**, 473–488.
- LI, G.C. and LAZLO, A. (1985). "Thermotolerance in mammalian cells: A possible role for the heat shock proteins," pages 349 to 371 in *Changes in Eukaryotic Gene Expression in Response to Environmental Stress*, Atkinson, B.C. and Walden, D.B., Eds. (Academic Science Press, New York).
- LI, Z.L. and SHIOTA, K. (1999). "Stage-specific homeotic vertebral transformations in mouse fetuses induced by maternal hyperthermia during somitogenesis," *Dev. Dyn.* **216**, 336–348.
- LI, G.C., HAHN, G.M. and TOLMACH, L.J. (1977). "Cellular inactivation by ultrasound," *Nature* **267**, 163–165.
- LIEBERMANN, L.N. (1949). "The second viscosity of liquids," *Phys. Rev.* **75**, 1415–1422.
- LIEBESKIND, D., BASES, R., MENDEZ, F., ELEQUIN, F. and KOENIGSBERG, M. (1979a). "Sister chromatid exchanges in human lymphocytes after exposure to diagnostic ultrasound," *Science* **205**, 1273–1275.

- LIEBESKIND, D., BASES, R., ELEQUIN, F., NEUBORT, S., LEIFER, R., GOLDBERG, R. and KOENIGSBERG, M. (1979b). "Diagnostic ultrasound: Effects on the DNA and growth patterns of animals cells," *Radiology* **131**, 177–184.
- LIEBESKIND, D., PADAWER, J., WOLLEY, R. and BASES, R. (1982). "Diagnostic ultrasound: Time-lapse and transmission electron microscopic studies of cells insonated *in vitro*," *Br. J. Cancer (Suppl.)* **45**, 176–186.
- LIMB, C.J. and HOLMES, L.B. (1994). "Anencephaly: Changes in prenatal detection and birth status, 1972-1990," *Am. J. Obstet. Gynecol.* **170**, 1333–1338.
- LIN, T., OPHIR, J. and POTTER, G. (1987). "Frequency-dependent ultrasonic differentiation of normal and diffusely diseased liver," *J. Acoust. Soc. Am.* **82**, 1131–1138.
- LINDGREN, D. (1972). "The temperature influence on the spontaneous mutation rate. II. Investigation by the aid of waxy mutants," *Hereditas* **70**, 179–184.
- LINDQUIST, S. and CRAIG, E.A. (1988). "The heat-shock proteins," *Ann. Rev. Genet.* **22**, 631–677.
- LIPSON, A.H. and EDWARDS, M.J. (1993). "Maternal sauna and hyperthermia during pregnancy and cardiovascular and other malformations in offspring," *Eur. J. Epidemiol.* **9**, 676–678.
- LIU, D.L. and WAAG, R.C. (1997). "Harmonic amplitude distribution in a wideband ultrasonic wavefront after propagation through human abdominal wall and breast specimens," *J. Acoust. Soc. Am.* **101**, 1172–1183.
- LIZZI, F.L., COLEMAN, D.J., DRILLER, J., FRANZEN, L.A. and JAKOBIEC, F.A. (1978). "Experimental, ultrasonically induced lesions in the retina, choroid, and sclera," *Invest. Ophthalmol. Vis. Sci.* **17**, 350–360.
- LIZZI, F.L., COLEMAN, D.J., DRILLER, J., FRANZEN, L.A. and LEOPOLD, M. (1981). "Effects of pulsed ultrasound on ocular tissue," *Ultrasound Med. Biol.* **7**, 245–252.
- LIZZI, F.L., DRILLER, J., LUNZER, B., KALISZ, A. and COLEMAN, D.J. (1992). "Computer model of ultrasonic hyperthermia and ablation for ocular tumors using B-mode data," *Ultrasound Med. Biol.* **18**, 59–73.
- LOCH, E.G., FISCHER, A.B. and KUWERT, E. (1971). "Effect of diagnostic and therapeutic intensities of ultrasonics on normal and malignant human cells *in vitro*," *Am. J. Obstet. Gynecol.* **110**, 457–460.
- LOPEZ, H. (1998). *How to Interpret the Ultrasound Output Display Standard for Higher Acoustic Output Diagnostic Ultrasound Devices* (American Institute of Ultrasound in Medicine, Laurel, Maryland).
- LOTMAR, R. (1952). "Die wirkung von ultraschall auf verschiedene entwicklungsstadien von *Drosophila melanogaster* (Dipt.)," *Strahlentherapie* **87**, 497–516.
- LOTSBERG, O., HOVEM, J.M. and AKSUM, B. (1996). "Experimental observation of subharmonic oscillations in Infuson bubbles," *J. Acoust. Soc. Am.* **99**, 1366–1369.
- LOVEROCK, P. and TER HAAR, G. (1991). "Synergism between hyperthermia, ultrasound and gamma irradiation," *Ultrasound Med. Biol.* **17**, 607–612.

- LOVEROCK, P., TER HAAR, G., ORMEROD, M.G. and IMRIE, P.R. (1990). "The effect of ultrasound on the cytotoxicity of adriamycin," *Br. J. Radiol.* **63**, 542–546.
- LYONS, E.A. and COGGRAVE-TOMS, M. (1979). "Abstract: Long term follow-up study of children exposed to ultrasound *in utero*," page 112 in *Proceedings of the 24th Annual Meeting of AIUM* (American Institute of Ultrasound in Medicine, Laurel, Maryland).
- LYONS, M.E. and PARKER, K.J. (1988). "Absorption and attenuation in soft tissues. II. Experimental results," *IEEE Trans. UFFC* **35**, 511–521.
- LYONS, E.A., COGGRAVE, M. and BROWN, R.E. (1980). "Abstract: Follow-up study in children exposed to ultrasound *in utero*-analysis of height and weight and weight in the first six years of life," page 49 in *Proceedings of the 25th Annual Meeting of AIUM* (American Institute of Ultrasound in Medicine, Laurel, Maryland).
- LYONS, E.A., DYKE, C., TOMS, M. and CHEANG, M. (1988). "*In utero* exposure to diagnostic ultrasound: A 6-year follow-up," *Radiology* **166**, 687–690.
- MACAULAY, J.H., BOND, K. and STEER, P.J. (1992a). "Epidural analgesia in labor and fetal hyperthermia," *Obstet. Gynecol.* **80**, 665–669.
- MACAULAY, J.H., RANDALL, N.R., BOND, K. and STEER, P.J. (1992b). "Continuous monitoring of fetal temperature by noninvasive probe and its relationship to maternal temperature, fetal heart rate, and cord arterial oxygen and pH," *Obstet. Gynecol.* **79**, 469–474.
- MACINTOSH, I.J.C. and DAVEY, D.A. (1970). "Chromosome aberrations induced by an ultrasonic fetal pulse detector," *BMJ* **4**, 92–93.
- MACKOWIAK, P.A., WASSERMAN, S.S. and LEVINE, M.M. (1992). "A critical appraisal of 98.6 °F, the upper limit of the normal body temperature, and other legacies of Carl Reinhold August Wunderlich," *JAMA* **268**, 1578–1580.
- MACMAHON, B. and PUGH, T.F. (1970). *Epidemiology: Principles and Methods* (Little, Brown and Company, Boston).
- MACROBBIE, A.G., RAEMAN, C.H., CHILD, S.Z. and DALECKI, D. (1997). "Thresholds for premature contractions in murine hearts exposed to pulsed ultrasound," *Ultrasound Med. Biol.* **23**, 761–765.
- MADSEN, E.L., ZAGZEBSKI, J.A. and FRANK, G.R. (1982). "Oil-in-gelatin dispersions for use as ultrasonically tissue-mimicking materials," *Ultrasound Med. Biol.* **8**, 277–287.
- MAGEE, T.R. and DAVIES, A.H. (1993). "Auditory phenomena during transcranial Doppler insonation of the basilar artery," *J. Ultrasound Med.* **12**, 747–750.
- MAKINO, K., MOSSOBA, M.M. and RIESZ, P. (1983). "Chemical effects of ultrasound on aqueous solutions. Formation of hydroxyl radicals and hydrogen atoms," *J. Phys. Chem.* **87**, 1369–1377.
- MANN, T.P. (1968). "Observations on temperatures of mothers and babies in the perinatal period," *J. Obstet. Gynaecol. Br. Commonw.* **75**, 316–321.
- MARSH, J.A., HALL, C.S., HUGHES, M.S., MOBLEY, J., MILLER, J.G. and BRANDENBURGER, G.H. (1997). "Broadband through-transmission

- signal loss measurements of Alburnex suspensions at concentrations approaching *in vivo* doses," *J. Acoust. Soc. Am.* **101**, 1155–1161.
- MARSH, J.N., HUGHES, M.S., BRANDENBURGER, G.H. and MILLER, J.G. (1999). "Broadband measurement of the scattering-to-attenuation ratio for Alburnex at 37 °C," *Ultrasound Med. Biol.* **25**, 1321–1324.
- MARTIN, C.J., PRATT, B.M. and WATMOUGH, D.J. (1983). "Observations of ultrasound-induced effects in the fish *Xiphophorus maculatus*," *Ultrasound Med. Biol.* **9**, 177–183.
- MARTINS, B.I., RAJU, M.R., HAYES, T.L. and TOBIAS, C.A. (1977). "Survival of cultured mammalian cells exposed to ultrasound," *Radiat. Environ. Biophys.* **14**, 243–250.
- MASAOKA, H., AKAMATSU, N., NUMOTO, A., FUJITA, T., KAWAHARA, Y., FUKUMOTO, S., KAWAI, J. and SEKIBA, K. (1987). "Ultrasonic attenuation coefficient of uterine myomas," pages 309 to 310 in *Euroson '87: Proceedings of the Sixth Congress of the European Federation of Societies for Ultrasound in Medicine and Biology* (Finnish Society Ultrasound in Medicine and Biology, Helsinki).
- MASATOSHI, M. and HASEGAWA, H. (1988). "Operative ultrasound during liver surgery," pages 51 to 91 in *Operative Ultrasonography*, Sigel, B., Ed. (Raven Press, New York).
- MASON, T.J. and LORIMER, J.P. (1988). *Sonochemistry: Theory, Applications and Uses of Ultrasound in Chemistry* (John Wiley & Sons, New York).
- MASON, G.C., LILFORD, R.J., PORTER, J., NELSON, E. and TYRELL, S. (1993). "Randomized comparison of routine versus highly selective use of Doppler ultrasound in low risk pregnancies," *Br. J. Obstet. Gynaecol.* **100**, 130–133.
- MATTREY, R.F. and PELURA, T.J. (1997). "Perfluorocarbon-based ultrasound contrast agents," pages 83 to 99 in *Ultrasound Contrast Agents*, Goldberg, B.B., Ed. (Martin Duntiz Ltd., London).
- MATTREY, R.F., LEOPOLD, G.R., VAN SONNENBERG, E., GOSINK, B.B., SCHEIBLE, F.W. and LONG, D.M. (1983). "Perfluorochemicals as liver- and spleen-seeking ultrasound contrast agents," *J. Ultrasound Med.* **2**, 173–176.
- MAYER, R., SCHENK, E., CHILD, S., NORTON, S., COX, C., HARTMAN, C., COX, C. and CARSTENSEN, E. (1990). "Pressure threshold for shock wave induced renal hemorrhage," *J. Urol.* **144**, 1505–1509.
- MCCLAIN, R.M., HOAR, R.M. and SALTZMAN, M.B. (1972). "Teratologic study of rats exposed to ultrasound," *Am. J. Obstet. Gynecol.* **114**, 39–42.
- MCINTIRE, L.G. and RAJAGOPALAN, S. (1993). "Fluid stress effects on suspended cells," pages 275 to 290 in *Physical Forces and the Mammalian Cell*, Frangos, J.A., Ed. (Academic Press, New York).
- MCKEE, J.R., CHRISTMAN, C.L., O'BRIEN, W.D. and WANG, S.Y. (1977). "Effects of ultrasound on nucleic acid bases," *Biochemistry* **16**, 4651–4654.
- MCKELVIE, M.L. and PALMER, S.B. (1987). "The interaction of ultrasound with cancellous bone," page 1 in *Ultrasonic Studies of Bone*, Palmer, S.B. and Langton, C.M., Eds. (Institute of Physics Publishing, Bristol, United Kingdom).

- MCLEAN, J.R. and MORTIMER, A.J. (1988). "A cavitation and free radical dosimeter for ultrasound," *Ultrasound Med. Biol.* **14**, 59-64.
- MCPARLAND, P. and PEARCE, J.M. (1988). "Doppler blood flow in pregnancy," *Placenta* **9**, 427-450.
- MEAD, E.L., SUTHERLAND, R.G. and VERRALL, R.E. (1975). "The effect of ultrasound on water in the presence of dissolved gases," *Can. J. Chem.* **53**, 2394.
- MELLETTTE, H.C., HUTT, B.K., ASKOVITZ, S.I. and HOVARTH, S.M. (1951). "Diurnal variations in body temperatures," *J. Appl. Physiol.* **3**, 665-675.
- MELLO FIKHO, A.C. and MENGHINI, R. (1984). "In vivo formation of single-strand breaks in DNA by hydrogen peroxide is mediated by the Haber-Weiss reaction," *Biochem. Biophys. Acta.* **781**, 56-63.
- MELTZER, R.S., TICKNER, E.G., SAHINES, T.P. and POPP, R.L. (1980). "The source of ultrasound contrast effect," *J. Clin. Ultrasound* **8**, 121-127.
- MELTZER, R.S., ADSUMELLI, R., RISHER, W.H., HICKS, G.L., JR., STERN, D.H., SHAH, P.M., WOJTCZAK, J.A., LUSTIK, S.J., GAYESKI, T.E., SHAPIRO, J.R. and CARSTENSEN, E.L. (1998). "Lack of lung hemorrhage in humans after intraoperative transesophageal echocardiography with ultrasound exposure conditions similar to those causing lung hemorrhage in laboratory animals," *J. Am. Soc. Echocardiogr.* **11**, 57-60.
- MEYER, E., BRENDER, K. and TAMM, K. (1958). "Pulsation oscillation of cavities in rubber," *J. Acoust. Soc. Am.* **30**, 1116-1124.
- MEYER, C.R., HERRON, D.S., CARSON, P.L., BANJAVIC, R.A., THIEME, G.A., BOOKSTEIN, F.L. and JOHNSON, M.L. (1984). "Estimation of ultrasonic attenuation and mean backscatterer size *via* digital signal processing," *Ultrason. Imaging* **6**, 13-23.
- MICHAELSON, S.M. (1982). "Physiologic regulation in electromagnetic fields," *Bioelectromagnetics* **3**, 91-103.
- MIHRAN, R.T., BARNES, F.S. and WACHTEL, H. (1990). "Temporally-specific modification of myelinated axon excitability *in vitro* following a single ultrasound pulse," *Ultrasound Med. Biol.* **16**, 297-309.
- MIHRAN, R.T., LINEAWEAVER, S.K., BARNES, F.S. and WACHTEL, H. (1996). "Effects of pulsed acoustic and mechanical stimuli on the excitability of isolated neuronal and cardiac cells," *Appl. Occup. Environ. Hyg.* **11**, 271-274.
- MILLER, D.L. (1977a). "Stable arrays of resonant bubbles in a 1 MHz standing wave acoustic field," *J. Acoust. Soc. Am.* **62**, 12-19.
- MILLER, D.L. (1977b). "The effects of ultrasonic activation of gas bodies in *Elodea* leaves during continuous and pulsed irradiation at 1 MHz," *Ultrasound Med. Biol.* **3**, 221-240.
- MILLER, D.L. (1979a). "Cell death thresholds in *Elodea* for 0.45-10 MHz ultrasound compared to gas-body resonance theory," *Ultrasound Med. Biol.* **5**, 351-357.
- MILLER, D.L. (1979b). "A cylindrical bubble model for the response of plant-tissue gas-bodies to ultrasound," *J. Acoust. Soc. Am.* **65**, 1313-1321.
- MILLER, D.L. (1980). "Acoustical interaction of spherical and cylindrical bubbles on plane sheets and ribbons," *Ultrasonics* **18**, 277-282.

- MILLER, D.L. (1981). "Ultrasonic detection of resonant cavitation bubbles in a flow tube by the second-harmonic emissions," *Ultrasonics* **19**, 217–224.
- MILLER, D.L. (1982). "Experimental investigation of the response of gas-filled micropores to ultrasound," *J. Acoust. Soc. Am.* **71**, 471–476.
- MILLER, D.L. (1983a). "The botanical effects of ultrasound: A review," *Environ. Exp. Botany* **23**, 1–27.
- MILLER, D.L. (1983b). "Further examination of the effects of ultrasonic activation of gas bodies in *Elodea* leaves," *Environ. Exp. Bot.* **23**, 393–405.
- MILLER, D.L. (1984). "Acoustic cavitation series: Part 6. Gas body activation," *Ultrasonics* **22**, 261–269.
- MILLER, D.L. (1985a). "Microstreaming shear as a mechanism of cell death in *Elodea* leaves exposed to ultrasound," *Ultrasound Med. Biol.* **11**, 285–292.
- MILLER, M.W. (1985b). "Does ultrasound induce sister chromatid exchanges?" *Ultrasound Med. Biol.* **11**, 561–570.
- MILLER, D.L. (1986). "Effects of high-amplitude 1-MHz standing ultrasonic field on the algae hydrodictyon," *IEEE Trans. UFFC* **33**, 165–170.
- MILLER, D.L. (1987). "A review of the ultrasonic bioeffects of microsonation, gas-body activation, and related cavitation-like phenomena," *Ultrasound Med. Biol.* **13**, 443–470.
- MILLER, D.L. (1988a). "The influence of hematocrit on hemolysis by ultrasonically activated gas-filled micropores," *Ultrasound Med. Biol.* **14**, 293–297.
- MILLER, D.L. (1988b). "Particle gathering and microstreaming near ultrasonically activated gas-filled micropores," *J. Acoust. Soc. Am.* **84**, 1378–1387.
- MILLER, D.L. (1998). "Frequency relationships for ultrasonic activation of free microbubbles, encapsulated microbubbles, and gas-filled micropores," *J. Acoust. Soc. Am.* **104**, 2498–2505.
- MILLER, D.L. (2000). "The safety of ultrasound contrast agents," pages 72 to 85 in *The Safety of Ultrasound in Medical Diagnostic*, ter Haar, G. and Duck, F.A., Eds. (British Medical Ultrasound Society/The British Institute of Radiology, London).
- MILLER, D.L. and BAO, S. (1998). "The relationship of scattered subharmonic, 3.3 MHz fundamental and second harmonic signals to damage of monolayer cells by ultrasonically activated Alunex," *J. Acoust. Soc. Am.* **103**, 1183–1189.
- MILLER, M.W. and BRAYMAN, A.A. (1997). "Comparative sensitivity of human erythrocytes and lymphocytes to sonolysis by 1-MHz ultrasound," *Ultrasound Med. Biol.* **23**, 635–638.
- MILLER, D.L. and GIES, R.A. (1998a). "Enhancement of ultrasonically-induced hemolysis by perfluorocarbon-based compared to air-based echo-contrast agents," *Ultrasound Med. Biol.* **24**, 285–292.
- MILLER, D.L. and GIES, R.A. (1998b). "Gas-body-based contrast agent enhances vascular bioeffects of 1.09 MHz ultrasound on mouse intestine," *Ultrasound Med. Biol.* **24**, 1201–1208.
- MILLER, D.L. and GIES, R.A. (1999). "Consequences of lithotripter shock-wave interaction with gas body contrast agent in mouse intestine," *J. Urol.* **162**, 606–609.

- MILLER, D.L. and GIES, R.A. (2000). "The influence of ultrasound frequency and gas-body composition on the contrast agent-mediated enhancement of vascular bioeffects in mouse intestine," *Ultrasound Med. Biol.* **26**, 307–313.
- MILLER, D.L. and LAMORE, B.J. (1987). "Ultrasonically activated gas-filled micropores release hemoglobin and antigens from human erythrocytes *in vitro*," *J. Ultrasound Med.* **6**, 231–236.
- MILLER, D.L. and NEPPIRAS, E.A. (1985). "On the oscillation mode of gas-filled micropores," *J. Acoust. Soc. Am.* **77**, 946–953.
- MILLER, D.L. and NYBORG, W.L. (1983). "Theoretical investigation of the response of gas-filled micropores and cavitation nuclei to ultrasound," *J. Acoust. Soc. Am.* **73**, 1537–1544.
- MILLER, D.L. and QUDDUS, J. (2000a). "Sonoporation of monolayer cells by diagnostic ultrasound activation of contrast-agent gas bodies," *Ultrasound Med. Biol.* **26**, 661–667.
- MILLER, D.L. and QUDDUS, J. (2000b). "Diagnostic ultrasound activation of contrast agent gas bodies induces capillary rupture in mice," *Proc. Natl. Acad. Sci. USA* **97**, 10178–10184.
- MILLER, D.L. and THOMAS, R.M. (1990). "The influence of variations in biophysical conditions on hemolysis near ultrasonically activated gas-filled micropores," *J. Acoust. Soc. Am.* **87**, 2225–2230.
- MILLER, D.L. and THOMAS, R.M. (1993a). "Frequency dependence of cavitation activity in a rotating tube exposure system compared to the mechanical index," *J. Acoust. Soc. Am.* **93**, 3475–3480.
- MILLER, D.L. and THOMAS, R.M. (1993b). "A comparison of hemolytic and sonochemical activity of ultrasonic cavitation in a rotating tube," *Ultrasound Med. Biol.* **19**, 83–90.
- MILLER, D.L. and THOMAS, R.M. (1993c). "Ultrasonic gas body activation in *Elodea* leaves and the mechanical index," *Ultrasound Med. Biol.* **19**, 343–351.
- MILLER, D.L. and THOMAS, R.M. (1994a). "Cavitation dosimetry: Estimates for single bubbles in a rotating-tube exposure system," *Ultrasound Med. Biol.* **20**, 187–193.
- MILLER, D.L. and THOMAS, R.M. (1994b). "Heating as a mechanism for ultrasonically-induced petechial hemorrhages in mouse intestine," *Ultrasound Med. Biol.* **20**, 493–503.
- MILLER, D.L. and THOMAS, R.M. (1995a). "Ultrasound contrast agents nucleate inertial cavitation *in vitro*," *Ultrasound Med. Biol.* **21**, 1059–1065.
- MILLER, D.L. and THOMAS, R.M. (1995b). "Thresholds for hemorrhages in mouse skin and intestine induced by lithotripter shock waves," *Ultrasound Med. Biol.* **21**, 249–257.
- MILLER, D.L. and THOMAS, R.M. (1996a). "Contrast-agent gas bodies enhance hemolysis induced by lithotripter shock waves and high-intensity focused ultrasound in whole blood," *Ultrasound Med. Biol.* **22**, 1089–1095.
- MILLER, D.L. and THOMAS, R.M. (1996b). "The role of cavitation in the induction of cellular DNA damage by ultrasound and lithotripter shock waves *in vitro*," *Ultrasound Med. Biol.* **22**, 681–687.

- MILLER, D.L. and WILLIAMS, A.R. (1983). "Further investigations of ATP release from human erythrocytes exposed to ultrasonically activated gas-filled pores," *Ultrasound Med. Biol.* **9**, 297-307.
- MILLER, D.L. and WILLIAMS, A.R. (1989). "Bubble cycling as an explanation of the promotion of ultrasonic cavitation in a rotating tube exposure system," *Ultrasound Med. Biol.* **15**, 641-648.
- MILLER, D.L. and WILLIAMS, A.R. (1992). "Nucleation and evolution of ultrasonic cavitation in a rotating exposure chamber," *J. Ultrasound Med.* **11**, 407-412.
- MILLER, M.W. and ZISKIN, M.C. (1989). "Biological consequences of hyperthermia," *Ultrasound Med. Biol.* **15**, 707-722.
- MILLER, D.L., NYBORG, W.L. and WHITCOMB, C.C. (1978). "*In vitro* clumping of platelets exposed to low intensity ultrasound," *Ultrasound Med.* **4**, 545-553.
- MILLER, D.L., NYBORG, W.L. and WHITCOMB, C.C. (1979). "Platelet aggregation induced by ultrasound under specialized conditions *in vitro*," *Science* **205**, 505-507.
- MILLER, D.L., WILLIAMS, A.R. and GROSS, D.R. (1984). "Characterization of cavitation in a flow-through exposure chamber by means of a resonant bubble detector," *Ultrasonics* **22**, 224-230.
- MILLER, D.L., REESE, J.A. and FRAZIER, M.E. (1989a). "Single strand DNA breaks in human leukocytes induced by ultrasound *in vitro*," *Ultrasound Med. Biol.* **15**, 765-771.
- MILLER, M.W., CHURCH C.C., BRAYMAN, A.A., MALCUIT, M.S. and BOYD, R.W. (1989b). "An explanation for the decrease in cell lysis in a rotating tube with increasing ultrasound intensity," *Ultrasound Med. Biol.* **15**, 67-72.
- MILLER, M.W., AZADNIV, M., PETTIT, S.E., CHURCH, C.C., CARSTENSEN, E.L. and HOFFMAN, D. (1989c). "Sister chromatid exchanges in Chinese hamster ovary cells exposed to high intensity pulsed ultrasound: Inability to confirm previous positive results," *Ultrasound Med. Biol.* **15**, 255-262.
- MILLER, M.W., CHURCH, C.C. and CIARAVINO, V. (1990). "Time lapse and microscopic examinations of insonated *in vitro* cells," *Ultrasound Med. Biol.* **16**, 73-79.
- MILLER, D.L., THOMAS, R.M. and WILLIAMS, A.R. (1991a). "Mechanisms for hemolysis by ultrasonic cavitation in the rotating exposure system," *Ultrasound Med. Biol.* **17**, 171-178.
- MILLER, D.L., THOMAS, R.M. and FRAZIER, M.E. (1991b). "Single strand breaks in CHO cell DNA induced by ultrasonic cavitation *in vitro*," *Ultrasound Med. Biol.* **17**, 401-406.
- MILLER, D.L., THOMAS, R.M. and FRAZIER, M.E. (1991c). "Ultrasonic cavitation indirectly induces single strand breaks in DNA of viable cells *in vitro* by the action of residual hydrogen peroxide," *Ultrasound Med. Biol.* **17**, 729-735.
- MILLER, M.W., AZADNIV, M., COX, C. and MILLER, W.M. (1991d). "Lack of induced increase in sister chromatid exchanges in human lymphocytes

- exposed to *in vivo* therapeutic ultrasound," *Ultrasound Med. Biol.* **17**, 81–83.
- MILLER, M.W., AZADNIV, M., DOIDA, Y. and BRAYMAN, A.A. (1995a). "Effect of a stabilized microbubble contrast agent on CW ultrasound induced red blood lysis *in vitro*," *Echocardiography* **12**, 1–11.
- MILLER, D.L., THOMAS, R.M. and BUSCHBOM, R.L. (1995b). "Comet assay reveals DNA strand breaks induced by ultrasonic cavitation *in vitro*," *Ultrasound Med. Biol.* **21**, 841–848.
- MILLER, D.L., THOMAS, R.M. and THRALL, B.D. (1996). "The role of ultraviolet light in the induction of cellular DNA damage by a spark-gap lithotripter *in vitro*," *J. Urol.* **156**, 286–290.
- MILLER, D.L., GIES, R.A. and CHRISLER, W.B. (1997). "Ultrasonically induced hemolysis at high cell and gas body concentrations in a thin-disc exposure chamber," *Ultrasound Med. Biol.* **23**, 625–633.
- MILLER, D.L., BAO, S. and MORRIS, J.E. (1999). "Sonoporation of cultured cells in the rotating tube exposure system," *Ultrasound Med. Biol.* **25**, 143–149.
- MILUNSKY, A., ULCICKAS, M., ROTHMAN, K.J., WILLETT, W., JICK, S.S. and JICK, H. (1992). "Maternal heat exposure and neural tube defects," *JAMA* **268**, 882–885.
- MOORE, J.A. (1968). "Vibratory stimulation of the skin by electrostatic field: Effects of size of electrode and site of stimulation on thresholds," *Am. J. Psychol.* **81**, 235–240.
- MOORE, R.M., JR., BARRICK, M.K. and HAMILTON, T.M. (1982). "Effect of sonic radiation on growth and development," *Am. J. Epidemiol.* **116**, 571.
- MOORE, R.M., JR., JENG, L.L., KACZMAREK, R.G. and PLACEK, P.J. (1990). "Use of diagnostic ultrasound, x-ray examinations, and electronic fetal monitoring in perinatal medicine," *J. Perinatol.* **10**, 361–365.
- MORISHIMA, H.O., GLASER, B., NIEMANN, W.H. and JAMES, L.S. (1975). "Increased uterine activity and fetal deterioration during maternal hyperthermia," *Am. J. Obstet. Gynecol.* **121**, 531–538.
- MORISHIMA, H.O., YEH, M.N., NIEMANN, W.H. and JAMES, L.S. (1977). "Temperature gradient between fetus and mother as an index for assessing intrauterine fetal condition," *Am. J. Obstet. Gynecol.* **129**, 443–448.
- MORNSTEIN, V. (1997). "Cavitation-induced risks associated with contrast agents used in ultrasonography," *Eur. J. Ultrasound* **5**, 101–111.
- MORRIS, J.V. and COAKLEY, W.T. (1980). "The non-thermal inhibition of growth and the detection of acoustic emissions from bean roots exposed to 1 MHz ultrasound," *Ultrasound Med. Biol.* **6**, 113–126.
- MORTIMER, A.J. and DYSON, M. (1988). "The effect of therapeutic ultrasound on calcium uptake in fibroblasts," *Ultrasound Med. Biol.* **14**, 499–506.
- MORTIMER, A.J. and TROLLOPE, B.J. (1987). "Altered myocardial contractility with pulsed ultrasound," *Ultrasound Med. Biol.* **13**, L567–L569.
- MORTIMER, A.J., ROY, O.Z., TAICHMAN, G.C., KEON, W.J. and TROLLOPE, B.J. (1978). "The effects of ultrasound on the mechanical properties of rat cardiac muscle," *Ultrasonics* **16**, 179–182.

- MORTIMER, A.J., FORESTER, G.V., TROLLOPE, B.J., VILLENEUVE, E.J. and ROY, O.Z. (1986). "Improved performance of the paced cat heart *in situ* with therapeutic ultrasound," *IEEE Trans. UFFC* **33**, 210–217.
- MORTON, K.I., TER HAAR, G.R., STRATFORD, I.J. and HILL, C.R. (1982). "The role of cavitation in the interaction of ultrasound with V79 Chinese hamster cells *in vitro*," *Br. J. Cancer (Suppl.)* **45**, 147–150.
- MULLER, J. (1851). "Ueber die temperature des kindes in mutterleibe," *Arch. Anat., Physiol. Wissenschaftliche Med.* **2**, 135–137.
- MULVAGH, S.L., FOLEY, D.A., AESCHBACHER, B.C., KLARICH, K.K. and SEWARD, J.B. (1996). "Second harmonic imaging of an intravenously administered echocardiographic contrast agent: Visualization of coronary arteries and measurement of coronary blood flow," *J. Am. Coll. Cardiol.* **27**, 1519–1525.
- MUSCARELLA, L.F., VASTHARE, U., TUMA, R.F., ABRAHAM, V. and ZISKIN, M.C. (1991). "Effect of ultrasound on regional cerebral blood flow in neonatal rats," *Ultrasound Med. Biol.* **17**, 893–899.
- NANDA, N.C., SCHLIEF, R. and GOLDBERG, B.B. (1997). *Advances in Echo Imaging Using Contrast Enhancement*, 2nd ed. (Kluwer Academic Publishers, New York).
- NAUMBURG, E., BELLOCCO, R., CNATTINGIUS, S., HALL, P. and EKBOM, A. (2000). "Prenatal ultrasound examinations and risk of childhood leukaemia: Case-control study," *BMJ* **320**, 282–283.
- NCRP (1977). National Council on Radiation Protection and Measurements. *Medical Radiation Exposure of Pregnant and Potentially Pregnant Women*, NCRP Report No. 54 (National Council on Radiation Protection and Measurements, Bethesda, Maryland).
- NCRP (1983). National Council on Radiation Protection and Measurements. *Biological Effects of Ultrasound: Mechanisms and Clinical Applications*, NCRP Report No. 74 (National Council on Radiation Protection and Measurements, Bethesda, Maryland).
- NCRP (1992). National Council on Radiation Protection and Measurements. *Exposure Criteria for Medical Diagnostic Ultrasound. I. Criteria Based on Thermal Mechanisms*, NCRP Report No. 113 (National Council on Radiation Protection and Measurements, Bethesda, Maryland).
- NEILSON, J.P. (1991). "Doppler ultrasound study of umbilical artery waveforms in high risk pregnancies," record 3889 in Oxford data base or perinatal trials [computer file], Chalmer, I., Ed. (Version 2.1, disk issue 6).
- NEMA (1992). National Electrical Manufacturers Association. *Acoustic Output Measurement Standard for Diagnostic Ultrasound Equipment*, NEMA UD-2-1992 (National Electrical Manufacturers Association, Washington).
- NEPPIRAS, E.A. and COAKLEY, W.T. (1976). "Acoustic cavitation in a focused field in water at 1 MHz," *J. Sound Vib.* **45**, 341–373.
- NEPPIRAS, E.A. and FILL, E.E. (1969). "A cyclic cavitation process," *J. Acoust. Soc. Am.* **46**, 1264–1271.
- NEPPIRAS, E.A., NYBORG, W.L. and MILLER, D.L. (1983). "Nonlinear behavior and stability of trapped micron-sized cylindrical gas bubbles in an ultrasound field," *Ultrasonics* **21**, 109–115.

- NESHEIM, B., BENSEN, I. and BRAKKEN, A. (1987). "Ultrasound in pregnancy: Consensus statement," *Int. J. Technol. Assess. Health Care* **3**, 463-470.
- NEWHOUSE, V.L., Ed. (1988). *Progress in Medical Imaging* (Springer-Verlag, New York).
- NEWHOUSE, V. and SHANKAR, P.M. (1984). "Bubble size measurements using the nonlinear mixing of two frequencies," *J. Acoust. Soc. Am.* **75**, 1473-1477.
- NEWNHAM, J.P., EVANS, S.F., MICHAEL, C.A., STANLEY, F.J. and LANDAU, L.I. (1993). "Effects of frequent ultrasound during pregnancy: A randomized controlled trial," *Lancet* **342**, 887-891.
- NICHOLAS, D. (1982). "Evaluation of backscattering coefficients for excised human tissues: Results, interpretation and associated measurements," *Ultrasound Med. Biol.* **8**, 17-28.
- NIGHTINGALE, K.R., KORNGUTH, P.J., WALKER, W.F., MCDERMOTT, B.A. and TRAHEY, G.E. (1995). "A novel ultrasonic technique for differentiating cysts from solid lesions: Preliminary results in the breast," *Ultrasound Med. Biol.* **21**, 745-751.
- NISHI, R.Y. (1972). "Ultrasonic detection of bubbles with Doppler flow transducers," *Ultrasonics* **10**, 173-179.
- NOCK, L. and TRAHEY, G.E. (1989). "Phase aberration correction in medical ultrasound using speckle brightness as a quality factor," *J. Acoust. Soc. Am.* **85**, 1819-1833.
- NYBORG, W.L. (1953). "Acoustic streaming due to attenuated plane waves," *J. Acoust. Soc. Am.* **25**, 68-75.
- NYBORG, W.L. (1965). "Acoustic streaming," pages 265 to 331 in *Physical Acoustics*, Mason, W.P., Ed. (Academic Press, New York).
- NYBORG, W.L. (1977). *Physical Mechanisms for Biological Effects of Ultrasound*, U.S. Department of Health, Education and Welfare Publication (FDA) 78-8062 (Food and Drug Administration, Rockville, Maryland).
- NYBORG, W.L. (1978). "Physical principles of ultrasound," pages 1 to 75 in *Ultrasound: Its Applications in Medicine and Biology, Part I*, Fry, F.J., Ed. (Elsevier Publishing Co., New York).
- NYBORG, W.L. (1986). "Sonically produced heat in a fluid with bulk viscosity and shear viscosity," *J. Acoust. Soc. Am.* **80**, 1133-1139.
- NYBORG, W.L. (1988). "Solutions of the bio-heat transfer equation," *Phys. Med. Biol.* **33**, 785-792.
- NYBORG, W.L. (1989). "Theoretical criterion for acoustic aggregation," *Ultrasound Med. Biol.* **15**, 93-99.
- NYBORG, W.L. (1991). "Biological effects of sound and ultrasound," pages 403 to 420 in *Encyclopedia of Applied Physics* (VCH Publishers, Inc., New York).
- NYBORG, W.L. (1992). "Scientifically based safety criteria for ultrasonography," *J. Ultrasound Med.* **11**, 425-432.
- NYBORG, W.L. (1996). "Human exposure to ultrasound," *Appl. Occup. Environ. Hyg.* **11**, 251-254.
- NYBORG, W.L. and HUGHES, D.E. (1967). "Bubble annihilation in cavitation streamers," *J. Acoust. Soc. Am.* **42**, 891-894.

- NYBORG, W.L. and MILLER, D.L. (1982a). "Biophysical implications of bubble dynamics," pages 17 to 24 in *The Mechanics and Physics of Bubbles in Liquids*, van Wijngaarden, L., Ed. (Kluwer, New York).
- NYBORG, W.L. and MILLER, D.L. (1982b). "Biophysical implications of bubble dynamics," *Appl. Sci. Res.* **38**, 17–24.
- NYBORG, W.L. and STEELE, R.B. (1983). "Temperature elevation in a beam of ultrasound," *Ultrasound Med. Biol.* **9**, 611–620.
- NYBORG, W.L. and WU, J. (1993). "Relevant field parameters with rationale," pages 85 to 112 in *Ultrasonic Exposimetry*, Ziskin, M.C. and Lewin, P.A., Eds. (CRC Press, Boca Raton, Florida).
- NYBORG, W.L. and WU, J. (1994). "Solution of the linear bio-heat transfer equation," *Phys. Med. Biol.* **39**, 924–925.
- NYBORG, W.L., MILLER, D.L. and GERSHOY, A. (1975). "Physical consequences of ultrasound in plant tissues and other bio-systems," pages 277 to 299 in *Fundamental and Applied Aspects of Nonionizing Radiation*, Michaelson, S.M. and Miller, M.W., Eds. (Plenum Press, New York).
- NYBORG, W.L., GERSHOY, A. and MILLER, D.L. (1977). "Interaction ultrasound with simple biological systems," pages 19 to 27 in *Ultrasonics International 1977 Conference Proceedings* (IPC Science and Technology Press, Guildford, Surrey, United Kingdom).
- O'BRIEN, W.D., JR., FRIZZELL, L.A., WEIGEL, R.M. and ZACHARY, J.F. (2000). "Ultrasound-induced lung hemorrhage is not caused by inertial cavitation," *J. Acoust. Soc. Am.* **108**, 1290–1297.
- O'CONNOR, M.E. (1980). "Mammalian teratogenesis and radio-frequency fields," *IEEE* **68**, 56–60.
- O'DONNELL, M. (1990). "Efficient parallel receive beam forming for phased array imaging using phase rotation," pages 95 to 98 in *IEEE Ultrasonics Symposium Proceedings* (Institute of Electronics and Electrical Engineers, Piscataway, New Jersey).
- O'DONNELL, M. and FLAX, S.W. (1988). "Phase aberration correction using signals from point reflectors and diffuse scatterers: Measurement," *IEEE Trans. UFFC* **35**, 768–774.
- OLSSON, S.B., JOHANSSON, B., NILSSON, A.M., OLSSON, C. and ROIJER, A. (1994). "Enhancement of thrombolysis by ultrasound," *Ultrasound Med. Biol.* **20**, 375–382.
- OMTZIGT, A.W. (1990). *Clinical Value of Umbilical Doppler Velocimetry: A Randomized Controlled Trial*, thesis (University of Utrecht, Utrecht, The Netherlands).
- O'NEILL, T.P., WINKLER, A.J. and WU, J. (1994). "Ultrasound heating in a tissue-bone phantom," *Ultrasound Med. Biol.* **20**, 579–588.
- OPHIR, J. and MEHTA, D. (1988). "Elimination of diffraction error in acoustic attenuation estimation *via* axial beam translation," *Ultrason. Imaging* **10**, 139–152.
- OPHIR, J. and PARKER, K.J. (1989). "Contrast agents in diagnostic ultrasound," *Ultrasound Med. Biol.* **15**, 319–333.
- PAELINCK, B.P. and KASPRZAK, J.D. (1999). "Contrast-enhanced echocardiography: Review and current role," *Acta Cardiol.* **54**, 195–201.

- PARKER, K.J. (1983). "Ultrasound attenuation and absorption in liver tissue," *Ultrasound Med. Biol.* **9**, 363–369.
- PARKER, K.J., TUTHILL, T.A., LERNER, R.M. and VIOLANTE, M.R. (1987). "A particulate contrast agent with potential for ultrasound imaging of liver," *Ultrasound Med. Biol.* **13**, 555–566.
- PATTON, C.A., HARRIS, G.R. and PHILLIPS, R.A. (1994). "Output levels and bioeffects indices from diagnostic ultrasound exposure data reported to the FDA," *IEEE Trans. UFFC* **41**, 353–359.
- PAY, T.L. and BARRICK, M.K. (1987). "The effect of pulsed ultrasound on the survival of *Drosophila*," *Ultrasound Med. Biol.* **13**, 93–95.
- PEDERSEN, P.C. and OZCAN, H.S. (1986). "Ultrasound properties of lung tissue and their measurements," *Ultrasound Med. Biol.* **12**, 483–499.
- PENNEY, D.P., SCHENK, E.A., MALTBY, K., HARTMAN-RAEMAN, C., CHILD, S.Z. and CARSTENSEN, E.L. (1993). "Morphological effects of pulsed ultrasound in the lung," *Ultrasound Med. Biol.* **19**, 127–135.
- PENNYCUIK, P.R. (1965). "The effects of acute exposure to high temperatures on prenatal development in the mouse with particular reference to secondary vibrissae," *Aust. J. Biol. Sci.* **18**, 97–113.
- PFIRSCH, F. (1958). "Role des meats gazeux dans l'action des ultrasons sur les cellules foliaires d' *Elodea* et de *Minium*," *C.R. Acad. Sci. Paris* **247**, 349–351.
- PHILLIP, A., DELIUS, M., SCHEFFCZYK, C., VOGEL, A. and LAUTERBORN, W. (1993). "Interaction of lithotripter-generated shock waves with air bubbles," *J. Acoust. Soc. Am.* **93**, 2496–2509.
- PIERCY, J.E. and LAMB, J. (1954). "Acoustic streaming in liquids," *Proc. Roy. Soc. A* **226**, 43–50.
- PILLA, A.A., MONT, M.A., NASSER, P.R., KHAN, S.A., FIGUEIREDO, M., KAUFMAN, J.J. and SIFFERT, R.S. (1990). "Non-invasive low-intensity pulsed ultrasound accelerates bone healing in the rabbit," *J. Orthop. Trauma* **4**, 246–253.
- PINAMONTI, S., GALLENGA, P.E. and MAZZEO, V. (1982). "Effect of pulsed ultrasound on human erythrocytes *in vitro*," *Ultrasound Med. Biol.* **8**, 631–638.
- PINAMONTI, S., CARUSO, A., MAZZEO, V., ZEBINI, E. and ROSSI, A. (1986). "DNA damage from pulsed sonication of human leukocytes *in vitro*," *IEEE Trans. UFFC* **33**, 179–185.
- PIZZARELLO, D.J., VIVINO, A., MADDEN, B., WOLSKY, A., KEEGAN, A.F. and BECKER, M. (1978). "Effect of pulsed low-power ultrasound on growing tissues," *Exptl. Cell Biol.* **46**, 179–191.
- PLESSET, M.S. and CHAPMAN, R.B. (1971). "Collapse of an initially spherical vapour cavity in the neighborhood of a solid boundary," *J. Fluid Mech.* **47**, 283–290.
- POHL, E.E., ROSENFELD, E.H., POHL, P. and MILLNER, R. (1995). "Effects of ultrasound on agglutination and aggregation of human erythrocytes *in vitro*," *Ultrasound Med. Biol.* **21**, 711–719.
- POLIACHIK, S.L., CHANDLER, W.L., MOURAD, P.D., BAILEY, M.R., BLOCH, S., CLEVELAND, R.O., KACZKOWSKI, P., KEILMAN, G., PORTER, T. and CRUM, L.A. (1999). "Effect of high-intensity focused

- ultrasound on whole blood with and without microbubble contrast agent," *Ultrasound Med. Biol.* **25**, 991–998.
- PORTER, T.R., XIE, F., KRICSFELD, D. and ARMBRUSTER, R.W. (1996). "Improved myocardial contrast with second harmonic transient ultrasound response imaging in humans using intravenous perfluorocarbon-exposed sonicated dextrose Albumin," *J. Am. Coll. Cardiol.* **27**, 1497–1501.
- PORTER, T.R., HISER, W.L., KRICSFELD, D., DELIGONUL, U., XIE, F., IVERSEN, P. and RADIO, S. (2001). "Inhibition of carotid artery neointimal formation with intravenous microbubbles," *Ultrasound Med. Biol.* **27**, 259–265.
- POSTERT, T., MUHS, A., MEVES, S., FEDERLEIN, J., PRZUNTEK, H. and BUTTNER, T. (1998). "Transient response harmonic imaging: An ultrasound technique related to brain perfusion," *Stroke* **29**, 1901–1907.
- POWELL-PHILLIPS, W.D. and TOWELL, M.E. (1979). "Doppler ultrasound and subjective assessment of fetal activity," *BMJ* **2**, 101–102.
- PRAT, F., CHAPELON, J.Y., CHAUFFERT, B., PONCHON, T. and CATHIGNOL, D. (1991). "Cytotoxic effects of acoustic cavitation on HT-29 cells and a rat peritoneal carcinomatosis *in vitro*," *Cancer Res.* **51**, 3024–3029.
- PRAT, F., CHAPELON, J.Y., EL FADIL, F.A., THEILLERE, Y., PONCHON, T. and CATHIGNOL, D. (1993). "*In vivo* effects of cavitation alone or in combination with chemotherapy in a peritoneal carcinomatosis in the rat," *Br. J. Cancer* **68**, 13–17.
- PRAT, F., SIBILLE, A., LUCCIONI, C., PANSU, D., CHAPELON, J.Y., BEAUMATIN, J., PONCHON, T. and CATHIGNOL, D. (1994). "Increased chemocytotoxicity to colon cancer cells by shock wave-induced cavitation," *Gastroenterology* **106**, 937–944.
- PRESTON, R.C. (1991). *Output Measurements for Medical Ultrasound* (Springer Verlag, New York).
- PRESTON, R.C., SHAW, A. and ZEQRIRI, B. (1991). "Prediction of *in situ* exposure to ultrasound: A proposed standard experimental method," *Ultrasound Med. Biol.* **17**, 333–339.
- PRICE, R.J., SKYBA, D.M., KAUL, S. and SKALAK, T.C. (1998). "Delivery of colloidal particles and red blood cells to tissue through microvessel ruptures created by targeted microbubble destruction with ultrasound," *Circulation* **98**, 1264–1267.
- PRIONAS, S.D., RAFTERY, K.A., EDMONDS, P.D. and CONSTANTINOU, C.E. (1991). "Flow dependence of 2-D temperature distributions induced in the perfused canine kidney by ultrasound," *Int. J. Hyperthermia* **7**, 367–383.
- PRISE, K.M., DAVIES, S. and MICHAEL, B.D. (1989). "Cell killing and DNA damage in Chinese hamster V79 cells treated with hydrogen peroxide," *Int. J. Radiat. Biol.* **55**, 583–592.
- PROHASKA, S.S., RIMER, V.G., TUSE, D., PRYOR, G.T. and EDMONDS, P.D. (1992a). "Conservation of bactericidal activity in ultrasound-exposed murine peritoneal phagocytic cells," *Ultrasound Med. Biol.* **18**, 601–606.
- PROHASKA, S.S., RIMER, V.G., WINTERS, M.A., HUMPHRES, R.C., TUSE, D. and EDMONDS, P.D. (1992b). "Conservation of receptor

- expression and phagocytic activity of murine macrophages exposed to various ultrasonic regimens *in vitro*," *J. Ultrasound Med.* **11**, 93–101.
- PURNELL, E.W., SOKOLLU, A., TORCHIA, R. and TANER, N. (1964a). "Focal chorioretinitis produced by ultrasound," *Invest. Ophthalmol.* **3**, 657–664.
- PURNELL, E.W., SOKOLLU, A. and HOLASEK, E. (1964b). "The production of focal chorioretinitis by ultrasound," *Am. J. Ophthalmol.* **58**, 953–957.
- PUTTERMAN, S.J. (1995). "Sonoluminescence: Sound to light," *Sci. Am.* February, 46–51.
- QUAIN, R.M., WAAG, R.C. and MILLER, M.W. (1991). "The use of frequency mixing to distinguish size distributions of gas-filled micropores," *Ultrasound Med. Biol.* **17**, 71–79.
- RAEMAN, C.H., CHILD, S.Z. and CARSTENSEN, E.L. (1993). "Timing of exposures in ultrasonic hemorrhage of murine lung," *Ultrasound Med. Biol.* **19**, 507–512.
- RAEMAN, C.H., CHILD, S.Z., DALECKI, D., MAYER, R., PARKER, K.J. and CARSTENSEN, E.L. (1994). "Damage to murine kidney and intestine from exposure to the fields of a piezoelectric lithotripter," *Ultrasound Med. Biol.* **20**, 589–594.
- RAEMAN, C.H., CHILD, S.Z., DALECKI, D., COX, C. and CARSTENSEN, E.L. (1996). "Exposure-time dependence of the threshold for ultrasonically induced murine lung hemorrhage," *Ultrasound Med. Biol.* **22**, 139–141.
- RAEMAN, C.H., DALECKI, D., CHILD, S.Z., MELTZER, R.S. and CARSTENSEN, E.L. (1997). "Albunex does not increase the sensitivity of the lung to pulsed ultrasound," *Echocardiography* **14**, 553–558.
- RAJAGOPALAN, B., GREENLEAF, J.F., THOMAS, P.J., JOHNSON, S.A. and BAHN, R.C. (1979). "Variation of acoustic speed with temperature in various excised human tissues studied by ultrasound computerized tomography," pages 227 to 233 in *Ultrasonic Tissue Characterization, II: A Collection of Reviewed Papers Based on Talks Presented at the Second Symposium on Ultrasonic Tissue Characterization*, Linzer, M., Ed., NBS Publication 525 (U.S. Government Printing Office, Washington).
- RAMNARINE, K.V., NASSIRI, D.K., PEARCE, J.M., JOSEPH, A.E.A., PATEL, R.H. and VARMA, T.R. (1993). "Estimation of *in situ* ultrasound exposure during obstetric examinations," *Ultrasound Med. Biol.* **19**, 319–329.
- RAMSEY, E.M. and DONNER, W.M. (1980). "Maternal circulation and fetal circulation," pages 56 to 70 in *Placental Vasculature and Circulation: Anatomy, Physiology, Radiology, Clinical Aspects* (Saunders, Philadelphia).
- RANDALL, N.J., BOND, K., MACAULAY, J. and STEER, P.J. (1991). "Measuring fetal and maternal temperature differentials: A probe for clinical use during labour," *J. Biomed. Eng.* **13**, 481–485.
- RANDAZZO, R.F., CHAUSSY, C.G., FUCHS, G.J., BHUTA, S.M., LOVREKOVICH, H. and DEKERNION, J.B. (1988). "The *in vitro* and *in vivo* effects of extracorporeal shock waves on malignant cells," *Urol. Res.* **16**, 419–426.
- RAYLEIGH, LORD (1917). "On the pressure developed in a liquid during the collapse of a spherical cavity," *Phil. Mag.* **34**, 94–98.

- RICHARDS, W.T. and LOOMIS, A.L. (1927). "The chemical effects of high frequency sound waves. I. A preliminary survey," *J. Am. Chem. Soc.* **49**, 3086–3100.
- RIDGE, B.R. and BUDD, G.M. (1990). "Letter: How long is too long in a spa pool?" *N. Engl. J. Med.* **323**, 835–836.
- RIESZ, P. and KONDO, T. (1992). "Free radical formation induced by ultrasound and its biological implications," *Free Radic. Biol. Med.* **13**, 247–270.
- ROELANDT, J.R.T.C. (1982). "Contrast echocardiography," *Ultrasound Med. Biol.* **8**, 471–492.
- ROONEY, J.A. (1970). "Hemolysis near an ultrasonically pulsating gas bubble," *Science* **169**, 869–871.
- ROONEY, J.A. (1972). "Shear as a mechanism for sonically induced biological effects," *J. Acoust. Soc. Am.* **52**, 1718–1724.
- ROONEY, J.A. (1973). "Hydrodynamic shearing of biological cells," *J. Biol. Phys.* **2**, 26–40.
- ROONEY, J.A. (1981). "Nonlinear phenomena," pages 299 to 353 in *Methods of Experimental Physics*, Edmonds, P.D., Ed. (Academic Press, New York).
- ROSENSCHEIN, U., BERNSTEIN, J.J., DISEGNI, E., KAPLINSKY, E., BERNHEIM, J. and ROZENSAJN, L.A. (1990). "Experimental ultrasonic angioplasty: Disruption of atherosclerotic plaques and thrombi *in vitro* and arterial recanalization *in vivo*," *J. Am. Coll. Cardiol.* **15**, 711–717.
- ROY, R.A., MADANSHETTY, S.I. and APFEL, R.E. (1990). "An acoustic backscattering technique for the detection of transient cavitation produced by microsecond pulses of ultrasound," *J. Acoust. Soc. Am.* **87**, 2451–2458.
- RSCHEVKIN, S.N. (1963). *The Theory of Sound*, English translation, Blunn, O.M. and Doak, P.E., Eds. (Pergamon Press, New York).
- RUDELSTORFER, R., SIMBRUNER, G., SZALAY, S. and JANISCH, H. (1981). "Heatflux from the fetus during delivery," *J. Perinat. Med.* **9**, 311–313.
- RUDELSTORFER, R., SIMBRUNER, G., BERNASCHEK, G., ROGAN, A.M., SZALAY, S. and JANISCH, H. (1983). "Heat flux from the fetal scalp during labor and fetal outcome," *Arch. Gynecol.* **233**, 85–91.
- RUDELSTORFER, R., SIMBRUNER, G., SHARMA, V. and JANISCH, H. (1987). "Scalp heat flux and its relationship to scalp blood pH of the fetus," *Am. J. Obstet. Gynecol.* **157**, 372–377.
- RUDENKO, O.V., SARVAZYAN, A.P. and EMELIANOV, S.Y. (1996). "Acoustic radiation force and streaming induced by focused nonlinear ultrasound in a dissipative medium," *J. Acoust. Soc. Am.* **99**, 2791–2798.
- RYAN, L.K. and FOSTER, F.S. (1997). "Tissue equivalent vessel phantoms for intravascular ultrasound," *Ultrasound Med. Biol.* **23**, 261–273.
- SAAD, A.H. (1983). *Some Biological Effects of Ultrasound*, Ph.D. thesis (University of Manchester, United Kingdom).
- SAAD, A.H. and HAHN, G.M. (1989). "Ultrasound enhanced drug toxicity on Chinese hamster ovary cells *in vitro*," *Cancer Res.* **49**, 5931–5934.
- SAAD, A.H. and WILLIAMS, A.R. (1985). "Possible mechanisms for the agitation-induced enhancement of acoustic cavitation *in vitro*," *J. Acoust. Soc. Am.* **78**, 429–434.

- SAARI-KEMPPAINEN, A., KARJALAINEN, O., YLOSTALO, P. and HEINONEN, O.P. (1990). "Ultrasound screening and perinatal mortality: Controlled trial of systematic one-state screening in pregnancy," *Lancet* **336**, 387–391.
- SACKS, P.G., MILLER, M.W. and CHURCH, C.C. (1982). "The exposure vessel as a factor in ultrasonically-induced mammalian cell lysis—I. A comparison of tube and chamber systems," *Ultrasound Med. Biol.* **8**, 289–298.
- SACKS, P.G., MILLER, M.W. and SUTHERLAND, R.M. (1983). "Response of multicell spheroids to 1-MHz ultrasonic irradiation: Cavitation-related damage," *Radiat. Res.* **93**, 545–559.
- SAFAR, M.H. (1968). "Comment on papers concerning rectified diffusion of cavitation bubbles," *J. Acoust. Soc. Am.* **43**, 1188–1189.
- SALVESEN, K.A. and EIK-NES, S.H. (1995). "Is ultrasound unsound? A review of epidemiological studies of human exposure to ultrasound," *Ultrasound Obstet. Gynecol.* **6**, 293–298.
- SALVESEN, K.A. and EIK-NES, S.H. (1999a). "Ultrasound during pregnancy and subsequent childhood non-right handedness: A meta-analysis," *Ultrasound Obstet. Gynecol.* **13**, 241–246.
- SALVESEN, K.A. and EIK-NES, S.H. (1999b). "Ultrasound during pregnancy and birthweight, childhood malignancies and neurological development," *Ultrasound Med. Biol.* **25**, 1025–1031.
- SALVESEN, K.A., BAKKETEIG, L.S., EIK-NES, S.H., UNDHEIM, J.O. and OKLAND, O. (1992a). "Routine ultrasonography *in utero* and school performance at age 8-9 years," *Lancet* **339**, 85–89.
- SALVESEN, K.A., VATTEN, L.J., JACOBSEN, G., EIK-NES, S.H., OKLAND, O., MOLNE, K. and BAKKETEIG, L.S. (1992b). "Routine ultrasonography *in utero* and subsequent vision and hearing at primary school age," *Ultrasound Obstet. Gynecol.* **2**, 243–247.
- SALVESEN, K.A., JACOBSEN, G., VATTEN, L.J., EIK-NES, S.H. and BAKKETEIG, L.S. (1993a). "Routine ultrasonography *in utero* and subsequent growth during childhood," *Ultrasound Obstet. Gynecol.* **1**, 6–10.
- SALVESEN, K.A., VATTEN, L.J., EIK-NES, S.H., HUGDAHL, K. and BAKKETEIG, L.S. (1993b). "Routine ultrasonography *in utero* and subsequent handedness and neurological development," *BMJ* **307**, 159–164.
- SALVESEN, K.A., VATTEN, L.J., BAKKETEIG, L.S. and EIK-NES, S.H. (1994). "Routine ultrasonography *in utero* and speech development," *Ultrasound Obstet. Gynecol.* **4**, 101–103.
- SALZ, H., ROSENFELD, E.H. and WUSSLING, M. (1997). "Effect of ultrasound on the contraction of isolated myocardial cells of adult rats," *Ultrasound Med. Biol.* **23**, 143–149.
- SAPARETO, S.A. and DEWEY, W.C. (1984). "Thermal dose determination in cancer therapy," *Int. J. Radiat. Oncol. Biol. Phys.* **10**, 787–800.
- SARGE, K.D., BRAY, A.E. and GOODSON, M.L. (1995). "Letter: Altered stress response in testis," *Nature* **374**, 126.
- SASAKI, J., YAMAGUCHI, A., NABESHIMA, Y., SHIGEMITSU, S., MESAKI, N. and KUBO, T. (1995). "Exercise at high temperatures causes

- maternal hyperthermia and fetal anomalies in rats," *Teratology* **51**, 233–236.
- SASS, W., DREYER, H.P., KETTERMANN, S. and SEIFERT, J. (1992). "The role of cavitation activity in fragmentation processes by lithotripters," *J. Stone Dis.* **4**, 193–207.
- SATO, M. (1961). "Response of Pacinian corpuscles to sinusoidal vibration," *J. Physiol.* **159**, 391–409.
- SAXEN, L., HOLMBERG, P.C., NURMINEN, M. and KUOSMA, E. (1982). "Sauna and congenital defects," *Teratology* **25**, 309–313.
- SCHEIDT, P.C. and LUNDIN, F.E. (1977). "Investigations for effects of intrauterine ultrasound in humans," pages 19 to 26 in *Proceedings of the Symposium on Biological Effects and Characterizations of Ultrasound Sources*, Hazzard, D.G. and Litz, M.L., Eds., U.S. Department of Health, Education and Welfare Publication (FDA) 78-8048 (U.S. Government Printing Office, Washington).
- SCHEIDT, P.C., STANLEY, F. and BRYLA, D.A. (1978). "One-year follow-up of infants exposed to ultrasound *in utero*," *Am. J. Obstet. Gynecol.* **131**, 743–748.
- SCHLANSKY-GOLDBERG, R., LEVEEN, R.F. and SEHGAL, C.M. (1991). "The use of ultrasound to enhance thrombolysis," *Circulation* **84**, 442a.
- SCHLIEF, R. (1991). "Ultrasound contrast agents," *Curr. Opin. Radiol.* **3**, 198–207.
- SCHLIEF, R., SCHURMANN, R., BALZER, T., ZOMACK, M. and NIENDORF, H. (1993). "Saccharide based contrast agents," pages 71 to 96 in *Advances in Echo Imaging Using Contrast Enhancement*, Nanda, N.C. and Schlief, R., Eds. (Kluwer Academic Publishers, New York).
- SCHNEIDER, M., BUSSAT, P., BARRAU, M.D., ARDITI, M., YAN, F. and HYBL, E. (1992). "Polymeric microballoons as ultrasound contrast agents: Physical and ultrasonic properties compared with sonicated albumin," *Invest. Radiol.* **27**, 134–139.
- SCHNEIDER, M., ARDITI, M., BARRAU, M.B., BROCHOT, J., BROILLET, A., VENTRONE, R. and YAN, F. (1995). "BR1: A new ultrasonographic contrast agent based on sulfur hexafluoride-filled microbubbles," *Invest. Radiol.* **30**, 451–457.
- SCHRODER, H., GILBERT, R.D. and POWER, G.G. (1988). "Computer model of fetal-maternal heat exchange in sheep," *J. Appl. Physiol.* **65**, 460–468.
- SCHROPE, B.A. and NEWHOUSE, V.L. (1993). "Second harmonic ultrasonic blood perfusion measurement," *Ultrasound Med. Biol.* **19**, 567–579.
- SCHROPE, B., SHANKAR, P.M. and NEWHOUSE, V.L. (1990). "*In vitro* detection and sizing of microbubbles in blood using a two frequency ultrasonic system," *Innov. Tech. Biol. Med.* **11**, 613–619.
- SCHROPE, B., NEWHOUSE, V.L. and UHLENDORF, V. (1992). "Simulated capillary blood flow measurement using a nonlinear ultrasonic contrast agent," *Ultrason. Imaging* **14**, 134–158.
- SCHWAN, H.P., CARSTENSEN, E.L. and LI, K. (1953). "Heating of fat-muscle layers by electromagnetic and ultrasonic diathermy," *Trans. Am. Inst. Elec. Eng.* **72**, 483–488.

- SCHWARZ, K.Q., CHEN, X., BEZANTE, G.P., PHILLIPS, D. and SCHLIEF, R. (1996). "The Doppler kinetics of microbubble echo contrast," *Ultrasound Med. Biol.* **22**, 453–462.
- SEGIL, L.J., HARPER, P.V., METZ, C.E. and FEINSTEIN, S.B. (1988). "Abstract: Enhancement of arterial blood flow imaging in color-encoded duplex sonography after intravenous injection of a lung-crossing ultrasound contrast agent," *J. Ultrasound Med.* **7**, S121.
- SEHGAL, C., SUTHERLAND, R.G. and VERVALL, R.E. (1980a). "Sonoluminescence intensity as a function of bulk solution temperature," *J. Phys. Chem.* **84**, 525–528.
- SEHGAL, C., SUTHERLAND, R.G. and VERVALL, R.E. (1980b). "Cavitation-induced oxidation of aerated aqueous Fe^{2+} in the presence of aliphatic alcohols," *J. Phys. Chem.* **84**, 2920–2922.
- SEHGAL, C.M., BROWN, G.M., BAHN, R.C. and GREENLEAF, J.F. (1986). "Measurement and use of acoustic nonlinearity and sound speed to estimate composition of excised livers," *Ultrasound Med. Biol.* **12**, 865–874.
- SEHGAL, C.M., LEVEEN, R.F. and SHLANSKY-GOLDBERG, R.D. (1993). "Ultrasound-assisted thrombolysis," *Invest. Radiol.* **28**, 939–943.
- SEIDEL, G., BELLER, K.D., AASLID, R., HUMMEL, R.P., THIBAUT, U., VIDAL-LANGWASSER, M., KUKAT, B. and KAPS, M. (1998). "The influence of different gases on acoustic properties of a spherosome-based ultrasound contrast agent (BY963). "A transcranial Doppler sonography study," *J. Neuroimaging* **8**, 83–87.
- SEIP, R. and EBBINI, E.S. (1995). "Noninvasive estimation of tissue temperature response to heating fields using diagnostic ultrasound," *IEEE Trans. Biomed. Eng.* **42**, 828–839.
- SELLER, M.J. and HANCOCK, P.C. (1985). "Letter: Is recurrence rate of neural tube defects declining?" *Lancet* **1**, 175.
- SELMAN, G.G. and COUNCE, S.J. (1953). "Abnormal embryonic development in *Drosophila* induced by ultrasonic treatment," *Nature* **172**, 503–504.
- SERR, D.M., PADEH, B., ZAKAT, H., SHAKI, R., MANNOR, S.M. and KALNER, B. (1971). "Studies on the effect of ultrasonic waves on the fetus," page 302 in *Proceedings of the Second European Congress on Perinatal Medicine*, Huntington, P.J., Beard, R.W., Hutten, E.E. and Seaoes, J.W., Eds. (European Association on Perinatal Medicine, Porto, Portugal).
- SHANKAR, P.M., KRISHNA, P.D. and NEWHOUSE, V.L. (1998). "Advantages of subharmonic over second harmonic backscatter for contrast-to-tissue echo enhancement," *Ultrasound Med. Biol.* **24**, 395–399.
- SHANKAR, P.M., KRISHNA, P.D. and NEWHOUSE, V.L. (1999). "Subharmonic backscattering from ultrasound contrast agents," *J. Acoust. Soc. Am.* **106**, 2104–2110.
- SHANNON, C.E. (1948). "A mathematical theory of communication," *Bell Syst. Tech. J.* **27**, 379–423, 623–656.
- SHAW, A. (1994). "Prediction of temperature rise in layered media from measured ultrasonic intensity data," *Phy. Med. Biol.* **39**, 1203–1218.
- SHAW, A., PRESTON, R.C. and BACON, D.R. (1996). "Perfusion corrections for ultrasonic heating in nonperfused media," *Ultrasound Med. Biol.* **22**, 203–216.

- SHAW, A., PAY, N.M. and PRESTON, R.C. (1998). *Assessment of the Likely Thermal Index Values for Pulsed Doppler Ultrasonic Equipment—Stages II and III: Experimental Assessment of Scanner/Transducer Combinations*, Report CMAM 12 (National Physical Laboratory, Teddington, Middlesex, United Kingdom).
- SHEN, J. and EBBINI, E.S. (1994). "An optimal image operator design technique for coded excitation ultrasound imaging system," pages 1777 to 1781 in *1994 IEEE Ultrasonics Symposium Proceedings* (Institute of Electrical and Electronic Engineers, Piscataway, New Jersey).
- SHEPARD, T.H. (1989). *Catalog of Teratogenic Agents* (Johns Hopkins University Press, Baltimore, Maryland).
- SHI, W.T. and FORSBERG, F. (2000). "Ultrasonic characterization of the nonlinear properties of contrast microbubbles," *Ultrasound Med. Biol.* **26**, 93–104.
- SHI, W.T., FORSBERG, F., HALL, A.L., CHIAO, R.Y., LIU, J.B., MILLER, S., THOMENIUS, K.E., WHEATLEY, M.A. and GOLDBERG, B.B. (1999a). "Subharmonic imaging with microbubble contrast agents: Initial results," *Ultrason. Imaging* **21**, 79–94.
- SHI, W.T., FORSBERG, F., RAICHLIN, J.S., NEEDLEMAN, L. and GOLDBERG, B.B. (1999b). "Pressure dependence of subharmonic signals from contrast microbubbles," *Ultrasound Med. Biol.* **25**, 275–283.
- SHIMA, A. and TSUJINO, T. (1978). "The behavior of gas bubbles in the Casson fluid," *J. Appl. Mech.* **45**, 37–42.
- SHIMA, A., TAKAYAMA, K. and TOMITA, Y. (1983). "Mechanisms of impact pressure generation from spark-generated bubble collapse near a wall," *Am. Inst. Aeron. Astron. J.* **21**, 55–59.
- SHIMA, A., RAJVANSHI, S.C. and TSUJINO, T. (1985). "Study of nonlinear oscillations of bubbles in Powell-Eyring fluids," *J. Acoust. Soc. Am.* **77**, 1702–1709.
- SHIMM, D.S., HYNENEN, K.H., ANHALT, D.P., ROEMER, R.B. and CASADY, J.R. (1988). "Scanned focussed ultrasound hyperthermia: Initial clinical results," *Int. J. Radiat. Oncol. Biol. Phys.* **15**, 1203–1208.
- SHIOTA, K. (1988). "Induction of neural tube defects and skeletal malformations in mice following brief hyperthermia *in utero*," *Biol. Neonate* **53**, 86–97.
- SHIRAN, M.B., QUAN, K.M., WATMOUGH, D.J., ABDELLATIF, K., MALLARD, J.R., MARSHALL, D. and GREGORY, D.W. (1990). "Some of the factors involved in the Sarvazyan method for recording ultrasound field distributions with special reference to the application of ultrasound in physiotherapy," *Ultrasonics* **28**, 411–414.
- SHOJI, R., MURAKAMI, U. and SHIMIZU, T. (1975). "Influence of low-intensity ultrasonic irradiation on prenatal development of two inbred mouse strains," *Teratology* **12**, 227–231.
- SHOMBERT, D.G., SMITH, S.W. and HARRIS, G.R. (1982). "Angular response of miniature ultrasonic hydrophones," *Med. Phys.* **9**, 484–492.
- SIDDIQI, T.A., O'BRIEN, W.D., JR., MEYER, R.A., SULLIVAN, J.M. and MIODOVNIK, M. (1991). "*In-situ* exposimetry: The ovarian ultrasound examination," *Ultrasound Med. Biol.* **17**, 257–263.

- SIDDIQI, T.A., O'BRIEN, W.D., JR., MEYER, R.A., SULLIVAN, J.M. and MODOVNIK, M. (1992). "Human *in situ* dosimetry: Differential insertion loss during passage through abdominal wall and myometrium," *Ultrasound Med. Biol.* **18**, 681–689.
- SIDDIQI, F., BLINC, A., BRAATEN, J. and FRANCIS, C.W. (1995a). "Ultrasound increases flow through fibrin gels," *Thromb. Haemost.* **73**, 495–498.
- SIDDIQI, T.A., O'BRIEN, W.D., JR., MEYER, R.A., SULLIVAN, J.M. and MODOVNIK, M. (1995b). "*In situ* human obstetrical ultrasound exposimetry: Estimates of derating factors for each of three different tissue models," *Ultrasound Med. Biol.* **21**, 379–391.
- SIDDIQI, F., ODR LJIN, T.M., FAY, P.J., COX, C. and FRANCIS, C.W. (1998). "Binding of tissue-plasminogen activator to fibrin: Effect of ultrasound," *Blood* **91**, 2019–2025.
- SIKOV, M.R. and HILDEBRAND, B.P. (1976). "Effects of ultrasound on the prenatal development of the rat. Part 1. 3.2 MHz continuous wave at nine days of gestation," *J. Clin. Ultrasound* **4**, 357–363.
- SIMON, R.H., HO, S.Y., PERKINS, C.R. and D'ARRIGO, J.S. (1992). "Quantitative assessment of tumor enhancement by ultrastable lipid-coated microbubbles as a sonographic contrast agent," *Invest. Radiol.* **27**, 29–34.
- SIMONS, J.W.I.M. (1982). "Effect of temperature on mutations in cultured human skin fibroblasts," *Mutat. Res.* **92**, 417–426.
- SKINNER, L.A. (1970). "Acoustically induced gas bubble growth," *J. Acoust. Soc. Am.* **51**, 378–382.
- SKOLNIK, M.I. (1990). *Radar Handbook*, 2nd ed. (McGraw-Hill, New York).
- SKYBA, D.M., PRICE, R.J., LINKA, A.Z., SKALAK, T.C. and KAUL, S. (1998). "Direct *in vivo* visualization of intravascular destruction of microbubbles by ultrasound and its local effects on tissue," *Circulation* **98**, 290–293.
- SMALES, O.R.C. and KIME, R. (1978). "Thermoregulation in babies immediately after birth," *Arch. Dis. Child.* **53**, 58–61.
- SMITH, R.A. (1989). "Are hydrophones of diameter 0.5 mm small enough to characterise diagnostic ultrasound equipment?" *Phys. Med. Biol.* **34**, 1593–1607.
- SMITH, P.F. and HUNTER, W.L. (1980). *On the Effects of Exposure to Intense Underwater Sound on Navy Divers*, NSMRL Memorandum Report 80-1 (Naval Submarine Medical Research Laboratory, Groton, Connecticut).
- SMITH, M.D., KWAN, O.L., REISER, H.J. and DEMARIA, A.N. (1984). "Superior intensity and reproducibility of SHU-454, a new right heart contrast agent," *J. Am. Coll. Cardiol.* **3**, 992–998.
- SMITH, S.W., STEWART, H.F. and JENKINS, D.P. (1985). "A plane layered model to estimate *in situ* ultrasound exposures," *Ultrasonics* **23**, 31–40.
- SMITS, G.A., OOSTERHOF, G.O., DE RUYTER, A.E., SCHALKEN, J.A. and DEBRUYNE, F.M. (1991). "Cytotoxic effects of high energy shock waves in different *in vitro* models: Influence of the experimental set-up," *J. Urol.* **145**, 171–175.
- SOETANTO, K. and CHAN, M. (2000). "Fundamental studies on contrast images from different-sized microbubbles: Analytical and experimental studies," *Ultrasound Med. Biol.* **26**, 81–91.

- SOHAR, E., SHOENFELD, Y.T., SHAPIRO, Y., OHRY, A. and CABILI, S. (1976). "Effects of exposure to Finnish sauna," *Isr. J. Med. Sci.* **12**, 1275–1282.
- SOMMER, F.G. and POUNDS, D. (1982). "Transient cavitation in tissues during ultrasonically induced hyperthermia," *Med. Phys.* **9**, 1–3.
- SONTUM, P.C., OSTENSEN, J., DYRSTAD, K. and HOFF, L. (1999). "Acoustic properties of NC100100 and their relation with the microbubble size distribution," *Invest. Radio.* **34**, 268–275.
- SPRAGGETT, K. and FRASER, F.C. (1982). "Sauna-induced hyperthermia in women," *Teratology* **25**, 77A.
- STARK, C.R., ORLEANS, M., HAVERKAMP, A.D. and MURPHY, J. (1984). "Short- and long-term risks after exposure to diagnostic ultrasound *in utero*," *Obstet. Gynecol.* **63**, 194–200.
- STARRITT, H.C. and DUCK, F.A. (1992). "Letter: Quantification of acoustic shock in routine exposure measurement," *Ultrasound Med. Biol.* **18**, 513–515.
- STARRITT, H.C., PERKINS, M.A., DUCK, F.A. and HUMPHREY, V.F. (1985). "Evidence for ultrasonic finite-amplitude distortion in muscles using medical equipment," *J. Acoust. Soc. Am.* **77**, 302–306.
- STARRITT, H.C., DUCK, F.A. and HUMPHREY, V.F. (1989). "An experimental investigation of streaming in pulsed diagnostic ultrasound beams," *Ultrasound Med. Biol.* **15**, 363–373.
- STARRITT, H.C., DUCK, F.A. and HUMPHREY, V.F. (1991). "Forces acting in the direction of propagation in pulsed ultrasound fields," *Phys. Med. Biol.* **36**, 1465–1474.
- STAVROS, A.T. and DENNIS, M.A. (1993). "The ultrasound of breast pathology," pages 111 to 115 in *Percutaneous Breast Biopsy*, Parker, S.H. and Jobe, W.E., Eds. (Raven Press, Ltd., New York).
- STEINBACH, P., HOFSTADTER, F., NICOLAI, H., ROSSLER, W. and WIELAND, W. (1992). "*In vitro* investigations on cellular damage induced by high energy shock waves," *Ultrasound Med. Biol.* **18**, 691–699.
- STELLA, M., TREVISAN, L., MONTALDI, A., ZACCARIA, G., ROSSI, G., BIANCHI, V. and LEVIS, A.G. (1984). "Induction of sister-chromatid exchanges in human lymphocytes exposed *in vitro* and *in vivo* to therapeutic ultrasound," *Mutat. Res.* **138**, 75–85.
- STOLZENBERG, S.J., TORBIT, C.A., EDMONDS, P.D. and TAENZER, J.C. (1980). "Effects of ultrasound on the mouse exposed at different stages of gestation: Acute studies," *Radiat. Environ. Biophys.* **17**, 245–270.
- STORM, D.L. (1974). "Interfacial distortions of a pulsating bubble," pages 234 to 239 in *Proceedings of the 1973 Symposium on Finite Amplitude Wave Effects in Fluids*, Bjorno, L., Ed. (IPC Science and Technology Press, Copenhagen, Denmark).
- STORTI, R.V., SCOTT, M.P., RICH, A. and PARDUE, M.L. (1980). "Translational control of protein synthesis in response to heat shock in *D. melanogaster* cells," *Cell* **22**, 825–834.
- STRASBERG, M. (1961). "Rectified diffusion: Comments on a paper by Hsieh and Plesset," *J. Acoust. Soc. Am.* **33**, 359L.

- STRATFORD, I.A. and ADAMS, G.E. (1977). "Effect of hyperthermia on differential cytotoxicity of a hypoxic cell radiosensitizer, Ro-07-0582, on mammalian cells *in vitro*," *Br. J. Cancer* **35**, 307–313.
- STUMPF, U. (1979). "Ultrasonic thrombolysis," *J. Acoust. Soc. Am.* **65**, 541–544.
- SUCHKOVA, V., SIDDIQI, F.N., CARSTENSEN, E.L., DALECKI, D., CHILD, S. and FRANCIS, C.W. (1998). "Enhancement of fibrinolysis with 40-kHz ultrasound," *Circulation* **98**, 1030–1035.
- SUCHKOVA, V.N., BAGGS, R.B. and FRANCIS, C.W. (2000). "Effect of 40-kHz ultrasound on acute thrombotic ischemia in a rabbit femoral artery thrombosis model: Enhancement of thrombolysis and improvement in capillary muscle perfusion," *Circulation* **101**, 2296–2301.
- SUHR, D., BRUMMER, F., IRMER, U., SCHLACHTER, M. and HULSER, D.F. (1994) "Reduced cavitation-induced cellular damage by the antioxidative effect of vitamin E," *Ultrasonics* **32**, 301–307.
- SUN, Y., DONG, Y. and SHAO, H. (1985). "Study of the acoustic nonlinearity parameter in highly attenuating biological media," pages 891 to 894 in *1985 IEEE Ultrasonics Symposium Proceedings*, McAvoy, B.R., Ed. (Institute of Electronics and Electrical Engineers, Piscataway, New Jersey).
- SUN, Y., DONG, Y., TONG, J. and TANG, Z. (1986). "Ultrasonic propagation parameters in human tissues," pages 905 to 908 in *1986 IEEE Ultrasonics Symposium Proceedings*, McAvoy, B.R., Ed. (Institute of Electronics and Electrical Engineers, Piscataway, New Jersey).
- SUSLICK, K.S. (1988). "Homogeneous sonochemistry," pages 123 to 163 in *Ultrasound: Its Chemical, Physical, and Biological Effects*, Suslick, K.S., Ed. (VCH Publishers, New York).
- SUSLICK, K.S. and HAMMERTON, D.A. (1986). "The site of sonochemical reactions," *IEEE Trans. UFFC* **33**, 143–147.
- SUSLICK, K.S., HAMMERTON, D.A. and CLINE, R.E. (1985). "Determination of local temperatures caused by acoustic cavitation," pages 1116 to 1121 in *1985 Ultrasonics Symposium Proceedings* (Institute of Electronics and Electrical Engineers, Piscataway, New Jersey).
- SUSLICK, K.A., HAMMERTON, D.A. and CLINE, R.E. (1986). "The sonochemical hot spot," *J. Am. Chem. Soc.* **108**, 5641–5642.
- TACHIBANA, S. (1985). "Application of ultrasonic vibration for boosting fibrinolytic effect of urokinase in rats," *Blood Vessel* **16**, 46–49.
- TACHIBANA, K. (1992). "Enhancement of fibrinolysis with ultrasound energy," *J. Vasc. Interv. Radiol.* **3**, 299–303.
- TACHIBANA, S. and KOGA, E. (1981). "Ultrasonic vibration for boosting fibrinolytic effect of urokinase," *Blood Vessel* **12**, 450–453.
- TACHIBANA, K. and TACHIBANA, S. (1995). "Albumin microbubble echo-contrast material as an enhancer for ultrasound accelerated thrombolysis," *Circulation* **92**, 1148–1150.
- TAKABAYASHI, Y.A., SATO, S., SATO, A. and SUZUKI, M. (1981). "Effects of pulse-wave ultrasonic irradiation on mouse embryo," *Cho-Onpo Igaku (Supersonic Medicine)* **8**, 286–288.
- TAKEUCHI, H., NAKAZAWA, T., KUMAKIRI, K. and KUSANO, R. (1970). "Experimental studies on ultrasonic Doppler method in obstetrics," *Acta. Obstet. Gynecol. Jpn.* **17**, 11–16.

- TANAKA, K., MIYAJIMA, G., WAGAI, T., YASUHURA, M., KIKUCHI, Y. and UCHIDA, R. (1952). "Detection of intracranial abnormalities by ultrasound," (Japan) Tokyo Med. J. **69**, 525.
- TANASAWA, I. and YANG, W. (1970). "Dynamic behavior of a gas bubble in viscoelastic liquids," J. Appl. Physics **41**, 4526–4531.
- TARANTAL, A.F. and CANFIELD, D.R. (1994). "Ultrasound-induced lung hemorrhage in the monkey," Ultrasound Med. Biol. **20**, 65–72.
- TARANTAL, A.F. and HENDRICKX, A.G. (1989). "Evaluation of the bioeffects of prenatal ultrasound exposure in the cynomolgus macaque (*Macaca fascicularis*): I. Neonatal/infant observations," and "II. Growth and behavior during the first year," Teratology **39**, 137–147; 149–162.
- TARANTAL, A.F., CHU, F., O'BRIEN, W.D., JR. and HENDRICKX, A.G. (1993). "Sonographic heat generation *in vivo* in the gravid long-tailed macaque (*Macaca fascicularis*)," J. Ultrasound Med. **12**, 285–295.
- TAYLOR, K.J. (1986). "Experience with ultrasound output settings and adequacy of diagnostic examinations," in presentation and panel discussion by Carson, P., Larsen, H., Stewart, H. and Taylor, K. (American Institute of Ultrasound in Medicine, Laurel, Maryland).
- TAYLOR, K.J. and POND, J.B. (1972). "A study of the production of haemorrhagic injury and paraplegia in rat spinal cord by pulsed ultrasound of low megahertz frequencies in the context of the safety for clinical usage," Br. J. Radiol. **45**, 343–353.
- TER HAAR, G.R. (1986). "Ultrasonic biophysics," pages 378 to 435 in *Physical Principles of Medical Ultrasound*, Hill, C.R., Ed. (Ellis Horwood Limited, Chichester, United Kingdom).
- TER HAAR, G. (1995). "Ultrasound focal beam surgery," Ultrasound Med. Biol. **21**, 1089–1100.
- TER HAAR, G.R. and DANIELS, S. (1981). "Evidence for ultrasonically induced cavitation *in vivo*," Phys. Med. Biol. **26**, 1145–1149.
- TER HAAR, G., DYSON, M. and SMITH, S.P. (1979). "Ultrastructural changes in the mouse uterus brought about by ultrasonic irradiation at therapeutic intensities in standing wave fields," Ultrasound Med. Biol. **5**, 167–179.
- TER HAAR, G., STRATFORD, I.J. and HILL, C.R. (1980). "Ultrasonic irradiation of mammalian cells *in vitro* at hyperthermic temperatures," Br. J. Radiol. **53**, 784–789.
- TER HAAR, G., DANIELS, S., EASTAUGH, K.C. and HILL, C.R. (1982). "Ultrasonically induced cavitation *in vivo*," Br. J. Cancer (Suppl.) **45**, 151–155.
- TER HAAR, G., WALLING, J., LOVEROCK, P. and TOWNSEND, S. (1988). "The effect of combined heat and ultrasound on multicellular tumour spheroids," Int. J. Radiat. Biol. Relat. Stud. Phys. Chem. Med. **53**, 813–827.
- TESTART, J., THEBAULT, A., SOUDERES, E. and FRYDMAN, R. (1982). "Premature ovulation after ovarian ultrasonography," Br. J. Obstet. Gynaecol. **89**, 694–700.
- THACKER, J. (1985a). "Investigations into genetic and inherited changes produced by ultrasound," pages 67 to 76 in *Biological Effects of Ultrasound*, Nyborg, W.L. and Ziskin, M.C., Eds. (Churchill Livingstone, New York).

- THACKER, S.B. (1985b). "Quality of controlled trials. The case of imaging ultrasound in obstetrics: A review," *Br. J. Obstet. Gynaecol.* **92**, 437-444.
- THIEME, G.A., BANJAVIC, R.A., JOHNSON, M.L., MEYER, C.R., SILVERS, G.W., HERRON, D.S. and CARSON, P.L. (1983). "Sonographic identification of lung maturation in the fetal lamb," *Invest. Radiol.* **18**, 18-26.
- THIEME, G.A., CARSON, P.L., MEYER, C.R. and BOWERMAN, R. (1993). "In vivo fetal lung tissue characterization by scattering," pages 409 to 449 in *Ultrasonic Scattering in Biological Tissues*, Shung, K.K. and Thieme, G.A., Eds. (CRC Press, Boca Raton, Florida).
- THOMAS, N.E. and COAKLEY, W.T. (1996). "Measurement of antigen concentration by an ultrasound-enhanced latex immunoagglutination assay," *Ultrasound Med. Biol.* **22**, 1277-1284.
- THOMENIUS, K.E. (1993). "Estimation of the potential for bioeffects," pages 372 to 407 in *Ultrasonic Exposimetry*, Ziskin, M.C. and Lewin, P.A., Eds. (CRC Press, Boca Raton, Florida).
- TIMMERMANS, L. (1973). "Les ultrasons dans le diagnostic des maladies des reins de la vessie et de la prostate," *Acta. Ural. Belg.* **41**, 337-354.
- TOMITA, Y. and SHIMA, A. (1986). "Mechanisms of impulsive pressure generation and damage pit formation by bubble collapse," *J. Fluid Mech.* **164**, 535-564.
- TRAMPLER, F., PUI, P., SONDERHOFF, S.A., KILBURN, D.G., BENES, E., GROSCHL, M., BURGER, W. and PIRET, J.M. (1993). "Aggregation and separation of hybridoma cells by ultrasonic resonance fields: Effect on viability, growth rate and productivity," pages 511 to 514 in *Ultrasonics International '93 Conference Proceedings* (Butterworth-Heinemann Ltd., Oxford).
- TRENCHARD, P.M. (1987). "Ultrasound-induced orientation of discoid platelets and simultaneous changes in light transmission: Preliminary characterisation of the phenomenon," *Ultrasound Med. Biol.* **13**, 183-195.
- TRIER, H.G., DECKER, D., LEPPER, R.D., IRION, K.M., REUTER, R., KOTTOW, M., MULLER-BREITENKAMP, R. and OTTO, K.J. (1984). "Ocular tissue characterization by RF-signal analysis: Summary of the Bonn/Stuttgart in vivo study," pages 455 to 466 in *Proceedings SIDUO IX, Ophthalmic Ultrasonography*, Hillman, J.S. and Le May, M.M., Eds. (W. Junk Publishing, The Hague).
- TRIMBLE, B.K. and DOUGHTY, J.H. (1974). "The amount of hereditary disease in human populations," *Ann. Hum. Genet.* **38**, 199-233.
- TRUBESTEIN, G., ENGEL, C., ETZEL, F., SOBBE, A., CREMER, H. and STUMPF, U. (1976). "Thrombolysis by ultrasound," *Clin. Sci. Mol. Med. (Suppl.)* **3**, 697S-698S.
- TRUDINGER, B.J., COOK, C.M., GILES, W.B., CONNELLY, A. and THOMPSON, R.S. (1987). "Umbilical artery flow velocity waveforms in high-risk pregnancy. Randomised controlled trial," *Lancet* **1**, 188-190.
- TSIRULNIKOV, E.M., VARTANYAN, I.A., GERSUNI, G.V., ROSENBLYUM, A.S., PUDOV, V.I. and GAVRILOV, L.R. (1988). "Use of amplitude-modulated focused ultrasound for diagnosis of hearing disorders," *Ultrasound Med. Biol.* **14**, 277-285.

- TSUJINO, T. (1987). "Cavitation damage and noise spectra in a polymer solution," *Ultrasonics* **25**, 67–72.
- TSUJINO, T. and SHIMA, A. (1980). "The behaviour of gas bubbles in blood subjected to an oscillating pressure," *J. Biomech.* **13**, 407–416.
- TYLER, T.D., OPHIR, J., MAKLAD, N.F. and GOBUTY, A. (1981). "In vivo enhancement of ultrasonic image luminance by aqueous solutions with high speed of sound," *Ultrason. Imaging* **3**, 323–329.
- TYRRELL, S.N., LILFORD, R.J., MACDONALD, H.N., NELSON, E.J., PORTER, J. and GUPTA, J.K. (1990). "Randomized comparison of routine vs highly selective use of Doppler ultrasound and biophysical scoring to investigate high risk pregnancies," *Br. J. Obstet. Gynaecol.* **97**, 909–916.
- UHLENDORF, V. (1994). "Physics of ultrasound contrast imaging: Scattering in the linear range," *IEEE Trans. UFFC* **41**, 70–79.
- UHLENDORF, V. and HOFFMANN, C. (1994). "Non-linear acoustic response of coated microbubbles in diagnostic ultrasound," pages 1559 to 1562 in *1994 Ultrasonics Symposium Proceedings* (Institute of Electrical and Electronic Engineers, Piscataway, New Jersey).
- UHLENDORF, V. and SCHOLLE, F.D. (1996). "Imaging of spatial distribution and flow of microbubbles using nonlinear acoustic properties," pages 233 to 238 in *Acoustical Imaging*, **22**, Tortoli, P. and Masotti, L., Eds. (Plenum Press, New York).
- UMEMURA, S. (1994). "Sonochemical application of ultrasound to tumor treatment," *Jpn. J. Appl. Phys.* **33**, 2846–2851.
- UMEMURA, S. and KAWABATA, K. (1993). "Enhancement of sonochemical reactions by second-harmonic superimposition," in *1993 IEEE Ultrasonics Symposium Proceedings* (Institute of Electrical and Electronic Engineers, Piscataway, New Jersey).
- UMEMURA, S., YUMITA, N., NISHIGAKI, R. and UMEMURA, K. (1990). "Mechanism of cell damage by ultrasound in combination with hemato-porphyrin," *Jpn. J. Cancer Res.* **81**, 962–966.
- UMEMURA, S., KAWABATA, K. and SASAKI, K. (1997). "In vitro and in vivo enhancement of sonodynamically active cavitation by second-harmonic superimposition," *J. Acoust. Soc. Am.* **101**, 569–577.
- UNGER, E.C., LUND, P.J., SHEN, D.K., FRITZ, T.A., YELLOWHAIR, D. and NEW, T.E. (1992). "Nitrogen-filled liposomes as a vascular US contrast agent: Preliminary evaluation," *Radiology* **185**, 453–456.
- UNGER, E., FRITZ, T., MCCREERY, T., SAHN, D., BARRETTE, T., YELLOWHAIR, D. and NEW, T. (1997). "Liposomes as myocardial perfusion ultrasound contrast agents," pages 57 to 74 in *Ultrasound Contrast Agents*, Goldberg, B.B., Ed. (Martin Duntiz Ltd., London).
- UNGER, E.C., MCCREERY, T.P., SWEITZER, R.H., CALDWELL, V.E. and WU, Y. (1998). "Acoustically active lipospheres containing paclitaxel: A new therapeutic ultrasound contrast agent," *Invest. Radiol.* **33**, 886–892.
- USSING, H.H. and ZEHRAN, K. (1951). "Sodium transport in frog skin," *Acta. Physiol. Scand.* **23**, 110–127.
- VAKIL, N. and EVERBACH, E.C. (1991). "Gas in gallstones: Quantitative determinations and possible effects on fragmentation by shock waves," *Gastroenterology* **101**, 1628–1634.

- VAKIL, N. and EVERBACH, E.C. (1993). "Transient acoustic cavitation in gallstone fragmentation: A study of gallstones fragmented *in vivo*," *Ultrasound Med. Biol.* **19**, 331–342.
- VANDENBERG, B.F. and MELTON, H.E. (1994). "Acoustic liability of albumin microspheres," *J. Am. Soc. Echocardiogr.* **7**, 582–589.
- VAN DER WOUW, P.A., BRAUNS, A.C., BAILEY, S.E., POWERS, J.E. and WILDE, A.A. (2000). "Premature ventricular contractions during triggered imaging with ultrasound contrast," *J. Am. Soc. Echocardiogr.* **13**, 288–294.
- VAN ZELST, S.J., ZUPP, J.L., HAYMAN, D.L. and SETCHELL, B.P. (1995). "X-Y chromosome dissociation in mice and rats exposed to increased testicular or environmental temperatures," *Reprod. Fertil. Dev.* **7**, 1117–1121.
- VERESS, E. and VINCENZE, J. (1977). "The haemolysing action of ultrasound on erythrocytes," *Acustica* **36**, 100–103.
- VERRALL, R.E. and SEHGAL, C.M. (1988). "Sonoluminescence," pages 227 to 286 in *Ultrasound: Its Chemical, Physical, and Biological Effects*, Suslick, K.S., Ed. (VCH Publishers, New York).
- VERRILLO, R.T. (1962). "Investigation of some parameters of the cutaneous threshold for vibration," *J. Acoust. Soc. Am.* **34**, 1768–1773.
- VERRILLO, R.T. (1963). "Effect of contactor area on the vibrotactile threshold," *J. Acoust. Soc. Am.* **35**, 1962–1966.
- VERRILLO, R.T. (1965). "Temporal summation in vibrotactile sensitivity," *J. Acoust. Soc. Am.* **37**, 843–846.
- VIVINO, A.A., BORAKER, D.K., MILLER, D. and NYBORG, W. (1985). "Stable cavitation at low ultrasonic intensities induces cell death and inhibits 3H-TdR incorporation by Con-A stimulated murine lymphocytes *in vitro*," *Ultrasound Med. Biol.* **11**, 751–759.
- VOGEL, A. and LAUTERBORN, W. (1988). "Acoustic transient generation by laser-generated cavitation bubbles near solid boundaries," *J. Acoust. Soc. Am.* **84**, 719–731.
- VOGEL, A., LAUTERBORN, W. and TIMM, R. (1989). "Optical and acoustic investigations of the dynamics of laser-produced cavitation bubbles near a solid boundary," *J. Fluid Mech.* **206**, 299–338.
- VOKURKA, K. (1986). "Comparison of Rayleigh's, Herring's and Gilmore's models of gas bubbles," *Acustica* **59**, 214–219.
- VONA, D.F., MILLER, M.W., MAILLIE, H.D. and RAEMAN, C.H. (1995). "A test of the hypothesis that cavitation at the focal area of an extracorporeal shock wave lithotripter produces far ultraviolet and soft x-ray emissions," *J. Acoust. Soc. Am.* **98**, 706–711.
- VON BEKESY, G. (1960). *Experiments in Hearing*, translated by Weaver, E.G., Ed. (McGraw-Hill, New York).
- VUILLE, C., NIDORF, M., MORRISSEY, R.L., NEWELL, J.B., WEYMAN, A.E. and PICARD, M.H. (1994). "Effect of static pressure on the disappearance rate of specific echocardiographic contrast agents," *J. Am. Soc. Echocardiogr.* **7**, 347–354.
- VYAS, R. and RUSTGI, M.L. (1992). "Green's function solution to the tissue bioheat equation," *Med. Phys.* **19**, 1319–1324.

- VYKHODTSEVA, N.I., HYNYNEN, K. and DAMIANOU, C. (1994). "Pulse duration and peak intensity during focused ultrasound surgery: Theoretical and experimental effects in rabbit brain *in vivo*," *Ultrasound Med. Biol.* **20**, 987–1000.
- VYKHODTSEVA, N.I., HYNYNEN, K. and DAMIANOU, C. (1995). "Histologic effects of high intensity pulsed ultrasound exposure with subharmonic emission in rabbit brain *in vivo*," *Ultrasound Med. Biol.* **21**, 969–979.
- WAGAI, T. and KIKUCHI, Y. (1965). "Destruction of transplantable ascites tumors by means of intense ultrasound," pages 179 to 189 in *Ultrasonic Energy: Biological Investigations and Medical Applications*, Kelly, E., Ed. (University of Illinois Press, Urbana).
- WALDAY, P., OSTENSEN, J., TOLLESHAUG, H. and HOLTZ, E. (1994a). "Albunex—a new ultrasound contrast agent. Effects on hemodynamics, contrast, and biodistribution in different species," *Invest. Radiol. (Suppl.)* **29**, S142–S144.
- WALDAY, P., TOLLESHAUG, H., GJOEN, T., KINDBERG, G.M., BERG, T., SKOTLAND, T. and HOLTZ, E. (1994b). "Biodistributions of air-filled albumin microspheres in rats and pigs," *Biochem. J.* **299**, 437–443.
- WALKER, D., WALKER, A. and WOOD, C. (1969). "Temperature of the human fetus," *J. Obstet. Gynecol. Br. Commonw.* **76**, 503–511.
- WALKER, K.W., PANTELY, G.A. and SAHN, D.J. (1997). "Ultrasound-mediated destruction of contrast agents. Effect of ultrasound intensity, exposure, and frequency," *Invest. Radiol.* **32**, 728–734.
- WALL, P.D., FRY, W.J., STEPHENS, R., TUCKER, D. and LETTVIN, J.Y. (1951). "Changes produced in the central nervous system by ultrasound," *Science* **114**, 686–687.
- WALSH, D.A., KLEIN, N.W., HIGHTOWER, L.E. and EDWARDS, M.J. (1987). "Heat shock and thermotolerance during early rat embryo development," *Teratology* **36**, 181–191.
- WALSH, D.A., LI, K., SPEIRS, J., CROWTHER, C.E. and EDWARDS, M.J. (1989). "Regulation of the inducible heat shock 71 genes in early neural development of cultured rat embryos," *Teratology* **40**, 321–334.
- WANG, S.J., LEWALLEN, D.G., BOLANDER, M.E., CHAO, E.Y.S., ILSTRUP, D.M. and GREENLEAF, J.F. (1994). "Low intensity ultrasound treatment increases strength in a rat femoral fracture model," *J. Orthop. Res.* **12**, 40–47.
- WARD, B., BAKER, A.C. and HUMPHREY, V.F. (1997). "Nonlinear propagation applied to the improvement of resolution in diagnostic medical ultrasound," *J. Acoust. Soc. Am.* **101**, 143–154.
- WARD, M., WU, J. and CHIU, J.F. (1999). "Ultrasound-induced cell lysis and sonoporation enhanced by contrast agents," *J. Acoust. Soc. Am.* **105**, 2951–2957.
- WATKIN, N.A., TER HAAR, G.R. and RIVENS, I. (1996). "The intensity dependence of the site of maximal energy deposition in focused ultrasound surgery," *Ultrasound Med. Biol.* **22**, 483–491.
- WATMOUGH, D.J., QUAN, K.M. and SHIRAN, M.B. (1990). "Possible explanation for the unexpected absence of gross biological damage to

- membranes of cells insonated in suspension and in surface culture in chambers exposed to standing and progressive wave fields," *Ultrasonics* **28**, 142–148.
- WATMOUGH, D.J., DAVIES, H.M., QUAN, K.M., WYTCH, R. and WILLIAMS, A.R. (1991). "Imaging microbubbles and tissues using a linear focussed scanner operating at 20 MHz: Possible implications for the detection of cavitation thresholds," *Ultrasonics* **29**, 312–318.
- WATMOUGH, D.J., LAKSHMI, R., GHEZZI, F., QUAN, K.M., WATMOUGH, J.A., KHIZHNYAK, E., PASHOVKIN, T.N. and SARVAZYAN, A.P. (1993). "The effect of gas bubbles on the production of ultrasound hyperthermia at 0.75 MHz: A phantom study," *Ultrasound Med. Biol.* **19**, 231–241.
- WATTS, P.L. and STEWART, C.R. (1972). "The effect of fetal heart monitoring by ultrasound on maternal and fetal chromosomes," *J. Obstet. Gynaecol. Br. Commonw.* **79**, 715–716.
- WEBSTER, W.S. and EDWARDS, M.J. (1984). "Hyperthermia and the induction of neural tube defects in mice," *Teratology* **29**, 417–425.
- WEBSTER, W.S., GERMAIN, M.A. and EDWARDS, M.J. (1985). "The induction of microphthalmia, encephalocele, and other head defects following hyperthermia during the gastrulation process in the rat," *Teratology* **31**, 73–82.
- WEGNER, R.D. and LANG, R. (1986). "Absence of a mutagenic effect of diagnostic ultrasound in the salmonella mutagenicity test (Ames Test)," *IEEE Trans. UFFC* **33**, 171–178.
- WEISER, M.A. and APFEL, R.E. (1982). "Extension of acoustic levitation to include the study of micron-sized particles in a more compressible host liquid," *J. Acoust. Soc. Am.* **71**, 1261–1268.
- WEISER, M.A., APFEL, R.E. and NEPPIRAS, E.A. (1984). "Interparticle forces on red cells in a standing wave field," *Acustica* **56**, 114–119.
- WEISSLER, A. (1958). "Formation of hydrogen peroxide by ultrasonic waves: Free radical," *J. Am. Chem. Soc.* **81**, 1077–1081.
- WEISSLER, A., COOPER, H.W. and SNYDER, S. (1950). "Chemical effect of ultrasonic waves: Oxidation of potassium iodide solution by carbon tetrachloride," *Am. Chem. Soc. J.* **72**, 1769–1775.
- WEISSMAN, N.J., COHEN, M.C., HACK, T.C., GILLAM, L.D., COHEN, J.L. and KITZMAN, D.W. (2000). "Infusion versus bolus contrast echocardiography: A multicenter, open-label, crossover trial." *Am. Heart J.* **139**, 399–404.
- WELLS, P.N., HARRIS, R.A. and HALLIWELL, M. (1992). "The envelope that tissue imposes on achievable ultrasonic imaging," *J. Ultrasound Med.* **11**, 433–439.
- WESTON, D.E. (1966). "Acoustic interaction effects in arrays of small spheres," *J. Acoust. Soc. Am.* **39**, 316–322.
- WESTWOOD, J.T., CLOS, J. and WU, C. (1991). "Stress-induced oligomerization and chromosomal relocalization of heat-shock factor," *Nature* **353**, 822–827.
- WFUMB (1989). World Federation for Ultrasound in Medicine and Biology. *Second World Federation of Ultrasound in Medicine and Biology*

- Symposium on Safety and Standardization in Medical Ultrasound*, *Ultrasound Med. Biol. (Suppl.)* **15**, 1–115.
- WFUMB (1992). World Federation for Ultrasound in Medicine and Biology. *WFUMB Symposium on Safety of Ultrasound in Medicine. Issues and Recommendations Regarding Thermal Mechanisms for Biological Effects of Ultrasound*, *Ultrasound Med. Biol.* **18**, 731–810.
- WFUMB (1998). World Federation for Ultrasound in Medicine and Biology. *WFUMB Symposium on Safety of Ultrasound in Medicine. Conclusions and Recommendations on Thermal and Nonthermal Mechanisms for Biological Effects of Ultrasound*, *Ultrasound Med. Biol. (Suppl.)* **24**, S1–S58.
- WHITTINGHAM, T.A. (2000). “Acoustic output of diagnostic machines,” pages 16 to 31 in *Safety of Diagnostic Ultrasound*, ter Harr, G. and Duck, F.A., Eds. (British Institute of Radiology, London).
- WHITWORTH, G. and COAKLEY, W.T. (1992). “Particle column formation in a stationary ultrasonic field,” *J. Acoust. Soc. Am.* **91**, 79–85.
- WHITWORTH, G., GRUNDY, M.A. and COAKLEY, W.T. (1991). “Transport and harvesting of suspended particles using modulated ultrasound,” *Ultrasonics* **29**, 439–444.
- WHO (1991). World Health Organization. *Congenital Malformations Worldwide. A Report from the International Clearinghouse for Birth Defects Monitoring Systems*, Erickson, J.D., Vollset, S.E. and Peters, P., Eds. (Elsevier, New York).
- WIGHT, P.S. (1995). “Intensifying ultrasound’s acoustic properties with microbubble contrast agents,” *Adv. Admin. Radiol.* **5**, 1–6.
- WILD, J.J. (1950). “The use of ultrasonic pulses for the measurement of biological tissues and the detection of tissue density changes,” *Surgery* **27**, 183–188.
- WILLIAMS, A.R. (1973a). “Viscoelasticity of the human erythrocyte membrane,” *Biorheology* **10**, 313–319.
- WILLIAMS, A.R. (1973b). “A possible alteration in the permeability of ascites cell membranes after exposure to acoustic microstreaming,” *J. Cell Sci.* **12**, 875–885.
- WILLIAMS, A.R. (1982). “Absence of meaningful thresholds for bioeffect studies on cell suspensions *in vitro*,” *Br. J. Cancer (Suppl.)* **45**, 192–195.
- WILLIAMS, A.R. (1983). *Ultrasound: Biological Effects and Potential Hazards* (Academic Press, New York).
- WILLIAMS, A.R. (1985). “Effects of ultrasound on blood and the circulation,” pages 49 to 65 in *Clinics in Diagnostic Ultrasound*, Nyborg, W.L. and Ziskin, M.C., Eds. (Churchill Livingstone, New York).
- WILLIAMS, A.R. and MILLER, D.L. (1980). “Photometric detection of ATP release from human erythrocytes exposed to ultrasonically activated gas-filled pores,” *Ultrasound Med. Biol.* **6**, 251–256.
- WILLIAMS, A.R. and MILLER, D.L. (1989). “The role of non-acoustic factors in the induction and proliferation of cavitation activity *in vitro*,” *Phys. Med. Biol.* **34**, 1561–1569.
- WILLIAMS, A.R., HUGHES, D.E. and NYBORG, W.L. (1970). “Hemolysis near a transversely oscillating wire,” *Science* **169**, 871–873.

- WILLIAMS, A.R., MILLER, D.L. and GROSS, D.R. (1986). "Haemolysis *in vivo* by therapeutic intensities of ultrasound," *Ultrasound Med. Biol.* **12**, 501–509.
- WILLIAMS, A.R., DELIUS, M., MILLER, D.L. and SCHWARZE, W. (1989). "Investigation of cavitation in flowing media by lithotripter shock waves both *in vitro* and *in vivo*," *Ultrasound Med. Biol.* **15**, 53–60.
- WILLIAMS, A.R., KUBOWICZ, G., CRAMER, E. and SCHLIEF, R. (1991). "The effects of the microbubble suspension SH U 454 (Echovist) on ultrasound-induced cell lysis in a rotating tube exposure system," *Echocardiography* **8**, 423–433.
- WILLIAMS, A.R., KUBOWICZ, G. and SCHLIEF, R. (1993). "Gas bubble dynamics in acoustic fields and their biological consequences," pages 113 to 134 in *Advances in Echo Imaging Using Contrast Enhancement*, Nanda, N.C. and Schlief, R., Eds. (Kluwer Academic Publishers, New York).
- WILLIAMS, J.C., WOODWARD, J.F., STONEHILL, M.A., EVAN, A.P. and MCATEER, J.A. (1999). "Cell damage by lithotripter shock waves at high pressure to preclude cavitation," *Ultrasound Med. Biol.* **25**, 1445–1449.
- WILSON, L.S., ROBINSON, D.E., GRIFFITHS, K.A., MANOHARAN, A. and DOUST, B.D. (1987). "Evaluation of ultrasonic attenuation in diffuse diseases of spleen and liver," *Ultrason. Imaging* **9**, 236–247.
- WLADIMIROFF, J.W., CRAFT, I.L. and TALBERT, D.G. (1975). "*In vitro* measurements of sound velocity in human fetal brain tissue," *Ultrasound Med. Biol.* **1**, 377–382.
- WONG, Y.S. and WATMOUGH, D.J. (1983). "Hemolysis of red blood cells *in vitro* and *in vivo* induced by ultrasound at 0.75 MHz and at therapeutic levels," pages 179 to 184 in *Ultrasound Interactions in Biology and Medicine*, Millner, R., Rosenfeld, E. and Cobet, U., Eds. (Plenum Press, New York).
- WOOD, C. and BEARD, R.W. (1964). "Temperature of the human fetus," *J. Obstet. Gynecol.* **71**, 768–769.
- WU, J.R. (1991). "Acoustical tweezers," *J. Acoust. Soc. Am.* **89**, 2140–2143.
- WU, J. (1998). "Temperature rise generated by ultrasound in the presence of contrast agent," *Ultrasound Med. Biol.* **24**, 267–274.
- WU, J. and CUBBERLEY, F. (1997). "Measurement of velocity and attenuation of shear waves in bovine compact bone using ultrasonic spectroscopy," *Ultrasound Med. Biol.* **23**, 129–134.
- WU, J. and DU, G. (1990). "Temperature elevation generated by a focused Gaussian beam of ultrasound," *Ultrasound Med. Biol.* **16**, 489–497.
- WU, J.R. and NYBORO, W.L. (1989). "Experimental frequency spectra of ultrasound transmission through two-dimensional ensembles of trapped microbubbles," *J. Acoust. Soc. Am.* **86**, 2250–2256.
- WU, J. and NYBORO, W.L. (1992). "Temperature rise generated by a focused Gaussian beam in a two-layer medium," *Ultrasound Med. Biol.* **18**, 293–302.
- WU, J., CHASE, J.D., ZHU, Z. and HOLZAPFEL, T.P. (1992). "Temperature rise in a tissue-mimicking material generated by unfocused and focused ultrasonic transducers," *Ultrasound Med. Biol.* **18**, 495–512.

- WU, J., WINKLER, A.J. and O'NEILL, T.P. (1994). "Effect of acoustic streaming on ultrasonic heating," *Ultrasound Med. Biol.* **20**, 195–201.
- WU, J., CUBBERLEY, F., GORMLEY, G. and SZABO, T.L. (1995). "Temperature rise generated by diagnostic ultrasound in a transcranial phantom," *Ultrasound Med. Biol.* **21**, 561–568.
- WU, Y., UNGER, E.C., MCCREERY, T.P., SWEITZER, R.H., SHEN, D., WU, G. and VIELHAUER, M.D. (1998). "Binding and lysing of blood clots using MRX-408," *Invest. Radiol.* **33**, 880–885.
- WULFF, V.J., FRY, W.J., TUCKER, D., FRY, F.J. and MELTON, C. (1951). "Effects of ultrasonic vibrations on nerve tissue," *Proc. Soc. Exp. Biol. Med.* **76**, 361–366.
- YAGITA, Y., ETANI, H., HANDA, N., ITOH, T., IMUTA, N., OKAMOTO, M., MATSUMOTO, M., KINOSHITA, N. and NUKADA, T. (1996). "Effect of transcranial Doppler intensity on successful recording in Japanese patients," *Ultrasound Med. Biol.* **22**, 701–705.
- YANG, W. and LAWSON, M.L. (1974). "Bubble pulsation and cavitation in viscoelastic liquids," *J. Appl. Phys.* **45**, 754–758.
- YAO, L.X., ZAGZEBSKI, J.A. and MADSEN, E.L. (1990). "Backscatter coefficient measurements using a reference phantom to extract depth-dependent instrumentation factors," *Ultrason. Imaging* **12**, 58–70.
- YASU, T., SCHMID-SCHONBEIN, G.W., COTTER, B. and DEMARIA, A.N. (1999). "Flow dynamics of QW7437, a new dodecafluoropentane ultrasound contrast agent, in the microcirculation: Microvascular mechanisms for persistent tissue echo enhancement," *J. Am. Coll. Cardiol.* **34**, 578–586.
- YE, Z. (1996). "On sound scattering and attenuation of Alunex bubbles," *J. Acoust. Soc. Am.* **100**, 2011–2028.
- YOON, H.S. and KATZ, J.L. (1979). "Temperature dependence of the ultrasonic velocities in bone," pages 395 to 398 in *1979 IEEE Ultrasonics Symposium Proceedings*, McAvoy, B.R., Ed. (Institute Electronics and Electrical Engineers, Piscataway, New Jersey).
- YOUNG, F.R. (1989). *Cavitation* (McGraw-Hill, New York).
- YOUNG, S.R. and DYSON, M. (1990). "Macrophage responsiveness to therapeutic ultrasound," *Ultrasound Med. Biol.* **16**, 809–816.
- YUAN, Y.W. and SHUNG, K.K. (1988). "Ultrasonic backscatter from flowing whole blood. I: Dependence on shear rate and hematocrit," *J. Acoust. Soc. Am.* **84**, 52–58.
- YUMITA, N., NISHIGAKI, R., UMEMURA, K. and UMEMURA, S. (1990). "Synergistic effect of ultrasound and hematoporphyrin on sarcoma 180," *Jpn. J. Cancer Res.* **81**, 304–308.
- ZACHARY, J.F. and O'BRIEN, W.D., JR. (1995). "Lung lesions induced by continuous- and pulsed-wave (diagnostic) ultrasound in mice, rabbits and pigs," *Vet. Pathol.* **32**, 43–54.
- ZAGZEBSKI, J.A., BANJAVIC, R.A., MADSEN, E.L. and SCHWABE, M. (1982). "Focused transducer beams in tissue-mimicking material," *J. Clin. Ultrasound* **10**, 159–166.
- ZANA, R. and LANG, J. (1974). "Interaction of ultrasound and amniotic liquid," *Ultrasound Med. Biol.* **1**, 253–258.

- ZHANG, L.J., CHENG, L.M., XU, N., ZHAO, N.M., LI, C.G., YUAN, J. and JIA, S.R. (1991). "Efficient transformation of tobacco by ultrasonication," *Biotechnology* **9**, 996–997.
- ZHU, W.H., MILLER, M.W. and COX, C. (1991). "Lack of increase in cell transformation frequency of C3H cells after exposure to pulsed ultrasound," *Ultrasonics* **29**, 81–84.
- ZILIANI, M., CABELLO, F., CHACON, N.R., RINCON, C.S. and SALAZAR, J.R. (1983). "Fetal scalp temperature during labor and its relation to acid-base balance and condition of the newborn," *Obstet. Gynecol.* **61**, 474–479.
- ZIMMER, J.E., HYNENEN, K., HE, D.S. and MARCUS, F. (1995). "The feasibility of using ultrasound for cardiac ablation," *IEEE Trans. Biomed. Eng.* **42**, 891–897.
- ZIMMER, E.Z., AVRAHAM, Z., SUJOY, P., GOLDSTEIN, I. and BRONSHTEIN, M. (1997). "The influence of prenatal ultrasound on the prevalence of congenital anomalies at birth," *Prenat. Diagn.* **17**, 623–628.
- ZISKIN, M.C. (1972). "Survey of patient exposure to diagnostic ultrasound," pages 203 to 205 in *Workshop on the Interaction of Ultrasound and Biological Tissues*, Reid, J.M. and Sikov, M.R., Eds., U.S. Department of Health, Education and Welfare Publication (FDA) 73–8008 (U.S. Government Printing Office, Washington).
- ZISKIN, M.C., BONAKDARPOUR, A., WEINSTEIN, D.P. and LYNCH, P.R. (1972). "Contrast agents for diagnostic ultrasound," *Invest. Radiol.* **7**, 500–505.

The NCRP

The National Council on Radiation Protection and Measurements is a nonprofit corporation chartered by Congress in 1964 to:

1. Collect, analyze, develop and disseminate in the public interest information and recommendations about (a) protection against radiation and (b) radiation measurements, quantities and units, particularly those concerned with radiation protection.
2. Provide a means by which organizations concerned with the scientific and related aspects of radiation protection and of radiation quantities, units and measurements may cooperate for effective utilization of their combined resources, and to stimulate the work of such organizations.
3. Develop basic concepts about radiation quantities, units and measurements, about the application of these concepts, and about radiation protection.
4. Cooperate with the International Commission on Radiological Protection, the International Commission on Radiation Units and Measurements, and other national and international organizations, governmental and private, concerned with radiation quantities, units and measurements and with radiation protection.

The Council is the successor to the unincorporated association of scientists known as the National Committee on Radiation Protection and Measurements and was formed to carry on the work begun by the Committee in 1929.

The participants in the Council's work are the Council members and members of scientific and administrative committees. Council members are selected solely on the basis of their scientific expertise and serve as individuals, not as representatives of any particular organization. The scientific committees, composed of experts having detailed knowledge and competence in the particular area of the committee's interest, draft proposed recommendations. These are then submitted to the full membership of the Council for careful review and approval before being published.

The following comprise the current officers and membership of the Council:

Officers

President
Vice President
Secretary and Treasurer
Assistant Secretary

Thomas S. Tenforde
Kenneth R. Kase
William M. Beckner
Michael F. McBride

Members

John F. Ahearne	Ethel S. Gilbert	Bruce A. Napier
Larry E. Anderson	Joel E. Gray	Carl J. Paperiello
Benjamin R. Archer	Andrew J. Grosovsky	Ronald C. Petersen
Mary M. Austin-Seymour	Raymond A. Guilmette	R. Julian Preston
Harold L. Beck	William R. Hendee	Jerome S. Puskin
Eleanor A. Blakely	John W. Hirshfeld	Marvin Rosenstein
John D. Boice, Jr.	David G. Hoel	Lawrence N. Rothenberg
Thomas B. Borak	F. Owen Hoffman	Henry D. Royal
André Bouville	Geoffrey R. Howe	Michael T. Ryan
Leslie A. Braby	Kenneth R. Kase	Jonathan M. Samet
Davi J. Brenner	Ann R. Kennedy	Stephen M. Seltzer
Antone L. Brooks	David C. Kocher	Roy E. Shore
Jerrold T. Bushberg	Ritsuko Komaki	Edward A. Sickles
John F. Cardella	Amy Kronenberg	David H. Sliney
Shih-Yew Chen	Charles E. Land	Paul Slovic
Chung-Kwang Chou	Susan M. Langhorst	Daniel J. Strom
Mary E. Clark	Richard W. Leggett	Louise C. Strong
James E. Cleaver	Howard L. Liber	Thomas S. Tenforde
J. Donald Cossairt	James C. Lin	Lawrence W. Townsend
Allen G. Croff	Jill Lipoti	Lois B. Travis
Francis A. Cucinotta	John B. Little	Robert L. Ullrich
Paul M. DeLuca	Jay H. Lubin	Richard J. Vetter
Carter Denniston	C. Douglas Maynard	Daniel Wartenberg
Gail de Planque	Claire M. Mays	David A. Weber
John F. Dicello	Barbara J. McNeil	F. Ward Whicker
Sarah S. Donaldson	Fred A. Mettler, Jr.	Chris G. Whipple
William P. Dornsife	Charles W. Miller	J. Frank Wilson
Stephen A. Feig	Jack Miller	Susan D. Wiltshire
H. Keith Florig	Kenneth L. Miller	Marco Zaidier
Kenneth R. Foster	William F. Morgan	Pasquale Zanonico
John F. Frazier	John E. Moulder	Marvin C. Ziskin
Thomas F. Gesell	David S. Myers	

Honorary Members

Lauriston S. Taylor, *Honorary President*
 Warren K. Sinclair, *President Emeritus*; Charles B. Meinhold, *President Emeritus*
 S. James Adelstein, *Honorary Vice President*
 W. Roger Ney, *Executive Director Emeritus*

Seymour Abrahamson	Patricia W. Durbin	Robert J. Nelsen
Edward L. Alpen	Keith F. Eckerman	Wesley L. Nyborg
Lynn R. Anspaugh	Thomas S. Ely	John W. Poston, Sr.
John A. Auxier	Richard F. Foster	Andrew K. Poznanski
William J. Bair	R.J. Michael Fry	Chester R. Richmond
Bruce B. Boecker	Robert O. Gorson	William L. Russell
Victor P. Bond	Arthur W. Guy	Eugene L. Saenger
Robert L. Brent	Eric J. Hall	William J. Schull
Reynold F. Brown	Naomi H. Harley	J. Newell Stannard
Melvin C. Carter	Donald G. Jacobs	John B. Storer
Randall S. Caswell	Bernd Kahn	John E. Till
Frederick P. Cowan	Roger O. McClellan	Arthur C. Upton
James F. Crow	Dade W. Moeller	George L. Voelz
Gerald D. Dodd	A. Alan Moghissi	Edward W. Webster

Lauriston S. Taylor Lecturers

- Herbert M. Parker (1977) *The Squares of the Natural Numbers in Radiation Protection*
- Sir Edward Pochin (1978) *Why be Quantitative about Radiation Risk Estimates?*
- Hymer L. Friedell (1979) *Radiation Protection—Concepts and Trade Offs*
- Harold O. Wyckoff (1980) *From “Quantity of Radiation” and “Dose” to “Exposure” and “Absorbed Dose”—An Historical Review*
- James F. Crow (1981) *How Well Can We Assess Genetic Risk? Not Very*
- Eugene L. Saenger (1982) *Ethics, Trade-offs and Medical Radiation*
- Merril Eisenbud (1983) *The Human Environment—Past, Present and Future*
- Harald H. Rossi (1984) *Limitation and Assessment in Radiation Protection*
- John H. Harley (1985) *Truth (and Beauty) in Radiation Measurement*
- Herman P. Schwan (1986) *Biological Effects of Non-ionizing Radiations: Cellular Properties and Interactions*
- Seymour Jablon (1987) *How to be Quantitative about Radiation Risk Estimates*
- Bo Lindell (1988) *How Safe is Safe Enough?*
- Arthur C. Upton (1989) *Radiobiology and Radiation Protection: The Past Century and Prospects for the Future*
- J. Newell Stannard (1990) *Radiation Protection and the Internal Emitter Saga*
- Victor P. Bond (1991) *When is a Dose Not a Dose?*
- Edward W. Webster (1992) *Dose and Risk in Diagnostic Radiology: How Big? How Little?*
- Warren K. Sinclair (1993) *Science, Radiation Protection and the NCRP*
- R.J. Michael Fry (1994) *Mice, Myths and Men*
- Albrecht Kellerer (1995) *Certainty and Uncertainty in Radiation Protection*
- Seymour Abrahamson (1996) *70 Years of Radiation Genetics: Fruit Flies, Mice and Humans*
- William J. Bair (1997) *Radionuclides in the Body: Meeting the Challenge!*
- Eric J. Hall (1998) *From Chimney Sweeps to Astronauts: Cancer Risks in the Workplace*
- Naomi H. Harley (1999) *Back to Background*
- S. James Adelstein (2000) *Administered Radioactivity: Unde Venimus Quoquo Imus*
- Wesley L. Nyborg (2001) *Assuring the Safety of Medical Diagnostic Ultrasound*
- R. Julian Preston (2002) *Developing Mechanistic Data for Incorporation into Cancer Risk Assessment: Old Problems and New Approaches*

Currently, the following committees are actively engaged in formulating recommendations:

- SC 1 Basic Criteria, Epidemiology, Radiobiology and Risk
- SC 1-4 Extrapolation of Risks from Non-Human Experimental Systems to Man
- SC 1-7 Information Needed to Make Radiation Protection Recommendations for Travel Beyond Low-Earth Orbit
- SC 1-8 Risk to Thyroid from Ionizing Radiation
- SC 1-10 Review of Cohen’s Radon Research Methods
- SC 1-11 Radiation Protection and Measurement for Neutron Surveillance Scanners

- SC 9 SC 1-12 Exposure Limits for Security Surveillance Devices
Structural Shielding Design and Evaluation for Medical Use of
X Rays and Gamma Rays of Energies Up to 10 MeV
- SC 46 Operational Radiation Safety
 - SC 46-8 Radiation Protection Design Guidelines for Particle
Accelerator Facilities
 - SC 46-13 Design of Facilities for Medical Radiation Therapy
 - SC 46-16 Radiation Protection in Veterinary Medicine
 - SC 46-17 Radiation Protection in Educational Institutions
 - SC 57-15 Uranium Risk
 - SC 57-17 Radionuclide Dosimetry Models for Wounds
- SC 64 Environmental Issues
 - SC 64-22 Design of Effective Effluent and Environmental
Monitoring Programs
 - SC 64-23 Cesium in the Environment
- SC 66 Biological Effects and Exposure Criteria for Ultrasound
- SC 72 Radiation Protection in Mammography
- SC 85 Risk of Lung Cancer from Radon
- SC 87 Radioactive and Mixed Waste
 - SC 87-1 Waste Avoidance and Volume Reduction
 - SC 87-3 Performance Assessment
 - SC 87-5 Risk Management Analysis for Decommissioned Sites
- SC 89 Nonionizing Electromagnetic Fields
 - SC 89-3 Biological Effects of Extremely Low-Frequency Electric
and Magnetic Fields
 - SC 89-4 Biological Effects and Exposure Recommendations for
Modulated Radiofrequency Fields
 - SC 89-5 Biological Effects and Exposure Criteria for
Radiofrequency Electromagnetic Fields
 - SC 89-6 Wireless Telecommunications Safety Issues for Building
Owners and Managers
- SC 91 Radiation Protection in Medicine
 - SC 91-1 Precautions in the Management of Patients Who Have
Received Therapeutic Amounts of Radionuclides
 - SC 91-2 Radiation Protection in Dentistry
- SC 92 Public Policy and Risk Communication
- SC 93 Radiation Measurement and Dosimetry

In recognition of its responsibility to facilitate and stimulate cooperation among organizations concerned with the scientific and related aspects of radiation protection and measurement, the Council has created a category of NCRP Collaborating Organizations. Organizations or groups of organizations that are national or international in scope and are concerned with scientific problems involving radiation quantities, units, measurements and

effects, or radiation protection may be admitted to collaborating status by the Council. Collaborating Organizations provide a means by which the NCRP can gain input into its activities from a wider segment of society. At the same time, the relationships with the Collaborating Organizations facilitate wider dissemination of information about the Council's activities, interests and concerns. Collaborating Organizations have the opportunity to comment on draft reports (at the time that these are submitted to the members of the Council). This is intended to capitalize on the fact that Collaborating Organizations are in an excellent position to both contribute to the identification of what needs to be treated in NCRP reports and to identify problems that might result from proposed recommendations. The present Collaborating Organizations with which the NCRP maintains liaison are as follows:

Agency for Toxic Substances and Disease Registry
 American Academy of Dermatology
 American Academy of Environmental Engineers
 American Academy of Health Physics
 American Association of Physicists in Medicine
 American College of Medical Physics
 American College of Nuclear Physicians
 American College of Occupational and Environmental Medicine
 American College of Radiology
 American Dental Association
 American Industrial Hygiene Association
 American Institute of Ultrasound in Medicine
 American Insurance Services Group
 American Medical Association
 American Nuclear Society
 American Pharmaceutical Association
 American Podiatric Medical Association
 American Public Health Association
 American Radium Society
 American Roentgen Ray Society
 American Society for Therapeutic Radiology and Oncology
 American Society of Health-System Pharmacists
 American Society of Radiologic Technologists
 Association of University Radiologists
 Bioelectromagnetics Society
 Campus Radiation Safety Officers
 College of American Pathologists
 Conference of Radiation Control Program Directors, Inc.
 Council on Radionuclides and Radiopharmaceuticals
 Defense Threat Reduction Agency
 Electric Power Research Institute
 Federal Communications Commission
 Federal Emergency Management Agency
 Genetics Society of America

Health Physics Society
 Institute of Electrical and Electronics Engineers, Inc.
 Institute of Nuclear Power Operations
 International Brotherhood of Electrical Workers
 National Aeronautics and Space Administration
 National Association of Environmental Professionals
 National Electrical Manufacturers Association
 National Institute for Occupational Safety and Health
 National Institute of Standards and Technology
 Nuclear Energy Institute
 Office of Science and Technology Policy
 Oil, Chemical and Atomic Workers
 Radiation Research Society
 Radiological Society of North America
 Society for Risk Analysis
 Society of Chairmen of Academic Radiology Departments
 Society of Nuclear Medicine
 Society of Skeletal Radiology
 U.S. Air Force
 U.S. Army
 U.S. Coast Guard
 U.S. Department of Energy
 U.S. Department of Housing and Urban Development
 U.S. Department of Labor
 U.S. Department of Transportation
 U.S. Environmental Protection Agency
 U.S. Navy
 U.S. Nuclear Regulatory Commission
 U.S. Public Health Service
 Utility Workers Union of America

The NCRP has found its relationships with these organizations to be extremely valuable to continued progress in its program.

Another aspect of the cooperative efforts of the NCRP relates to the Special Liaison relationships established with various governmental organizations that have an interest in radiation protection and measurements. This liaison relationship provides: (1) an opportunity for participating organizations to designate an individual to provide liaison between the organization and the NCRP; (2) that the individual designated will receive copies of draft NCRP reports (at the time that these are submitted to the members of the Council) with an invitation to comment, but not vote; and (3) that new NCRP efforts might be discussed with liaison individuals as appropriate, so that they might have an opportunity to make suggestions on new studies and related matters. The following organizations participate in the Special Liaison Program:

Australian Radiation Laboratory
 Bundesamt für Strahlenschutz (Germany)

Canadian Nuclear Safety Commission
 Central Laboratory for Radiological Protection (Poland)
 China Institute for Radiation Protection
 Commissariat à l'Énergie Atomique
 Commonwealth Scientific Instrumentation Research Organization
 (Australia)
 European Commission
 Health Council of the Netherlands
 International Commission on Non-Ionizing Radiation Protection
 Japan Radiation Council
 Korea Institute of Nuclear Safety
 National Radiological Protection Board (United Kingdom)
 Russian Scientific Commission on Radiation Protection
 South African Forum for Radiation Protection
 World Association of Nuclear Operations

The NCRP values highly the participation of these organizations in the Special Liaison Program.

The Council also benefits significantly from the relationships established pursuant to the Corporate Sponsor's Program. The program facilitates the interchange of information and ideas and corporate sponsors provide valuable fiscal support for the Council's program. This developing program currently includes the following Corporate Sponsors:

3M Corporate Health Physics
 Amersham Health
 Duke Energy Corporation
 ICN Biomedicals, Inc.
 Landauer, Inc.
 Nuclear Energy Institute
 Philips Medical Systems
 Southern California Edison

The Council's activities are made possible by the voluntary contribution of time and effort by its members and participants and the generous support of the following organizations:

3M Health Physics Services
 Agfa Corporation
 Alfred P. Sloan Foundation
 Alliance of American Insurers
 American Academy of Dermatology
 American Academy of Health Physics
 American Academy of Oral and Maxillofacial Radiology
 American Association of Physicists in Medicine
 American Cancer Society
 American College of Medical Physics
 American College of Nuclear Physicians
 American College of Occupational and Environmental Medicine

American College of Radiology
American College of Radiology Foundation
American Dental Association
American Healthcare Radiology Administrators
American Industrial Hygiene Association
American Insurance Services Group
American Medical Association
American Nuclear Society
American Osteopathic College of Radiology
American Podiatric Medical Association
American Public Health Association
American Radium Society
American Roentgen Ray Society
American Society of Radiologic Technologists
American Society for Therapeutic Radiology and Oncology
American Veterinary Medical Association
American Veterinary Radiology Society
Association of University Radiologists
Battelle Memorial Institute
Canberra Industries, Inc.
Chem Nuclear Systems
Center for Devices and Radiological Health
College of American Pathologists
Committee on Interagency Radiation Research and Policy
Coordination
Commonwealth Edison
Commonwealth of Pennsylvania
Consolidated Edison
Consumers Power Company
Council on Radionuclides and Radiopharmaceuticals
Defense Nuclear Agency
Eastman Kodak Company
Edison Electric Institute
Edward Mallinckrodt, Jr. Foundation
EG&G Idaho, Inc.
Electric Power Research Institute
Electromagnetic Energy Association
Federal Emergency Management Agency
Florida Institute of Phosphate Research
Florida Power Corporation
Fuji Medical Systems, U.S.A., Inc.
Genetics Society of America
Health Effects Research Foundation (Japan)
Health Physics Society
Institute of Nuclear Power Operations
James Picker Foundation
Martin Marietta Corporation
Motorola Foundation

National Aeronautics and Space Administration
National Association of Photographic Manufacturers
National Cancer Institute
National Electrical Manufacturers Association
National Institute of Standards and Technology
Picker International
Public Service Electric and Gas Company
Radiation Research Society
Radiological Society of North America
Richard Lounsbury Foundation
Sandia National Laboratory
Siemens Medical Systems, Inc.
Society of Nuclear Medicine
Society of Pediatric Radiology
U.S. Department of Energy
U.S. Department of Labor
U.S. Environmental Protection Agency
U.S. Navy
U.S. Nuclear Regulatory Commission
Victoreen, Inc.
Westinghouse Electric Corporation

Initial funds for publication of NCRP reports were provided by a grant from the James Picker Foundation.

The NCRP seeks to promulgate information and recommendations based on leading scientific judgment on matters of radiation protection and measurement and to foster cooperation among organizations concerned with these matters. These efforts are intended to serve the public interest and the Council welcomes comments and suggestions on its reports or activities from those interested in its work.

NCRP Publications

Information on NCRP publications may be obtained from the NCRP website (<http://www.ncrp.com>), e-mail (ncrppubs@ncrp.com), by telephone (800-229-2652, Ext. 25), or fax (301-907-8768). The address is:

NCRP Publications
7910 Woodmont Avenue
Suite 400
Bethesda, MD 20814-3095

Abstracts of NCRP reports published since 1980, abstracts of all NCRP commentaries, and the text of all NCRP statements are available at the NCRP website. Currently available publications are listed below.

NCRP Reports

No.	Title
8	<i>Control and Removal of Radioactive Contamination in Laboratories</i> (1951)
22	<i>Maximum Permissible Body Burdens and Maximum Permissible Concentrations of Radionuclides in Air and in Water for Occupational Exposure</i> (1959) [Includes Addendum 1 issued in August 1963]
25	<i>Measurement of Absorbed Dose of Neutrons, and of Mixtures of Neutrons and Gamma Rays</i> (1961)
27	<i>Stopping Powers for Use with Cavity Chambers</i> (1961)
30	<i>Safe Handling of Radioactive Materials</i> (1964)
32	<i>Radiation Protection in Educational Institutions</i> (1966)
35	<i>Dental X-Ray Protection</i> (1970)
36	<i>Radiation Protection in Veterinary Medicine</i> (1970)
37	<i>Precautions in the Management of Patients Who Have Received Therapeutic Amounts of Radionuclides</i> (1970)
38	<i>Protection Against Neutron Radiation</i> (1971)
40	<i>Protection Against Radiation from Brachytherapy Sources</i> (1972)
41	<i>Specification of Gamma-Ray Brachytherapy Sources</i> (1974)
42	<i>Radiological Factors Affecting Decision-Making in a Nuclear Attack</i> (1974)

- 44 *Krypton-85 in the Atmosphere—Accumulation, Biological Significance, and Control Technology* (1975)
- 46 *Alpha-Emitting Particles in Lungs* (1975)
- 47 *Tritium Measurement Techniques* (1976)
- 49 *Structural Shielding Design and Evaluation for Medical Use of X Rays and Gamma Rays of Energies Up to 10 MeV* (1976)
- 50 *Environmental Radiation Measurements* (1976)
- 52 *Cesium-137 from the Environment to Man: Metabolism and Dose* (1977)
- 54 *Medical Radiation Exposure of Pregnant and Potentially Pregnant Women* (1977)
- 55 *Protection of the Thyroid Gland in the Event of Releases of Radioiodine* (1977)
- 57 *Instrumentation and Monitoring Methods for Radiation Protection* (1978)
- 58 *A Handbook of Radioactivity Measurements Procedures*, 2nd ed. (1985)
- 60 *Physical, Chemical, and Biological Properties of Radiocerium Relevant to Radiation Protection Guidelines* (1978)
- 61 *Radiation Safety Training Criteria for Industrial Radiography* (1978)
- 62 *Tritium in the Environment* (1979)
- 63 *Tritium and Other Radionuclide Labeled Organic Compounds Incorporated in Genetic Material* (1979)
- 64 *Influence of Dose and Its Distribution in Time on Dose-Response Relationships for Low-LET Radiations* (1980)
- 65 *Management of Persons Accidentally Contaminated with Radionuclides* (1980)
- 67 *Radiofrequency Electromagnetic Fields—Properties, Quantities and Units, Biophysical Interaction, and Measurements* (1981)
- 68 *Radiation Protection in Pediatric Radiology* (1981)
- 69 *Dosimetry of X-Ray and Gamma-Ray Beams for Radiation Therapy in the Energy Range 10 keV to 50 MeV* (1981)
- 70 *Nuclear Medicine—Factors Influencing the Choice and Use of Radionuclides in Diagnosis and Therapy* (1982)
- 72 *Radiation Protection and Measurement for Low-Voltage Neutron Generators* (1983)
- 73 *Protection in Nuclear Medicine and Ultrasound Diagnostic Procedures in Children* (1983)
- 74 *Biological Effects of Ultrasound: Mechanisms and Clinical Implications* (1983)
- 75 *Iodine-129: Evaluation of Releases from Nuclear Power Generation* (1983)
- 77 *Exposures from the Uranium Series with Emphasis on Radon and Its Daughters* (1984)
- 78 *Evaluation of Occupational and Environmental Exposures to Radon and Radon Daughters in the United States* (1984)

- 79 *Neutron Contamination from Medical Electron Accelerators* (1984)
- 80 *Induction of Thyroid Cancer by Ionizing Radiation* (1985)
- 81 *Carbon-14 in the Environment* (1985)
- 82 *SI Units in Radiation Protection and Measurements* (1985)
- 83 *The Experimental Basis for Absorbed-Dose Calculations in Medical Uses of Radionuclides* (1985)
- 84 *General Concepts for the Dosimetry of Internally Deposited Radionuclides* (1985)
- 85 *Mammography—A User's Guide* (1986)
- 86 *Biological Effects and Exposure Criteria for Radiofrequency Electromagnetic Fields* (1986)
- 87 *Use of Bioassay Procedures for Assessment of Internal Radionuclide Deposition* (1987)
- 88 *Radiation Alarms and Access Control Systems* (1986)
- 89 *Genetic Effects from Internally Deposited Radionuclides* (1987)
- 90 *Neptunium: Radiation Protection Guidelines* (1988)
- 92 *Public Radiation Exposure from Nuclear Power Generation in the United States* (1987)
- 93 *Ionizing Radiation Exposure of the Population of the United States* (1987)
- 94 *Exposure of the Population in the United States and Canada from Natural Background Radiation* (1987)
- 95 *Radiation Exposure of the U.S. Population from Consumer Products and Miscellaneous Sources* (1987)
- 96 *Comparative Carcinogenicity of Ionizing Radiation and Chemicals* (1989)
- 97 *Measurement of Radon and Radon Daughters in Air* (1988)
- 99 *Quality Assurance for Diagnostic Imaging* (1988)
- 100 *Exposure of the U.S. Population from Diagnostic Medical Radiation* (1989)
- 101 *Exposure of the U.S. Population from Occupational Radiation* (1989)
- 102 *Medical X-Ray, Electron Beam and Gamma-Ray Protection for Energies Up to 50 MeV (Equipment Design, Performance and Use)* (1989)
- 103 *Control of Radon in Houses* (1989)
- 104 *The Relative Biological Effectiveness of Radiations of Different Quality* (1990)
- 105 *Radiation Protection for Medical and Allied Health Personnel* (1989)
- 106 *Limit for Exposure to "Hot Particles" on the Skin* (1989)
- 107 *Implementation of the Principle of As Low As Reasonably Achievable (ALARA) for Medical and Dental Personnel* (1990)
- 108 *Conceptual Basis for Calculations of Absorbed-Dose Distributions* (1991)
- 109 *Effects of Ionizing Radiation on Aquatic Organisms* (1991)
- 110 *Some Aspects of Strontium Radiobiology* (1991)

- 111 *Developing Radiation Emergency Plans for Academic, Medical or Industrial Facilities* (1991)
- 112 *Calibration of Survey Instruments Used in Radiation Protection for the Assessment of Ionizing Radiation Fields and Radioactive Surface Contamination* (1991)
- 113 *Exposure Criteria for Medical Diagnostic Ultrasound: I. Criteria Based on Thermal Mechanisms* (1992)
- 114 *Maintaining Radiation Protection Records* (1992)
- 115 *Risk Estimates for Radiation Protection* (1993)
- 116 *Limitation of Exposure to Ionizing Radiation* (1993)
- 117 *Research Needs for Radiation Protection* (1993)
- 118 *Radiation Protection in the Mineral Extraction Industry* (1993)
- 119 *A Practical Guide to the Determination of Human Exposure to Radiofrequency Fields* (1993)
- 120 *Dose Control at Nuclear Power Plants* (1994)
- 121 *Principles and Application of Collective Dose in Radiation Protection* (1995)
- 122 *Use of Personal Monitors to Estimate Effective Dose Equivalent and Effective Dose to Workers for External Exposure to Low-LET Radiation* (1995)
- 123 *Screening Models for Releases of Radionuclides to Atmosphere, Surface Water, and Ground* (1996)
- 124 *Sources and Magnitude of Occupational and Public Exposures from Nuclear Medicine Procedures* (1996)
- 125 *Deposition, Retention and Dosimetry of Inhaled Radioactive Substances* (1997)
- 126 *Uncertainties in Fatal Cancer Risk Estimates Used in Radiation Protection* (1997)
- 127 *Operational Radiation Safety Program* (1998)
- 128 *Radionuclide Exposure of the Embryo/Fetus* (1998)
- 129 *Recommended Screening Limits for Contaminated Surface Soil and Review of Factors Relevant to Site-Specific Studies* (1999)
- 130 *Biological Effects and Exposure Limits for "Hot Particles"* (1999)
- 131 *Scientific Basis for Evaluating the Risks to Populations from Space Applications of Plutonium* (2001)
- 132 *Radiation Protection Guidance for Activities in Low-Earth Orbit* (2000)
- 133 *Radiation Protection for Procedures Performed Outside the Radiology Department* (2000)
- 134 *Operational Radiation Safety Training* (2000)
- 135 *Liver Cancer Risk from Internally-Deposited Radionuclides* (2001)
- 136 *Evaluation of the Linear-Nonthreshold Dose-Response Model for Ionizing Radiation* (2001)
- 137 *Fluence-Based and Microdosimetric Event-Based Methods for Radiation Protection in Space* (2001)
- 138 *Management of Terrorist Events Involving Radioactive Material* (2001)
- 139 *Risk-Based Classification of Radioactive and Hazardous Chemical Wastes* (2002)
- 140 *Exposure Criteria for Medical Diagnostic Ultrasound: II. Criteria Based on All Known Mechanisms* (2002)
- 141 *Managing Potentially Radioactive Scrap Metal* (2002)
- 142 *Operational Radiation Safety Program for Astronauts in Low-Earth Orbit: A Basic Framework* (2002)

Binders for NCRP reports are available. Two sizes make it possible to collect into small binders the "old series" of reports (NCRP Reports Nos. 8-30) and into large binders the more recent publications (NCRP Reports Nos. 32-142). Each binder will accommodate from five to seven reports. The binders carry the identification "NCRP Reports" and come with label holders which permit the user to attach labels showing the reports contained in each binder.

The following bound sets of NCRP reports are also available:

- Volume I. NCRP Reports Nos. 8, 22
- Volume II. NCRP Reports Nos. 23, 25, 27, 30
- Volume III. NCRP Reports Nos. 32, 35, 36, 37
- Volume IV. NCRP Reports Nos. 38, 40, 41
- Volume V. NCRP Reports Nos. 42, 44, 46
- Volume VI. NCRP Reports Nos. 47, 49, 50, 51
- Volume VII. NCRP Reports Nos. 52, 53, 54, 55, 57
- Volume VIII. NCRP Report No. 58
- Volume IX. NCRP Reports Nos. 59, 60, 61, 62, 63
- Volume X. NCRP Reports Nos. 64, 65, 66, 67
- Volume XI. NCRP Reports Nos. 68, 69, 70, 71, 72
- Volume XII. NCRP Reports Nos. 73, 74, 75, 76
- Volume XIII. NCRP Reports Nos. 77, 78, 79, 80
- Volume XIV. NCRP Reports Nos. 81, 82, 83, 84, 85
- Volume XV. NCRP Reports Nos. 86, 87, 88, 89
- Volume XVI. NCRP Reports Nos. 90, 91, 92, 93
- Volume XVII. NCRP Reports Nos. 94, 95, 96, 97
- Volume XVIII. NCRP Reports Nos. 98, 99, 100
- Volume XIX. NCRP Reports Nos. 101, 102, 103, 104
- Volume XX. NCRP Reports Nos. 105, 106, 107, 108
- Volume XXI. NCRP Reports Nos. 109, 110, 111
- Volume XXII. NCRP Reports Nos. 112, 113, 114
- Volume XXIII. NCRP Reports Nos. 115, 116, 117, 118
- Volume XXIV. NCRP Reports Nos. 119, 120, 121, 122
- Volume XXV. NCRP Report No. 123I and 123II
- Volume XXVI. NCRP Reports Nos. 124, 125, 126, 127
- Volume XXVII. NCRP Reports Nos. 128, 129, 130
- Volume XXVIII. NCRP Reports Nos. 131, 132, 133
- Volume XXIX. NCRP Reports Nos. 134, 135, 136, 137

(Titles of the individual reports contained in each volume are given above.)

NCRP Commentaries

No.	Title
1	<i>Krypton-85 in the Atmosphere—With Specific Reference to the Public Health Significance of the Proposed Controlled Release at Three Mile Island</i> (1980)
4	<i>Guidelines for the Release of Waste Water from Nuclear Facilities with Special Reference to the Public Health Significance of the Proposed Release of Treated Waste Waters at Three Mile Island</i> (1987)
5	<i>Review of the Publication, Living Without Landfills</i> (1989)
6	<i>Radon Exposure of the U.S. Population—Status of the Problem</i> (1991)
7	<i>Misadministration of Radioactive Material in Medicine—Scientific Background</i> (1991)
8	<i>Uncertainty in NCRP Screening Models Relating to Atmospheric Transport, Deposition and Uptake by Humans</i> (1993)
9	<i>Considerations Regarding the Unintended Radiation Exposure of the Embryo, Fetus or Nursing Child</i> (1994)
10	<i>Advising the Public about Radiation Emergencies: A Document for Public Comment</i> (1994)
11	<i>Dose Limits for Individuals Who Receive Exposure from Radionuclide Therapy Patients</i> (1995)
12	<i>Radiation Exposure and High-Altitude Flight</i> (1995)
13	<i>An Introduction to Efficacy in Diagnostic Radiology and Nuclear Medicine (Justification of Medical Radiation Exposure)</i> (1995)
14	<i>A Guide for Uncertainty Analysis in Dose and Risk Assessments Related to Environmental Contamination</i> (1996)
15	<i>Evaluating the Reliability of Biokinetic and Dosimetric Models and Parameters Used to Assess Individual Doses for Risk Assessment Purposes</i> (1998)

Proceedings of the Annual Meeting

No.	Title
1	<i>Perceptions of Risk</i> , Proceedings of the Fifteenth Annual Meeting held on March 14-15, 1979 (including Taylor Lecture No. 3) (1980)
3	<i>Critical Issues in Setting Radiation Dose Limits</i> , Proceedings of the Seventeenth Annual Meeting held on April 8-9, 1981 (including Taylor Lecture No. 5) (1982)
4	<i>Radiation Protection and New Medical Diagnostic Approaches</i> , Proceedings of the Eighteenth Annual Meeting held on April 6-7, 1982 (including Taylor Lecture No. 6) (1983)

- 5 *Environmental Radioactivity*, Proceedings of the Nineteenth Annual Meeting held on April 6-7, 1983 (including Taylor Lecture No. 7) (1983)
- 6 *Some Issues Important in Developing Basic Radiation Protection Recommendations*, Proceedings of the Twentieth Annual Meeting held on April 4-5, 1984 (including Taylor Lecture No. 8) (1985)
- 7 *Radioactive Waste*, Proceedings of the Twenty-first Annual Meeting held on April 3-4, 1985 (including Taylor Lecture No. 9) (1986)
- 8 *Nonionizing Electromagnetic Radiations and Ultrasound*, Proceedings of the Twenty-second Annual Meeting held on April 2-3, 1986 (including Taylor Lecture No. 10) (1988)
- 9 *New Dosimetry at Hiroshima and Nagasaki and Its Implications for Risk Estimates*, Proceedings of the Twenty-third Annual Meeting held on April 8-9, 1987 (including Taylor Lecture No. 11) (1988)
- 10 *Radon*, Proceedings of the Twenty-fourth Annual Meeting held on March 30-31, 1988 (including Taylor Lecture No. 12) (1989)
- 11 *Radiation Protection Today—The NCRP at Sixty Years*, Proceedings of the Twenty-fifth Annual Meeting held on April 5-6, 1989 (including Taylor Lecture No. 13) (1990)
- 12 *Health and Ecological Implications of Radioactively Contaminated Environments*, Proceedings of the Twenty-sixth Annual Meeting held on April 4-5, 1990 (including Taylor Lecture No. 14) (1991)
- 13 *Genes, Cancer and Radiation Protection*, Proceedings of the Twenty-seventh Annual Meeting held on April 3-4, 1991 (including Taylor Lecture No. 15) (1992)
- 14 *Radiation Protection in Medicine*, Proceedings of the Twenty-eighth Annual Meeting held on April 1-2, 1992 (including Taylor Lecture No. 16) (1993)
- 15 *Radiation Science and Societal Decision Making*, Proceedings of the Twenty-ninth Annual Meeting held on April 7-8, 1993 (including Taylor Lecture No. 17) (1994)
- 16 *Extremely-Low-Frequency Electromagnetic Fields: Issues in Biological Effects and Public Health*, Proceedings of the Thirtieth Annual Meeting held on April 6-7, 1994 (not published).
- 17 *Environmental Dose Reconstruction and Risk Implications*, Proceedings of the Thirty-first Annual Meeting held on April 12-13, 1995 (including Taylor Lecture No. 19) (1996)
- 18 *Implications of New Data on Radiation Cancer Risk*, Proceedings of the Thirty-second Annual Meeting held on April 3-4, 1996 (including Taylor Lecture No. 20) (1997)
- 19 *The Effects of Pre- and Postconception Exposure to Radiation*, Proceedings of the Thirty-third Annual Meeting held on April 2-3, 1997, *Teratology* **59**, 181–317 (1999)

- 20 *Cosmic Radiation Exposure of Airline Crews, Passengers and Astronauts*, Proceedings of the Thirty-fourth Annual Meeting held on April 1-2, 1998, Health Phys. **79**, 466–613 (2000)
- 21 *Radiation Protection in Medicine: Contemporary Issues*, Proceedings of the Thirty-fifth Annual Meeting held on April 7-8, 1999 (including Taylor Lecture No. 23) (1999)
- 22 *Ionizing Radiation Science and Protection in the 21st Century*, Proceedings of the Thirty-sixth Annual Meeting held on April 5-6, 2000, Health Phys. **80**, 317–402 (2001)
- 23 *Fallout from Atmospheric Nuclear Tests—Impact on Science and Society*, Proceedings of the Thirty-seventh Annual Meeting held on April 4-5, 2001, Health Phys. **82**, 573–748 (2002)

Lauriston S. Taylor Lectures

- | No. | Title |
|-----|--|
| 1 | <i>The Squares of the Natural Numbers in Radiation Protection</i> by Herbert M. Parker (1977) |
| 2 | <i>Why be Quantitative about Radiation Risk Estimates?</i> by Sir Edward Pochin (1978) |
| 3 | <i>Radiation Protection—Concepts and Trade Offs</i> by Hymer L. Friedell (1979) [Available also in <i>Perceptions of Risk</i> , see above] |
| 4 | <i>From “Quantity of Radiation” and “Dose” to “Exposure” and “Absorbed Dose”—An Historical Review</i> by Harold O. Wyckoff (1980) |
| 5 | <i>How Well Can We Assess Genetic Risk? Not Very</i> by James F. Crow (1981) [Available also in <i>Critical Issues in Setting Radiation Dose Limits</i> , see above] |
| 6 | <i>Ethics, Trade-offs and Medical Radiation</i> by Eugene L. Saenger (1982) [Available also in <i>Radiation Protection and New Medical Diagnostic Approaches</i> , see above] |
| 7 | <i>The Human Environment—Past, Present and Future</i> by Merrill Eisenbud (1983) [Available also in <i>Environmental Radioactivity</i> , see above] |
| 8 | <i>Limitation and Assessment in Radiation Protection</i> by Harald H. Rossi (1984) [Available also in <i>Some Issues Important in Developing Basic Radiation Protection Recommendations</i> , see above] |
| 9 | <i>Truth (and Beauty) in Radiation Measurement</i> by John H. Harley (1985) [Available also in <i>Radioactive Waste</i> , see above] |
| 10 | <i>Biological Effects of Non-ionizing Radiations: Cellular Properties and Interactions</i> by Herman P. Schwan (1987) [Available also in <i>Nonionizing Electromagnetic Radiations and Ultrasound</i> , see above] |

- 11 *How to be Quantitative about Radiation Risk Estimates* by Seymour Jablon (1988) [Available also in *New Dosimetry at Hiroshima and Nagasaki and its Implications for Risk Estimates*, see above]
- 12 *How Safe is Safe Enough?* by Bo Lindell (1988) [Available also in *Radon*, see above]
- 13 *Radiobiology and Radiation Protection: The Past Century and Prospects for the Future* by Arthur C. Upton (1989) [Available also in *Radiation Protection Today*, see above]
- 14 *Radiation Protection and the Internal Emitter Saga* by J. Newell Stannard (1990) [Available also in *Health and Ecological Implications of Radioactively Contaminated Environments*, see above]
- 15 *When is a Dose Not a Dose?* by Victor P. Bond (1992) [Available also in *Genes, Cancer and Radiation Protection*, see above]
- 16 *Dose and Risk in Diagnostic Radiology: How Big? How Little?* by Edward W. Webster (1992) [Available also in *Radiation Protection in Medicine*, see above]
- 17 *Science, Radiation Protection and the NCRP* by Warren K. Sinclair (1993) [Available also in *Radiation Science and Societal Decision Making*, see above]
- 18 *Mice, Myths and Men* by R.J. Michael Fry (1995)
- 19 *Certainty and Uncertainty in Radiation Research* by Albrecht M. Kellerer. *Health Phys.* **69**, 446–453 (1995).
- 20 *70 Years of Radiation Genetics: Fruit Flies, Mice and Humans* by Seymour Abrahamson. *Health Phys.* **71**, 624–633 (1996).
- 21 *Radionuclides in the Body: Meeting the Challenge* by William J. Bair. *Health Phys.* **73**, 423–432 (1997).
- 22 *From Chimney Sweeps to Astronauts: Cancer Risks in the Work Place* by Eric J. Hall. *Health Phys.* **75**, 357–366 (1998).
- 23 *Back to Background: Natural Radiation and Radioactivity Exposed* by Naomi H. Harley. *Health Phys.* **79**, 121–128 (2000).
- 24 *Administered Radioactivity: Unde Venimus Quoque Imus* by S. James Adelstein. *Health Phys.* **80**, 317–324 (2001).
- 25 *Assuring the Safety of Medical Diagnostic Ultrasound* by Wesley L. Nyborg. *Health Phys.* **82**, 578–587 (2002)

Symposium Proceedings

No.	Title
1	<i>The Control of Exposure of the Public to Ionizing Radiation in the Event of Accident or Attack</i> , Proceedings of a Symposium held April 27-29, 1981 (1982)
2	<i>Radioactive and Mixed Waste—Risk as a Basis for Waste Classification</i> , Proceedings of a Symposium held November 9, 1994 (1995)

- 3 *Acceptability of Risk from Radiation—Application to Human Space Flight*, Proceedings of a Symposium held May 29, 1996 (1997)
- 4 *21st Century Biodosimetry: Quantifying the Past and Predicting the Future*, Proceedings of a Symposium held on February 22, 2001, *Radiat. Prot. Dosim.* **97**, No. 1, 7–80 (2001)

NCRP Statements

No.	Title
1	“Blood Counts, Statement of the National Committee on Radiation Protection,” <i>Radiology</i> 63 , 428 (1954)
2	“Statements on Maximum Permissible Dose from Television Receivers and Maximum Permissible Dose to the Skin of the Whole Body,” <i>Am. J. Roentgenol., Radium Ther. and Nucl. Med.</i> 84 , 152 (1960) and <i>Radiology</i> 75 , 122 (1960)
3	<i>X-Ray Protection Standards for Home Television Receivers, Interim Statement of the National Council on Radiation Protection and Measurements</i> (1968)
4	<i>Specification of Units of Natural Uranium and Natural Thorium, Statement of the National Council on Radiation Protection and Measurements</i> (1973)
5	<i>NCRP Statement on Dose Limit for Neutrons</i> (1980)
6	<i>Control of Air Emissions of Radionuclides</i> (1984)
7	<i>The Probability That a Particular Malignancy May Have Been Caused by a Specified Irradiation</i> (1992)
8	<i>The Application of ALARA for Occupational Exposures</i> (1999)
9	<i>Extension of the Skin Dose Limit for Hot Particles to Other External Sources of Skin Irradiation</i> (2001)

Other Documents

The following documents of the NCRP were published outside of the NCRP report, commentary and statement series:

Somatic Radiation Dose for the General Population, Report of the Ad Hoc Committee of the National Council on Radiation Protection and Measurements, 6 May 1959, *Science*, February 19, 1960, Vol. 131, No. 3399, pages 482-486

Dose Effect Modifying Factors In Radiation Protection, Report of Subcommittee M-4 (Relative Biological Effectiveness) of the National Council on Radiation Protection and Measurements, Report BNL 50073 (T-471) (1967) Brookhaven National Laboratory (National Technical Information Service Springfield, Virginia)

Index

- Accuracy of Output Display Standard (ODS) indices 445–450
 - acoustic-pressure spatial distribution 449
 - bone thermal index 447
 - cranial thermal index 447
 - estimation of attenuation 446
 - nonlinear propagation 445
 - nonthermal-damage threshold, frequency dependence 449
 - recent tests, thermal indices 450
 - soft-tissue thermal index 448
- Acoustic cavitation, bioeffects in mammalian tissues 213–239
 - bioeffects of speculative relevance 233
 - blood 219, 224, 231
 - brain 213
 - diagnostic fields 226
 - embryos 222
 - fetal hemorrhage near bone 225, 232
 - heart 223, 231
 - intestine 218, 223, 230
 - kidney 221
 - lithotripsy 220
 - liver 213, 221
 - lung 222, 226, 230
 - muscle 215
 - paraplegia 217
 - sonoluminescence 216
 - synergism 232
 - urine 220
- Acoustic microstreaming 38, 40
 - cells 38
 - cell suspensions 38
 - in vivo* experiments 40
- Acoustic outputs 280–282, 284, 287–289, 292, 294, 298–303, 305, 307, 310–318, 454, 456
 - additional data in operator's and reference manuals 294
 - AIUM standard 284
 - bioeffects relevant to equipment design changes 303
 - conclusions of NCRP Report No. 113 (1992) 454
 - data for compliance with Output Display Standard (ODS) 289
 - diagnostic information content relative to acoustic pressure 305
 - effective penetration relative to increased output 307
 - equipment output data, further information 298–302
 - existing diagnostic systems 282
 - FDA 510(k) guidance 282
 - historical trends 282
 - IEC 61157 standard 292
 - mechanical index 289
 - mechanical index data 288
 - NEMA standard 284
 - nonlinear propagation in tissue 456
 - output-labeling guidance and standards 282
 - possible image and signal quality improvement 310–313
 - possible peak-pressure reduction 314–318
 - reporting-table example 287
 - risk, outputs versus image quality 280
 - thermal index data 288
 - thermal indices 289
- Acoustic outputs, current equipment 280–302

- Acoustic outputs, diagnostic equipment 280–318
- Acoustic outputs, rationale for current and desired use 302–318
- Acoustical predictors 138
 - for safety guidelines 138
- Acoustic pressure 464
 - nonlinear propagation 464
- Acoustic radiation force 24, 26, 30, 95
 - banding of red cells 26
 - bubble vibration 95
 - pearl chains 30
 - response by eye 24
 - response by heart 26
 - torques on small particles 26
- Acoustic streaming 31, 33–34, 36–38
 - agglutination and aggregation 36
 - cells 38
 - cell suspension 38
 - cellular inactivation 34
 - heat transport 34
 - in diagnostic ultrasound 33
 - myocardial cells 37
 - theory 31, 37
- American Institute of Ultrasound in Medicine (AIUM) standard 284
- Auditory response 17–22
 - basilar artery 21
 - bone conduction 20
 - cat auditory system 17
 - human sensing 18
 - in utero* by ultrasound scanning 21
- Bioeffects 213, 215–226, 230–233, 303, 319–378, 383, 388–389, 392, 395, 397, 402
 - acoustic cavitation 226
 - blood 219, 224, 231
 - brain 213
 - Campbell study 395
 - diagnostic fields 226
 - embryo 222
 - fetal activity 388
 - fetal exposure 383
 - fetal hemorrhage near bone 225, 232
 - heart 223, 231
 - intestine 218, 223, 230
 - kidney 221
 - lithotripsy 220
 - liver 213, 221
 - lung 222, 226
 - muscle 215
 - Newnham study 392
 - nonthermal 319
 - paraplegia 217
 - RADIUS study 389
 - relevance to equipment design
 - changes 303
 - sonoluminescence 216
 - speculative relevance to cavitation 233
 - statistical considerations 397
 - status current human studies 402
 - temperature elevation 319
 - thermal 319
 - urine 220
- Bioeffects in cell suspensions 147, 150
 - contrast agents 150
 - gas-filled micropores 147
- Bioeffects in mammalian tissues 213–239
- Bioeffects, internal gas bodies 159
- Bioeffects, *in vitro* 171–212
 - cell lysis 176
 - cell morphology 202
 - effects on deoxyribonucleic acid 204
 - electrical excitability 202
 - exposure systems 173
 - growth 204
 - inertial cavitation 171
 - influence of cells and media 192
 - lithotriptors 208
 - membrane permeability 206
 - on surviving cells 176
 - phagocytic activity 202
 - sublethal 202

- Bioeffects, non-mammalian
 - 146–170
 - noninertial cavitation 146
- Bioeffects on 17–18, 20–24, 26, 28, 30, 36–37, 40–44, 47, 68, 69, 213, 215–226, 230–233, 302
 - bone repair 44
 - cardiac performance 44
 - cat auditory system 17
 - Drosophila* larva 69
 - Elodea* leaf 69
 - eye 24
 - fetal hearing 21
 - fetal hemorrhage 47
 - frog skin 43
 - hearing 20
 - heart 26
 - Hydrodictyon reticulatum* 40
 - membrane potential 22
 - middle ear 18
 - mouse mesenteric blood vessel 41
 - myocardial cells 37
 - red cells 28, 30, 36
 - skin 23
 - viscoelastic media 68
- Bioeffects, shear-stress hypothesis 165
- Biophysical analysis 165
 - shear-stress hypothesis 165
- Bubble detection 62
- Bubble radial pulsation 52
- Bubble response 107
 - nonlinear 107
- Bubble stability 60
- Bubble vibration 92–93, 95, 99–100, 187
 - acoustic microstreaming 100
 - acoustic radiation force 95
 - bubble motion 95
 - effect on nearby particles 99
 - effect on nearby red blood cells 99
 - heat generated 93
 - hydrodynamic shear 95
 - radiated acoustic power 93
- Campbell study 395
- Cell lysis, *in vitro* 179–180, 183–184, 186–190, 192, 196, 198–201, 208
 - alternating direction of ultrasound direction 186
 - attenuation of ultrasound by bubbles 180
 - bubble implosion and jets 189
 - bubble recycling 184
 - cell-bubble collisions 188
 - cell concentration 196
 - chemotherapeutic agents 201
 - contrast agents 198
 - free radicals 190
 - gas content of the medium 200
 - influence of cells and media 192
 - influence of exposure conditions 179
 - lithotrippers 208
 - mechanical stirring 183
 - mechanisms of lysis 187
 - nucleation 192
 - other sonochemicals 190
 - rotation of exposure tube 180
 - shear near moving bubbles 188
 - standing waves 183
 - superposed ionizing radiation 201
 - temperature 200
 - viscosity of the medium 199
- Cell studies 171
 - advantages and disadvantages 171
 - in vitro* 171
- Cell studies, *in vitro* 177
 - cavitation 177
 - heat production 177
 - sonochemistry 177
- Cell suspensions 147, 150, 156
 - hemolysis 150
 - monolayers 156
- Cellular inactivation 34
 - heat and shear 34
- Clinical surveys 382–383, 388–389, 392, 395, 397, 402
 - Campbell study 395
 - fetal activity 388

- fetal exposure 383
- Newnham study 392
- RADIUS study 389
- statistical considerations 397
- status current human studies 402
- ultrasound exposure 382
- Computations of temperature rise 351
- Contrast agents 78, 80–82, 84, 88, 150, 254
 - commercial examples 80
 - diagnostic ultrasound 78
 - encapsulated bubbles 82
 - engineering stability 78
 - in vivo* cavitation in blood 81
 - limits to exposure estimation 254
 - medical exploitation 88
 - nucleation 84
 - physics of excitation 81
 - stability 84
- Damping constant 56
- Derating intensities, nonlinear propagation 458
- Derating pressure, nonlinear propagation 466
- Diagnostic fields, mammalian
 - bioeffects 226, 230–233, 254
 - acoustic cavitation 226
 - blood 231
 - fetal hemorrhage near bone 232
 - heart 231
 - intestine 230
 - lung 226
 - obstetrics 254
 - synergism 232
- Diagnostic fields, speculative
 - bioeffects 233–235, 237
 - blood vessel endothelial damage 233
 - enhanced effects by contrast agents 235
 - perfusion 234
 - sonochemical tumor treatment 237
 - thrombolysis 234
- Diagnostic ultrasound 33, 78
 - acoustic streaming 33
 - contrast agents 78
- Diffusion 60
- Drosophila* eggs and larvae 161
 - internal gas bodies 161
- Elodea* 159, 168
 - internal gas bodies 159
 - shear-stress hypothesis 168
- Epidemiology 379–403
 - Campbell study 395
 - causality 382
 - clinical surveys 382
 - fetal activity 388
 - fetal exposure 383
 - methodology 380
 - Newnham study 392
 - pregnancy outcomes 379
 - RADIUS study 389
 - statistical considerations 397
 - status current human studies 402
- Epidemiology, ultrasound exposure (see Epidemiology)
- Equipment, acoustic outputs (see Acoustic outputs)
- Equipment design, possible changes 303–305, 307, 310–318
 - duty factor 304
 - dwell time 304, 305
 - effective penetration relative to increased output 307
 - polarity 303
 - possible image- and signal-quality improvement 310–313
 - possible peak-pressure reduction 314–318
 - pulse duration 303, 305
 - relevant to bioeffects 303
 - repetition rate 304, 305
 - wave shape 303
- Equipment output data 298–301
 - beam dimensions 301
 - focal gain 301
 - frequency range 299
 - historical trends 298

- manufacturer supplied versus independently measured data 298
 - pulse duration 300
 - pulse repetition rates 300
- Exposure estimation 240–245, 247–257, 262, 270, 272–277
 - acoustic properties of tissues 247–251
 - air cavities in intestines 274
 - attenuation 241
 - attenuation in obstetrics 257
 - bone thermal index (TIB) 243
 - digestive tract 274
 - direct lung studies 273
 - during echocardiography 272
 - esophagus 275
 - fixed-path models 242
 - homogeneous models 242
 - indirect lung exposures 272, 273
 - insertion-loss measurements in obstetrics 257
 - intensity 240
 - limits to accuracy 252
 - mechanical index (MI) 243
 - minimally attenuating fluid paths 272
 - near surface bone thermal index (TIC) 243
 - neonatal head 276
 - nonlinear propagation, limits on accuracy 252
 - obstetrical attenuation models 262
 - obstetrical patient-specific attenuation models 270
 - obstetrics 254
 - ophthalmology 277
 - other effects, limits on accuracy 252
 - Output Display Standard (ODS) 243
 - path lengths in obstetrics 256
 - patient-specific adjustment of the homogeneous attenuation model 247
 - power 240
 - pressure 240
 - propagation-path models 241
 - scanning sensitive tissues 272
 - soft-tissue thermal index (TIS) 243
 - specialized tissue models 243–245
 - thermal index (TI) 243
 - tissue characteristics 240
 - transcranial 276
 - using probes 275
- Exposure estimation, human beings 240–279
- Exposure models 240, 282
- Fetal activity 388
- Fetal core temperature 321
- Fetal exposures 383, 389, 392, 395, 397
 - Campbell study 395
 - Newnham study 392
 - RADIUS study 389
 - statistical considerations 397
- Food and Drug Administration (FDA) 510(k) guidance 282
- Free bubbles 435
 - mechanical equilibrium 435
- Gas-body activation 52, 56, 60, 64, 65, 66, 68, 71, 76, 77, 78, 92, 104
 - acoustic microstreaming 104
 - bubble stability 60
 - contrast agents 78
 - damping constant 56
 - definition 65
 - diagnostic ultrasound 78
 - diffusion 60
 - engineering of stabilized gas bodies 78
 - gas-filled channels 76
 - in mammals 77
 - in viscoelastic media 68
 - radial pulsation 52
 - rectified diffusion 56
 - spherical gas bubble 52
 - stability 66
 - structures 66

- surface waves 64
- trapped gas theory 71
- vibration of bubbles 92
- vibration of stabilized gas bodies 92
- viscoelastic media 68
- Gas-body vibration 92, 104
 - acoustic microstreaming 104
- Gas-filled channels in 76
 - Elodea* leaves 76
 - fruit-fly larvae 76
 - plant roots 76
- Gas-filled micropores 147
- Genetic effects 204

- Harmonics 62
- Heating rates 459
 - nonlinear propagation 459
- Heat-shock proteins 332
- Hemolysis 150, 151–156
- Human studies 402
 - current epidemiological status 402

- Inertial cavitation 107–109, 125, 127, 129, 131, 135, 138, 171, 173, 177, 179, 187
 - acoustical predictors 138
 - bioeffects 171
 - cell lysis, *in vitro* 179
 - cells, *in vitro* 171
 - chaos 125
 - definition 108
 - experimental repetitive cavitation 129
 - exposure systems 173
 - indeterminate motion 125
 - jet formation 127
 - mechanisms of action, *in vitro* 177
 - mechanisms of lysis 187
 - nonlinear bubble response 107
 - Rayleigh collapse curve 108
 - sonochemistry 135
 - sonoluminescence 131
 - surface disturbances 127
- Inertial cavitation *in vitro* 192, 202, 208
 - influence of cells and media 192
 - lithotriptors 208
 - sublethal cell effects 202
- Inertial cavitation theory 109, 113, 116, 120
 - by very short pulses 120
 - general 109
 - spherical symmetry 116
 - stable noninertial cavitation, spherical symmetry 113
- Intensity 456
 - nonlinear propagation 456
- Internal gas bodies 159, 161
 - Drosophila* eggs and larvae 161
 - insects 161
 - plants 159
- International Electrochemical Commission (IEC) 61157
 - standard 292

- Lithotripsy 220–225
 - acoustic cavitation *in vivo* 220
 - blood 224
 - embryos 222
 - fetal hemorrhage near bone 225
 - heart 223
 - intestine 223
 - kidney 221
 - liver 221
 - lung 222
 - negative pressures 224
- Lithotriptors 208
 - cell lysis *in vitro* 208

- Mammalian tissues 213
 - acoustic cavitation 213
 - bioeffects 213
- Maternal core temperature 321
- Measurements of temperature rise 357, 362
 - mammalian tissues 362
 - models 357
- Mechanical index 440, 468
 - calculation 440
 - nonlinear propagation 468
- Membrane damage 147
- Minimally attenuating fluid paths 272

- Models for exposure estimation 240–279
- Monolayers 156–158
- National Electrical Manufacturers Association (NEMA) standard 284
- Newnham study 392
- Noninertial cavitation 50–106, 146, 435
- activation of stabilized gas bodies 65
 - bioeffects 146
 - bubble detection 62
 - free bodies 50
 - gas-body activation 50
 - harmonics 62
 - mechanical equilibrium of free bubbles 435
 - non-mammalian systems 146
 - scattering 62
- Noninertial cavitation bioeffects 147, 150, 159, 165
- biophysical analysis 165
 - cell suspensions 147
 - contrast agents 150
 - internal gas bodies 159
 - shear-stress hypothesis 165
- Nonlinear bubble response 107–145
- inertial cavitation 107
- Nonlinear propagation 252, 454, 456, 458–459, 462, 464, 466, 468
- acoustic pressures 464
 - conclusions of NCRP Report No. 113 (1992) 454
 - derating intensities 458
 - derating pressures 466
 - effect of apodization on intensity 458
 - focal intensity relative to source intensity 456
 - heating rates 459
 - limits to exposure estimation 252
 - mechanical index 468
 - temperature increments 462
- Nonlinear propagation: An update 454–472
- Nonthermal mechanisms in
- absence of cavitation 16–49
 - acoustic power measurement 16
 - acoustic radiation force 16, 26
 - acoustic streaming 31
 - banding of red cells 26
 - pearl chains 30
 - radiation pressure 16
 - response by eye 24
 - response by heart 26
 - reversible modification of membrane potential 22
 - tactile perception 23
 - torques on small particles 26
 - unidentified mechanisms 42
- Nucleation 192, 194
- endogenous 194
 - exogenous 194
- Obstetrics 254, 256, 257, 262, 266, 269, 270
- attenuation measurements 257
 - attenuation models 262
 - displayed thermal and mechanical indices 266
 - exposure estimation 254
 - insertion-loss measurements 257
 - path-length measurements 256
 - patient-specific attenuation models 270
 - summary of attenuation models 269
- Output display guidance 283
- Output Display Standard (ODS) 284, 289, 299, 439–451
- acoustic-pressure spatial distribution 449
 - accuracy of ODS indices 445
 - bone thermal index 447
 - cranial thermal index 447
 - data for compliance 289
 - equations for thermal and mechanical indices 440
 - estimation of attenuation 446
 - frequency range 299

- labeling 284
- maximal values of thermal indices 444
- measurement 284
- nonlinear propagation 445
- nonthermal damage threshold, frequency dependence 449
- recent tests, thermal indices 450
- soft-tissue thermal index 448
- Output-labeling guidance and standards 282

- Pregnancy outcomes 379
 - epidemiology 379

- RADIUS study 389
- Rayleigh collapse curve 108
- Recommendations of this Report 430–434
- Rectified diffusion 60
- Risk, equipment outputs versus image quality 280

- Scanning sensitive tissues 272
- Scattering 62
- Shear-stress hypothesis 165, 167, 168, 169
 - applications of 167
 - Elodea* 168
 - other mechanisms 169
- Sonochemistry 135
- Sonoluminescence 131, 134, 136
 - detection of cavitation 136
 - multibubble 134
- Statistical considerations 397–398, 400–401
 - calculation prospective significance 398
 - calculation retrospective significance 397
 - incidence detection in medical practice 400–401
 - number of subjects required 397
- Summary and conclusions of this Report 404–429

- Surface waves 64
- Surgery, temperature related 369

- Temperature elevation 319–378
 - basic information 320
 - bioeffects 319
 - computations of temperature rise 351
 - heat-shock proteins 332
 - mammalian embryo and fetus ultrasound exposures *in vivo* and *in vitro* 334
 - maternal and fetal core-temperature relations 321
 - measurements of temperature rise in mammalian tissues 362
 - measurements of temperature rise in models 357
 - nonthermal bioeffects 319
 - role of temperature during ultrasound exposure 349
 - temperature-related surgery 369
 - thermal bioeffects 319
 - thermally induced teratogenesis re-evaluated 337
 - ultrasonic hyperthermia 369
- Temperature increments 462
 - nonlinear propagation 462
- Temperature-rise computations 351
- Teratogenesis, thermally induced 324
- Teratogenesis, thermally induced re-evaluation 337
- Thermal bioeffects 319
- Thermal elevation 324, 332
 - heat-shock proteins 332
 - thermally induced teratogenesis 324
- Thermal indices 440
 - calculation 440
- Thermally induced teratogenesis 324
- Thermally induced teratogenesis re-evaluated 337

- Ultrasonic hyperthermia, surgery 369
- Ultrasound exposure, epidemiology (see Epidemiology)
- Ultrasound exposures of mammalian embryos and fetuses *in vivo* and *in vitro* 334
- Unidentified mechanisms 42, 44, 47, 48
- bone repair 44
- cardiac performance 44
- electrical potentials and currents 42
- fetal hemorrhage 47
- lithotripsy 47
- lithotripsy under noncavitating conditions 48
- Viscoelastic media 68

akusher-lib.ru